STRUCTURE AND FUNCTION OF CHLOROPLASTS

EDITED BY: Hongbo Gao, Rebecca L. Roston, Juliette Jouhet and Fei Yu

PUBLISHED IN: Frontiers in Plant Science

frontiers Research Topics

ISSN 1664-8714
ISBN 978-2-88945-713-7
DOI 10.3389/978-2-88945-713-7

About Frontiers

Frontiers is more than just an open-access publisher of scholarly articles: it is a pioneering approach to the world of academia, radically improving the way scholarly research is managed. The grand vision of Frontiers is a world where all people have an equal opportunity to seek, share and generate knowledge. Frontiers provides immediate and permanent online open access to all its publications, but this alone is not enough to realize our grand goals.

Frontiers Journal Series

The Frontiers Journal Series is a multi-tier and interdisciplinary set of open-access, online journals, promising a paradigm shift from the current review, selection and dissemination processes in academic publishing. All Frontiers journals are driven by researchers for researchers; therefore, they constitute a service to the scholarly community. At the same time, the Frontiers Journal Series operates on a revolutionary invention, the tiered publishing system, initially addressing specific communities of scholars, and gradually climbing up to broader public understanding, thus serving the interests of the lay society, too.

Dedication to Quality

Each Frontiers article is a landmark of the highest quality, thanks to genuinely collaborative interactions between authors and review editors, who include some of the world's best academicians. Research must be certified by peers before entering a stream of knowledge that may eventually reach the public - and shape society; therefore, Frontiers only applies the most rigorous and unbiased reviews.
Frontiers revolutionizes research publishing by freely delivering the most outstanding research, evaluated with no bias from both the academic and social point of view. By applying the most advanced information technologies, Frontiers is catapulting scholarly publishing into a new generation.

What are Frontiers Research Topics?

Frontiers Research Topics are very popular trademarks of the Frontiers Journals Series: they are collections of at least ten articles, all centered on a particular subject. With their unique mix of varied contributions from Original Research to Review Articles, Frontiers Research Topics unify the most influential researchers, the latest key findings and historical advances in a hot research area! Find out more on how to host your own Frontiers Research Topic or contribute to one as an author by contacting the Frontiers Editorial Office: researchtopics@frontiersin.org

STRUCTURE AND FUNCTION OF CHLOROPLASTS

Topic Editors:
Hongbo Gao, Beijing Forestry University, China
Rebecca L. Roston, University of Nebraska-Lincoln, United States
Juliette Jouhet, Laboratoire de Physiologie Cellulaire Vegetale, France
Fei Yu, Northwest A&F University, China

Citation: Gao, H., Roston, R. L., Jouhet, J., Yu, F., eds. (2019). Structure and Function of Chloroplasts. Lausanne: Frontiers Media. doi: 10.3389/978-2-88945-713-7

Table of Contents

III. METHODS

IV. PERSPECTIVES

V. HYPOTHESIS

frontiers in Plant Science

EDITORIAL
published: 14 November 2018
doi: 10.3389/fpls.2018.01656

Editorial: Structure and Function of Chloroplasts

*Rebecca L. Roston[1], Juliette Jouhet[2], Fei Yu[3] and Hongbo Gao[4]**

[1] University of Nebraska-Lincoln, Lincoln, NE, United States, [2] UMR5168 Laboratoire de Physiologie Cellulaire Vegetale (LPCV), Grenoble, France, [3] Northwest A&F University, Xianyang, China, [4] Beijing Forestry University, Beijing, China

Keywords: chloroplast, photosynthesis, lipid, envelope, thylakoid, development

Editorial on the Research Topic

Structure and Function of Chloroplasts

The primary energy resource of life on earth is the sun, whose energy is captured in the form of usable carbons by a process called photosynthesis. Photosynthesis occurs within a cellular organelle adapted to that purpose, called the chloroplast. Chloroplasts are unique metabolic and sensory organelles restricted to plants, algae, and a few protists. In this special topic, we aimed to gather new research, hypotheses, and reviews that would help us to better understand the important role of chloroplasts in all photosynthetic organisms. We were fortunate enough to have submissions from many talented chloroplast researchers. This topic contains a total of 24 papers of which 13 are original research, 3 are methods, 5 are reviews or mini-reviews, 2 are perspectives and one is a hypothesis.

Chloroplasts developed in an ancient eukaryotic symbiosis, which has since evolved into many divergent organisms. Because of this, studies on algae and other early endosymbionts are particularly relevant as they help us to triangulate back to a better understanding of that first endosymbiotic event. From *Euglena gracilis*, a unique protist with an evolutionarily recent algal endosymbiont, the importance of balancing energy needs with organelle abundance was demonstrated (Shibata et al.) From the model green alga species *Chlamydomonas reinhardtii*, are included three advances. First, a protein conserved in green lineages and diatoms was found to regulate chloroplast redox and be important for the accumulation of Photosystem II (PSII; Xing et al.) Second, a ferredoxin-dependent biliverdin reductase was discovered to function both in retrograde bilin biosynthesis and interaction with light-dependent protochlorophyllide oxidoreductase (Zhang et al.) Third, a new method to isolate intact chloroplasts after nitrogen stress as monitored by ultrastructure observation and fatty acid biomarkers analysis was developed (Yang et al.)

Chloroplasts make many major metabolic contributions to the cell. Photosynthesis has been studied for many decades, but the finer details remain to be established. Recent advances in single-particle cryo-electron microscopy, X-ray free electron laser, and other techniques have revealed unprecedented structural and catalytic details of the photosynthetic protein complexes, which are reviewed by Gao et al. with an emphasis on the light-harvesting complex of PSII. Chlorophyll fluorescence imaging is one of the most important tools for studying photosynthesis. Ruhle et al. reviewed various chlorophyll fluorescence-based genetic screening strategies in *Arabidopsis* and *Chlamydomonas*. Type 1 NADPH dehydrogenase is a protein interacts with Photosystem I (PSI) and has a known role in respiration, cyclic electron transport around PSI and CO_2 acquisition. This protein was also shown to be important for stabilizing the PSI complex in *Synechocystis* under stress conditions by Zhao et al. Other chloroplast metabolic outputs covered by this special issue include vitamin E/tocopherol and its precursors which is reviewed by Pellaud and Mene-Saffrane and the role of vitamin E/tocopherol in phosphate stress tolerance which was probed by Allu et al.

OPEN ACCESS

Edited and reviewed by:
Cornelia Spetea,
University of Gothenburg, Sweden

****Correspondence:***
Hongbo Gao
gaohongbo@bjfu.edu.cn

Specialty section:
This article was submitted to Plant Physiology, a section of the journal Frontiers in Plant Science

Received: *15 October 2018*
Accepted: *25 October 2018*
Published: *14 November 2018*

Citation:
Roston RL, Jouhet J, Yu F and Gao H (2018) Editorial: Structure and Function of Chloroplasts. Front. Plant Sci. 9:1656. doi: 10.3389/fpls.2018.01656

The assembly and transfer of iron-sulfur clusters critical for many aspects of plant metabolism was reviewed by Lu. An important methodological advance in generating cell suspension cultures with which to investigate photosynthesis and other chloroplast metabolic outputs was provided by Sello et al.

Chloroplasts have a number of structures that allow photosynthesis to occur. One of these is the photosynthetic (thylakoid) membrane, which is composed primarily of galactolipids. The role of galactolipids in chloroplast biogenesis was nicely reviewed by Rocha et al. Kobayashi et al. added their perspective on thylakoid phosphatidylglycerol content, and Phosphatidic Acid Phosphohydrolases were shown to be critical for the maintenance of chloroplast membranes (Yoshitake et al.) A natural consequence of positioning highly desaturated membrane lipids near to highly-reactive photosynthetically-derived reactive oxygen species is the production of oxylipins, a subset of which are highly toxic. These can be reduced by the chloroplast envelope quinone oxidoreductase homolog, and its structure was solved by Mas et al. A perspective on the extent to which a thylakoid metalloprotease called FtsH2 controls reactive oxygen signaling was contributed by Dogra et al. An outstanding question in the field of thylakoid structure is how the thylakoid membranes are developed, and a new mechanistic hypothesis regarding the involvement of dynamin-like proteins was contributed by Jilly et al.

The photosynthetic thylakoid membranes are encapsulated within the chloroplast double envelope membranes. All of these must divide together to propagate, and the gene *GIANT CHLOROPLAST 1* was previously suggested to play a critical role in this process. However, Li et al. used CRISPR-mediated gene editing to show that it rarely has giant chloroplasts and likely only has a minor role in chloroplast division. Interestingly, Giant Chloroplast 1 is an inner envelope protein well conserved in plants and its true function awaits further investigation. Encapsulated by the envelopes is a special environment called the stroma which has a strongly variable pH, due to the movement of protons during photosynthesis. Su and Lai established a simple and non-destructive method to measure the stromal pH using a fluorescent dye. Several other genes affecting chloroplast development are reported. The first was previously known only through its mutant phenotype as *variegated5-1*. Its function was defined as a likely Mg^{2+} transporter by Liang et al. leading to interesting new avenues to investigate the role of Mg in chloroplast development. The role of Mg in chlorophyll biosynthesis is well known and was expanded in soybean by Zhang et al. where a complex regulatory system may be needed to control Mg incorporation into chlorophyll. The second, *Dwarf and Yellow 1* may represent a new regulatory mechanism of chloroplast biogenesis and was reported by Huang et al. The third, *Shikimate Kinase-Like 1*, which seems to lack function in the shikimate pathway, was shown to be important for chloroplast development and also to be involved in auxin-related pathways by Xu et al. The majority of the above studies rely on the excellent genetic systems available in model species. In some non-model plants, like the peach tree *Prunus persica*, chloroplast development varies widely by the highly defined tissue types. The strong divergence of the tissues was taken advantage of by Chen et al. which mapped the roles of transcription factors in controlling tissue-specific development. Clearly, further studies are needed to uncover all of the critical components of chloroplast biogenesis.

Together, the papers span a wide breadth of chloroplast structure and function advances from investigations of photosystem structures and the membranes on which they reside, to development within non-model protists and trees. It is our hope that these exciting advances prompt research into the new avenues of research begun here.

AUTHOR CONTRIBUTIONS

All authors listed have made a substantial and intellectual contribution to the work, and approved it for publication.

FUNDING

HG was supported by National Nature Science Foundation of China (Grant No. 31570182).

ACKNOWLEDGMENTS

We thank all the authors and reviewers that have contributed to this Research Topic.

Conflict of Interest Statement: The authors declare that the research was conducted in the absence of any commercial or financial relationships that could be construed as a potential conflict of interest.

frontiers in Plant Science

REVIEW
published: 30 January 2018
doi: 10.3389/fpls.2018.00055

Chlorophyll Fluorescence Video Imaging: A Versatile Tool for Identifying Factors Related to Photosynthesis

Thilo Rühle, Bennet Reiter and Dario Leister*

Plant Molecular Biology, Department of Biology, Ludwig Maximilian University of Munich, Munich, Germany

Measurements of chlorophyll fluorescence provide an elegant and non-invasive means of probing the dynamics of photosynthesis. Advances in video imaging of chlorophyll fluorescence have now made it possible to study photosynthesis at all levels from individual cells to entire crop populations. Since the technology delivers quantitative data, is easily scaled up and can be readily combined with other approaches, it has become a powerful phenotyping tool for the identification of factors relevant to photosynthesis. Here, we review genetic chlorophyll fluorescence-based screens of libraries of Arabidopsis and Chlamydomonas mutants, discuss its application to high-throughput phenotyping in quantitative genetics and highlight potential future developments.

Keywords: photosynthesis, Arabidopsis, Chlamydomonas, chloroplast, screening, chlorophyll fluorescence, forward genetic screen, reverse genetic screen

OPEN ACCESS

Edited by:
Juliette Jouhet, UMR5168 Laboratoire de Physiologie Cellulaire Vegetale (LPCV), France

Reviewed by:
Dimitris Petroutsos, Univ. Grenoble Alpes, CNRS, CEA, INRA, BIG-LPCV, Grenoble, France
Katarzyna Glowacka, University of Illinois at Urbana–Champaign, United States

****Correspondence:***
Thilo Rühle
thilo.ruehle@biologie.uni-muenchen.de;
thiloruehle@hotmail.com

Specialty section:
This article was submitted to Plant Physiology, a section of the journal Frontiers in Plant Science

Received: *26 October 2017*
Accepted: *10 January 2018*
Published: *30 January 2018*

Citation:
Rühle T, Reiter B and Leister D (2018) Chlorophyll Fluorescence Video Imaging: A Versatile Tool for Identifying Factors Related to Photosynthesis. Front. Plant Sci. 9:55. doi: 10.3389/fpls.2018.00055

INTRODUCTION

Since the discovery of the rapid fluorescence transient associated with the initial exposure of dark-adapted leaves to light (the Kautsky effect) in 1931, chlorophyll (Chl) fluorescence has emerged as an indispensable probe in photosynthesis research. There are several reasons for this remarkable development: (i) measurements of Chl fluorescence dynamics can be carried out on intact plants or algal cell cultures in an essentially non-invasive manner, (ii) multiple quantitative photosynthetic parameters can be extracted in short measuring times, (iii) Chl fluorescence measurements can be easily combined with other analytical tools, (iv) instrumentation capable of automated quantification and analysis of Chl fluorescence is now commercially available to a broad range of plant scientists and the technique is no longer restricted to a small group of experts, (v) technical advances achieved in recent decades now permit investigations from the single-cell level (Oxborough and Baker, 1997; Küpper et al., 2000; Tseng and Chu, 2017) to crop plants in the field (Virlet et al., 2017), and open up numerous applications, such as the use of Chl fluorescence-derived parameters as indicators of abiotic (Baker, 2008; Rungrat et al., 2016) or biotic stress (reviewed in: Chaerle et al., 2009). A particularly important technological breakthrough in this field was the development of video imaging systems (Omasa et al., 1987; Fenton and Crofts, 1990), which not only paved the way for the examination of the spatial heterogeneity within a sample, but also made it possible to assess large numbers of samples (e.g., individual plants or cell colonies) in a

single experimental run. Thus, Chl fluorescence video imaging (CFVI) can be regarded as an ideal phenotyping technology for the identification of mutants affected in photosynthesis.

In the following, we will give an overview of CFVI-based screens which have been carried out on plant and green algal mutant libraries in the past, discuss recent progress and consider how the technology may be further developed in the future. Technical and theoretical aspects of Chl fluorescence imaging have been described in detail in Nedbal and Whitmarsh (2004), as well as in Oxborough (2004). The interested reader is also referred to several excellent review articles for introductions to the biophysical basis and biochemical implications of Chl fluorescence-derived photosynthetic parameters (Maxwell and Johnson, 2000; Roháček, 2002; Baker, 2008; Kalaji et al., 2017).

In brief, a typical state-of-the-art CFVI analysis is based on the application of pulse-amplitude-modulated (PAM), measuring light (ML), which is generated by a powerful array of LEDs placed in a defined working distance to the sample. Those LEDs can also serve for the generation of short saturation pulses (SPs) and for actinic illumination (AL) of the samples to drive photosynthesis. Emitted red Chl fluorescence is detected by a computer-connected charge-coupled device (CCD) video camera which is protected from excitation light or near-infrared radiation by appropriate color glass filters. Custom software allows the conversion of Chl fluorescence signals into false color images, calculation of different photosynthetic parameters and quantitative analyses of the results. In general, plant or algal samples are dark-adapted prior to the measurements to open all PSII reaction centers. Then, samples are exposed to ML for dark fluorescence yield (F_0) determination and to a short SP for maximum fluorescence yield (F_m) measurement, respectively (see also **Figure 1A**). In this state, the PSII quantum yield (F_v/F_m) is maximal and can be calculated according to the equation $F_v/F_m = (F_m - F_0)/F_m$. AL is switched on and application of SPs provides maximum fluorescence yields (F_m') of illuminated samples. Effective PSII quantum yields (Φ_{II}) are calculated by the equation $\Phi_{II} = (F_m' - F)/F_m'$ (Genty et al., 1989), whereas the fluorescence yield (F) is recorded every time shortly before a SP and represents an average of several current fluorescence yield (F_t) pictures. Electron transport rates through PSII [ETR(II)] at a given photosynthetically active radiation (PAR) can be calculated according to Schreiber et al. (1995), using the equation $ETR(II) = \Phi_{II} \times PAR \times 0.84 \times 0.5$. Maximum ETR(II) measured at saturating light intensity provides an estimate of the maximum photosynthesis rate (P_{max}). F_m' values of illuminated samples are in general lowered compared to Fm by non-photochemical quenching (NPQ), which can be quantified according to the equation $NPQ = (F_m - F_m')/F_m'$ (Bilger and Björkman, 1990). NPQ mechanisms can be further examined in dark relaxation experiments. To this end, actinic light is switched off after a period of actinic light exposure and minimum fluorescence (F_0'') and maximum fluorescence yields (F_m'') are determined by application of SPs in the dark relaxation phase (**Figure 1A**). The two NPQ components qE (ΔpH-dependent feedback de-excitation, the major component of NPQ), and qI (photo-inhibitory quenching) can be calculated according to the equations $qE = F_m/F_m' - F_m/F_m''$ (Thiele et al., 1997) and $qI = (F_v - F_v'')/F_v$ (Björkman and Demmig, 1987).

Chl FLUORESCENCE VIDEO IMAGING IN FORWARD GENETIC APPROACHES

Screens for Chlamydomonas and Arabidopsis Mutants Defective in Photochemical Quenching

The first instance of the successful use of Chl fluorescence imaging to identify photosynthetic mutants was the detection of a '*high-chlorophyll-fluorescence*' (*hcf*) phenotype in a population of methyl-methane sulfonate-mutagenized *Chlamydomonas reinhardtii* cells by Bennoun and Levine (1967) (**Table 1**). The screen was based on the fact that severe perturbations in photosynthetic electron transport, such as those caused by incubating algal cells in the presence of the photosynthetic electron transport inhibitor 3-(3,4-dichlorophenyl)-1,1-dimethylurea (DCMU), lead to high steady-state levels of Chl fluorescence. Following its application for screening of Chlamydomonas mutant libraries (see for example Harris, 1989) the concept was tested in higher plants (Miles and Daniel, 1973) and employed for the screening of maize (Miles and Daniel, 1974; Barkan et al., 1986; Taylor et al., 1987) and Arabidopsis mutant libraries (Dinkins et al., 1994; Meurer et al., 1996b). Several factors involved in chloroplast biogenesis were identified using the *hcf* phenotyping method, including the maize proteins HCF106, HCF60, and HCF136 (reviewed in: Belcher et al., 2015) and the Arabidopsis proteins HCF5 (Dinkins et al., 1997), HCF101 (Lezhneva et al., 2004), HCF107 (Felder et al., 2001), HCF109 (Meurer et al., 1996a), HCF145 (Lezhneva and Meurer, 2004; Manavski et al., 2015), HCF152 (Meierhoff et al., 2003) and LPA1 (Peng et al., 2006).

Even though such *hcf* mutant screens can be performed rapidly and efficiently, and have significantly enhanced our knowledge of the molecular repertoire required for photosynthesis and chloroplast biogenesis, only mutants with severe defects can be unequivocally detected, and these are often lethal under photoautotrophic conditions. However, technological progress in Chl fluorescence analyses during the 1980s and 1990s allowed the technique to be employed for more elaborate modes of screening, and led to the identification of algal or plant mutants with relatively modest alterations in photosynthetic performance. For example, Varotto et al. (2000a,b) identified '*photosynthesis affected mutants*' (*pam*) in Arabidopsis on the basis of their lower effective quantum yields (Φ_{II}) (Genty et al., 1989) using a combination of a pulse-amplitude-modulation fluorometer (Schreiber et al., 1986) and an automated screening system. This set-up facilitated the screening of large *En* transposon or T-DNA mutagenized Arabidopsis populations, and *pam* mutants disrupted in the nucleus-encoded photosystem I subunits PsaE1 (*pam4*) (Varotto et al., 2000b) and PsaD1 (*pam62*)

TABLE 1 | Chronology of Chl fluorescence phenotyping based gene discovery studies.

Phenotype/principle	Organism	Authors
hcf	Chlamydomonas	Bennoun and Levine, 1967
hcf	Maize	Miles and Daniel, 1974
hcf	Maize	Barkan et al., 1986
hcf	Maize	Taylor et al., 1987
hcf	Arabidopsis	Dinkins et al., 1994
hcf	Arabidopsis	Meurer et al., 1996b
Low NPQ after high light treatment	Chlamydomonas	Niyogi et al., 1997
Low NPQ after high light treatment	Arabidopsis	Niyogi et al., 1998
Deficiency in state transition	Chlamydomonas	Fleischmann et al., 1999
Deficiency in state transition	Chlamydomonas	Kruse et al., 1999
Low NPQ after high light treatment	Arabidopsis	Shikanai et al., 1999
Alterations in Φ_{II}	Arabidopsis	Varotto et al., 2000a
Lack of NDH complex activity	Arabidopsis	Hashimoto et al., 2003
Identification of mutants with unchanged Φ_{II} after acclimation to high light	Arabidopsis	Walters et al., 2003
Low NPQ after high light treatment	Arabidopsis	Kalituho et al., 2006
hcf	Arabidopsis	Peng et al., 2006
Identification of photorespiration mutants by comparison of F_v/F_m values under varying CO_2 concentrations	Arabidopsis	Badger et al., 2009
Identification of NDH complex mutants in a guilt-by-association approach	Arabidopsis	Takabayashi et al., 2009
Quantitative genetic analysis of thermal dissipation	Arabidopsis	Jung and Niyogi, 2009
Identification of CEF mutants with a high qE	Arabidopsis	Livingston et al., 2010
Affected Chl fluorescence transients	Chlamydomonas	Houille-Vernes et al., 2011
Affected Chl fluorescence transients	Chlamydomonas	Tolleter et al., 2011
Identification of hydrogenase-deficient mutants using Φ_{II} measurements under anaerobiosis	Chlamydomonas	Godaux et al., 2013
Suppressor screen of mutants with a high NPQ in the absence of PsbS	Arabidopsis	Brooks et al., 2013
Identification of mutants with altered mitochondrial respiration using F_v/F_m measurements	Chlamydomonas	Massoz et al., 2015
Quantitative genetic analysis of variations in Φ_{II} acclimation to irradiance changes in different natural Arabidopsis accessions	Arabidopsis	van Rooijen et al., 2015
High transient NPQ after a dark-light shift	Arabidopsis	Zhang et al., 2016
Identification of mutants with emergent photosynthetic phenotypes under dynamic environmental conditions	Arabidopsis	Cruz et al., 2016
Identification of mitochondrial complex I mutants in a Φ_{II}-based screening of a mutagenized *pgrl1* library	Chlamydomonas	Massoz et al., 2017
Identification of mutants affected in the slowly reversible photoprotective form of NPQ termed qH	Arabidopsis	Malnoë et al., 2017

hcf, high chlorophyll fluorescence; NPQ, non-photochemical quenching; Φ_{II}, effective quantum yield of PSII; NDH complex, NADH dehydrogenase-like complex; F_v/F_m, maximal quantum yield of PSII; qE, energy-dependent quenching; CEF, cyclic electron flow.

(Ihnatowicz et al., 2004), the metal-ion transporter IRT1 (*pam25*) (Varotto et al., 2002), and the cytoplasmic *N*-acetyltransferase AtMAK3 (*pam21*) (Pesaresi et al., 2003), as well as the PSII assembly factor PAM68 (*pam68*) (Armbruster et al., 2010), were isolated and functionally characterized in subsequent studies.

Screens for Chlamydomonas and Arabidopsis Mutants Affected in Non-Photochemical Quenching (NPQ)

Due to their sessile lifestyle, many multicellular photosynthetic organisms have evolved various strategies to cope with light stress (Ort, 2001). When the photosynthetic machinery is exposed to excessively high levels of light, short- and long-term adaptive responses are triggered at the molecular level, which allow for the thermal dissipation of excited energy by NPQ mechanisms to prevent over-reduction of the electron transport chain. At least four processes contribute to NPQ: qE, qZ (zeaxanthin-dependent quenching), qT (state-transition-dependent quenching) and qI (reviewed in: Ruban, 2016). Several CFVI-based screens have been performed on mutagenized Chlamydomonas and Arabidopsis populations with the aim of dissecting the genetics of NPQ (**Table 1**). Mutant identification was essentially based on the comparison of two video images of Chl fluorescence captured under different illumination conditions. The first picture was taken in the dark-adapted state during a saturating light pulse (F_m), or shortly after the onset of high-light treatment (F). The second image was recorded after several minutes of exposure to high light either during a saturating light pulse (F_m') or not (F'). The NPQ values derived using the equation $(F - F')/F'$ or $(F_m - F_m')/F_m'$ were then visualized as false-color images, and several Chlamydomonas and Arabidopsis mutants affected in NPQ of excited Chl states could be identified. Subsequent analyses revealed three distinct groups of mutants with aberrant

NPQ (reviewed in: Golan et al., 2004). Mutants in the first group were impaired in the generation of a proton gradient across the thylakoid membrane, which is a prerequisite for the induction of qE (the ΔpH-dependent quenching component of NPQ), and were consequently defined as '*proton gradient regulation*' mutants (*pgr*). One such mutant, *pgr1*, was further characterized, and shown to be defective in the photosynthetic electron transfer C (*PETC*) gene, which encodes the Rieske subunit of the cytochrome b_6f complex (Munekage et al., 2001). Another mutant line impaired in the build-up of the proton gradient is *pgr5* (Shikanai et al., 1999; Munekage et al., 2002). It lacks a component of the antimycin A-sensitive cyclic electron flow (CEF) pathway, which is mediated by the ferredoxin-plastoquinone reductase PGRL1/PGR5 (Hertle et al., 2013). The second group with aberrant NPQ comprised the mutants *npq1* and *npq2*, which display defects in the xanthophyll cycle and are disrupted in the violaxanthin de-epoxidase and zeaxanthin epoxidase, respectively (Niyogi et al., 1997). The third type of mutant (*npq4*) showed normal pigment composition, xanthophyll cycle activity and photosynthetic electron transport, but this mutant was nevertheless specifically affected at the level of qE (Li et al., 2000). It turned out that the *npq4* mutant lacks the PSII-associated protein S (PsbS), which is now known to be the luminal pH sensor that triggers NPQ within the PSII antenna in plants (Li et al., 2000). In a subsequent study, which was designed to isolate Arabidopsis lines affected in other slowly reversible NPQ components, CFVI was used to screen mutagenized seedlings for suppressors of the *npq4* phenotype (Brooks et al., 2013). This screen yielded the *suppressor of quenching 1* (*soq1*), which has a high NPQ even in the absence of PsbS and lacks a thylakoid membrane protein (SOQ1) that harbors a thioredoxin-like, a β-propeller and a haloacid-dehalogenase domain. SOQ1 maintains light-harvesting efficiency and prevents formation of a slow, reversible NPQ mechanism that is independent of qE, qZ, and qT, but participates in a photoprotective, 'qI-like' mechanism termed qH (Malnoë et al., 2017). To identify factors involved in qH, suppressors of *soq1 npq4* were screened for by CFVI and two mutants affected either in chlorophyllide *a* oxygenase (CAO) or the plastid lipocalin (LCNP) showed a reversion to the low NPQ phenotype of *npq4*. In-depth analyses of both mutants provided evidence that qH operates under high-light and cold stress, and can be localized to the peripheral LHCII antenna of PSII and requires LCNP (Malnoë et al., 2017).

A further step toward an understanding of the molecular basis of NPQ was the identification of so-called '*state transition*' (*stt*) mutants with alterations in qT. State transitions involve the reversible association of the mobile pool of light-harvesting-complex II proteins (LHCIIs) with either PSII (state 1) or PSI (state 2) and re-establish a balanced distribution of light energy between the photosystems. Several studies (Fleischmann et al., 1999; Kruse et al., 1999) took advantage of the fact that the green alga Chlamydomonas undergoes large changes in Chl fluorescence during state transitions, which can be attributed to its significantly higher fraction of mobile LHCIIs (about 80%, Delosme et al., 1996) compared to land plants (15–20%) (Allen, 1992). Mutants affected in state transitions were identified by comparing fluorescence images taken under state-1 and state-2 conditions, and this type of differential fluorescence screen enabled Fleischmann et al. (1999) to isolate four *stt* mutants (*stt2, stt3, stt5,* and *stt7*). These mutants were characterized by high Chl fluorescence levels at room temperature even under state-2 conditions, indicating that they were physiologically locked in state 1. Further analyses showed that *stt7* lacks the thylakoid serine-threonine protein kinase Stt7, which is required for phosphorylation of LHCII in response to state-2 conditions (Depège et al., 2003).

Screening for Chlororespiratory Arabidopsis Mutants

In addition to the predominant linear electron flow pathway, which results in the production of both NADPH and ATP, two CEF routes around PSI have been described that are important for balancing the ATP/NADPH budget of photosynthesis, as well as for protecting the photosystems from photodamage in plants (reviewed in: Yamori and Shikanai, 2016). One of these pathways is mediated by the NADH-like dehydrogenase (NDH) complex, which is also responsible for chlororespiration in the dark. To identify '*chlororespiratory reduction*' mutants (*crr*) which are disrupted in NDH function, Hashimoto et al. (2003) established a CFVI-based screening system, in which the post-illumination rise of Chl fluorescence (PIF) after a low-light treatment was monitored in an Arabidopsis mutant population. Under such conditions, the fluorescence signal is almost proportional to the reduction state of the plastoquinone pool (Krause and Weis, 1991), so that the chlororespiratory activity of the NDH complex can be derived from the degree to which the PIF is depressed in mutants with a dysfunctional NDH complex (Shikanai et al., 1998). Screening of over 50,000 M2 seedlings for aberrant PIFs led to the identification of 17 *crr* mutants in Arabidopsis. These could be assigned to at least 11 loci, and further analyses revealed the existence of novel NDH subunits and allowed the functional characterization of factors required for efficient NDH complex biogenesis (reviewed in: Peng et al., 2011).

Screening for Arabidopsis Mutants Affected in Acclimation of Photosynthesis to the Environment

Plants and algae can undergo photosynthetic acclimation processes which take place over periods of hours or days and entail substantial changes in plastid and nuclear gene expression, as well as adjustments of the photosynthetic apparatus. For instance, the long-term response to high light levels has been thoroughly studied and, instead of reducing the demands on light harvesting, it actually enhances the capacity for electron transport and carbon dioxide fixation. To investigate the molecular mechanisms behind the signal cascades that activate the acclimation response to high light, Walters et al. (2003) screened an Arabidopsis mutant population for alterations in '*acclimation of photosynthesis to the environment*' (*ape*). Their CFVI screen was based on the observation that in wild-type Arabidopsis plants a 3-day exposure to high light raises effective quantum yields (Φ_{II}), and its goal was to

identify mutants that were unable to increase P_{max} under these conditions. Among the three *ape* mutants obtained, which showed distinct acclimation-defective phenotypes, *ape2* exhibited a lower P_{max} under all light regimes, and was disrupted in the chloroplast envelope triose-phosphate/phosphate translocator (TPT). Subsequent studies using Arabidopsis double and triple mutants altered in the day and night modes of photoassimilate export from the chloroplast provided evidence that carbohydrates act as chloroplast-to-nucleus retrograde signals and modulate the acclimation response to high light (Schmitz et al., 2012, 2014).

Screening for Arabidopsis Mutants Affected in Photorespiration

Ribulose-1,5-bisphosphate carboxylase/oxygenase (RuBisCO) not only fixes atmospheric CO_2 but also oxygen. The phosphoglycolate generated by the latter reaction must be degraded via a complex mechanism which is known as photorespiration, because CO_2 is released during the process. The photorespiratory pathway is distributed between four compartments (chloroplasts, cytosol, peroxisomes and mitochondria) and requires the action of several transporters and enzymes. Most of the early mutants affected in photorespiration were identified by their ability to grow normally in a high concentration (1%) of CO_2, while becoming chlorotic when shifted to ambient air (Somerville, 1986). Recently, it was shown that mutations in components involved in the photorespiratory pathway also impair photosynthetic light reactions, as revealed by the observation that photorespiratory mutants transferred from high to ambient CO_2 concentrations showed a decline in PSII functionality (Takahashi et al., 2007). Thus, Badger et al. (2009) set up a CFVI screen designed to detect mutants with more subtle photorespiratory phenotypes. To this end, levels of PSII function in mutagenized Arabidopsis seedlings grown under high concentrations of CO_2, and in its absence, were compared. Two major mutant phenotype classes could be distinguished. One group comprised 'photorespiration-like' mutants, which were characterized by F_v/F_m values that were close to those of wild-type plants under high CO_2 concentrations, but significantly lower than normal in the absence of CO_2. The second group consisted of lines in which F_v/F_m values were depressed even under high concentrations of CO_2. Remarkably, some members of the second group were able to partially recover PSII functionality after exposure to zero CO_2 concentrations, and were therefore named for this 'reverse photorespiration' phenotype (Badger et al., 2009).

Screening for Chlamydomonas Mutants Impaired in Hydrogenase Activity

As aquatic organisms, many unicellular green algae are characterized by a remarkably flexible metabolism, and can acclimate rapidly to anaerobic conditions (Terashima et al., 2010; Grossman et al., 2011). As part of an extensive response to anaerobiosis, expression and synthesis of oxygen-labile [Fe–Fe] hydrogenases are induced in *C. reinhardtii* and hydrogen production is linked to photosynthesis by ferredoxin-mediated electron supply. Several factors required for expression, maturation and activity of [Fe–Fe] hydrogenases have been identified, most of them through a H_2-sensing, chemochromic screening system that can discriminate Chlamydomonas mutants with aberrant H_2 production capacities (reviewed in: Hemschemeier et al., 2009). An alternative, less time-consuming approach has been demonstrated by Godaux et al. (2013), and takes advantage of the observation that mutants with defects in [Fe–Fe] hydrogenase activity exhibit low effective PSII quantum yields shortly after a shift from dark anaerobiosis to saturating light conditions. As a proof of concept, screening of a small Chlamydomonas population of about 3000 strains generated by insertional mutagenesis yielded five mutants with a Chl fluorescence signature similar to that of the [Fe–Fe] hydrogenase-deficient control strain, and one of them turned out to be defective in the previously characterized [Fe–Fe] hydrogenase assembly factor G (HydG) (Posewitz et al., 2004). Moreover, in various mutants affected in anaerobic energy metabolism, the effective quantum yield of PSII was shown to be correlated with the level of [Fe–Fe] hydrogenase activity. Thus, the screening system represents a time-saving, alternative approach to the chemochromic method, and is capable of detecting mutants impaired in [Fe–Fe] hydrogenase biogenesis, regulation or activity.

Screening for Chlamydomonas Mutants Altered in Mitochondrial Respiration

Although respiration and photosynthesis take place in different organelles in photosynthetic eukaryotes, the energy metabolisms of mitochondria and chloroplasts are intertwined at multiple levels. Not only do these organelles share over 100 dual-targeted proteins (reviewed in: Carrie and Small, 2013), provide both ATP and contribute to photorespiration, chloroplasts can shuttle reducing power to mitochondria via the malate valve (reviewed in: Scheibe, 2004; Kramer and Evans, 2011). Functional cooperation between mitochondria and chloroplasts in balancing the cellular ATP/NADPH ratio becomes even more obvious when compensatory acclimation processes are studied in mutants affected in photosynthesis or respiration. For instance, in Chlamydomonas mutants defective in different complexes of the respiratory electron transport chain, the resulting ATP deficiency is counterbalanced by increased non-photochemical reduction of the plastoquinone pool mediated by the chlororespiratory pathway, LHCII protein association to PSI and cyclic photophosphorylation (Cardol et al., 2003). Furthermore, the Chlamydomonas strain *pgrl1* disrupted in the proton regulation 5 like 1 protein (PGRL1), which was identified as a CEF mutant in CFVI-based screen (Tolleter et al., 2011), compensates for ATP deficiency by increasing oxygen photoreduction downstream of PSI and shows higher susceptibility to mitochondrial inhibitors (Dang et al., 2014). These results are consistent with the finding that overall fitness and yields of photosynthesis were only significantly reduced when state transitions and mitochondrial respiration were concomitantly impaired in the Chlamydomonas double mutant *stt7-9 dum22* (Cardol et al., 2009). Thus, increased cyclic electron transport rates induced by state 2 transitions can supply extra ATP when respiratory ATP production becomes

limiting and, conversely, mitochondrial cooperation is increased when CEF is downregulated in Chlamydomonas. One important conclusion that could be drawn from these studies was that PSII efficiencies were reduced in respiratory mutants and was explained by enhanced rates of non-photochemical reduction of plastoquinone mediated by the chlororespiratory pathway and preferential association of LHCII proteins with PSI (Cardol et al., 2003). Massoz et al. (2015) therefore used F_v/F_m values as an initial criterion to select mutants affected in mitochondrial respiration. Several mutants disrupted in subunits of the respiratory complex I or the isocitrate lyase were isolated from a collection of about 2900 insertional mutants generated in either a wild-type or a state transition-defective strain (*stt7-9*). A later refinement of the screening procedure used the CEF mutant *pgrl1* as the starting strain with a view to isolating mutants impaired in mitochondrial complex I (Massoz et al., 2017). As proof of concept, the double mutant *pgrl1*Δ*nd4*, which is deficient in both CEF and complex 1, was generated and shown to exhibit a lower PSII efficiency than either of the single mutants. Subsequent screening of about 3000 insertional mutants created in the *pgrl1* background resulted in 46 mutants with reduced PSII efficiency, of which three were complex I mutants. Further analyses revealed that one of these was disrupted in NADH dehydrogenase [ubiquinone] 1 alpha subcomplex assembly factor 3 (NDUFAF3), a complex I assembly factor also conserved in humans (Massoz et al., 2017).

Chl FLUORESCENCE VIDEO IMAGING IN REVERSE GENETIC APPROACHES

Forward genetic approaches still dominated mutant searches in the late 1990s and early 2000s (Lloyd and Meinke, 2012), but thanks to advances in genome sequencing technologies, the establishment of large mutant libraries and the development of new genetic tools such as RNA silencing techniques (Mohr et al., 2014), and more recently genome editing tools (Yin et al., 2017), reverse genetics has since come to the fore. Indeed, in conjunction with the tremendous rise in the availability of myriad 'omics' datasets, reverse genetic strategies have become the more practicable choice, since laborious screens of large mutant libraries are circumvented and the underlying genetic defects are already known. Relative to classical forward genetic approaches, reverse genetic screens start with a significantly reduced number of lines or strains, which are generally disrupted in genes with poorly characterized or unknown functions. Depending on the stringency of preselection criteria (e.g., coregulation or phylogenomic studies), 'the starting material' can be narrowed down to a reasonable number of candidates which is compatible with the complexity of the required screening procedure. One example for the power of such 'guilt-by-association' approaches is the identification of three subunits of the NDH complex – NDF1, NDF2, and NDF4 (Takabayashi et al., 2009) now called photosynthetic NDH subcomplex B subunit PnsB1, PnsB2, and PnsB3 (Ifuku et al., 2011). In that study, genes of unknown function were selected on the basis of their co-expression with nucleus-encoded NDH subunits L, N, and O (NDHL, NDHN, and NDHO). In addition, Arabidopsis genes (of unknown function) were considered together with homologs found in cyanobacteria but not in green algae, since *C. reinhardtii* lacks a plant-type NDH complex. Insertion lines were identified for 21 of the 36 genes pre-selected by means of the bioinformatics screen, and these were tested for NDH activity. Remarkably, four of them (nearly 20%) failed to exhibit the post-illumination rise in fluorescence. Further studies provided evidence that the respective genes indeed code for the NDH subunits NDF1 (PnsB1), NDF2 (PnsB2), and NDF4 (PnsB3), whereas NDF3 corresponds to the chlororespiratory reduction protein 6 (CRR6), which is involved in NDH subcomplex A assembly (Munshi et al., 2006).

Chl Fluorescence Image Analyses in Combined Screening Protocols

Since Chl fluorescence-based phenotyping is no longer as time-consuming as it once was, and manageable numbers of candidates can be examined in reverse genetics projects, contemporary screening approaches can be extended to more elaborate protocols in which subtle or multiple photosynthetic phenotypes can be detected in a single, albeit longer, experimental run. Commercial Chl video imaging systems now make it possible to set up automated measuring routines composed of several analytical blocks that can last for days. One example of such a combined screening protocol is shown in **Figure 1**, which we use routinely for initial phenotyping of selected Arabidopsis mutant lines.

In principle, the approach comprises six phases, in which most of the previously described Chl fluorescence signatures of photosynthetic mutants can be identified (**Figure 1A**). In the first block, the F_v/F_m measurement allows one to assess PSII functionality and pinpoint mutants with an *hcf* phenotype, such as the Arabidopsis PSII subunit O (PsbO) knockdown mutant *psbO1 psbO2* (**Figure 1B**) (Steinberger et al., 2015). The second analytical block was designed to identify mutant lines with a *crr* phenotype, and detects NDH activity by means of a PIF measurement (**Figure 1C**). Block 3 implements a standard slow induction experiment, which is carried out under moderate actinic light intensities. Several informative parameters can be extracted in block 3 which reveal aspects of the transient dynamics of photosynthesis upon a dark-light shift. For instance, *pgr* mutants can be already identified at this stage by their low transient NPQ phenotype (DalCorso et al., 2008). Conversely, mutants affected in chloroplast F_1F_0-ATP synthase activity can be identified on the basis of their high NPQ (**Figure 1D**) (Rühle et al., 2014; Grahl et al., 2016; Zhang et al., 2016). The increased NPQ in such mutants can be attributed to a high operating qE, which is established as a result of proton accumulation in the thylakoid lumen already under moderate light intensities. Parameters determined at the end of block 3 reflect photosynthetic performance in the steady state, and an analysis of effective quantum yields (Φ_{II}) uncovers *pam* mutants (**Figure 1E**). Samples in block 4 are shifted back into the dark and NPQ relaxation kinetics provide values of qI

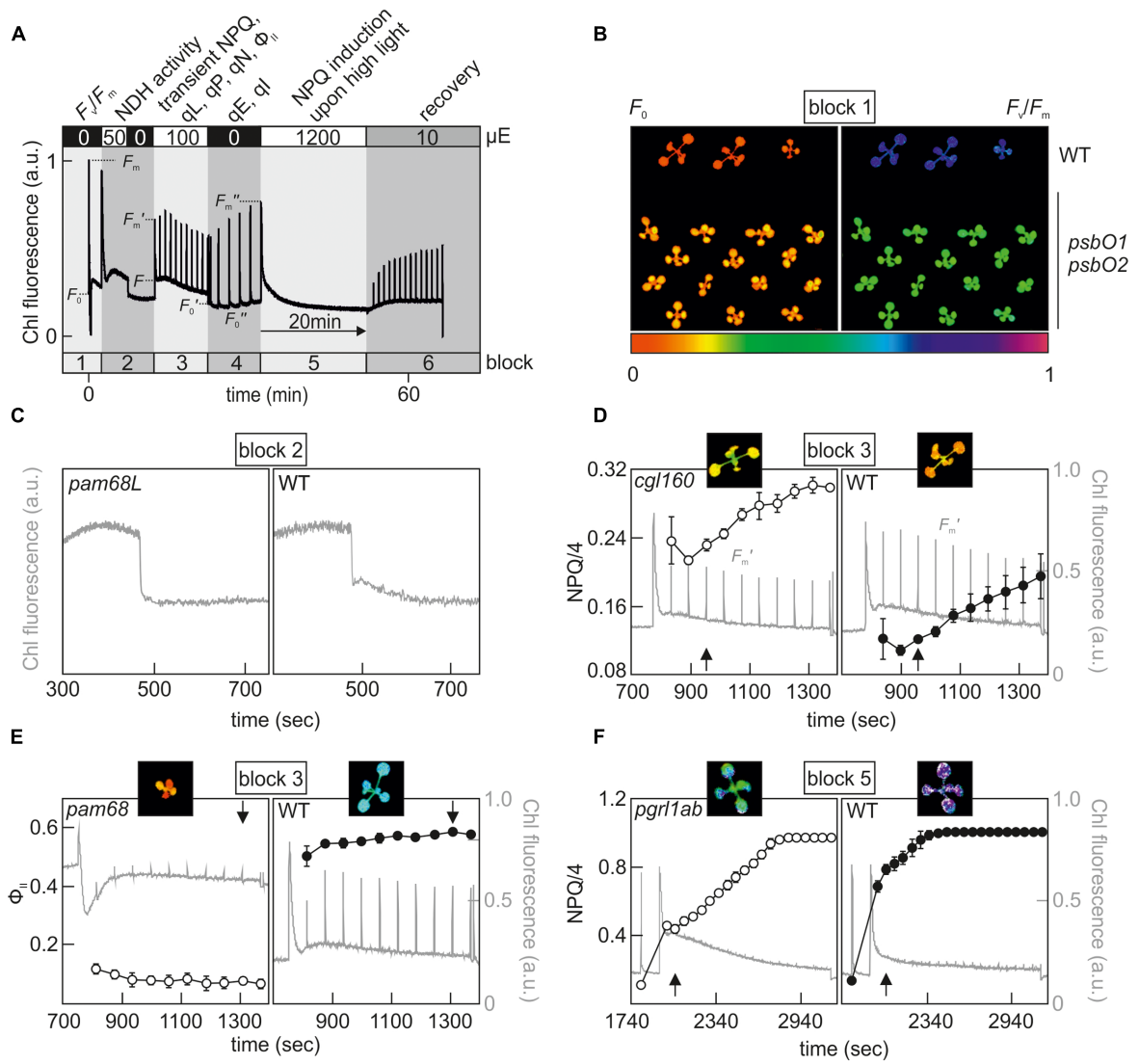

FIGURE 1 | Example of a combined screening protocol based on Chl fluorescence video imaging which is able to identify *hcf, crr, npq, pam* and PSII repair mutants. **(A)** Chl fluorescence was monitored using an Imaging PAM system (Walz®) and the indicated sequence of actinic light conditions was executed in series to determine, in a single experimental run, the various photosynthetic parameters listed at the top. Plants were dark-adapted for 20 min and acclimated to measuring light for 5 min prior to the analysis. For further explanations, see the main text. F_v/F_m, maximum quantum yield of PSII; NPQ, non-photochemical quenching; qL, fraction of open PSII centers; qP, photochemical quenching coefficient; qN non-photochemical quenching coefficient; Φ_{II}, effective quantum yield of PSII; qE, energy-dependent quenching; qI, photo-inhibitory quenching. **(B)** Example of an *hcf* mutant phenotype, which can be detected in measurement block 1. F_0 and F_v/F_m images of wild-type and *psbO1 psbO2* (Steinberger et al., 2015) Arabidopsis plants. **(C)** Identification of a *crr* mutant phenotype in block 2. Detail of the post-illumination fluorescence rise (PIF) analysis of *pam68L* (Armbruster et al., 2013), which is disrupted in NDH complex assembly. **(D)** Detection of a high NPQ phenotype in block 3. F_m' values were recorded every minute by applying saturating light pulses after a dark-light transition (100 µE m^{-2} s^{-1}) and calculated NPQ values of the chloroplast ATP synthase-deficient mutant *cgl160* (Rühle et al., 2014) were compared to a wild-type control. **(E)** Example of a *pam* mutant phenotype, which can be distinguished at the end of block 3. Φ_{II} values of the PSII assembly mutant *pam68* (Armbruster et al., 2010) were compared to a wild-type control. **(F)** Detection of an *npq* phenotype in measurement block 5. NPQ analyses were carried out with the CEF mutant *pgrl1ab* (DalCorso et al., 2008) and compared to a wild-type control. False-color images for F_0, F_v/F_m, NPQ/4, and Φ_{II} depicted at the time points highlighted by a black arrow represent values on a rainbow scale from 0 to 1 shown below **(B)**. Note that NPQ parameters in **(D,F)** are displayed in NPQ/4 to fit the standard color code ranging from 0 to 1. Chl fluorescence signals were normalized to F_m and are shown in gray on a scale from 0 to 1 in **(D–F)**.

and qE, which was recently determined in an initial screening step to identify '*high cyclic electron flow around PSI*' (*hcef)* mutants with altered CEF (Livingston et al., 2010). Block 5 also implements a dark-light shift experiment, but using excessive light intensities (1200 µE m^{-2} s^{-1}) and longer exposure times (20 min), which allow the detection of *npq* mutants due to their aberrant NPQ induction patterns under high light (Niyogi et al., 1998). After the photodamage-inducing high-light treatment in block 5, the protocol ends with a recovery phase from high light (block 6) under low light intensities (10 µE m^{-2} s^{-1}) and

was designed to pick up mutants that are defective in the PSII repair mechanism (Schroda et al., 1999; Malnoe et al., 2014). Overall, the CFVI protocol outlined above can already uncover a wide range of phenotypes, but can be further expanded to cover a larger collection of photosynthetic parameters, such as the determination of P_{max} from light saturation curves (van Rooijen et al., 2015) and measurements of qT in state transitions (Pribil et al., 2010) or effective quantum yields/NPQ parameters under fluctuating light conditions (Cruz et al., 2016).

Chl Fluorescence Image Phenotyping under Simulated Environmental Conditions

The photosynthetic lifestyle of plants and algae requires a high degree of flexibility and the ability to adapt to rapidly fluctuating environments. However, for reasons of scalability and reproducibility most of the screening studies referred to here were conducted with small Arabidopsis plants or algae grown in stable, standardized laboratory settings and would have been impossible with fully developed crops under field conditions. Furthermore, phenotyping of mutant collections involved measurements of only one or a few photosynthetic parameters, which were determined at one or more time points, thus providing a rather static picture of the highly dynamic process of photosynthesis. It is therefore obvious that many factors that contribute to the fine tuning of photosynthesis in response to dynamic environmental changes will have not been identified by previous screening procedures (Cruz et al., 2016). This assertion is also supported by the observation that plant lines lacking PsbS (Külheim et al., 2002), the LHCII serine/threonine-protein kinase STN7 (Grieco et al., 2012) or PGR5 (Suorsa et al., 2012) showed higher levels of photodamage and notable reductions in their growth rates (or lethality) only under fluctuating light conditions that were not observed under unchanging conditions. One logical and straightforward way to bypass this limitation would be to carry out phenotyping of mutant collections in the field, and suitable large-scale Chl fluorescence image analyzers are now available for this task (e.g., Field Scanalyzer) (Virlet et al., 2017). However, besides the fact that in several countries the cultivation of genetically modified plants in the field is either prohibited or subject to legal restrictions, such studies are complicated by a multitude of overlapping, unpredictable abiotic and biotic stress factors, and statistical evaluation of the results become particularly challenging. For these reasons, the dynamic environmental photosynthesis imager (DEPI) platform was developed for replication of natural, fluctuating growth conditions in the laboratory (Cruz et al., 2016). Several parameters can be controlled (light intensity, CO_2 concentration, humidity and temperature) in the growth chamber, and rapid responses as well as long-term acclimation processes of photosynthesis can be assessed *in situ* by the integrated CFVI system in more than two hundred plants simultaneously. As a proof of concept, a library of over 300 T-DNA Arabidopsis lines disrupted in nuclear genes coding for chloroplast-targeted proteins (Ajjawi et al., 2010) was exposed to a 5-day regime of fluctuating light levels and screened for alterations in photosynthetic performance. As a result, *psb33* plants lacking PSII protein 33 (PSB33) (Fristedt et al., 2015) and several other conditional mutant lines showed transient, spatiotemporal-dependent phenotypes which could not be detected or were not reliably expressed under standard growth conditions. PSB33 is a green-lineage-specific protein (Merchant et al., 2007) predominantly found in non-appressed thylakoids of Arabidopsis chloroplasts and sustains D1 of PSII under fluctuating light conditions (Fristedt et al., 2017). Thus, the DEPI system can reveal new, complex and previously unseen phenotypes, and provides a versatile experimental platform with which to identify factors required for remodeling and regulation of photosynthesis under dynamic environmental conditions.

Chl FLUORESCENCE VIDEO IMAGING IN QUANTITATIVE GENETIC APPROACHES

Forward and reverse genetics are efficient strategies for elucidating the functions of a single gene or of small gene families, but these approaches reach their limits when the genetic architecture of a quantitative trait and its interaction with the environment needs to be determined. Most agronomically important traits (e.g., grain yield, grain size, ripening or flowering time) are controlled by multiple genes which have to be analyzed by quantitative genetic approaches, such as classical linkage mapping or genome-wide association studies (GWAS) (reviewed in: Bazakos et al., 2017). Natural variation also exists for photosynthetic traits and can be roughly divided into morphological and physiological variations, which have been investigated in several studies with different plant species (reviewed in: Flood et al., 2011). For instance, Jung and Niyogi (2009) examined natural NPQ variation in different Arabidopsis accessions and provided evidence that thermal dissipation is a quantitative trait that depends on multiple, nucleus-encoded genetic factors. Two high-NPQ QTLs (*HQE1* and *HQE2*) were identified in a quantitative trait locus (QTL) analysis which was performed with a F2 mapping population generated from a cross between a low-NPQ and a high-NPQ Arabidopsis accession (Jung and Niyogi, 2009). Remarkably, *HQE1* and *HQE2* were not mapped to previously characterized factors identified in forward genetic approaches, indicating that quantitative genetics can serve as a complementary strategy to dissect the genetic architecture of thermal dissipation.

Even though quantitative genetic approaches have a long history in plant science, their potential for photosynthesis research has not yet been fully explored. This may simply reflect the high complexity of the genetic architecture of photosynthesis, which not only comprises the several hundred genes directly involved in biogenesis processes, regulation or acclimation of photosynthesis, but also involves two quite distinct genetic systems (plastid and nuclear genome) with different inheritance modes. Moreover, successful quantitative genetic approaches in photosynthesis research require reproducible, non-invasive, high-throughput phenotyping pipelines that were not available until recently. However, several platforms have been developed

in recent years. Examples include FluorImager (Barbagallo et al., 2003), GROWSCREEN FLUORO (Jansen et al., 2009), PlantScreen (Humplík et al., 2015), Phenovator (Flood et al., 2016), the DEPI system (Cruz et al., 2016) or the crop population growth information detection system (Wang et al., 2017), which now integrate CFVI analyses into their phenotyping facilities. As an example for the combination of a GWAS and a high-throughput Chl fluorescence phenotyping approach, van Rooijen et al. (2015) have explored the natural genetic variation for acclimation of photosynthetic light use efficiency (Φ_{II}) in 344 Arabidopsis accessions. Of 63 newly identified gene candidates, 13 encode chloroplast-localized proteins, most of which are either associated with abiotic stress responses or have unknown functions.

GENE DISCOVERY THROUGH CHLOROPHYLL FLUORESCENCE VIDEO IMAGING – A BRIEF OUTLOOK

Due to the advances in imaging and data acquisition technologies in the last two decades, Chl fluorescence-based analyses have entered the 'phenomics' field and promise to increase our knowledge of photosynthesis substantially. Modern phenotyping systems are highly flexible and will allow the identification of new genotype-phenotype-environment relationships and accelerate gene discovery studies significantly.

The next obvious step will be to determine photosynthetic parameters of large-scale, indexed mutant collections like the Arabidopsis unimutant (O'Malley and Ecker, 2010), the Arabidopsis Chloroplast 2010 Project (Ajjawi et al., 2010) and the GABI-DUPLO double mutant (Bolle et al., 2013) collections, or the recently generated Chlamydomonas mutant collection CLiP (Li et al., 2016). Consequently, with the exception of screening approaches under highly specialized conditions, tedious forward genetic screening procedures, which were carried out by single researchers or research groups in the past, will become obsolete. A major task in the future will lie in the processing, handling, quality control, maintenance, storage, analysis and sharing of the vast amount of data collected by CFVI-based phenotyping studies, which will become even more challenging when such screens are combined with other non-invasive phenotyping technologies (Walter et al., 2015; Tardieu et al., 2017). But computational techniques for assessing the quality of phenotypic data (Xu et al., 2015) and analyzing massive amounts of data in order to reveal dynamic relationships between phenotypes and environment (Yang et al., 2017) have already been developed, and these will eventually replace manual evaluation methods.

Chl fluorescence video imaging also has the potential to be an important technological driver in crop science, since it offers an efficient screening technology for rapid evaluation of plant performance under stress conditions such as drought, salinity, freezing, chilling, high temperature or nutrient deficiency (reviewed in: Baker and Rosenqvist, 2004). CFVI is of particular interest in plant breeding programs, since low-cost and precise high-throughput phenotyping technologies have been regarded as one of the major bottleneck in the postgenomic era of plant breeding (reviewed in: Araus and Cairns, 2014). A further challenge is the difficulty to extrapolate results gained under a strictly controlled environment (such as a growth chamber or greenhouse) to field conditions. It is therefore inevitable to establish high throughput phenotyping technologies under heterogeneous field conditions to analyze quantitative traits and to elucidate their underlying genetic architecture for future breeding efforts. Significant progress in non-invasive sensor and imaging technology has been made (reviewed in: White et al., 2012; Fiorani and Schurr, 2013) and the Field Scanalyzer system installed at Rothamsted Research (United Kingdom) by LemnaTec GmbH (Germany) is one example, which now employs Chl fluorescence based measurements for high-throughput phenotyping in the field (Virlet et al., 2017).

While recent work has mainly focused on scaling up CFVI screening systems for simultaneous evaluation of large sample collections, a future direction might be to explore the potential of screening single cells by exploiting their Chl fluorescence fingerprints. Flow cytometry technologies are well established for unicellular microalgae in environmental and toxicological studies (reviewed in: Hyka et al., 2013) and several flow cytometry studies with plant protoplasts have been reported (Harkins et al., 1990; Galbraith, 2007; Berendzen et al., 2012; You et al., 2015). Flow cytometry is generally coupled to fluorescence-activated cell sorting, which permits the isolation of a desired cell population with specific physiological properties. Recently, this technique has been successfully employed to screen high-lipid Chlamydomonas mutants that were stained with the lipid-sensitive dye Nile Red prior to screening (Xie et al., 2014; Terashima et al., 2015) or to identify protein-protein interactions in plant protoplasts by combining bimolecular fluorescence complementation with flow cytometry (Berendzen et al., 2012). Moreover, Chl autofluorescence has been used in flow cytometry studies as an endogenous probe to sort tobacco mesophyll protoplasts (Harkins et al., 1990) and to discriminate between different phytoplankton species by cytometric approaches (Hildebrand et al., 2016). Although implementation will be challenging, the combination of flow cytometry and Chl fluorescence kinetics-based cell sorting can provide a fast means of screening mutagenized cell populations for specific Chl fluorescence phenotypes.

AUTHOR CONTRIBUTIONS

TR designed and wrote the article. BR and DL wrote the article.

FUNDING

This work was funded by the German Science Foundation (DFG, Research Unit FOR2092, grant RU 1945/2-1).

ACKNOWLEDGMENTS

We thank Paul Hardy for critical comments on the manuscript.

REFERENCES

Ajjawi, I., Lu, Y., Savage, L. J., Bell, S. M., and Last, R. L. (2010). Large-scale reverse genetics in Arabidopsis: case studies from the Chloroplast 2010 Project. *Plant Physiol.* 152, 529–540. doi: 10.1104/pp.109.148494

Allen, J. F. (1992). Protein phosphorylation in regulation of photosynthesis. *Biochim. Biophys. Acta* 1098, 275–335. doi: 10.1016/S0005-2728(09)91014-3

Araus, J. L., and Cairns, J. E. (2014). Field high-throughput phenotyping: the new crop breeding frontier. *Trends Plant Sci.* 19, 52–61. doi: 10.1016/j.tplants.2013.09.008

Armbruster, U., Rühle, T., Kreller, R., Strotbek, C., Zühlke, J., Tadini, L., et al. (2013). The photosynthesis affected mutant68-like protein evolved from a PSII assembly factor to mediate assembly of the chloroplast NAD(P)H dehydrogenase complex in Arabidopsis. *Plant Cell* 25, 3926–3943. doi: 10.1105/tpc.113.114785

Armbruster, U., Zühlke, J., Rengstl, B., Kreller, R., Makarenko, E., Rühle, T., et al. (2010). The Arabidopsis thylakoid protein PAM68 is required for efficient D1 biogenesis and photosystem II assembly. *Plant Cell* 22, 3439–3460. doi: 10.1105/tpc.110.077453

Badger, M. R., Fallahi, H., Kaines, S., and Takahashi, S. (2009). Chlorophyll fluorescence screening of *Arabidopsis thaliana* for CO_2 sensitive photorespiration and photoinhibition mutants. *Funct. Plant Biol.* 36, 867–873. doi: 10.1071/FP09199

Baker, N. R. (2008). Chlorophyll fluorescence: a probe of photosynthesis in vivo. *Annu. Rev. Plant Biol.* 59, 89–113. doi: 10.1146/annurev.arplant.59.032607.092759

Baker, N. R., and Rosenqvist, E. (2004). Applications of chlorophyll fluorescence can improve crop production strategies: an examination of future possibilities. *J. Exp. Bot.* 55, 1607–1621. doi: 10.1093/jxb/erh196

Barbagallo, R. P., Barbagallo, R. P., Oxborough, K., Oxborough, K., Pallett, K. E., Pallett, K. E., et al. (2003). Rapid noninvasive screening for perturbations of metabolism and plant growth using chlorophyll fluorescence imaging. *Plant Physiol.* 132, 485–493. doi: 10.1104/pp.102.018093

Barkan, A., Miles, D., and Taylor, W. C. (1986). Chloroplast gene expression in nuclear, photosynthetic mutants of maize. *EMBO J.* 5, 1421–1427. doi: 10.1002/j.1460-2075.1986.tb04378.x

Bazakos, C., Hanemian, M., Trontin, C., Jiménez-Gómez, J. M., and Loudet, O. (2017). New strategies and tools in quantitative genetics: How to go from the phenotype to the genotype. *Annu. Rev. Plant Biol.* 68, 435–455. doi: 10.1146/annurev-arplant-042916-40820

Belcher, S., Williams-Carrier, R., Stiffler, N., and Barkan, A. (2015). Large-scale genetic analysis of chloroplast biogenesis in maize. *Biochim. Biophys. Acta* 1847, 1004–1016. doi: 10.1016/j.bbabio.2015.02.014

Bennoun, P., and Levine, R. P. (1967). Detecting mutants that have impaired photosynthesis by their increased level of fluorescence. *Plant Physiol.* 42, 1284–1287.

Berendzen, K. W., Bohmer, M., Wallmeroth, N., Peter, S., Vesic, M., Zhou, Y., et al. (2012). Screening for in planta protein-protein interactions combining bimolecular fluorescence complementation with flow cytometry. *Plant Methods* 8:25. doi: 10.1186/1746-4811-8-25

Bilger, W., and Björkman, O. (1990). Role of the xanthophyll cycle in photoprotection elucidated by measurements of light-induced absorbance changes, fluorescence and photosynthesis in leaves of *Hedera canariensis*. *Photosynth. Res.* 25, 173–185. doi: 10.1007/BF00033159

Björkman, O., and Demmig, B. (1987). Photon yield of O2 evolution and chlorophyll fluorescence characteristics at 77 K among vascular plants of diverse origins. *Planta* 170, 489–504. doi: 10.1007/BF00402983

Bolle, C., Huep, G., Kleinbölting, N., Haberer, G., Mayer, K., Leister, D., et al. (2013). GABI-DUPLO: A collection of double mutants to overcome genetic redundancy in *Arabidopsis thaliana*. *Plant J.* 75, 157–171. doi: 10.1111/tpj.12197

Brooks, M. D., Sylak-Glassman, E. J., Fleming, G. R., and Niyogi, K. K. (2013). A thioredoxin-like/β-propeller protein maintains the efficiency of light harvesting in Arabidopsis. *Proc. Natl. Acad. Sci. U.S.A.* 110, E2733–E2740. doi: 10.1073/pnas.1305443110

Cardol, P., Alric, J., Girard-Bascou, J., Franck, F., Wollman, F.-A., and Finazzi, G. (2009). Impaired respiration discloses the physiological significance of state transitions in Chlamydomonas. *Proc. Natl. Acad. Sci. U.S.A.* 106, 15979–15984. doi: 10.1073/pnas.0908111106

Cardol, P., Gloire, G., Havaux, M., Remacle, C., Matagne, R., and Franck, F. (2003). Photosynthesis and state transitions in mitochondrial mutants of *Chlamydomonas reinhardtii* affected in respiration. *Plant Physiol.* 133, 2010–2020. doi: 10.1104/pp.103.028076

Carrie, C., and Small, I. (2013). A reevaluation of dual-targeting of proteins to mitochondria and chloroplasts. *Biochim. Biophys. Acta* 1833, 253–259. doi: 10.1016/j.bbamcr.2012.05.029

Chaerle, L., Lenk, S., Leinonen, I., Jones, H. G., Van Der Straeten, D., and Buschmann, C. (2009). Multi-sensor plant imaging: towards the development of a stress-catalogue. *Biotechnol. J.* 4, 1152–1167. doi: 10.1002/biot.200800242

Cruz, J. A., Savage, L. J., Zegarac, R., Hall, C. C., Satoh-Cruz, M., Davis, G. A., et al. (2016). Dynamic environmental photosynthetic imaging reveals emergent phenotypes. *Cell Syst.* 2, 365–377. doi: 10.1016/j.cels.2016.06.001

DalCorso, G., Pesaresi, P., Masiero, S., Aseeva, E., Schünemann, D., Finazzi, G., et al. (2008). A complex containing PGRL1 and PGR5 is involved in the switch between linear and cyclic electron flow in Arabidopsis. *Cell* 132, 273–285. doi: 10.1016/j.cell.2007.12.028

Dang, K.-V., Plet, J., Tolleter, D., Jokel, M., Cuiné, S., Carrier, P., et al. (2014). Combined increases in mitochondrial cooperation and oxygen photoreduction compensate for deficiency in cyclic electron flow in *Chlamydomonas reinhardtii*. *Plant Cell* 26, 3036–3050. doi: 10.1105/tpc.114.126375

Delosme, R., Olive, J., and Wollman, F. A. (1996). Changes in light energy distribution upon state transitions: an in vivo photoacoustic study of the wild type and photosynthesis mutants from *Chlamydomonas reinhardtii*. *Biochim. Biophys. Acta* 1273, 150–158. doi: 10.1016/0005-2728(95)00143-3

Depège, N., Bellafiore, S., and Rochaix, J. D. (2003). Role of chloroplast protein kinase Stt7 in LHCII phosphorylation and state transition in Chlamydomonas. *Science* 299, 1572–1575. doi: 10.1126/science.1081397

Dinkins, R. D., Bandaranayake, H., Baeza, L., Griffiths, A. J., and Green, B. R. (1997). *hcf5*, a nuclear photosynthetic electron transport mutant of *Arabidopsis thaliana* with a pleiotropic effect on chloroplast gene expression. *Plant Physiol.* 113, 1023–1031. doi: 10.1104/pp.113.4.1023

Dinkins, R. D., Bandaranayake, H., Green, B. R., and Griffiths, A. J. (1994). A nuclear photosynthetic electron transport mutant of *Arabidopsis thaliana* with altered expression of the chloroplast petA gene. *Curr. Genet.* 25, 282–288. doi: 10.1007/BF00357174

Felder, S., Meierhoff, K., Sane, A. P., Meurer, J., Driemel, C., Plücken, H., et al. (2001). The nucleus-encoded HCF107 gene of Arabidopsis provides a link between intercistronic RNA processing and the accumulation of translation-competent *psbH* transcripts in chloroplasts. *Plant Cell* 13, 2127–2141. doi: 10.1105/TPC.010090

Fenton, J. M., and Crofts, A. R. (1990). Computer aided fluorescence imaging of photosynthetic systems - Application of video imaging to the study of fluorescence induction in green plants and photosynthetic bacteria. *Photosynth. Res.* 26, 59–66. doi: 10.1007/BF00048977

Fiorani, F., and Schurr, U. (2013). Future scenarios for plant phenotyping. *Annu. Rev. Plant Biol.* 64, 267–291. doi: 10.1146/annurev-arplant-050312-120137

Fleischmann, M. M., Ravanel, S., Delosme, R., Olive, J., Zito, F., Wollman, F.-A., et al. (1999). Isolation and characterization of photoautotrophic mutants of *Chlamydomonas reinhardtii* deficient in state transition. *J. Biol. Chem.* 274, 30987–30994. doi: 10.1074/jbc.274.43.30987

Flood, P. J., Harbinson, J., and Aarts, M. G. M. (2011). Natural genetic variation in plant photosynthesis. *Trends Plant Sci.* 16, 327–335. doi: 10.1016/j.tplants.2011.02.005

Flood, P. J., Kruijer, W., Schnabel, S. K., van der Schoor, R., Jalink, H., Snel, J. F. H., et al. (2016). Phenomics for photosynthesis, growth and reflectance in *Arabidopsis thaliana* reveals circadian and long-term fluctuations in heritability. *Plant Methods* 12:14. doi: 10.1186/s13007-016-0113-y

Fristedt, R., Herdean, A., Blaby-Haas, C. E., Mamedov, F., Merchant, S. S., Last, R. L., et al. (2015). PHOTOSYSTEM II PROTEIN33, a protein conserved in the plastid lineage, is associated with the chloroplast thylakoid membrane and provides stability to photosystem II supercomplexes in Arabidopsis. *Plant Physiol.* 167, 481–492. doi: 10.1104/pp.114.253336

Fristedt, R., Trotta, A., Suorsa, M., Nilsson, A. K., Croce, R., Aro, E.-M., et al. (2017). PSB33 sustains photosystem II D1 protein under fluctuating light conditions. *J. Exp. Bot.* 68, 4281–4293. doi: 10.1093/jxb/erx218

Galbraith, D. W. (2007). *Protoplast Analysis Using Flow Cytometry and Sorting. Flow Cytometry with Plant Cells*. Weinheim: Wiley-VCH, 231–250. doi: 10.1002/9783527610921.ch10

Genty, B., Briantais, J.-M., and Baker, N. R. (1989). The relationship between the quantum yield of photosynthetic electron transport and quenching of chlorophyll fluorescence. *Biochim. Biophys. Acta* 990, 87–92. doi: 10.1016/S0304-4165(89)80016-9

Godaux, D., Emonds-Alt, B., Berne, N., Ghysels, B., Alric, J., Remacle, C., et al. (2013). A novel screening method for hydrogenase-deficient mutants in *Chlamydomonas reinhardtii* based on in vivo chlorophyll fluorescence and photosystem II quantum yield. *Int. J. Hydrogen Energy* 38, 1826–1836. doi: 10.1016/j.ijhydene.2012.11.081

Golan, T., Li, X.-P., Muller-Moule, P., and Niyogi, K. K. (2004). "Using mutants to understand light stress acclimation in plants,"," in *Chlorophyll a Fluorescence: A Signature of Photosynthesis*, eds G. C. Papageorgiou and Govindjee (Dordrecht: Springer Netherlands), 525–554.

Grahl, S., Reiter, B., Gügel, I. L., Vamvaka, E., Gandini, C., Jahns, P., et al. (2016). The Arabidopsis protein CGLD11 is required for chloroplast ATP synthase accumulation. *Mol. Plant* 9, 885–899. doi: 10.1016/j.molp.2016.03.002

Grieco, M., Tikkanen, M., Paakkarinen, V., Kangasjarvi, S., and Aro, E.-M. (2012). Steady-state phosphorylation of light-harvesting complex II proteins preserves photosystem I under fluctuating white light. *Plant Physiol.* 160, 1896–1910. doi: 10.1104/pp.112.206466

Grossman, A. R., Catalanotti, C., Yang, W., Dubini, A., Magneschi, L., Subramanian, V., et al. (2011). Multiple facets of anoxic metabolism and hydrogen production in the unicellular green alga *Chlamydomonas reinhardtii*. *New Phytol.* 190, 279–288. doi: 10.1111/j.1469-8137.2010.03534.x

Harkins, K. R., Jefferson, R. A., Kavanagh, T. A., Bevan, M. W., and Galbraith, D. W. (1990). Expression of photosynthesis-related gene fusions is restricted by cell type in transgenic plants and in transfected protoplasts. *Proc. Natl. Acad. Sci. U.S.A.* 87, 816–820. doi: 10.1073/pnas.87.2.816

Harris, E. H. (1989). "Nuclear mutations described in *C. reinhardtii*," in *The Chlamydomonas Sourcebook: A Comprehensive Guide to Biology and Laboratory Use*, ed. E. H. Harris (San Diego, CA: Academic Press, Inc.), 461–542.

Hashimoto, M., Endo, T., Peltier, G., Tasaka, M., and Shikanai, T. (2003). A nucleus-encoded factor, CRR2, is essential for the expression of chloroplast *ndhB* in Arabidopsis. *Plant J.* 36, 541–549. doi: 10.1046/j.1365-313X.2003.01900.x

Hemschemeier, A., Melis, A., and Happe, T. (2009). Analytical approaches to photobiological hydrogen production in unicellular green algae. *Photosynth. Res.* 102, 523–540. doi: 10.1007/s11120-009-9415-5

Hertle, A. P., Blunder, T., Wunder, T., Pesaresi, P., Pribil, M., Armbruster, U., et al. (2013). PGRL1 is the elusive ferredoxin-plastoquinone reductase in photosynthetic cyclic electron flow. *Mol. Cell* 49, 511–523. doi: 10.1016/j.molcel.2012.11.030

Hildebrand, M., Davis, A., Abbriano, R., Pugsley, H. R., Traller, J. C., Smith, S. R., et al. (2016). "Applications of imaging flow cytometry for microalgae," in *Imaging Flow Cytometry*, eds N. Barteneva and I. Vorobjev (New York, NY: Humana Press), 47–67.

Houille-Vernes, L., Rappaport, F., Wollman, F.-A., Alric, J., and Johnson, X. (2011). Plastid terminal oxidase 2 (PTOX2) is the major oxidase involved in chlororespiration in Chlamydomonas. *Proc. Natl. Acad. Sci. U.S.A.* 108, 20820–20825. doi: 10.1073/pnas.1110518109

Humplík, J. F., Lazár, D., Fürst, T., Husičková, A., Hýbl, M., and Spíchal, L. (2015). Automated integrative high-throughput phenotyping of plant shoots: a case study of the cold-tolerance of pea (*Pisum sativum* L.). *Plant Methods* 11:20. doi: 10.1186/s13007-015-0063-9

Hyka, P., Lickova, S., Přibyl, P., Melzoch, K., and Kovar, K. (2013). Flow cytometry for the development of biotechnological processes with microalgae. *Biotechnol. Adv.* 31, 2–16. doi: 10.1016/j.biotechadv.2012.04.007

Ifuku, K., Endo, T., Shikanai, T., and Aro, E.-M. (2011). Structure of the chloroplast NADH dehydrogenase-like complex: nomenclature for nuclear-encoded subunits. *Plant Cell Physiol.* 52, 1560–1568. doi: 10.1093/pcp/pcr098

Ihnatowicz, A., Pesaresi, P., Varotto, C., Richly, E., Schneider, A., Jahns, P., et al. (2004). Mutants for photosystem I subunit D of *Arabidopsis thaliana*: effects on photosynthesis, photosystem I stability and expression of nuclear genes for chloroplast functions. *Plant J.* 37, 839–852. doi: 10.1111/j.1365-313X.2003.02011.x

Jansen, M., Gilmer, F., Biskup, B., Nagel, K. A., Rascher, U., Fischbach, A., et al. (2009). Simultaneous phenotyping of leaf growth and chlorophyll fluorescence via Growscreen Fluoro allows detection of stress tolerance in *Arabidopsis thaliana* and other rosette plants. *Funct. Plant Biol.* 36, 902–914. doi: 10.1071/FP09095

Jung, H.-S., and Niyogi, K. K. (2009). Quantitative genetic analysis of thermal dissipation in Arabidopsis. *Plant Physiol.* 150, 977–986. doi: 10.1104/pp.109.137828

Kalaji, H. M., Schansker, G., Brestic, M., Bussotti, F., Calatayud, A., Ferroni, L., et al. (2017). Frequently asked questions about chlorophyll fluorescence, the sequel. *Photosynth. Res.* 132, 13–66. doi: 10.1007/s11120-016-0318-y

Kalituho, L., Graßes, T., Graf, M., Rech, J., and Jahns, P. (2006). Characterization of a nonphotochemical quenching-deficient Arabidopsis mutant possessing an intact PsbS protein, xanthophyll cycle and lumen acidification. *Planta* 223, 532–541. doi: 10.1007/s00425-005-0093-z

Kramer, D. M., and Evans, J. R. (2011). The importance of energy balance in improving photosynthetic productivity. *Plant Physiol.* 155, 70–78. doi: 10.1104/pp.110.166652

Krause, G. H., and Weis, E. (1991). Chlorophyll fluorescence and photosynthesis: the basics. *Annu. Rev. Plant Physiol. Plant Mol. Biol.* 42, 313–349. doi: 10.1146/annurev.pp.42.060191.001525

Kruse, O., Nixon, P. J., Schmid, G. H., and Mullineaux, C. W. (1999). Isolation of state transition mutants of *Chlamydomonas reinhardtii* by fluorescence video imaging. *Photosynth. Res.* 61, 43–51. doi: 10.1023/A:1006229308606

Külheim, C., Agren, J., and Jansson, S. (2002). Rapid regulation of light harvesting and plant fitness in the field. *Science* 297, 91–93. doi: 10.1126/science.1072359

Küpper, H., Šetlík, I., Trtílek, M., and Nedbal, L. (2000). A microscope for two-dimensional measurements of in vivo chlorophyll fluorescence kinetics using pulsed measuring radiation, continuous actinic radiation, and saturating flashes. *Photosynthetica* 38, 553–570. doi: 10.1023/A:1012461407557

Lezhneva, L., Amann, K., and Meurer, J. (2004). The universally conserved HCF101 protein is involved in assembly of [4Fe-4S]-cluster-containing complexes in *Arabidopsis thaliana* chloroplasts. *Plant J.* 37, 174–185. doi: 10.1046/j.1365-313X.2003.01952.x

Lezhneva, L., and Meurer, J. (2004). The nuclear factor HCF145 affects chloroplast *psaA-psaB-rps14* transcript abundance in *Arabidopsis thaliana*. *Plant J.* 38, 740–753. doi: 10.1111/j.1365-313X.2004.02081.x

Li, X., Zhang, R., Patena, W., Gang, S. S., Blum, S. R., Ivanova, N., et al. (2016). An indexed, mapped mutant library enables reverse genetics studies of biological processes in *Chlamydomonas reinhardtii*. *Plant Cell* 28, 367–387. doi: 10.1105/tpc.16.00465

Li, X. P., Björkman, O., Shih, C., Grossman, A. R., Rosenquist, M., Jansson, S., et al. (2000). A pigment-binding protein essential for regulation of photosynthetic light harvesting. *Nature* 403, 391–395. doi: 10.1038/35000131

Livingston, A. K., Cruz, J. A., Kohzuma, K., Dhingra, A., and Kramer, D. M. (2010). An Arabidopsis mutant with high cyclic electron flow around photosystem I (hcef) involving the NADPH dehydrogenase complex. *Plant Cell* 22, 221–233. doi: 10.1105/tpc.109.071084

Lloyd, J., and Meinke, D. (2012). A comprehensive dataset of genes with a loss-of-function mutant phenotype in Arabidopsis. *Plant Physiol.* 158, 1115–1129. doi: 10.1104/pp.111.192393

Malnoë, A., Schultink, A., Shahrasbi, S., Rumeau, D., Havaux, M., and Niyogi, K. K. (2017). The plastid lipocalin LCNP is required for sustained photoprotective energy dissipation in Arabidopsis. *Plant Cell* doi: 10.1105/tpc.17.00536 [Epub ahead of print].

Malnoe, A., Wang, F., Girard-Bascou, J., Wollman, F.-A., and de Vitry, C. (2014). Thylakoid FtsH protease contributes to photosystem II and cytochrome b_6f remodeling in *Chlamydomonas reinhardtii* under stress conditions. *Plant Cell* 26, 373–390. doi: 10.1105/tpc.113.120113

Manavski, N., Torabi, S., Lezhneva, L., Arif, M. A., Frank, W., and Meurer, J. (2015). HIGH CHLOROPHYLL FLUORESCENCE145 binds to and stabilizes the *psaA* 5′ UTR via a newly defined repeat motif in Embryophyta. *Plant Cell* 27, 2600–2615. doi: 10.1105/tpc.15.00234

Massoz, S., Hanikenne, M., Bailleul, B., Coosemans, N., Radoux, M., Miranda-Astudillo, H., et al. (2017). In vivo chlorophyll fluorescence screening allows the isolation of a Chlamydomonas mutant defective for NDUFAF3, an assembly factor involved in mitochondrial complex I assembly. *Plant J.* 17, 2045–2054. doi: 10.1111/tpj.13677

Massoz, S., Larosa, V., Horrion, B., Matagne, R. F., Remacle, C., and Cardol, P. (2015). Isolation of *Chlamydomonas reinhardtii* mutants with altered mitochondrial respiration by chlorophyll fluorescence measurement. *J. Biotechnol.* 215, 27–34. doi: 10.1016/j.jbiotec.2015.05.009

Maxwell, K., and Johnson, G. N. (2000). Chlorophyll fluorescence–a practical guide. *J. Exp. Bot.* 51, 659–668. doi: 10.1093/jexbot/51.345.659

Meierhoff, K., Felder, S., Nakamura, T., Bechtold, N., and Schuster, G. (2003). HCF152, an Arabidopsis RNA binding pentatricopeptide repeat protein involved in the processing of chloroplast *psbB-psbT-psbH-petB-petD* RNAs. *Plant Cell* 15, 1480–1495. doi: 10.1105/tpc.010397

Merchant, S. S., Prochnik, S. E., Vallon, O., Harris, E. H., Karpowicz, S. J., Witman, G. B., et al. (2007). The Chlamydomonas genome reveals the evolution of key animal and plant functions. *Science* 318, 245–250. doi: 10.1126/science.1143609

Meurer, J., Berger, A., and Westhoff, P. (1996a). A nuclear mutant of Arabidopsis with impaired stability on distinct transcripts of the plastid *psbB, psbD/C, ndhH*, and *ndhC* operons. *Plant Cell* 8, 1193–1207. doi: 10.1105/tpc.8.7.1193

Meurer, J., Meierhoff, K., and Westhoff, P. (1996b). Isolation of high-chlorophyll-fluorescence mutants of *Arabidopsis thaliana* and their characterisation by spectroscopy, immunoblotting and northern hybridisation. *Planta* 198, 385–396. doi: 10.1007/BF00620055

Miles, C. D., and Daniel, D. J. (1973). A rapid screening technique for photosynthetic mutants of higher plants. *Plant Sci. Lett.* 1, 237–240. doi: 10.1016/0304-4211(73)90025-4

Miles, C. D., and Daniel, D. J. (1974). Chloroplast reactions of photosynthetic mutants in *Zea mays*. *Plant Physiol.* 53, 589–595. doi: 10.1104/pp.53.4.589

Mohr, S. E., Smith, J. A., Shamu, C. E., Neumüller, R. A., and Perrimon, N. (2014). RNAi screening comes of age: improved techniques and complementary approaches. *Nat. Rev. Mol. Cell Biol.* 15, 591–600. doi: 10.1038/nrm3860

Munekage, Y., Hojo, M., Meurer, J., Endo, T., Tasaka, M., and Shikanai, T. (2002). PGR5 Is involved in cyclic electron flow around photosystem I and is essential for photoprotection in Arabidopsis. *Cell* 110, 361–371. doi: 10.1016/S0092-8674(02)00867-X

Munekage, Y., Takeda, S., Endo, T., Jahns, P., Hashimoto, T., and Shikanai, T. (2001). Cytochrome b6f mutation specifically affects thermal dissipation of absorbed light energy in Arabidopsis. *Plant J.* 28, 351–359. doi: 10.1046/j.1365-313X.2001.01178.x

Munshi, M. K., Kobayashi, Y., and Shikanai, T. (2006). CHLORORESPIRATORY REDUCTION 6 is a novel factor required for accumulation of the chloroplast NAD(P)H dehydrogenase complex in Arabidopsis. *Plant Physiol.* 141, 737–744. doi: 10.1104/pp.106.080267.1

Nedbal, L., and Whitmarsh, J. (2004). "Chlorophyll fluorescence imaging of leaves and fruits," in *Chlorophyll a Fluorescence: A Signature of Photosynthesis*, eds G. C. Papageorgiou and Govindjee (Dordrecht: Springer Netherlands), 389–407. doi: 10.1007/978-1-4020-3218-9

Niyogi, K., Bjorkman, O., and Grossman, A. (1997). Chlamydomonas xanthophyll cycle mutants identified by video imaging of chlorophyll fluorescence quenching. *Plant Cell* 9, 1369–1380. doi: 10.1105/tpc.9.8.1369

Niyogi, K. K., Grossman, A. R., and Bjorkman, O. (1998). Arabidopsis mutants define a central role for the xanthophyll cycle in the regulation of photosynthetic energy conversion. *Plant Cell* 10, 1121–1134. doi: 10.1105/tpc.10.7.1121

O'Malley, R. C., and Ecker, J. R. (2010). Linking genotype to phenotype using the Arabidopsis unimutant collection. *Plant J.* 61, 928–940. doi: 10.1111/j.1365-313X.2010.04119.x

Omasa, K., Shimazaki, K., Aiga, I., Larcher, W., and Onoe, M. (1987). Image analysis of chlorophyll fluorescence transients for diagnosing the photosynthetic system of attached leaves. *Plant Physiol.* 84, 748–752. doi: 10.1104/pp.84.3.748

Ort, D. R. (2001). When there is too much light. *Plant Physiol.* 125, 29–32. doi: 10.1104/pp.125.1.29

Oxborough, K. (2004). "Using chlorophyll a fluorescence imaging to monitor photosynthetic performance," in *Chlorophyll a Fluorescence: A Signature of Photosynthesis*, eds G. C. Papageorgiou and Govindjee (Dordrecht: Springer Netherlands), 409–428.

Oxborough, K., and Baker, N. R. (1997). An instrument capable of imaging chlorophyll a fluorescence from intact leaves at very low irradiance and at cellular and subcellular levels of organization. *Plant Cell Environ.* 20, 1473–1483. doi: 10.1046/j.1365-3040.1997.d01-42.x

Peng, L., Ma, J., Chi, W., Guo, J., Zhu, S., Lu, Q., et al. (2006). LOW PSII ACCUMULATION1 is involved in efficient assembly of photosystem II in *Arabidopsis thaliana*. *Plant Cell* 18, 955–969. doi: 10.1105/tpc.105.037689

Peng, L., Yamamoto, H., and Shikanai, T. (2011). Structure and biogenesis of the chloroplast NAD(P)H dehydrogenase complex. *Biochim. Biophys. Acta* 1807, 945–953. doi: 10.1016/j.bbabio.2010.10.015

Pesaresi, P., Gardner, N. A., Masiero, S., Dietzmann, A., Eichacker, L., Wickner, R., et al. (2003). Cytoplasmic N-terminal protein acetylation is required for efficient photosynthesis in Arabidopsis. *Plant Cell* 15, 1817–1832. doi: 10.1105/tpc.012377.NatA

Posewitz, M. C., King, P. W., Smolinski, S. L., Zhang, L., Seibert, M., and Ghirardi, M. L. (2004). Discovery of two novel radical S-adenosylmethionine proteins required for the assembly of an active [Fe] hydrogenase. *J. Biol. Chem.* 279, 25711–25720. doi: 10.1074/jbc.M403206200

Pribil, M., Pesaresi, P., Hertle, A., Barbato, R., and Leister, D. (2010). Role of plastid protein phosphatase TAP38 in LHCII dephosphorylation and thylakoid electron flow. *PLOS Biol.* 8:e1000288. doi: 10.1371/journal.pbio.1000288

Roháček, K. (2002). Chlorophyll fluorescence parameters: the definitions, photosynthetic meaning, and mutual relationships. *Photosynthetica* 40, 13–29. doi: 10.1023/A:1020125719386

Ruban, A. V. (2016). Nonphotochemical chlorophyll fluorescence quenching: mechanism and effectiveness in protecting plants from photodamage. *Plant Physiol.* 170, 1903–1916. doi: 10.1104/pp.15.01935

Rühle, T., Razeghi, J. A., Vamvaka, E., Viola, S., Gandini, C., Kleine, T., et al. (2014). The Arabidopsis protein CONSERVED ONLY IN THE GREEN LINEAGE160 promotes the assembly of the membranous part of the chloroplast ATP synthase. *Plant Physiol.* 165, 207–226. doi: 10.1104/pp.114.237883

Rungrat, T., Awlia, M., Brown, T., Cheng, R., Sirault, X., Fajkus, J., et al. (2016). Using phenomic analysis of photosynthetic function for abiotic stress response gene discovery. *Arabidopsis Book* 14:e0185. doi: 10.1199/tab.0185

Scheibe, R. (2004). Malate valves to balance cellular energy supply. *Physiol. Plant.* 120, 21–26. doi: 10.1111/j.0031-9317.2004.0222.x

Schmitz, J., Heinrichs, L., Scossa, F., Fernie, A. R., Oelze, M. L., Dietz, K. J., et al. (2014). The essential role of sugar metabolism in the acclimation response of *Arabidopsis thaliana* to high light intensities. *J. Exp. Bot.* 65, 1619–1636. doi: 10.1093/jxb/eru027

Schmitz, J., Schöttler, M., Krueger, S., Geimer, S., Schneider, A., Kleine, T., et al. (2012). Defects in leaf carbohydrate metabolism compromise acclimation to high light and lead to a high chlorophyll fluorescence phenotype in *Arabidopsis thaliana*. *BMC Plant Biol.* 12:8. doi: 10.1186/1471-2229-12-8

Schreiber, U., Bilger, W., and Neubauer, C. (1995). "Chlorophyll fluorescence as a nonintrusive indicator for rapid assessment of *In Vivo* photosynthesis," in *Ecophysiology of Photosynthesis*, eds E. D. Schulze and M. Caldwell (Berlin: Springer), 49–70.

Schreiber, U., Schliwa, U., and Bilger, W. (1986). Continuous recording of photochemical and non-photochemical chlorophyll fluorescence quenching with a new type of modulation fluorometer. *Photosynth. Res.* 10, 51–62.

Schroda, M., Vallon, O., Wollman, F. A., and Beck, C. F. (1999). A chloroplast-targeted heat shock protein 70 (HSP70) contributes to the photoprotection and repair of photosystem II during and after photoinhibition. *Plant Cell Online* 11, 1165–1178. doi: 10.1105/tpc.11.6.1165

Shikanai, T., Endo, T., Hashimoto, T., Yamada, Y., Asada, K., and Yokota, A. (1998). Directed disruption of the tobacco *ndhB* gene impairs cyclic electron flow around photosystem I. *Proc. Natl. Acad. Sci. U.S.A.* 95, 9705–9709.

Shikanai, T., Munekage, Y., Shimizu, K., Endo, T., and Hashimoto, T. (1999). Identification and characterization of Arabidopsis mutants with reduced quenching of chlorophyll fluorescence. *Plant Cell Physiol.* 40, 1134–1142.

Somerville, C. R. (1986). Analysis of photosynthesis with mutants of higher plants and algae. *Annu. Rev. Plant Physiol.* 37, 467–506. doi: 10.1146/annurev.pp.37.060186.002343

Steinberger, I., Egidi, F., and Schneider, A. (2015). Chlorophyll fluorescence measurements in Arabidopsis wild-type and photosystem II mutant leaves. *Bio-protocol* 5:e1532. doi: 10.21769/BioProtoc.1532

Suorsa, M., Jarvi, S., Grieco, M., Nurmi, M., Pietrzykowska, M., Rantala, M., et al. (2012). PROTON GRADIENT REGULATION5 is essential for proper acclimation of Arabidopsis photosystem I to naturally and artificially fluctuating light conditions. *Plant Cell* 24, 2934–2948. doi: 10.1105/tpc.112.097162

Takabayashi, A., Ishikawa, N., Obayashi, T., Ishida, S., Obokata, J., Endo, T., et al. (2009). Three novel subunits of Arabidopsis chloroplastic NAD(P)H dehydrogenase identified by bioinformatic and reverse genetic approaches. *Plant J.* 57, 207–219. doi: 10.1111/j.1365-313X.2008.03680.x

Takahashi, S., Bauwe, H., and Badger, M. (2007). Impairment of the photorespiratory pathway accelerates photoinhibition of photosystem II by suppression of repair but not acceleration of damage processes in Arabidopsis. *Plant Physiol.* 144, 487–494. doi: 10.1104/pp.107.097253

Tardieu, F., Cabrera-Bosquet, L., Pridmore, T., and Bennett, M. (2017). Plant phenomics, from sensors to knowledge. *Curr. Biol.* 27, R770–R783. doi: 10.1016/j.cub.2017.05.055

Taylor, W. C., Barkan, A., and Martienssen, R. A. (1987). Use of nuclear mutants in the analysis of chloroplast development. *Dev. Genet.* 8, 305–320. doi: 10.1002/dvg.1020080503

Terashima, M., Freeman, E. S., Jinkerson, R. E., and Jonikas, M. C. (2015). A fluorescence-activated cell sorting-based strategy for rapid isolation of high-lipid Chlamydomonas mutants. *Plant J.* 81, 147–159. doi: 10.1111/tpj.12682

Terashima, M., Specht, M., Naumann, B., and Hippler, M. (2010). Characterizing the anaerobic response of *Chlamydomonas reinhardtii* by quantitative proteomics. *Mol. Cell. Proteomics* 9, 1514–1532. doi: 10.1074/mcp.M900421-MCP200

Thiele, A., Winter, K., and Krause, G. H. (1997). Low inactivation of D1 protein of photosystem II in young canopy leaves of *Anacardium excelsum* under high-light stress. *J. Plant Physiol.* 151, 286–292. doi: 10.1016/S0176-1617(97)80254-4

Tolleter, D., Ghysels, B., Alric, J., Petroutsos, D., Tolstygina, I., Krawietz, D., et al. (2011). Control of hydrogen photoproduction by the proton gradient generated by cyclic electron flow in *Chlamydomonas reinhardtii*. *Plant Cell* 23, 2619–2630. doi: 10.1105/tpc.111.086876

Tseng, Y.-C., and Chu, S.-W. (2017). High spatio-temporal-resolution detection of chlorophyll fluorescence dynamics from a single chloroplast with confocal imaging fluorometer. *Plant Methods* 13:43. doi: 10.1186/s13007-017-0194-2

van Rooijen, R., Aarts, M. G. M., and Harbinson, J. (2015). Natural genetic variation for acclimation of photosynthetic light use efficiency to growth irradiance in Arabidopsis. *Plant Physiol.* 167, 1412–1429. doi: 10.1104/pp.114.252239

Varotto, C., Maiwald, D., Pesaresi, P., Jahns, P., Salamini, F., and Leister, D. (2002). The metal ion transporter IRT1 is necessary for iron homeostasis and efficient photosynthesis in *Arabidopsis thaliana*. *Plant J.* 31, 589–599. doi: 10.1046/j.1365-313X.2002.01381.x

Varotto, C., Pesaresi, P., Maiwald, D., Kurth, J., Salamini, F., and Leister, D. (2000a). Identification of photosynthetic mutants of Arabidopsis by automatic screening for altered effective quantum yield of photosystem 2. *Photosynthetica* 38, 497–504. doi: 10.1023/A:1012445020761

Varotto, C., Pesaresi, P., Meurer, J., Oelmüller, R., Steiner-Lange, S., Salamini, F., et al. (2000b). Disruption of the Arabidopsis photosystem I gene *psaE1* affects photosynthesis and impairs growth. *Plant J.* 22, 115–124. doi: 10.1046/j.1365-313x.2000.00717.x

Virlet, N., Sabermanesh, K., Sadeghi-Tehran, P., and Hawkesford, M. J. (2017). Field Scanalyzer: An automated robotic field phenotyping platform for detailed crop monitoring. *Funct. Plant Biol.* 44, 143–153. doi: 10.1071/FP16163

Walter, A., Liebisch, F., and Hund, A. (2015). Plant phenotyping: from bean weighing to image analysis. *Plant Methods* 11:14. doi: 10.1186/s13007-015-0056-8

Walters, R. G., Shephard, F., Rogers, J. J. M., Rolfe, S. A., and Horton, P. (2003). Identification of mutants of Arabidopsis defective in acclimation of photosynthesis to the light environment. *Plant Physiol.* 131, 472–481. doi: 10.1104/pp.015479

Wang, H., Qian, X., Zhang, L., Xu, S., Li, H., Xia, X., et al. (2017). Detecting crop population growth using chlorophyll fluorescence imaging. *Appl. Opt.* 56, 9762–9769. doi: 10.1364/AO.56.009762

White, J. W., Andrade-Sanchez, P., Gore, M. A., Bronson, K. F., Coffelt, T. A., Conley, M. M., et al. (2012). Field-based phenomics for plant genetics research. *Field Crop Res.* 133, 101–112. doi: 10.1016/j.fcr.2012.04.003

Xie, B., Stessman, D., Hart, J. H., Dong, H., Wang, Y., Wright, D. A., et al. (2014). High-throughput fluorescence-activated cell sorting for lipid hyperaccumulating *Chlamydomonas reinhardtii* mutants. *Plant Biotechnol. J.* 12, 872–882. doi: 10.1111/pbi.12190

Xu, L., Cruz, J. A., Savage, L. J., Kramer, D. M., and Chen, J. (2015). Plant photosynthesis phenomics data quality control. *Bioinformatics* 31, 1796–1804. doi: 10.1093/bioinformatics/btu854

Yamori, W., and Shikanai, T. (2016). Physiological functions of cyclic electron transport around photosystem I in sustaining photosynthesis and plant growth. *Annu. Rev. Plant Biol.* 67, 81–106. doi: 10.1146/annurev-arplant-043015-112002

Yang, Y., Xu, L., Feng, Z., Cruz, J. A., Savage, L. J., Kramer, D. M., et al. (2017). PhenoCurve: capturing dynamic phenotype-environment relationships using phenomics data. *Bioinformatics* 33, 1370–1378. doi: 10.1093/bioinformatics/btw673

Yin, K., Gao, C., and Qiu, J.-L. (2017). Progress and prospects in plant genome editing. *Nat. Plants* 3:17107. doi: 10.1038/nplants.2017.107

You, M. K., Lim, S. H., Kim, M. J., Jeong, Y. S., Lee, M. G., and Ha, S. H. (2015). Improvement of the fluorescence intensity during a flow cytometric analysis for rice protoplasts by localization of a green fluorescent protein into chloroplasts. *Int. J. Mol. Sci.* 16, 788–804. doi: 10.3390/ijms16010788

Zhang, L., Duan, Z., Zhang, J., and Peng, L. (2016). BIOGENESIS FACTOR REQUIRED FOR ATP SYNTHASE 3 facilitates assembly of the chloroplast ATP synthase complex in Arabidopsis. *Plant Physiol.* 171, 1291–1306. doi: 10.1104/pp.16.00248

Conflict of Interest Statement: The authors declare that the research was conducted in the absence of any commercial or financial relationships that could be construed as a potential conflict of interest.

frontiers in Plant Science

REVIEW
published: 14 March 2018
doi: 10.3389/fpls.2018.00336

Assembly and Transfer of Iron–Sulfur Clusters in the Plastid

*Yan Lu**

Department of Biological Sciences, Western Michigan University, Kalamazoo, MI, United States

Iron-Sulfur (Fe-S) clusters and proteins are essential to many growth and developmental processes. In plants, they exist in the plastids, mitochondria, cytosol, and nucleus. Six types of Fe-S clusters are found in the plastid: classic 2Fe-2S, NEET-type 2Fe-2S, Rieske-type 2Fe-2S, 3Fe-4S, 4Fe-4S, and siroheme 4Fe-4S. Classic, NEET-type, and Rieske-type 2Fe-2S clusters have the same 2Fe-2S core; similarly, common and siroheme 4Fe-4S clusters have the same 4Fe-4S core. Plastidial Fe-S clusters are assembled by the sulfur mobilization (SUF) pathway, which contains cysteine desulfurase (EC 2.8.1.7), sulfur transferase (EC 2.8.1.3), Fe-S scaffold complex, and Fe-S carrier proteins. The plastidial cysteine desulfurase-sulfur transferase-Fe-S-scaffold complex system is responsible for *de novo* assembly of all plastidial Fe-S clusters. However, different types of Fe-S clusters are transferred to recipient proteins via respective Fe-S carrier proteins. This review focuses on recent discoveries on the molecular functions of different assembly and transfer factors involved in the plastidial SUF pathway. It also discusses potential points for regulation of the SUF pathway, relationships among the plastidial, mitochondrial, and cytosolic Fe-S assembly and transfer pathways, as well as several open questions about the carrier proteins for Rieske-type 2Fe-2S, NEET-type 2Fe-2S, and 3F-4S clusters.

Keywords: iron–sulfur cluster, cysteine desulfurase, sulfur transferase, iron–sulfur scaffold complex, iron–sulfur carrier protein

OPEN ACCESS

Edited by:
Fei Yu,
Northwest A&F University, China

Reviewed by:
Aigen Fu,
Northwest University, China
Stefano Santabarbara,
Consiglio Nazionale Delle Ricerche (CNR), Italy

***Correspondence:**
Yan Lu
yan.1.lu@wmich.edu

Specialty section:
This article was submitted to Plant Physiology, a section of the journal Frontiers in Plant Science

Received: *03 October 2017*
Accepted: *28 February 2018*
Published: *14 March 2018*

Citation:
Lu Y (2018) Assembly and Transfer of Iron–Sulfur Clusters in the Plastid. Front. Plant Sci. 9:336. doi: 10.3389/fpls.2018.00336

INTRODUCTION

Iron–Sulfur (Fe-S) clusters are sulfide (S^{2-})-linked di-iron, tri-iron, or tetra-iron clusters found in metalloproteins. Iron (Fe) is a transition metal, which can form cations with an incomplete *d* subshell. This property makes Fe show a variable valency (e.g., Fe^{2+} and Fe^{3+}) and the ability to form coordination units, such as Fe-S clusters. Depending on the ligands, organic structures, and protein folds, the redox potential of Fe-containing cofactors may range between −650 and +450 mV (Beinert, 2000).

Due to the varying redox potential of Fe, Fe-S clusters have the ability to transfer electrons, especially when they are arranged sequentially with individual distances of <14 Å (Balk and Schaedler, 2014). Fe-S clusters are best known for participating in oxidation-reduction reactions in photosynthetic electron transport in thylakoid membranes and respiratory electron transport in the inner mitochondrial membrane (Johnson et al., 2005; Balk and Pilon, 2011; Couturier et al., 2013). Examples of Fe-S proteins involved in photosynthetic electron transport include the photosynthetic electron transfer C (PetC) protein in the cytochrome b_6f complex, Photosystem I (PSI) core subunits PsaA, PsaB, and PsaC, and ferredoxins (Balk and Pilon, 2011). Examples of Fe-S complexes involved in respiratory electron transport include NADH dehydrogenase (Complex I, EC 1.6.99.3), succinate dehydrogenase (Complex II, EC 1.3.5.1), and cytochrome *bc*1 complex (Complex III, EC 1.10.2.2) (Couturier et al., 2013).

COMMON TYPES OF Fe-S CLUSTERS AND EXAMPLES OF Fe-S PROTEINS IN THE PLASTID

Common types of Fe-S clusters found in the plastid include (1) classic 2Fe-2S coordinated by four cysteine (Cys) residues; (2) NEET-type 2Fe-2S coordinated by three Cys and one His residues; (3) Rieske-type 2Fe-2S coordinated by two Cys and two His residues; (4) 3Fe-4S coordinate by three Cys residues; (5) 4Fe-4S coordinated by four Cys residues (or three Cys residues and the hydroxide group from water); and (6) 4Fe-4S coordinated by four Cys residues with one Cys cross-bridging a siroheme (**Figure 1**) (Johnson et al., 2005; Balk and Pilon, 2011; Couturier et al., 2013; Balk and Schaedler, 2014). 3Fe-4S and 4Fe-4S clusters are cubane-type clusters. The three 2Fe-2S clusters are rhombic-type clusters, containing the same 2Fe-2S core. Therefore, the relative abundances of the three rhombic-type clusters depend not on the rate of cluster assembly, but on the availability of appropriate carriers and recipient proteins.

The plant-type ferredoxin (Fd) is a classic 2Fe-2S protein. It is a small and soluble protein with four conserved Cys residues capable of ligating one 2Fe-2S cluster (Hanke and Mulo, 2013). In the chloroplast stroma, Fd acts as a mobile electron carrier during photosynthetic electron transport, carrying electrons from PSI to PSI-associated Fd-$NADP^+$ reductase, for the reduction of $NADP^+$ to NADPH (Hase et al., 2006). The plant-type Fd also serves as an electron donor to a number of chloroplast stromal proteins, such as nitrite reductase (NiR, EC 1.7.7.1), sulfite reductase (SiR, EC 1.8.7.1), and Fd-dependent glutamine:2-oxyoglutarate aminotransferases (Fd-GOGATs, EC 1.4.7.1) (Hase et al., 2006). Whether Fd serves as an electron carrier or electron donor, the electron is actually carried by the 2Fe-2S cluster within the protein (Hase et al., 2006).

Abbreviations: ABA, abscisic acid deficient 3; ABC, ATP binding cassette; ACO, aconitase; APR1, adenosine 5′-phosphosulfate reductase 1; At, *Arabidopsis thaliana*; ATPase, adenosine triphosphatase; BIO, biotin synthase; BolA, DNA-binding transcriptional regulator BolA; CAO, chlorophyllide a oxygenase; CIA, cytosolic iron–sulfur pathway; COG0354m and COG0354p, mitochondrial and plastidial Clusters of Orthologous Groups 0354 proteins; CpNifS, chloroplastic nitrogen fixation S-like; CpIscA1, chloroplast iron–sulfur cluster protein A1; CpSufS, chloroplastic sulfur mobilization protein S; DUF59 and DUF971, domain of unknown function 59 and 971; Fd, ferredoxin; Fd-GOGAT1 and Fd-GOGAT2, ferredoxin-dependent Gln oxoglutarate aminotransferase 1 and 2; FER1, FER2, and FER3, ferritin 1, 2, and 3; FNR, fumarate and nitrate reduction regulatory protein; FTR, ferredoxin-thioredoxin reductase; GFP, green fluorescent protein; GIY-YIG, GlyIleTyr-TyrIleGly; GRX, glutaredoxin; GRXS14 and GRXS16, glutaredoxin S14 and S16; HCAR, 7-hydroxymethyl chlorophyll *a* reductase; HCF101, high chlorophyll fluorescence 101; IRP1, iron regulatory protein 1; ISC, iron–sulfur cluster pathway; IscS, iron–sulfur cluster protein S; ISU1, iron sulfur cluster assembly protein 1; LEU1, 3-isopropylmalate isomerase 1; LIP, lipoic acid synthase; MiaB, isopentenyl-adenosine A37 tRNA methylthiolase; NadA, quinolinate synthase; NAP1, NAP6, and NAP7, non-intrinsic ABC protein 1, 6, and 7; NFU1, NFU2, and NFU3, nitrogen fixation subunit U 1, 2, and 3; NFS1/NifS1 and NFS2, nitrogen fixation S-like 1 and 2; NiR, nitrite reductase; NTPase, nucleotide phosphatase; PetC, photosynthetic electron transfer C; PAO, pheophorbide *a* oxygenase; PSI, Photosystem I; PsaA, PsaB, and PsaC, Photosystem I proteins A, B, and C; RNAi, RNA interference; SiR, sulfite reductase; SUF, sulfur mobilization pathway; SufA1, SufB, SufC, SufD, SufE1, SufE2, and SufE3, sulfur mobilization protein A1, B, C, D, E1, E2, and E3; TP, transit peptide; YFP, yellow fluorescent protein.

One example of NEET-type 2Fe-2S proteins is At-NEET, a CDGSH motif-containing *Arabidopsis thaliana* protein dually targeted to the chloroplast stroma and mitochondria (Nechushtai et al., 2012; Su et al., 2013). The CDGSH motif contains a 16-amino acid consensus sequence (C-X-C-X_2-[S/T]-X_3-P-X-C-D-G-[S/A/T]-H, where the three Cys [C^{74}, C^{76}, and C^{85}] residues and one His [H^{89}] residue for NEET-type 2Fe-2S cluster coordination are underlined). The recombinant At-NEET homodimer coordinates two labile 2Fe-2S clusters, which are readily transferred to apo Fd in *in vivo* assays (Nechushtai et al., 2012). Therefore, Nechushtai et al. (2012) proposed that AT-NEET may serve as a NEET-type 2Fe-2S carrier for plastidial and mitochondrial Fe-S assembly and transfer pathways. Compared to classic 2Fe-2S, NEET-type 2Fe-2S is relatively unstable due to its atypical coordination with three Cys and one His residues (Wiley et al., 2007). Protonation of the ligating His residue could trigger cluster release, indicating that His ligation is also important for the pH lability of NEET-type 2Fe-2S (Wiley et al., 2007).

PetC is an example of Rieske-type 2Fe-2S proteins. The Rieske-type 2Fe-2S cluster in PetC is essential to photosynthetic electron transport. It accepts electrons from plastoquinol and transfers to the heme Fe of the cytochrome *f* protein (Madueño et al., 1992). Riesk-type 2Fe-2S proteins contain a Rieske-type 2Fe-2S-binding domain (CXHXGCX_{12-44}CXCH, where the two Cys and two His residues for cluster coordination are underlined) (Link, 1999). The asymmetric coordination pattern (**Figure 1C**) of Rieske-type 2Fe-2S results in distinctive redox and spectroscopic properties (Kounosu et al., 2004). Compared to classic 2Fe-2S, Rieske-type 2Fe-2S has a relatively positive midpoint redox potential and its visible spectrum is red-shifted (Mason and Cammack, 1992).

Fd-GOGATs are examples of 3Fe-4S proteins. Plants have two Fd-GOGAT isoforms: Fd-GOGAT1 and Fd-GOGAT2 (Coschigano et al., 1998). Fd-GOGAT1 is expressed in leaf chloroplasts and its primary role is photorespiration and nitrogen assimilation in leaves; Fd-GOGAT2 is expressed in root plastids and its primary role is nitrogen assimilation in roots (Coschigano et al., 1998). Fd-GOGATs function via non-covalent binding of Fd and subsequent delivery of reducing equivalents from Fd to FMN (another cofactor) via the 3Fe-4S cluster (van den Heuvel et al., 2002). Both FMN and 3Fe-4S are located in the catalytic centers of Fd-GOGATs (van den Heuvel et al., 2002).

PSI core proteins PsaA, PsaB, and PsaC are examples of 4Fe-4S proteins. PSI has three 4Fe-4S clusters, each coordinated by four Cys residues. One is known as F_X, which is bound to the PsaA/PsaB heterodimer. The other two are known as F_A and F_B, both are bound to PsaC (Saenger et al., 2002). These 4Fe-4S clusters are essential to photosynthetic electron transport: they serve as sequential electron carriers ($F_X \rightarrow F_A \rightarrow F_B$) within PSI.

NiR and SiR, two enzymes catalyzing the six electron reduction of nitrite and sulfite respectively (Raux-Deery et al., 2005), are siroheme 4Fe-4S proteins. The active site of these enzymes has a siroheme attached to the 4Fe-4S cluster via a Cys residue (Crane et al., 1995; Crane and Getzoff, 1996). Therefore, the siroheme 4Fe-4S cluster is central to the reductive activity of NiR and SiR. The insertion of Fe into siroheme is carried out by

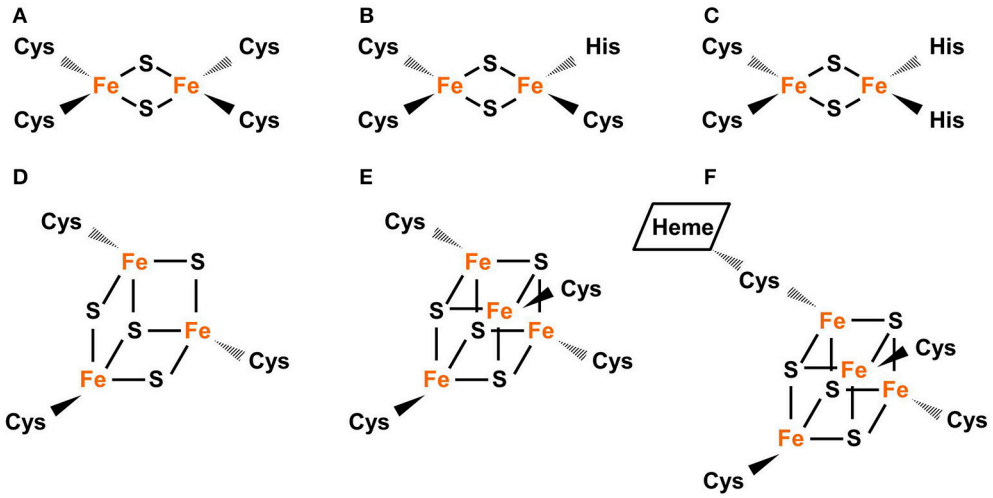

FIGURE 1 | Common types of Fe-S clusters found in the plastid. **(A)** Classic 2Fe-2S coordinated by four Cys residues, as in the plant-type Fd (ferredoxin). **(B)** NEET-type 2Fe-2S coordinated by three Cys and one His residues, as in NEET. **(C)** Rieske-type 2Fe-2S coordinated by two Cys and two His residues, as in PetC (photosynthetic electron transfer **C)**. **(D)** 3Fe-4S coordinated by three Cys residues as in Fd-GOGATs (ferredoxin-dependent Gln oxoglutarate aminotransferases). **(E)** 4Fe-4S coordinated by four Cys residues, as in PsaA, PsaB, and PsaC (Photosystem I proteins **A–C)**. **(F)** 4Fe-4S coordinated by four Cys residues with a thiolate ligand serving also for siroheme, as in NiR (nitrite reductase) and SiR (sulfite reductase). In Fe-S clusters, the oxidation state of Fe could be +2 or +3 while the oxidation state of S is −2.

sirohydrochlorin ferrochelatase (EC 4.99.1.4), which contains a 2Fe-2S cluster (Saha et al., 2012).

In Fe-S clusters, Fe^{2+} or Fe^{3+} is combined with sulfide (S^{2-}). The valency of the entire cluster could be indicated with square brackets (e.g., $[2Fe\text{-}2S]^{2+}$, in which both Fe ions exist as Fe^{3+}). After S^{2-} is incorporated into the cluster, it does not undergo redox transitions. However, Fe^{3+} in the cluster may be reduced to Fe^{2+} and *vice versa*. For example, $[2Fe\text{-}2S]^{2+}$ may receive an electron and become reduced to $[2Fe\text{-}2S]^{1+}$ and $[2Fe\text{-}2S]^{1+}$ may lose an electron and become oxidized to $[2Fe\text{-}2S]^{2+}$.

Different types of Fe-S clusters are inter-convertible. $[4Fe\text{-}4S]^{2+}$ (a common oxidation state of 4Fe-4S) could be converted to $[2Fe\text{-}2S]^{2+}$ (a common oxidation state of 2Fe-2S) via oxidative cleavage (Holm and Lo, 2016). For example, $[4Fe\text{-}4S]^{2+}$-containing fumarate and nitrate reduction regulatory protein (FNR) is a DNA-binding homodimer under anaerobic conditions (Zhang et al., 2012). Under high oxygen, the $[4Fe\text{-}4S]^{2+}$ cluster is quickly converted to a classic $[2Fe\text{-}2S]^{2+}$ cluster, with the release of one Fe^{3+} ion, one Fe^{2+} ion, two S^{2-} ions, and a superoxide ion (O_2^-), via a two-step process (Crack et al., 2008; Zhang et al., 2012). In the first step, $[4Fe\text{-}4S]^{2+}$ is oxidized by one electron from molecular oxygen, producing an intermediate $[3Fe\text{-}4S]^{1+}$, an Fe^{2+} ion, and a O_2^- ion. In the second step, the intermediate $[3Fe\text{-}4S]^{1+}$ converts spontaneously to $[2Fe\text{-}2S]^{2+}$, releasing an Fe^{3+} ion and two S^{2-} ions. This two-step conversion causes the transition of FNR from dimer to monomer and the loss of DNA-binding ability. The $[4Fe\text{-}4S]^{2+}$-to-$[2Fe\text{-}2S]^{2+}$ conversion could be reversed via reductive coupling. For example, two $[2Fe\text{-}2S]^{2+}$ clusters in FNR could receive two electrons and be reverted to $[4Fe\text{-}4S]^{2+}$ after incubation with DTT under anaerobic conditions (Zhang et al., 2012).

Fe-S clusters are sensitive to oxygen and reactive oxygen species (ROS) (Couturier et al., 2013; Balk and Schaedler, 2014) and the assembly of Fe-S clusters is influenced by the availability of Fe and S (Vigani et al., 2009). The inter-convertibility among different types of Fe-S clusters may represent a route to repair damaged Fe-S clusters and/or a regulatory process in response to changes in cellular and external environments, especially redox status. As discussed below, loss-of-function mutations in a specific plastidial Fe-S carrier protein do not result in uniform reductions in the levels of different types of plastidial Fe-S clusters. These observations suggest that cluster inter-conversion may not be sufficient to compensate for the loss of a specific Fe-S carrier protein.

Fe-S ASSEMBLY AND TRANSFER PATHWAYS IN PLANTS

The Fe-S assembly and transfer process can be separated into two sequential steps (**Figure 2**). The first step is the assembly of Fe-S clusters on a scaffold complex by Cys desulfurase (EC 2.8.1.7), with the help from sulfur transferase (EC 2.8.1.3). The second step is the transfer of Fe-S clusters from the scaffold complex to recipient proteins via carrier proteins. The initial identification of proteins involved in Fe-S assembly was from the analysis of proteins required for nitrogen fixation in Gram-negative bacterium *Azotobacteria vinelandii* (Frazzon and Dean, 2003; Dos Santos et al., 2004). The work on the synthesis of nitrogenase (molybdenum [Mo])-Fe-S cofactors led to the discovery of the NIF (nitrogen fixation) system and established the requirement of Cys desulfurase, sulfur transferase, and Fe-S scaffold protein(s) during Fe-S assembly (Frazzon and Dean, 2003). While the NIF

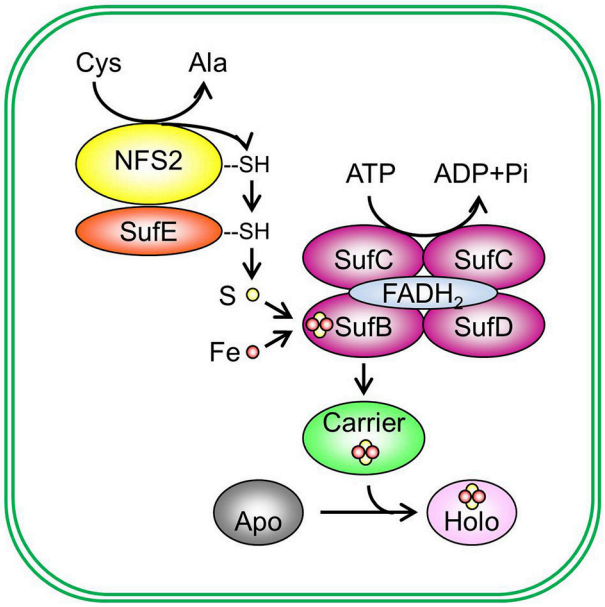

FIGURE 2 | *De novo* assembly and transfer of Fe-S clusters in the plastid. In the plastid, Cys desulfurase NFS2 (nitrogen fixation S-like 2) removes sulphane (S^0) from Cys and converts cysteine (Cys) to alanine (Ala). Sulphane (S^0) is transferred from Cys desulfurase to sulfur transferase SufE (sulfur mobilization protein E) and then to SufB (sulfur mobilization protein B) of the $SufBC_2D$ scaffold complex. On the $SufBC_2D$ scaffold complex, whose function requires cofactor $FADH_2$, sulphane (S^0) is reduced to sulfide (S^{2-}) and is incorporated in Fe-S clusters. The $SufBC_2D$ complex has ATPase activity, thus coupling ATP hydrolysis with the formation of Fe-S clusters. The source of Fe is not yet known. The newly assembled Fe-S cluster is then transferred to a carrier protein, which delivers the Fe-S cluster to recipient apoproteins and converts recipient apoproteins (Apo) into holoproteins (Holo). Plastidial sulfur transferases include SufE1, SufE2, and SufE3. The Suf scaffold complex is composed of three different proteins: SufB, sulfur mobilization protein C (SufC), and sulfur mobilization protein D (SufD), primarily in a 1:2:1 (BC_2D) ratio. Potential plastidial Fe-S carriers include sulfur mobilization protein A1 (SufA1), nitrogen fixation subunit U 1, 2, and 3 (NFU1, NFU2, and NFU3), high chlorophyll fluorescence 101 (HCF101), plastidial Clusters of Orthologous Groups 0354 protein (COG0354p), and glutaredoxin S14 and S16 (GRXS14 and GRXS16). Pi, inorganic phosphate.

system specifically deals with nitrogenase cofactor synthesis in nitrogen-fixing bacteria (Jacobson et al., 1989; Frazzon and Dean, 2003), the assembly of Fe-S clusters for other Fe-S proteins in bacteria is carried out by the iron–sulfur cluster (ISC) system and the sulfur mobilization (SUF) system (Takahashi and Tokumoto, 2002; Outten et al., 2004). The bacterial ISC system contains the following proteins: Cys desulfurase IscS, scaffold protein IscU, DnaK-like chaperone HscA (heat shock cognate protein A), DnaJ-like co-chaperone HscB (heat shock cognate protein B), and possibly Fd (Ayala-Castro et al., 2008; Roche et al., 2013). The bacterial SUF system contains two complexes: SufSE (where SufS is Cys desulfurase and SufE is sulfur transferase), and $SufBC_2D$ (the scaffold complex). The bacterial ISC and SUF systems have different tolerance to oxidative stress (Dai and Outten, 2012). In SufS, the catalytic active Cys residue is deeply buried and thus not easily accessed by O_2 or H_2O_2 (Lima, 2002). On the contrary, the catalytic active Cys residue in IscS is exposed to the surface of the protein (Cupp-Vickery et al., 2003). Therefore, it was proposed that the ISC system is the housekeeping system for Fe-S assembly and the SUF system is adapted to assemble Fe-S clusters under Fe or S starvation, or oxidative stress (Outten et al., 2004). Consistent with this hypothesis, SufS was found to express under Fe starvation, low S availability, and oxidative stress conditions (Outten et al., 2004). If readers are interested in detailed information on the regulation of bacterial ISC and SUF systems and the functions of individual Fe-S assembly proteins, they may refer to reviews on bacterial Fe-S assembly pathways, for example, Ayala-Castro et al. (2008) and Roche et al. (2013), and the references therein.

There are three Fe-S assembly and transfer pathways in the plant cell: the SUF pathway in the plastid, the ISC pathway in the mitochondrion, and the cytosolic iron–sulfur assembly (CIA) pathway (Balk and Pilon, 2011; Couturier et al., 2013; Balk and Schaedler, 2014). These pathways supply Fe-S clusters to the plastids, mitochondria, and cytosol plus nucleus, respectively. It is worth mentioning that the ISC pathway in plants evolved from the bacterial ISC system, which has poor tolerance to oxidative stress, and the SUF pathway in plants evolved from the bacterial SUF system, which has higher tolerance to oxidative stress (Takahashi and Tokumoto, 2002; Outten et al., 2004). Oxygenic phototrophs such as cyanobacteria and plants generate oxygen in photosynthetic cells or tissues. Therefore, it is likely that cyanobacteria and plants inherited the bacterial SUF system to tolerate the high oxidative environment at the site of photosynthesis. The plastidial SUF pathway appears to be independent from the mitochondrial ISC pathway and the CIA pathway (Van Hoewyk et al., 2007; Bernard et al., 2013). However, the CIA pathway requires the function of the mitochondrial ISC pathway: the sulfide compound from the ISC way is exported from the mitochondrion to the cytosol via ATM3 (ATP binding cassette transporter of the mitochondrion 3) and it serves as the S source for the CIA pathway (Kushnir et al., 2001; Kim et al., 2006; Bernard et al., 2009). This review focuses on recent discoveries on the molecular functions of different types of proteins involved in the plastidial SUF pathway. Detailed information about the ISC and ICA pathways in plants could be found in the following excellent reviews: Balk and Pilon (2011), Couturier et al. (2013), and Balk and Schaedler (2014).

Cys Desulfurase

Cys desulfurase removes S from Cys and converts Cys to alanine (Ala) (**Figure 2**) (Zheng et al., 1993, 1994; Zheng and Dean, 1994). The newly released sulphane S (S^0) is bound to the active site of Cys desulfurase in the form of persulfide ($R\text{-}S\text{-}S^0H$). The bound sulphane (S^0) is then transferred in the same form to the Fe-S scaffold complex with the help from sulfur transferase.

Cys desulfurases can be classified into two groups according to their sequences and structures (Mihara et al., 1997; Mihara and Esaki, 2002; Roret et al., 2014). The two groups differ in the β-hairpin loop and the extended lobe containing the catalytic Cys residue. In group I, the extended loop lacks the β-hairpin structure and it is long and sufficiently flexible to transfer S^{2-} to sulfur transferase (Kaiser et al., 2000). Thus the sulfur transferase

associated with a group I Cys desulfurase does not need to be flexible to acquire S^{2-}. On the contrary, group II Cys desulfurases have a β-hairpin structure constraining the catalytic site and their extended loop is short and insufficiently flexible (Mihara et al., 2002; Outten et al., 2003; Singh et al., 2013). Therefore, the sulfur transferase associated with a group II Cys desulfurase needs additional flexibility to acquire S^{2-} (Kim and Park, 2013).

Plants have three Cys desulfurases: nitrogen fixation S-like 1 (NFS1/NifS1, referred to as NFS1 hereafter) (Frazzon et al., 2007), nitrogen fixation S-like 2/chloroplastic nitrogen fixation S-like/chloroplastic sulfur mobilization protein S (NFS2/CpNifS/CpSufS, referred to as NFS2 hereafter) (Pilon-Smits et al., 2002; Ye et al., 2005; Van Hoewyk et al., 2007), and abscisic acid deficient 3 (ABA3) (Heidenreich et al., 2005). Among them, ABA3 is involved in Mo cofactor sulfuration but not in Fe-S assembly (Bernard et al., 2013). NFS1 is a group I Cys desulfurase (Mihara et al., 1997; Mihara and Esaki, 2002) and it is targeted to the mitochondrion (Kushnir et al., 2001). NFS2 is a group II Cys desulfurase (Mihara et al., 1997; Mihara and Esaki, 2002) and it is located to the chloroplast (**Table 1**) (Léon et al., 2002; Pilon-Smits et al., 2002). Full-length NFS2 has a 35-amino acid plastid transit peptide and a C-terminal Cys desulfurase domain (**Figure 3**) (Pilon-Smits et al., 2002). Gel filtration of the purified NFS2 protein showed this protein forms a dimer (**Table 2**) (Pilon-Smits et al., 2002; Ye et al., 2005). Recombinant NFS2 demonstrated Cys desulfurase activity toward Cys and seleno-Cys lyase activity toward seleno-Cys, with a much high activity on seleno-Cys (Pilon-Smits et al., 2002). Absorption spectrum indicated the presence of a pyridoxal 5′-phosphate cofactor in the purified protein (Pilon-Smits et al., 2002). NFS2 silencing via RNA interference (RNAi) is lethal (Van Hoewyk et al., 2007). Immunoblot analysis showed that the levels of Fe-S proteins representing different types of plastidial Fe-S clusters were reduced in the RNAi lines. However, mitochondrial Fe-S proteins and respiration were not affected in the RNAi lines. Taken together, these data indicate that NFS2 is required in *de novo* assembly of all plastidial Fe-S clusters and that the plastidial and mitochondrial Fe-S assembly pathways operate independently (Van Hoewyk et al., 2007).

Sulfur Transferase

The Cys desulfurase activity of NFS2 is activated by sulfur transferases, which accept the persulfide (R-S-S^0H) from NFS2 and transfer it to the Fe-S scaffold complex (**Figure 2**). Plants have three sulfur transferases: sulfur mobilization protein E1, E2, and E3, i.e., SufE1, SufE2, and SufE3 (**Table 1**) (Xu and Møller, 2006; Ye et al., 2006; Murthy et al., 2007). Full-length SufE1 contains a transit peptide, a SufE domain, and a BolA domain (**Figure 3**) (Xu and Møller, 2006; Ye et al., 2006). *In silico* analysis of the transit peptide suggests that SufE1 is dual-targeted to plastids and mitochondria. This prediction was confirmed with confocal microscopic analysis of tobacco and Arabidopsis leaves transiently expressing the AtSufE1-YFP (At stands for *A. thaliana*; YFP stands for yellow fluorescent protein) fusion protein (Xu and Møller, 2006). AtSufE1 was able to complement the growth defects of ΔSufE *Escherichia coli*. *In vitro* Cys desulfurization assays demonstrated that AtSufE1 interacts with and activates both plastid-targeted NFS2 and mitochondrion-targeted NFS1 (**Table 2**) (Xu and Møller, 2006; Ye et al., 2006). Loss-of-function AtSufE1 mutants are embryo lethal, indicating that SufE1 and Fe-S cluster assembly in plastids and mitochondria are essential during embryo development (Xu and Møller, 2006; Ye et al., 2006).

The function of the BolA domain in SufE1 was intriguing. BolA proteins are known as morphogens, whose overexpression results in spherical cell morphology in *E. coli* (Aldea et al., 1988). Surprisingly, overexpression of the BolA domain of AtSufE1 showed no effects on the morphology of *E. coli* or Arabidopsis (Xu and Møller, 2006). Therefore, Xu and Møller (2006) proposed that the BolA domain in SufE1 is not functional. However, recent yeast-two-hybrid and bimolecular fluorescence complementation assays demonstrated that the BolA domain allows SufE1 to interact with monothiol glutaredoxins (GRXs), including plastid-targeted GRXS14 and GRXS16 (Couturier et al., 2014). In addition, *in vitro* experiments showed that the binding of GRXs promotes the deglutathionation of SufE1, and thereby facilitates the activation of NFS2 by deglutathionated SufE1 (Couturier et al., 2014). Taken together, the interactions between the SufE1 BolA domain and GRXs suggest possible redox regulation of SufE1 activity and Fe-S cluster assembly by GRXs.

Full-length SufE2 and SufE3 have a plastid transit peptide and a SufE domain (**Figure 3**). Confocal microscopic analysis of Arabidopsis protoplasts expressing GFP (green fluorescent protein)-tagged AtSufE2 and AtSufE3 confirmed their plastidial localization (Murthy et al., 2007). The SufE domain of AtSufE2 and AtSufE3 was found to interact with and activate the Cys desulfurase activity of NFS2 (**Table 2**) (Murthy et al., 2007). SufE3 has a C-terminal NadA domain. In bacteria, the *NadA* gene encodes quinolinate synthase A (EC 2.5.1.72), an enzyme required for NAD biosynthesis (Foster and Moat, 1980). Expression of AtSufE3 complemented the *E. coli* ΔNadA mutant, suggesting that SufE3 contains a functional NadA domain (Murthy et al., 2007). Consistent with this hypothesis, recombinant AtSufE3 demonstrated quinolinate synthase (QS) activity. The expression of the NadA domain of AtSufE3 alone could not complement the *E. coli* ΔNadA mutant, indicating that the SufE domain of SufE3 is required for QS activity. Apparently, QS activity requires the 4Fe-4S cluster in the NadA domain; and the SufE domain is responsible for reconstituting the cluster by interacting with NFS2 (Murthy et al., 2007).

The phenotype of loss-of-function AtSufE2 mutants has not yet been reported. Loss-of-function AtSufE3 mutants are embryo lethal (Murthy et al., 2007), suggesting that SufE3 is an essential protein. This is somewhat surprising because there are three SufE proteins in plants. It is possible that the BolA domain in SufE1 and the NadA domain in SufE3 make the two proteins irreplaceable (Murthy et al., 2007). Differential expression could be another reason why the three SufE proteins cannot complement each other (Murthy et al., 2007). For example, SufE1 and SufE3 are expressed in vegetative tissues while SufE2 is only expressed in pollen. Furthermore, SufE1 is

TABLE 1 | Proteins involved in *de novo* assembly and transfer of Fe-S clusters in the Arabidopsis plastid.

Functional category	Protein name	Locus ID	Activity of purified recombinant protein	Phenotype of loss-of-function mutants	References
Cys desulfurase	NFS2	At1g08490	Cys desulfurase activity	Seedling lethal	Pilon-Smits et al., 2002; Ye et al., 2005; Van Hoewyk et al., 2007
Activation of Cys desulfurase; sulfur transferase	SufE1	At4g26500	Activates Cys desulfurase; complements *E. coli* ΔSufE mutant	Embryo lethal	Xu and Møller, 2006; Ye et al., 2006
Activation of Cys desulfurase; sulfur transferase	SufE2	At1g67810	Activates Cys desulfurase	Not yet described	Murthy et al., 2007
Activation of Cys desulfurase; sulfur transferase	SufE3	At5g50210	Activates Cys desulfurase; quinolinate synthase activity; complements *E. coli* ΔNadA mutant	Embryo lethal	Katoh et al., 2006; Murthy et al., 2007
Scaffold complex	SufB	At4g04770	ATPase activity; complements *E. coli* ΔSufB mutant	Embryo lethal (strong alleles); pale green and growth retardation (weak alleles)	Møller et al., 2001; Ahn et al., 2005; Xu et al., 2005; Nagane et al., 2010; Saini et al., 2010; Wollers et al., 2010; Hu et al., 2017a,b
Scaffold complex	SufC	At3g10670	ATPase activity; complements *E. coli* ΔSufC mutant	Embryo lethal	Xu and Møller, 2004; Saini et al., 2010; Wollers et al., 2010; Hu et al., 2017a
Scaffold complex	SufD	At1g32500	Fe acquisition	Seed abortion; reduced chlorophyll content; defects in plastid morphology	Xu and Møller, 2004; Hjorth et al., 2005; Saini et al., 2010; Wollers et al., 2010; Hu et al., 2017a
Carrier protein	SufA1	At1g10500	Carrier of classic 2Fe-2S	No visible phenotype	Abdel-Ghany et al., 2005; Yabe and Nakai, 2006
Carrier protein	NFU1	At4g01940	Complements yeast *isu1 nfu1* double mutant	Not yet described	Léon et al., 2003
Carrier protein	NFU2	At5g49940	Carrier of classic 2Fe-2S and 4Fe-4S; complements yeast *isu1 nfu1* double mutant	Pale green; growth retardation; reduced levels of 2Fe-2S and 4Fe-4S proteins	Léon et al., 2003; Touraine et al., 2004; Yabe et al., 2004; Gao et al., 2013; Hu et al., 2017a
Carrier protein	NFU3	At4g25910	Carrier of 3Fe-4S and 4Fe-4S	Pale green; growth retardation; reduced levels of 3Fe-4S and 4Fe-4S proteins	Léon et al., 2003; Nath et al., 2016, 2017
Carrier protein	HCF101	At3g24430	Carrier of 4Fe-4S	Seedling lethal (strong alleles); reduced levels of 4Fe-4S proteins	Lezhneva et al., 2004; Stöckel and Oelmuller, 2004; Schwenkert et al., 2010; Hu et al., 2017a
Carrier protein	COG0354p	At1g60990	Complements *E. coli* ΔYgfZ and ΔMiaB mutants	Not yet described	Waller et al., 2010, 2012
Carrier protein; regulation of redox status	GRXS14	At3g54900	Carrier of 2Fe-2S; complements yeast *grx5* mutant; activates SufE1 by deglutathionating	Defects in early seedling growth under oxidative stresses; increased protein carbonylation in the chloroplast; no growth defects in adult plants under normal conditions	Cheng and Hirschi, 2003; Cheng et al., 2006; Bandyopadhyay et al., 2008; Yadav et al., 2012; Couturier et al., 2014; Rey et al., 2017
Carrier protein; regulation of redox status	GRXS16	At2g38270	Carrier of 2Fe-2S; GIY-YIG endonuclease activity; complements yeast *grx5* mutant; activates SufE1 by deglutathionating	No growth defects in adult plants under normal conditions	Cheng and Hirschi, 2003; Bandyopadhyay et al., 2008; Liu et al., 2013; Couturier et al., 2014; Rey et al., 2017
Carrier protein; regulation of redox status	At-NEET	At5g51720	Carrier of NEET-type 2Fe-2S	Delayed growth and development, accelerated senescence, and elevated ROS under normal conditions; increased sensitivity to low Fe; reduced sensitivity to high Fe	Nechushtai et al., 2012; Su et al., 2013

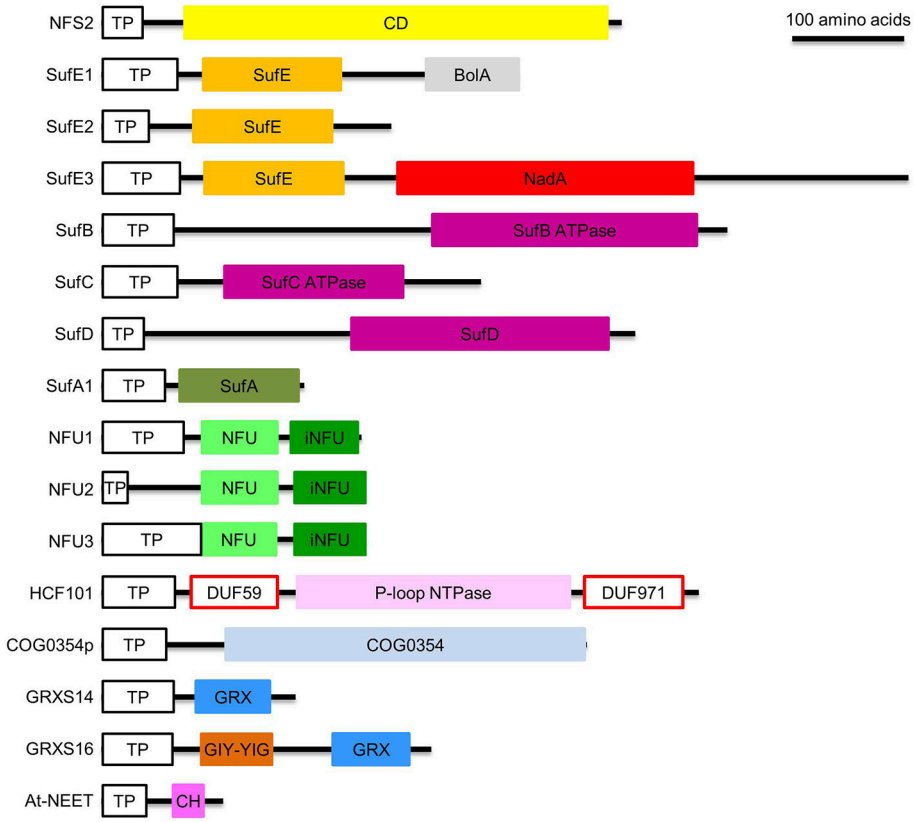

FIGURE 3 | Domain composition of proteins involved in *de novo* assembly and transfer of Fe-S clusters in the plastid. ATPase, adenosine triphosphatase; BolA, DNA-binding transcriptional regulator BolA; CD, Cys desulfurase; CH, CDGSH motif; COG0354, Clusters of Orthologous Groups 0354 protein; COG0354p, plastidial Clusters of Orthologous Groups 0354 protein; DUF59 and DUF971; domain of unknown function 59 and 971; GIY-YIG, GlyIleTyr-TyrIleGly; GRX, glutaredoxin; GRXS14 and GRXS16, glutaredoxin S14 and S16; HCF101, high chlorophyll fluorescence 101; iNFU, redox-inactive nitrogen fixation subunit U; NadA, quinolinate synthase A; NFU, nitrogen fixation subunit U; NFU1, NFU2, and NFU3, nitrogen fixation subunit U 1, 2, and 3; NFS2, nitrogen fixation S-like 2; P-loop NTPase, P-loop nucleotide phosphatase; SufA1, SufB, SufC, SufD, SufE1, SufE2, and SufE3, sulfur mobilization protein A1, B, C, D, E1, E2, and E3; TP, transit peptide. Note that SufE1 and At-NEET are dually targeted to plastids and mitochondria. Bar = 100 amino acids.

dual-targeted to both plastids and mitochondria while SufE2 and SufE3 are targeted to the plastid.

The Fe-S Scaffold Complex

Persulfide (R-S-S^0H) groups are transferred to the scaffold complex for Fe-S cluster assembly (**Figure 2**). During this step, sulphane (S^0) accepts electrons from electron donors and is reduced to sulfide (S^{2-}), the final form of S in Fe-S clusters. The scaffold complex of the SUF pathway is composed of three different proteins: sulfur mobilization protein B/non-intrinsic ABC protein 1 (SufB/NAP1; referred to as SufB hereafter; ABC stands for ATP binding cassette), sulfur mobilization protein C/non-intrinsic ABC protein 7 (SufC/NAP7; referred to as SufC hereafter), and sulfur mobilization protein D/non-intrinsic ABC protein 6 (SufD/NAP6; referred to as SufD hereafter), primarily in a 1:2:1 (BC_2D) ratio (Xu et al., 2005; Hu et al., 2017a). However, other subcomplexes may form as well (Wollers et al., 2010; Roche et al., 2013; Hu et al., 2017a). Extensive protein-protein interactions have been observed among SufB, SufC, and SubD proteins (**Table 2**) (Xu and Møller, 2004; Xu et al., 2005; Hu et al., 2017a). Although all three proteins are required for *in vivo* assembly of Fe-S clusters (**Table 1**), formation of Fe-S clusters occurs directly on SufB (Saini et al., 2010). Each $SufBC_2D$ complex binds to one molecule of $FADH_2$ via SufB (Wollers et al., 2010). $FADH_2$ was thought to provide electrons to reduce sulphane (S^0) to sulfide (S^{2-}) (Wollers et al., 2010). However, Wollers et al. (2010) reported that $FADH_2$ actually plays a role in reductive mobilization of Fe, which is equally important for the assembly of Fe-S clusters. Using lysed and intact chloroplasts, Takahashi et al. showed that plastidial formation of Fe-S clusters on the scaffold complex requires ATP and NADPH (Takahashi et al., 1986, 1991a,b). These observations were re-confirmed by the activation of the SUF pathway in cell lysates by the addition of ATP and NADPH (Saini et al., 2010). The hydrolysis of ATP is likely carried out by the $SufBC_2D$ complex, because the SufB and SufC subunits of this complex have ATPase activity (Xu and Møller, 2004; Xu et al., 2005). While ATP hydrolysis by the $SufBC_2D$ complex provides energy for the formation of Fe-S clusters (Xu and Møller, 2004; Xu et al., 2005), NADPH may serve as the reducing agent for redox cycling of $FADH_2$/FAD (Saini

TABLE 2 | Protein-protein interactions among different plastidial Fe-S assembly and transfer factors.

	NFS2	SufE1	SufE2	SufE3	SufB	SufC	SufD	SufA1	NFU1	NFU2	NFU3	HCF101	COG0354p	GRXS14	GRXS16	At-NEET
NFS2	+	+	+	+				+								
SufE1	+					−		−						+	+	
SufE2	+															
SufE3	+															
SufB					+	+	+									
SufC					+	+	+									
SufD					+	+										
SufA1	+	−						+								
NFU1																
NFU2										+						
NFU3																
HCF101																
COG0354p																
GRXS14		+												+		
GRXS16		+													+	
At-NEET																+

et al., 2010). In addition to NADPH, another possible source of reducing agents is plant-type Fds. Because plant-type Fds participate in many plastidial reactions, direct evidence for their role in the SUF pathway is still lacking. However, mitochondrial Fd has been shown to be essential for *de novo* assembly of Fe-S clusters in yeast mitochondria (Takahashi and Nakamura, 1999).

The source of Fe for plastidial Fe-S assembly is not yet known. Universal Fe-storage protein ferritin was previously considered as a candidate to supply Fe to the Fe-S scaffold complex (Lobreaux and Briat, 1991; Briat and Lobréaux, 1997). However, the triple loss-of-function Arabidopsis mutant of three major chloroplastic ferritins FER1, FER3, and FER4 had normal photosynthetic apparatus, which is extremely dependent on proper assembly of Fe-S clusters (Ravet et al., 2009). These results suggest that chloroplastic ferritins do not constitute a major Fe pool for the plastidial SUF pathway. Interestingly, the triple mutant exhibited increased sensitivity to excess Fe, suggesting that chloroplastic ferritins may actually act as Fe scavengers.

Full-length SufB contains a plastid transit peptide and an adenosine triphosphatase (ATPase, EC 3.6.1.3) domain with degenerative Walker A (also known as P-loop) and Walker B motifs (**Figure 3**) (Xu et al., 2005). The plastidial localization of AtSufB was confirmed with confocal microscopic analysis of onion epidermal cells expressing the AtSufB-GFP fusion protein (Møller et al., 2001). AtSufB expression complemented the growth defects of *E. coli* ΔSufB mutant, suggesting that AtSufB is a functional SufB protein (Xu et al., 2005). However, the absence of either SufD or both SufC and SufD caused substantial reduction in the *in vivo* cluster-assembly ability of SufB (Hu et al., 2017a). These results indicate that SufC and SufD are required for *in vivo* Fe-S cluster formation on SufB. Recombinant AtSufB demonstrated Fe^{2+}-stimulated ATPase activity (Xu et al., 2005). This is somewhat surprising because ATPase activity was not reported for prokaryotic SufB (Roche et al., 2013). SufB was previously classified as a non-intrinsic ABC protein; however its ATPase domain does not contain the conserved ABC signature motif. In addition, SufB is capable of forming homodimers (**Table 2**), which also is different from its prokaryotic counterparts. The strong loss-of-function AtSufB mutant is embryo lethal, suggesting that SufB and the SUF pathway are essential to embryogenesis (Nagane et al., 2010). Weak SufB alleles in Arabidopsis and *Nicotiana benthamiana* had pale green leaves and retarded growth, due to defects in chlorophyll biosynthesis and chloroplast development (Møller et al., 2001; Ahn et al., 2005; Nagane et al., 2010; Hu et al., 2017a,b). These data demonstrate that insufficient supply of Fe-S clusters in the plastid will lead to defects in chlorophyll biosynthesis, chloroplast development, growth retardation, and embryo development.

Full-length SufC contains a plastid transit peptide and an ATPase domain with degenerative Walker A and Walker B motifs and an ABC signature motif (**Figure 3**) (Xu and Møller, 2004). The plastidial localization of SufC was confirmed by microscopic analysis of tobacco leaves expressing the AtSufC-YFP fusion protein (Xu and Møller, 2004). AtSufC expression complemented the growth defects of *E. coli* ΔSufC mutant, suggesting that AtSufC is a functional SufC protein (Xu and Møller, 2004). Consistent with this observation, recombinant AtSufC demonstrated Mg^{2+}-stimulated ATPase activity (Xu and Møller, 2004). Loss of AtSufC resulted in an embryo-lethal phenotype, suggesting that SufC and the SUF pathway are essential to embryogenesis (Xu and Møller, 2004). The RNAi lines of SufB demonstrated pale green leaves, because of their defects in chlorophyll biosynthesis (Hu et al., 2017a). Due to similarity to the ISC pathway, it was proposed that ATP hydrolysis by SufB and SufC induces conformational changes of the $SufBC_2D$ scaffold complex to release newly assembled Fe-S clusters (Markley et al., 2013). However, Saini et al. (2010) reported that the ATPase activity is instead necessary for Fe acquisition during *in vivo* assembly of Fe-S clusters.

Full-length SufD contains a plastid transit peptide and a SufD domain (**Figure 3**). The plastidial localization of SufD was confirmed by microscopic analysis of tobacco leaves expressing the AtSufD-YFP fusion protein (Xu and Møller, 2004). Unlike SufB or SufC, the SufD domain does not contain Walker A, Walker B, or the ABC signature motif. Saini et al. (2010) reported that SufD is not required for *in vivo* sulfur transfer from the NFS2-SufE system, but it is required during *in vivo* Fe acquisition and *in vivo* formation of Fe-S clusters on SufB (Saini et al., 2010). The loss-of-function mutation in the *SufD* gene resulted in seed abortion, reduced chlorophyll content, and defects in plastid morphology (Hjorth et al., 2005). Consistent with these observations, RNAi lines of this protein showed defective chlorophyll biosynthesis (Hu et al., 2017a). Taken together, these data indicate that SufD may have a general house-keeping role (e.g., chlorophyll biosynthesis and chloroplast development), instead of functioning only in embryogenesis (Hjorth et al., 2005).

Fe-S Carrier Proteins

Fe-S clusters assembled on the $SufBC_2D$ scaffold complex are transferred to recipient proteins via carrier proteins (**Figure 2**). When exogenous Fe^{2+} and S^{2-} are supplied, Fe-S carrier proteins may serve as scaffold proteins for *in vitro* Fe-S cluster assembly. Examples of plastidial Fe-S carrier proteins include: sulfur mobilization protein A1/chloroplast ISC protein A1 (SufA1/CpIscA1, referred to as SufA1 hereafter) (Abdel-Ghany et al., 2005; Yabe and Nakai, 2006); nitrogen-fixation-subunit-U-type proteins NFU1, NFU2, and NFU3 (Léon et al., 2003; Touraine et al., 2004; Yabe et al., 2004; Gao et al., 2013; Nath et al., 2016, 2017); P-loop nucleotide phosphatase (NTPase) HCF101 (high chlorophyll fluorescence 101) (Lezhneva et al., 2004; Stöckel and Oelmuller, 2004; Schwenkert et al., 2010); plastidial-type COG0354 (COG0354p, COG stands for Clusters of Orthologous Groups; p stands for plastidial) (Waller et al., 2010, 2012); and monothiol GRXS14 and GRXS16 (S refers to the Ser residue in the CGFS active site motif of GRXs) (**Table 1**) (Cheng and Hirschi, 2003; Cheng et al., 2006; Bandyopadhyay et al., 2008; Yadav et al., 2012; Couturier et al., 2014).

SufA1

The Arabidopsis genome encodes four SufA proteins: SufA1 is plastid-targeted (**Figure 3**; **Table 1**) while SufA2, SufA3, and SufA4 are mitochondrion-targeted (Yabe and Nakai, 2006). All four SufA proteins contain three conserved Cys residues: one in the GCXGXXY motif and the other two in the C-terminal C(G/S)CXSF motif (Yabe and Nakai, 2006). These conserved Cys residues may serve as ligands for Fe-S clusters. The plastidial localization of SufA1 was confirmed with a number of independent techniques, including confocal microscopic analysis of GFP-fusion protein, import assays, as well as chloroplast sub-fractionation and subsequent immunodetection (Abdel-Ghany et al., 2005). SufA1 is ubiquitously expressed in all the Arabidopsis tissues tested, with higher expression in green tissues such as leaves and flower stalks (Abdel-Ghany et al., 2005; Yabe and Nakai, 2006). Gel filtration analysis showed that SufA1 tends to form homodimers (**Table 2**). Recombinant SufA1 was capable of enhancing NFS2-mediated *in vitro* assembly of 2Fe-2S clusters on apo Fd (Abdel-Ghany et al., 2005). This observation suggests a possible interaction between SufA1 and NFS2 (**Table 2**), during which SufA1 may act as a scaffold protein for *in vitro* assembly of 2Fe-2S clusters. However, loss-of-function mutation in the *SufA1* gene does not cause any defect in plant growth and development or in the abundance of classic 2Fe-2S protein Fd (Yabe and Nakai, 2006). It is likely that SufA1 serves as a back-up carrier for classic 2Fe-2S (**Figure 4A**), when other classic 2Fe-2S carriers are insufficient, e.g., under stress conditions.

NFU1, NFU2, and NFU3

The Arabidopsis genome encodes five NFU proteins: NFU1, NFU2, and NFU3 are plastid-localized (**Figure 3**; **Table 1**) and NFU4 and NFU5 are mitochondrion-localized (Léon et al., 2003; Yabe et al., 2004; Gao et al., 2013; Nath et al., 2016). Their subcellular localization was confirmed with confocal microscopic analysis of Arabidopsis protoplasts expressing GFP-tagged NFU proteins (Léon et al., 2003). Reverse transcription-PCR analysis showed that NFU1 is expressed in flower stalks and siliques, NFU2 is expressed in flower stalks and leaves, and NFU3 is expressed in flower stalks, leaves, flowers, and roots (Léon et al., 2003).

Mature NFU1, NFU2, and NFU3 contain an N-terminal redox-active NFU domain with a conserved CXXC motif and a C-terminal redox-inactive NFU domain (Léon et al., 2003; Gao et al., 2013; Nath et al., 2016). The two Cys residues in the conserved CXXC motif of the redox-active NFU domain are used to coordinate Fe-S clusters. Both NFU1 and NFU2 were able to complement the growth defects of the yeast *isu1 nfu1* double mutant, suggesting that NFU1 and NFU2 are functional NFU proteins (Léon et al., 2003). The oligomerization and activity of recombinant NFU1 has not yet been tested *in vitro*. Recombinant NFU2 may form homodimers and homotetramers (**Table 2**) (Yabe et al., 2004; Gao et al., 2013). It served as a scaffold protein during *in vitro* reconstitution of classic 2Fe-2S and 4Fe-4S clusters (**Figure 4A**) and a carrier protein during subsequent *in vitro* transfer to apo GRXS16 and APR1 (adenosine 5′-phosphosulfate reductase 1, EC 1.8.99.2) proteins (Léon et al., 2003; Yabe et al., 2004; Gao et al., 2013). The unidirectional and intact transfer of classic 2Fe-2S from NFU2 to apo GRXS16 *in vitro* suggests that NFU2 may work upstream of GRXS16 during *in vivo* delivery of classic 2Fe-2S clusters to recipient proteins (**Figure 4C**) (Gao et al., 2013). NFU3 also is a functional NFU protein. Recombinant NFU3 served as a scaffold protein during *in vitro* reconstitution of 3Fe-4S and 4Fe-4S clusters (**Figure 4A**) (Nath et al., 2016).

The phenotype of loss-of-function mutants of NFU1 has not been described. Therefore, it is not clear which Fe-S cluster(s) NFU1 is able to carry. Loss-of-function mutations of the *NFU2* gene resulted in smaller and pale green leaves, a smaller plant size, as well as stunted growth and development (Touraine et al., 2004; Yabe et al., 2004). SDS-PAGE and immunoblot analysis showed that the levels of classic 2Fe-2S protein Fd, 4Fe-4S proteins PsaA, PsaB, and PsaC, and siroheme 4Fe-4S proteins NiR and SiR were largely reduced in the *nfu2* mutants while the level of Rieske-type 2Fe-2S protein PetC was substantially

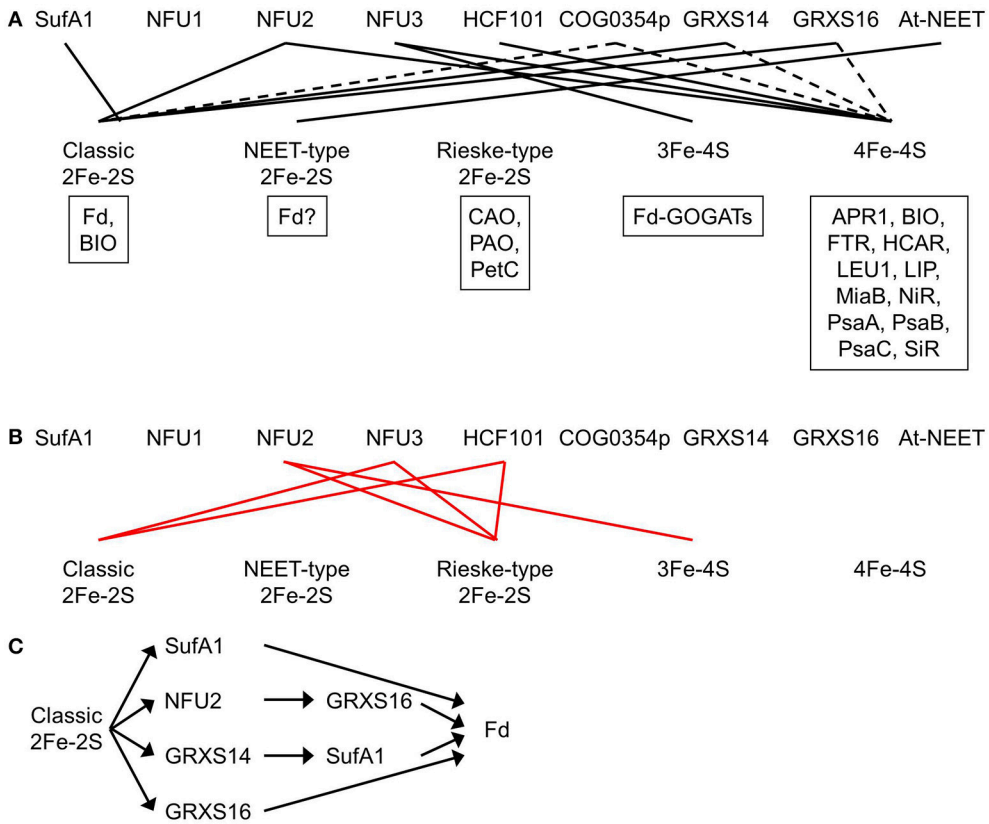

FIGURE 4 | Plastidial Fe-S clusters and the corresponding Fe-S carrier proteins**. (A)** Plastidial Fe-S clusters, the corresponding Fe-S carrier proteins, and exemplar Fe-S proteins. Solid black lines indicate that the Fe-S carrier protein has been shown to act as a carrier for that type of Fe-S clusters. Dashed lines indicate that the Fe-S carrier protein could be a possible carrier for that type of Fe-S clusters. Exemplar Fe-S proteins containing that type of Fe-S clusters are shown in boxes. APR1, adenosine 5′-phosphosulfate reductase 1; At-NEET, *Arabidopsis thaliana* NEET; BIO, biotin synthase; CAO, chlorophyllide *a* oxygenase; COG0354p, plastidial Clusters of Orthologous Groups 0354 protein; Fd, ferredoxin; Fd-GOGATs, ferredoxin-dependent Gln oxoglutarate aminotransferases; FTR, ferredoxin-thioredoxin reductase; GRXS14 and GRXS16, glutaredoxin S14 and S16; HCAR, 7-hydroxymethyl chlorophyll *a* reductase; HCF101, high chlorophyll fluorescence 101; LEU1, 3-isopropylmalate isomerase 1; LIP, lipoic acid synthase; MiaB, isopentenyl-adenosine A37 tRNA methylthiolase; NFU1, NFU2, and NFU3, nitrogen fixation subunit U 1, 2, and 3; NiR, nitrite reductase; PetC, photosynthetic electron transfer C; PAO, pheophorbide *a* oxygenase; PsaA, PsaB, and PsaC, Photosystem I proteins A, B, and C; SiR, sulfite reductase. Note that BIO contains one classic 2Fe-2S and one 4Fe-4S. Recombinant At-NEET was able to transfer the NEET-type 2Fe-2S cluster to the plant-type Fd under *in vitro* conditions. However, it is not clear whether the plant-type Fd is able to serve as a recipient protein for the NEET-type 2Fe-2S cluster under *in vivo* conditions, because plant-type Fds are known as classic 2Fe-2S proteins. Therefore, a question mark is placed next to Fd in the box for exemplar NEET-type 2Fe-2S proteins. **(B)** Experimental evidence showed that NFU2 does not act as a carrier for Rieske-type 2Fe-2S and 3Fe-4S cluster and that NFU3 and HCF101 do not act as carriers for classic and Rieske-type 2Fe-2S clusters. Solid red lines indicate that the Fe-S carrier protein does not transfer that type of Fe-S clusters. **(C)** The transfer network of carrier proteins for classic 2Fe-2S clusters in the plastid. Fd is used as an example of recipient proteins.

increased. Consistent with the immunoblot data, the activities of PSI and SiR were substantially reduced in the *nfu2* mutants while the activity of 3Fe-4S enzyme Fd-GOGAT was significantly increased. Taken together, these data demonstrate that NFU2 is required in the assembly and transfer of classic 2Fe-2S and 4Fe-4S clusters (**Figure 4A**). Excess Fe and S in the *nfu2* mutants could be used to make other Fe-S clusters such as Rieske-type 2Fe-2S and 3Fe-4S, hence, increased levels of Rieske-type 2Fe-2S protein PetC and 3Fe-4S proteins Fd-GOGATs. The elevated contents of PetC and Fd-GOGATs suggest that NFU2 does not serve as a carrier protein for Rieske-type 2Fe-2S or 3Fe-4S (**Figure 4B**).

Loss-of-function mutants of NFU3 exhibited retarded growth and development, along with smaller and pale green leaves and a smaller plant size (Nath et al., 2016, 2017). SDS-PAGE and immunoblot analysis showed that the levels of 4Fe-4S proteins PsaA, PsaB, and PsaC and 3Fe-4S proteins Fd-GOGATs were substantially reduced in the *nfu3* mutants while the levels of classic 2Fe-2S protein Fd and Rieske-type 2Fe-2S protein PetC were significantly increased. Consistent with the immunoblot data, PSI activity was nearly abolished in the *nfu3* mutants. Taken together, these results demonstrate that NFU3 is required in the assembly and transfer of 4Fe-4S and 3Fe-4S clusters (**Figure 4A**). Excess Fe and S in the *nfu3* mutants could be used to make other Fe-S clusters such as classic and Rieske-type 2Fe-2S, hence, increased levels of classic 2Fe-2S protein Fd and Rieske-type 2Fe-2S protein PetC. The elevated levels of Fd and PetC suggest that NFU3 does not serve as a carrier protein for classic or Rieske-type 2Fe-2S (**Figure 4B**).

HCF101

HCF101 is a plastid-localized P-loop NTPase with an N-terminal domain of unknown function 59 (DUF59) and a C-terminal domain of unknown function 971 (DUF971) (**Figure 3**; **Table 1**) (Lezhneva et al., 2004; Stöckel and Oelmuller, 2004; Schwenkert et al., 2010). The P-loop NTPase domain contains a Walker A motif (i.e., P-loop, CKGGVGKS), an A' motif (GARVGIFDADV), and a B motif (DYLVID) (Stöckel and Oelmuller, 2004; Schwenkert et al., 2010). Via site-directed mutagenesis, three Cys residues were found to be required for the assembly and/or stability of Fe-S clusters: C^{128}, C^{347}, and C^{419} (Schwenkert et al., 2010). C^{347} and C^{419} exist in the presence of a second Cys residue: $C^{339}X_7C^{347}$ and $C^{414}X_4C^{419}$. These Cys residues and motifs might be binding sites for Fe-S clusters. Analysis of Fe and S contents in reconstituted HCF101 showed that this protein may bind to one 4Fe-4S cluster per monomer (Schwenkert et al., 2010).

The plastidial localization of HCF101 was confirmed with import assays (Lezhneva et al., 2004). Recombinant HCF101 served as a scaffold protein during *in vitro* reconstitution of 4Fe-4S clusters and a carrier protein during subsequent *in vitro* transfer to apo LEU1 (3-isopropylmalate isomerase 1, EC 4.2.1.33) (Schwenkert et al., 2010). Complete loss-of-function mutations in the *HCF101* gene resulted in a seedling-lethal phenotype (Lezhneva et al., 2004; Stöckel and Oelmuller, 2004). In the *hcf101* mutants, the levels of 4Fe-4S proteins PsaA, PsaB, and PsaC were < 4% of those in the wild type (Lezhneva et al., 2004). In addition, the content of Fd-thioredoxin reductase (FTR, EC 1.8.7.2), another plastidial 4Fe-4S protein, was significantly reduced in the *hcf101* mutants. On the contrary, the amount of Rieske-type 2Fe-2S protein PetC was not reduced in the *hcf101* mutants and the amount of classic 2Fe-2S protein Fd was actually increased. Taken together, these data show that HCF101 is required in the assembly and transfer of 4Fe-4S (**Figure 4A**), but not classic or Rieske-type 2Fe-2S (Lezhneva et al., 2004) (**Figure 4B**). Because the amounts of representative 3Fe-4S proteins were not determined in the *hcf101* mutants, it is not clear whether HCF101 can serve as a carrier protein for 3Fe-4S.

COG0354p

COG0354 is a family of proteins classified in the Clusters of Orthologous Groups database (Waller et al., 2010). COG0354 proteins are found in all domains of life. IBA57 in yeast and YgfZ in *E. coli* are two well-studied COG0354 proteins. Mitochondrion-targeted IBA57 is required for the assembly of Fe-S clusters on mitochondrial aconitase (ACO, EC 4.2.1.3), as well as the activation of radical S-adenosylmethionine enzymes, such as isopentenyl-adenosine A37 tRNA methylthiolase (MiaB, EC 2.8.4.3), biotin synthase (BIO, EC 2.8.1.6), and lipoic acid synthase (LIP, EC 2.8.1.8) (Gelling et al., 2008). These four enzymes contain one 4Fe-4S, two 4Fe-4S, one classic 2Fe-2S plus one 4Fe-4S, and two 4Fe-4S clusters, respectively (Balk and Pilon, 2011). IBA57 physically interacted with mitochondrial Fe-S assembly protein 1 and 2 (ISA1 and ISA2) (Gelling et al., 2008), further demonstrating that COG0354 family proteins are part of the Fe-S assembly machinery. YgfZ, which is targeted to the mitochondria as well, is required for the activities of MiaB and some other Fe-S enzymes (Waller et al., 2010).

Plants have two COG0354 proteins: one is plastid-targeted (COG0354p; **Figure 3**; **Table 1**) and the other is mitochondrion-targeted (COG0354m) (Waller et al., 2010, 2012). Their subcellular localization was confirmed with import assays and confocal microscopic analysis of GFP fusion proteins (Waller et al., 2012). Both COG0354p and COG0354m were capable of complementing the growth defects of *E. coli* ΔYgfZ and ΔMiaB mutants (Waller et al., 2010, 2012). Similar to IBA57 and YgfZ, the activity of COG0354p and COG0354m is folate-dependent (Waller et al., 2012). Inactivation of COG0354m resulted in embryo lethality, indicating that COG0354m is an essential protein (Waller et al., 2012). The phenotype of loss-of-function mutants of COG0354p has not yet been described (**Table 1**). Therefore, it is not clear which Fe-S clusters are carried by COG0354p and COG0354m. However, because inactivation of IBA57 affects 4Fe-4S and classic 2Fe-2S enzymes (Gelling et al., 2008), it is possible that COG0354p and COG0354m are involved in the assembly and transfer of 4Fe-4S and/or classic 2Fe-2S clusters (**Figure 4A**).

GRXS14 and GRXS16

Higher plants have two plastidial GRXs: GRXS14 and GRXS16 (**Figure 3**; **Table 1**) (Bandyopadhyay et al., 2008). They were previously thought as activators of vacuolar H^+/Ca^{2+} antiporters (Cheng and Hirschi, 2003). However, *in silico* analysis showed that full-length GRXS14 and GRXS16 contain a plastid transit peptide and a GRX domain with a CGFS active site motif (Cheng et al., 2006; Bandyopadhyay et al., 2008). The plastidial localization of GRXS14 and GRXS16 was confirmed by confocal microscopic analysis of GFP fusion proteins. After careful examination of the subcellular localization and physiological function, Cheng et al. (2006) reported that GRXS14 and GRXS16 do not act as activators of vacuolar H^+/Ca^{2+} antiporters.

Both GRXS14 and GRXS16 were able to complement the growth defects of yeast *grx5* mutant, suggesting that these two proteins are functional GRXs (Bandyopadhyay et al., 2008). Analytical, absorption, and circular dichroism spectral data showed that GRXS14 and GRXS16 bind to one 2Fe-2S cluster per homodimer via the CGFS active site (**Table 2**) and the binding is assisted by the Cys residues of two glutathione molecules (Bandyopadhyay et al., 2008). In addition, apo GRXS14 served as the scaffold protein during Cys desulfurase-mediated *in vitro* 2Fe-2S cluster assembly and the 2Fe-2S cluster in GRXS14 could be readily transferred to apo Fd (**Figure 4A**) (Bandyopadhyay et al., 2008). Furthermore, a unidirectional and intact transfer of 2Fe-2S clusters from GRXS14 to SufA1 was observed, suggesting that GRXS14 may work upstream of SufA1 during *in vivo* delivery of 2Fe-2S to recipient proteins (**Figure 4C**) (Mapolelo et al., 2013). It should be noticed that introducing GRXS14 and GRXS16 into yeast *grx5* mutant also restores the activity of mitochondrial ACO (Bandyopadhyay et al., 2008). Because mitochondrial ACO requires a 4Fe-4S cluster to function, it is possible that GRXS14 and GRXS16 act as 4Fe-4S carriers as well (**Figure 4A**) (Rouhier et al., 2010).

In Arabidopsis, GRXS14 and GRXS16 have a similar expression profile: both are expressed in green photosynthetic tissues and flowers (Rey et al., 2017). Consistent with the expression profile, GRXS14 knockout lines and GRXS16 knockdown lines did not exhibit any phenotypic defects under standard growth conditions (Rey et al., 2017). However, the combination of GRXS14 knockout and GRXS16 knockdown resulted in retarded growth, suggesting that GRXS14 and GRXS16 have an overlapping role in the plastid.

Environmental constraints, such as oxidative stress, prolonged darkness, high irradiance, and high salt, change cellular redox status (Rey et al., 2017). Under oxidative stress, GRXS14 knockout lines displayed growth defects in early seedlings (Cheng et al., 2006). Prolonged darkness causes GRXS14 oxidation and reduced contents of proteins involved in maturation of Fe-S proteins (Rey et al., 2017). Under prolonged darkness, GRXS14 knockout lines exhibited accelerated chlorophyll loss. These data suggest that GRXS14 is important in protecting proteins again oxidative stress during early seedling growth and maintaining the chlorophyll level under prolonged darkness. Interestingly, GRXS14 overexpression lines demonstrated a reduce chlorophyll content under standard, high irradiance, and high salt conditions (Rey et al., 2017). Therefore, Rey et al. (2017) proposed that GRXS14 may regulate the redox status of chlorophyll biosynthetic enzymes and/or participate in the assembly and transfer of 2Fe-2S in the plastid, especially under stress conditions. A number of enzymes involved in chlorophyll metabolism contain Fe-S clusters as cofactors: chlorophyllide *a* oxygenase (CAO, EC 1.14.13.122), 7-hydroxymethyl chlorophyll *a* reductase (HCAR, EC 1.17.7.2), and pheophorbide *a* oxygenase (PAO, EC 1.14.15.17) (Oster et al., 2000; Pruzinská et al., 2003; Meguro et al., 2011). Plastidial GRXs may control the redox status of chlorophyll biosynthetic enzymes by regulating the assembly and transfer pathway of Fe-S clusters in the plastids. Consistent with this hypothesis, GRXs, including GRXS14 and GRXS16, could interact with the BolA domain of SufE1 (**Table 2**) and thereby deglutathionate SufE1, which facilities the activation of plastidial Cys desulfurase (Couturier et al., 2014).

GRXS16 has an N-terminal GlyIleTyr-TyrIleGly (GIY-YIG) endonuclease domain (**Figure 3**), which confers GRXS16 unique functions, such as coordinating redox regulation and DNA cleavage (Liu et al., 2013). The GIY-YIG domain of GRXS16 alone has endonuclease activity and the activity is decreased substantially in GRXS16 (Liu et al., 2013). On the other hand, the presence of the GIY-YIG domain reduces the ability of GRXS16 to suppress the susceptibility of yeast *grx5* mutant to oxidative stress. These data suggest that the two functional domains in GRXS16 negatively regulate each other. Furthermore, Liu et al. (2013) found that Cys^{123} in the GIY-YIG domain may form an intramolecular disulfide bond with Cys^{219} in the CGFS motif of the GRX domain, which explains the negative regulation between the two functional domains.

At-NEET

As mentioned previously, At-NEET has a CDGSH motif (**Figure 3**; **Table 1**), which contains the three Cys and one His residues necessary for NEET-type 2Fe-2S coordination (Nechushtai et al., 2012; Su et al., 2013). The first two Cys residues (C^{74} and C^{76}) have been shown to be essential for cluster coordination (Su et al., 2013), while the His residue (H^{89}) has been shown to be essential for the transferability of the 2Fe-2S cluster (Nechushtai et al., 2012). At-NEET forms homodimers (**Table 2**) and each homodimer coordinates two labile 2Fe-2S clusters, which are readily transferred to apo Fd in *in vivo* assays (Nechushtai et al., 2012). Knockdown and RNAi lines of At-NEET showed delayed growth and development, accelerated senescence, and elevated ROS accumulation under standard conditions, increased sensitivity to low Fe conditions, and reduced sensitivity to high Fe conditions (Nechushtai et al., 2012). These data suggest that At-NEET is important in Fe metabolism, ROS homeostasis, as well as plant growth, development, and senescence. Therefore, At-NEET might be a carrier protein for the assembly and transfer of NEET-type 2Fe-2S clusters (Nechushtai et al., 2012).

REGULATION OF THE PLASTIDIAL Fe-S ASSEMBLY AND TRANSFER PATHWAY

Due to the toxicity of free Fe, the biosynthesis of Fe-S clusters has to be regulated together with Fe uptake (Balk and Schaedler, 2014). Hierarchical clustering analysis of Arabidopsis genes involved in Fe-S assembly and transfer pathways with publicly available microarray data showed that genes for the plastidial SUF pathway form one cluster and genes for the mitochondrial ISC pathway and the cytosolic CIA pathway form another (Balk and Schaedler, 2014). For example, the *SufA1*, *SufB*, *SufC*, *SufD*, and *SufE1* genes cluster together, possibly due to their high expression in photosynthetic tissues (Balk and Schaedler, 2014). These observations suggest that the expression of *SUF* genes is coordinated and that the plastidial SUF pathway and the ISC/CIA pathways might be differentially regulated. The latter is consistent with the relative independency of the SUF pathway from the ISC/CIA pathways (Van Hoewyk et al., 2007; Bernard et al., 2013).

Balk and Schaedler (2014) also found that under pathogen infection (*Pseudomonas syringae*) or oxygen deficiency, the expression of *ISC* and *SUF* genes is down-regulated (Balk and Schaedler, 2014). Following recognition of the pathogen, the host plant immediately up-regulates ROS production, as part of the defense responses (Torres et al., 2006; Torres, 2010). The rapid rise in ROS tends to destroy Fe-S clusters (Balk and Schaedler, 2014). Therefore, down-regulation of Fe-S cluster assembly at the transcriptional level could be viewed as a preventive method to minimize the content of toxic free Fe released from Fe-S clusters (Balk and Schaedler, 2014).

Several studies showed that *SufB* gene expression in Arabidopsis is down-regulated under Fe-deficient conditions (Xu et al., 2005; Balk and Schaedler, 2014). This trend was also observed in rice (Liang et al., 2014). Because SufB is an essential Fe-S scaffold protein (Nagane et al., 2010), a decrease in *SufB*

gene expression may quickly decrease the overall rate of Fe-S synthesis in the plastid (Balk and Schaedler, 2014). Further studies are needed to understand the molecular mechanism for Fe deficiency-induced down-regulation of *SufB* gene expression.

Among Fe-S assembly-related genes, *SufE2* was very responsive to a wide range of environmental stimuli (Balk and Schaedler, 2014). As mentioned above, SufE2 only has a single SufE domain, unlike SufE1 and SufE3, which have an additional BolA and NadA domain, respectively (Murthy et al., 2007). Therefore, Balk and Schaedler (2014) proposed that SufE2 may regulate the flux of persulfide (R-S-S^0H) groups between BolA, the C-terminal domain of SufE1, and NadA, the C-terminal domain of SufE3.

As mentioned above, the two plastid-targeted GRX proteins, GRXS14 and GRXS16, have two Fe-S assembly-related roles. On one hand, GRXS14 and GRXS16 serve as Fe-S carriers in the plastidial Fe-S assembly and transfer pathway (Bandyopadhyay et al., 2008). On the other hand, GRXS14 and GRXS16 are important regulators of redox homeostasis inside the plastid (Rey et al., 2017). GRXS14 and GRXS16 were found to interact with the BolA domain of SufE1 (Couturier et al., 2014). These observations indicate that SufE1 activity and overall Fe-S cluster assembly in the plastid may be subject to redox regulation by GRXS14 and GRXS16 (Couturier et al., 2014). In addition, the interactions between the SufE1 BolA domain and the two plastidial GRX proteins suggest potential link or regulation between the upstream persulfide (R-S-S^0H) flux at the SufSE complex and the downstream Fe-S transfer steps via Fe-S carrier proteins.

Another protein with a potential regulatory role is At-NEET, a NEET-type 2Fe-2S-containing protein dually targeted to plastids and mitochondria (Nechushtai et al., 2012; Su et al., 2013). As mentioned in a previous paragraph, knockdown and RNAi of At-NEET expression resulted in delayed growth and developmental retardation, enhanced senescence, and increased ROS under standard conditions (Nechushtai et al., 2012). The same mutants also displayed elevated sensitivity to low Fe and decreased sensitivity to high Fe (Nechushtai et al., 2012). Therefore, Nechushtai et al. (2012) concluded that At-NEET is important in Fe metabolism and ROS homeostasis. Additional studies are needed to investigate whether and how At-NEET plays a role in regulating Fe-S assembly.

CONCLUDING REMARKS AND OUTSTANDING QUESTIONS

Fe-S clusters and proteins are essential to many biological processes. They are found in the plastids, mitochondria, cytosol, and nucleus of plant cells. Plastidial Fe-S clusters are assembled by the SUF pathway, which consists of Cys desulfurase NFS2, sulfur transferases SufE1, SufE2, and SufE3, $SufBC_2D$ scaffold complex, and carrier proteins. Cys is the S source for *in vivo* assembly of Fe-S clusters. However, it is not yet known what the *in vivo* Fe source is and how Fe is delivered to the scaffold complex. The NFS2-SufE1/2/3-$SufBC_2D$ system is responsible for *de novo* assembly of all plastidial Fe-S clusters, because no other Fe-S cluster assembly pathway has been found in the plastid. Single loss-of-function mutations of the NFS2-SufE1/2/3-$SufBC_2D$ system often result in an embryo- or seedling-lethal phenotype, suggesting that the NFS2-SufE1/2/3-$SufBC_2D$ system is essential. After assembly, Fe-S clusters need to be delivered to appropriate recipient proteins via carrier proteins. A total of nine potential plastidial Fe-S carriers have been identified thus far: SufA1, NFU1, NFU2, NFU3, HCF101, COG0354p, GRXS14, GRXS16, and At-NEET. SufA1, NFU2, GRXS14, and GRXS16 have been shown to act as carrier proteins transferring classic 2Fe-2S from the $SufBC_2D$ scaffold complex to recipient proteins. NFU3 has been shown to act as the carrier protein for 3Fe-4S. NFU2, NFU3, and HCF101 have been shown to act as 4Fe-4S carriers. At-NEET is a possible carrier protein for NEET-type 2Fe-2S.

Although NFU1 is a functional NFU protein, it is not clear which Fe-S clusters are transferred by this protein. It is possible that NFU1 plays a role in transferring 2Fe-2S, 3Fe-4S, and/or 4Fe-4S clusters because this protein contains a redox-active NFU domain with a conserved CXXC motif capable of coordinating 2Fe-2S, 3Fe-4S, and 4Fe-4S clusters. Functional analysis of recombinant NFU1 protein as well as immunodetection and activity assays of representative plastidial Fe-S proteins in loss-of-function *nfu1* mutants will help address these questions. The types of Fe-S clusters COG0354p transfers are also elusive. It is possible that COG0354p plays a role in transferring 4Fe-4S and classic 2Fe-2S clusters, because inactivation of COG0354 family protein IBA57 reduces the activities of 4Fe-4S and classic 2Fe-2S-containing enzymes.

AT-NEET is listed as a carrier protein for NEET-type 2Fe-2S. The recombinant AT-NEET homodimer contains two labile 2Fe-2S clusters, which can be transferred to apo Fd *in vitro* (Nechushtai et al., 2012). However, whether plant-type Fds act as an *in vivo* recipient protein for NEET-type 2Fe-2S from AT-NEET is still questionable, because plant-type Fds are known as classic 2Fe-2S proteins. Additional experiments are necessary to identify the *in vivo* recipient proteins for NEET-type 2F-2S and to test whether AT-NEET is capable of transferring NEET-type 2Fe-2S to recipient proteins under *in vivo* conditions.

It is not yet known which plastidial carriers are responsible for transferring Rieske-type 2Fe-2S to recipient proteins. NFU1 does not seem to be a good candidate because it does not contain the appropriate binding domain ($\underline{C}X\underline{H}XGCX_{12-44}\underline{C}X\underline{C}\underline{H}$) for Rieske-type 2Fe-2S. Although it is well-established that GRXS14 and GRXS16 transfer classic 2Fe-2S, it is possible that these two GRXs may transfer other Fe-S clusters as well. The expression of plastidial GRXS14 and GRXS16 in yeast *grx5* mutant restores the activity of mitochondrial ACO, whose function requires 4Fe-4S. These results suggest that GRXS14 and GRXS16 may act as carrier proteins for 4Fe-4S as well. Functional analysis of recombinant GRXS14 and GRXS16 as well as immunodetection and activity assays of representative plastidial 4Fe-4S proteins in loss-of-function *grxs14* and *grxs16* mutants will help test this hypothesis.

3Fe-4S and 4Fe-4S have similar absorption spectra, with a broad peak around 410 nm (Kennedy et al., 1984; Nakamaru-Ogiso et al., 2002). Therefore, it is challenging

to distinguish the specific types of Fe-S clusters transferred by a Fe-S carrier protein simply via absorption spectral characterization of as-purified and reconstituted Fe-S carrier proteins. Immunodetection and activity assays of representative plastidial proteins for each type of Fe-S clusters in loss-of-function mutants will provide complementary information.

Furthermore, the unidirectional and intact transfer of Fe-S clusters from one carrier to another raises the possibly that some Fe-S carriers may work together in a sequence when delivering Fe-S clusters to the appropriate recipient proteins.

Lastly, although several possible regulation routes have been proposed for the SUF pathway, it is a relatively understudied area. Further investigations are needed to gain a more holistic understanding of the regulatory network of Fe-S assembly and transfer pathways in plants.

AUTHOR CONTRIBUTIONS

The author confirms being the sole contributor of this work and approved it for publication.

ACKNOWLEDGMENTS

This work was supported by US National Science Foundation Grant MCB-1244008.

REFERENCES

Abdel-Ghany, S. E., Ye, H., Garifullina, G. F., Zhang, L., Pilon-Smits, E. A., and Pilon, M. (2005). Iron-sulfur cluster biogenesis in chloroplasts. Involvement of the scaffold protein CpIscA. *Plant Physiol.* 138, 161–172. doi: 10.1104/pp.104.058602

Ahn, C. S., Lee, J. H., and Pai, H. S. (2005). Silencing of NbNAP1 encoding a plastidic SufB-like protein affects chloroplast development in *Nicotiana benthamiana*. *Mol. Cells* 20, 112–118.

Aldea, M., Hernandez-Chico, C., de la Campa, A. G., Kushner, S. R., and Vicente, M. (1988). Identification, cloning, and expression of *bolA*, an *ftsZ*-dependent morphogene of *Escherichia coli*. *J. Bacteriol.* 170, 5169–5176. doi: 10.1128/jb.170.11.5169-5176.1988

Ayala-Castro, C., Saini, A., and Outten, F. W. (2008). Fe-S cluster assembly pathways in bacteria. *Microbiol. Mol. Biol. Rev.* 72, 110–125. doi: 10.1128/MMBR.00034-07

Balk, J., and Pilon, M. (2011). Ancient and essential: the assembly of iron-sulfur clusters in plants. *Trends Plant Sci.* 16, 218–226. doi: 10.1016/j.tplants.2010.12.006

Balk, J., and Schaedler, T. A. (2014). Iron cofactor assembly in plants. *Annu. Rev. Plant Biol.* 65, 125–153. doi: 10.1146/annurev-arplant-050213-035759

Bandyopadhyay, S., Gama, F., Molina-Navarro, M. M., Gualberto, J. M., Claxton, R., Naik, S. G., et al. (2008). Chloroplast monothiol glutaredoxins as scaffold proteins for the assembly and delivery of [2Fe−2S] clusters. *EMBO J.* 27, 1122–1133. doi: 10.1038/emboj.2008.50

Beinert, H. (2000). Iron-sulfur proteins: ancient structures, still full of surprises. *J. Biol. Inorg. Chem.* 5, 2–15. doi: 10.1007/s007750050002

Bernard, D. G., Cheng, Y., Zhao, Y., and Balk, J. (2009). An allelic mutant series of ATM3 reveals its key role in the biogenesis of cytosolic iron-sulfur proteins in Arabidopsis. *Plant Physiol.* 151, 590–602. doi: 10.1104/pp.109.143651

Bernard, D. G., Netz, D. J., Lagny, T. J., Pierik, A. J., and Balk, J. (2013). Requirements of the cytosolic iron–sulfur cluster assembly pathway in Arabidopsis. *Phil. Trans. R. Soc. B* 368:20120259. doi: 10.1098/rstb.2012.0259

Briat, J.-F., and Lobréaux, S. (1997). Iron transport and storage in plants. *Trends Plant Sci.* 2, 187–193. doi: 10.1016/S1360-1385(97)85225-9

Cheng, N. H., and Hirschi, K. D. (2003). Cloning and characterization of CXIP1, a novel PICOT domain-containing Arabidopsis protein that associates with CAX1. *J. Biol. Chem.* 278, 6503–6509. doi: 10.1074/jbc.M210883200

Cheng, N.-H., Liu, J.-Z., Brock, A., Nelson, R. S., and Hirschi, K. D. (2006). AtGRXcp, an Arabidopsis chloroplastic glutaredoxin, is critical for protection against protein oxidative damage. *J. Biol. Chem.* 281, 26280–26288. doi: 10.1074/jbc.M601354200

Coschigano, K. T., Melo-Oliveira, R., Lim, J., and Coruzzi, G. M. (1998). Arabidopsis gls mutants and distinct Fd-GOGAT genes. Implications for photorespiration and primary nitrogen assimilation. *Plant Cell* 10, 741–752. doi: 10.2307/3870661

Couturier, J., Touraine, B., Briat, J. F., Gaymard, F., and Rouhier, N. (2013). The iron-sulfur cluster assembly machineries in plants: current knowledge and open questions. *Front. Plant Sci.* 4:259. doi: 10.3389/fpls.2013.00259

Couturier, J., Wu, H. C., Dhalleine, T., Pegeot, H., Sudre, D., Gualberto, J. M., et al. (2014). Monothiol glutaredoxin-BolA interactions: redox control of *Arabidopsis thaliana* BolA2 and SufE1. *Mol. Plant* 7, 187–205. doi: 10.1093/mp/sst156

Crack, J. C., Jervis, A. J., Gaskell, A. A., White, G. F., Green, J., Thomson, A. J., et al. (2008). Signal perception by FNR: the role of the iron-sulfur cluster. *Biochem. Soc. Trans.* 36, 1144–1148. doi: 10.1042/BST0361144

Crane, B. R., and Getzoff, E. D. (1996). The relationship between structure and function for the sulfite reductases. *Curr. Opin. Struc. Biol.* 6, 744–756. doi: 10.1016/S0959-440X(96)80003-0

Crane, B. R., Siegel, L. M., and Getzoff, E. D. (1995). Sulfite reductase structure at 1.6 Å: evolution and catalysis for reduction of inorganic anions. *Science* 270, 59–67. doi: 10.1126/science.270.5233.59

Cupp-Vickery, J. R., Urbina, H., and Vickery, L. E. (2003). Crystal structure of IscS, a cysteine desulfurase from *Escherichia coli*. *J. Mol. Biol.* 330, 1049–1059. doi: 10.1016/S0022-2836(03)00690-9

Dai, Y., and Outten, F. W. (2012). The *E. coli* SufS-SufE sulfur transfer system is more resistant to oxidative stress than IscS-IscU. *FEBS Lett.* 586, 4016–4022. doi: 10.1016/j.febslet.2012.10.001

Dos Santos, P. C., Smith, A. D., Frazzon, J., Cash, V. L., Johnson, M. K., and Dean, D. R. (2004). Iron-sulfur cluster assembly: NifU-directed activation of the nitrogenase Fe protein. *J. Biol. Chem.* 279, 19705–19711. doi: 10.1074/jbc.M400278200

Foster, J. W., and Moat, A. G. (1980). Nicotinamide adenine dinucleotide biosynthesis and pyridine nucleotide cycle metabolism in microbial systems. *Microbiol. Rev.* 44, 83–105.

Frazzon, A. P., Ramirez, M. V., Warek, U., Balk, J., Frazzon, J., Dean, D. R., et al. (2007). Functional analysis of Arabidopsis genes involved in mitochondrial iron-sulfur cluster assembly. *Plant Mol. Biol.* 64, 225–240. doi: 10.1007/s11103-007-9147-x

Frazzon, J., and Dean, D. R. (2003). Formation of iron–sulfur clusters in bacteria: an emerging field in bioinorganic chemistry. *Curr. Opin. Chem. Biol.* 7, 166–173. doi: 10.1016/S1367-5931(03)00021-8

Gao, H., Subramanian, S., Couturier, J., Naik, S. G., Kim, S. K., Leustek, T., et al. (2013). *Arabidopsis thaliana* Nfu2 accommodates [2Fe-2S] or [4Fe-4S] clusters and is competent for *in vitro* maturation of chloroplast [2Fe-2S] and [4Fe-4S] cluster-containing proteins. *Biochemistry* 52, 6633–6645. doi: 10.1021/bi4007622

Gelling, C., Dawes, I. W., Richhardt, N., Lill, R., and Muhlenhoff, U. (2008). Mitochondrial Iba57p is required for Fe/S cluster formation on aconitase and activation of radical SAM enzymes. *Mol. Cell. Biol.* 28, 1851–1861. doi: 10.1128/MCB.01963-07

Hanke, G., and Mulo, P. (2013). Plant type ferredoxins and ferredoxin-dependent metabolism. *Plant Cell Environ.* 36, 1071–1084. doi: 10.1111/pce.12046

Hase, T., Schürmann, P., and Knaff, D. B. (2006). "The interaction of ferredoxin with ferredoxin-dependent enzymes," in *Photosystem I: The Light-Driven Plastocyanin:Ferredoxin Oxidoreductase*, ed J. H. Golbeck (Dordrecht: Springer Netherlands), 477–498.

Heidenreich, T., Wollers, S., Mendel, R. R., and Bittner, F. (2005). Characterization of the NifS-like domain of ABA3 from *Arabidopsis thaliana* provides Insight into the mechanism of molybdenum cofactor sulfuration. *J. Biol. Chem.* 280, 4213–4218. doi: 10.1074/jbc.M411195200

Hjorth, E., Hadfi, K., Zauner, S., and Maier, U. G. (2005). Unique genetic compartmentalization of the SUF system in cryptophytes and characterization of a SufD mutant in *Arabidopsis thaliana*. *FEBS Lett.* 579, 1129–1135. doi: 10.1016/j.febslet.2004.12.084

Holm, R. H., and Lo, W. (2016). Structural conversions of synthetic and protein-bound iron–sulfur clusters. *Chem. Rev.* 116, 13685–13713. doi: 10.1021/acs.chemrev.6b00276

Hu, X., Kato, Y., Sumida, A., Tanaka, A., and Tanaka, R. (2017a). The $SUFBC_2D$ complex is required for the biogenesis of all major classes of plastid Fe-S proteins. *Plant J.* 90, 235–248. doi: 10.1111/tpj.13483

Hu, X., Page, M. T., Sumida, A., Tanaka, A., Terry, M. J., and Tanaka, R. (2017b). The iron–sulfur cluster biosynthesis protein SUFB is required for chlorophyll synthesis, but not phytochrome signaling. *Plant J.* 89, 1184–1194. doi: 10.1111/tpj.13455

Jacobson, M. R., Cash, V. L., Weiss, M. C., Laird, N. F., Newton, W. E., and Dean, D. R. (1989). Biochemical and genetic analysis of the nifUSVWZM cluster from *Azotobacter vinelandii*. *Mol. Gen. Genet.* 219, 49–57. doi: 10.1007/BF00261156

Johnson, D. C., Dean, D. R., Smith, A. D., and Johnson, M. K. (2005). Structure, function, and formation of biological iron-sulfur clusters. *Annu. Rev. Biochem.* 74, 247–281. doi: 10.1146/annurev.biochem.74.082803.133518

Kaiser, J. T., Clausen, T., Bourenkow, G. P., Bartunik, H.-D., Steinbacher, S., and Huber, R. (2000). Crystal structure of a NifS-like protein from *Thermotoga maritima*: implications for iron sulphur cluster assembly. *J. Mol. Biol.* 297, 451–464. doi: 10.1006/jmbi.2000.3581

Katoh, A., Uenohara, K., Akita, M., and Hashimoto, T. (2006). Early steps in the biosynthesis of NAD in Arabidopsis start with aspartate and occur in the plastid. *Plant Physiol.* 141, 851–857. doi: 10.1104/pp.106.081091

Kennedy, M. C., Kent, T. A., Emptage, M., Merkle, H., Beinert, H., and Munck, E. (1984). Evidence for the formation of a linear [3Fe-4S] cluster in partially unfolded aconitase. *J. Biol. Chem.* 259, 14463–14471.

Kim, D.-Y., Bovet, L., Kushnir, S., Noh, E. W., Martinoia, E., and Lee, Y. (2006). AtATM3 is involved in heavy metal resistance in Arabidopsis. *Plant Physiol.* 140, 922–932. doi: 10.1104/pp.105.074146

Kim, S., and Park, S. (2013). Structural changes during cysteine desulfurase CsdA and sulfur acceptor CsdE interactions provide insight into the trans-persulfuration. *J. Biol. Chem.* 288, 27172–27180. doi: 10.1074/jbc.M113.480277

Kounosu, A., Li, Z., Cosper, N. J., Shokes, J. E., Scott, R. A., Imai, T., et al. (2004). Engineering a three-cysteine, one-histidine ligand environment into a new hyperthermophilic archaeal Rieske-type [2Fe-2S] ferredoxin from *Sulfolobus solfataricus*. *J. Biol. Chem.* 279, 12519–12528. doi: 10.1074/jbc.M305923200

Kushnir, S., Babiychuk, E., Storozhenko, S., Davey, M. W., Papenbrock, J., De Rycke, R., et al. (2001). A mutation of the mitochondrial ABC transporter Sta1 leads to dwarfism and chlorosis in the Arabidopsis mutant starik. *Plant Cell* 13, 89–100. doi: 10.1105/tpc.13.1.89

Léon, S., Touraine, B., Briat, J. F., and Lobreaux, S. (2002). The AtNFS2 gene from *Arabidopsis thaliana* encodes a NifS-like plastidial cysteine desulphurase. *Biochem. J.* 366, 557–564. doi: 10.1042/bj20020322

Léon, S., Touraine, B., Ribot, C., Briat, J. F., and Lobréaux, S. (2003). Iron-sulphur cluster assembly in plants: distinct NFU proteins in mitochondria and plastids from *Arabidopsis thaliana*. *Biochem. J.* 371, 823–830. doi: 10.1042/bj20021946

Lezhneva, L., Amann, K., and Meurer, J. (2004). The universally conserved HCF101 protein is involved in assembly of [4Fe-4S]-cluster-containing complexes in *Arabidopsis thaliana* chloroplasts. *Plant J.* 37, 174–185. doi: 10.1046/j.1365-313X.2003.01952.x

Liang, X., Qin, L., Liu, P., Wang, M., and Ye, H. (2014). Genes for iron-sulphur cluster assembly are targets of abiotic stress in rice, *Oryza sativa*. *Plant Cell Environ.* 37, 780–794. doi: 10.1111/pce.12198

Lima, C. D. (2002). Analysis of the *E. coli* NifS CsdB protein at 2.0 A reveals the structural basis for perselenide and persulfide intermediate formation. *J. Mol. Biol.* 315, 1199–1208. doi: 10.1006/jmbi.2001.5308

Link, T. A. (1999). The structures of Rieske and Rieske-type proteins. *Adv. Inorg. Chem.* 47, 83–157. doi: 10.1016/S0898-8838(08)60077-X

Liu, X., Liu, S., Feng, Y., Liu, J. Z., Chen, Y., Pham, K., et al. (2013). Structural insights into the N-terminal GIY-YIG endonuclease activity of Arabidopsis glutaredoxin AtGRXS16 in chloroplasts. *Proc. Natl. Acad. Sci. U.S.A.* 110, 9565–9570. doi: 10.1073/pnas.1306899110

Lobreaux, S., and Briat, J. F. (1991). Ferritin accumulation and degradation in different organs of pea (*Pisum sativum*) during development. *Biochem. J.* 274, 601–606. doi: 10.1042/bj2740601

Madueño, F., Napier, J. A., Cejudo, F. J., and Gray, J. C. (1992). Import and processing of the precursor of the Rieske FeS protein of tobacco chloroplasts. *Plant Mol. Biol.* 20, 289–299. doi: 10.1007/BF00014496

Mapolelo, D. T., Zhang, B., Randeniya, S., Albetel, A. N., Li, H., Couturier, J., et al. (2013). Monothiol glutaredoxins and A-type proteins: partners in Fe-S cluster trafficking. *Dalton Trans.* 42, 3107–3115. doi: 10.1039/c2dt32263c

Markley, J. L., Kim, J. H., Dai, Z., Bothe, J. R., Cai, K., Frederick, R. O., et al. (2013). Metamorphic protein IscU alternates conformations in the course of its role as the scaffold protein for iron–sulfur cluster biosynthesis and delivery. *FEBS Lett.* 587, 1172–1179. doi: 10.1016/j.febslet.2013.01.003

Mason, J. R., and Cammack, R. (1992). The electron-transport proteins of hydroxylating bacterial dioxygenases. *Annu. Rev. Microbiol.* 46, 277–305. doi: 10.1146/annurev.mi.46.100192.001425

Meguro, M., Ito, H., Takabayashi, A., Tanaka, R., and Tanaka, A. (2011). Identification of the 7-hydroxymethyl chlorophyll a reductase of the chlorophyll cycle in Arabidopsis. *Plant Cell* 23, 3442–3453. doi: 10.1105/tpc.111.089714

Mihara, H., and Esaki, N. (2002). Bacterial cysteine desulfurases: their function and mechanisms. *Appl. Microbiol. Biotechnol.* 60, 12–23. doi: 10.1007/s00253-002-1107-4

Mihara, H., Fujii, T., Kato, S., Kurihara, T., Hata, Y., and Esaki, N. (2002). Structure of external aldimine of *Escherichia coli* CsdB, an IscS/NifS homolog: implications for its specificity toward selenocysteine. *J. Biochem.* 131, 679–685. doi: 10.1093/oxfordjournals.jbchem.a003151

Mihara, H., Kurihara, T., Yoshimura, T., Soda, K., and Esaki, N. (1997). Cysteine sulfinate desulfinase, a NIFS-like protein of Escherichia coli with selenocysteine lyase and cysteine desulfurase activities. Gene cloning, purification, and characterization of a novel pyridoxal enzyme. *J. Biol. Chem.* 272, 22417–22424. doi: 10.1074/jbc.272.36.22417

Møller, S. G., Kunkel, T., and Chua, N. H. (2001). A plastidic ABC protein involved in intercompartmental communication of light signaling. *Genes Dev.* 15, 90–103. doi: 10.1101/gad.850101

Murthy, N. U. M., Ollagnier-de-Choudens, S., Sanakis, Y., Abdel-Ghany, S. E., Rousset, C., Ye, H., et al. (2007). Characterization of *Arabidopsis thaliana* SufE2 and SufE3: functions in chloroplast iron-sulfur cluster assembly and NAD synthesis. *J. Biol. Chem.* 282, 18254–18264. doi: 10.1074/jbc.M701428200

Nagane, T., Tanaka, A., and Tanaka, R. (2010). Involvement of AtNAP1 in the regulation of chlorophyll degradation in *Arabidopsis thaliana*. *Planta* 231, 939–949. doi: 10.1007/s00425-010-1099-8

Nakamaru-Ogiso, E., Yano, T., Ohnishi, T., and Yagi, T. (2002). Characterization of the iron-sulfur cluster coordinated by a cysteine cluster motif (CXXCXXXCX27C) in the Nqo3 subunit in the proton-translocating NADH-quinone oxidoreductase (NDH-1) of *Thermus thermophilus* HB-8. *J. Biol. Chem.* 277, 1680–1688. doi: 10.1074/jbc.M108796200

Nath, K., O'Donnell, J. P., and Lu, Y. (2017). Chloroplastic iron-sulfur scaffold protein NFU3 is essential to overall plant fitness. *Plant Signal. Behav.* 12:e1282023. doi: 10.1080/15592324.2017.1282023

Nath, K., Wessendorf, R. L., and Lu, Y. (2016). A nitrogen-fixing subunit essential for accumulating 4Fe-4S-containing Photosystem I core proteins. *Plant Physiol.* 172, 2459–2470. doi: 10.1104/pp.16.01564

Nechushtai, R., Conlan, A. R., Harir, Y., Song, L., Yogev, O., Eisenberg-Domovich, Y., et al. (2012). Characterization of Arabidopsis NEET reveals an ancient role for NEET proteins in iron metabolism. *Plant Cell* 24, 2139–2154. doi: 10.1105/tpc.112.097634

Oster, U., Tanaka, R., Tanaka, A., and Rudiger, W. (2000). Cloning and functional expression of the gene encoding the key enzyme for chlorophyll b biosynthesis (CAO) from *Arabidopsis thaliana*. *Plant J.* 21, 305–310. doi: 10.1046/j.1365-313x.2000.00672.x

Outten, F. W., Djaman, O., and Storz, G. (2004). A suf operon requirement for Fe-S cluster assembly during iron starvation in *Escherichia coli*. *Mol. Microbiol.* 52, 861–872. doi: 10.1111/j.1365-2958.2004.04025.x

Outten, F. W., Wood, M. J., Muñoz, F. M., and Storz, G. (2003). The SufE protein and the SufBCD complex enhance SufS cysteine desulfurase activity as part of

a sulfur transfer pathway for Fe-S cluster assembly in *Escherichia coli*. *J. Biol. Chem.* 278, 45713–45719. doi: 10.1074/jbc.M308004200

Pilon-Smits, E. A., Garifullina, G. F., Abdel-Ghany, S., Kato, S., Mihara, H., Hale, K. L., et al. (2002). Characterization of a NifS-like chloroplast protein from Arabidopsis. Implications for its role in sulfur and selenium metabolism. *Plant Physiol.* 130, 1309–1318. doi: 10.1104/pp.102.010280

Pruzinská, A., Tanner, G., Anders, I., Roca, M., and Hortensteiner, S. (2003). Chlorophyll breakdown: pheophorbide *a* oxygenase is a Rieske-type iron-sulfur protein, encoded by the accelerated cell death 1 gene. *Proc. Natl. Acad. Sci. U.S.A.* 100, 15259–15264. doi: 10.1073/pnas.2036571100

Raux-Deery, E., Leech, H. K., Nakrieko, K. A., McLean, K. J., Munro, A. W., Heathcote, P., et al. (2005). Identification and characterization of the terminal enzyme of siroheme biosynthesis from *Arabidopsis thaliana*: a plastid-located sirohydrochlorin ferrochelatase containing a 2Fe-2S center. *J. Biol. Chem.* 280, 4713–4721. doi: 10.1074/jbc.M411360200

Ravet, K., Touraine, B., Boucherez, J., Briat, J. F., Gaymard, F., and Cellier, F. (2009). Ferritins control interaction between iron homeostasis and oxidative stress in Arabidopsis. *Plant J.* 57, 400–412. doi: 10.1111/j.1365-313X.2008.03698.x

Rey, P., Becuwe, N., Tourrette, S., and Rouhier, N. (2017). Involvement of Arabidopsis glutaredoxin S14 in the maintenance of chlorophyll content. *Plant Cell Environ.* 40, 2319–2332. doi: 10.1111/pce.13036

Roche, B., Aussel, L., Ezraty, B., Mandin, P., Py, B., and Barras, F. (2013). Iron/sulfur proteins biogenesis in prokaryotes: formation, regulation and diversity. *Biochim. Biophys. Acta* 1827, 455–469. doi: 10.1016/j.bbabio.2012.12.010

Roret, T., Pegeot, H., Couturier, J., Mulliert, G., Rouhier, N., and Didierjean, C. (2014). X-ray structures of Nfs2, the plastidial cysteine desulfurase from *Arabidopsis thaliana*. *Acta Crystallogr. Sect. F Struct. Biol. Cryst. Commun.* 70, 1180–1185. doi: 10.1107/S2053230X14017026

Rouhier, N., Couturier, J., Johnson, M. K., and Jacquot, J.-P. (2010). Glutaredoxins: roles in iron homeostasis. *Trends Biochem. Sci.* 35:43. doi: 10.1016/j.tibs.2009.08.005

Saenger, W., Jordan, P., and Krauss, N. (2002). The assembly of protein subunits and cofactors in Photosystem, I. *Curr. Opin. Struc. Biol.* 12, 244–254. doi: 10.1016/S0959-440X(02)00317-2

Saha, K., Webb, M. E., Rigby, S. E., Leech, H. K., Warren, M. J., and Smith, A. G. (2012). Characterization of the evolutionarily conserved iron-sulfur cluster of sirohydrochlorin ferrochelatase from *Arabidopsis thaliana*. *Biochem. J.* 444, 227–237. doi: 10.1042/BJ20111993

Saini, A., Mapolelo, D. T., Chahal, H. K., Johnson, M. K., and Outten, F. W. (2010). SufD and SufC ATPase activity are required for iron acquisition during *in vivo* Fe-S cluster formation on SufB. *Biochemistry* 49, 9402–9412. doi: 10.1021/bi1011546

Schwenkert, S., Netz, D. J., Frazzon, J., Pierik, A. J., Bill, E., Gross, J., et al. (2010). Chloroplast HCF101 is a scaffold protein for [4Fe-4S] cluster assembly. *Biochem. J.* 425, 207–214. doi: 10.1042/BJ20091290

Singh, H., Dai, Y., Outten, F. W., and Busenlehner, L. S. (2013). *Escherichia coli* SufE sulfur transfer protein modulates the SufS cysteine desulfurase through allosteric conformational dynamics. *J. Biol. Chem.* 288, 36189–36200. doi: 10.1074/jbc.M113.525709

Stöckel, J., and Oelmuller, R. (2004). A novel protein for Photosystem I biogenesis. *J. Biol. Chem.* 279, 10243–10251. doi: 10.1074/jbc.M309246200

Su, L. W., Chang, S. H., Li, M. Y., Huang, H. Y., Jane, W. N., and Yang, J. Y. (2013). Purification and biochemical characterization of Arabidopsis At-NEET, an ancient iron-sulfur protein, reveals a conserved cleavage motif for subcellular localization. *Plant Sci.* 213, 46–54. doi: 10.1016/j.plantsci.2013.09.001

Takahashi, Y., Mitsui, A., Fujita, Y., and Matsubara, H. (1991a). Roles of ATP and NADPH in formation of the Fe-S cluster of spinach ferredoxin. *Plant Physiol.* 95, 104–110. doi: 10.1104/pp.95.1.104

Takahashi, Y., Mitsui, A., Hase, T., and Matsubara, H. (1986). Formation of the iron-sulfur cluster of ferredoxin in isolated chloroplasts. *Proc. Natl. Acad. Sci. U.S.A.* 83, 2434–2437. doi: 10.1073/pnas.83.8.2434

Takahashi, Y., Mitsui, A., and Matsubara, H. (1991b). Formation of the Fe-S cluster of ferredoxin in lysed spinach chloroplasts. *Plant Physiol.* 95, 97–103. doi: 10.1104/pp.95.1.97

Takahashi, Y., and Nakamura, M. (1999). Functional assignment of the ORF2-iscS-iscU-iscA-hscB-hscA-fdx-ORF3 gene cluster involved in the assembly of Fe-S clusters in *Escherichia coli*. *J. Biochem.* 126, 917–926. doi: 10.1093/oxfordjournals.jbchem.a022535

Takahashi, Y., and Tokumoto, U. (2002). A third bacterial system for the assembly of iron-sulfur clusters with homologs in archaea and plastids. *J. Biol. Chem.* 277, 28380–28383. doi: 10.1074/jbc.C200365200

Torres, M. A. (2010). ROS in biotic interactions. *Physiol. Plant.* 138, 414–429. doi: 10.1111/j.1399-3054.2009.01326.x

Torres, M. A., Jones, J. D., and Dangl, J. L. (2006). Reactive oxygen species signaling in response to pathogens. *Plant Physiol.* 141, 373–378. doi: 10.1104/pp.106.079467

Touraine, B., Boutin, J. P., Marion-Poll, A., Briat, J. F., Peltier, G., and Lobreaux, S. (2004). Nfu2: a scaffold protein required for [4Fe-4S] and ferredoxin iron-sulphur cluster assembly in Arabidopsis chloroplasts. *Plant J.* 40, 101–111. doi: 10.1111/j.1365-313X.2004.02189.x

van den Heuvel, R. H., Ferrari, D., Bossi, R. T., Ravasio, S., Curti, B., Vanoni, M. A., et al. (2002). Structural studies on the synchronization of catalytic centers in glutamate synthase. *J. Biol. Chem.* 277, 24579–24583. doi: 10.1074/jbc.M202541200

Van Hoewyk, D., Abdel-Ghany, S. E., Cohu, C. M., Herbert, S. K., Kugrens, P., Pilon, M., et al. (2007). Chloroplast iron-sulfur cluster protein maturation requires the essential cysteine desulfurase CpNifS. *Proc. Natl. Acad. Sci. U.S.A.* 104, 5686–5691. doi: 10.1073/pnas.0700774104

Vigani, G., Maffi, D., and Zocchi, G. (2009). Iron availability affects the function of mitochondria in cucumber roots. *New Phytol.* 182, 127–136. doi: 10.1111/j.1469-8137.2008.02747.x

Waller, J. C., Alvarez, S., Naponelli, V., Lara-Nunez, A., Blaby, I. K., Da Silva, V., et al. (2010). A role for tetrahydrofolates in the metabolism of iron-sulfur clusters in all domains of life. *Proc. Natl. Acad. Sci. U.S.A.* 107, 10412–10417. doi: 10.1073/pnas.0911586107

Waller, J. C., Ellens, K. W., Alvarez, S., Loizeau, K., Ravanel, S., and Hanson, A. D. (2012). Mitochondrial and plastidial COG0354 proteins have folate-dependent functions in iron-sulphur cluster metabolism. *J. Exp. Bot.* 63, 403–411. doi: 10.1093/jxb/err286

Wiley, S. E., Murphy, A. N., Ross, S. A., van der Geer, P., and Dixon, J. E. (2007). MitoNEET is an iron-containing outer mitochondrial membrane protein that regulates oxidative capacity. *Proc. Natl. Acad. Sci. U.S.A.* 104, 5318–5323. doi: 10.1073/pnas.0701078104

Wollers, S., Layer, G., Garcia-Serres, R., Signor, L., Clemancey, M., Latour, J. M., et al. (2010). Iron-sulfur (Fe-S) cluster assembly: the SufBCD complex is a new type of Fe-S scaffold with a flavin redox cofactor. *J. Biol. Chem.* 285, 23331–23341. doi: 10.1074/jbc.M110.127449

Xu, X. M., Adams, S., Chua, N. H., and Møller, S. G. (2005). AtNAP1 represents an atypical SufB protein in Arabidopsis plastids. *J. Biol. Chem.* 280, 6648–6654. doi: 10.1074/jbc.M413082200

Xu, X. M., and Møller, S. G. (2004). AtNAP7 is a plastidic SufC-like ATP-binding cassette/ATPase essential for Arabidopsis embryogenesis. *Proc. Natl. Acad. Sci. U.S.A.* 101, 9143–9148. doi: 10.1073/pnas.0400799101

Xu, X. M., and Møller, S. G. (2006). AtSufE is an essential activator of plastidic and mitochondrial desulfurases in *Arabidopsis*. *EMBO J.* 25, 900–909. doi: 10.1038/sj.emboj.7600968

Yabe, T., Morimoto, K., Kikuchi, S., Nishio, K., Terashima, I., and Nakai, M. (2004). The Arabidopsis chloroplastic NifU-like protein CnfU, which can act as an iron-sulfur cluster scaffold protein, is required for biogenesis of ferredoxin and Photosystem, I. *Plant Cell* 16, 993–1007. doi: 10.1105/tpc.020511

Yabe, T., and Nakai, M. (2006). Arabidopsis AtIscA-I is affected by deficiency of Fe-S cluster biosynthetic scaffold AtCnfU-V. *Biochem. Biophys. Res. Commun.* 340, 1047–1052. doi: 10.1016/j.bbrc.2005.12.104

Yadav, S., Kushwaha, H. R., Kumar, K., and Verma, P. K. (2012). Comparative structural modeling of a monothiol GRX from chickpea: insight in iron-sulfur cluster assembly. *Int. J. Biol. Macromol.* 51, 266–273. doi: 10.1016/j.ijbiomac.2012.05.014

Ye, H., Abdel-Ghany, S. E., Anderson, T. D., Pilon-Smits, E. A., and Pilon, M. (2006). CpSufE activates the cysteine desulfurase CpNifS for chloroplastic Fe-S cluster formation. *J. Biol. Chem.* 281, 8958–8969. doi: 10.1074/jbc.M512737200

Ye, H., Garifullina, G. F., Abdel-Ghany, S. E., Zhang, L., Pilon-Smits, E. A., and Pilon, M. (2005). The chloroplast NifS-like protein of *Arabidopsis thaliana* is required for iron-sulfur cluster formation in ferredoxin. *Planta* 220, 602–608. doi: 10.1007/s00425-004-1388-1

Zhang, B., Crack, J. C., Subramanian, S., Green, J., Thomson, A. J., Le Brun, N. E., et al. (2012). Reversible cycling between cysteine persulfide-ligated [2Fe-2S] and cysteine-ligated [4Fe-4S] clusters in the FNR regulatory protein. *Proc. Natl. Acad. Sci. U.S.A.* 109, 15734–15739. doi: 10.1073/pnas.1208787109

Zheng, L., and Dean, D. R. (1994). Catalytic formation of a nitrogenase iron-sulfur cluster. *J. Biol. Chem.* 269, 18723–18726.

Zheng, L., White, R. H., Cash, V. L., and Dean, D. R. (1994). Mechanism for the desulfurization of L-cysteine catalyzed by the nifS gene product. *Biochemistry* 33, 4714–4720. doi: 10.1021/bi00181a031

Zheng, L., White, R. H., Cash, V. L., Jack, R. F., and Dean, D. R. (1993). Cysteine desulfurase activity indicates a role for NIFS in metallocluster biosynthesis. *Proc. Natl. Acad. Sci. U.S.A.* 90, 2754–2758. doi: 10.1073/pnas.90.7.2754

Conflict of Interest Statement: The author declares that the research was conducted in the absence of any commercial or financial relationships that could be construed as a potential conflict of interest.

frontiers in Plant Science

MINI REVIEW
published: 14 November 2017
doi: 10.3389/fpls.2017.01959

Metabolic Origins and Transport of Vitamin E Biosynthetic Precursors

*Sébastien Pellaud and Laurent Mène-Saffrané**

Department of Biology, University of Fribourg, Fribourg, Switzerland

Tocochromanols are organic compounds mostly produced by photosynthetic organisms that exhibit vitamin E activity in animals. They result from the condensation of homogentisate with four different polyprenyl side chains derived all from geranylgeranyl pyrophosphate. The core tocochromanol biosynthesis has been investigated in several photosynthetic organisms and is now well-characterized. In contrast, our current knowledge of the biosynthesis and transport of tocochromanol biosynthetic precursors is much more limited. While tocochromanol synthesis occurs in plastids, converging genetic data in Arabidopsis and soybean demonstrate that the synthesis of the polar precursor homogentisate is located in the cytoplasm. These data implies that tocochromanol synthesis involves several plastidic membrane transporter(s) that remain to be identified. In addition, the metabolic origin of the lipophilic isoprenoid precursor is not fully elucidated. While some genetic data exclusively attribute the synthesis of the prenyl component of tocochromanols to the plastidic methyl erythritol phosphate pathway, multiple lines of evidence provided by feeding experiments and metabolic engineering studies indicate that it might partially originate from the cytoplasmic mevalonate pathway. Although this question is still open, these data demonstrate the existence of membrane transporter(s) capable of importing cytosolic polyprenyl pyrophosphate such as farnesyl pyrophosphate into plastids. Since the availability of both homogentisate and polyprenyl pyrophosphates are currently accepted as major mechanisms controlling the type and amount of tocochromanols produced in plant tissues, we summarized our current knowledge and research gaps concerning the biosynthesis, metabolic origins and transport of tocochromanol biosynthetic precursors in plant cells.

Keywords: vitamin E, tocochromanols, mevalonate pathway, methyl erythritol phosphate pathway, homogentisate, prenyl pyrophosphate, Arabidopsis, nutrigenomics

OPEN ACCESS

Edited by:
Rebecca L. Roston, University of Nebraska Lincoln, United States

Reviewed by:
Beatrycze Anna Nowicka, Jagiellonian University, Poland
Dan Siehl, Pioneer Hi-Bred, United States

***Correspondence:**
Laurent Mène-Saffrané
laurent.mene-saffrane@unifr.ch

Specialty section:
This article was submitted to Plant Physiology, a section of the journal Frontiers in Plant Science

Received: *13 October 2017*
Accepted: *31 October 2017*
Published: *14 November 2017*

Citation:
Pellaud S and Mène-Saffrané L (2017) Metabolic Origins and Transport of Vitamin E Biosynthetic Precursors. Front. Plant Sci. 8:1959. doi: 10.3389/fpls.2017.01959

INTRODUCTION

Tocochromanols are amphipathic compounds typified by a chromanol ring (**Figure 1**). To date, four types of tocochromanols, namely tocopherols, tocotrienols, plastochromanol-8 (PC-8) and tocomonoenols, have been identified in higher plants. These organic compounds drew the attention because tocopherols and tocotrienols exhibit vitamin E activity that is notably essential for animal reproduction (Evans and Bishop, 1922). Tocochromanols are mostly produced by photosynthetic organisms such as plants, algae and some cyanobacteria, and by the non-photosynthetic parasite causing malaria *Plasmodium falciparum* (Sussmann et al., 2011;

Mène-Saffrané and Pellaud, 2017). Tocochromanol biosynthesis is initiated by the condensation of two biosynthetic precursors, the polar homogentisate (HGA) and a lipophilic polyprenyl pyrophosphate that varies according to the type of tocochromanol. The polyprenyl precursor of tocopherols is phytyl pyrophosphate (PPP), geranylgeranyl pyrophosphate (GGPP) for tocotrienols, solanesyl pyrophosphate (SPP) for PC-8, and tetrahydrogeranylgeranyl pyrophosphate (THGGPP) for tocomonoenols (**Figure 1**; Pellaud et al., 2018). The core tocochromanol biosynthetic pathway has been widely investigated and is now well-characterized (Mène-Saffrané and DellaPenna, 2010; DellaPenna and Mène-Saffrané, 2011; Mène-Saffrané and Pellaud, 2017). In contrast, our knowledge of the biosynthesis and transport of tocochromanol precursors is currently much more limited. This topic is central in understanding and manipulating tocochromanol metabolism as it is now largely accepted that precursor availability is a major mechanism determining both the type and amount of tocochromanols produced by plants (Mène-Saffrané and Pellaud, 2017). This review summarizes both consensual knowledge and divided views on the biosynthesis and metabolic origins of the tocochromanol precursors HGA and polyprenyl pyrophosphates. It notably highlights the current research gaps on chloroplast membrane transporters required for exchanging tocochromanol precursors between the cytoplasm and plastids.

BIOSYNTHESIS AND ORIGIN OF HOMOGENTISATE

Homogentisate is an aromatic compound resulting from the degradation of L-tyrosine (tyr; **Figure 2**). Following its synthesis by the plastidic shikimate pathway, tyr is converted into 4-hydroxyphenylpruvate (HPP) by tyrosine aminotransferases (TATs), a class of enzymes that catalyze the transamination between tyr and 2-oxoglutarate, and HPP and L-glutamate (Maeda and Dudareva, 2012). Based on sequence similarities, 6–10 *TAT* genes have been identified in the Arabidopsis genome (Riewe et al., 2012; Wang et al., 2016). However, the enzymatic activity has been experimentally confirmed only for *AtTAT1* and *AtTAT2* (Prabhu and Hudson, 2010; Grossmann et al., 2012; Wang et al., 2016). AtTAT1 (also named TAT7) controls 35–50% of the leaf tocopherol biosynthesis (Riewe et al., 2012). The other TAT(s) involved in the biosynthesis of the 50–65% TAT1-independent tocochromanols remain to be identified. They might include the cytosolic AtTAT2 and/or plastidic TAT(s) whose activity has been detected but the corresponding gene(s) has not yet been identified (Wang et al., 2016). It was recently shown that AtTAT1 is localized in the cytoplasm, indicating that HGA synthesis occurs, in total or in part, in this compartment (Wang et al., 2016). This data implies that tocochromanol synthesis involves a yet unknown transporter that brings cytoplasmic HGA back into plastids (**Figure 2**). The TAT isoform(s) involved in seed tocochromanol synthesis remains to be identified.

Hydroxyphenylpruvate is converted into HGA by the 4-hydroxyphenylpyruvate dioxygenase (HPPD), an Fe(II)-containing non-heme oxygenase encoded by a single gene in Arabidopsis (Norris et al., 1995; Tsegaye et al., 2002). Several studies investigating the subcellular localization of HPPD showed that it varies according to the plant species. Early work on *Spinacia oleracea* and *Lemna gibba* localized the HPPD activity in chloroplasts (Löffelhardt and Kindl, 1979; Fiedler et al., 1982). In tomato and cotton, *HPPD* sequence analyses identified a chloroplast transit peptide (Moshiri et al., 2007). In maize, transient expression of the full length *HPPD* gene localized the protein in chloroplasts (Siehl et al., 2014). In contrast, HPPD activity and/or protein is localized in the cytoplasm of both carrot and Arabidopsis cells (Garcia et al., 1997; Wang et al., 2016). Besides these species, soybean HPPD was demonstrated to be localized in both compartments. The single copy *GmHPPD* gene exhibits two transcription start sites that produce a long and a short polypeptide, respectively. Transient and stable expression of both transcripts confirmed that the long version was imported in chloroplasts while the shorter one remained in the cytoplasm (Siehl et al., 2014). The recent identification of the soybean MO12 mutant further supports the cytoplasmic synthesis of the tocochromanol precursor HGA in some plant species. This mutant, which carries a defective *HOMOGENTISATE-1,2-DIOXYGENASE 1* (*HGO1*) gene degrading HGA into 4-maleyl acetoacetate, overaccumulated free HGA and tocochromanols in seeds (Stacey et al., 2016). Interestingly, *GmHGO1* sequence analysis did not detect any obvious targeting peptide suggesting that HGO1 is likely localized in the cytoplasm. This was experimentally confirmed with transient expression of the HGO1:GFP fusion protein that accumulated exclusively in the cytoplasm. Since the cytoplasmic HGA catabolism directly impacts tocochromanol accumulation in soybean seeds, this implies that cytoplasmic HGA substantially contributes to tocochromanol synthesis, at least in soybean (**Figure 2**). These data further support the existence of a mechanism transferring cytoplasmic HGA into plastids where it is notably used for tocochromanol synthesis. To date, the identity of this membrane transporter(s) remains to be identified. Interestingly, the Arabidopsis *HGO* gene is also predicted to be localized in the cytoplasm (TAIR10).

BIOSYNTHESIS OF THE TOCOCHROMANOL ISOPRENOID SIDE CHAINS

All four polyprenyl tocochromanol precursors (PPP, GGPP, SPP, and THGGPP) derive from GGPP produced by GERANYLGERANYL PYROPHOSPHATE SYNTHASEs (GGPPS; **Figure 2**). Among the 10 GGPPS identified in Arabidopsis, seven are predicted to be localized in plastids, notably GGPPS11 that is the main paralog responsible for the synthesis of GGPP used for tocochromanol production (Ruiz-Sola et al., 2016).

The prenyl precursor PPP used for tocopherol synthesis mostly comes from chlorophyll catabolism during which its side chain is cleaved off and recycled (Valentin et al., 2006; Vom Dorp et al., 2015). To date, four hydrolases active on chlorophylls and/or on their Mg-free derivative pheophytines

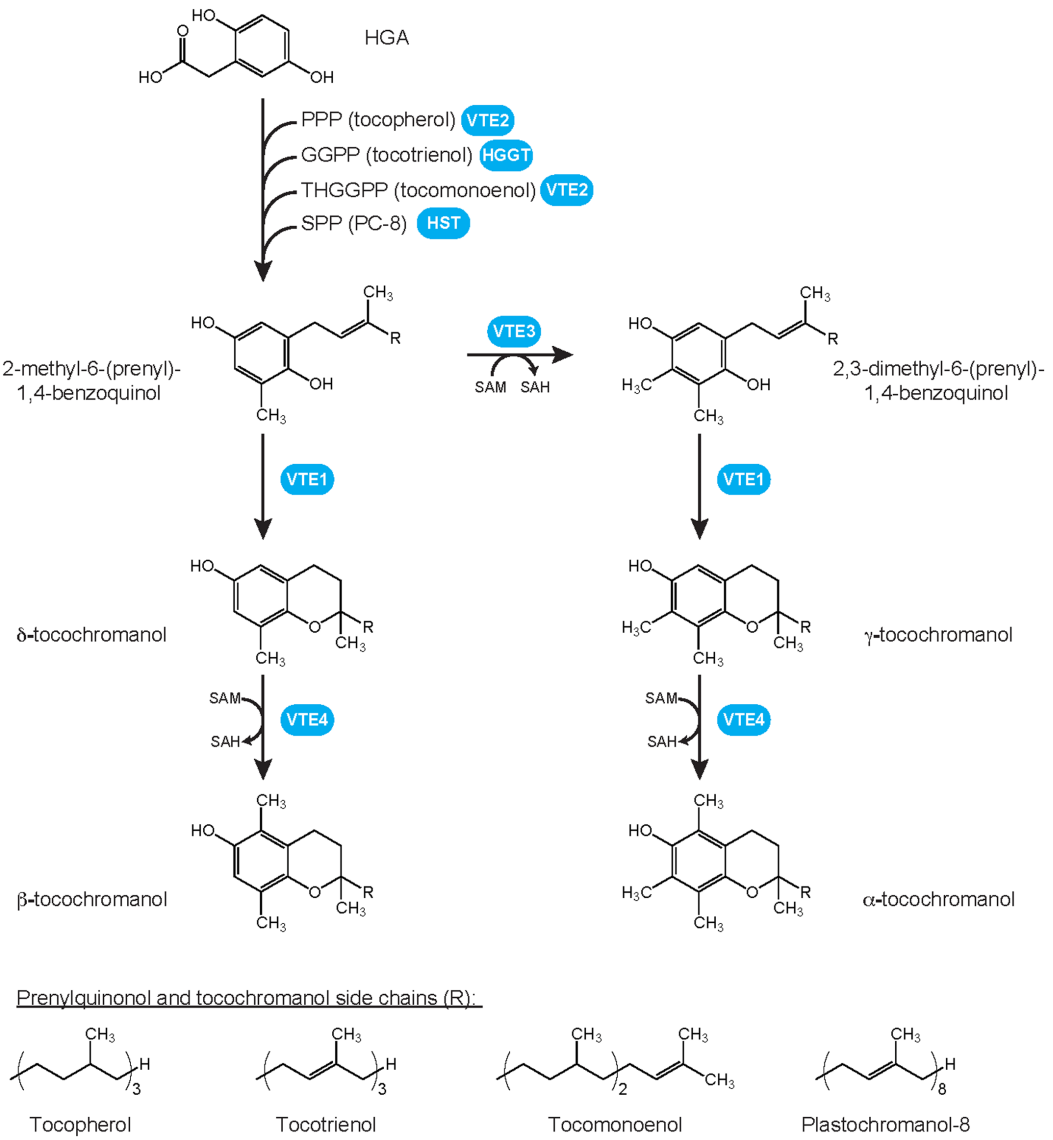

FIGURE 1 | Plant tocochromanol biosynthetic pathways and chemical structures of prenylquinols and tocochromanols. Whereas all four methylated forms, i.e., α-, β-, γ- and δ-tocochromanol, have been identified in wild-type plants for tocopherols, tocotrienols, and tocomonoenols, only the γ- form of solanesyl-derived tocochromanol PC-8 has been identified in wild-type plants. Its methylated form, methyl PC-8, has been found only in transgenic plants overexpressing *VTE4*. GGPP, geranylgeranyl pyrophosphate; HGA, homogentisate; HGGT, HGA geranylgeranyl transferase; HST, HGA solanesyl transferase; PC-8, plastochromanol-8; PPP, phytyl pyrophosphate; SAH, *S*-adenosylhomocystein; SAM, *S*-adenosylmethionine; SPP, solanesyl pyrophosphate; THGGPP, tetrahydrogeranylgeranyl pyrophosphate; VTE, vitamin E biosynthetic enzyme.

have been identified. Two *CHLOROPHYLLASEs AtCLH1* and *AtCLH2* genes have been isolated in Arabidopsis based on sequence homologies with the *Citrus sinensis* and *Chenopodium album CLH* genes, respectively (Jacob-Wilk et al., 1999; Tsuchiya et al., 1999). The chlorophyllase activities of CsCLH, CaCLH, and AtCLH1 have been demonstrated *in vitro*. Intriguingly, neither *AtCLH1* nor *AtCLH2* genes exhibit the typical chloroplast transit peptide targeting them into plastids where chlorophyll catabolism occurs. In addition, both AtCLH1 and AtCLH2 have been shown to have a very limited role in chlorophyll catabolism occurring during senescence (Schelbert et al., 2009).

The hydrolase responsible for chlorophyll dephytylation during leaf senescence is encoded by the *PHEOPHYTINASE* gene (Schelbert et al., 2009). This enzyme is localized in plastids and is specifically expressed during senescence. Consequently, leaves of *pph* mutants exhibit a stay-green phenotype and accumulate pheophytin upon dark-induced senescence. Although it has not been experimentally tested yet, it is very likely that the tocopherol accumulation observed in senescent leaves is dependent on this enzyme (Rise et al., 1989). Recently, it was shown that the chlorophyll dephytylase CLD1 catalyzes the dephytylation of chlorophylls both *in vitro* and *in vivo* (Lin et al., 2016). The

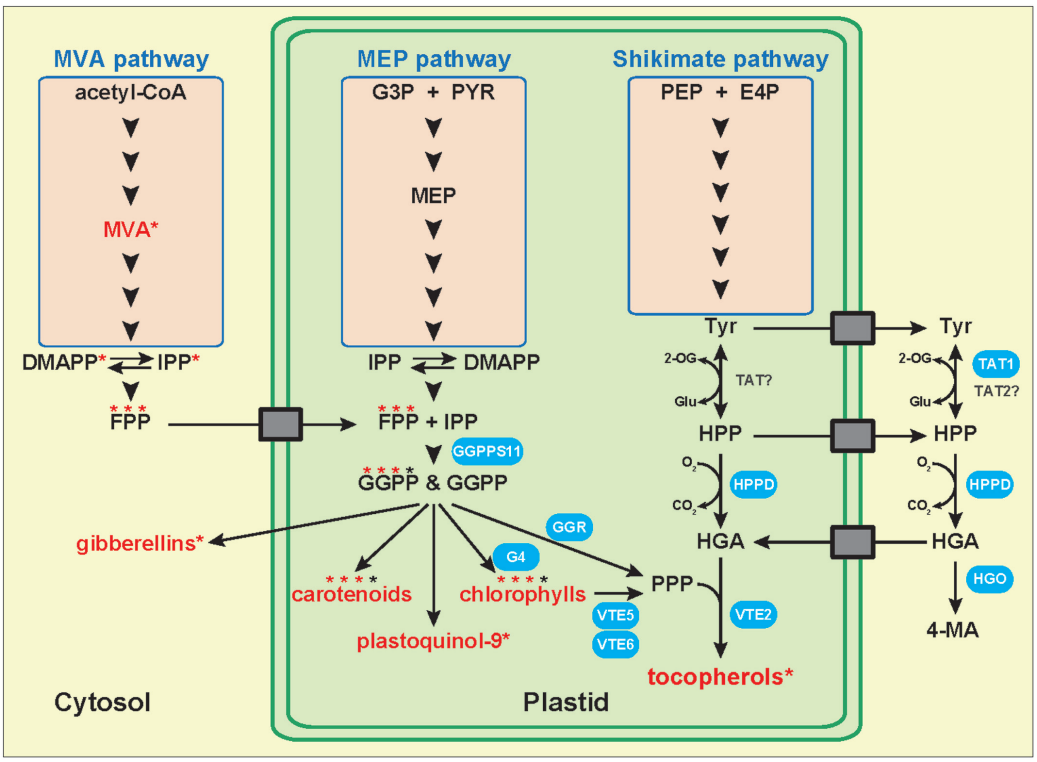

FIGURE 2 | Metabolic origins of tocopherol biosynthetic precursors. Model representing the biosynthetic pathways, cellular compartments, and membrane transport proteins involved in the biosynthesis and transport of tocopherol precursors. Several studies suggest that the cytoplasmic MVA pathway might supply prenyl biosynthetic precursors such as farnesyl pyrophosphate for the synthesis of plastidic isoprenoids including carotenoids, plastoquinol-9, chlorophylls, and tocopherols. Compound names in red with an asterisk indicate that the corresponding radiolabeled molecule has been detected following feeding with radiolabeled mevalonate (cytoplasmic MVA pathway). Compound names topped with three red stars and one black star indicate that three quarters of the prenyl side chain of the molecule was radiolabeled following radiolabeled MVA feeding, while one quarter remained unlabeled. Biosynthetic enzymes in blue indicate that they have been demonstrated to be involved in tocopherol metabolism and that their subcellular localization was confirmed. In contrast, enzyme names in black have not been demonstrated involved in tocochromanol metabolism yet. Genetic and biochemical evidence in Arabidopsis and soybean show that HGA synthesis is localized in the cytoplasm. This implies the existence of membrane transport proteins exporting tyrosine and potentially HPP from plastids to the cytoplasm, and of transporter(s) importing HGA back into plastids. None of the transporters symbolized by gray boxes have been identified yet. CoA, coenzyme A; DMAPP, dimethylallyl pyrophosphate; E4P, D-erythrose-4-phosphate; FPP, farnesyl pyrophosphate; G3P, glyceraldehyde-3-phosphate; G4, chlorophyll synthase; GGPP, geranylgeranyl pyrophosphate; GGPPS, geranylgeranyl pyrophosphate synthase; GGR, geranylgeranyl reductase; Glu, L-glutamate; HGA, homogentisic acid; HGO, homogentisic acid dioxygenase; HPP, 4-hydroxyphenylpyruvate; HPPD, 4-hydroxyphenylpyruvate dioxygenase; IPP, isopentenyl pyrophosphate; 4-MA, 4-maleylacetoacetate; MEP, methylerythritol phosphate; MVA, mevalonate; 2-OG, 2-oxoglutarate; PEP, phosphoenolpyruvate; PPP, phytyl pyrophosphate; PYR, pyruvate; TAT, tyrosine aminotransferase; Tyr, tyrosine; VTE, vitamin E biosynthetic enzyme.

CLD1 gene is strongly expressed in green leaves where the corresponding protein is associated with thylakoids in plastids. As for chlorophyll catabolism in Arabidopsis seeds, it has been shown that PPH, CLH1, and CLH2 are not involved in supplying phytol for seed tocopherol synthesis (Zhang et al., 2014). The enzyme catalyzing this step in seeds of chloroembryophytes is currently unknown.

Once cleaved from chlorophyll/pheophytin, phytol needs to be phosphorylated twice to produce PPP. This reaction is catalyzed by the phytol kinase VTE5 and the phytyl phosphate kinase VTE6 (**Figure 2**). Seed and leaf tocopherols of *vte5* mutants are reduced by 80 and 65%, respectively, while *vte6* leaves fully lack tocopherols (Valentin et al., 2006; Vom Dorp et al., 2015). Since phytol content was significantly increased in *vte6* mutants, it has been suggested that VTE6 might also directly phosphorylate phytol. Thus, according to this later biosynthetic model, tocopherol synthesis would fully rely on chlorophyll catabolism and recycling. This is only partially supported by data obtained with mutants of the chlorophyll synthase *G4/CHLSYN1*, the enzyme catalyzing the last step of chlorophyll biosynthesis. Indeed, while leaves of *g4/chlsyn1* mutants maintained for 5 weeks on 2% sucrose were nearly devoid of tocopherols, their seeds still accumulated 25% wild-type tocopherols (Zhang et al., 2015). These results support the idea that leaf tocopherol synthesis is fully dependent on chlorophyll catabolism and phytol recycling. In contrast, they suggest that seed tocopherol synthesis might partially depend on a source of polyprenyl other than chlorophylls that has not been identified yet.

The PC-8 prenyl precursor SPP is produced by the plastidic SOLANESYL PYROPHOSPHATE SYNTHASEs (SPS) 1 and 2 (Block et al., 2013). *In vitro* experiments with recombinant AtSPS1 and 2 and various polyprenyl pyrophosphates in

combination to either isopentenyl pyrophosphate (IPP) or dimethylallyl pyrophosphate (DMAPP) showed that both enzymes poorly utilize geranyl pyrophosphate and DMAPP (Hirooka et al., 2003, 2005). In contrast, both efficiently utilize farnesyl pyrophosphate and GGPP in combination to IPP with the highest affinity for GGPP/IPP. Double *sps1 sps2* mutants are albino and lack plastoquinol-9, the prenylated benzoquinol notably involved in the electron transfer chain of photosynthesis, and PC-8, the tocochromanol resulting from plastoquinol-9 cyclization.

The tocomonoenol prenyl precursor THGGPP is an intermediate of the reductive pathway converting GGPP into PPP (Kruk et al., 2011; Pellaud et al., 2018). This process is mediated by a geranylgeranyl reductase (GGR) that sequentially converts both geranylgeranylated chlorophyll *a* and GGPP into phytylated chlorophyll *a* and PPP, respectively (Keller et al., 1998; Takahashi et al., 2014). This biosynthetic model originates from biochemical experiments in which both dihydro- and tetrahydrogeranylgeranyl intermediates were identified together with phytylated chlorophyll and PPP following the incubation of geranylgeranyl chlorophyll *a* or GGPP with recombinant GGR, respectively (Keller et al., 1998). Recently, the sequential reduction of geranylgeranyl intermediates has been further confirmed *in planta* with the functional study of LIGHT-HARVESTING CHLOROPHYLL-BINDING-LIKE (LIL) 3:1 and 3:2 that both stabilize GGR (Takahashi et al., 2014). Mutations in either *LIL3:1* or *LIL3:2* lead to the reduction of GGR activity and to the concomitant accumulation of dihydro- and tetrahydrogeranylgeranyl chlorophylls in leaves. Moreover, leaves of *lil3:1 lil3:2* double mutants exhibit further lower GGR activity and mostly accumulate geranylgeranylated chlorophylls. Since tocomonoenols were not identified in Arabidopsis seeds at the time of that study, which focused exclusively on leaves, it is currently unknown whether tocomonoenol contents increase in seeds of *lil3:1* and *lil3:2* single mutants. In line with this tocomonoenol biosynthetic model, we recently showed that γ-tocomonoenol content significantly increased in segregating *GGR ggr* seeds (Pellaud et al., 2018).

METABOLIC ORIGINS OF THE TOCOCHROMANOL ISOPRENOID SIDE CHAINS

Most articles on plant tocochromanol metabolism attribute the origin of the prenyl component of tocochromanols exclusively to the plastidic methylerythritol phosphate (MEP) pathway. These references cite two significant review articles published right after the discovery of this non-mevalonate isoprenoid pathway that did not support the exchange of isoprenoid precursor(s) between the plastidic MEP and cytoplasmic mevalonate (MVA) pathways at that time (Lichtenthaler, 1998, 1999). Recently, another landmark review article on the MVA and MEP pathways also supported the MEP pathway origin of the prenyl component of plastidic isoprenoids by using two lines of genetic evidences (Vranová et al., 2013). Germinating homozygous mutants of MEP biosynthetic genes are albino indicating that the MVA pathway is not capable of complementing chlorophyll synthesis during germination of MEP pathway mutants. In addition, mutants of MVA biosynthetic genes are male sterile indicating that the MEP pathway is not capable of complementing the defective pollen of MVA pathway mutants. Besides these genetic data, much evidence shows that the prenyl component of plastidic isoprenoids might also come from the cytosolic MVA pathway. Independent feeding experiments using radiolabeled MVA, an intermediate of the cytoplasmic MVA pathway, resulted in the production of radiolabeled isoprenoids typically produced in plastids. It was shown for instance that maize shoots, calendula leaves, and barley leaves treated with [2-^{14}C]MVA produced radiolabeled α-tocopherol (Threlfall et al., 1967; Janiszowska et al., 1976; Schultz, 1990). This suggests that cytoplasmic MVA pathway-derived IPP/DMAPP and/or prenyl pyrophosphates might be imported into plastids and incorporated into plastidic isoprenoids such as tocopherols. Similarly, treatment of pine seedlings, etiolated maize and oat seedlings, potato sprouts, and barley leaves with [2-^{14}C]MVA resulted in the synthesis of chlorophylls with labeled phytyl side chains (Treharne et al., 1966; Wieckowski and Goodwin, 1967; Schultz, 1990; Kozukue et al., 2001). These results were recently confirmed in cotton leaves in which up to 19 and 44% of the phytyl side chains of chlorophyll *a* and *b*, respectively, were labeled following [2-^{13}C]MVA feeding (Opitz et al., 2014). Since the phytyl side chain of chlorophylls is a significant prenyl source for tocopherol synthesis, these data further indicate that the prenyl component of tocopherols likely does not originate exclusively from the plastidic MEP pathway and might also originate from the cytoplasmic MVA pathway. Moreover, labeled β-carotene has been independently detected in maize and barley shoots, in etiolated maize and oat seedlings, in pine seedlings, in barley leaves, and in cultured cells of liverworts treated with [2-^{14}C]MVA (Treharne et al., 1966; Threlfall et al., 1967; Wieckowski and Goodwin, 1967; Schultz, 1990; Nabeta et al., 1997). A quantitative study recently estimated that 34% of β-carotene in cotton leaves was labeled following [2-^{13}C]MVA feeding (Opitz et al., 2014). While these feeding studies do not firmly demonstrate the existence of a systematic cross-flow between the cytoplasmic and plastidic isoprenoid pathways, they undoubtedly demonstrate that cytoplasmic isoprenoid precursor(s), when available in large amount, are incorporated into plastidic isoprenoids such as tocopherols, carotenoids, and chlorophylls. These data also indicate that a transport system allowing the import of cytoplasmic isoprenoid precursor(s) into plastids exists in plants (**Figure 2**). To date, this transporter(s) remains to be identified.

Recent feeding experiments with radiolabeled MVA combined to NMR analysis further refined our understanding of the import of cytoplasmic MVA pathway-derived isoprenoid precursors into plastids. It was independently shown that three quarters of the prenyl units composing the phytyl side chain of chlorophylls, β-carotene or other plastidic isoprenoids produced after [2-^{13}C]MVA feeding were labeled whereas the terminal C5 unit was not (Itoh et al., 2000; Karunagoda et al., 2001; **Figure 2**). This suggests that MVA pathway-derived radiolabeled IPP is concatenated in the cytoplasm into radiolabeled FPP that is imported into plastids where it is condensed with non-labeled

MEP pathway-derived IPP. This biosynthetic model is supported by data showing the import of cytosolic FPP into plastids and its incorporation into the phytyl side chain of chlorophylls and into β-carotene (Nabeta et al., 1995, 1997). Moreover, comparison of plastid uptakes of several radiolabeled polyprenyl pyrophosphates showed that FPP was 6–8 and 2–5 times more incorporated into the side chains of chlorophylls than IPP or GPP, respectively (Karunagoda and Nabeta, 2004). Collectively, these data indicate that FPP is likely the preferential cytoplasmic isoprenoid precursor imported into plastids and used for the synthesis of plastidic isoprenoids (**Figure 2**).

Several metabolic engineering studies overexpressing cytoplasmic isoprenoid biosynthetic genes further support the utilization of cytoplasmic MVA-derived isoprenoid precursors for the synthesis of plastidic isoprenoids. It was shown for instance that overexpression of *Brassica juncea 3-HYDROXY-3-METHYLGLUTARYL-COA SYNTHASE1*, an MVA pathway biosynthetic gene, did not only increase the accumulation of cytoplasmic phytosterols in transgenic tomato fruits, but also strongly increased the synthesis of plastidic isoprenoids such as α-tocopherol (fivefold) and carotenoids (twofold; Liao et al., 2017). Overexpression of a *Salvia miltiorrhiza* 3-HYDROXY-3-METHYLGLUTARYL-COA REDUCTASE, a rate-limiting enzyme of the MVA pathway, strongly increased the synthesis of tanshinone, a diterpene produced by the MEP pathway (Kai et al., 2011). Similarly, overexpression in spike lavender of the Arabidopsis 3-HYDROXY-3-METHYLGLUTARYL-COA REDUCTASE1, an MVA pathway biosynthetic gene, doubled the synthesis of monoterpenes produced by the MEP pathway (Muñoz-Bertomeu et al., 2007). Together with the feeding experiment data presented above, these metabolic engineering studies further support the concept that MVA-derived isoprenoid precursors are used for the synthesis of plastidic isoprenoid compounds when they are available in sufficient amounts. This conclusion might explain why the MVA pathway does not complement chlorophyll synthesis in albino seedlings of MEP pathway mutants, and why the MEP pathway does not complement the defective pollen of MVA pathway mutants. Indeed, analysis of MEP and MVA biosynthetic gene expression with ePlant (The Bio-Analytic Resources for Plant Biology; University of Toronto) shows that MVA biosynthetic genes are very weakly expressed in seedlings, notably the mevalonate kinase encoded by a single gene (At5g27450). Similarly, MEP biosynthetic genes are very weakly expressed in pollen, notably the 1-deoxy-D-xylulose-5-phosphate reductoisomerase also encoded by a single gene (At5g62790). Thus, if both pathways are not fully functional at a given physiological stage, they cannot complement the one disrupted by the mutation, and this, despite the possible exchange of isoprenoid precursor(s) showed by feeding experiments and metabolic engineering. Importantly, there is currently no report in the literature demonstrating the dual origin of the prenyl side chain of tocochromanols in wild-type plants.

CONCLUSIONS AND PERSPECTIVES

From the cloning of the first tocopherol biosynthetic genes to the recent identification of the tocomonoenol ones, substantial progress has been made in understanding the core tocochromanol biosynthetic pathways in plants (Shintani and DellaPenna, 1998; Pellaud et al., 2018). In contrast, major knowledge gaps highlighted in the present review currently exist on the metabolic origin(s) of tocochromanol biosynthetic precursors and on transporters involved in exchanges of polar and lipophilic metabolites between the cytoplasm and plastids. For instance, the cytoplasmic biosynthesis of HGA notably implies the existence of membrane transport proteins exporting tyr and potentially HPP from plastids to the cytoplasm, and of transporters importing back HGA into plastids. Since HGA availability is a potent mechanism controlling tocochromanol synthesis in plants, future challenges will be to identify these transporters and modulate their expression to investigate their role in tocochromanol biosynthesis. Similarly, although the existence of mechanisms importing cytoplasmic MVA-derived isoprenoid precursors into plastids is no longer to be demonstrated, these transporters remain to be identified and characterized. In addition, since the incorporation of MVA pathway-derived prenyls into tocochromanols has not been demonstrated yet in wild-type plants, it is still an open question whether the cytoplasmic MVA pathway contributes or not to tocochromanol biosynthesis in plants.

AUTHOR CONTRIBUTIONS

SP and LM-S designed and wrote the manuscript.

ACKNOWLEDGMENT

We are grateful to the University of Fribourg, Switzerland for supporting our work.

REFERENCES

Block, A., Fristedt, R., Rogers, S., Kumar, J., Barnes, B., Barnes, J., et al. (2013). Functional modelling identifies paralogous solanesyl-diphosphate synthases that assemble the side chain of plastoquinone-9 in plastids. *J. Biol. Chem.* 288, 27594–27606. doi: 10.1074/jbc.M113.492769

DellaPenna, D., and Mène-Saffrané, L. (2011). Vitamin E. *Adv. Bot. Res.* 59, 179–227. doi: 10.1016/B978-0-12-385853-5.00002-7

Evans, H. M., and Bishop, K. S. (1922). On the existence of a hitherto unrecognized dietary factor essential for reproduction. *Science* 56, 650–651. doi: 10.1126/science.56.1458.650

Fiedler, E., Soll, J., and Schultz, G. (1982). The formation of homogentisate in the biosynthesis of tocopherol and plastoquinone in spinach chloroplasts. *Planta* 155, 511–515. doi: 10.1007/BF01607575

Garcia, I., Rodgers, M., Lenne, C., Rolland, A., Sailland, A., and Matringe, M. (1997). Subcellular localization and purification of a *p*-hydroxyphenylpyruvate

dioxygenase from cultured carrot cells and characterization of the corresponding cDNA. *Biochem. J.* 325, 761–769. doi: 10.1042/bj3250761

Grossmann, K., Hutzler, J., Tresch, S., Christiansen, N., Looser, R., and Ehrhardt, T. (2012). On the mode of action of the herbicides cinmethylin and 5-benzyloxymethyl-1, 2-isoxazolines: putative inhibitors of plant tyrosine aminotransferase. *Pest Manag. Sci.* 68, 482–492. doi: 10.1002/ps.2319

Hirooka, K., Bamba, T., Fukusaki, E.-I., and Kobayashi, A. (2003). Cloning and kinetic characterization of *Arabidopsis thaliana* solanesyl diphosphate synthase. *Biochem. J.* 370, 679–686. doi: 10.1042/bj20021311

Hirooka, K., Izumi, Y., An, C.-I., Nakazawa, Y., Fukusaki, E.-I., and Kobayashi, A. (2005). Functional analysis of two solanesyl diphosphate synthases from *Arabidopsis thaliana*. *Biosci. Biotechnol. Biochem.* 69, 592–601. doi: 10.1271/bbb.69.592

Itoh, D., Karunagoda, R. P., Fushie, T., Katoh, K., and Nabeta, K. (2000). Nonequivalent labelling of the phytyl side chain of chlorophyll *a* in callus of the Hornwort *Anthoceros punctatus*. *J. Nat. Prod.* 63, 1090–1093. doi: 10.1021/np000089m

Jacob-Wilk, D., Holland, D., Goldschmidt, E. E., Riov, J., and Eyal, Y. (1999). Chlorophyll breakdown by chlorophyllase: isolation and functional expression of the Chlase1 gene from ethylene-treated *Citrus* fruit and its regulation during development. *Plant J.* 20, 653–661. doi: 10.1046/j.1365-313X.1999.00637.x

Janiszowska, W., Michalski, W., and Kasprzyk, Z. (1976). Polyprenyl quinones and αα-tocopherol in *Calendula officinalis*. *Phytochemistry* 15, 125–127. doi: 10.1016/S0031-9422(00)89066-4

Kai, G., Xu, H., Zhou, C., Liao, P., Xiao, J., Luo, X., et al. (2011). Metabolic engineering tanshinone biosynthetic pathway in *Salvia miltiorrhiza* hairy root cultures. *Metab. Eng.* 13, 319–327. doi: 10.1016/j.ymben.2011.02.003

Karunagoda, R., and Nabeta, K. (2004). Biosynthesis of chloroplastidic isoprenoids in liverworts: uptake of farnesyl diphosphate by the chloroplasts of *Heteroscyphus planus* and *Ptychanthus striatus*. *Trop. Agric. Res.* 16, 214–222.

Karunagoda, R. P., Itoh, D., Katoh, K., and Nabeta, K. (2001). Labeling patterns of chloroplastidic isoprenoids in cultured cells of liverwort *Ptychanthus striatus*. *Biosci. Biotechnol. Biochem.* 65, 1076–1081. doi: 10.1271/bbb.65.1076

Keller, Y., Bouvier, F., D'Harlingue, A., and Camara, B. (1998). Metabolic compartmentation of plastid prenyllipid biosynthesis. *Eur. J. Biochem.* 251, 416–417. doi: 10.1046/j.1432-1327.1998.2510413.x

Kozukue, N., Tsuchida, H., and Friedman, M. (2001). Tracer studies on the incorporation of [2-14C]-DL-mevalonate into chlorophylls *a* and *b*, α-chaconine, and α-solanine of potato sprouts. *J. Agric. Food Chem.* 49, 92–97. doi: 10.1021/jf0003348

Kruk, J., Pisarski, A., and Szymanska, R. (2011). Novel vitamin E forms in leaves of *Kalanchoe daigremontiana* and *Phaseolus coccineus*. *J. Plant Physiol.* 168, 2021–2027. doi: 10.1016/j.jplph.2011.06.015

Liao, P., Chen, X., Wang, M., Bach, T. J., and Chye, M. L. (2017). Improved fruit α-tocopherol, carotenoid, squalene and phytosterol content through manipulation of *Brassica juncea* 3-HYDROXY-3-METHYLGLURARYL-COA SYNTHASE1 in transgenic tomato. *Plant Biotechnol. J.* doi: 10.1111/pbi.12828 [Epub ahead of print]. doi: 10.1111/pbi.12828

Lichtenthaler, H. K. (1998). The plants' 1-deoxy-D-xylulose-5-phosphate pathway for biosynthesis of isoprenoids. *Lipid* 100, 128–138. doi: 10.1002/(SICI)1521-4133(19985)100:4/5<128::AID-LIPI128>3.0.CO;2-D

Lichtenthaler, H. K. (1999). The 1-deoxy-D-xylulose-5-phosphate pathway of isoprenoid biosynthesis in plants. *Annu. Rev. Physiol. Plant Mol. Biol.* 50, 47–65. doi: 10.1146/annurev.arplant.50.1.47

Lin, Y. P., Wu, M. C., and Chang, Y. Y. (2016). Identification of a chlorophyll dephytylase involved in chlorophyll turnover in Arabidopsis. *Plant Cell* 28, 2974–2990. doi: 10.1105/tpc.16.00478

Löffelhardt, W., and Kindl, H. (1979). Conversion of 4-hydroxyphenylpyruvic acid into homogentisic acid at the thylakoid membrane of Lemna gibba. *FEBS Lett.* 104, 332–334. doi: 10.1016/0014-5793(79)80845-5

Maeda, H., and Dudareva, N. (2012). The shikimate pathway and aromatic amino acid biosynthesis in plants. *Annu. Rev. Plant Biol.* 63, 73–105. doi: 10.1146/annurev-arplant-042811-105439

Mène-Saffrané, L., and DellaPenna, D. (2010). Biosynthesis, regulation and functions of tocochromanols in plants. *Plant Physiol. Biochem.* 48, 301–309. doi: 10.1016/j.plaphy.2009.11.004

Mène-Saffrané, L., and Pellaud, S. (2017). Current strategies for vitamin E biofortification of crops. *Curr. Opin. Biotechnol.* 44, 189–197. doi: 10.1016/j.copbio.2017.01.007

Moshiri, F., Hao, M., Karunanandaa, B., Valentin, H. E., Venkatesh, T. V., and Wong, Y. H. H. (2007). Genes encoding 4-hydroxyphenylpyruvate dioxygenase (HPPD) enzymes for plant metabolic engineering. U.S. Patent No US20080127371 A1.

Muñoz-Bertomeu, J., Sales, E., Ros, R., Arrillaga, I., and Segura, J. (2007). Up-regulation of an N-terminal truncated 3-hydroxy-3-methylglutaryl CoA reductase enhances production of essential oils and sterols in transgenic *Lavandula latifolia*. *Plant Biotechnol. J.* 5, 746–758. doi: 10.1111/j.1467-7652.2007.00286.x

Nabeta, K., Kawae, T., Kikuchi, T., Saitoh, T., and Okuyama, H. (1995). Biosynthesis of chlorophyll a from 13C-labelled mevalonates and glycine in liverwort. Nonequivalent labelling of phytyl side chain. *J. Chem. Soc., Chem. Commun.* 2529–2530.

Nabeta, K., Kawae, T., Saitoh, T., and Kikuchi, T. (1997). Synthesis of chlorophyll a and β-carotene from 2H- and 13C-labelled mevalonates and 13C-labelled glycine in cultured cells of liverworts, Heteroscyphus planus and Lophocolea heterophylla. *J. Chem. Soc. Perkin Trans.* 1, 261–267. doi: 10.1039/a604562f

Norris, S. R., Barrette, T. R., and DellaPenna, D. (1995). Genetic dissection of carotenoid synthesis in Arabidopsis defines plastoquinone as an essential component of phytoene desaturation. *Plant Cell* 7, 2139–2149. doi: 10.1105/tpc.7.12.2139

Opitz, S., Nes, W. D., and Gershenzon, J. (2014). Both methylerythritol phosphate and mevalonate pathways contribute to biosynthesis of each of the major isoprenoid classes in young cotton seedlings. *Phytochemistry* 98, 110–119. doi: 10.1016/j.phytochem.2013.11.010

Pellaud, S., Bory, A., Chabert, V., Romanens, J., Chaisse-Leal, L., Doan, A. V., et al. (2018). WRI1 and DGAT1 regulate tocochromanol metabolism in Arabidopsis. *New Phytol.* doi: 10.1111/nph.14856 [Epub ahead of print].

Prabhu, P. R., and Hudson, A. O. (2010). Identification and partial characterization of an L-tyrosine aminotransferase (TAT) from *Arabidopsis thaliana*. *Biochem. Res. Inter.* 2010:549572. doi: 10.1155/2010/549572

Riewe, D., Koohi, M., Lisec, J., Pfeiffer, M., Lippmann, R., Schmeichel, J., et al. (2012). A tyrosine aminotransferase involved in tocopherol synthesis in Arabidopsis. *Plant J.* 71, 850–859. doi: 10.1111/j.1365-313X.2012.05035.x

Rise, M., Cojocaru, M., Gottlieb, H. E., and Goldschmidt, E. E. (1989). Accumulation of α-tocopherol in senescing organs as related to chlorophyll degradation. *Plant Physiol.* 89, 1028–1030. doi: 10.1104/pp.89.4.1028

Ruiz-Sola, M. A., Coman, D., Beck, G., Barja, M. V., Colinas, M., Graf, A., et al. (2016). Arabidopsis GERANYLGERANYL DIPHOSPHATE SYNTHASE 11 is a hub isozyme required for the production of most photosynthesis-related isoprenoids. *New Phytol.* 209, 252–264. doi: 10.1111/nph.13580

Schelbert, S., Aubry, S., Burla, B., Agne, B., Kessler, F., Krupinska, K., et al. (2009). Pheophytin pheophorbide hydrolase (pheophytinase) is involved in chlorophyll breakdown during leaf senescence in *Arabidopsis*. *Plant Cell* 21, 767–785. doi: 10.1105/tpc.108.064089

Schultz, G. (1990). Biosynthesis of α-tocopherol in chloroplasts of higher plants. *Fat Sci. Technol.* 92, 86–91. doi: 10.1002/lipi.19900920209

Shintani, D., and DellaPenna, D. (1998). Elevating the vitamin E content of plants through metabolic engineering. *Science* 282, 2098–2100. doi: 10.1126/science.282.5396.2098

Siehl, D. L., Tao, Y., Albert, H., Dong, Y., Heckert, M., Madrigal, A., et al. (2014). Broad 4-hydroxyphenylpyruvate dioxygenase inhibitor herbicide tolerance in soybean with an optimized enzyme and expression cassette. *Plant Physiol.* 166, 1162–1176. doi: 10.1104/pp.114.247205

Stacey, M. G., Cahoon, R. E., Nguyen, H. T., Cui, Y., Sato, S., Nguyen, C. T., et al. (2016). Identification of homogentisate dioxygenase as a target for vitamin E biofortification in oilseeds. *Plant Physiol.* 172, 1506–1518. doi: 10.1104/pp.16.00941

Sussmann, R. A. C., Angeli, C. B., Peres, V. J., Kimura, E. A., and Katzin, A. M. (2011). Intraerythrocytic stages of *Plasmodium falciparum* biosynthesize vitamin E. *FEBS Lett.* 585, 3985–3991. doi: 10.1016/j.febslet.2011.11.005

Takahashi, K., Takabayashi, A., Tanaka, A., and Tanaka, R. (2014). Functional analysis of light-harvesting-like protein 3 (LIL3) and its light-harvesting chlorophyll-binding motif in *Arabidopsis*. *J. Biol. Chem.* 289, 987–999. doi: 10.1074/jbc.M113.525428

Threlfall, D. R., Griffiths, W. T., and Goodwin, T. W. (1967). Biosynthesis of the prenyl side chains of plastoquinone and related compounds in maize and barley shoots. *Biochem. J.* 103, 831–851. doi: 10.1042/bj1030831

Treharne, K. J., Mercer, E. I., and Goodwin, T. W. (1966). Incorporation of [14C]carbon dioxide and [2-14C]mevalonic acid into terpenoids of higher plants during chloroplast development. *Biochem. J.* 99, 239–245. doi: 10.1042/bj0990239

Tsegaye, Y., Shintani, D. K., and DellaPenna, D. (2002). Overexpression of the enzyme p-hydroxyphenolpyruvate dioxygenase in Arabidopsis and its relation to tocopherol biosynthesis. *Plant Physiol. Biochem.* 40, 913–920. doi: 10.1016/S0981-9428(02)01461-4

Tsuchiya, T., Ohta, H., Okawa, K., Iwamatsu, A., Shimada, H., Masuda, T., et al. (1999). Cloning of chlorophyllase, the key enzyme in chlorophyll degradation: Finding of a lipase motif and the induction by methyl jasmonate. *Proc. Nat. Acad. Sci. U.S.A.* 96, 15362–15367. doi: 10.1073/pnas.96.26.15362

Valentin, H., Lincoln, K., Moshiri, F., Jensen, P. K., Qi, Q., Venkatesh, T. V., et al. (2006). The *Arabidopsis vitamin E pathway gene5-1* mutant reveals a critical role for phytol kinase in seed tocopherol biosynthesis. *Plant Cell* 18, 212–224. doi: 10.1105/tpc.105.037077

Vom Dorp, K., Hölzl, G., Plohmann, C., Eisenhut, M., Abraham, M., Weber, A. P. M., et al. (2015). Remobilization of phytol from chlorophyll degradation is essential for tocopherol synthesis and growth of Arabidopsis. *Plant Cell* 27, 2846–2859. doi: 10.1105/tpc.15.00395

Vranová, E., Coman, D., and Wilhelm, G. (2013). Network analysis of the MVA and MEP pathways for isoprenoid synthesis. *Annu. Rev. Biol.* 64, 665–700. doi: 10.1146/annurev-arplant-050312-120116

Wang, M., Toda, K., and Maeda, H. A. (2016). Biochemical properties and subcellular localization of tyrosine aminotransferases in *Arabidopsis thaliana*. *Phytochemistry* 132, 16–25. doi: 10.1016/j.phytochem.2016.09.007

Wieckowski, S., and Goodwin, T. W. (1967). Incorporation of DL-[2-14C]mevalonic acid lactone into β-carotene and the phytol side chain of chlorophyll in cotyledons of four species of pine seedlings. *Biochem. J.* 105, 89–92. doi: 10.1042/bj1050089

Zhang, C., Zhang, W., Ren, G., Li, D., Cahoon, R. E., Chen, M., et al. (2015). Chlorophyll synthase under epigenetic surveillance is critical for vitamin E synthesis, and altered expression affects tocopherol levels in Arabidopsis. *Plant Physiol.* 168, 1503–1511. doi: 10.1104/pp.15.00594

Zhang, W., Liu, T., Ren, G., Hörstensteiner, S., Zhou, Y., Cahoon, E. B., et al. (2014). Chlorophyll degradation: the tocopherol biosynthesis-related phytol hydrolase in Arabidopsis seeds is still missing. *Plant Physiol.* 166, 70–79. doi: 10.1104/pp.114.243709

Conflict of Interest Statement: The authors declare that the research was conducted in the absence of any commercial or financial relationships that could be construed as a potential conflict of interest.

frontiers in Plant Science

MINI REVIEW
published: 08 February 2018
doi: 10.3389/fpls.2018.00126

Do Galactolipid Synthases Play a Key Role in the Biogenesis of Chloroplast Membranes of Higher Plants?

*Joana Rocha[1,2], Milène Nitenberg[1,2], Agnès Girard-Egrot[3], Juliette Jouhet[1,4], Eric Maréchal[1,4], Maryse A. Block[1,4] and Christelle Breton[1,2]**

[1] Université Grenoble Alpes, Grenoble, France, [2] CERMAV, CNRS, Grenoble, France, [3] GEMBAS Team, ICBMS, UMR 5246 CNRS, University of Lyon, Lyon, France, [4] LPCV, UMR 5168 CNRS/CEA/INRA/UGA, Université Grenoble Alpes, Grenoble, France

A unique feature of chloroplasts is their high content of the galactolipids monogalactosyldiacylglycerol (MGDG) and digalactosyldiacylglycerol (DGDG), which constitute up to 80% of their lipids. These galactolipids are synthesized in the chloroplast envelope membrane through the concerted action of galactosyltransferases, the so-called 'MGDG synthases (MGDs)' and 'DGDG synthases (DGDs),' which use uridine diphosphate (UDP)-galactose as donor. In Arabidopsis leaves, under standard conditions, the enzymes MGD1 and DGD1 provide the bulk of galactolipids, necessary for the massive expansion of thylakoid membranes. Under phosphate limited conditions, plants activate another pathway involving MGD2/MGD3 and DGD2 to provide additional DGDG that is exported to extraplastidial membranes where they partly replace phospholipids, a phosphate-saving mechanism in plants. A third enzyme system, which relies on the UDP-Gal-independent GGGT (also called SFR2 for SENSITIVE TO FREEZING 2), can be activated in response to a freezing stress. The biosynthesis of galactolipids by these multiple enzyme sets must be tightly regulated to meet the cellular demand in response to changing environmental conditions. The cooperation between MGD and DGD enzymes with a possible substrate channeling from diacylglycerol to MGDG and DGDG is supported by biochemical and biophysical studies and mutant analyses reviewed herein. The fine-tuning of MGDG to DGDG ratio, which allows the reversible transition from the hexagonal II to lamellar α phase of the lipid bilayer, could be a key factor in thylakoid biogenesis.

Keywords: galactolipids, MGDG, DGDG, chloroplast, biosynthesis, Arabidopsis

OPEN ACCESS

Edited by:
Benoit Schoefs,
The University of Maine, France

Reviewed by:
Koichi Kobayashi,
The University of Tokyo, Japan
Agnieszka Mostowska,
University of Warsaw, Poland

***Correspondence:**
Christelle Breton
breton@cermav.cnrs.fr

Specialty section:
This article was submitted to Plant Physiology, a section of the journal Frontiers in Plant Science

Received: *25 November 2017*
Accepted: *23 January 2018*
Published: *08 February 2018*

Citation:
Rocha J, Nitenberg M, Girard-Egrot A, Jouhet J, Maréchal E, Block MA and Breton C (2018) Do Galactolipid Synthases Play a Key Role in the Biogenesis of Chloroplast Membranes of Higher Plants?. Front. Plant Sci. 9:126. doi: 10.3389/fpls.2018.00126

INTRODUCTION

Photosynthetic membranes, or thylakoids, have a unique lipid composition that has been remarkably conserved from cyanobacteria to chloroplast-containing eukaryotes (**Figure 1**). The bulk of lipids is composed of the non-phosphorous and uncharged galactoglycerolipids monogalactosyldiacylglycerol (MGDG) and digalactosyldiacylglycerol (DGDG), which represent up to 80% of total lipids (Block et al., 1983). Other lipids mostly consist of the anionic

Abbreviations: DGDG, digalactosyldiacylglycerol; IEM, inner envelope membrane; MGDG, monogalactosyldiacylglycerol; OEM, outer envelope membrane; PA, phosphatidic acid; PG, phosphatidylglycerol; SQDG, sulfoquinovosyl diacylglycerol.

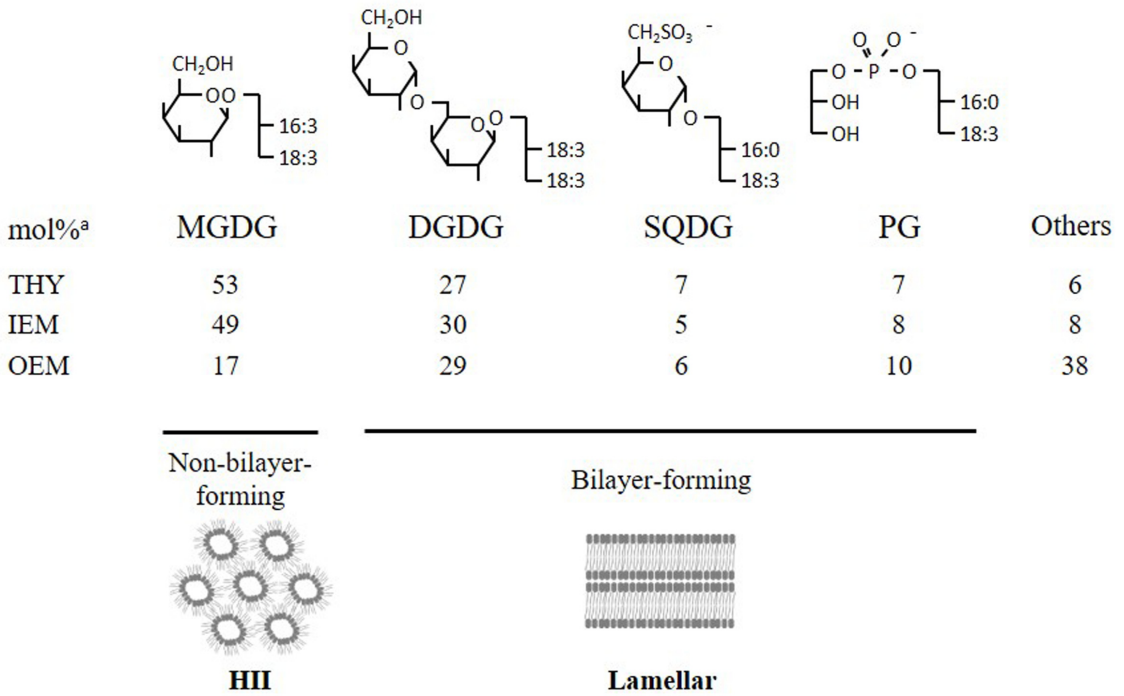

FIGURE 1 | Structures of the conserved quartet of lipids and their abundance (expressed in mol%) in chloroplast membranes. The small polar head of MGDG resembles a truncated cone, which induces a negative curvature favoring its organization into inverted micelles (HII phase). DGDG, SQDG, and PG form lamellar phases. THY, thylakoids; IEM, inner envelope membrane; OEM, outer envelope membrane. [a]From Block et al., 1983.

sulfoquinovosyl diacylglycerol (SQDG) and phosphatidylglycerol (PG). MGDG is exclusively found in plastids, but DGDG can also be found in non-plastidial membranes, under specific conditions such as phosphate (Pi) deprivation, where it can substitute phospholipids (Härtel et al., 2000; Jouhet et al., 2004; Andersson et al., 2005). Galactolipids are believed to play essential roles in the light-dependent conversion of prolamellar bodies to thylakoid membranes in germinating seeds and in the dynamic organization of highly stacked grana membranes and photosynthetic machinery in response to light variations (Fujii et al., 2017; Gabruk et al., 2017). MGDG and DGDG are also known to stabilize the photosystem protein complexes in chloroplasts (Jones, 2007; Mizusawa and Wada, 2012; Kobayashi, 2016).

The MGDG and DGDG have also a major role in determining the physicochemical properties of thylakoid membranes. MGDG, which accounts for half of the total lipids, is a 'non-bilayer forming lipid' due to its cone-like shape, whereas the three other major components DGDG, SQDG, and PG are 'bilayer-forming lipids' (**Figure 1**). Maintaining a constant MGDG/DGDG ratio in thylakoid membranes (at least under standard growth conditions) seems crucial for the stability and functional integrity of photosynthetic membranes (Dörmann and Benning, 2002).

The efficiency of light energy capture and its conversion relies on the rapid expansion of thylakoids, thus requiring an effective and efficient system for providing the bulk of galactolipids. In Arabidopsis, the four major lipid components of photosynthetic membranes are synthesized in the chloroplast envelope (Boudière et al., 2014; Kobayashi, 2016). DAG is the direct precursor for galactolipid formation and it can be produced within the chloroplast via the 'prokaryotic' pathway or from extra-plastidial phosphatidylcholine (PC) via the 'eukaryotic' pathway in the ER (Siebertz et al., 1979; Browse et al., 1986). The flux of DAG must therefore be tightly controlled to meet the dramatic demand of the chloroplast without adversely impacting the needs of other cell membranes.

Although galactolipids represent the major lipid components of oxygenic photosynthetic organisms, their biosynthesis differs between cyanobacteria and plants (Awai, 2016). In plants, MGDG synthesis is carried out by MGDG synthases (MGD), which transfer a galactose residue from uridine diphosphate (UDP)-α-D-galactose (UDP-Gal) to the *sn-3* position of diacylglycerol (DAG), to form Galβ-DAG (MGDG). In cyanobacteria, MGDG is formed in two steps. The first step involves a glucosyltransferase, which transfers a glucose residue from UDP-α-D-glucose to DAG to yield Glcβ-DAG (MGlcDG) (Awai et al., 2006). In a second step, an epimerase converts the glucose moiety of MGlcDG to galactose, yielding MGDG (Awai et al., 2014). DGDG biosynthesis occurs by the same general mechanism in plants and in cyanobacteria, although using distantly related enzymes (Awai et al., 2007; Sakurai et al., 2007). The reaction is catalyzed by DGDG synthases that transfer a galactose from UDP-Gal to MGDG to produce Galα1,6Galβ-DAG (DGDG).

These gluco/galactolipid synthases belong to the large glycosyltransferase (GT) family. The transfer of the monosaccharide to the acceptor is regio- and stereo-specific. GTs

can be classified as retaining or inverting enzymes depending on the stereochemical issue of the transfer reaction (i.e., retention or inversion of the anomeric configuration of the transferred sugar). Another classification has been proposed that groups GTs into families based on amino acid sequence similarities, i.e., CAZy database[1]. The same fold and reaction mechanism are expected to occur within one GT family. The database currently comprises ∼340,000 entries divided into ∼100 GT families (designated GTx, x being the family number). Despite the considerable diversity of GT sequences and function, the three-dimensional structure of GTs is remarkably conserved since only two types of folds (designated as GT-A and GT-B) have been described to date for all nucleotide sugar dependent GTs (Breton et al., 2012). The GT-A and GT-B topologies are variations around a common α/β/α scaffold, the so-called 'Rossmann fold.' Despite the similarities of their folds, GT-A and GT-B enzymes are unrelated and they probably evolved independently (Hashimoto et al., 2010). GTs are also characterized by an amazing conformational plasticity, which may explain their tremendous potential for accommodating a myriad of acceptor substrates (Albesa-Jové and Guerin, 2016). The gluco- and galactolipid synthases that have been described above fall into three GT families: the MGDG and DGDG synthases belong to GT28 (inverting) and GT4 (retaining), respectively, where members of both families are predicted to adopt a GT-B fold. Surprisingly, the bacterial MGlcDG synthase belongs to the inverting GT2 family, and is expected to adopt a GT-A fold. Because it is widely accepted that plastids in plants and algae originate from an ancestral cyanobacteria, the existence of two different pathways for MGDG synthesis involving two unrelated GTs raises the question of the importance of conserving MGDG in photosynthetic membranes and on the evolution history of eukaryotic MGDG synthases. The hypothesis of a lateral transfer of a MGDG synthase gene from an ancestral Chloroflexi has been proposed (Yuzawa et al., 2012).

In the past years, a number of reviews have been published covering various aspects of galactoglycerolipid metabolism and chloroplast biogenesis both in cyanobacteria and in plants (Boudière et al., 2014; Petroutsos et al., 2014; Awai, 2016; Bastien et al., 2016; Kobayashi, 2016). The present review will focus on recent developments in the biochemical and structural characterization of galactolipid synthases and of their products MGDG and DGDG, with a special focus on Arabidopsis enzymes, and how these data can be integrated in the broader context of chloroplast membrane biogenesis.

THE MGDG SYNTHASES

The MGDG synthase activity was first ascribed to a minor membrane protein localized in the chloroplast envelope (Maréchal et al., 1994a,b). Shimojima et al. (1997) first succeeded in the cloning of the MGDG synthase from cucumber. This has led to the identification in the Arabidopsis genome of a multigenic family of MGDG synthases that were designated as type A (or MGD1) and type B (or MGD2 and MGD3) (Awai et al., 2001). The type A protein is characterized by the presence at its N-terminus of a cleavable chloroplast transit peptide of ∼100 amino acids, whereas type B displays a short addressing sequence of ∼30 residues. MGD1 is a monotopic membrane protein that was shown to localize to the outer leaflet of the inner envelope membrane (IEM) (Miège et al., 1999; Xu et al., 2005; Vojta et al., 2007). Whether the MGD1 protein faces the stromal side or the intermembrane space of the IEM is still a matter of debate. This assumption has to be revisited with the demonstration that an epimerase catalyzing the conversion of UDP-Glucose into UDP-Gal in the chloroplast stroma is essential for the biosynthesis of galactolipids in rice (Li et al., 2011). This suggests that the UDP-Gal substrate for MGD1 can be produced *in situ* in chloroplasts and that MGD1 may have access to the IEM stroma side. MGD1 was shown to be the most active isoform responsible for the synthesis of the bulk of MGDG needed for the massive expansion of thylakoids. Indeed, a MGD1 knock-out mutant (*mgd1-2*) could only grow on sucrose-supplemented media and demonstrated a complete lack of chlorophyll as well as a growth arrest after embryogenesis (Kobayashi et al., 2007).

The other Arabidopsis MGD isoforms (MGD2, MGD3) are mostly produced in non-photosynthetic tissues and, more specifically, they are induced in response to phosphate shortage (Awai et al., 2001; Kobayashi et al., 2009). In contrast to MGD1, MGD2 and MGD3 are localized in the outer leaflet of the outer envelope membrane (OEM) (Awai et al., 2001). Knock-out mutants of MGD2 and MGD3 have no striking phenotype in standard growth conditions (Kobayashi et al., 2009).

The MGD1 has been the most extensively studied galactolipid synthase. Biochemical data obtained on the purified spinach enzyme showed a sequential, random or ordered, mechanism with independent donor and acceptor binding sites (Maréchal et al., 1994a). Major advance was recently obtained in the production and crystallization of the catalytic domain of MGD1 (Rocha et al., 2013, 2016). The recombinant protein produced in *Escherichia coli* is fully active but it behaves as a monomer in solution and not as a dimer as previously proposed (Miège et al., 1999). As expected for GTs belonging to family GT28, the MGD1 protein adopts a GT-B fold (Rocha et al., 2016). The GT-B fold is characterized by two Rossmann-type domains with the catalytic site between the two domains. Perhaps the most striking feature in MGD1 was the presence of a long and flexible region of ∼50 amino acids residues in the N-terminal domain. This region seems to contribute to the anchoring MGD1 in the membrane and is essential to capture the DAG acceptor (Rocha et al., 2016). MGD1 requires anionic lipids, such as phosphatidic acid (PA) and PG for its activity (Coves et al., 1988; Dubots et al., 2010). Interestingly, it was shown that PA and PG proceed through different mechanisms, thus suggesting distinct binding sites (Dubots et al., 2010). Mutational studies indicated that PG binds to MGD1 in a region close to the DAG-binding site (Rocha et al., 2016). When tested on biomimetic langmuir monolayers, MGD1 showed a contrasted behavior toward MGDG and DGDG (Sarkis et al., 2014). The reaction product MGDG exerts a positive effect on MGD1, facilitating its binding to the membrane, whereas DGDG has a negative effect and tends

[1]http://www.cazy.org/

to exclude the enzyme. These opposite effects illustrate the importance of the MGDG/DGDG ratio in maintaining the enzyme bound to the membrane and they also suggest that MGD1 localizes to specific microdomains (see below). Particularly, in presence of MGDG, MGD1 tends to self-organize forming elongated and reticulated lipoproteic structures (Sarkis et al., 2014). This type of organization is believed to optimize the massive production of MGDG needed for thylakoid expansion and, possibly, to contribute to the scaffolding of prothylakoids originating from the IEM (Bastien et al., 2016). MGD1 also demonstrated high affinity for DAG and PG monolayers (Sarkis et al., 2014). PG which represents ∼10% of total lipids of IEM probably plays an important role in MGD1 binding. Its role as MGD1 activator and the proximity of PG and DAG binding sites suggest that PG could help the enzyme to trap its DAG substrate. The role of PA in MGD1 activity is less clear. PA is barely detectable in chloroplast membranes but it acts as an allosteric activator of MGD1 (Dubots et al., 2010) and is the direct precursor for DAG of prokaryotic origin. A conformational change of the bilobal MGD1 enzyme may explain this allosteric effect, or alternatively, PA may induce protein dimerization. It is clear that PA plays a central role in the metabolism of lipids of photosynthetic membrane (Dubots et al., 2012).

THE DGDG SYNTHASES

In Arabidopsis, two genes coding for DGDG synthases have been identified and characterized (Dörmann et al., 1999; Kelly and Dörmann, 2002). DGD1 is responsible for the synthesis of the bulk of DGDG (>90%) in chloroplasts under normal growth conditions, whereas DGD2 only produces minor amounts of DGDG (Kelly et al., 2003). Only the part of MGDG with a eukaryotic signature is used by DGDG synthases to form DGDG. A *dgd1* mutant shows severe dwarfism and loss of photosynthesis efficiency (Dörmann et al., 1995), whereas *dgd2* mutants were much less affected (Kelly et al., 2003). Although the expression of both DGD1 and DGD2 is induced during phosphate deprivation, DGD2 seems to be the major enzyme to provide DGDG for the extraplastidial membranes (Härtel et al., 2000; Kelly and Dörmann, 2002). Both enzymes are localized to the OEM (Froehlich et al., 2001; Kelly et al., 2003), with their catalytic domains oriented to the cytosolic side, thus raising the question of the trafficking of their substrate MGDG synthesized in the IEM. DGD1 seems to use MGDG formed by MGD1 in the IEM whereas DGD2, under Pi shortage, preferably uses MGDG generated by MGD2/MGD3 in the OEM (Benning, 2009).

The catalytic domain of DGDG synthases is predicted to adopt a similar GT-B fold as MGD1. DGD1 has a unique feature that is not observed in DGD2. The catalytic domain is preceded by a large N-terminal region comprising about 330 amino acids. This domain does not contribute to the galactosyltransferase reaction but is required for insertion of DGD1 into the OEM (Froehlich et al., 2001). Very recently, the role of this N-terminal extension (N-DGD1), predicted all-α with coiled-coil domains, was addressed (Kelly et al., 2016). Using a series of chimeric constructs to complement a *dgd1* mutant, the authors demonstrated that N-DGD1 was essential for enabling galactolipid transfer between envelope membranes. Also, N-DGD1 mediates a PA-dependent membrane fusion *in vitro*. These data represent a breakthrough in our understanding of MGDG and DGDG trafficking between IEM and OEM. In the case of DGD2, it was proposed that the enzyme interacts with the membrane through its N-terminal domain, via interactions with negatively charged lipids (Szpryngiel et al., 2011), but also with part of its C-terminal domain which could act as a lipid sensing switch (Szpryngiel and Mäler, 2016).

Another pathway for DGDG synthesis is mediated by the GGGT, an enzyme that transfers a galactose from one molecule of MGDG to another MGDG with concomitant release of a DAG moiety (Moellering and Benning, 2011). However, it must be noted that DGDG produced is different with respect to the glycosidic linkage formed (ββ-DGDG instead of αβ-DGDG). Although the GGGT enzyme was found localized to the OEM, it does not contribute to the net synthesis of galactolipids in normal growth conditions and during Pi deprivation (Kelly et al., 2003). GGGT also demonstrates a processive activity leading to the formation of tri- and tetra-galactolipids. The role of GGGT has been enigmatic for many years. Recently, this GGGT was shown to be involved in freezing tolerance (Moellering et al., 2010). The GGGT encoding gene has been identified as SENSITIVE TO FREEZING 2 (SFR2) in Arabidopsis. SFR2 is not vital for normal growth and development but the freezing sensitivity of the *sfr2* mutant suggested that the enzyme was involved in lipid remodeling of chloroplast membranes. Changing the ratio of bilayer-/non-bilayer-forming lipids to favor the formation of lamellar bilayers is a mechanism to stabilize membranes during freezing stress. One can reasonably speculate a role of SFR2 as a sensor of biophysical and compositional changes in membranes, triggering lipid remodeling in response to abiotic stress.

ROLES OF GALACTOLIPIDS IN THE STRUCTURE AND BIOGENESIS OF THYLAKOIDS

The lipid composition of chloroplast membranes has been remarkably conserved through evolution from cyanobacteria to plants (Petroutsos et al., 2014). Particularly the MGDG/DGDG ratio appears to be highly stable (Boudière et al., 2014). The hypothesis of a specific contribution of galactolipids in the organization of thylakoid membranes as stacked flattened cisternae that can pile up to form grana was steadily addressed. This type of organization appears crucial to ensure enough density of photosystems to capture light energy. By reconstituting membranes made of natural thylakoid lipid extracts, it was found that the lipid mixture can self-organize as a membrane bilayer and can reversibly switch from the hexagonal II (HII) to the lamellar (Lα) phase (Demé et al., 2014). The transition can be fine-tuned by the lipid composition, particularly the MGDG/DGDG ratio, and hydration. These studies highlighted

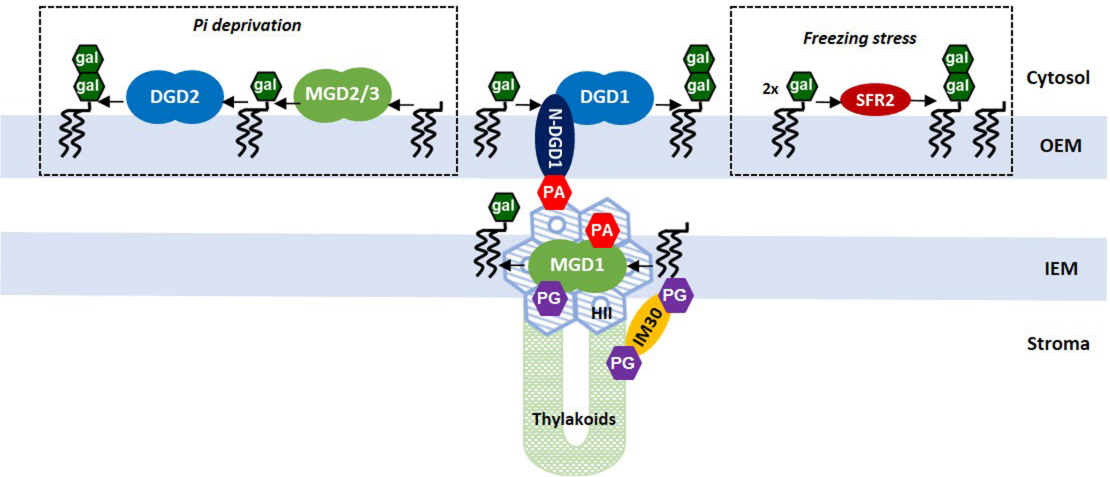

FIGURE 2 | Biosynthesis of galactolipids in the chloroplast envelope membranes in Arabidopsis. The three enzyme systems are represented. The main pathway is mediated by MGD1 and DGD1 which provide the bulk of galactolipids for all chloroplast membranes in normal growth conditions. MGD2/3 and DGD2 are activated in response to Pi deprivation, and SFR2 is activated in response to a freezing stress. Flux of galactolipids between IEM and OEM are facilitated by PA-mediated contacts with N-DGD1 (as proposed by Kelly et al., 2016). The MGD1-MGDG association in the IEM forms a HII platform that allows the transit of galactolipids to newly synthesized thylakoids through a non-lamellar/non-vesicular process (as proposed by Bastien et al., 2016). This process might involve other cellular partners such as the IM30/VIPP1 protein (Hennig et al., 2015). Can MGD1, inserted in a locally non-lamellar microdomain, have access on one side or the other side of the IEM, or even both, has yet to be determined.

the critical role of the bilayer-forming DGDG, described as a galactolipid zipper (Demé et al., 2014), in membrane stacking via hydrogen bonds between polar heads of adjacent bilayers. These interactions also contribute to balance the repulsive electrostatic effects of the anionic lipids PG and SQDG, thus favoring grana stacking (Demé et al., 2014; Kanduč et al., 2017). The biophysical properties of galactolipids could explain the conservation of thylakoid membrane composition throughout evolution.

Thylakoid biogenesis results in etioplasts from light activation of the cubic phase tubular structure of prolamellar bodies where a critical level of MGDG is required for the formation of the photoactive protochlorophyllide-LPOR-NADPH complex and its oligomerization (Fujii et al., 2017; Gabruk et al., 2017). Alternatively, in most types of plastids, thylakoid biogenesis results also from formation of *de novo* structures from the IEM. Different scenarios have been proposed for formation from IEM, including the budding of vesicles or flattened invaginations from the IEM and HII intermediate structures (Bastien et al., 2016). The unique localization of MGD1 in the IEM and the propensity of MGDG to self-organize in inverse micelles (HII) rather than in bilayers are important clues in the context of thylakoid biogenesis. A HII↔Lα phase transition triggered by subtle variations in the MGDG/DGDG ratio, as a result of favored or disfavored MGD1 binding to the IEM, can be a driving force that governs thylakoid membrane expansion. To support this assumption, membrane connections were observed between the IEM and thylakoids in the severe genetic background of *mgd1-2* mutant (Kobayashi et al., 2007), and in wild-type Arabidopsis plants treated with galvestin-1, an inhibitor of MGDG synthases (Botté et al., 2011). Based on these observations, a non-lamellar/non-vesicular model has been proposed in which the transit of lipids between the IEM and thylakoids operates, at least in the early stage of thylakoid biogenesis, through HII regions enriched in MGD1-MGDG (Bastien et al., 2016). This model does not exclude the contribution of other cellular partners such as IM30/VIPP1, a protein triggering membrane fusion in chloroplasts, and which was shown to bind to anionic lipids (i.e., PG and SQDG) (Hennig et al., 2015).

This review highlights the unique and irreplaceable roles of MGDG and DGDG, which have very contrasted biophysical properties, in the biogenesis and architecture of chloroplast membranes. **Figure 2** gives an overview of our current knowledge on galactolipid synthases, particularly their localization in the chloroplast envelope, and highlights the central roles of MGD1 and DGD1 in regulating the flux of galactolipids between IEM and OEM, and between IEM and thylakoid membranes. The fine-tuning of these enzymes, by controlling HII↔Lα phase transitions, appears important for nascent thylakoid development, for membrane–membrane interactions and the development of flattened cisternae. This also raises the major but still unresolved question of the coexistence of HII+Lα phases. In particular, the location and regulation of MGDG-rich HII regions, required for the functional violaxanthin/asthaxanthin cycle (Goss et al., 2017), and the relation with domains containing the photosystems, is clearly a major puzzling question for the future.

AUTHOR CONTRIBUTIONS

The subject was the result of a fruitful collaboration involving all co-authors. JR, MN, AG-E, JJ, EM, MB, and CB agreed to contribute this review and participated in delineating the content of the topic, and in the writing and preparation of figures.

ACKNOWLEDGMENTS

The authors were supported by the French National Research Agency (ANR-10-Blan-1524 ReGal, ANR-13-ADAP-0008 Reglisse, ANR-13-BSV8-0011, and ANR-10-LABEX-04 GRAL Grenoble Alliance for Integrated Structural Cell Biology); Grenoble Alpes (AGIR 2015); and Communauté Université Grenoble Alpes (Cross-Disciplinary project Glyco@Alps).

REFERENCES

Albesa-Jové, D., and Guerin, M. E. (2016). The conformational plasticity of glycosyltransferases. *Curr. Opin. Struct. Biol.* 40, 23–32. doi: 10.1016/j.sbi.2016.07.007

Andersson, M. X., Larsson, K. E., Tjellstrom, H., Liljenberg, C., and Sandelius, A. S. (2005). The plasma membrane and the tonoplast as major targets for phospholipid-to-glycolipid replacement and stimulation of phospholipases in the plasma membrane. *J. Biol. Chem.* 280, 27578–27586. doi: 10.1074/jbc.M503273200

Awai, K. (2016). "Thylakoid development and galactolipid synthesis in cyanobacteria," in *Lipids in Plant and Algae Development: Subcellular Biochemistry*, Vol. 86, eds Y. Nakamura and Y. Li-Beisson (Cham: Springer), 85–101. doi: 10.1007/978-3-319-25979-6_4

Awai, K., Kakimoto, T., Awai, C., Kaneko, T., Nakamura, Y., Takamiya, K., et al. (2006). Comparative genomic analysis revealed a gene for monoglucosyldiacylglycerol synthase, an enzyme for photosynthetic membrane lipid synthesis in cyanobacteria. *Plant Physiol.* 141, 1120–1127. doi: 10.1104/pp.106.082859

Awai, K., Maréchal, E., Block, M. A., Brun, D., Masuda, T., Shimada, H., et al. (2001). Two types of MGDG synthase genes, found widely in both 16:3 and 18:3 plants, differentially mediate galactolipid syntheses in photosynthetic and nonphotosynthetic tissues in *Arabidopsis thaliana*. *Proc. Natl. Acad. Sci. U.S.A.* 98, 10960–10965. doi: 10.1073/pnas.181331498

Awai, K., Ohta, H., and Sato, N. (2014). Oxygenic photosynthesis without Galactolipids. *Proc. Natl. Acad. Sci. U.S.A.* 111, 13571–13575. doi: 10.1073/pnas.1403708111

Awai, K., Watanabe, H., Benning, C., and Nishida, I. (2007). Digalactosyldiacylglycerol is required for better photosynthetic growth of *Synechocystis* sp. PCC6803 under phosphate limitation. *Plant Cell Physiol.* 48, 1517–1523. doi: 10.1093/pcp/pcm134

Bastien, O., Botella, C., Chevalier, F., Block, M. A., Jouhet, J., Breton, C., et al. (2016). New insights on thylakoid biogenesis in plant cells. *Int. Rev. Cell Mol. Biol.* 323, 1–30. doi: 10.1016/bs.ircmb.2015.12.001

Benning, C. (2009). Mechanisms of lipid transport involved in organelle biogenesis in plant cells. *Annu. Rev. Cell Dev. Biol.* 25, 71–91. doi: 10.1146/annurev.cellbio.042308.113414

Block, M. A., Dorne, A.-J., Joyard, J., and Douce, R. (1983). Preparation and characterization of membrane fractions enriched in outer and inner envelope membranes from spinach chloroplasts. 2. Biochemical characterization. *J. Biol. Chem.* 258, 3281–3286.

Botté, C. Y., Deligny, M., Roccia, A., Bonneau, A. L., Saïdani, N., Hardré, H., et al. (2011). Chemical inhibitors of monogalactosyldiacylglycerol synthases in *Arabidopsis thaliana*. *Nat. Chem. Biol.* 7, 834–842. doi: 10.1038/nchembio.658

Boudière, L., Michaud, M., Petroutsos, D., Rébeillé, F., Falconet, D., Bastien, O., et al. (2014). Glycerolipids in photosynthesis: composition, synthesis and trafficking. *Biochim. Biophys. Acta* 1837, 470–480. doi: 10.1016/j.bbabio.2013.09.007

Breton, C., Fournel-Gigleux, S., and Palcic, M. M. (2012). Recent structures, evolution and mechanisms of glycosyltransferases. *Curr. Opin. Struct. Biol.* 22, 540–549. doi: 10.1016/j.sbi.2012.06.007

Browse, J., Warwick, N., Somerville, C. R., and Slack, C. R. (1986). Fluxes through the prokaryotic and eukaryotic pathways of lipid synthesis in the 16-3 plant *Arabidopsis thaliana*. *Biochem. J.* 235, 25–31. doi: 10.1042/bj2350025

Coves, J., Joyard, J., and Douce, R. (1988). Lipid requirement and kinetic studies of solubilized UDP-galactose:diacylglycerol galactosyltransferase activity from spinach chloroplast envelope membranes. *Proc. Natl. Acad. Sci. U.S.A.* 85, 4966–4970. doi: 10.1073/pnas.85.14.4966

Demé, B., Cataye, C., Block, M. A., Maréchal, E., and Jouhet, J. (2014). Contribution of galactoglycerolipids to the 3-dimensional architecture of thylakoids. *FASEB J.* 28, 3373–3383. doi: 10.1096/fj.13-247395

Dörmann, P., Balbo, I., and Benning, C. (1999). *Arabidopsis* galactolipid biosynthesis and lipid trafficking mediated by DGD1. *Science* 284, 2181–2184. doi: 10.1126/science.284.5423.2181

Dörmann, P., and Benning, C. (2002). Galactolipids rule in seed plants. *Trends Plant Sci.* 7, 112–118. doi: 10.1016/S1360-1385(01)02216-6

Dörmann, P., Hoffmann-Benning, S., Balbo, I., and Benning, C. (1995). Isolation and characterization of an Arabidopsis mutant deficient in the thylakoid lipid digalactosyl diacylglycerol. *Plant Cell* 7, 1801–1810. doi: 10.1105/tpc.7.11.1801

Dubots, E., Audry, M., Yamaryo, Y., Bastien, O., Ohta, H., Breton, C., et al. (2010). Activation of the chloroplast monogalactosyldiacylglycerol synthase MGD1 by phosphatidic acid and phosphatidylglycerol. *J. Biol. Chem.* 285, 6003–6011. doi: 10.1074/jbc.M109.071928

Dubots, E., Botté, C., Boudière, L., Yamaryo-Botté, Y., Jouhet, J., Maréchal, E., et al. (2012). Role of phosphatidic acid in plant galactolipid synthesis. *Biochimie* 94, 86–93. doi: 10.1016/j.biochi.2011.03.012

Froehlich, J. E., Benning, C., and Dörmann, P. (2001). The digalactosyldiacylglycerol (DGDG) synthase DGD1 is inserted into the outer envelope membrane of chloroplasts in a manner independent of the general import pathway and does not depend on direct interaction with monogalactosyldiacylglycerol synthase for DGDG biosynthesis. *J. Biol. Chem.* 276, 31806–31812. doi: 10.1074/jbc.M104652200

Fujii, S., Kobayashi, K., Nagata, N., Masuda, T., and Wada, H. (2017). Monogalactosyldiacylglycerol facilitates synthesis of photoactive protochlorophyllide in etioplasts. *Plant Physiol.* 174, 2183–2198. doi: 10.1104/pp.17.00304

Gabruk, M., Mysliwa-Kurdziel, B., and Kruk, J. (2017). MGDG, PG and SQDG regulate the activity of light-dependent protochlorophyllide oxidoreductase. *Biochem. J.* 474, 1307–1320. doi: 10.1042/BCJ20170047

Goss, R., Greifenhagen, A., Bergner, J., Volke, D., Hoffmann, R., Wilhelm, C., et al. (2017). Direct isolation of a functional violaxanthin cycle domain from thylakoid membranes of higher plants. *Planta* 245, 793–806. doi: 10.1007/s00425-016-2645-9

Härtel, H., Dörmann, P., and Benning, C. (2000). DGD1-independent biosynthesis of extraplastidic galactolipids after phosphate deprivation in *Arabidopsis*. *Proc. Natl. Acad. Sci. U.S.A.* 97, 10649–10654. doi: 10.1073/pnas.180320497

Hashimoto, K., Madej, T., Bryant, S. H., and Panchenko, A. R. (2010). Functional states of homooligomers: insights from the evolution of glycosyltransferases. *J. Mol. Biol.* 399, 196–206. doi: 10.1016/j.jmb.2010.03.059

Hennig, R., Heidrich, J., Saur, M., Schmüser, L., Roeters, S. J., Hellmann, N., et al. (2015). IM30 triggers membrane fusion in cyanobacteria and chloroplasts. *Nat. Commun.* 6:7018. doi: 10.1038/ncomms8018

Jones, M. R. (2007). Lipids in photosynthetic reaction centres: structural roles and functional holes. *Prog. Lipid Res.* 46, 56–87. doi: 10.1016/j.plipres.2006.06.001

Jouhet, J., Maréchal, E., Baldan, B., Bligny, R., Joyard, J., and Block, M. A. (2004). Phosphate deprivation induces transfer of DGDG galactolipid from chloroplast to mitochondria. *J. Cell Biol.* 167, 863–874. doi: 10.1083/jcb.200407022

Kanduč, M., Schlaich, A., de Vries, A. H., Jouhet, J., Maréchal, E., Demé, B., et al. (2017). Tight cohesion between glycolipid membranes results from balanced water-headgroup interactions. *Nat. Commun.* 8:14899. doi: 10.1038/ncomms14899

Kelly, A. A., and Dörmann, P. (2002). *DGD2*, an *Arabidopsis* gene encoding a UDP-galactose-dependent digalactosyldiacylglycerol synthase is expressed during growth under phosphate-limiting conditions. *J. Biol. Chem.* 277, 1166–1173. doi: 10.1074/jbc.M110066200

Kelly, A. A., Froehlich, J. E., and Dormann, P. (2003). Disruption of the two digalactosyldiacylglycerol synthase genes *DGD1* and *DGD2* in Arabidopsis

reveals the existence of an additional enzyme of galactolipid synthesis. *Plant Cell* 15, 2694–2706. doi: 10.1105/tpc.016675

Kelly, A. A., Kalisch, B., Hölzl, G., Schulze, S., Thiele, J., Melzer, M., et al. (2016). Synthesis and transfer of galactolipids in the chloroplast envelope membranes of *Arabidopsis thaliana*. *Proc. Natl. Acad. Sci. U.S.A.* 113, 10714–10719. doi: 10.1073/pnas.1609184113

Kobayashi, K. (2016). Role of membrane glycerolipids in photosynthesis, thylakoid biogenesis and chloroplast development. *J. Plant Res.* 129, 565–580. doi: 10.1007/s10265-016-0827-y

Kobayashi, K., Awai, K., Nakamura, M., Nagatani, A., Masuda, T., and Ohta, H. (2009). Type-B monogalactosyldiacylglycerol synthases are involved in phosphate starvation-induced lipid remodeling, and are crucial for low-phosphate adaptation. *Plant J.* 57, 322–331. doi: 10.1111/j.1365-313X.2008.03692.x

Kobayashi, K., Kondo, M., Fukuda, H., Nishimura, M., and Ohta, H. (2007). Galactolipid synthesis in chloroplast inner envelope is essential for proper thylakoid biogenesis, photosynthesis, and embryogenesis. *Proc. Natl. Acad. Sci. U.S.A.* 104, 17216–17221. doi: 10.1073/pnas.0704680104

Li, C., Wang, Y., Liu, L., Hu, Y., Zhang, F., Mergen, S., et al. (2011). A rice plastidial nucleotide sugar epimerase is involved in galactolipid biosynthesis and improves photosynthetic efficiency. *PLOS Genet.* 7:e1002196. doi: 10.1371/journal.pgen.1002196

Maréchal, E., Block, M. A., Joyard, J., and Douce, R. (1994a). Comparison of the kinetic properties of MGDG synthase in mixed micelles and in envelope membranes from spinach chloroplast. *FEBS Lett.* 352, 307–310.

Maréchal, E., Block, M. A., Joyard, J., and Douce, R. (1994b). Kinetic properties of monogalactosyldiacylglycerol synthase from spinach chloroplast envelope membranes. *J. Biol. Chem.* 269, 5788–5798.

Miège, C., Maréchal, E., Shimojima, M., Awai, K., Block, M. A., Ohta, H., et al. (1999). Biochemical and topological properties of type A MGDG synthase, a spinach chloroplast envelope enzyme catalyzing the synthesis of both prokaryotic and eukaryotic MGDG. *Eur. J. Biochem.* 265, 990–1001. doi: 10.1046/j.1432-1327.1999.00801.x

Mizusawa, N., and Wada, H. (2012). The role of lipids in photosystem II. *Biochim. Biophys. Acta* 1817, 194–208. doi: 10.1016/j.bbabio.2011.04.008

Moellering, E. R., and Benning, C. (2011). Galactoglycerolipid metabolism under stress: a time for remodeling. *Trends Plant Sci.* 16, 98–107. doi: 10.1016/j.tplants.2010.11.004

Moellering, E. R., Muthan, B., and Benning, C. (2010). Freezing tolerance in plants requires lipid remodeling at the outer chloroplast membrane. *Science* 330, 226–228. doi: 10.1126/science.1191803

Petroutsos, D., Amiar, S., Abida, H., Dolch, L. J., Bastien, O., Rébeillé, F., et al. (2014). Evolution of galactoglycerolipid biosynthetic pathways–from cyanobacteria to primary plastids and from primary to secondary plastids. *Prog. Lipid Res.* 54, 68–85. doi: 10.1016/j.plipres.2014.02.001

Rocha, J., Audry, M., Pesce, G., Chazalet, V., Block, M. A., Maréchal, E., et al. (2013). Revisiting the expression and purification of MGD1, the major galactolipid synthase in Arabidopsis to establish a novel standard for biochemical and structural studies. *Biochimie* 95, 700–708. doi: 10.1016/j.biochi.2012.11.011

Rocha, J., Sarkis, J., Thomas, A., Pitou, L., Radzimanowski, J., Audry, M., et al. (2016). Structural insights and membrane binding properties of MGD1, the major galactolipid synthase in plants. *Plant J.* 85, 622–633. doi: 10.1111/tpj.13129

Sakurai, I., Mizusawa, N., Wada, H., and Sato, N. (2007). Digalactosyldiacylglycerol is required for stabilization of the oxygen-evolving complex in photosystem II. *Plant Physiol.* 145, 1361–1370. doi: 10.1104/pp.107.106781

Sarkis, J., Rocha, J., Maniti, O., Jouhet, J., Vie, V., Block, M. A., et al. (2014). The influence of lipids on MGD1 membrane binding highlights novel mechanisms for galactolipid biosynthesis regulation in chloroplasts. *FASEB J.* 28, 3114–3123. doi: 10.1096/fj.14-250415

Shimojima, M., Ohta, H., Iwamatsu, A., Masuda, T., Shioi, Y., and Takamiya, K. (1997). Cloning of the gene for monogalactosyldiacylglycerol synthase and its evolutionary origin. *Proc. Natl. Acad. Sci. U.S.A.* 94, 333–337. doi: 10.1073/pnas.94.1.333

Siebertz, H. P., Heinz, E., Linscheid, M., Joyard, J., and Douce, R. (1979). Characterization of lipids from chloroplast envelopes. *Eur. J. Biochem.* 101, 429–438. doi: 10.1111/j.1432-1033.1979.tb19736.x

Szpryngiel, S., Ge, C., Iakovleva, I., Georgiev, A., Lind, J., Wieslander, A., et al. (2011). Lipid interacting regions in phosphate stress glycosyltransferase atDGD2 from *Arabidopsis thaliana*. *Biochemistry* 50, 4451–4466. doi: 10.1021/bi200162f

Szpryngiel, S., and Mäler, L. (2016). Insights into the membrane interacting properties of the C-terminal domain of the monotopic glycosyltransferase DGD2 in *Arabidopsis thaliana*. *Biochemistry* 55, 6776–6786. doi: 10.1021/acs.biochem.6b00559

Vojta, L., Soll, J., and Bölter, B. (2007). Protein transport in chloroplasts - targeting to the intermembrane space. *FEBS J.* 274, 5043–5054. doi: 10.1111/j.1742-4658.2007.06023.x

Xu, C., Fan, J., Froehlich, J. E., Awai, K., and Benning, C. (2005). Mutation of the TGD1 chloroplast envelope protein affects phosphatidate metabolism in *Arabidopsis*. *Plant Cell* 17, 3094–3110. doi: 10.1105/tpc.105.035592

Yuzawa, Y., Nishihara, H., Haraguchi, T., Masuda, S., Shimojima, M., Shimoyama, A., et al. (2012). Phylogeny of galactolipid synthase homologs together with their enzymatic analyses revealed a possible origin and divergence time for photosynthetic membrane biogenesis. *DNA Res.* 19, 91–102. doi: 10.1093/dnares/dsr044

Conflict of Interest Statement: The authors declare that the research was conducted in the absence of any commercial or financial relationships that could be construed as a potential conflict of interest.

frontiers in Plant Science

MINI REVIEW
published: 20 March 2018
doi: 10.3389/fpls.2018.00357

Structure and Function of the Photosystem Supercomplexes

*Jinlan Gao[1], Hao Wang[2], Qipeng Yuan[2] and Yue Feng[2]**

[1] State Key Laboratory of Plant Genomics, Institute of Microbiology, Chinese Academy of Sciences, Beijing, China,
[2] College of Life Science and Technology, Beijing University of Chemical Technology, Beijing, China

Photosynthesis converts solar energy into chemical energy to sustain all life on earth by providing oxygen and food, and controlling the atmospheric carbon dioxide. During this process, the water-splitting and oxygen-evolving reaction is catalyzed by photosystem II (PSII), while photosystem I (PSI) generates the reducing power for the reduction of $NADP^+$ to NADPH. Together with their peripheral light-harvesting complexes (LHCs), photosystems function as multisubunit supercomplexes located in the thylakoid membranes of cyanobacteria, algae, and plants. Recent advances in single-particle cryo-electron microscopy (cryoEM), X-ray free electron laser (XFEL) and other techniques have revealed unprecedented structural and catalytic details concerning the two supercomplexes. Several high-resolution structures of the complexes from plants were solved, and serial time-resolved crystallography and "radiation-damage-free" femtosecond XFEL also provided important insights into the mechanism of water oxidation. Here, we review these exciting advances in the studies of the photosystem supercomplexes with an emphasis on PSII-LHCII, propose presently unresolved problems in this field, and suggest potential tendencies for future studies.

Keywords: chloroplast, photosynthesis, structure, photosystem II protein complex, protein complex

OPEN ACCESS

Edited by:
Juliette Jouhet, UMR5168 Laboratoire de Physiologie Cellulaire Vegetale (LPCV), France

Reviewed by:
Stefano Santabarbara, Consiglio Nazionale delle Ricerche (CNR), Italy
Luning Liu, University of Liverpool, United Kingdom

****Correspondence:***
Yue Feng
fengyue@mail.buct.edu.cn;
forest66318@163.com

Specialty section:
This article was submitted to Plant Physiology, a section of the journal Frontiers in Plant Science

Received: *31 October 2017*
Accepted: *02 March 2018*
Published: *20 March 2018*

Citation:
Gao J, Wang H, Yuan Q and Feng Y (2018) Structure and Function of the Photosystem Supercomplexes. Front. Plant Sci. 9:357. doi: 10.3389/fpls.2018.00357

INTRODUCTION

Photosynthesis carries out a series of biophysical and biochemical processes, finally converting solar energy into chemical energy. Oxygenic photosynthesis split water molecules to oxygen, which is indispensable for maintaining aerobic life on earth (Dismukes et al., 2001). It is believed that photosynthesis has evolved only once during the evolution history in cyanobacteria. For algae and higher plants, they acquired photosynthesis capacity via cyanobacteria endosymbionts which evolved to chloroplasts in plants (Tomioka and Sugiura, 1983). Plant leaves are the major organs of photosynthesis with about 100 chloroplasts in each mesophyll cell (Woodson, 2016). Due to their essential roles in light harvesting and energy production, chloroplasts are vital organelles of photosynthetic cells in algae and higher plants, acting as the suppliers of carbon sources and energy. Chloroplast is a large organelle with a complex structure harboring two outer membranes called the chloroplast envelope and a third extensively folded internal membrane system called thylakoid (Arvidsson and Sundby, 1999; Kirchhoff, 2013). The thylakoid membrane is composed of two morphologically distinct domains, the grana domain which is characterized by ~5–20 layers of cylindrical stacks of thylakoid membrane disks (Mullineaux, 2005; Mustárdy et al., 2008), and the stroma lamellae domain which are stroma-exposed membrane pairs connecting the grana stacks (Dekker and Boekema, 2005).

There are two types of photosystems in cyanobacteria, algae and higher plants, called photosystem I (PSI, plastocyanin-ferredoxin oxidoreductase) and photosystem II (PSII, water-plastoquinone oxidoreductase), both of which are multisubunit membrane complexes. The PSI is located in the stroma lamella of thylakoid while the PSII is in the stacked grana domain (Albertsson, 2001; Dekker and Boekema, 2005). Each photosystem is composed of a core complex and a peripheral antenna system, light harvesting complex I (LHCI) for PSI and light harvesting complex II (LHCII) for PSII, respectively. Recently, new atom-resolution structures of the photosystems and detailed insights into the water-splitting process have been reported, with the development of single-particle cryo-electron microscopy, serial time-resolved crystallography and other techniques. Here, we will review the recent progress in the studies into the structures and functions of photosystems of different origins, with an emphasis on PSII-LHCII.

BIOCHEMISTRY OF PHOTOSYSTEMS

The complete photosynthetic reactions in cyanobacteria, algae and plants are executed by four major protein supercomplexes including PSI, PSII, cytochrome b_6f (plastoquinone-plastocyanin oxidoreductase) and F-ATPase (proton-motive force-driven ATP synthase) (Nelson and Benshem, 2004; Nelson and Yocum, 2006). Both PSI and PSII supercomplexes bind chlorophyll molecules to sense different spectrums and intensities of light (Remelli et al., 1999; Nelson and Yocum, 2006; Croce and van Amerongen, 2013; van Amerongen and Croce, 2013; Caffarri et al., 2014; Ruban, 2015). Light harvested by the chlorophylls and other pigments in PSI and PSII is transferred to the photosynthetic reaction center (RC), further inducing the excitation of chlorophylls known as P680 for PSII and P700 for PSI to initiate the proton translocation across the membrane (Nelson and Junge, 2015). In PSII, P680 undergoes charge separation and the generated electrons are transferred to the quinone acceptor pheophytin and plastoquinone sequentially (Grabolle and Dau, 2005; Johnson, 2016). Meanwhile, water molecule, the authentic electron donor, is oxidized to molecular oxygen and P680 is eventually reduced. After the reaction, the electrons are ultimately transferred to the thylakoid-embedded cytochrome b_6f, which oxidizes plastoquinols to plastoquinones and reduces plastocyanins (Cramer et al., 1996). And then, the plastocyanin is oxidized by PSI, during which the reduced electron carrier protein ferredoxin, is used to reduce $NADP^+$ to NADPH by ferredoxin–$NADP^+$ reductase (FNR) enzyme (Brettel and Leibl, 2001; Sétif, 2001; Golbeck, 2006). Together, PSII generates the most positive redox potential, while PSI generates the powerful naturally occurring reductant NADPH (Hope, 2000; Holzwarth et al., 2006; Nelson, 2011). The photocatalytic activity of PSII and PSI is linked by the cytochrome b_6f complex, and the proton-motive force generated during the process are utilized by the F-ATPase to generate ATP, which together with NADPH are supplied as energy compounds for sugar synthesis from carbon dioxide by the dark reaction (Pfannschmidt, 2003).

The first PSI structure from the thermophilic cyanobacterium *Synechococcus elongatus* (*S. elongatus*) displayed a complex with 12 protein subunits and 127 cofactors (96 chlorophylls, 22 carotenoids, 2 phylloquinones, 3 Fe_4S_4 clusters, and 4 lipids), providing the very first detailed molecular architecture of PSI (Fromme et al., 2001; Jordan et al., 2001). *S. elongatus* PSI is a trimer with a diameter of 210 Å and a maximum height of 90 Å (Jordan et al., 2001), while the plant PSI supercomplex is a monomer (Ben-Shem et al., 2003). The core complex is largely conserved from cyanobacteria to plants with nine membrane-embedded subunits, whereas the LHCI complexes are variable in subunit composition, binding pigments and sizes due to the different habitats of cyanobacteria, algae, and plants (Ben-Shem et al., 2003; Qin et al., 2015). However, although PSI and PSII evolved from the same ancestor, belonging to the same superfamily, their structures are largely different.

STRUCTURE OF THE CYANOBACTERIAL PSII SUPERCOMPLEX

The PS II homodimer from *Thermosynechococcus elongatus* (*T. elongatus*) has dimensions of 105 Å in depth (45 Å in membrane), 205 Å in length, and 110 Å in width (Ferreira et al., 2004). The PSII supercomplex in cyanobacteria comprises the reaction center (RC) proteins D1 and D2, the antenna subunits CP47 and CP43, 13 membrane-intrinsic small subunits (PsbE, PsbF, PsbH-M, PsbN, PsbX, PsbY, PsbZ, and PsbYcf12) and 3 extrinsic subunits (PsbO, PsbU, and PsbV). The structures of D1 and D2 are similar to each other, both containing five helices all tilted against the membrane planes (Zouni et al., 2001; Kamiya and Shen, 2003), and they form the center of the PSII complex. CP43 and CP47 surround the D1-D2 core with similar structures of six helices, respectively. Afterward, Loll et al. (2005) provided the first complete structure of cyanobacterial photosystem II, providing a full glimpse of the PSII cofactors. They displayed the positions of 20 protein subunits and their interactions with 77 cofactors (**Figure 1A**). The overall structures of the supercomplex and protein subunits are similar to those previously reported (Zouni et al., 2001; Kamiya and Shen, 2003; Biesiadka et al., 2004). Lipids have long been thought to play a role in the assembly and function of PSII, and for the first time the authors showed the lipid integrally bound to PSII. Eleven lipids surrounding the RC form a belt to separate it from the antenna and small protein subunits, while the remaining lipids are mostly located at the monomer-monomer interface. The lipid-rich property renders PSII both structural flexibility for local mobility and convenience in subunit-subunit recognition (Guskov et al., 2009). Eleven carotenoid molecules were modeled as β-carotenes in all-trans configurations in their study and an additional Car15 was identified in the study by Guskov et al. (2009). In the study by Guskov et al. (2009), they also successfully assigned the small protein subunits Psbycf12, PsbY, and PsbX to the previously unassigned positions (Loll et al., 2005; Guskov et al., 2009). A summary of the subunit composition information, including the subunit-cofactor interactions in PSII from *T. elongatus*, is presented in **Table 1** (Guskov et al., 2009). In 2009, Broser

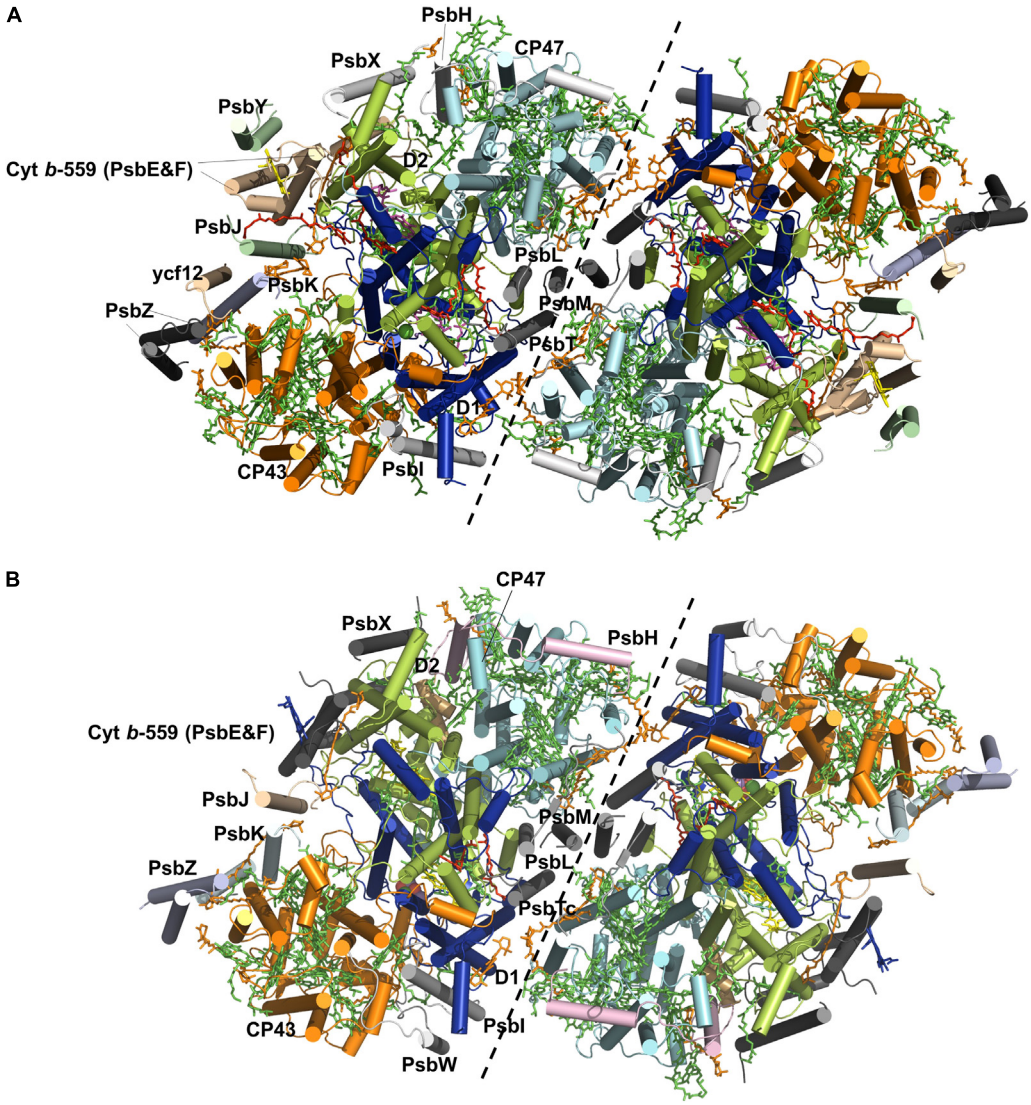

FIGURE 1 | Overall structures of the PSII core complex from *Tynechococcus elongatus* **(A)** and spinach **(B)**. The monomer-monomer interface is indicated by a black dashed line. Only the four large subunits and the intrinsic subunits of PSIIs are shown. The subunits D1 (blue), D2 (lime), CP43 (yellow), and CP47 (cyan) and the other small subunits are labeled in the monomer on the left. Cofactors are shown in sticks, including Chl (green), Car (orange), heme (light magenta) and lipids (red). The Mn cluster is shown in spheres.

et al. presented the first structure of a monomeric form of PSII core complex (PSIIcc) with high oxygen-evolution capacity from *T. elongatus* (Broser et al., 2010). The assembly of the protein subunits, tetrapyrrole cofactors and the non-heme iron in the monomeric PSIIcc are all identical to those in the dimer structure.

During photosynthesis, water oxidation happens in the oxygen-evolving complex (OEC), which comprises the Mn_4CaO_5 cluster as the catalytic center. Water splitting is a process fulfilled in five consecutive stages named S_0 to S_4. It has been a model system for synthesizing catalysts for inorganic water oxidation and dioxygen evolution (Kanady and Agapie, 2011; Mukherjee et al., 2012). In the work of Ferreira et al. (2004), they reported that the OEC harbors a "cubane-like" Mn_3CaO_4 cluster linked to a fourth Mn by a mono-μ-oxo bridge which had not been specifically suggested before. However, neither water nor hydroxide could be observed to find the water oxidation site accurately in their study. In the first complete PSII structure, the Mn_4Ca cluster was proposed as a "Y-shaped hook," considerably differed from the "cubane-like" model (Loll et al., 2005). Then a 1.9-Å resolution X-ray structure of PSII from *T. vulcanus* revealed a clear picture of the Mn_4CaO_5 cluster, in which the electron densities for each metal ion and the oxo-bridged oxygen atoms were totally separated, thus allowing the clear assignment of each of the atoms. They found that the OEC Mn_4CaO_5 cluster displayed a "distorted chair" conformation with three Mn, one Ca and four oxygen atoms forming an asymmetric cubane-like seat base and the fourth Mn (Mn_4) together with the fifth oxygen atom (O_4) forming the chair back (Umena et al., 2011).

TABLE 1 | Transmembrane (TM) helices, chlorophylls, and other cofactors of PSII RCs from cyanobacteria and plants[1].

Subunits	TM helices		Chlorophylls		Other cofactors in plant PSII RC			
	Cyano	Plant	Cyano	Plant	Carotenoid	Heme	Lipid	Others
A (D1)	5	5	4	6[2]	1		3	1 Mn_4CaO_5
B (CP47)	6	6	16	16	3		2	
C (CP43)	6	6	13	13	3		4	
D (D2)	5	5	4	2	1		4	1 plastoquinone
E	1	1				1[3]		
F	1	1						
H	1	1			1		1	
I	1	1						
J	1	1						
K	1	1			1			
L	1	1					1	
M	1	1						
O	0	0						
P		0						
Q		0						
T	1							
U	0							
V	0							
W		1						
Tc		1						
Tn		0						
X	1	1						
Y	1							
Z	1	2					1	
Ycf12	1							

[1] *The subunit composition and the number of TM helices are based on the structures of PSIIs from Tynechococcus elongatus and spinach (Guskov et al., 2009; Wei et al., 2016).* [2] *These include 4 Chl a and 2 pheophytin.* [3] *This heme is bound by both PsbE and PsbF.*

Subsequently, a simultaneous femtosecond X-ray spectroscopy and diffraction of the PSII system showed that the electron density maps of the dark and illuminated states are similar with an overall correlation coefficient (CC) of 0.77 (a CC of 0 means no correlation; a CC of 1 indicates full correlation), suggesting no significant conformational changes between the S_1 and S_2 states (Kern et al., 2013). However, with a serial time-resolved crystallography, the authors acquired PSII structures in the dark S_1 and putative S_3 states, in which they found that the distance between the Mn_3O_xCa cubane and the distant protruding Mn (dangler Mn) increased in the putative S_3 state, allowing the binding of the second water molecule during the S_2 to S_3 state transition (Kupitz et al., 2014). Moreover, with a "radiation-damage-free" femtosecond X-ray free electron laser (XFEL), Suga et al. (2015, 2017) found that the Mn-Mn and Mn-O distances showed marked differences in the OEC from XFEL: all the distances are about 0.1–0.2 Å shorter than those from the X-ray diffraction (XRD) structures. In addition, the position of O5 is also unusual. The results showed that it functions more as a hydroxide ion instead of a normal oxygen dianion to serve as one of the substrate oxygen atoms (Suga et al., 2015). Their recent work described the light-induced structural changes in PSII by two-flash illumination, modeled a sixth oxygen atom (O6) close to O5, and provided important implications for the O=O bond formation mechanism (Suga et al., 2017). Furthermore, it was reported that the chloride ion is essential for oxygen evolution, and there are two anion binding sites positioned on the two sides of the MnCa cluster with the same distance from the cluster to stabilize its structure (Kawakami et al., 2009).

STRUCTURE OF THE PLANT PSII SUPERCOMPLEX

Plant PSII has a similar overall structure of a dimeric supercomplex as cyanobacterial PSII. The first structure of plant PSII-LHCII complex from spinach was obtained 17 years ago at 17 Å (Nield et al., 2000), and recently a 3.2 Å spinach C_2S_2-type (C: PSII core complex; S: strongly associated LHCII trimer) supercomplex structure was reported with the development of single-particle cryo-electron microscopy techniques (Wei et al., 2016) (**Figure 1B**). More recently, structure of the dominant type of supercomplex in plants, the $C_2S_2M_2$-type (M: moderately bound LHCIIs) was also solved at 2.7 and 3.2 Å for the stacked and unstacked forms from *Pisum sativum* (pea), and at 5.3 Å from *Arabidopsis thaliana*, respectively (Su et al., 2017; van Bezouwen et al., 2017). Compared to the structure of the spinach C_2S_2-type supercomplex, the structure reported by Su et al. (2017)

was determined under more physiological conditions, containing three light-harvesting complex (LHC) monomers (CP29, CP26, and CP24) and two trimers (S-LHCII and M-LHCII) per core. In contrast, CP24 and M-LHCII are missing in the previous structure of Wei et al. (2016). The plant PSII indeed exhibits the same composition and organizations of the subunits and cofactors as their cyanobacterial counterparts (**Table 1**). The catalytic center within the core complex is composed of four largest membrane intrinsic subunits PsbA (D1), PsbB (CP47), PsbC (CP43), and PsbD (D2). Specifically, D1 and D2 form the photochemical RC, which is responsible for the charge separation and electron transfer, and CP47 and CP43 act as internal antenna proteins involved in light harvesting and energy transportation from peripheral antenna to the RC. In the core complex, there are also 12 low molecular-mass (MM) membrane-spanning subunits surrounding the reaction center, forming a belt-like structure. In the spinach PSII-LHCII complex, these subunits are PsbE, PsbF, PsbH-M, PsbTc, PsbW, PsbX, and PsbZ. Most of these subunits are structurally conserved with a single transmembrane helix except PsbZ with two helices. These subunits are essential for both the dimerization and stabilization of the core complex and the association between the core complex and the peripheral antenna complex. In addition, they bind cytochrome *b*-559 to protect the PSII complex from photo-damage. Three extrinsic subunits PsbO, PsbP, and PsbQ constitute the OEC, which also encompasses the luminal domain of CP43 and the C-terminal domain of D1, shielding the water splitting machinery. Among them, PsbO stabilizes the Mn complex while PsbP and PsbQ are involved in optimizing the oxygen evolution at physical concentration of calcium and chloride ions. Structure comparison also revealed that the flexible regions of these subunits experience significant conformational changes when they bind to the core complex (Wei et al., 2016). Outside the core complex is the LHCII, the structure of which in the PSII supercomplex is almost the same as the pea LHCII complex (Standfuss et al., 2005).

Plant LHCII occupies about 30% of total proteins in the chloroplast membrane, therefore representing the most abundant membrane protein on earth (Peter and Thornber, 1991; Standfuss et al., 2005). LHCII acts as a heterotrimer constituted by Lhcb1, Lhcb2, and Lhcb3. Each polypeptide spans the thylakoid membrane three times with its C terminus positioned on the luminal side (Kuhlbrandt et al., 1994). The LHCII complex is vital for both photosynthesis and chloroplast grana formation. For the first function, the LHCII heterotrimers are linked to the photosystem core complex by the minor antenna subunits Lhcb4 (CP29), Lhcb5 (CP26), and Lhcb6 (CP24). In spinach PSII-LHCII supercomplex, two LHCII heterotrimer together with two CP26 proteins flank the core dimer complex from both sides (Wei et al., 2016). Whereas in the $C_2S_2M_2$ supercomplex from *Arabidopsis* and pea, there are four LHCII trimers, out of which the two strongly bound LHCII trimers (S_2) along with CP26 and CP24, and the moderately bound trimers (M_2) with CP29, together encompass the core complex for electron transportation (Su et al., 2017; van Bezouwen et al., 2017). For the second function, the stromal surface of the LHCII trimer is negatively charged whereas its N-terminal first 15 residues contain 4 positively charged residues. This striking charge pattern resembles a "Velcro-like" mode, guaranteeing non-specific interactions of LHCII trimers in the adjacent thylakoid membranes (Standfuss et al., 2005), which seems essential for the chloroplast grana formation. It has been reported that constitutively expression of Lhcb1 robustly increased grana stacks in the transgenic tobacco plants (Labate et al., 2004), while knock-down of Lhcb1 and Lhcb2 impede formation of grana stacks (Andersson et al., 2003; Garab, 2014, 2016). In a recent work, in order to figure out how PSII-LHCII supercomplexes interact with each other in the chloroplast thylakoid, the authors isolated the PSII-LHCII supercomplexes in an ionic concentration that resembles the chloroplast native environment, and found that most of the supercomplexes are existed in a paired C_2S_2M form (Albanese et al., 2017). This study provided new insights into how adjacent thylakoids might be linked to mediate the stacking of grana membranes by interactions between pairs of PSII-LHCII supercomplexes.

Cofactors within the PSII-LHCII supercomplex are indispensable for their appropriate functions. Similar to those in cyanobacteria, these cofactors mainly include chlorophylls, carotenoids, lipids etc. (**Table 1**). In spinach C_2S_2 PSII-LHCII supercomplex, there are in total 105 chlorophyll molecules, 28 β-carotenes and xanthophylls, one heme, one Mn_4CaO_5 cluster, one plastoquinone and numerous lipids. Interestingly, the LHCII monomer shows both amino acid sequence and structure similarities to those of CP29, however, the type, quantity and location of the chlorophylls they bind are significantly different (Liu et al., 2004; Standfuss et al., 2005; Pan et al., 2011). As the largest chromophore-bound antenna subunits, the LHCII harbors Chls which absorb solar radiation of different wavelengths of 660 ± 20 nm.

CONCLUSIONS AND PERSPECTIVES

Photosynthesis plays very important roles in molecular oxygen production, atmospheric carbon dioxide control and global food supply. Structural information of the photosystems is invaluable for our understanding of photosynthesis, probably the most important process on earth. The information will also help design artificial photosynthetic system for the improvement of bioenergy production and the enhancement of agricultural productivity. Most recently, the structure of the largest light-harvesting complex, the phycobilisome (PBS) from *Griffithsia pacifica* was also reported (Zhang et al., 2017). As the main light-harvesting antenna in cyanobacteria and red algae, it exhibits a very fast energy transfer rate with a high quantum yield (Glazer, 1989). The structural information of the PBS will provide a firm basis for understanding its energy transfer pathways and further applications in the designs of artificial light-harvesting machineries.

Recent advances in single-particle cryo-EM have provided unprecedented structural information about these huge membrane complexes. However, there are also several open questions to be answered. First, the exact reaction mechanism underlying water oxidation and possible structural rearrangements during the S-state transitions still await the

structures of PSII in more intermediate S states. Second, it is still not well understood why in PSII only one electron transfer chain is functional (as in bacterial RC), whereas in PSI both are functional (Santabarbara et al., 2010). Since static structures solved thus far has provided no conclusive clues in this respect, new studies investigating the dynamic nature of PSII might shed more light on this, which is very relevant to make PSII not only a proton pump but also the site of O_2 evolution. Third, more structural information is needed to figure out the localizations and functions of PsbR and PsbS, PSII subunits that are essential for oxygen-evolving activity (Allahverdiyeva et al., 2007) and photoprotection of plants (Fan et al., 2015), respectively. Last, new high-resolution structures of the photosystems from cyanobacteria, algae, and plants will provide more insights into the evolution of oxygenic photosynthesis, based on which better artificial photosynthetic machineries could be developed.

AUTHOR CONTRIBUTIONS

JG wrote the manuscript with the help of HW and QY. YF reviewed and revised the manuscript.

FUNDING

This work was supported by the National Natural Science Foundation of China (Grant Nos. 31400635 and 31670766).

ACKNOWLEDGMENTS

We apologize to colleagues whose work could not be cited due to space limitations.

REFERENCES

Albanese, P., Melero, R., Engel, B. D., Grinzato, A., Berto, P., Manfredi, M., et al. (2017). Pea PSII-LHCII supercomplexes form pairs by making connections across the stromal gap. *Sci. Rep.* 7:10067. doi: 10.1038/s41598-017-10700-8

Albertsson, P. (2001). A quantitative model of the domain structure of the photosynthetic membrane. *Trends Plant Sci.* 6, 349–354. doi: 10.1016/S1360-1385(01)02021-0

Allahverdiyeva, Y., Mamedov, F., Suorsa, M., Styring, S., Vass, I., and Aro, E. M. (2007). Insights into the function of PsbR protein in *Arabidopsis thaliana*. *Biochim. Biophys. Acta* 1767, 677–685. doi: 10.1016/j.bbabio.2007.01.011

Andersson, J., Wentworth, M., Walters, R. G., Howard, C. A., Ruban, A. V., Horton, P., et al. (2003). Absence of the Lhcb1 and Lhcb2 proteins of the light-harvesting complex of photosystem II-effects on photosynthesis, grana stacking and fitness. *Plant J. Cell Mol. Biol.* 35, 350–361. doi: 10.1046/j.1365-313X.2003.01811.x

Arvidsson, P. O., and Sundby, C. (1999). A model for the topology of the chloroplast thylakoid membrane. *Funct. Plant Biol.* 26, 687–694. doi: 10.1071/PP99072

Ben-Shem, A., Frolow, F., and Nelson, N. (2003). Crystal structure of plant photosystem I. *Nature* 426, 630–635. doi: 10.1038/nature02200

Biesiadka, J., Loll, B., Kern, J., Irrgang, K. D., and Zouni, A. (2004). Crystal structure of cyanobacterial photosystem II at 3.2 Å resolution: a closer look at the Mn-cluster. *Phys. Chem. Chem. Phys.* 6, 4733–4736. doi: 10.1039/B406989G

Brettel, K., and Leibl, W. (2001). Electron transfer in photosystem I. *Biochim. Biophys. Acta* 1507, 100–114. doi: 10.1016/S0005-2728(01)00202-X

Broser, M., Gabdulkhakov, A., Kern, J., Guskov, A., Müh, F., Saenger, W., et al. (2010). Crystal structure of monomeric photosystem II from *Thermosynechococcus elongatus* at 3.6-Å resolution. *J. Biol. Chem.* 285, 26255. doi: 10.1074/jbc.M110.127589

Caffarri, S., Tibiletti, T., Jennings, R. C., and Santabarbara, S. (2014). A comparison between plant photosystem I and photosystem II architecture and functioning. *Curr. Prot. Peptide Sci.* 15, 296–331. doi: 10.2174/1389203715666140327102218

Cramer, W. A., Soriano, G. M., Ponomarev, M., Huang, D., Zhang, H., Martinez, S. E., et al. (1996). Some new structural aspects and old controversies concerning the cytochrome b6f complex of oxygenic photosynthesis. *Annu. Rev. Plant Physiol. Plant Mol. Biol.* 47, 477–508. doi: 10.1146/annurev.arplant.47.1.477

Croce, R., and van Amerongen, H. (2013). Light-harvesting in photosystem I. *Photosynth. Res.* 116, 153–166. doi: 10.1007/s11120-013-9838-x

Dekker, J. P., and Boekema, E. J. (2005). Supramolecular organization of thylakoid membrane proteins in green plants. *Biochim. Biophys. Acta* 1706, 12–39. doi: 10.1016/j.bbabio.2004.09.009

Dismukes, G. C., Klimov, V. V., Baranov, S. V., Kozlov, Y. N., DasGupta, J., and Tyryshkin, A. (2001). The origin of atmospheric oxygen on Earth: the innovation of oxygenic photosynthesis. *Proc. Natl. Acad. Sci. U.S.A.* 98, 2170–2175. doi: 10.1073/pnas.061514798

Fan, M., Li, M., Liu, Z., Cao, P., Pan, X., Zhang, H., et al. (2015). Crystal structures of the PsbS protein essential for photoprotection in plants. *Nat. Struct. Mol. Biol.* 22, 729–735. doi: 10.1038/nsmb.3068

Ferreira, K. N., Iverson, T. M., Maghlaoui, K., Barber, J., and Iwata, S. (2004). Architecture of the photosynthetic oxygen-evolving center. *Science* 303, 1831–1838. doi: 10.1126/science.1093087

Fromme, P., Jordan, P., and Krauss, N. (2001). Structure of photosystem I. *Biochim. Biophys. Acta* 1507, 5–31. doi: 10.1016/S0005-2728(01)00195-5

Garab, G. (2014). Hierarchical organization and structural flexibility of thylakoid membranes. *Biochim. Biophys. Acta* 1837, 481–494. doi: 10.1016/j.bbabio.2013.12.003

Garab, G. (2016). Self-assembly and structural-functional flexibility of oxygenic photosynthetic machineries: personal perspectives. *Photosynth. Res.* 127, 131–150. doi: 10.1007/s11120-015-0192-z

Glazer, A. N. (1989). Directional energy transfer in a photosynthetic antenna. *J. Biol. Chem.* 264, 1–4.

Golbeck, J. H. (2006). *Photosystem I: The Light-Driven Plastocyanin: Ferredoxin Oxidoreductase*. Dordrecht: Springer.

Grabolle, M., and Dau, H. (2005). Energetics of primary and secondary electron transfer in Photosystem II membrane particles of spinach revisited on basis of recombination-fluorescence measurements. *Biochim. Biophys. Acta* 1708, 209–218. doi: 10.1016/j.bbabio.2005.03.007

Guskov, A., Kern, J., Gabdulkhakov, A., Broser, M., Zouni, A., and Saenger, W. (2009). Cyanobacterial photosystem II at 2.9-Å resolution and the role of quinones, lipids, channels and chloride. *Nat. Struct. Mol. Biol.* 16, 334–342. doi: 10.1038/nsmb.1559

Holzwarth, A. R., Müller, M. G., Reus, M., Nowaczyk, M., Sander, J., and Rögner, M. (2006). Kinetics and mechanism of electron transfer in intact photosystem II and in the isolated reaction center: pheophytin is the primary electron acceptor. *Proc. Natl. Acad. Sci. U.S.A.* 103, 6895–6900. doi: 10.1073/pnas.0505371103

Hope, A. B. (2000). Electron transfers amongst cytochrome f, plastocyanin and photosystem I: kinetics and mechanisms. *Biochim. Biophys. Acta* 1456, 5–26. doi: 10.1016/S0005-2728(99)00101-2

Johnson, M. P. (2016). Photosynthesis. *Essays Biochem.* 60, 255–273. doi: 10.1042/EBC20160016

Jordan, P., Fromme, P., Witt, H. T., Klukas, O., Saenger, W., and Krauss, N. (2001). Three-dimensional structure of cyanobacterial photosystem I at 2.5 Å resolution. *Nature* 411, 909–917. doi: 10.1038/35082000

Kamiya, N., and Shen, J. R. (2003). Crystal structure of oxygen-evolving photosystem II from *Thermosynechococcus vulcanus* at 3.7-Å resolution. *Proc. Natl. Acad. Sci. U.S.A.* 100, 98–103. doi: 10.1073/pnas.0135651100

Kanady, J. S., and Agapie, T. (2011). A synthetic model of the Mn3Ca subsite of the oxygen-evolving complex in photosystem II. *Science* 333, 733–736. doi: 10.1126/science.1206036

Kawakami, K., Umena, Y., Kamiya, N., and Shen, J. R. (2009). Location of chloride and its possible functions in oxygen-evolving photosystem II revealed by X-ray

crystallography. *Proc. Natl. Acad. Sci. U.S.A.* 106, 8567. doi: 10.1073/pnas.0812797106

Kern, J., Alonso-Mori, R., Tran, R., Hattne, J., Gildea, R. J., Echols, N., et al. (2013). Simultaneous femtosecond X-ray spectroscopy and diffraction of photosystem II at room temperature. *Science* 340, 491–495. doi: 10.1126/science.1234273

Kirchhoff, H. (2013). Architectural switches in plant thylakoid membranes. *Photosynth. Res.* 116, 481–487. doi: 10.1007/s11120-013-9843-0

Kuhlbrandt, W., Wang, D. N., and Fujiyoshi, Y. (1994). Atomic model of plant light-harvesting complex by electron crystallography. *Nature* 367, 614–621. doi: 10.1038/367614a0

Kupitz, C., Basu, S., Grotjohann, I., Fromme, R., Zatsepin, N. A., Rendek, K. N., et al. (2014). Serial time-resolved crystallography of photosystem II using a femtosecond X-ray laser. *Nature* 513, 261–265. doi: 10.1038/nature13453

Labate, M. T., Ko, K., Ko, Z. W., Pinto, L. S., Real, M. J., Romano, M. R., et al. (2004). Constitutive expression of pea Lhcb 1-2 in tobacco affects plant development, morphology and photosynthetic capacity. *Plant Mol. Biol.* 55, 701–714. doi: 10.1007/s11103-004-1963-7

Liu, Z., Yan, H., Wang, K., Kuang, T., Zhang, J., Gui, L., et al. (2004). Crystal structure of spinach major light-harvesting complex at 2.72 Å resolution. *Nature* 428, 287–292. doi: 10.1038/nature02373

Loll, B., Kern, J., Saenger, W., Zouni, A., and Biesiadka, J. (2005). Towards complete cofactor arrangement in the 3.0 Å resolution structure of photosystem II. *Nature* 438, 1040–1044. doi: 10.1038/nature04224

Mukherjee, S., Stull, J. A., Yano, J., Stamatatos, T. C., Pringouri, K., Stich, T. A., et al. (2012). Synthetic model of the asymmetric [Mn3CaO4] cubane core of the oxygen-evolving complex of photosystem II. *Proc. Natl. Acad. Sci. U.S.A.* 109, 2257–2262. doi: 10.1073/pnas.1115290109

Mullineaux, C. W. (2005). Function and evolution of grana. *Trends Plant Sci.* 10, 521–525. doi: 10.1016/j.tplants.2005.09.001

Mustárdy, L., Buttle, K., Steinbach, G., and Garab, G. (2008). The three-dimensional network of the thylakoid membranes in plants: quasihelical model of the granum-stroma assembly. *Plant Cell* 20, 2552–2557. doi: 10.1105/tpc.108.059147

Nelson, N. (2011). Photosystems and global effects of oxygenic photosynthesis. *Biochim. Biophys. Acta* 1807, 856–863. doi: 10.1016/j.bbabio.2010.10.011

Nelson, N., and Benshem, A. (2004). The complex architecture of oxygenic photosynthesis. *Nat. Rev. Mol. Cell Biol.* 5, 971–982. doi: 10.1038/nrm1525

Nelson, N., and Junge, W. (2015). Structure and energy transfer in photosystems of oxygenic photosynthesis. *Annu. Rev. Biochem.* 84, 659–683. doi: 10.1146/annurev-biochem-092914-041942

Nelson, N., and Yocum, C. F. (2006). Structure and function of photosystems I and II. *Annu. Rev. Plant Biol.* 57, 521–565. doi: 10.1146/annurev.arplant.57.032905.105350

Nield, J., Orlova, E. V., Morris, E. P., Gowen, B., van Heel, M., and Barber, J. (2000). 3D map of the plant photosystem II supercomplex obtained by cryoelectronmicroscopy and single particle analysis. *Nat. Struct. Biol.* 7, 44–47. doi: 10.1038/71242

Pan, X., Li, M., Wan, T., Wang, L., Jia, C., Hou, Z., et al. (2011). Structural insights into energy regulation of light-harvesting complex CP29 from spinach. *Nat. Struct. Mol. Biol.* 18, 309–315. doi: 10.1038/nsmb.2008

Peter, G. F., and Thornber, J. P. (1991). Biochemical composition and organization of higher plant photosystem II light-harvesting pigment-proteins. *J. Biol. Chem.* 266, 16745–16754.

Pfannschmidt, T. (2003). Chloroplast redox signals: how photosynthesis controls its own genes. *Trends Plant Sci.* 8, 33–41. doi: 10.1016/S1360-1385(02)00005-5

Qin, X., Suga, M., Kuang, T., and Shen, J. R. (2015). Photosynthesis. Structural basis for energy transfer pathways in the plant PSI-LHCI supercomplex. *Science* 348, 989–995. doi: 10.1126/science.aab0214

Remelli, R., Varotto, C., Sandonà, D., Croce, R., and Bassi, R. (1999). Chlorophyll binding to monomeric light-harvesting complex. A mutation analysis of chromophore-binding residues. *J. Biol. Chem.* 274, 33510–33521. doi: 10.1074/jbc.274.47.33510

Ruban, A. V. (2015). Evolution under the sun: optimizing light harvesting in photosynthesis. *J. Exp. Bot.* 66, 7–23. doi: 10.1093/jxb/eru400

Santabarbara, S., Galuppini, L., and Casazza, A. P. (2010). Bidirectional electron transfer in the reaction centre of photosystem I. *J. Integr. Plant Biol.* 52, 735–749. doi: 10.1111/j.1744-7909.2010.00977.x

Sétif, P. (2001). Ferredoxin and flavodoxin reduction by photosystem I. *Biochim. Biophys. Acta* 1507, 161–179. doi: 10.1016/S0005-2728(01)00205-5

Standfuss, J., Ac, T. V. S., Lamborghini, M., and Kühlbrandt, W. (2005). Mechanisms of photoprotection and nonphotochemical quenching in pea light-harvesting complex at 2.5 Å resolution. *EMBO J.* 24, 919–928. doi: 10.1038/sj.emboj.7600585

Su, X., Ma, J., Wei, X., Cao, P., Zhu, D., Chang, W., et al. (2017). Structure and assembly mechanism of plant C2S2M2-type PSII-LHCII supercomplex. *Science* 357, 815–820. doi: 10.1126/science.aan0327

Suga, M., Akita, F., Hirata, K., Ueno, G., Murakami, H., Nakajima, Y., et al. (2015). Native structure of photosystem II at 1.95 Å resolution viewed by femtosecond X-ray pulses. *Nature* 517, 99–103. doi: 10.1038/nature13991

Suga, M., Akita, F., Sugahara, M., Kubo, M., Nakajima, Y., Nakane, T., et al. (2017). Light-induced structural changes and the site of O = O bond formation in PSII caught by XFEL. *Nature* 543, 131–135. doi: 10.1038/nature21400

Tomioka, N., and Sugiura, M. (1983). The complete nucleotide sequence of a 16S ribosomal RNA gene from a blue-green alga, *Anacystis nidulans*. *Mol. Gen. Genet.* 191, 46–50. doi: 10.1007/BF00330888

Umena, Y., Kawakami, K., Shen, J. R., and Kamiya, N. (2011). Crystal structure of oxygen-evolving photosystem II at a resolution of 1.9 Å. *Nature* 473, 55–60. doi: 10.1038/nature09913

van Bezouwen, L. S., Caffarri, S., Kale, R. S., Kouřil, R., Thunnissen, A. W. H., Oostergetel, G. T., et al. (2017). Subunit and chlorophyll organization of the plant photosystem II supercomplex. *Nat. Plants* 3:17080. doi: 10.1038/nplants.2017.80

van Amerongen, H., and Croce, R. (2013). Light harvesting in photosystem II. *Photosynth. Res.* 116, 251–263. doi: 10.1007/s11120-013-9824-3

Wei, X., Su, X., Cao, P., Liu, X., Chang, W., Li, M., et al. (2016). Structure of spinach photosystem II-LHCII supercomplex at 3.2 Å resolution. *Nature* 534, 69–74. doi: 10.1038/nature18020

Woodson, J. D. (2016). Chloroplast quality control – balancing energy production and stress. *New Phytol.* 212, 36–41. doi: 10.1111/nph.14134

Zhang, J., Ma, J., Liu, D., Qin, S., Sun, S., Zhao, J., et al. (2017). Structure of phycobilisome from the red alga *Griffithsia pacifica*. *Nature* 551, 57–63. doi: 10.1038/nature24278

Zouni, A., Witt, H. T., Kern, J., Fromme, P., Krauss, N., Saenger, W., et al. (2001). Crystal structure of photosystem II from *Synechococcus elongatus* at 3.8 Å resolution. *Nature* 409, 739–743. doi: 10.1038/35055589

Conflict of Interest Statement: The authors declare that the research was conducted in the absence of any commercial or financial relationships that could be construed as a potential conflict of interest.

frontiers in Plant Science

ORIGINAL RESEARCH
published: 09 March 2017
doi: 10.3389/fpls.2017.00329

Crystal Structure of the Chloroplastic Oxoene Reductase ceQORH from *Arabidopsis thaliana*

*Sarah Mas y mas[1], Gilles Curien[2], Cécile Giustini[2], Norbert Rolland[2], Jean-Luc Ferrer[1] and David Cobessi[1]**

[1] *Institut de Biologie Structurale (IBS), Univ. Grenoble Alpes, CEA, Centre National de la Recherche Scientifique (CNRS), Grenoble, France,* [2] *Laboratoire de Physiologie Cellulaire & Végétale, BIG, Univ. Grenoble Alpes, CEA, Centre National de la Recherche Scientifique (CNRS), INRA, Grenoble, France*

Enzymatic and non-enzymatic peroxidation of polyunsaturated fatty acids give rise to accumulation of aldehydes, ketones, and α,β-unsaturated carbonyls of various lengths, known as oxylipins. Oxylipins with α,β-unsaturated carbonyls are reactive electrophile species and are toxic. Cells have evolved several mechanisms to scavenge reactive electrophile oxylipins and decrease their reactivity such as by coupling with glutathione, or by reduction using NAD(P)H-dependent reductases and dehydrogenases of various substrate specificities. Plant cell chloroplasts produce reactive electrophile oxylipins named γ-ketols downstream of enzymatic lipid peroxidation. The chloroplast envelope quinone oxidoreductase homolog (ceQORH) from *Arabidopsis thaliana* was previously shown to reduce the reactive double bond of γ-ketols. In marked difference with its cytosolic homolog alkenal reductase (AtAER) that displays a high activity toward the ketodiene 13-oxo-9(Z),11(E)-octadecadienoic acid (13-KODE) and the ketotriene 13-oxo-9(Z), 11(E), 15(Z)-octadecatrienoic acid (13-KOTE), ceQORH binds, but does not reduce, 13-KODE and 13-KOTE. Crystal structures of apo-ceQORH and ceQORH bound to 13-KOTE or to $NADP^+$ and 13-KOTE have been solved showing a large ligand binding site, also observed in the structure of the cytosolic alkenal/one reductase. Positioning of the α,β-unsaturated carbonyl of 13-KOTE in ceQORH-$NADP^+$-13-KOTE, far away from the $NADP^+$ nicotinamide ring, provides a rational for the absence of activity with the ketodienes and ketotrienes. ceQORH is a monomeric enzyme in solution whereas other enzymes from the quinone oxidoreductase family are stable dimers and a structural explanation of this difference is proposed. A possible *in vivo* role of ketodienes and ketotrienes binding to ceQORH is also discussed.

Keywords: chloroplast envelope quinone oxidoreductase homolog, oxylipins, γ-ketols, α, β-unsaturated carbonyls, X-ray crystallography

OPEN ACCESS

Edited by:
Rebecca L. Roston, University of Nebraska–Lincoln, USA

Reviewed by:
Christophe Wirth, University of Freiburg, Germany
Jinpeng Gao, Washington State University, USA

****Correspondence:***
David Cobessi
david.cobessi@ibs.fr

Specialty section:
This article was submitted to Plant Cell Biology, a section of the journal Frontiers in Plant Science

Received: *18 January 2017*
Accepted: *24 February 2017*
Published: *09 March 2017*

Citation:
Mas y mas S, Curien G, Giustini C, Rolland N, Ferrer J-L and Cobessi D (2017) Crystal Structure of the Chloroplastic Oxoene Reductase ceQORH from Arabidopsis thaliana. Front. Plant Sci. 8:329. doi: 10.3389/fpls.2017.00329

INTRODUCTION

Plants lack an immune system like animals. However, they possess mechanisms that recognize pathogens and initiate defense responses. Some of these mechanisms involve various types of oxygenated fatty acids, termed "oxylipins." These molecules are involved in responses to physical damage by animals or insects, stress, and attack by pathogens. Oxylipins are derived

from linoleic and α-linolenic acids, released from their lipid associations by poorly defined acyl hydrolases (lipases) of various kinds (**Figure 1**). A first key step in oxidation is the action of lipoxygenases. For example, depending on the source of the enzyme, lipoxygenases (e.g., LOX1, a 9-lipoxygenase from the cytosol, or LOX2, a 13-lipoxygenase from the chloroplast stroma) catalyze the oxidation of linoleic (C18:2) or linolenic acids (C18:3) into either 9- or 13-hydroperoxy-octadecatrienoic acids (HPODE). Such compounds are highly reactive, and they are quickly metabolized by various enzymes into series of oxylipins, with a range of distinct biological activities (Blée, 2002; Mosblech et al., 2009; Joyard et al., 2010). Some oxylipins such as 4-oxononenal, 4-hydroxynonenal, ketodienes [the 9-oxo-10(E), 12(E)-octadecadienoic acid (9-KODE), and 13-oxo-9(Z), 11(E)-octadecadienoic acid (13-KODE)], ketotrienes [the 9-oxo-10(E), 12(Z), 15(Z)-octadecatrienoic acid (9-KOTE) and 13-oxo-9(Z), 11(E), 15(Z)-octadecatrienoic acid (13-KOTE)], or the plant specific γ-ketols (**Figure 1** and **Figure S1**) are α,β-unsaturated carbonyls and reactive electrophile species (RES). RES can act as signaling molecules (Farmer and Mueller, 2013) and also react with important cellular nucleophiles such as thiols of proteins and nucleic acids, modifying their biochemical properties, and are potentially toxic (Esterbauer et al., 1991; Szweda et al., 1993). Due to this potential toxicity, cells have developed an armory of defense to decrease their activity. One class of enzymes involved in detoxification of reactive electrophile oxylipins are NADPH-oxidoreductases belonging to the zinc-independent medium-chain dehydrogenase/reductase (MDR) superfamily and more specifically to the quinone oxidoreductase (QOR) subfamily to which alkenal/one reductases belong (Porté et al., 2009). These enzymes can decrease the activity of reactive electrophile oxylipins by reducing the unsaturated carbon-carbon bond located in α,β of the carbonyl group to a single bond (Yamauchi et al., 2011) (**Figure 1**).

The chloroplast envelope Quinone Oxidoreductase Homolog (ceQORH; At4g13010; molecular weight 34,034 Da) from *Arabidopsis thaliana* is associated to the inner membrane of the chloroplast envelope (**Figure 1**) where it represents 1–2% of the crude envelope proteins (Miras et al., 2002). It is encoded by the nuclear genome and is targeted to the chloroplast by an alternative import pathway, without cleavage of its internal chloroplast targeting sequence (Miras et al., 2002, 2007). Despite its original annotation as a "QOR," ceQORH is inactive on quinones but preferentially reduces γ-ketols in the presence of NADPH (Curien et al., 2016) (**Figure 1** and **Figure S1**). γ-ketols (**Figure 1** and **Figure S1**) are long-chain reactive electrophile oxylipins and are potentially toxic (Kuga et al., 1993). They are spontaneously produced in the jasmonate biosynthetic pathway, downstream of lipoxygenase specific peroxidation by hydrolysis of an allene oxide intermediate (Grechkin et al., 1991). ceQORH is also active though to a lesser extent on the highly toxic (Lin et al., 2005) C9 α,β-unsaturated carbonyl 4-oxononenal (Curien et al., 2016). ceQORH is thus probably dedicated to detoxification of γ-ketols which can be produced in plants under normal growth conditions (Theodoulou et al., 2005), and accumulate in damaged tissues (Buseman et al., 2006) or at a distance from bite zone when plants are attacked by caterpillars (Schulze et al., 2007). ceQORH bears similar characteristics and sequence homology with members of the MDR superfamily, which includes chloroplastic alkenone reductase [At1g23740, AtAOR (Yamauchi et al., 2012), **Figure 1**], Arabidopsis ζ-crystallin [alkenal reductase, AT5G16970, AtAER (Mano et al., 2005), **Figure 1**], yeast ζ-crystallin (Crosas et al., 2011), human eye ζ-crystallin (Porté et al., 2011), and *Escherichia coli* quinone reductase (Thorn et al., 1995) (**Figure S2**).

Unlike the chloroplastic AtAOR (Yamauchi et al., 2012) (**Figure 1**), which is active on short-chain α,β-unsaturated carbonyls ($C < 5$), ceQORH does not reduce short chain unsaturated carbonyls ($C < 9$). In addition, compared to the cytosolic broad specific alkenal/one reductase AtAER (**Figure 1**), ceQORH showed a restricted substrate specificity, being inactive on the ketodienes 9-KODE and 13-KODE, or on the ketotrienes 9-KOTE and 13-KOTE (**Figure S1**) and virtually inactive on 4-hydroxynonenal and traumatin [12-oxo-10(E) dodecenoate] (Curien et al., 2016). ceQORH is encoded by the nuclear genome and is targeted to the chloroplast by an alternative import pathway independent from the trimeric TOC159/75/34 complex, without cleavage of its internal chloroplast targeting sequence (Miras et al., 2002, 2007). This peculiarity, together with the ceQORH restricted substrate specificity, prompted us to carry out crystallographic studies of ceQORH. No crystal was obtained either in the presence of γ-ketols or NADPH but the protein crystallized in the absence of ligands as well as bound to 13-KODE and NADPH, 13-KOTE and $NADP^+$ and 13-KOTE alone. Structure comparisons with AtAER (Youn et al., 2006) and the enone oxidoreductase from *Fragaria x ananassa* (Schiefner et al., 2013) provided insights into the molecular basis of substrate specificity.

Abbreviations: 9-KODE, 9-oxo-10(E), 12(E)-octadecadienoic acid; 13-KODE, 13-oxo-9(Z),11(E)-octadecadienoic acid; 9-KOTE, 9-oxo-10(E), 12(Z), 15(Z)-octadecatrienoic acid; 13-KOTE, 13-oxo-9(Z), 11(E), 15(Z)-octadecatrienoic acid; ceQORH, chloroplast envelope quinone oxidoreductase homolog; AtAER, alkenal/one reductase from *Arabidopsis thaliana* (cytosolic enzyme); AtAOR, alkenone oxidoreductase from *Arabidopsis thaliana* (chloroplastic enzyme)

MATERIALS AND METHODS

Tryptophan Fluorescence Anisotropy Measurements

Tryptophan fluorescence anisotropy measurements of ceQORH were carried out in the same experimental conditions as *in vitro* kinetics (Curien et al., 2016). Assays were carried out with a MOS-450 spectrometer (BioLogic, Inc.) in a 150 μL quartz cuvette, under temperature control (25°C). Excitation and emission wavelengths were set at 280 and 350 nm respectively. Assay conditions were: 10 mM HEPES pH 7.5, 150 mM KCl. Protein concentration was 200 nM. Changes in fluorescence anisotropy were probed following addition of NADPH (200 μM), 13-KODE (50 μM), or γ-ketols (100 μM).

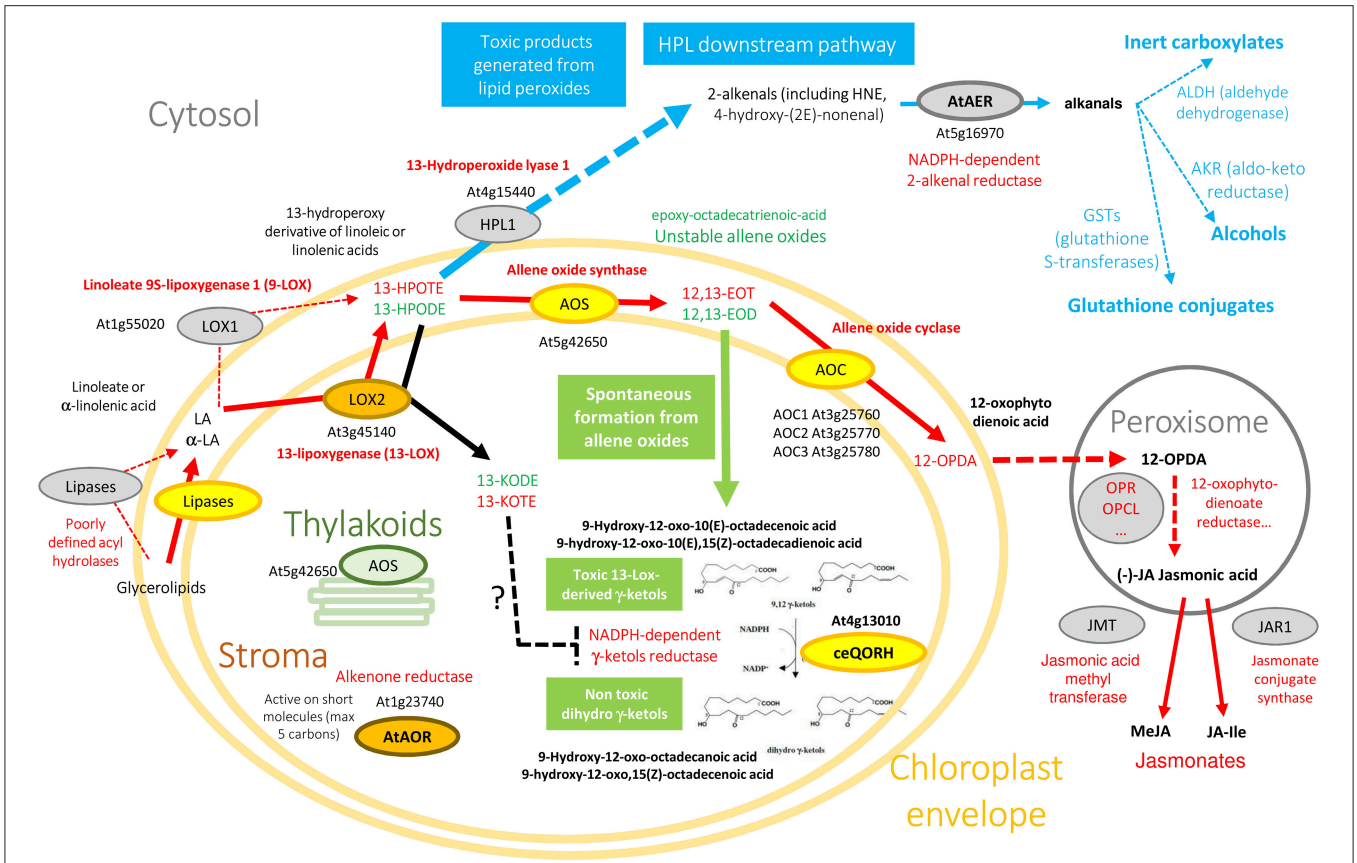

FIGURE 1 | Oxylipin metabolism engenders essential, but also toxic molecules. Color code originates from experimental information about the subplastidial localization of enzymes (see AT_CHLORO database; Ferro et al., 2010). Yellow enzymes (AOS, AOC, ceQORH) are associated to the chloroplast envelope while brown ones (LOX2, AtAOR) are found in the chloroplast stroma. Note that AOS is associated with both envelope (yellow) and thylakoid membranes (green). Non-plastid enzymes (cytosol, peroxisomes), or proteins suspected to interact with the outer surface of chloroplasts, are colored in gray. Due to space constraints, some specific data are absent from this figure. For example, from the cytosolic 9-LOX (LOX1), derive 9-HPOTE and 9,10-EOT that are not indicated here, and α and γ-ketols also derive from 9,10-EOT. 13(*S*)-HPODE and 12,13-EOD derive from linoleic acid (18:2) while 13(*S*)-HPOTE and 12,13-EOT derive from linolenic acid (18:3). Note that from 13(*S*)-HPODE and 13(*S*)-HPOTE, LOX2 synthesize 13-KODE and 13-KOTE, respectively (black arrow).

Crystallization and Data Collection

Expression, purification, crystallization, and data collection of apo-ceQORH were described previously (Mas y mas et al., 2015). ceQORH-13-KOTE (1.45 mM 13-KOTE) and ceQORH-13-KOTE-NADP$^+$ (1.45 mM NADP$^+$, 1.45 mM 13-KOTE) at 5 mg/ml in 50 mM Tris-HCl, pH 7.5, 200 mM KCl, 2 mM DTT, 1 mM EDTA, 10% (v/v) glycerol were subjected to crystallization using the sitting-drop vapor-diffusion technique and high throughput crystallization facility at EMBL, Grenoble, at 4°C. Crystallization hits were optimized using Limbro plates, at 20°C. Crystals of ceQORH-13-KOTE-NADP$^+$ were obtained in 0.2 M sodium chloride, 0.1 M Tris-HCl pH 8.5, 15.5% (w/v) PEG 4K. Crystals of ceQORH-13-KOTE were obtained in 0.2 M ammonium tartrate pH 7.2, 20% (w/v) PEG3350. Crystals of ceQORH-NADPH-13-KODE (1.45 mM NADPH, 1.45 mM 13-KODE) were also obtained in 0.2 M sodium chloride, 0.1 M Tris-HCl pH 7.5, 28% (w/v) PEG3500, but despite all our efforts, it was not possible to obtain diffraction good enough and the resulting structure was not used here. All the diffraction data were collected on FIP-BM30A (Roth et al., 2002) at the European Synchrotron Radiation Facility, Grenoble, France, at 100 K, using an ADSC 315r detector. The data (**Table 1**) were processed and scaled using XDS (Kabsch, 2010).

Phasing and Model Refinement

Phasing was performed by molecular replacement using Phaser (McCoy et al., 2007) from CCP4 (CCP4, 1994). The structure of the QOR from *Coxiella burnetii* (PDB entry: 3TQH) (Franklin et al., 2015) was used as model and modified based on sequence alignment with ceQORH using CHAINSAW (Stein, 2008) from CCP4 to calculate the phases for the data of ceQORH-13-KOTE. The other structures were solved using the monomer of ceQORH-13-KOTE as search model for molecular replacement. All the model refinements were performed with non-crystallographic symmetry. The refinements and rebuilding were done using PHENIX (Adams et al., 2010) and COOT (Emsley et al., 2010) respectively. Water molecules were added in apo-ceQORH using PHENIX. Refinement statistics are summarized in **Table 2**. Structure of ceQORH-NADPH-13-KODE was not used for analyses since statistics of X-ray data

TABLE 1 | Statistics of data collection.

	CeQORH-13-KOTE	CeQORH-NADP$^+$-13-KOTE
Resolution range (Å)	40.21–2.78 (2.94–2.78)	49.58–2.81 (2.98–2.81)
Wavelength (Å)	0.9796	1.04
Space group	P1	$P2_1$
Unit cell parameters (Å,°)	a = 82.87, b = 121.01, c = 122.94, α = 66.73, β = 79.10, γ = 79.99	a = 82.16, b = 128.60, c = 150.12, β = 97.76
Molecules in au	12	8
Number of total reflections	186,642 (27,138)	283,856 (45,069)
Unique reflections	102,756 (15,212)	75,277 (11,943)
Average multiplicity	1.8 (1.8)	3.8 (3.8)
Data completeness (%)	94.8 (87.0)	99.4 (98.2)
Rsym (%)	14.5 (75.4)	8.6 (62.6)
<I/σ(I)>	6.1 (1.1)	13.7 (2.2)
CC(1/2)	ND	99.7 (77.0)

Rsym = ΣΣ|Ii-Im|/ΣΣIi, where Ii is the intensity of the measured reflection and Im is the mean intensity of this reflection. Values indicated in parentheses correspond to the statistics in the highest resolution shell.

TABLE 2 | Refinement statistics.

	Apo-ceQORH	CeQORH-13-KOTE	CeQORH-NADP$^+$-13-KOTE
Resolution (Å)	42.26–2.34 (2.42–2.34)	40.21–2.78 (2.81–2.78)	49.58–2.81 (2.84–2.81)
R_{cryst} ($\sigma_F = 0$) (%)	18.14 (22.19)	20.03 (32.28)	18.82 (32.46)
R_{free} ($\sigma_F = 0$) (%)	25.05 (32.92)	25.75 (36.90)	22.47 (38.87)
Number of atoms	5,275	28,354	19,576
Water molecules	387	0	0
B average (Å^2)	25.64	45.46	72.36
Rmsd bonds (Å)	0.011	0.011	0.008
Rmsd angle (°)	1.350	1.286	1.214
Ramachandran favored (%)	98.04	97.02	97.80
Ramachandran outliers (%)	1.06	1.05	0.42

Values indicated in parentheses correspond to the statistics in the highest resolution shell. R_{cryst} = Σ||Fobs|-|Fcalc||/Σ|Fobs|. Rfree (Brünger, 1992) is the same as Rcryst but calculated for 5% data omitted from the refinement.

were poor. It is roughly similar to that of ceQORH-NADP$^+$-13-KOTE and 13-KODE is located at a similar position than 13-KOTE.

Atomic coordinates and X-ray data were deposited in the PDB with the accession numbers: apo-ceQORH (5A3V), ceQORH-13-KOTE (5A3J), and ceQORH-NADP$^+$-13-KOTE (5A4D).

RESULTS

Analysis of ceQORH Oligomerization State

The oligomeric forms of ceQORH (i.e., dimers and tetramers, see later) observed in the different crystals raised the question of their physiological relevance. Indeed, we previously showed by analytical ultracentrifugation analyses (AUC) (Mas y mas et al., 2015) that ceQORH in the presence of NADPH is a monomer while apo-ceQORH displayed several oligomerization forms, i.e., monomeric, dimeric, and tetrameric. As NADPH is always present *in vivo*, ceQORH is probably a monomer at least in the absence of the other substrates. To see whether γ-ketols (substrates) or the ketodiene and ketotriene (ligands) affected the ceQORH oligomerization state, tryptophan fluorescence anisotropy measurements of ceQORH were carried out in the same experimental conditions as *in vitro* kinetics (Curien et al., 2016). No change in fluorescence anisotropy was observed upon addition of NADPH, NADP$^+$, 13-KOD(T)E or substrates, either alone or in combination. The same results were obtained when the fluorescence anisotropy was measured with a *C*-terminal GFP-fusion form of ceQORH taking opportunity of the fluorescence of GFP. Since ceQORH-NADPH is a monomer (Mas y mas et al., 2015) even at high concentration and no change in fluorescence anisotropy is observed upon addition of ligands we can conclude that ceQORH is active with its substrates and binds ligands as a monomer. The oligomeric states observed in AUC and in crystals (see after) thus result from the use of high ceQORH concentrations (17.5 and 174.9 μM in AUC and 145.8 μM in crystallogenesis) and probably do not have any physiological significance. The oligomerization state is however described and discussed in the context of structure comparison with other QORs that form stable dimers.

The ceQORH Oligomers

In crystals of apo-ceQORH, the asymmetric unit contains two monomers related by a non-crystallographic two-fold axis (**Figures 2A,B**) that form a dimer. The monomers are very similar with a value of root mean square deviation (rmsd) of 0.25 Å between monomers. The buried area in the dimer interface is 2,410 Å^2. The dimer of apo-ceQORH crystallized whereas monomers and tetramers observed in AUC did not. No crystallization could be observed with the following complexes, ceQORH-NADPH, ceQORH-γ-ketol, and ceQORH-NADP$^+$-γ-ketols using either 18:1 or 18:2 γ-ketols. We could obtain crystals with 13-KODE and 13-KOTE without and with NADPH or NADP$^+$. In the crystals of the binary and ternary complexes ceQORH-13-KOTE and ceQORH-NADP$^+$-13-KOTE, the asymmetric unit contains 12 and 8 ceQORH molecules, respectively. They assemble into tetramers (**Figures 3A,B**). As indicated above the tetramers observed in the crystals do not have any physiological significance. The structure of the tetramers is similar as characterized by low values of rmsd when the tetramers are superimposed, in a range from 0.62 to 1.19 Å. The monomers of the three ceQORH structures can be superimposed with low rmsd going from 0.03 to 0.80 Å. The highest differences in rmsd are observed between the monomers of apo-ceQORH and those in complexes. The dimer of apo-ceQORH does not superimpose on any dimers of the tetramers (**Figure 4**). The interactions between monomers are therefore the main differences between the apo-ceQORH dimer and the tetramers.

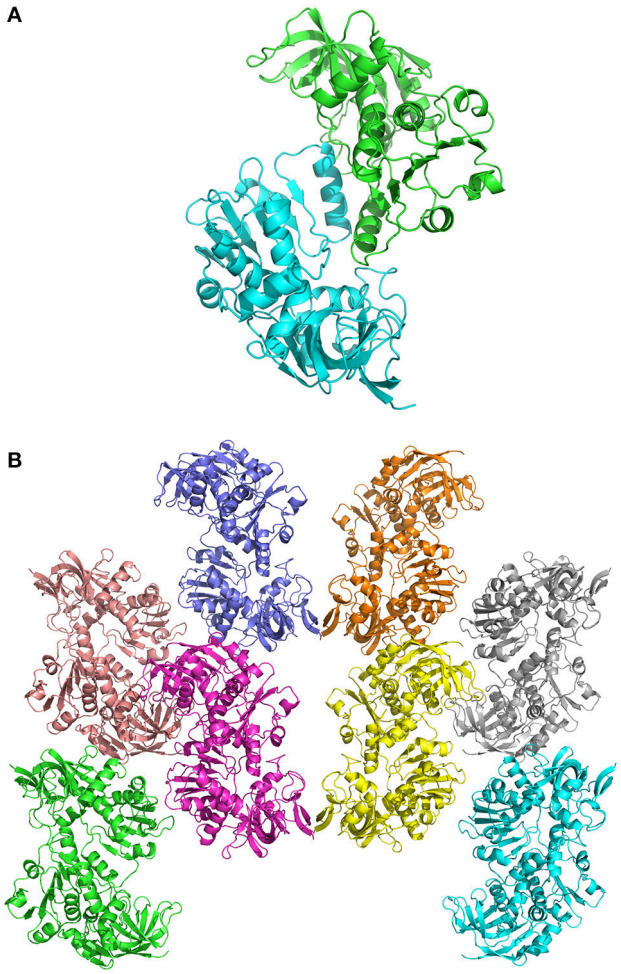

FIGURE 2 | (A) view of the ceQORH dimer (apo-ceQORH) with each monomer in a different color. The β-strands are drawn in arrows and the α-helices are represented in ribbons. **(B)** crystal packing of the apo-ceQORH in the space group $C222_1$. Two molecules are in the asymmetric unit.

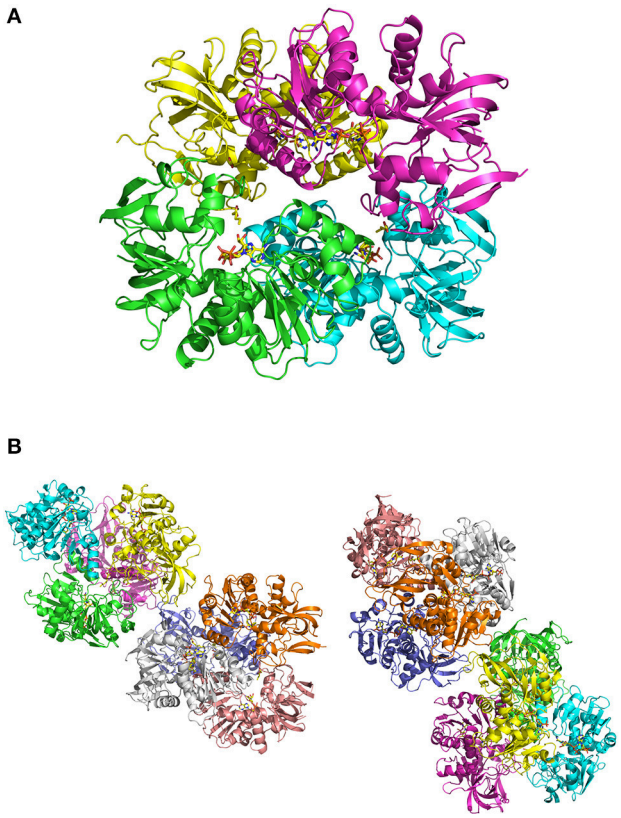

FIGURE 3 | (A) view of ceQORH-$NADP^+$-13-KOTE tetramer. Each monomer is displayed with a different color. The β-strands are drawn in arrows and the α-helices are represented in ribbons. $NADP^+$ and 13-KOTE are drawn in sticks. **(B)** crystal packing of the ceQORH-$NADP^+$-13-KOTE in the space group $P2_1$. Eight molecules of ceQORH-$NADP^+$-13-KOTE are in the asymmetric unit.

Comparison of apo-ceQORH and ceQORH Bound to Ligands

Overall Description of the Monomers

The ceQORH monomer is formed of two domains (**Figure 5**) with (i) the catalytic domain including residues from Gly3 to Pro132 and from Leu277 to Pro329 and (ii) the cofactor binding domain (Val133 to Leu276) showing the classical motif of Rossmann fold. No major overall conformational change is observed in monomers following ligand binding, as shown by the low values of rmsd between monomers. Minor local changes could be observed following ligands binding, as described below.

Description of the Ligand Binding Sites

Figure 6 shows that $NADP^+$ is well-defined in the electron density map of the ternary complex (ceQORH-$NADP^+$-13-KOTE). $NADP^+$ is bound at the interface of the two domains and the nicotinamide ring is in the vicinity of the catalytic site. Comparison of apo-ceQORH and ceQORH-$NADP^+$-13-KOTE monomers shows that $NADP^+$ binding introduces local changes in the vicinity of the cofactor. The orientation of the Arg190 side chain is modified, stabilizing the 2′-phosphate of the $NADP^+$ adenosine moiety. The loop containing Thr251 in the Rossmann fold shifts and stabilizes the ribose group of the $NADP^+$ nicotinamide moiety by interacting with the Thr251 hydroxyl group.

The quality of the electron density map for 13-KOTE differs depending on the monomers in the binary and ternary complexes, suggesting flexibility of the 13-KOTE aliphatic chain (**Figure 6**). The 13-KOTE binding site is large and solvent accessible (**Figure 7**). Upon 13-KOTE binding, the loop from Leu97 to Gly103 moves, thus stabilizing the ligand (**Figure S3**).

13-KOTE is not a substrate of ceQORH (Curien et al., 2016) though it displays an unsaturated double bond in α,β of a carbonyl group. Analyses of the ceQORH structures provide a possible explanation for this absence of activity. In the ceQORH-$NADP^+$-13-KOTE structure, the aliphatic

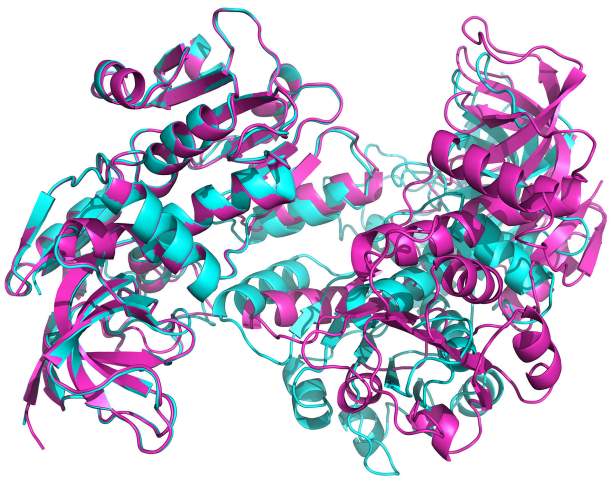

FIGURE 4 | View of the superimposition of apo-ceQORH (blue) onto ceQORH-NADP$^+$-13-KOTE (purple). For clarity a single dimer of the tetramer was drawn.

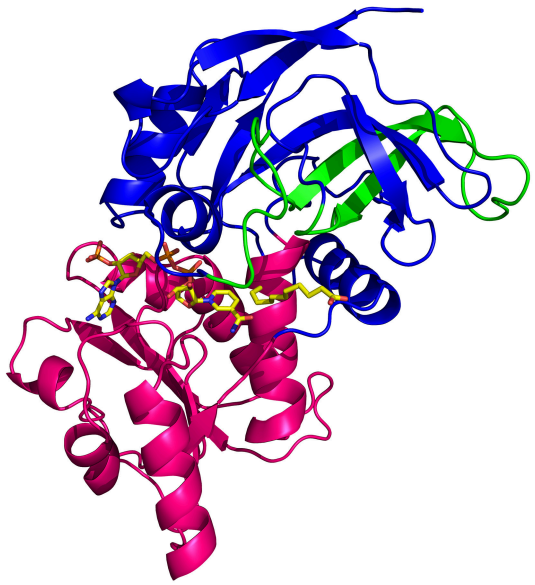

FIGURE 5 | View of the ceQORH monomer from ceQORH-NADP$^+$-13-KOTE. The catalytic domain (Gly3-Pro132, Leu277-Pro329) is colored in blue. The cofactor binding domain (Val133-Leu276) is colored in magenta. The internal chloroplast targeting sequence peptide (Pro59-Leu100) is colored in green. NADP$^+$ and 13-KOTE are drawn in sticks.

chain of 13-KOTE is observed in electron density up to the C11 atom of the α,β-unsaturated carbon-carbon bond (C11 = C12) (**Figure 6**). The distance average between the C11 atom and the C4 atom of the NADP$^+$ nicotinamide ring bearing the hydride is 6.84 Å. The flexibility of 13-KOTE and the large distance between the α,β-unsaturated carbon-carbon bond (C11 = C12) and the C4 atom of NADP$^+$ nicotinamide ring are not compatible with a hydride transfer.

Changes in the ceQORH Oligomerization States

We previously showed (Mas y mas et al., 2015) that addition of NADPH to apo-ceQORH changes the oligomerization state of ceQORH from a mixture of monomers, dimers and tetramers to a solution of monomers. NADPH is always present *in vivo* and the dimeric apo-ceQORH probably never forms in cell. In the apo-ceQORH dimer, interactions between monomers mainly involve residues in the α-helix Pro254-Met267 belonging to the cofactor binding domain. Each α-helix in the dimer contributes for 723 Å^2 to the buried area, being 60% of the overall buried area at the dimer interface. When the apo-ceQORH structure is compared either to the ceQORH-13-KOTE or ceQORH-NADP$^+$-13-KOTE structure, the main chain from Asn46 to Leu61 and from Ile250 to Lys269, containing the α-helix Pro254-Met267 involved in the dimer interface, are shifted. The shift of the main chain from Ile250 to Lys269 is even larger in the ceQORH-NADP$^+$-13-KOTE structure compared to the ceQORH-13-KOTE complex due to the NADP$^+$ binding. The new position of the α-helix Pro254-Met267 observed in ceQORH-NADP$^+$-13-KOTE could prevent the dimer formation when ceQORH binds NADPH (**Figure S3**) and may explain why ceQORH-NADPH behaves as a monomer in solution (Mas y mas et al., 2015).

As our results suggest that the tetrameric forms of ceQORH in the presence of 13-KOTE or 13-KOTE with NADP$^+$ are non-physiological (see first paragraph), we briefly describe the structures. In the complexes ceQORH-13-KOTE and ceQORH-NADP$^+$-13-KOTE complexes, residues of three ceQORH monomers interact with 13-KOTE by hydrogen bonds and van der Waals interactions. The 13-KOTE carboxylate group from one monomer is hydrogen bonded to the Arg58 guanidinium group and Tyr14 hydroxyl group from another monomer (**Figure 8**). Thus, the 13-KOTE carboxylate group is an anchoring point allowing for oligomerization in the crystals.

Comparisons with Other Quinone Oxidoreductases (QORs)

The apo-ceQORH monomer was used for searching homolog and comparisons with structures from the PDB using PDBefold (Krissinel and Henrick, 2004). When monomers are superimposed the values of rmsd go from 1.42 Å (comparison with the QOR from *C. burnetii*, PDB entry: 3TQH) (Franklin et al., 2015) to 2.65 Å (comparison with a putative NADPH quinone reductase from *Mesorhizobium loti*, PDB entry: 3PI7). The sequence identity based on structure comparison goes from 20 to 32%. The fold of QORs is roughly conserved and also similar to that of alcohol dehydrogenases belonging to the MDR family.

Comparison of Oligomeric State

Proteins in the QOR family display two different oligomeric states, being either monomers (such as the QOR from *C. burnetii)* or dimers [*E. coli* QOR (Thorn et al., 1995), *A. thaliana* alkenal reductase AtAER (Youn et al., 2006), *Saccharomyces cerevisiae* ζ-crystallin (Zta1) (Guo et al., 2011)]. Structure

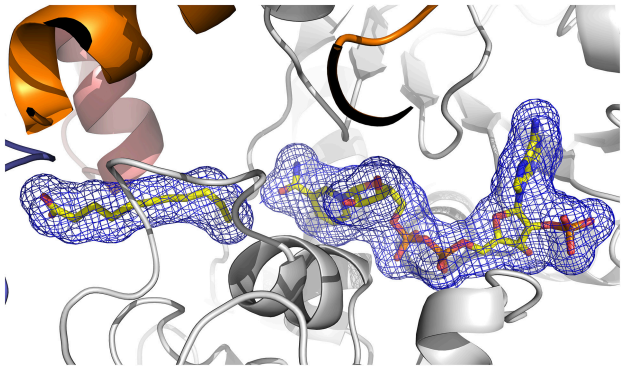

FIGURE 6 | View of the 2Fo-Fc electron density omit map (blue) at 2.8 Å resolution contoured at 1.2 σ level, calculated using PHENIX, surrounding 13-KOTE and NADP$^+$. The β-strands are drawn in arrows and the α-helices are represented in ribbons. 13-KOTE until the carbon C11 and NADP$^+$ are drawn in stick.

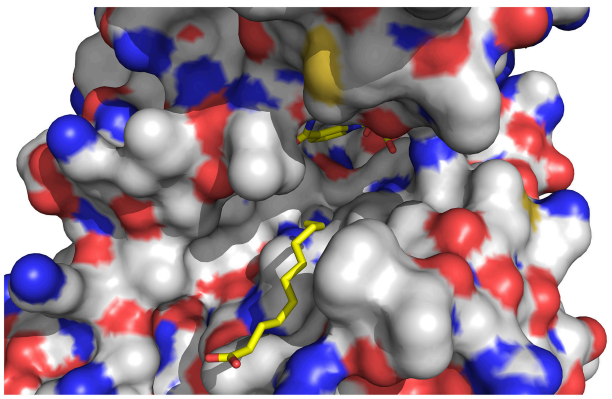

FIGURE 7 | View of the ligand binding site of ceQORH. 13-KOTE until the carbon C11 and NADP$^+$ are drawn in stick.

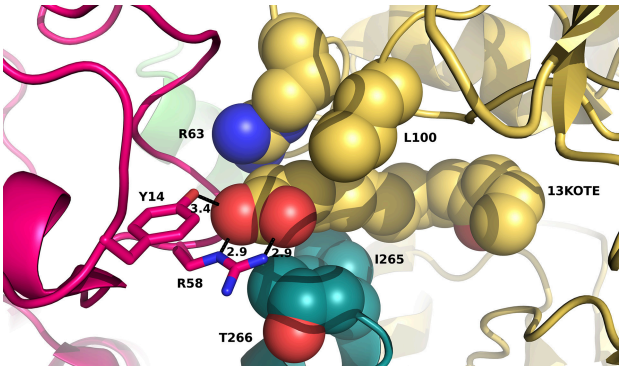

FIGURE 8 | View of residues stabilizing the first atoms of 13-KOTE in the ceQORH-13-KOTE. 13-KOTE tetramer, Arg63 and Leu100 from one monomer, and Ile265, Thr266 from a second monomer are represented in van der Waals spheres. Arg58 and Tyr14 from a third monomer are drawn in stick. Hydrogen bonds between the 13-KOTE carboxylate group and Tyr14 and Arg58 are drawn in dashed lines and distances are given in Å.

analysis provides an explanation for these differences. The main difference is observed when dimeric QORs are compared with apo-ceQORH. The analysis of dimeric QORs of known structures showed that interactions between the monomers occur by involving a β-strand of the Rossmann fold leading to the formation of a QOR dimer displaying a 12 stranded β-sheet. In ceQORH, the residues (Thr251-Lys269) are folded in a loop-α-helix(Pro254-Met267)-loop. This α-helix interacts with the non-crystallographic symmetry related α-helix in the apo-ceQORH dimer, as described above. Thr251-Lys269 from ceQORH do not superimpose onto the corresponding residues (Gly239 to Ser258) of QOR from *E. coli* (PDB entry: 1QOR) (Thorn et al., 1995) (**Figure 9**). The orientation of the α-helix (Pro254-Met267) prevents the monomer of ceQORH to interact with another monomer to form a dimer similar to that observed in dimeric QORs. When bound to NADP$^+$ or NADPH, dimeric QORs remain in the dimeric state while AUC studies (Mas y mas et al., 2015) and tryptophan fluorescence anisotropy measurements showed that ceQORH is a monomer. Thus, dimeric QORs are stable dimers, which is not the case of ceQORH.

Comparison of the Binding Sites

When the cofactor binding site of other QORs is compared with that of ceQORH several interactions between these proteins and NADP$^+$ are observed in the ceQORH-NADP$^+$-13-KOTE structure. However, the residues in the catalytic site are not conserved at the exception of Asn46 which was proposed for substrate stabilization in *S. cerevisiae* ζ-crystallin (Zta1) (Guo et al., 2011). Ile50, Tyr59, and Leu131 proposed for quinone orientation in catalytic site of Zta1 correspond to the hydrophobic amino acids Val47, Ile56, and Val132 in ceQORH.

Insights into the Discrimination of Substrate Length of the Alkenal/Alkenone Reductases

To gain a deeper understanding of the ligand specificity at the molecular level, structures of the *Arabidopsis* alkenal double bond reductase At5g16970 (AtAER) bound to *p*-coumaryl aldehyde or 4-hydroxy-2-nonenal (PDB entries: 2J3J and 2J3K, respectively) (Youn et al., 2006), of the enone oxidoreductase from *Fragaria x ananassa* (PDB entry: 4IDF) (Schiefner et al., 2013) and of ceQORH were compared. The enone oxidoreductase from *Fragaria x ananassa* (PDB entry: 4IDF) (Schiefner et al., 2013) displays 70.8% sequence identity with AtAOR (**Figure S4**). ceQORH shares 33% sequence identity with AtAOR and 32% with the enone oxidoreductase from *Fragaria x ananassa*. The rmsd values between the monomers of ceQORH-NADP$^+$-13KOTE and the enone oxidoreductase from *Fragaria x ananassa* (PDB code: 4IDF) are between 1.48 and 1.52 Å. Analysis of the structures shows that the enzymes have a large substrate binding site. In 4IDF, the loop Leu104-Glu120 (Val112-Glu128 in AtAOR), corresponding to Leu97-Glu107 in ceQORH or Ile103-Glu108 in AtAER, is located in the vicinity of the binding site and is larger than in ceQORH and AtAER. In the six structures of enone oxidoreductase from *Fragaria x ananassa*, the conformation of this loop (B average of 13.3 Å^2) does not change upon ligand binding and the loop protrudes inside the ligand binding site. Superimposition of the enone

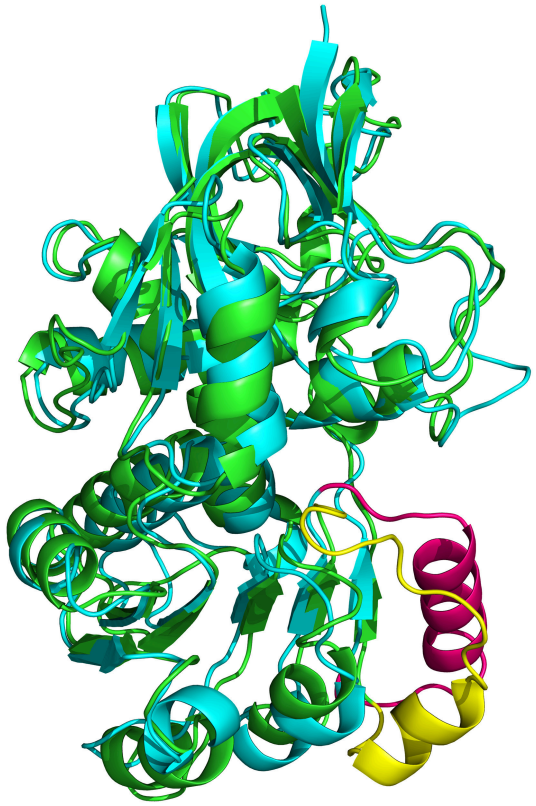

FIGURE 9 | Superimposition of the monomer from *E. coli* 1QOR (green) (Thorn et al., 1995) onto that of *A. thaliana* ceQORH (cyan). Gly239 to Ser258 in 1QOR is colored in yellow and the corresponding zone (Thr251-Lys269) in ceQORH is colored in pink.

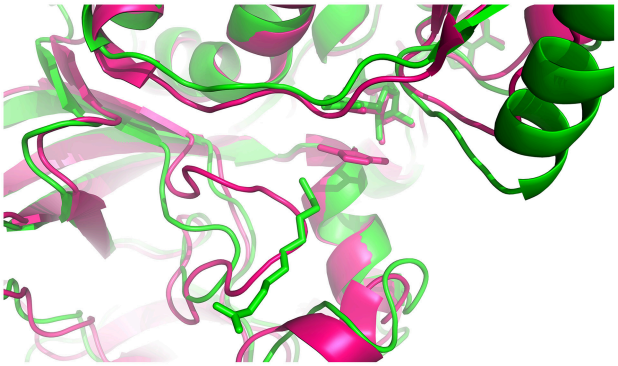

FIGURE 10 | Superimposition of the monomer from ceQORH-NADP$^+$-13-KOTE (green) onto the enone reductase from *Fragaria x ananassa* (pink) (Schiefner et al., 2013). The cofactors and ligands are drawn in sticks. 4-hydroxy-5-methylfuran-3(2H)-one and NADPH from enone oxidoreductase are colored in pink. NADP$^+$ and 13-KOTE from ceQORH are colored in green.

oxidoreductase from *Fragaria x ananassa* with the structures of AtAER and ceQORH shows clashes between the loop Leu104-Glu120 (Val112-Glu128 in AtAOR) and 13-KOTE of ceQORH-NADP$^+$-13-KOTE (**Figure 10**), or with the *p*-coumaryl aldehyde in 2J3J and 4-hydroxy-2-nonenal in 2J3K of AtAER. The substrate specificity of AtAOR, restricted to small chain α,β-unsaturated carbonyl (C < 5), could therefore result from the length of the loop (Val112-Glu128) which could prevent binding of large substrates.

ceQORH Import Sequence

ceQORH has the peculiar property to possess an internal signal sequence (Pro59-Leu100), for its import into the chloroplast, which is not cleaved after import (Miras et al., 2002, 2007). In the ceQORH structure, the internal chloroplast targeting sequence is folded as a two anti-parallel β-strands (Thr71 to Gly81 and Asp91 to Leu97) connected by a long loop (Ser82 to Gly90) (**Figure 5**). The chloroplast targeting sequence is partially solvent exposed and forms part of a larger 4-stranded β-sheet with the catalytic domain. Clearly, cleavage of this sequence would affect the active site and obviously had to be retained for the protein to be active. The internal chloroplast targeting sequence described for ceQORH has a similar fold in the other QORs. Therefore, the information for the ceQORH targeting likely does not rely on the structure of its internal chloroplast targeting sequence but rather on its primary structure.

DISCUSSION

9,12 γ-ketols are plant specific reactive electrophile oxylipins produced spontaneously in chloroplasts (Grechkin et al., 1991). Until recently, no enzyme able to detoxify γ-ketol in the chloroplast could be identified. Previously, we showed that ceQORH, a chloroplast inner envelope membrane associated protein, efficiently reduces γ-ketol but is inactive with the ketodienes 13-KODE and 13-KOTE and small reactive aldehydes (less than 9 carbon atoms) (Curien et al., 2016). Structure analyses of ceQORH crystallized bound to ligands showed that the ligand binding site is large and solvent exposed. These features are consistent with the binding of medium-sized (C > 9) molecules such as 1,3-diphenyl-2-propenone or 4-oxononenal but also with the binding of the long-chain molecules 9,12 γ-ketols (18 carbon atoms) (Curien et al., 2016). The structure analysis of the ternary complex ceQORH-NADP$^+$-13-KOTE provides a structural explanation for the absence of activity with 13-KOTE with a positioning inconsistent with a hydride transfer from NADPH to the C=C bond positioned in α,β of the ketone. This observation also suggests that positioning of γ-ketol in the ligand binding site of ceQORH is different from that observed for 13-KOTE, γ-ketol being necessarily closer from the C4 of NADPH to be reduced. Structure comparisons and kinetic studies revealed that ceQORH shares structural similarities and overlapping substrate specificity with the cytoplasmic NADPH-dependent 2-alkenal reductase (AtAER) from *A. thaliana* (PDB entries: 2J3J and 2J3K) (Mano et al., 2005; Youn et al., 2006). AtAER is able to reduce the same substrates as ceQORH with similar efficiencies. However, AtAER substrate specificity is much larger than that of ceQORH, being active on ketodiene and ketotriene and showing much higher affinity for 4-hydroxy-2-nonenal and the C12 molecule traumatin (Curien et al., 2016).

The structure comparison shows that both enzymes have a large ligand binding site. More generally, structure comparison with QORs and sequence alignments showed that the residues of ceQORH binding site are not well-conserved. Only co-crystallization of ceQORH and other QORs with substrates would allow understanding the basis of ceQORH restricted substrate specificity. Unfortunately we could not obtain crystals in the presence of γ-ketols. Nonetheless, by comparing different structures of QORs we could highlight a molecular basis allowing selection of the substrate length in the soluble stromal AtAOR, an enzyme that only reduces short-chain α,β unsaturated carbonyls. The AtAOR specificity for small compounds probably results from the presence of a long loop located in the vicinity of the binding site of AtAOR, which could prevent the binding of large molecules.

By comparison with other QORs that are stable dimers, all our results indicate that ceQORH is a monomer in solution and is active as a monomer. Oligomerization observed in crystals and in AUC experiments only occurs at high protein concentrations under conditions that are probably irrelevant of physiological conditions. Comparison of ceQORH structure with other dimeric QORs shows that the ceQORH dimer is different from the stable dimer of QORs due to structural differences in the Rossmann fold. A dimerization mode similar to that of AtAER is prevented in ceQORH by the orientation of the α-helix Pro254-Met267. Analysis of QOR from *C. Burnetii* (PDB entry: 3TQH) (Franklin et al., 2015) bound to NADPH, which is also a monomeric QOR supports this explanation as an α-helix equivalent to the ceQORH Pro254-Met267 α-helix is also observed. As ceQORH is associated to the inner membrane of chloroplast envelope (Miras et al., 2007), a monomeric state could increase its catalytic efficiency (higher mobility, better dispersion on the membrane surface) and might have been selected during evolution as this would favor the detoxification rate.

The successful crystallization of ceQORH in the presence of ketotriene and ketodiene raised the question of the physiological significance of this property. Kinetic experiments showed that ceQORH could be inhibited by 13-KODE. However, the inhibition was a slow process taking 400 s to reach completion A IC_{50} of 36 μM for 13-KODE could be determined in the presence of 25 μM substrate (**Figures S5**). 13-KODE and 13-KOTE are molecules that are produced during the hypersensitive response (HR) of plants attacked by a pathogen (Andersson et al., 2006). This response leads to local destruction of the plant tissues, preventing the spreading of the pathogen. Ketodiene and ketotriene can accumulate to 2.5–5 nmol per g fresh weight several hours after the hypersensitive response is initiated (Andersson et al., 2006). This value corresponds to 2.5–5 μM assuming a homogeneous distribution in the cell. As these compounds could be concentrated locally, they could reached concentration close to ceQORH IC_{50} and a first hypothesis might be that ceQORH sequesters ketodi(tri)enes quantitatively. However, this does not seem to be the case for the following reason: ceQORH is a low abundant protein at the cellular level. ceQORH represents about 1% of the chloroplast envelope proteins corresponding to about 50,000 copies per chloroplast, i.e., ∼1 μM assuming the protein is soluble. This is barely compatible with an efficient sequestering of sub-micromolar concentrations of ketodiene and ketotriene. Another model can be proposed. Some RES oxylipins are signaling molecules (Farmer and Mueller, 2013). Upon increase of the ketodiene and ketotriene levels, following the triggering of the HR (Andersson et al., 2006), ceQORH would become inactivated by these molecules and would then be unable to metabolize γ-ketols. γ-ketols would in turn accumulate and contribute either to signaling or to an additional chemical defense of the plant. ceQORH may thus have a dual function, detoxification of γ-ketols under normal conditions and indirect contribution to chemical defense/signaling after pathogen attack. This would be reminiscent of the "floodgate" hypothesis proposed for H_2O_2 signaling where inhibition of 2-Cys peroxiredoxins occurs at high concentration of H_2O_2 (Wood et al., 2003).

More work is required to determine how ceQORH handles 13-KODE, 13-KOTE and γ-ketols *in vivo*, and whether ceQORH is involved during the HR response to pathogen attacks.

AUTHOR CONTRIBUTIONS

SMM performed experiments, analyzed data and wrote the article. GC designed and performed experiments, analyzed data, and wrote the article. CG performed experiments. JLF and NR participated to the article writing. DC designed and performed experiments, analyzed data, and wrote the article. All authors read and approved the final manuscript.

ACKNOWLEDGMENTS

The diffraction experiments were conducted on beamline FIP-BM30A at the ESRF (Grenoble, France). We thank the beamline staff for technical help. This work used the platforms of the Grenoble Instruct centre (ISBG; UMS 3518 CNRS-CEA-UJF-EMBL) with support from FRISBI (ANR-10-INSB-05-02) and GRAL (ANR-10-LABX-49-01) within the Grenoble Partnership for Structural Biology (PSB).

SUPPLEMENTARY MATERIAL

The Supplementary Material for this article can be found online at: http://journal.frontiersin.org/article/10.3389/fpls.2017.00329/full#supplementary-material

Figure S1 | Skeletal formulas of γ-ketol 18:1, 13-KOTE, 13-KODE and drawing of the reaction catalyzed by ceQORH.

Figure S2 | Sequence alignment between ceQORH from *Arabidopsis thaliana*, and QORs from *Coxiella burnetii* (3TQH) (Franklin et al., 2015), *Escherichia coli* (1QOR) (Thorn et al., 1995), and *Saccharomyces cerevisiae* (3QWA) Guo et al., 2011. The ceQORH secondary structure is drawn. The β-strands are represented by arrows and the α-helices by curls. The conserved residues are highlighted in red. The sequences were aligned using Multalin (Corpet, 1988) and the drawing was generated using ESPript (Gouet et al., 1999).

Figure S3 | Superimposition of apo-ceQORH (green), ceQORH-13-KOTE (cyan), and ceQORH-$NADP^+$-13-KOTE (magenta) displaying conformational changes which occur upon binding of 13-KOTE and 13-KOTE + $NADP^+$.

Figure S4 | Sequence alignment between ceQORH, AtAER (Mano et al., 2002), AtAOR from *Arabidopsis thaliana* (Yamauchi et al., 2012), and the enone oxidoreductase from *Fragaria x ananassa* (4IDF) (Schiefner et al., 2013). The conserved residues are highlighted in red. The sequences were aligned using Multalin (Corpet, 1988) and the drawing was generated using ESPript (Gouet et al., 1999).

Figure S5 | Inhibition of ceQORH by the ketodiene 13-KODE; (A) activity (ΔAbs340 nm/s) was measured after different preincubation time of the enzyme with 13-KODE. 50 nM enzyme was pre-incubated in the presence of 10 mM HEPES-KOH pH 7.5, 150 mM KCl, 160 μM NADPH and 55 μM 13-KODE. The reaction was initiated by the addition of 25 μM *trans*-1,3 diphenyl-2-propenone. The *k*obs value was obtained by nonlinear least-square fitting of the progress curves using the following equation: At = At0–vs.t + (vs–vi). (1-exp(-*k*obs.t))/*k*obs, where At is the absorbance at time t, At0 is the absorbance at t0, *vi* is the initial velocity of the reaction, vs. is the steady-state velocity of the reaction, and *k*obs is an exponential decay constant. A *k*obs value of 0,01 s-1 was obtained by curve fitting and $t_{1/2}$ (i.e., ln2/*k*obs) was 70 s. **(B)** The enzyme (50 nM) was preincubated 400 s in the presence of 160 μM NADPH and 13-KODE at different concentrations as indicated in the graph before addition of the 25 μM *trans*-1,3 diphenyl-2-propenone. An IC50 of 36 μM (±3) μM was measured.

REFERENCES

Adams, P. D., Afonine, P. V., Bunkóczi, G., Chen, V. B., Davis, I. W., Echols, N., et al. (2010). PHENIX: a comprehensive Python-based system for macromolecular structure solution. *Acta Cryst. D* 66, 213–221. doi: 10.1107/S0907444909052925

Andersson, M. X., Hamberg, M., Kourtchenko, O., Brunnström, A., McPhail, K. L., Gerwick, W. H., et al. (2006). Oxylipin profiling of the hypersensitive response in *Arabidopsis thaliana*. *J. Biol. Chem.* 281, 31528–31537. doi: 10.1074/jbc.M604820200

Blée, E. (2002). Impact of phyto-oxylipins in plant defense. *Trends Plant Sci.* 7, 315–322. doi: 10.1016/S1360-1385(02)02290-2

Brünger, A. T. (1992). Free R value: a novel statistical quantity for assessing the accuracy of crystal structures. *Nature* 355, 472–475. doi: 10.1038/355472a0

Buseman, C. M., Tamura, P., Sparks, A. A., Baughman, E. J., Maatta, S., Zhao, J., et al. (2006). Wounding stimulates the accumulation of glycerolipids containing oxophytodienoic acid and dinor-oxophytodienoic acid in Arabidopsis leaves. *Plant Physiol.* 142, 28–39. doi: 10.1104/pp.106.082115

CCP4. Collaborative computational project, Number 4. (1994). The CCP4 suite: programs for protein crystallography. *Acta Cryst. D* 50, 760–763. doi: 10.1107/S0907444994003112

Corpet, F. (1988). Multiple sequence alignment with hierarchical clustering. *Nucleic Acids Res.* 16, 10881–10890. doi: 10.1093/nar/16.22.10881

Crosas, E., Porté, S., Moeini, A., Farrés, J., Biosca, J. A., Parés, X., et al. (2011). Novel alkenal/one reductase activity of yeast NADPH: quinone reductase Zta1p. Prospect of the functional role for the *ζ-crystallin family*. Chem. Biol. Interact. 191, 32–37. doi: 10.1016/j.cbi.2011.01.021

Curien, G., Giustini, C., Montillet, J.-L., Mas-y-mas, S., Cobessi, D., Ferrer, J.-L., et al. (2016). The chloroplast membrane associated ceQORH putative quinone oxidoreductase reduces long-chain, stress-related oxidized lipids. *Phytochemistry* 122, 45–55. doi: 10.1016/j.phytochem.2015.11.015

Emsley, P., Lohkamp, B., Scott, W. G., and Cowtan, K. (2010). Features and development of Coot. *Acta Cryst. D* 66, 486–501. doi: 10.1107/S0907444910007493

Esterbauer, H., Schaur, R. J., and Zollner, H. (1991). Chemistry and biochemistry of 4-hydroxynonenal, malondialdehyde and related aldehydes. *Free Radic. Biol. Med.* 11, 81–128. doi: 10.1016/0891-5849(91)90192-6

Farmer, E. E., and Mueller, M. J. (2013). ROS-mediated lipid peroxidation and RES activated signaling. *Annu. Rev. Plant Biol.* 64, 429–450. doi: 10.1146/annurev-arplant-050312-120132

Ferro, M., Brugière, S., Salvi, D., Seigneurin-Berny, D., Court, M., Moyet, L., et al. (2010). AT_CHLORO, a comprehensive chloroplast proteome database with subplastidial localization and curated information on envelope proteins. *Mol. Cell Proteomics* 9, 1063–1084. doi: 10.3389/fpls.2012.00205

Franklin, M. C., Cheung, J., Rudolph, M. J., Burshteyn, F., Cassidy, M., Gary, E., et al. (2015). Structural genomics for drug design against the pathogen *Coxiella burnetii*. *Proteins* 83, 2124–2136. doi: 10.1002/prot.24841

Gouet, P., Courcelle, E., Stuart, D. I., and Métoz, F. (1999). ESPript: analysis of multiple sequence alignments in PostScript. *Bioinformatics* 15, 305–308. doi: 10.1093/bioinformatics/15.4.305

Grechkin, A. N., Kuramshin, R. A., Safonova, E. Y., Latypov, S. K., and Ilyasov, A. V. (1991). Formation of ketols from linolenic acid 13-hydroperoxide via allene oxide. Evidence for two *distinct mechanisms of allene oxide hydrolysis*. Biochim. Biophys. Acta 1086, 317–325. doi: 10.1016/0005-2760(91)90176-I

Guo, P. C., Ma, X. X., Bao, Z. Z., Ma, J. D., Chen, Y., and Zhou, C. Z. (2011). Structural insights into the cofactor-assisted substrate recognition of yeast quinone oxidoreductase Zta1. *J. Struct. Biol.* 176, 112–118. doi: 10.1016/j.jsb.2011.07.010

Joyard, J., Ferro, M., Masselon, C., Seigneurin-Berny, D., Salvi, D., Garin, J., et al. (2010). Chloroplast proteomics highlights the subcellular compartmentation of lipid metabolism. *Prog. Lipid Res.* 49, 128–158. doi: 10.1016/j.plipres.2009.10.003

Kabsch, W. (2010). XDS. *Acta Cryst D* 66, 125–132. doi: 10.1107/S0907444909047337

Krissinel, E., and Henrick, K. (2004). Secondary-structure matching (SSM), a new tool for fast protein structure alignment in three dimensions. *Acta Cryst. D* 60, 2256–2268. doi: 10.1107/S0907444904026460

Kuga, H., Ejima, A., Mitui, I., Sato, K., Ishihara, N., Fukuda, K., et al. (1993). Isolation and characterization of cytotoxic compounds from corn. *Biosci. Biotech. Biochem.* 57, 1020–1021. doi: 10.1271/bbb.57.1020

Lin, D., Lee, H. G., Liu, Q., Perry, G., Smith, M. A., and Sayre, L. M. (2005). 4-oxo-2-nonenal is both more neurotoxic and more protein reactive than 4-hydroxy-2-nonenal. *Chem. Res. Toxicol.* 18, 1219–1231. doi: 10.1021/tx050080q

Mano, J., Torii, Y., Hayashi, S., Takimoto, K., Matsui, K., Nakamura, K., et al. (2002). The NADPH:quinone oxidoreductase P1-zeta-crystallin in Arabidopsis catalyzes the α,β-hydrogenation of 2-alkenals: detoxication of the lipid peroxide-derived reactive aldehydes. *Plant Cell. Physiol.* 43, 1445–1455. doi: 10.1093/pcp/pcf187

Mano, J., Belles-Boix, E., Babiychuk, E., Inzé, D., Torii, Y., Hiraoka, E., et al. (2005). Protection against photooxidative injury of tobacco leaves by 2-alkenal reductase. Detoxication of lipid peroxide-derived reactive carbonyls. *Plant Physiol.* 139, 1773–1783. doi: 10.1104/pp.105.070391

Mas y mas, S., Guistini, C., Ferrer, J.-L., Rolland, N., Curien, G., and Cobessi, D. (2015). Analytical ultracentrifugation and preliminary X-ray studies of the chloroplast envelope quinone oxidoreductase homologue from *Arabidopsis thaliana*. *Acta Cryst. F* 71, 455–458. doi: 10.1107/S2053230X1500480X

McCoy, A. J., Grosse-Kunstleve, R. W., Adams, P. D., Winn, M. D., Storoni, L. C., and Read, R. J. (2007). Phaser crystallographic software. *J. Appl. Cryst.* 40, 658–674. doi: 10.1107/S0021889807021206

Miras, S., Salvi, D., Ferro, M., Grunwald, D., Garin, J., Joyard, J., et al. (2002). Non-canonical transit peptide for import into the chloroplast. *J. Biol. Chem.* 277, 47770–47778. doi: 10.1074/jbc.M207477200

Miras, S., Salvi, D., Piette, L., Seigneurin-Berny, D., Grunwald, D., Reinbothe, C., et al. (2007). Toc159- and Toc75-independent import of a transit sequence-less precursor into the inner envelope of chloroplasts. *J. Biol. Chem.* 282, 29482–29492. doi: 10.1074/jbc.M611112200

Mosblech, A., Feussner, I., and Heilmann, I. (2009). Oxylipins: structurally diverse metabolites from fatty acid oxidation. *Plant Physiol. Biochem.* 47, 511–517. doi: 10.1016/j.plaphy.2008.12.011

Porté, S., Crosas, E., Yakovtseva, E., Biosca, J. A., Farrés, J., Fernández, M. R., et al. (2009). MDR quinone oxidoreductases: the human and yeast zeta-crystallins. *Chem. Biol. Interact.* 178, 288–294. doi: 10.1016/j.cbi.2008.10.018

Porté, S., Moeini, A., Reche, I., Shafqat, N., Oppermann, U., Farrés, J., et al. (2011). Kinetic and structural evidence of the alkenal/one reductase specificity of human *ζ*-crystallin. *Cell. Mol. Life Sci.* 68, 1065–1077. doi: 10.1007/s00018-010-0508-2

Roth, M., Carpentier, P., Kaïkati, O., Joly, J., Charrault, P., Pirocchi, M., et al. (2002). FIP: a highly automated beamline for multiwavelength

anomalous diffraction experiments. *Acta Cryst. D* 58, 805–814. doi: 10.1107/S0907444902003943

Schiefner, A., Sinz, Q., Neumaier, I., Schwab, W., and Skerra, A. (2013). Structural basis for the enzymatic formation of the key strawberry flavor compound 4-hydroxy-2,5-dimethyl-3(2H)-furanone. *J. Biol. Chem.* 288, 16815–16826. doi: 10.1074/jbc.M113.453852

Schulze, B., Dabrowska, P., and Boland, W. (2007). Rapid enzymatic isomerization of 12-oxophytodienoic acid in the gut of lepidopteran larvae. *Chembiochem* 8, 208–216. doi: 10.1002/cbic.200600379

Stein, N. (2008). CHAINSAW: a program for mutating pdb files used as templates in molecular replacement. *J. Appl. Cryst.* 41, 641–643. doi: 10.1107/S0021889808006985

Szweda, L. I., Uchida, K., Tsai, L., and Stadtman, E. R. (1993). Inactivation of glucose-6-phosphate-dehydrogenase by 4-hydroxy-2-nonenal. Selective modification of an active-site lysine. *J. Biol. Chem.* 268, 3342–3347.

Theodoulou, F. L., Job, K., Slocombe, S. P., Footitt, S., Holdsworth, M., Baker, A., et al. (2005). Jasmonic acid levels are reduced in comatose ATP binding cassette transporter mutants. Implications for transport of jasmonate precursors into peroxisomes. *Plant Physiol.* 137, 835–840. doi: 10.1104/pp.105.059352

Thorn, J. M., Barton, J. D., Dixon, N. E., Ollis, D. L., and Edwards, K. J. (1995). Crystal structure of *Escherichia coli* QOR quinone oxidoreductase complexed with NADPH. *J. Mol. Biol.* 249, 785–799. doi: 10.1006/jmbi.1995.0337

Wood, Z. A., Poole, L. B., and Karplus, P. A. (2003). Peroxiredoxin evolution and the regulation of hydrogen peroxide signaling. *Science* 300, 650–653. doi: 10.1126/science.1080405

Yamauchi, Y., Hasegawa, A., Taninaka, A., Mizutani, M., and Sugimoto, Y. (2011). NADPH-dependent reductases involved in the detoxification of reactive carbonyls in plants. *J. Biol. Chem.* 286, 6999–7009. doi: 10.1074/jbc.M110.202226

Yamauchi, Y., Hasegawa, A., Mizutani, M., and Sugimoto, Y. (2012). Chloroplastic NADPH-dependent alkenal/one oxidoreductase contributes to the detoxification of reactive carbonyls produced under oxidative stress. *FEBS Lett.* 586, 1208–1213. doi: 10.1016/j.febslet.2012.03.013

Youn, B., Kim, S. J., Moinuddin, S. G., Lee, C., Bedgar, D. L., Harper, A. R., et al. (2006). Mechanistic and structural studies of apoform, binary, and ternary complexes of the Arabidopsis alkenal double bond reductase At5g16970. *J. Biol. Chem.* 281, 40076–40088. doi: 10.1074/jbc.M605900200

Conflict of Interest Statement: The authors declare that the research was conducted in the absence of any commercial or financial relationships that could be construed as a potential conflict of interest.

frontiers in Plant Science

ORIGINAL RESEARCH
published: 10 August 2017
doi: 10.3389/fpls.2017.01396

Defense-Related Transcriptional Reprogramming in Vitamin E-Deficient Arabidopsis Mutants Exposed to Contrasting Phosphate Availability

Annapurna D. Allu[1,2†], Bárbara Simancas[3†], Salma Balazadeh[1,2] and Sergi Munné-Bosch[3]*

[1] Institute of Biochemistry and Biology, University of Potsdam, Potsdam-Golm, Germany, [2] Max-Planck-Institut für Molekulare Pflanzenphysiologie, Potsdam, Germany, [3] Department of Evolutionary Biology, Ecology and Environmental Sciences, Faculty of Biology, University of Barcelona, Barcelona, Spain

OPEN ACCESS

Edited by:
Hongbo Gao,
Beijing Forestry University, China

Reviewed by:
Deqiang Duanmu,
Huazhong Agricultural University, China
Keke Yi,
Chinese Academy of Agricultural Sciences, China

***Correspondence:**
Sergi Munné-Bosch
smunne@ub.edu

† These authors have contributed equally to this work.

Specialty section:
This article was submitted to Plant Physiology, a section of the journal Frontiers in Plant Science

Received: *17 April 2017*
Accepted: *26 July 2017*
Published: *10 August 2017*

Citation:
Allu AD, Simancas B, Balazadeh S and Munné-Bosch S (2017) Defense-Related Transcriptional Reprogramming in Vitamin E-Deficient Arabidopsis Mutants Exposed to Contrasting Phosphate Availability. Front. Plant Sci. 8:1396. doi: 10.3389/fpls.2017.01396

Vitamin E inhibits the propagation of lipid peroxidation and helps protecting photosystem II from photoinhibition, but little is known about its possible role in plant response to Pi availability. Here, we aimed at examining the effect of vitamin E deficiency in *Arabidopsis thaliana vte* mutants on phytohormone contents and the expression of transcription factors in plants exposed to contrasting Pi availability. Plants were subjected to two doses of Pi, either unprimed (controls) or previously exposed to low Pi (primed). In the wild type, α-tocopherol contents increased significantly in response to repeated periods of low Pi, which was paralleled by increased growth, indicative of a priming effect. This growth-stimulating effect was, however, abolished in *vte* mutants. Hormonal profiling revealed significant effects of Pi availability, priming and genotype on the contents of jasmonates and salicylates; remarkably, *vte* mutants showed enhanced accumulation of both hormones under low Pi. Furthermore, expression profiling of 1,880 transcription factors by qRT-PCR revealed a pronounced effect of priming on the transcript levels of 45 transcription factors mainly associated with growth and stress in wild-type plants in response to low Pi availability; while distinct differences in the transcriptional response were detected in *vte* mutants. We conclude that α-tocopherol plays a major role in the response of plants to Pi availability not only by protecting plants from photo-oxidative stress, but also by exerting a control over growth- and defense-related transcriptional reprogramming and hormonal modulation.

Keywords: antioxidants, photosystem II, plastochromanol-8, priming, retrograde signaling, tocochromanols, vitamin E

INTRODUCTION

Tocopherol cyclase (VTE1), which is located in plastoglobules (Vidi et al., 2006), is a key enzyme for the biosynthesis of both plastochromanol-8 and vitamin E compounds (Sattler et al., 2003; Szymanska and Kruk, 2010). As the content of plastoglobules is in equilibrium with thylakoid membranes (Austin et al., 2006), both plastochromanol-8 and vitamin E compounds are found in

thylakoids. These together fulfill an antioxidant function protecting lipids from the propagation of lipid peroxidation and prevent photosystem II damage, the latter function being performed together with carotenoids (Munné-Bosch and Alegre, 2002; Havaux et al., 2005; Falk and Munné-Bosch, 2010; Zbierzak et al., 2010; Kruk et al., 2014). Apart from this antioxidant function, tocochromanols may play a major role in cellular signaling by influencing redox, hormonal, and sugar regulatory networks, an aspect that has already been shown in key developmental processes such as seed germination (Mène-Saffrané et al., 2010) or leaf senescence (Abbasi et al., 2009), and plant responses to abiotic stresses, including salinity (Abbasi et al., 2007; Cela et al., 2011; Asensi-Fabado et al., 2015), osmotic stress (Abbasi et al., 2007), high light (Munné-Bosch et al., 2007), low temperatures (Maeda et al., 2008), and water deficit (Cela et al., 2011). Although a previous study has shown that vitamin E and inorganic phosphate (Pi) availability exert a complex interplay in the control of longevity in *Arabidopsis thaliana* (Simancas and Munné-Bosch, 2015), nothing is known about the possible influence of vitamin E on plant response to contrasting Pi availability.

The response of plants to several environmental stress factors, including low phosphate availability in soils, involves intricate regulatory networks governed by various signaling molecules. Pi is a major macro element source for plant growth; hence one of the most prominent effects of Pi starvation is reduced plant growth (Marschner, 2012). However, to maintain cellular Pi homeostasis under conditions of Pi starvation, plants have evolved a series of adaptive responses such as limiting Pi consumption and internally adjusting Pi recycling (Sato and Miura, 2011). Several hormones such as abscisic acid (ABA), ethylene, auxin, and cytokinin have been shown to be involved in plant response to varying Pi availability conditions (Franco-Zorrilla et al., 2004; Rubio et al., 2009). Plants coordinate Pi homeostasis with its carbon status and photosynthesis through sophisticated mechanisms and phytohormones play a crucial role in cross-talking the Pi starvation with sugar signaling (Franco-Zorrilla et al., 2004; Wissuwa et al., 2005; Rubio et al., 2009). Cytokinins negatively regulate Pi starvation responses and its content is reduced under Pi starvation (Yang and Finnegan, 2010). Cytokinins are also proposed to be interacting with sugars in Pi starvation signaling (Franco-Zorrilla et al., 2005). Both auxin (auxin-dependent and independent) and ethylene pathways are known to regulate root architecture in response to Pi availability (Franco-Zorrilla et al., 2004; Rouached et al., 2010). Impaired ABA sensitivity (*abi2-1*) or biosynthesis (*aba1*) mutants display reduced Pi-responsive gene expression and anthocyanin accumulation (Trull et al., 1997; Ciereszkoa and Kleczkowsk, 2002). Furthermore, the gibberellin-DELLA signaling pathway plays a role in the regulation of plant stature, root architecture changes, and anthocyanin accumulation under low Pi-conditions involving ubiquitin-mediated protein degradation (Jiang et al., 2007).

Extensive gene expression changes that integrate signals from external and internal factors are indispensable in the execution of evolved intricate adaptive strategies under low Pi conditions and are witnessed by transcriptome analysis in several plant species (Yang and Finnegan, 2010). Transcription factors (TFs) are the major regulators of stress-associated gene expression changes. Several recent studies have identified TFs involved in the regulation of Pi availability-related gene expression changes. PHOSPHATE STARVATION RESPONSE 1 (PHR1), a member of the MYB TF super family was identified in a mutant screen, where the mutants are impaired in Pi-responsive transcript and anthocyanin accumulation (Rubio et al., 2001; Bari et al., 2006). *OsPHR1* and *2*, the two *AtPHR1* orthologs in rice, have been identified to regulate the Pi-deficiency response similar to that in Arabidopsis (Zhou et al., 2008). Further, a Pi-starvation induced TF, MYB62, plays a major role during Pi limitation resulting in changes in root length, root phosphatase activity, and anthocyanin accumulation. The MYB62-mediated Pi starvation response has been proposed to act through the regulation of gibberellin levels (Devaiah et al., 2009; Yang and Finnegan, 2010). Few other TFs that were identified to have a functional role in the Pi starvation response include Arabidopsis ZAT6, bHLH32, PTF1, WRKY75, and rice OsWRKY74, among others (Yi et al., 2005; Chen et al., 2007; Devaiah et al., 2007a,b; Dai et al., 2016). Importantly, these TFs act as nodes in the crosstalk between Pi starvation- and hormone-signaling in regulating the plant response to Pi limitation (Rouached et al., 2010), but only a few TFs have been identified so far.

Despite Pi addition is a common practice to increase yield in cultivated plants and plant response to low Pi has been studied in detail, the underlying mechanisms explaining plant response to reiterated changes in Pi availability has been poorly studied to date. In poplar, it was found that stem cuttings derived from sites with lower Pi availability established worse, irrespective of Pi level after transplantation, which was correlated with differences in DNA methylation (Schönberger et al., 2016). Epigenetic modifications are of high interest to better understand priming or memory effects and may serve as an excellent basis to better exploit Pi resources, an important nutrient that is very likely to become limited in the near future (Herrera-Estrella and López-Arredondo, 2016). In this respect, current genetic resources in the model plant *A. thaliana* can be used to better understand priming effects in plant response to contrasting Pi availability.

Chloroplast-nuclear retrograde signaling regulates gene expression, but its integration with redox and hormonal signaling is still poorly understood (Pfannschmidt and Munné-Bosch, 2013). It has been shown that changes in the vitamin E composition in chloroplasts profoundly alters gene expression in the nucleus, particularly of ethylene-related signaling genes, including *ERF1* (Cela et al., 2011), an essential regulatory hub of ethylene, jasmonic acid, and ABA signaling (Müller and Munné-Bosch, 2015). Recently, transorganellar complementation has also revealed that vitamin E can access the lumen of the endoplasmic reticulum without necessarily involving transporters (Mehrshahi et al., 2013), which opens the possibility of vitamin E directly influencing redox signaling outside chloroplasts.

In the current study, with the aim of getting new insights into the possible retrograde signaling function of vitamin E as an antioxidant in chloroplasts, we examined the response of wild

type and vitamin E-deficient *A. thaliana* plants to contrasting levels of Pi availability, including a priming treatment. We aimed at understanding the effect of varying Pi availability on the expression of whole TFs that govern the downstream gene expression changes orchestrating plant growth and response to low Pi conditions. Emphasis was put on the possible effects of vitamin E deficiency on TFs and hormonal profiling.

MATERIALS AND METHODS

Plant Material, Treatments, and Sampling

Seeds of *A. thaliana* Columbia ecotype (Col-0), and *vte1* (GK_111D07) and *vte4* (SALK_036736) mutants were used in this study. *vte1* and *vte4* mutants have T-DNA insertions in the *VTE1* and *VTE4* genes (Porfirova et al., 2002; Bergmüller et al., 2003), which encode tocopherol cyclase and γ-tocopherol methyltransferase, respectively, so that the *vte1* mutant lacks both α- and γ-tocopherol, and the *vte4* mutant lacks α-tocopherol but accumulates γ-tocopherol (**Figure 1**).

Seeds were cold-stratified and sown in 0.1 L-pots in soil (Einheitserde GS90; Gebrüder Patzer) in a climate-controlled chamber with a 8-h day length provided by fluorescent light at 100 μmol m^{-2} s^{-1}, a day/night temperature of 20/16.8°C and a relative humidity of 60/75% (day/night). Prior to treatments, plants were watered every third day during 23 days with high Pi nutrient solution containing 5 mM $Ca(NO_3)_2$, 5 mM KNO_3, 2 mM $MgSO_4$, 1 mM KH2PO_4, and 5 g/L iron chelate (EDTA FeNa). Next, plants were divided into four sets and were subjected to varying phosphate treatments (**Figure 2**). One set of plants was supplied with the same high Pi nutrient solution (containing 1 mM KH_2PO_4) every other day throughout the experiment (high Pi-plants). Contrasting Pi levels were then supplied to the other three set of plants by using 0.5 mM instead of 1 mM KH_2PO_4 in the nutrient solution (low Pi). This nutrient solution was supplied with 0.5 mM KCl to compensate for K deficiency. Typically, low Pi (0.1 mM) and high Pi (ranging between 0.5 and 2.5 mM) are used in studies on Pi starvation in *A. thaliana* (Williamson et al., 2001). However, our studies indicated that 0.5 mM Pi is an adequate concentration to induce priming effects ultimately resulting in enhanced growth (**Figure 3**).

Samplings were performed at midday (in the middle of the photoperiod) at the end of treatments. Whole rosettes of six individuals were used to estimate leaf water contents, chlorophyll levels, the F_v/F_m ratio, and the levels of plastochromanol-8 and vitamin E, as well as the TFs and hormonal profiling. Samples for biochemical and transcriptional analyses were collected, immediately frozen in liquid nitrogen and stored at −80°C until analysis.

Leaf Water and Nutrient Content, Chlorophyll Level, F_v/F_m ratio and Lipid Peroxidation

Samples were weighed to estimate the fresh matter (FW), immersed in distilled water at 4°C for 24 h to estimate the turgid matter (TW) and then oven-dried at 80°C to constant weight to estimate the dry matter (DW). Relative water content (RWC) was then calculated as 100 × (FW − DW)/(TW − DW). For analyses of macro- and micronutrients (P, S, Ca, Mg, K, Na, Mn, Zn, Fe, Mo, B, Cu, and Si), dried samples were weighed, digested with HNO_3, and analyzed by inductively coupled plasma atomic emission spectroscopy (ICP-AES). For pigment analysis, measurements were performed using a SPAD 502 Plus chlorophyll meter. The maximum efficiency of the photosystem II (F_v/F_m ratio) was determined measuring the chlorophyll fluorescence of leaves by using a pulse-modulated fluorometer (Mini PAM; Walz, Effeltrich, Germany) as described by Genty et al. (1989). The extent of lipid peroxidation was estimated by measuring the levels of malondialdehyde (MDA) in leaves. MDA levels were estimated spectrophotometrically following the thiobarbituric acid-reactive assay considering the effect of potential interfering compounds, as described (Hodges et al., 1999).

Tocochromanol Contents

For analyses of vitamin E and plastochromanol-8 contents, leaf samples (50 mg) were ground in liquid nitrogen and extracted with cold methanol (v/v) using ultra-sonication. After centrifuging at 8000 rpm for 10 min and 4°C, the supernatant was collected and the pellet re-extracted with the same solvent until it was colorless; then, supernatants were pooled, filtered, and injected into the HPLC. Tocochromanols were separated isocratically on a normal-phase HPLC system using a fluorescent detector as described (Cela et al., 2011). Compounds were identified by co-elution with authentic standards and quantified by using a calibration curve.

Transcription Factor Profiling

For the large-scale TF (a total of 1,880 TFs) profiling using qRT-PCR, total RNA was extracted from whole rosette leaves. Primer sequences are provided in Supplementary Table 10. Total RNA extraction, synthesis of cDNA, and qRT-PCR were performed as described (Caldana et al., 2007). ACTIN2 was used as reference gene. PCR reactions were run on an ABI PRISM 7900HT sequence detection system (Applied Biosystems Applera), and SYBR Green (Life Technologies) was used for visualizing amplified products.

GO Enrichment Analysis

Gene ontology (GO) enrichment analysis for the priming specific TFs was performed using PLAZA 3.0 using default settings (Proost et al., 2015).

Clustering Analysis

Differentially expressed genes were visualized as heatmaps using multiple expression viewer (Mev[1]; Saeed et al., 2003). Cluster analysis for differentially expressed genes was performed with Short Time-series Expression Miner (STEM) software using default settings (Ernst and Bar-Joseph, 2006).

[1]http://www.tm4.org/

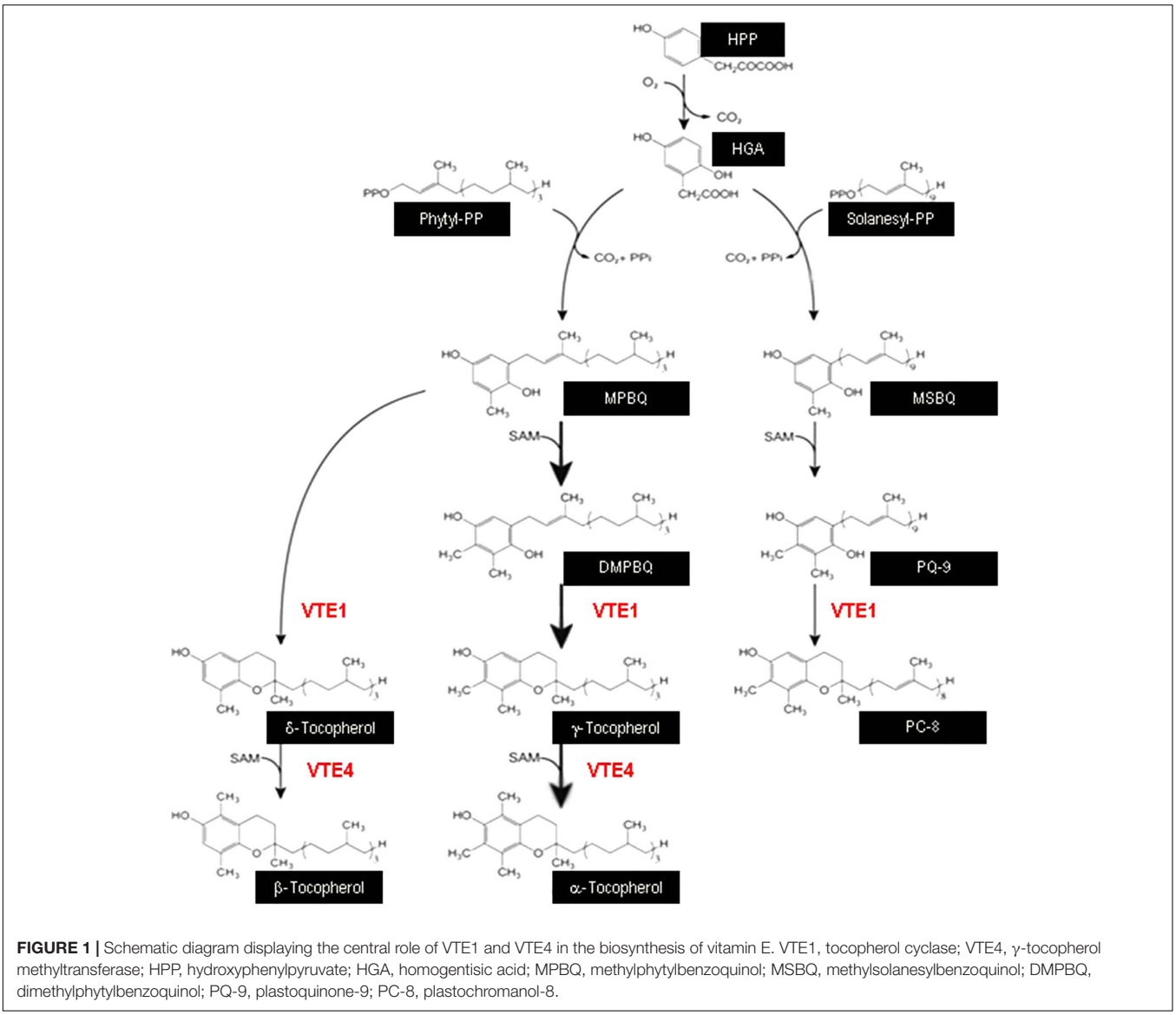

FIGURE 1 | Schematic diagram displaying the central role of VTE1 and VTE4 in the biosynthesis of vitamin E. VTE1, tocopherol cyclase; VTE4, γ-tocopherol methyltransferase; HPP, hydroxyphenylpyruvate; HGA, homogentisic acid; MPBQ, methylphytylbenzoquinol; MSBQ, methylsolanesylbenzoquinol; DMPBQ, dimethylphytylbenzoquinol; PQ-9, plastoquinone-9; PC-8, plastochromanol-8.

Hormonal Profiling

For analyses of cytokinins, auxin, gibberellins, ABA, salicylic acid, jasmonates, the ethylene precursor, 1-aminocyclopropane-1-carboxylic acid, and melatonin, leaf samples (50 mg) were ground in liquid nitrogen and extracted with cold methanol:isopropanol:acetic acid (50:49:1, v/v/v) using ultra-sonication. After centrifuging at 8000 rpm for 10 min and 4°C, the supernatant was collected and the pellet re-extracted with the same solvent until it was colorless; then, supernatants were pooled, filtered, and injected into the UHPLC-MS/MS. Phytohormones were separated using an elution gradient on a reverse-phase UHPLC system and quantified using tandem mass spectrometry in multiple reaction monitoring mode as described (Müller and Munné-Bosch, 2011). Recovery rates were calculated for each hormone on every sample by using deuterated compounds.

Statistical Analysis

Data was analyzed by using three-way and one-way factorial analysis of variance (ANOVA), and by additionally using Duncan *post hoc* tests to analyze for the effects of genotypes at each condition. In all cases, differences were considered significant at a probability level of $P < 0.05$. All statistical tests were carried out using the SPSS 20.0 statistical package.

RESULTS

Plant Response to Contrasting Phosphate Availability

In order to understand plant adaptive mechanisms to contrasting Pi availability, plants were grown in a controlled environment initially to attain uniform growth among all the genotypes under study. Later, one set of plants were supplied with the

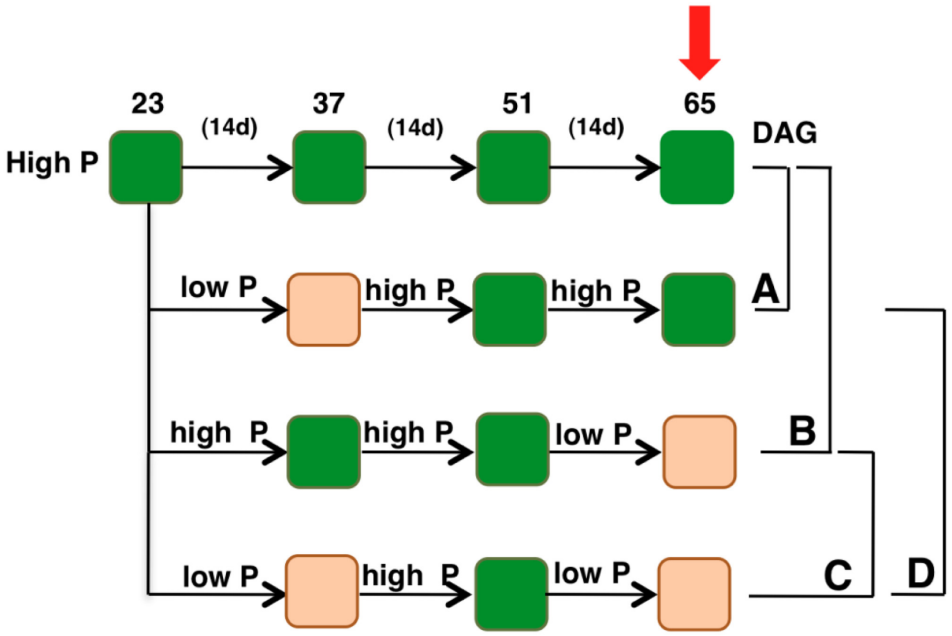

FIGURE 2 | Schematic diagram displaying the experimental plan. All the genotypes were grown with 1 mM potassium phosphate (hereafter called high Pi) for 23 days. Contrasting Pi levels were then supplied to the plants in three different sets. Orange blocks indicate periods during which the plants were supplied with 0.5 mM potassium phosphate (hereafter called low Pi). Arrow indicates the time point when sampling was performed. DAG, days after germination. (A–C) Show comparisons used for data analyses.

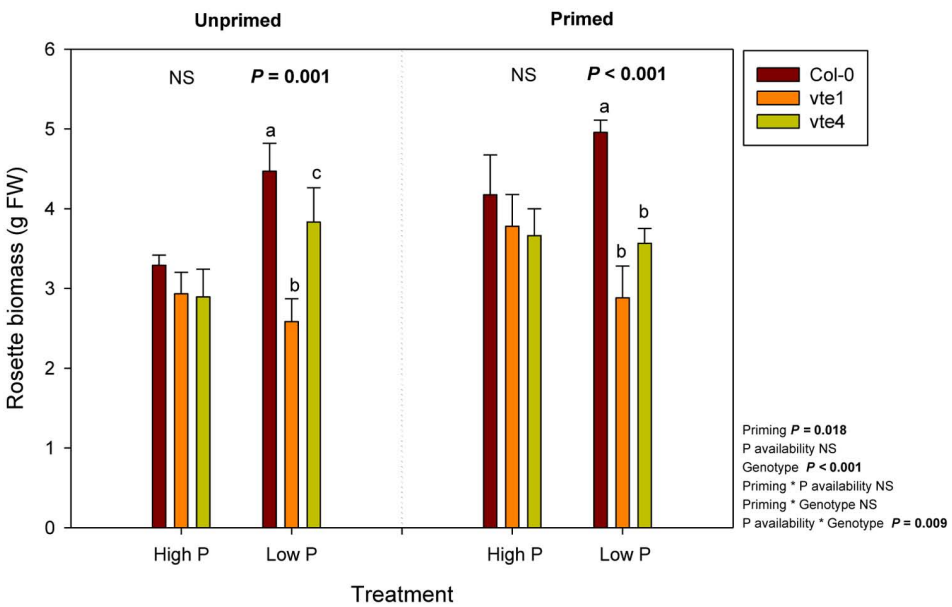

FIGURE 3 | Rosette biomass of vitamin E-deficient (*vte1* and *vte4* mutants) and wild-type plants of *Arabidopsis thaliana* exposed to contrasting Pi availability, including unprimed and primed plants. Data represent the mean ± SE of $n = 6$ individuals. Significant differences between groups were tested by three-way analysis of variance (ANOVA, $P < 0.05$). Different letters significant differences between genotypes at any given treatment (Duncan *post hoc* tests, $P < 0.05$). NS, not significant.

same Pi concentration (hereafter called high Pi), whereas half the concentration (hereafter called low Pi, see "Materials and Methods") was supplied to plants in three different sets to understand plant response to contrasting Pi availability and priming effects. The first set included plants supplied with low Pi for 2 weeks and then returned to high Pi; the second set

included plants grown under high Pi condition and then exposed to low Pi for 2 weeks just prior to samplings. To capture the effects of priming, plants were exposed to low Pi, returned to high Pi condition and then later exposed to second spell of low Pi (**Figure 2**).

Rosette biomass was not affected by Pi availability, but it was significantly influenced by the genotype and priming. Plant biomass did not differ between genotypes under high Pi, either in unprimed or primed plants. However, rosette biomass was lower in the *vte1* mutant compared to wild-type plants at low Pi in unprimed plants, and in both mutants relative to the wild type in primed plants (**Figure 3**). Wild-type plants were the ones better adapted to low Pi in terms of biomass accumulation, so that priming had positive effects on plant growth. α-Tocopherol deficiency prevented the mutants to benefit from low Pi availability, as indicated by the smaller rosette biomass in both *vte* mutants compared to wild-type plants under primed conditions at low Pi (**Figure 3**). Despite these effects on growth, endogenous Pi concentrations did not differ between genotypes at any tested conditions (**Figure 4**). Furthermore, none of the other nutrients measured revealed any significant genotype-related difference ($P < 0.05$, ANOVA, Supplementary Figures 1, 2).

Tocochromanols, including α- and γ-tocopherol, as well as plastochromanol-8, were not detected in the *vte1* mutant, while both γ-tocopherol and plastochromanol-8 accumulated in the absence of α-tocopherol in the *vte4* mutant (**Figure 5**). In contrast, wild-type plants accumulated α-tocopherol in leaves, particularly at low Pi in primed condition. The contents of this antioxidant doubled at low Pi availability in primed compared to unprimed plants (**Figure 5**). The contents of γ-tocopherol also increased to a similar extent in the *vte4* mutant at low Pi in primed plants only. Plastochromanol-8 contents did not follow the same variations (**Figure 5**).

Changes in photo-oxidative stress markers, including chlorophyll contents, the maximum efficiency of PSII photochemistry (F_v/F_m ratio), and the extent of lipid peroxidation, estimated as MDA accumulation (**Figure 6**) paralleled those of rosette biomass (**Figure 3**), though effects were observed to a much more limited extent, particularly at low Pi in primed plants. Both chlorophyll contents and the F_v/F_m ratio were lower in the *vte1* mutant compared to wild-type plants under primed condition at low Pi. However, reductions in the F_v/F_m ratio were very small, the values in all plant genotypes being always above 0.75 (**Figure 6**). No significant differences in the extent of lipid peroxidation were observed between genotypes, Pi availability or priming (**Figure 6**).

Differential Expression Pattern of TFs to Varying Pi Availability

Transcription factors, the major regulators of gene expression changes play a pivotal role in plant stress responses. To identify such transcriptional regulators that may have possible roles in the regulation of plant response to low Pi conditions and capture the priming effect on plant's response to contrasting Pi availability, 1,880 Arabidopsis TFs expression was profiled under experimental conditions described above using quantitative real-time PCR (qRT-PCR). Obtained data was analyzed to identify TFs that respond differentially to varying low Pi conditions: (A) TFs responding to low Pi pre-treatment at high Pi, (B) TFs responding to a single low Pi episode, (C) Priming responsive TFs, and (D) TFs responding to recurrent low Pi stimuli (**Figure 2**).

In wild-type plants, a total of 454 TFs were differentially expressed with a 3-$\log_2$ fold change as cut-off (either up- or down-regulated) in any of the four comparisons performed, representing ∼ 24% of TFs tested in this study (**Figure 7A** and Supplementary Table 1). Diverse expression patterns of these TFs under different conditions tested suggest a massive transcriptional re-programming involved in plant response to Pi availability. Differentially expressed TFs (DETFs) represented several TF families such as MYB, AP2-EREBP, bZIP, bHLH, AGL, and BBX, among others. These TFs were manually classified based on their expression pattern as either A, B or C specific (Supplementary Table 2). The "A" group contains 69 TFs that were specifically up- (43) or down-regulated (26) in response to low Pi pre-treatment at high Pi, representing ∼15% of total DETFs. Forty-six TFs (∼10% of total DETFs) expressed specifically to a single low Pi episode (B), but only four of them were up-regulated. Interestingly, ∼12% of DETFs (29 up- and 24 down-regulated) were specifically expressed in response to priming treatment (C). These include several TFs functioning in response to plant growth or stress responses. For example, *SWI2C,* a core component of the SWI/SNF-type chromatin-remodeling complex C (CRCs), was up-regulated in a priming specific manner. SWI2C is a growth regulator and has been identified to interact with DELLA proteins (Sarnowska et al., 2013). Anthocyanin accumulation is a typical phenotypic response under Pi starvation (Morcuende et al., 2007); interestingly MYB111 and MYB113 involved in the regulation of anthocyanin production (Tohge et al., 2013) were repressed specifically in primed plants. Next, GO enrichment analysis was performed for the DETFs that showed priming specific expression using PLAZA 3.0 (Proost et al., 2015). Significantly over-represented GO terms describing the biological process include "gibberellin biosynthesis process," "ABA-activated signaling pathway," "regulation of triglyceride catabolic process," and "histone H3- and H4-acetylation" (Supplementary Figure 3). These GO terms indicate the underlying mechanism of priming effect on plant response to low Pi (Supplementary Figures 4–6).

Additionally, in order to visualize cluster profiles of the DETFs based on their expression direction and magnitude, STEM (STEM) was employed. A comparison of observed groups with those expected in random permutation enables to determine enrichment of the obtained clusters (Ernst et al., 2005; Ernst and Bar-Joseph, 2006). Such comparison of expression patterns resulted in profiles classified into 50 categories in the response of wild-type plants to contrasting Pi availability (**Figure 7B**). Out of the 50 possible clusters, eight clusters were found to be significant (P-value ≤ 0.05). Colored blocks in (**Figure 7B** and Supplementary Table 3) display expression profiles of significant clusters (clusters 6, 11, 20, 24, 31, 34, 44, and 45) arranged based on their significance. MYB TF family represented the highest

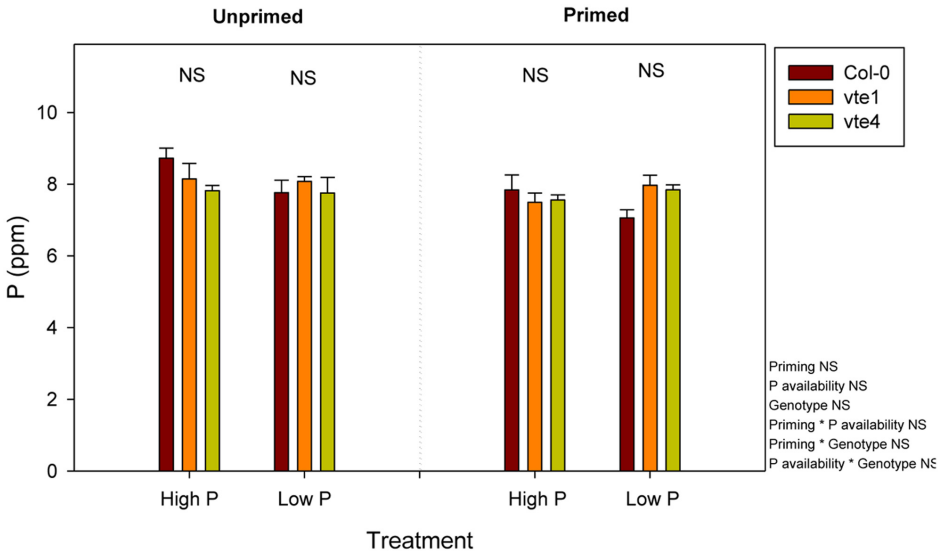

FIGURE 4 | Endogenous P contents in vitamin E-deficient (*vte1* and *vte4* mutants) and wild-type plants of *A. thaliana* exposed to contrasting Pi availability, including unprimed and primed plants. Data represent the mean ± SE of $n = 6$ individuals. Significant differences between groups were tested by three-way analysis of variance (ANOVA, $P < 0.05$). NS, not significant. Results are expressed as parts per million (ppm) on a dry matter basis.

number among the various cluster profiles, followed by AGL and bHLH TF families. Cluster profiles 6, 44, and 31 displayed 73, 67, and 47 TFs, respectively, representing larger cluster groups, among others. To understand the biological significance of the obtained cluster profiles, GO terms enriched in the TF clusters were analyzed. Profile 6 is enriched for TFs associated with GO terms "regulation of response to stimulus," "response to jasmonic acid, endogenous stimulus, hormone, stress, acid chemical, oxygen containing compound, gibberellin, salicylic acid, and ethylene," "regulation of signal transduction, jasmonic acid-mediated signaling pathway," and "chromatin modification and organization," among others. Profile 44 represents GO terms "regulation of cellular macromolecule biosynthetic process," "nucleobase-containing compound metabolic process," "organic substance biosynthesis and metabolic process," and "root system development," among others. Profile 31 represents "response to salt and osmotic stress, alcohol, lipid."

Vitamin E Deficiency Alters Plant Response to Contrasting Pi Availability

Given the extensive expression changes of TFs under varying Pi availability in wild-type plants (**Figure 7A**), it was interesting to study how an altered tocopherol composition affects the expression of those transcriptional regulators under contrasting Pi availability. Toward this, we performed whole TF profiling in *vte1* and *vte4* mutants under the above described conditions (**Figure 2**). A total of 568 and 583 TFs were differentially expressed (both up- and down-regulated with 3-$\log_2$ fold change as cut-off threshold) in *vte1* and *vte4* mutants compared to the wild type (**Figure 8** and Supplementary Tables 4, 5) representing ∼30 and ∼31% of the total TFs analyzed, respectively. DETFs in the *vte1* mutant are represented by a mixture of TF families, while TFs belonging to MYB, AGL, bZIP, bHLH TF families were abundant in the *vte4* mutant compared to the wild type. To identify TFs that exhibit condition specific expression patterns, manual classification was performed (Supplementary Tables 6, 7) as described above (see also **Figure 2**). In the *vte1* mutant, 49 TFs were specific to group A of which, 34 and 15 were up- and down-regulated, respectively, representing ∼9% of the total DETFs. *vte4* mutant displayed ∼8% TFs specific to group A with 14 and 29 up- and down-regulated, respectively. Contrasting to the wild type, the *vte1* mutant displayed more TFs specific to group B with 121 up-regulated and only 1 down-regulated (∼22% of DETFs). In the *vte4* mutant, around 8% (35 up- and 8 down-regulated) of total DETFs responded specifically to group B. The TFs involved in the regulation of anthocyanin were up-regulated in both the mutants compared to wild-type plants, suggesting that the mutants were experiencing stress under low Pi compared to the wild type. For example, in the *vte1* mutant, *MYB112* was induced in group A and *MYB114* up-regulated in both A and B, both known to be involved in the regulation of anthocyanin production (Tohge et al., 2013; Lotkowska et al., 2015). Furthermore, ∼8% TFs displayed a priming specific (group C) expression pattern, of which 28 and 16 were up- and down-regulated in the *vte1* mutant compared to the wild type. Interestingly, several of these TFs showed an opposite priming specific expression pattern in wild-type plants. Priming repressed TFs in the wild type, *MYB111* and *MYB113* expression was induced in *vte1* primed plants, which suggests that these plants could not benefit from priming.

Varying number of TFs representing group specific expression pattern among *vte1* and *vte4* mutants was observed which might suggest diverse roles for the different tocopherol forms. As contrasting to *vte1*, *vte4* mutants displayed ∼24%

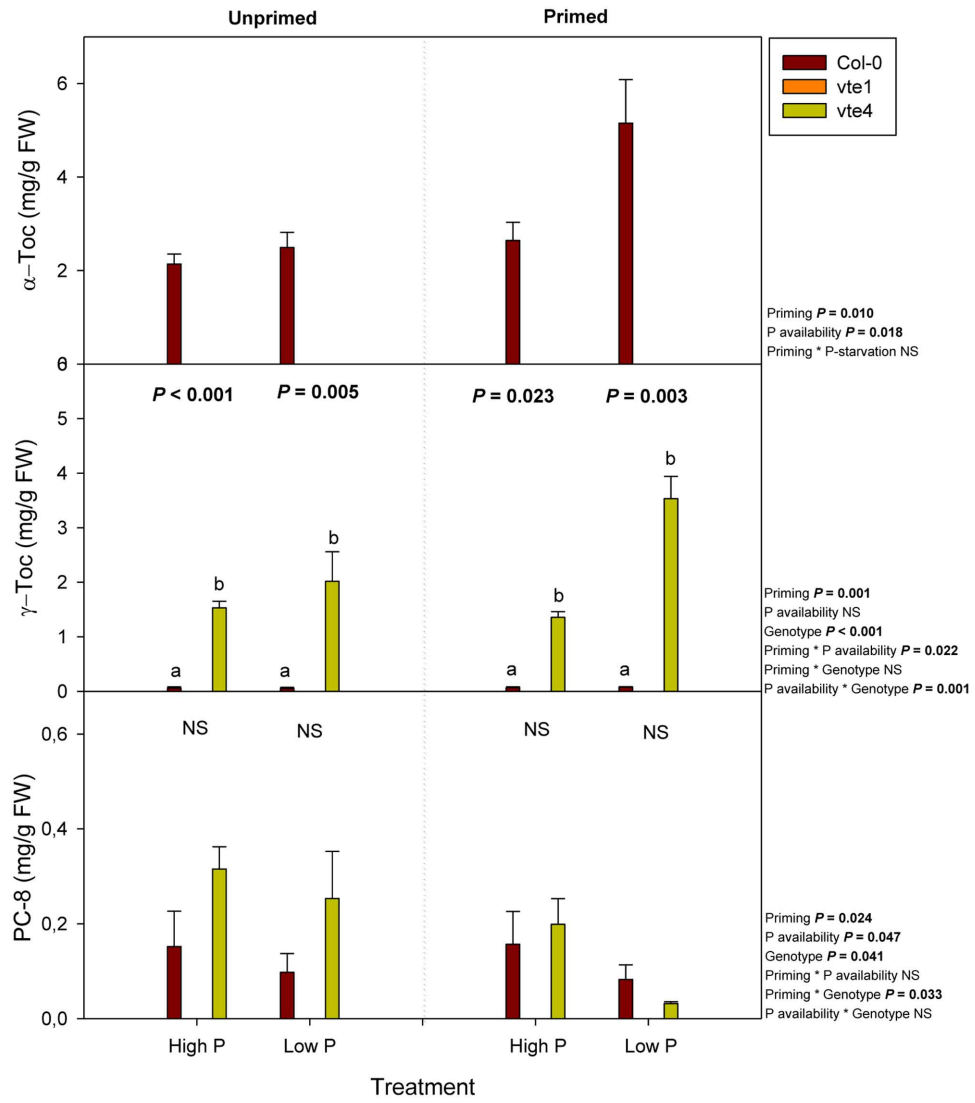

FIGURE 5 | Endogenous contents of α-tocopherol, γ-tocopherol, and PC-8 in vitamin E-deficient (*vte1* and *vte4* mutants) and wild-type plants of *A. thaliana* exposed to contrasting Pi availability, including unprimed and primed plants. Data represent the mean ± SE of $n = 6$ individuals. Significant differences between groups were tested by three-way analysis of variance (ANOVA, $P < 0.05$). Different letters significant differences between genotypes at any given treatment (Duncan *post hoc* tests, $P < 0.05$). NS, not significant.

(56 up- and 81 down-regulated) TFs with priming specific expression pattern compared to the wild type. *MYB111* expression was also increased in primed plants. Expression of *ZAT6*, a negative regulator of Pi homeostasis (Devaiah et al., 2007b) was up-regulated in the *vte4* mutant in a priming specific manner. Previously, expression of several ethylene signaling pathway genes such as *EIN2*, *EIN3*, *CTR1,* and *ERF1* has been reported to be up-regulated in the *vte4* mutant upon salt stress compared to wild-type plants (Cela et al., 2011). In the present study, expression of several ERFs was induced, while *EIN* and *EIL3* expression was repressed in primed *vte4* plants. GO enrichment analysis of the priming specifically expressed TFs revealed interesting over-represented GO terms such as "ethylene mediated signaling pathway," "cytokinin activated signaling pathway," "TF import to nucleus," and "histone H3 K27 methylation" in *vte1* mutant; "salicylic acid-mediated signaling pathway," "sucrose-induced translational repression," and "regulation of pectin biosynthesis and metabolism" in *vte4* mutant. Activation of cytokinin signaling pathway in *vte1* mutant indicate attenuated low Pi response in these plants, as cytokinins negatively regulate Pi starvation responses (Yang and Finnegan, 2010). Defense hormone SA-mediated signaling and pectin biosynthesis in the *vte4* mutant suggests activated defense response networks in *vte* mutants in response to priming. Further, positive effect of priming on the growth observed in the wild type was compromised in *vte* mutants possibly due to the tradeoff toward defense.

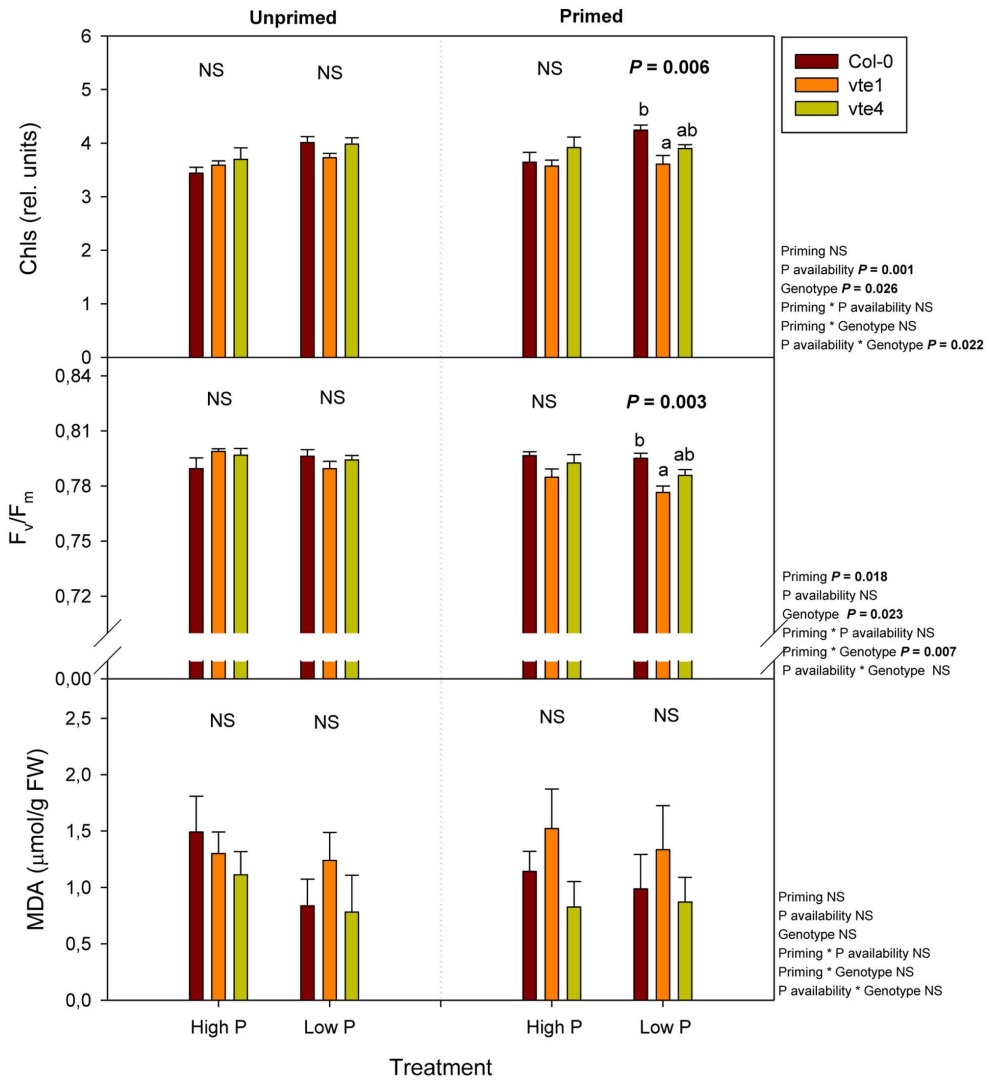

FIGURE 6 | Total chlorophyll contents (given as relative units), maximum efficiency of PSII photochemistry (F_v/F_m ratio), and malondialdehyde (MDA) accumulation, an indicator of the extent of lipid peroxidation in leaves, in vitamin E-deficient (*vte1* and *vte4* mutants) and wild-type plants of *A. thaliana* exposed to contrasting Pi availability, including unprimed and primed plants. Data represent the mean ± SE of $n = 6$ individuals. Significant differences between groups were tested by three-way analysis of variance (ANOVA, $P < 0.05$). Different letters significant differences between genotypes at any given treatment (Duncan *post hoc* tests, $P < 0.05$). NS, not significant.

Next, to understand those expression patterns observed among different Pi availability conditions in both the mutants, first we clustered the DETFs into profiles using STEM. A total of 50 possible cluster profiles were obtained for both mutants, of which, 7 (5, 6, 24, 27, 44, 45, and 47) and 9 (5, 6, 12, 14, 23, 24, 27, 28, and 44) clusters were found to be significant in *vte1* and *vte4* mutants, respectively (**Figures 9A,B** and Supplementary Tables 8, 9). Further, these significant clusters were compared with the significant clusters obtained from wild-type plants using STEM, where the TFs in each cluster from the mutants were compared with their magnitude of expression and direction in the wild type. Interestingly, such correlation revealed opposite patterns for many of the cluster profiles between the mutants and the wild type (**Figures 9A,B**). To learn about the involvement of tocopherols in mediating the plant response to contrasting Pi availability, these oppositely expressed TFs could serve as a valuable resource. Additionally, learning about the GO terms associated with these TFs would help to expand our knowledge in understanding the adaptive mechanisms associated with vitamin E under varying Pi availability. Interestingly, the largest cluster profiles 6 and 44 of wild-type plants showed good correlation with the cluster profiles of the *vte1* mutant. Wild type profile 6 and 44 in the *vte1* mutant displayed TFs representing similar GO terms such as "response to: gibberellin, hormone, endogenous stimulus, organic substance, ethylene, lipid, jasmonic acid, salicylic acid, auxin, ABA, organic cyclic compound," "regulation of: signaling, signal transduction, cell communication," and "negative regulation of: cellular, macromolecule biosynthesis

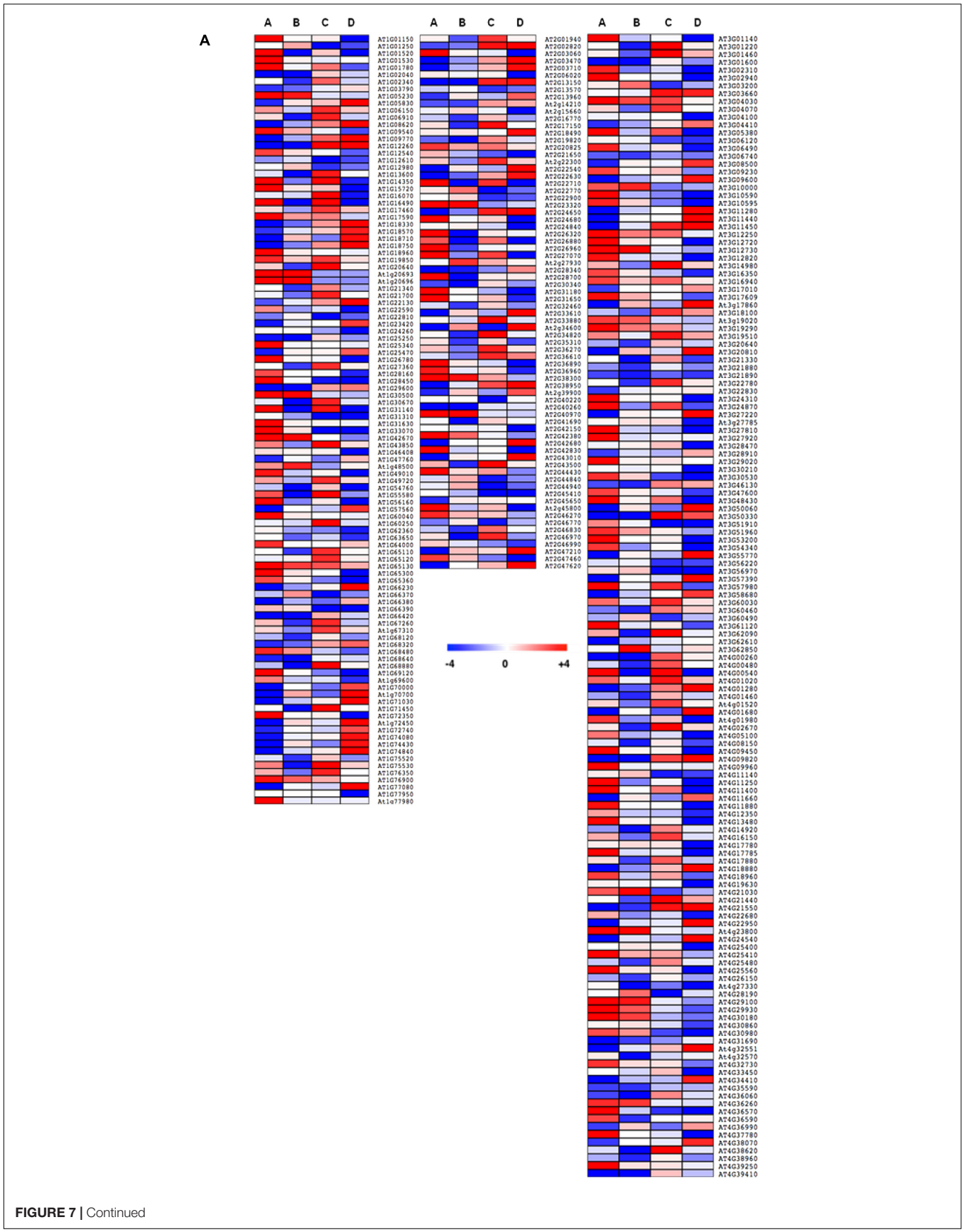

FIGURE 7 | Continued

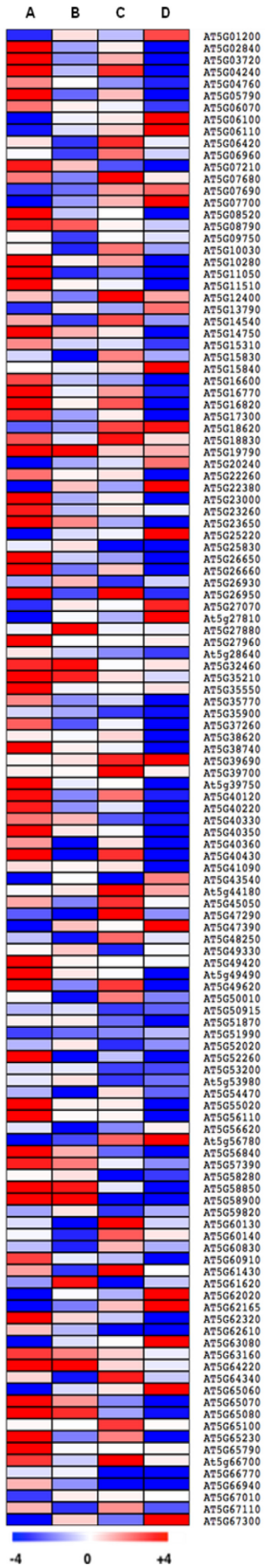

FIGURE 7 | Continued

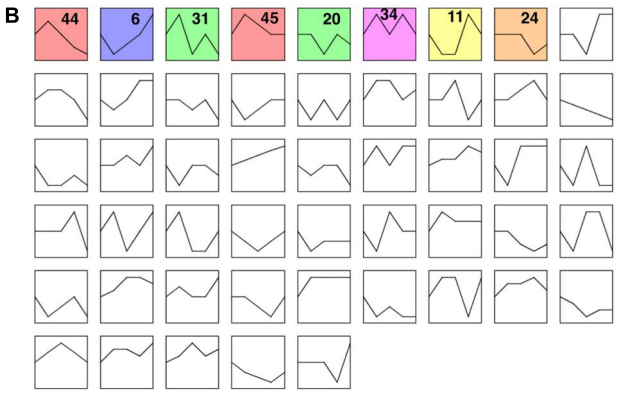

FIGURE 7 | Changes in Pi availability trigger massive alterations in transcription factors (TFs) gene expression. **(A)** Heatmap showing the expression pattern of differentially expressed TFs (DETFs) under varying Pi availability in the wild type (groups A–D, respectively, from left to right). **(B)** Clustering analysis of DETFs using Short Time-series Expression Miner (STEM) software resulted in eight distinct cluster profiles that were significant among the 50 possible clusters obtained. For each genotype and treatment, data was obtained from six individuals, using the mean of two independent measurements from three pooled plants each.

process, nucleobase-containing compound metabolic process" among others. Wild type profile 44 correlated with *vte1* profile 6 representing the GO terms "heterocyclic compound-, organic cyclic compound-, nucleic acid-binding," and "protein dimerization activity." Profile correlations between wild type and the *vte4* mutant as well showed significant GO enrichment terms. Wild type profile 6 and *vte4* profile 44 correlated TFs represented GO terms "response to gibberellin, stress, abiotic stress, osmotic stress, lipid, salicylates, ethylene," "chromatin modification, organization," and "histone modification," among others. Wild type profile 23 and *vte4* profile 24 displayed GO terms "cellular response to: ethylene stimulus, hormone stimulus, organic substance, endogenous and chemical stimulus," "ethylene activated signaling pathway,", "phosphorelay signal transduction system," and "hormone-mediated signaling pathway".

Hormonal Profiling Reveals Activated Defense Response in *vte* Mutants under Contrasting Pi Availability

Hormonal profiling revealed genotype-related differences, particularly for salicylic acid contents, which increased significantly in the *vte1* mutant compared to wild-type plants at low Pi, but in unprimed plants only. This effect was not observed in primed plants, because in this case salicylic acid contents increased similarly in the three genotypes at low Pi availability (**Figure 10**). Furthermore, enhanced jasmonic acid-isoleucine (JA-Ile) contents were observed in the *vte4* mutant compared to wild-type plants and the *vte1* mutant in primed plants at low Pi (**Figure 10**). No genotype-related differences were observed in the contents of cytokinins (Supplementary Figure 3), auxin (Supplementary Figure 7), gibberellins (Supplementary

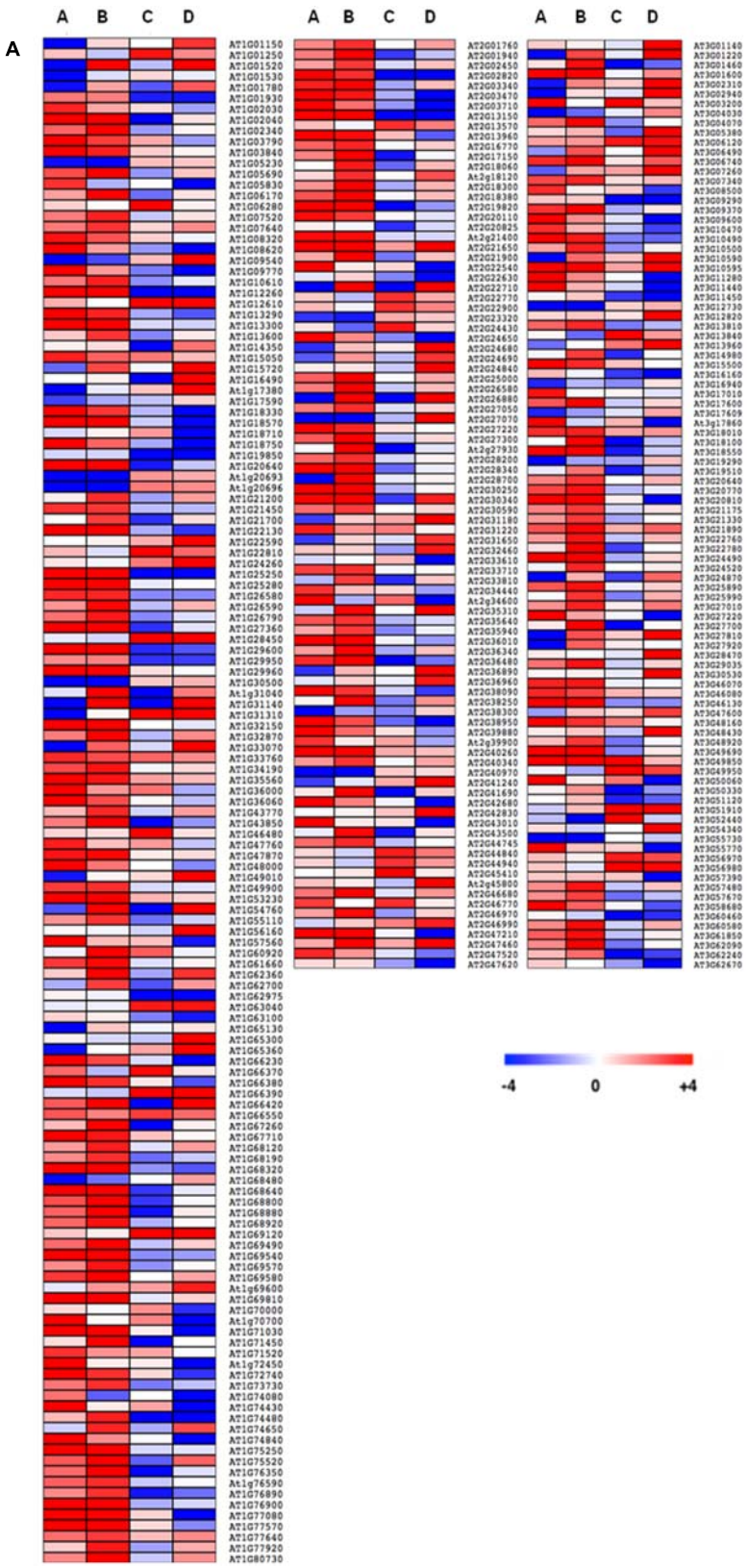

FIGURE 8 | Continued

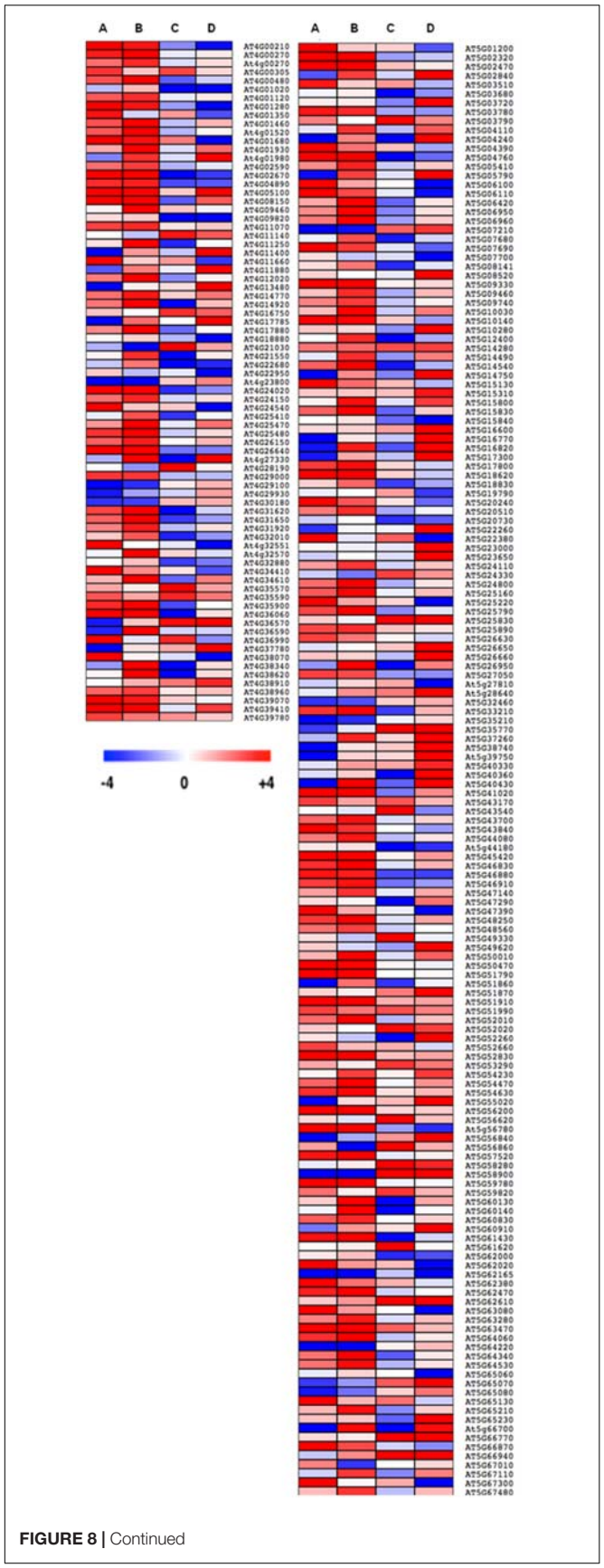

FIGURE 8 | Continued

Figure 8), ABA, the ethylene precursor, 1-amino-cyclopropane-1-carboxylic acid, or melatonin (Supplementary Figure 9). Priming had significant effects on jasmonates, salicylates, and auxin contents; defense-related compounds such as jasmonic acid in particular, increasing, and indole-3-acetic acid contents decreasing, in primed plants (**Figure 10** and Supplementary Figure 7). Low Pi availability increased the contents of *oxo*-phytodienoic acid and JA-Ile irrespective of priming, the latter particularly increasing in the *vte4* mutant in primed plants (**Figure 10**).

DISCUSSION

Phosphorus is one of the crucial macronutrients needed for the plants and its limitation leads to adaptations both at molecular, biochemical, and developmental level (Marschner, 2012). Our current study has shown that repeated exposure (priming) of plants to moderately low Pi availability condition improves growth in the model plant *A. thaliana*. Priming had a positive effect on plant growth in the wild type, but this effect was abolished in both *vte* mutants. Priming led to significant increases in α-tocopherol contents in the wild type, thus indicating α-tocopherol deficiency in both the *vte1* and *vte4* mutants may explain the genotype-related effects observed in the present study. It is noteworthy that both wild-type plants and the *vte4* mutant increased tocopherol levels (α- and γ-tocopherol, respectively) instead of those of plastochromanol-8 in response to priming, thus genotype-related effects on growth in primed plants may be related to changes in tocopherols rather than plastochromanol-8. Despite platochromanol-8 antioxidant role in thylakoid membranes (Kruk et al., 2014), it seems that tocopherols play a prominent role over plastochromanol-8 in regulating plant response to contrasting Pi availability in *A. thaliana*. Vitamin E deficiency had slight effects on photoinhibition (as indicated by reductions in chlorophyll levels and the F_v/F_m ratio), particularly in the *vte1* mutant, but differences between genotypes were very small and lipid peroxidation (as indicated by MDA accumulation) kept unaltered, thus indicating that genotype-related effects on growth in primed plants might be mostly associated with mechanisms other than a slightly enhanced photo-oxidative stress in leaves due to α-tocopherol deficiency. Here, it is shown that an alteration in the vitamin E composition and contents in chloroplasts may influence growth and defense though modulation of specific clusters of gene expression and hormones.

Transcription factors regulate the majority of gene expression changes and thus play a crucial role in regulating the plant response to various stresses including Pi limitation (Wu et al., 2003). Several studies have focused on identifying such TFs that are involved in the regulation of plant response to Pi limitation. For example, Arabidopsis MYB62, ZAT6, bHLH32, PTF1, WRKY75 and rice OsWRKY74 are of those TFs whose role in the regulation of Pi response have been identified (Yi et al., 2005; Chen et al., 2007; Devaiah et al., 2007a,b, 2009; Dai et al., 2016). Previously, genome wide expression profiling revealed

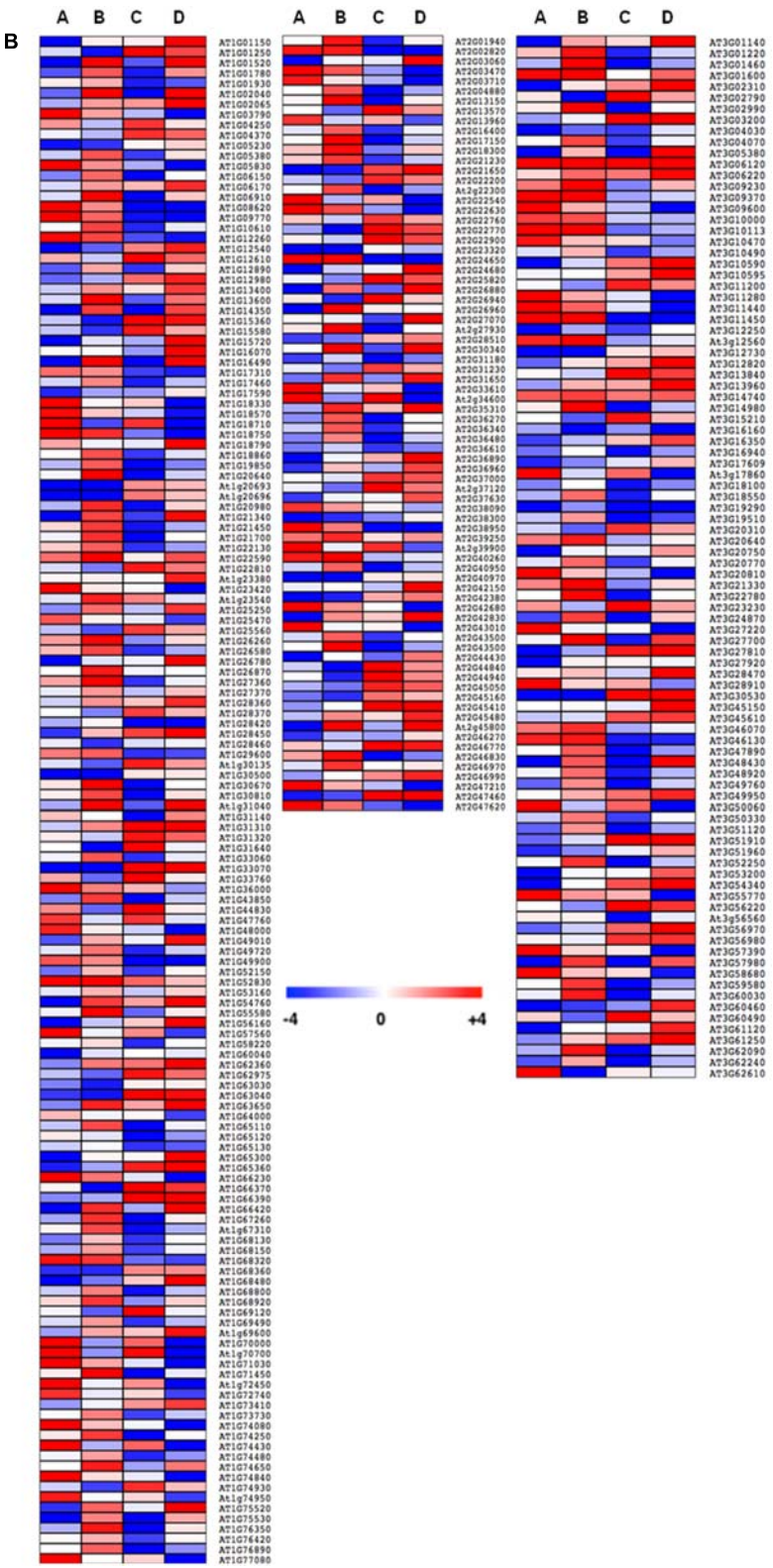

FIGURE 8 | Continued

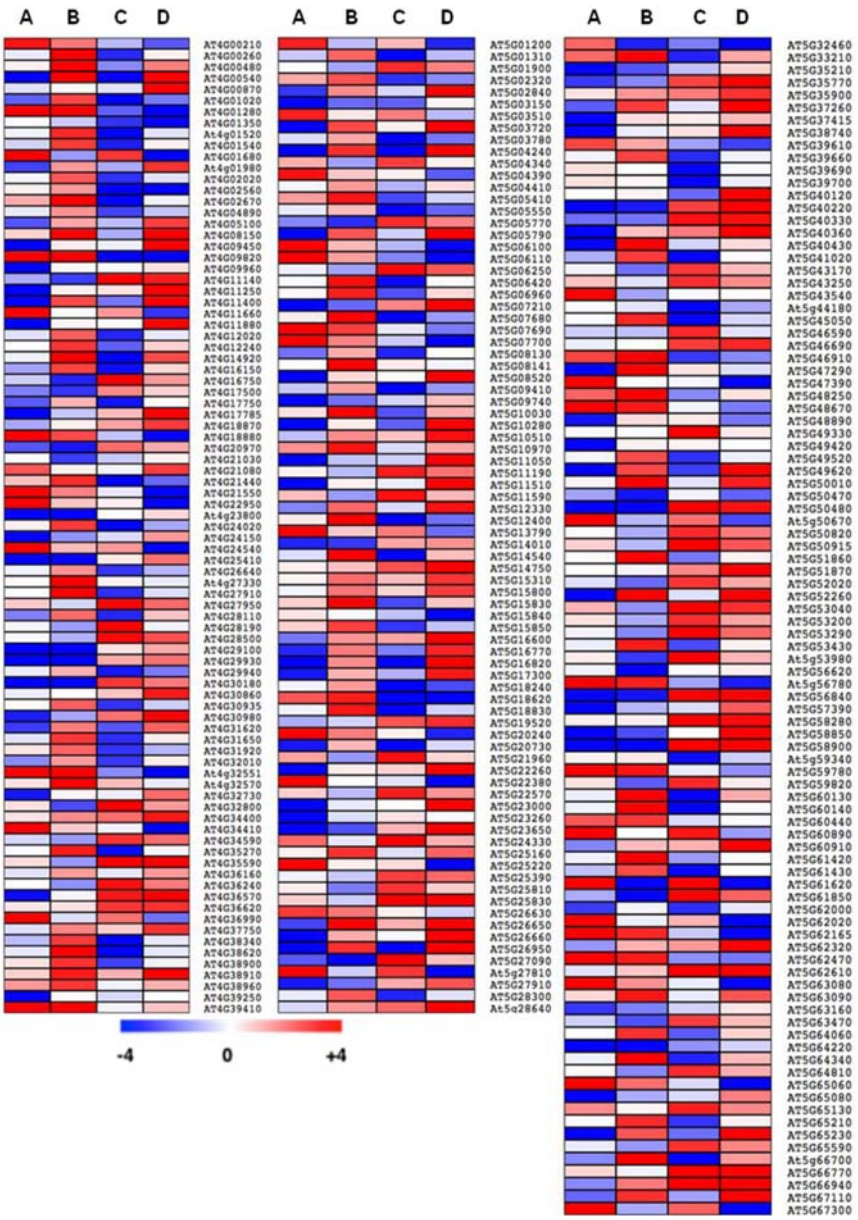

FIGURE 8 | Effect of vitamin E deficiency on TFs profile under contrasting Pi availability. Heatmap showing the expression pattern of DETFs under varying Pi conditions in *vte1*/wild type **(A)** and *vte4*/wild type **(B)**. Results for comparisons A–D, respectively, are shown from left to right. For each genotype and treatment, data was obtained from six individuals, using the mean of two independent measurements from three pooled plants each.

specific sets of TFs to be involved in regulation of early and late Pi deficiency responses (Misson et al., 2005). In this study, qRT-PCR analyses of 1,880 TF genes revealed massive transcriptional reprogramming in response to different phosphate regimes. Our data show that priming had a clear positive effect on the response to Pi limitation in wild-type plants. Transcript levels of 45 TFs were specifically deregulated (29 up- and 24 down-regulated) in response to priming treatment. These TFs are mainly associated with regulation of plant growth or response to stresses. Moreover, among TFs specifically repressed in response to priming, *MYB111* and *MYB113*, TFs involved in anthocyanin biosynthesis, were identified. This observation suggests that pre-exposure to a moderate Pi limitation renders the plant to efficiently safeguard when encountered with a second stress. Furthermore, priming specific induction of TF *SWI2C* involved in cross-talking with several hormonal pathways indicate a possible involvement of hormones in regulating the priming specific responses. Interestingly, priming specific TFs represent sets of TFs involved in stress responses such as *MYB102*, *ZAT12*, *MYB4R1*, *WOXY9A*, *HB22*, *HB52*, and *ANAC047*; disease responsive like *WRKY16* and *HAT3.1*; hormone related such as *AtABF1*, *ABI4*, *ABI5*, *ETHYLENE INSENSITIVE 3 FAMILY*

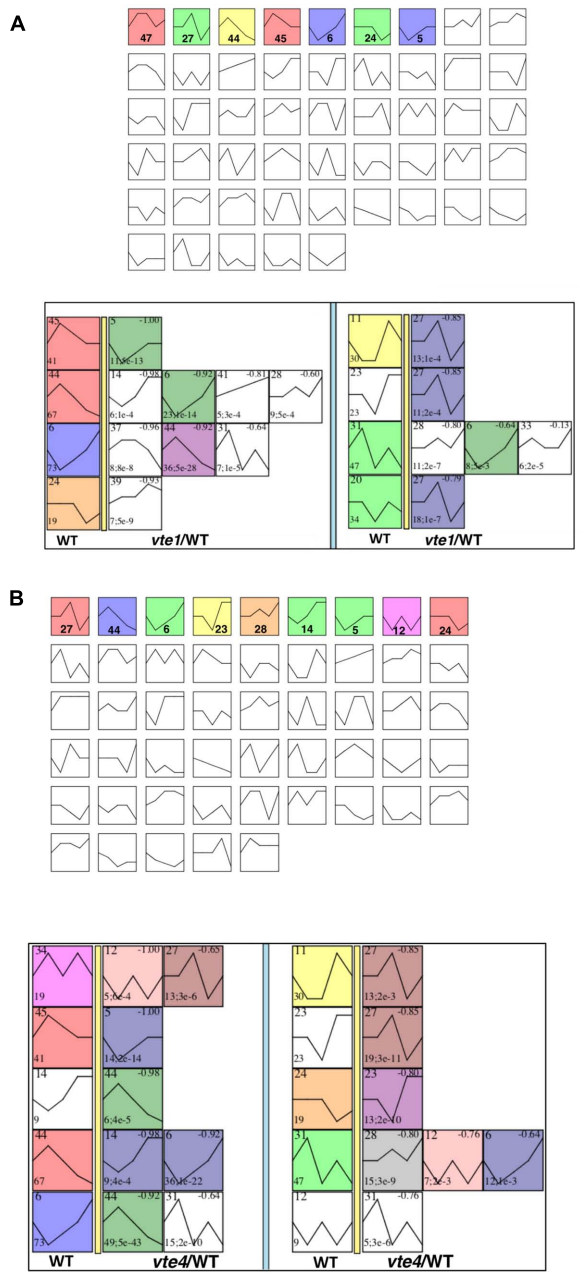

FIGURE 9 | Vitamin E deficiency alters the expression pattern of TFs to contrasting Pi availability. Cluster profiles of DETFs obtained using STEM software, significant profiles are represented in colored blocks (upper panel), blocks displaying the comparison of wild type with *vte* mutant profiles (lower panel). **(A)** *vte1*/wild type and **(B)** *vte4*/wild type. For each genotype and treatment, data was obtained from six individuals, using the mean of two independent measurements from three pooled plants each.

PROTEIN, and *ERF13*; development related like *SPL7*, *SPL12*, and *ULTULT1*; and *NLP5*, a TF involved in nitrate signaling. Enriched GO terms for the priming specifically expressed TFs display several interconnected pathways involved in the regulation of plant growth and stress responses. Regulation of growth promoting hormone (gibberellin) biosynthesis correlated well with the increased rosette biomass of the wild-type plants under primed condition. Previous studies reported ABA to have a minimal role in mediating low Pi responses (Franco-Zorrilla et al., 2004), whereas in the current study, enriched ABA-activated signaling in primed plants may suggest its possible role in regulating efficient stress response. Post-translational modifications of histones at specific amino acid residues such as acetylation, SUMOylation (Small ubiquitin-related modifier), ubiquitination, phosphorylation indicates the integrity of the nucleosome in that region (Berger, 2007). In Arabidopsis Pi deficiency response pathway, At-SIZ1 was identified to function as a SUMO E3 ligase, which can mediate SUMOylation of AtPHR1. It can also associate with a putative ubiquitin conjugase AtPHO1/UBC24 in the SUMOlylation pathway (Yang and Finnegan, 2010). Repression of target genes by endogenous or environmental cues can be achieved through reduction in histone acetylation levels, thus acetylation of histones is associated with gene activation (Dhar et al., 2014). Interestingly, histone H3 and H4 acetylation was over-represented in GO enrichment analysis for the priming specific TFs. It would be interesting to understand the possible link between histone acetylation and Pi responses, in particular upon priming.

Both *vte* mutants displayed distinct TF expression profile compared to wild-type plants under moderately low Pi availability. Induction of *MYB112* and *MYB114* (TFs involved in anthocyanin production) in the *vte1* mutant, and induction of *MYB62* (a repressor of Pi homeostasis) in both *vte1* and *vte4* mutants compared to the wild type indicate attenuated responses to Pi limitation in these plants. Furthermore, the *vte1* mutant displayed opposite expression pattern for several of the priming specific TFs found in wild-type plants, which may be linked to the lack of α-tocopherol in these mutants. Functional characterization of these TFs might give more insights into the role of α-tocopherol in regulating the plant response to Pi availability. Massive priming specific TF expression changes were also observed in the *vte4* mutant upon varying Pi availability, which include several TF families such as WRKY, bZIP, GATA, NAC, and ERF. GO enrichment analysis clearly indicates the potential role of tocopherols in regulating priming. Activated cytokinin-mediated signaling pathway marks the underlying attenuated low Pi response in *vte1* mutant. More interestingly, *vte1* mutants display heterochromatin state; as methylation of H3 lysine, especially H3K27me3 has been identified to be a major chromatin silencing modification associated with 1000s of genes at the 5′ region (Zhang et al., 2007; Dhar et al., 2014). Activated TF import into nucleus in the *vte1* mutant provides a mechanism to translate signals from the cytosol to the nucleus, thus indicating vitamin E deficiency may profoundly alter signaling processes. Activated defense responses in *vte4* mutants suggest a possible tradeoff regulation between growth and defense response. Furthermore, sucrose-induced translational repression in the *vte4* mutant indicates sugar signaling is strongly influenced by the tocopherol composition, an aspect that has also been shown in salt-stressed potato plants (Asensi-Fabado et al., 2015).

Further, comparing the cluster profiles of wild-type plants and the *vte* mutants displayed clusters enriched with opposite

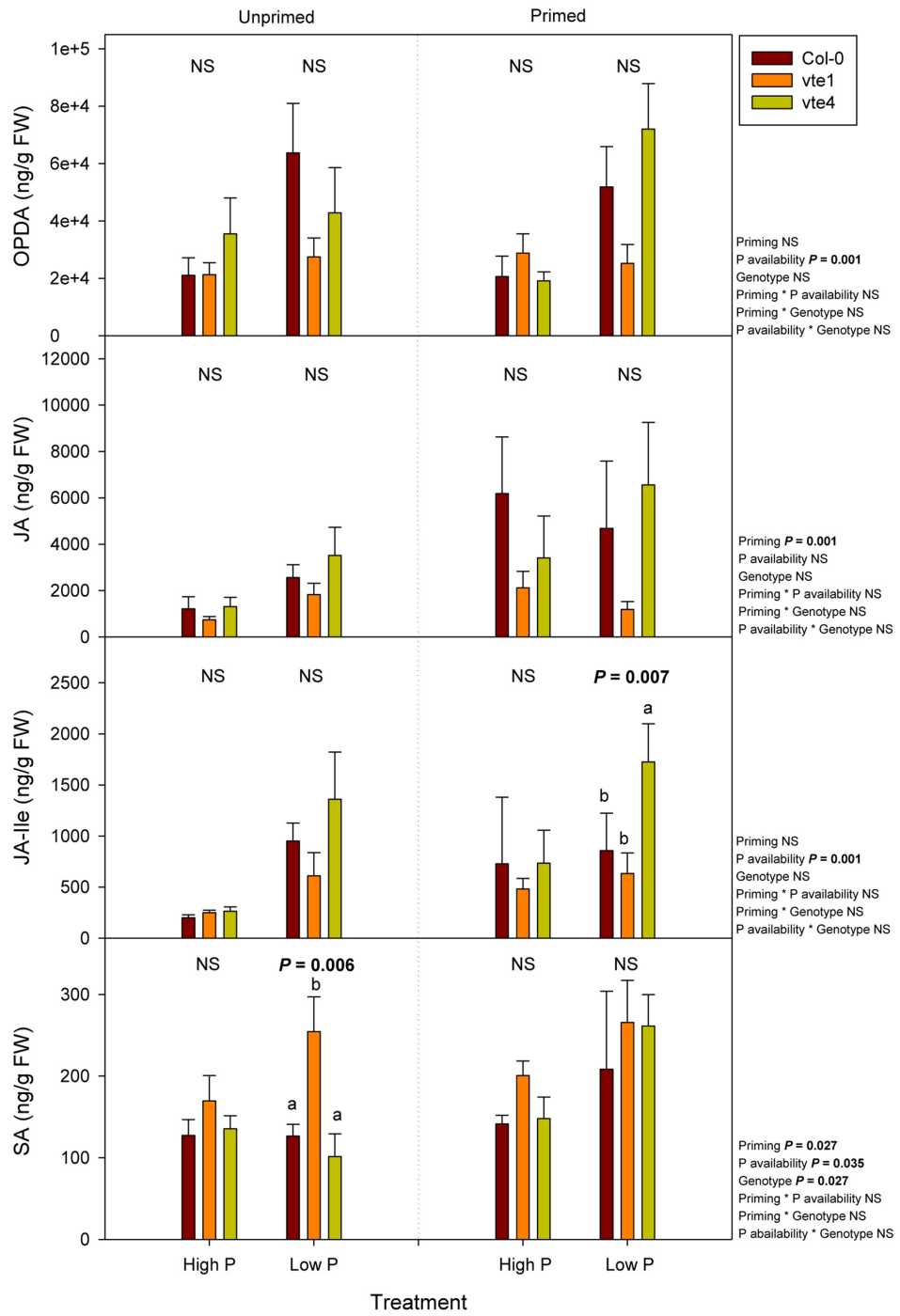

FIGURE 10 | Endogenous concentrations of jasmonates, including *oxo*-phytodienoic acid (OPDA), jasmonic acid (JA) and jasmonic acid isoleucine (JA-Ile), and salicylic acid (SA) in vitamin E-deficient (*vte1* and *vte4* mutants) and wild-type plants of *A. thaliana* exposed to contrasting Pi availability, including unprimed and primed plants. Data represent the mean ± SE of $n = 6$ individuals. Significant differences between groups were tested by three-way analysis of variance (ANOVA, $P < 0.05$). Different letters significant differences between genotypes at any given treatment (Duncan *post hoc* tests, $P < 0.05$). NS, not significant.

TF expression patterns. Interestingly, the GO terms associated with those clusters are "response to gibberellin, jasmonates, salicylates, ABA, ethylene, lipid, auxin, organic cyclic compound" and "negative regulation of cellular, macromolecular biosynthesis process," among others. Changes related to growth promoting hormone gibberellin and stress hormones such as salicylates, jasmonates, ABA, and ethylene may further support a possible tradeoff scenario in these mutants compared to the wild type.

Indeed, results of hormonal profiling confirms a tradeoff between response to contrasting Pi availability and activation of defense-related compounds with increases in endogenous salicylic acid concentrations in the *vte1* mutant compared to the wild type at low Pi in unprimed plants, and enhanced JA-Ile levels in the *vte4* mutant compared to the wild type at low Pi in primed plants. In these two cases, these mutants grew less than the wild type and activated more chemical defenses. It is therefore likely that reduced growth and photoprotection in vitamin E-deficient mutants favors the capacity to synthesize chemical defenses, such as salicylates and jasmonates, under abiotic stress conditions, thus suggesting a tradeoff between growth and different defense pathways in plants (growth and photoprotection versus potential chemical defense to biotrophs and necrotrophs through salicylates and jasmonates, respectively), which is in agreement with previous studies (Demmig-Adams et al., 2013, 2014; Morales et al., 2015; Simancas and Munné-Bosch, 2015).

The present study shows a link between the capacity of plants to synthesize chloroplastic antioxidants and massive changes in gene expression, therefore suggesting vitamin E influences retrograde signaling an aspect that has been previously proposed (Hofius et al., 2004; Sattler et al., 2004; Munné-Bosch, 2005; Cela et al., 2011; Pfannschmidt and Munné-Bosch, 2013). In this respect, it has been previously shown that tocopherols play a major role in the regulation of fatty acid metabolism, not only from chloroplasts, but also from the endoplasmic reticulum, due to a continuous exchange of information between endoplasmic reticulum and chloroplast membranes that may help transfer signals from chloroplasts to the nucleus (Sattler et al., 2006; Mehrshahi et al., 2013, 2014). In the present study, pre-treatment with moderately low Pi (condition A) led to down- and up-regulation of MYB30 in the wild type and the *vte4* mutant, respectively. MYB30 is a TF that regulates very-long-chain fatty acid biosynthesis (Raffaele et al., 2008), therefore suggesting a link between vitamin E and fatty acid metabolism in plant response to low Pi. Furthermore, alterations in fatty acid metabolism due to the effects of tocopherol deficiency (in the *vte1* mutant) or an altered tocopherol composition (in the *vte4* mutant) may lead to profound changes in lipid peroxidation products, including alterations in both enzymatic (as shown here with jasmonate levels in the *vte4* mutant) and non-enzymatic lipid peroxidation products, an aspect that warrants further investigation in *vte* mutants exposed to contrasting Pi availability. It is concluded that α-tocopherol may play a major role in plant response to contrasting Pi availability not only protecting plants from photo-oxidative stress, but also exerting a regulatory role on growth and defense though modulation of specific clusters of gene expression and hormones. Further research is, however, needed to better understand the metabolic and cellular processes linking vitamin E with retrograde signaling in plants.

AUTHOR CONTRIBUTIONS

SM-B and SB conceived the research plans. AA and BS performed the experiments. AA and SM-B wrote the article with contributions of BS and SB.

FUNDING

This work was supported by the Catalan Government (Institució Catalana de Recerca i Estudis Avançats Academia Award given to SM-B), the Spanish Government (project number BFU2015-64001-P/MINECO/FEDER), and the Max-Planck Institute of Molecular Plant Physiology.

ACKNOWLEDGMENTS

We are very grateful to Laura Siles and Maren Müller for their help with this work. We are also indebted to Serveis Científico-tècnics for technical assistance. Plastochromanol-8 standard was kindly provided by Jerzy Kruk (Jagiellonian University, Krakow, Poland).

SUPPLEMENTARY MATERIAL

The Supplementary Material for this article can be found online at: http://journal.frontiersin.org/article/10.3389/fpls.2017.01396/full#supplementary-material

REFERENCES

Abbasi, A.-R., Hajirezaei, M., Hofius, D., Sonnewald, U., and Voll, L. M. (2007). Specific roles of α- and γ-tocopherol in abiotic stress responses of transgenic tobacco. *Plant Physiol.* 143, 1720–1738. doi: 10.1104/pp.106.094771

Abbasi, A.-R., Saur, A., Hennig, P., Tschiersch, H., Hajirezaei, M., Hofius, D., et al. (2009). Tocopherol deficiency in transgenic tobacco (*Nicotiana tabacum* L.) plants leads to accelerated senescence. *Plant Cell Environ.* 32, 144–157. doi: 10.1111/j.1365-3040.2008.01907.x

Asensi-Fabado, M. A., Ammon, A., Sonnewald, U., Munné-Bosch, S., and Voll, L. M. (2015). Tocopherol deficiency reduces sucrose export from salt-stressed potato leaves independently of oxidative stress and symplastic obstruction by callose. *J. Exp. Bot.* 66, 957–971. doi: 10.1093/jxb/eru453

Austin, J. R., Frost, E., Vidi, P. A., Kessler, F., and Staehlin, L. A. (2006). Plastoglobules are lipoprotein subcompartments of the chloroplast that are permanently coupled to thylakoid membranes and contain biosynthetic enzymes. *Plant Cell* 18, 1693–1703. doi: 10.1105/tpc.105.039859

Bari, R., Pant, B. D., Stitt, M., and Scheible, W. R. (2006). PHO2, microRNA399, and PHR1 define a phosphate-signaling pathway in plants. *Plant Physiol.* 141, 988–999. doi: 10.1104/pp.106.079707

Berger, S. L. (2007). The complex language of chromatin regulation during transcription. *Nature* 447, 407–412. doi: 10.1038/nature05915

Bergmüller, E., Porfirova, S., and Dörmann, P. (2003). Characterization of an *Arabidopsis* mutant deficient in γ-tocopherol methyltransferase. *Plant Mol. Biol.* 52, 1181–1190. doi: 10.1023/B:PLAN.0000004307.62398.91

Caldana, C., Scheible, W. R., Mueller-Roeber, B., and Ruzicic, S. (2007). A quantitative RT-PCR platform for high-throughput expression profiling of 2500 rice transcription factors. *Plant Methods* 3:7 doi: 10.1186/1746-4811-3-7

Cela, J., Chang, C., and Munné-Bosch, S. (2011). Accumulation of γ- rather than α-tocopherol alters ethylene signaling gene expression in the *vte4* mutant of *Arabidopsis thaliana*. *Plant Cell Physiol.* 52, 1389–1400. doi: 10.1093/pcp/pcr085

Chen, Z. H., Nimmo, G. A., Jenkins, G. I., and Nimmo, H. G. (2007). BHLH32 modulates several biochemical and morphological processes that respond to Pi starvation in Arabidopsis. *Biochem. J.* 405, 191–198. doi: 10.1042/BJ20070102

Ciereszkoa, I., and Kleczkowsk, L. A. (2002). Effects of phosphate deficiency and sugars on expression of rab18 in Arabidopsis: hexokinase-dependent and okadaic acid-sensitive transduction of the sugar signal. *Biochim. Biophys. Acta* 1579, 43–49. doi: 10.1016/S0167-4781(02)00502-X

Dai, X., Wang, W., and Zhang, W. H. (2016). OsWRKY74, a WRKY transcription factor, modulates tolerance to phosphate starvation in rice. *J. Exp. Bot.* 67, 947–960. doi: 10.1093/jxb/erv515

Demmig-Adams, B., Cohu, C. M., Amiard, V., Zadelhoff, G., Veldink, G. A., Muller, O., et al. (2013). Emerging trade-offs – impact of photoprotectants (PsbS, xanthophylls, and vitamin E) on oxylipins and biotic defense. *New Phytol.* 197, 720–729. doi: 10.1111/nph.12100

Demmig-Adams, B., Stewart, J. J., and Adams, W. W. III (2014). "Chloroplast photoprotection and the trade-off between abiotic and biotic defense," in *Nonphotochemical Quenching and Energy Dissipation in Plants, Algae and Cyanobacteria. Advances in Photosynthesis and Respiration*, Vol. 40, eds B. Demmig-Adams, G. Garab, W. Adams III, and Govindjee (Dordrecht: Springer).

Devaiah, B. N., Karthikeyan, A. S., and Raghothama, K. G. (2007a). WRKY75 transcription factor is a modulator of phosphate acquisition and root development in Arabidopsis. *Plant Physiol.* 143, 1789–1801.

Devaiah, B. N., Nagarajna, V. K., and Raghothama, K. G. (2007b). Phosphate homeostasis and root development in Arabidopsis are synchronized by the zing finger transcription factor ZAT6. *Plant Physiol.* 145, 147–159.

Devaiah, B. N., Madhuvanthi, R., Karthikeyan, A. S., and Raghothama, K. G. (2009). Phosphate starvation responses and gibberellic acid biosynthesis are regulated by the MYB62 transcription factor in Arabidopsis. *Mol. Plant* 2, 43–58. doi: 10.1093/mp/ssn081

Dhar, M. K., Vishal, P., Sharma, R., and Kaul, S. (2014). Epigenetic dynamics: role of epimarks and underlying machinery in plants exposed to abiotic stress. *Int. J. Genomics* 2014:187146. doi: 10.1155/2014/187146

Ernst, J., and Bar-Joseph, Z. (2006). STEM: a tool for the analysis of short term series gene expression data. *BMC Bioinformatics* 7:191. doi: 10.1186/1471-2105-7-191

Ernst, J., Nau, G. J., and Bar-Joseph, Z. (2005). Clustering short time series gene expression data. *Bioinformatics* 21, i159–i168. doi: 10.1093/bioinformatics/bti1022

Falk, J., and Munné-Bosch, S. (2010). Tocochromanol functions in plants: antioxidation and beyond. *J. Exp. Bot.* 61, 1549–1566. doi: 10.1093/jxb/erq030

Franco-Zorrilla, J. M., González, A., Bustos, R., Linhares, F., Leyva, A., and Paz-Ares, J. (2004). The transcriptional control of plant responses to phosphate limitation. *J. Exp. Bot.* 55, 285–293. doi: 10.1093/jxb/erh009

Franco-Zorrilla, J. M., Martín, A. C., Leyva, A., and Paz-Ares, J. (2005). Interaction between phosphate-starvation, sugar, and cytokinin signaling in Arabidopsis and the roles of cytokinin receptors CRE1/AHK4 and AHK3. *Plant Physiol.* 138, 847–857. doi: 10.1104/pp.105.060517

Genty, B., Briantais, J., and Baker, N. R. (1989). The relationship between quantum yield of photosynthetic electron transport and quenching of chlorophyll fluorescence. *Biochim. Biophys. Acta* 990, 87–92. doi: 10.1016/S0304-4165(89)80016-9

Havaux, M., Eymery, F., Porfirova, S., Rey, P., and Dörmann, P. (2005). Vitamin E protects against photoinhibition and photooxidative stress in *Arabidopsis thaliana*. *Plant Cell* 17, 3451–3469. doi: 10.1105/tpc.105.037036

Herrera-Estrella, L., and López-Arredondo, D. (2016). Phosphorus: the underrated element for feeding the world. *Trends Plant Sci.* 21, 461–463. doi: 10.1016/j.tplants.2016.04.010

Hodges, D. M., DeLong, J. M., Forney, C. F., and Prange, R. K. (1999). Improving the thiobarbituric acid-reactive-substances assay for estimating lipid peroxidation in plant tissues containing anthocyanin and other interfering compounds. *Planta* 207, 604–611.

Hofius, D., Hajirezaei, M., Geiger, M., Tschiersch, H., Melzer, M., and Sonnewald, U. (2004). RNAi-mediated tocopherol deficiency impairs photoassimilate export in transgenic potato plants. *Plant Physiol.* 135, 1256–1268. doi: 10.1104/pp.104.043927

Jiang, C., Gao, X., Liao, L., Harberd, N. P., and Fu, X. (2007). Phosphate starvation root architecture and anthocyanin accumulation responses are modulated by the gibberellin–DELLA signaling pathway in Arabidopsis. *Plant Physiol.* 145, 1460–1467. doi: 10.1104/pp.107.103788

Kruk, J., Szymanska, R., Cela, J., and Munné-Bosch, S. (2014). Plastochromanol-8: fifty years of research. *Phytochemistry* 108, 9–16. doi: 10.1016/j.phytochem.2014.09.011

Lotkowska, M. E., Tohge, T., Fernie, A. R., Xue, G.-P., Balazadeh, S., and Mueller-Roeber, B. (2015). The Arabidopsis transcription factor MYB112 promotes anthocyanin formation during salinity and under high light stress. *Plant Physiol.* 169, 1862–1880. doi: 10.1104/pp.15.00605

Maeda, H., Sage, T. L., Isaac, G., Welti, R., and DellaPenna, D. (2008). Tocopherols modulate extraplastidic polyunsaturated fatty acid metabolism in Arabidopsis at low temperature. *Plant Cell* 20, 452–470. doi: 10.1105/tpc.107.054718

Marschner, P. (2012). *Marschner's Mineral Nutrition of Higher Plants*. Amsterdam: Elsevier.

Mehrshahi, P., Johnny, C., and DellaPenna, D. (2014). Redefining the metabolic continuity of chloroplasts and ER. *Trends Plant Sci.* 19, 501–507. doi: 10.1016/j.tplants.2014.02.013

Mehrshahi, P., Stefano, G., Andaloro, J. M., Brandizzi, F., Froehlich, J. E., and DellaPenna, D. (2013). Transorganellar complementation redefines the biochemical continuity of endoplasmic reticulum and chloroplasts. *Proc. Natl. Acad. Sci. U.S.A.* 110, 12126–12131. doi: 10.1073/pnas.1306331110

Mène-Saffrané, L., Jones, A. D., and DellaPenna, D. (2010). Plastochromanol-8 and tocopherols are essential lipid-soluble antioxidants during seed desiccation and quiescence in *Arabidopsis*. *Proc. Natl. Acad. Sci. U.S.A.* 107, 17815–17820. doi: 10.1073/pnas.1006971107

Misson, J., Raghothama, K. G., Jain, A., Jouhet, J., Block, M. A., Bligny, R., et al. (2005). A genome-wide transcriptional analysis using *Arabidopsis thaliana* Affymetrix gene chips determined plant responses to phosphate deprivation. *Proc. Natl. Acad. Sci. U.S.A.* 102, 11934–11939. doi: 10.1073/pnas.0505266102

Morales, M., Garcia, Q. S., and Munné-Bosch, S. (2015). Ecophysiological response to seasonal variations in water availability in the arborescent, endemic plant *Vellozia gigantea*. *Tree Physiol.* 35, 253–265. doi: 10.1093/treephys/tpv012

Morcuende, R., Bari, R., Gibon, Y., Zheng, W., Pant, B. D., Bläsing, O., et al. (2007). Genome-wide reprogramming of metabolism and regulatory networks of Arabidopsis in response to phosphorus. *Plant Cell Environ.* 30, 85–112. doi: 10.1111/j.1365-3040.2006.01608.x

Müller, M., and Munné-Bosch, S. (2011). Rapid and sensitive hormonal profiling of complex plant samples by liquid chromatography coupled to electrospray ionization tandem mass spectrometry. *Plant Methods.* 7:37. doi: 10.1186/1746-4811-7-37

Müller, M., and Munné-Bosch, S. (2015). Ethylene response factors: a key regulatory hub in hormone and stress signaling. *Plant Physiol.* 169, 32–41. doi: 10.1104/pp.15.00677

Munné-Bosch, S. (2005). Linking tocopherols with cellular signaling in plants. *New Phytol.* 166, 363–366. doi: 10.1111/j.1469-8137.2005.01411.x

Munné-Bosch, S., and Alegre, L. (2002). The function of tocopherols and tocotrienols in plants. *Crit. Rev. Plant Sci.* 21, 31–57. doi: 10.1080/0735-260291044179

Munné-Bosch, S., Weiler, E. W., Alegre, L., Müller, M., Düchting, P., and Falk, J. (2007). α-Tocopherol may influence cellular signaling by modulating jasmonic acid levels in plants. *Planta* 225, 681–691. doi: 10.1007/s00425-006-0375-0

Pfannschmidt, T., and Munné-Bosch, S. (2013). "Plastidial signaling during the plant life cycle," in *Plastid Development in Leaves during Growth and Senescence, Advances in Photosynthesis and Respiration*, Vol. 36, eds B. Biswal, K. Krupinska, and U. C. Biswal (Dordrecht: Springer), 503–528.

Porfirova, S., Bergmüller, E., Tropf, S., Lemke, R., and Dörmann, P. (2002). Isolation of an *Arabidopsis* mutant lacking vitamin E and identification of a cyclase essential for all tocopherol biosynthesis. *Proc. Natl. Acad. Sci. U.S.A.* 99, 12495–12500. doi: 10.1073/pnas.182330899

Proost, S., Van Bel, M., Vaneecchoutte, D., Van de Peer, Y., Inzé, D., Mueller-Roeber, B., et al. (2015). PLAZA 3.0: an access point for plant comparative genomics. *Nucleic Acids Res.* 43, D974–D981. doi: 10.1093/nar/gku986

Raffaele, S., Vailleau, F., Líger, A., Joubès, J., Miersch, O., Huard, C., et al. (2008). A MYB transcription factor regulates very-long-chain fatty acid biosynthesis for activation of the hypersensitive cell death response in Arabidopsis. *Plant Cell* 20, 752–767. doi: 10.1105/tpc.107.054858

Rouached, H., Arpat, A. B., and Poirier, Y. (2010). Regulation of phosphate starvation responses in plants: Signaling players and cross-talks. *Mol. Plant* 3, 288–299. doi: 10.1093/mp/ssp120

Rubio, V., Linhares, F., Solano, R., Martín, A. C., Iglesias, J., Leyva, A., et al. (2001). A conserved MYB transcription factor involved in phosphate starvation signaling both in vascular plants and in unicellular algae. *Genes Dev.* 15, 2122–2133. doi: 10.1101/gad.204401

Rubio, V., Bustos, R., Irigoyen, M. L., Cardona-Lopez, X., Rojas-Triana, M., and Paz-Ares, J. et al. (2009). Plant hormones and nutrient signaling. *Plant Mol. Biol.* 69, 361–373. doi: 10.1007/s11103-008-9380-y

Saeed, A. I., Sharov, V., White, J., Li, J., Liang, W., Bhagabati, N., et al. (2003). TM4: a free, open-source system for microarray data management and analysis. *Biotechniques* 34, 374–378.

Sarnowska, E. A., Rolicka, A. T., Bucior, E., Cwiek, P., Tohge, T., Fernie, A. R., et al. (2013). DELLA-interacting SWI3C core subunit of switch/sucrose nonfermenting chromatin remodeling complex modulates gibberellin responses and hormonal cross talk in Arabidopsis. *Plant Physiol.* 163, 305–317. doi: 10.1104/pp.113.223933

Sato, A., and Miura, K. (2011). Root architecture remodeling induced by phosphate starvation. *Plant Signal. Behav.* 6, 1122–1126. doi: 10.4161/psb.6.8.15752

Sattler, S. E., Cahoon, E. B., Coughlan, S. J., and Della Penna, D. (2004). Vitamin E is essential for seed longevity and for preventing lipid peroxidation during germination. *Plant Cell* 16, 1419–1432. doi: 10.1105/tpc.021360

Sattler, S. E., Cahoon, E. B., Coughlan, S. J., and DellaPenna, D. (2003). Characterization of tocopherol cyclases from higher plants and cyanobacteria. Evolutionary implications for tocopherol synthesis and function. *Plant Physiol.* 132, 2184–2195. doi: 10.1104/pp.103.024257

Sattler, S. E., Mène-Saffrané, L., Farmer, E. E., Krischke, M., Mueller, M. J., and DellaPenna, D. (2006). Nonenzymatic lipid peroxidation reprograms gene expression and activates defense markers in Arabidopsis tocopherol-deficient mutants. *Plant Cell* 18, 3706–3720. doi: 10.1105/tpc.106.044065

Schönberger, B., Chen, X., Mager, S., and Ludewig, U. (2016). Site-dependent differences in DNA methylation and their impact on plant establishment and phosphorus nutrition in *Populus trichocarpa*. *PLoS ONE* 11:e0168623. doi: 10.1371/journal.pone.0168623

Simancas, B., and Munné-Bosch, S. (2015). Interplay between Vitamin E and phosphorus availability in the control of longevity in *Arabidopsis thaliana*. *Ann. Bot.* 116, 511–518. doi: 10.1093/aob/mcv033

Szymanska, R., and Kruk, J. (2010). Plastoquinol is the main prenyllipid synthesized during acclimation to high light conditions in Arabidopsis and is converted to plastochromanol by tocopherol cyclase. *Plant Cell Physiol.* 51, 537–545. doi: 10.1093/pcp/pcq017

Tohge, T., Watanabe, M., Hoefgen, R., and Fernie, A. R. (2013). The evolution of phenylpropanoid metabolism in the green lineage. *Crit. Rev. Biochem. Mol. Biol.* 48, 123–152. doi: 10.3109/10409238.2012.758083

Trull, M. C., Guiltinan, M. J., Lynch, J. P., and Deikman, J. (1997). The responses of wild-type and ABA mutant *Arabidopsis thaliana* plants to phosphorus starvation. *Plant Cell Environ.* 20, 85–92. doi: 10.1046/j.1365-3040.1997.d01-4.x

Vidi, P. A., Kanwischer, M., Baginsky, S., Austin, J. R., Csucs, G., Dörmann, P., et al. (2006). Tocopherol cyclase (VTE1) localization and vitamin E accumulation in chloroplast plastoglobule lipoprotein particles. *J. Biol. Chem.* 281, 11225–11234. doi: 10.1074/jbc.M511939200

Williamson, L. C., Ribrioux, S. P. C. P., Fitter, A. H., and Leyser, H. M. O. (2001). Phosphate availability regulates root system architecture in Arabidopsis. *Plant Physiol.* 126, 875–882. doi: 10.1104/pp.126.2.875

Wissuwa, M., Gamat, G., and Ismail, A. M. (2005). Is root growth under phosphorus deficiency affected by source or sink limitations? *J. Exp. Bot.* 56, 1943–1950. doi: 10.1093/jxb/eri189

Wu, X., Li, Y., Crise, B., and Burgess, S. M. (2003). Transcription start regions in the human genome are favored targets for MLV integration. *Science* 300, 1749—1751. doi: 10.1126/science.1083413

Yang, X. J., and Finnegan, P. M. (2010). Regulation of phosphate starvation responses in higher plants. *Ann. Bot.* 105, 513–526. doi: 10.1093/aob/mcq015

Yi, K., Wu, Z., Zhou, J., Du, L., Guo, L., Wu, Y., et al. (2005). OsPTF1, a novel transcription factor involved in tolerance to phosphate starvation in rice. *Plant Physiol.* 138, 2087–2096. doi: 10.1104/pp.105.063115

Zbierzak, A. M., Kanwischer, M., Wille, C., Vidi, P. A., Giavalisco, P., Lohmann, A., et al. (2010). Intersection of the tocopherol and plastoquinol metabolic pathways at the plastoglobule. *Biochem. J.* 425, 389–399. doi: 10.1042/BJ20090704

Zhang, K., Sridhar, V. V., Zhu, J., and Kapoor, A. (2007). Distinctive core histone post-translational modification patterns in *Arabidopsis thaliana*. *PLoS ONE* 2:e1210. doi: 10.1371/journal.pone.0001210

Zhou, J., Jiao, F. C., Wu, Z. C., Li, Y., Wang, X., He, X., et al. (2008). *OsPHR2* is involved in phosphate-starvation signaling and excessive phosphate accumulation in shoots of plants. *Plant Physiol.* 146, 1673–1686. doi: 10.1104/pp.107.111443

Conflict of Interest Statement: The authors declare that the research was conducted in the absence of any commercial or financial relationships that could be construed as a potential conflict of interest.

frontiers in Plant Science

ORIGINAL RESEARCH
published: 31 October 2017
doi: 10.3389/fpls.2017.01847

Arabidopsis Phosphatidic Acid Phosphohydrolases Are Essential for Growth under Nitrogen-Depleted Conditions

*Yushi Yoshitake[1], Ryoichi Sato[2†], Yuka Madoka[3], Keiko Ikeda[4], Masato Murakawa[1], Ko Suruga[3], Daisuke Sugiura[5†], Ko Noguchi[6], Hiroyuki Ohta[1,7] and Mie Shimojima[1]**

[1] School of Life Science and Technology, Tokyo Institute of Technology, Yokohama, Japan, [2] Center for Biological Resources and Informatics, Tokyo Institute of Technology, Yokohama, Japan, [3] Graduate School of Bioscience and Biotechnology, Tokyo Institute of Technology, Yokohama, Japan, [4] Biomaterial Analysis Center, Technical Department, Tokyo Institute of Technology, Yokohama, Japan, [5] Graduate School of Science, The University of Tokyo, Tokyo, Japan, [6] School of Life Sciences, Tokyo University of Pharmacy and Life Sciences, Tokyo, Japan, [7] Earth-Life Science Institute, Tokyo Institute of Technology, Tokyo, Japan

The Arabidopsis homologs of mammalian lipin, PAH1 and PAH2, are cytosolic phosphatidic acid phosphohydrolases that are involved in phospholipid biosynthesis and are essential for growth under phosphate starvation. Here, *pah1 pah2* double-knockout mutants were found to be hypersensitive to nitrogen (N) starvation, whereas transgenic plants overexpressing PAH1 or PAH2 in the *pah1 pah2* mutant background showed a similar growth phenotype as compared with wild type (WT) under N starvation. The chlorophyll content of *pah1 pah2* was significantly lower than that of WT, whereas the chlorophyll content and photosynthetic activity of the transgenic plants were significantly higher than those of WT under N-depleted conditions. Membrane glycerolipid composition of the *pah1 pah2* mutants showed a significant decrease in the mole percent of chloroplast lipids to other phospholipids, whereas membrane lipid composition did not differ between transgenic plants and WT plants. Pulse-chase labeling experiments using plants grown under N-depleted conditions showed that, in *pah1 pah2* plants, the labeling percent of chloroplast lipids such as phosphatidylglycerol and monogalactosyldiacylglycerol in the total glycerolipids was significantly lower than in WT. Moreover, N starvation-induced degradation of chloroplast structure was enhanced in *pah1 pah2* mutants, and the membrane structure was recovered by complementation with PAH1. Thus, PAH is involved in maintaining chloroplast membrane structure and is required for growth under N-depleted conditions.

Keywords: phosphatidic acid phosphohydrolase, lipin, photosynthetic membrane, monogalactosyldiacylglycerol, nitrogen starvation, chloroplast, thylakoid membrane, *Arabidopsis thaliana*

OPEN ACCESS

Edited by:
Hongbo Gao,
Beijing Forestry University, China

Reviewed by:
Ruth Welti,
Kansas State University, United States
Jinpeng Gao,
Washington State University, United States
Wenqiang Yang,
Institute of Botany (CAS), China

****Correspondence:***
Mie Shimojima
shimojima.m.aa@m.titech.ac.jp

†Present address:
Ryoichi Sato,
Division of Environmental Photobiology, National Institute for Basic Biology, Okazaki, Japan
Daisuke Sugiura
Graduate School of Bioagricultural Sciences, Nagoya University, Nagoya, Japan

Specialty section:
This article was submitted to Plant Physiology, a section of the journal Frontiers in Plant Science

Received: *01 August 2017*
Accepted: *10 October 2017*
Published: *31 October 2017*

Citation:
Yoshitake Y, Sato R, Madoka Y, Ikeda K, Murakawa M, Suruga K, Sugiura D, Noguchi K, Ohta H and Shimojima M (2017) Arabidopsis Phosphatidic Acid Phosphohydrolases Are Essential for Growth under Nitrogen-Depleted Conditions. Front. Plant Sci. 8:1847. doi: 10.3389/fpls.2017.01847

INTRODUCTION

Nitrogen (N) is an essential macronutrient for plant growth and is used to produce many fundamental biological molecules such as nucleic acids, amino acids, proteins, and metabolites (Crawford and Forde, 2002; Peng et al., 2007). N starvation leads to severe growth retardation with concomitant decreases in the chlorophyll content and the efficiency of photosynthetic

activities (Vidal and Gutiérrez, 2008; Maathuis, 2009; Boussadia et al., 2010). Thus, to enhance N uptake under N-depleted conditions, plants alter their lateral root architecture (Little et al., 2005; Orsel et al., 2006; Remans et al., 2006) and increase the expression of genes responsible for nitrate transport (Guo et al., 2001). Plants also enhance N remobilization from older to younger leaves and from reproductive organs (Ono et al., 1996; Hanaoka et al., 2002; Remans et al., 2006; Peng et al., 2007). Plant lipid composition also changes in response to N availability. Photosynthetic membranes, namely thylakoid membranes of chloroplasts, are predominantly composed of galactolipids such as monogalactosyldiacylglycerol (MGDG) and digalactosyldiacylglycerol (DGDG), which constitute ∼80% of the total thylakoid membrane lipids (Block et al., 1983). However, the galactolipid composition is greatly affected by N starvation. In soybean leaves, the content of MGDG and DGDG is decreased under N starvation, whereas phospholipid content remains unchanged during N starvation (Narasimhan et al., 2013). In Arabidopsis, the relative amount of MGDG in membrane lipids is decreased under N starvation (Gaude et al., 2007). The synthesis of fatty acid phytyl esters is enhanced in chloroplasts to avoid the accumulation of toxic intermediates, such as tetrapyrroles, free phytols, and free fatty acids, as a result of chlorophyll and galactolipid degradation during N starvation (Gaude et al., 2007). N starvation also increases triacylglycerol accumulation in vegetative tissues (Martin et al., 2002; Gaude et al., 2007; Yang et al., 2011). In Arabidopsis and *Brassica napus*, the increased expression of phospholipase Dε (PLDε), which hydrolyzes membrane phospholipids to produce the cellular signaling molecule phosphatidic acid, has the potential to improve plant growth under N-depleted conditions (Hong et al., 2009; Lu et al., 2016). Thus, genetic modifications to lipid synthesis pathways could potentially improve plant tolerance to N starvation. However, little is known about the detailed mechanism of N-starvation tolerance mediated by lipids.

The soluble phosphatidic acid phosphohydrolase, lipin, is involved in triacylglycerol biosynthesis and was originally identified in yeast and humans. Arabidopsis has two lipin homologs, PAH1 and PAH2 (Nakamura et al., 2009). Although Arabidopsis single-knockout mutants of PAH1 or PAH2 do not show any notable phenotype as compared with wild type (WT), the double-knockout mutant *pah1 pah2* has a higher level of phospholipids and a severe phenotype when grown under inorganic phosphate (Pi)-depleted conditions as compared with WT (Nakamura et al., 2009). Plants often suffer from Pi starvation because of the scarcity of inorganic Pi in soil, and thus they have multiple mechanisms to overcome Pi deficiency (Raghothama, 1999). One of these mechanisms is membrane lipid remodeling in which the phospholipid phosphatidylcholine in extraplastidial membranes is replaced with the non-phosphorus-containing galactolipid DGDG (Härtel and Benning, 2000; Dörmann and Benning, 2002). One important membrane lipid remodeling pathway produces diacylglycerol (DAG), which is a substrate for MGDG synthase. During Pi starvation, galactolipid synthesis is upregulated via the activation of type B MGDG synthase (MGD2 and MGD3 in Arabidopsis), which is localized in the outer envelope membrane of chloroplasts (Awai et al., 2001; Kobayashi et al., 2009). The DAG generated via phospholipid degradation is supplied to the type B MGDG synthase, and the resultant MGDG is subsequently used for DGDG synthesis (Shimojima and Ohta, 2011; Nakamura, 2013). Because *pah1 pah2* plants show severe growth retardation under Pi-depleted conditions, PAH1 and PAH2 are considered to be key enzymes in Pi starvation-induced lipid remodeling, which plays a role in releasing Pi via phospholipid degradation (required for other essential biological processes) and in supplying DAG for galactolipid synthesis as a substrate of MGDG synthase (Nakamura et al., 2009).

Here, we found that Arabidopsis *pah1 pah2* mutants showed a severe growth phenotype, whereas transgenic plants overexpressing PAH1 or PAH2 in the *pah1 pah2* background showed slightly higher photosynthetic activity under N starvation as compared with WT. Our results showed that PAH1 and PAH2 are involved not only in phospholipid homeostasis in the endoplasmic reticulum (ER) but also in the maintenance of the thylakoid membrane in chloroplasts and its photosynthetic activity, especially under N starvation.

MATERIALS AND METHODS

Plant Material and Growth Conditions

The isolation of the *Arabidopsis thaliana pah1 pah2* mutant and the generation of transgenic plants overexpressing PAH1 or PAH2 and harboring GFP in a *pah1 pah2* background were previously described (Nakamura et al., 2009). Surface-sterilized seeds of WT *A. thaliana* (Columbia-0), the *pah1 pah2* mutant, and the transgenic mutant lines were incubated at 4°C in darkness for 3 days prior to plating on Murashige and Skoog medium (Murashige and Skoog, 1962) containing 0.8% (w/v) agar supplemented with 1% (w/v) sucrose. Plants were then incubated at 22°C under continuous white light (40–50 μmol m^{-2} s^{-1}) for all growth conditions. Arabidopsis seeds were grown on solidified Murashige and Skoog agar supplemented with 1% (w/v) sucrose for 10 days and then were grown for another 7 days on a solidified N-sufficient (4.5 mM N) or N-depleted (0 mM N) medium (Estelle and Somerville, 1987; Gaude et al., 2007) supplemented with 1% (w/v) sucrose, with KNO_3 and $Ca(NO_3)_2{\cdot}4H_2O$ replaced with KCl_2 and $CaCl_2$, respectively.

Quantitative Reverse Transcription-PCR

Total RNA was isolated from three independent plant samples using the SV Total RNA Isolation System (Promega). Reverse transcription was performed using the PrimeScript RT reagent kit (TaKaRa Bio), and cDNA amplification was carried out using SYBR PreMix Ex Taq (TaKaRa Bio). Signal detection and quantification were performed in duplicate using the Thermal Cycler Dice Real Time System (TaKaRa Bio). Quantitative PCR determination of *MGD1*, *MGD2*, *MGD3*, *DGD1, DGD2, PES1*, and *PES2* transcripts was normalized using the Arabidopsis *UBQ10* transcript level (Sun and Callis, 1997). Expression

levels were obtained from at least three replicates. The gene-specific primers used were as follows: PAH1 Fw (5′ GGATAA CGAGGACAGGAAGACTG 3′); PAH1 Rv (5′ AGCAGCTGCG CTAAGTCCCATAC 3′); PAH2 Fw (5′ CTCAAGCCTCAGTCA CAAGACAA 3′); PAH2 Rv (5′ AAGGAAAGAGACCATCAG GAGAGA 3′); PES1 Fw (5′ CCTGTCACCGCAACCAATC 3′); PES1 Rv (5′ ATTGTTGCACCAAACCGTGCT 3′); PES2 Fw (5′ CTCTTCTCCTATACTTACCTGG 3′); PES2 Rv (5′ CCT CAATAAGCTTCACCAAGT 3′); MGD1 Fw (5′ AGGTTTCA CTGCGATAAAGTGGTT 3′); MGD1 Rv (5′ AACGGCAAT CCCTCCTCAC 3′); MGD2 Fw (5′ GATTCGATCACTTC CTATCATCCTC 3′); MGD2 Rv (5′ TGTGCTAAACCATT CCCCAAC 3′); MGD3 Fw (5′ TCGTGGCGGATTGGTTTAG 3′); MGD3 Rv (5′ CGTTGTTGTTGTTGGGATAGATG 3′); DGD1 Fw (5′ CTGAAGAGAGATCCCGTGGTG 3′); DGD1 Rv (5′ TCCCAAGTTCGCTTTTGTGTT 3′); DGD2 Fw (5′ TGCAGAACCTATGACGATGGA 3′); DGD2 Rv (5′ GCT CTGTAAGTTGCGATGGTTG 3′); UBQ10 Fw (5′ GGCCTT GTATAATCCCTGATGAATAAG 3′); UBQ10 Rv (5′ AAAGA GATAACAGGAACGGAAACATAGT 3′).

Measurement of Chlorophyll Content

The 17-day-old seedlings were incubated in 1 mL dimethylformamide (Wako) at 4°C for 20 h in the dark, and then absorbance was measured at 646.8 and 663.8 nm. Chlorophyll content was calculated as follows: Chl*a* = ($13.43A_{663.8}$ – $3.47A_{646.8}$)/sample fresh weight, and Chl*b* = ($22.9A_{646.8}$ – $4.88A_{663.8}$)/sample fresh weight (Moran and Porath, 1980).

Analysis of Chlorophyll Fluorescence

The maximum quantum efficiency (F_v/F_m) of photosystem II was measured using a Dual-PAM system (Walz). The minimum chlorophyll fluorescence (F_o) was determined by measuring light (intensity set at 20). After the F_o determination, a saturating pulse of red light (intensity set at 15) was applied to determine the maximum chlorophyll fluorescence (F_m). F_v/F_m was calculated as $(F_m - F_o)/F_m$. Before the F_v/F_m measurements, samples were incubated for 10 min in the dark. Samples were in plastic plates when measured.

Determination of N Concentration

To determine N concentration, ∼0.1 g fresh weight of shoots from 10- or 17-day-old seedlings was washed and oven dried at 80°C for a minimum of 3 days and then ground into powder. The N concentration was determined using a CN analyzer (Vario ELIII; Elementar Analysensysteme GmbH) according to Hachiya and Noguchi (2008).

Electron Microscopy

Leaf segments were fixed with 2% (w/v) paraformaldehyde and 2.5% (w/v) glutaraldehyde in 0.067 M phosphate buffer (pH 7.4) for 2 h at room temperature and then for 16 h at 4°C. Samples were then washed six times in the phosphate buffer for 10 min each at room temperature. They were post-fixed with 2% (w/v) osmium tetroxide in 0.067 M phosphate buffer (pH 7.4) for 2 h at room temperature. The fixed samples were dehydrated in a graded ethanol series and embedded in an epoxy resin mixture (Quetol 651 mixture; Nisshin EM). Ultrathin 70-nm sections were cut with a diamond knife on a Leica EM-UC7 ultramicrotome and were transferred to copper grids. The sections were stained with EM stainer (Nisshin EM) for 1 h, followed by Reynolds's lead citrate for 9 min at room temperature. The specimens were observed with a JOEL JEM-1400 Plus transmission electron microscope at an accelerating voltage of 80 kV.

Lipid Analysis

Total lipids were extracted from tissues as described (Bligh and Dyer, 1959). Polar membrane lipids were separated by two-dimensional thin-layer chromatography (Kobayashi et al., 2007). Neutral glycerolipids were separated by one-dimensional thin-layer chromatography using the solvent system of hexane/diethyl ether/acetic acid (160:40:4, v/v/v). Lipids on silica gel plates were visualized with 0.01% (w/v) primuline in 80% (v/v) acetone under UV light. Lipids isolated from silica gel plates were methylated, and fatty acid methyl esters were quantified by gas chromatography using pentadecanoic acid as an internal standard (Kobayashi et al., 2006).

Pulse-Chase Labeling Experiments

In vivo labeling experiments with [^{14}C]acetate were conducted according to Nakamura et al. (2009), except that [^{14}C]acetate was diluted to 0.05 mCi mL^{-1} with N-depleted medium (Estelle and Somerville, 1987; Gaude et al., 2007). [^{14}C]acetate was spread with a micropipette in 3-μL droplets over the surface of the third and fourth leaves cut off from 15-day-old seedlings, and the leaves were placed on 3MM paper immersed in N-depleted medium and incubated for 2 h at 22°C. After the incubation, the leaves were washed twice in non-radioactive N-depleted medium to remove exogenous radioactivity and were placed on 3MM paper immersed in N-depleted medium. After the incubation, the samples were harvested and were frozen in liquid nitrogen. Lipids were extracted and separated by two-dimensional TLC as described above. Radioactive spots were analyzed by autoradiography (FLA7000, Fuji Film) and Imaging Plate (Fuji Film).

RESULTS

The *pah1 pah2* Mutants Are Hypersensitive to N Starvation

We previously produced Arabidopsis transgenic plants overexpressing PAH1 or PAH2 in the *pah1 pah2* background (Nakamura et al., 2009). Expression levels of *PAH1* and *PAH2* were analyzed for several lines for each transgenic combination, and PAH1OE 20-1 and PAH2OE 22-1 were selected and used as PAH1OE and PAH2OE, respectively, for further analyses (**Supplementary Figure S1**). Expression of *PAH1* in PAH1OE and *PAH2* in PAH2OE was 11-fold and 5-fold higher than that in WT, respectively, under normal growth conditions (+N), and these levels were 16-fold and 3-fold higher than that in

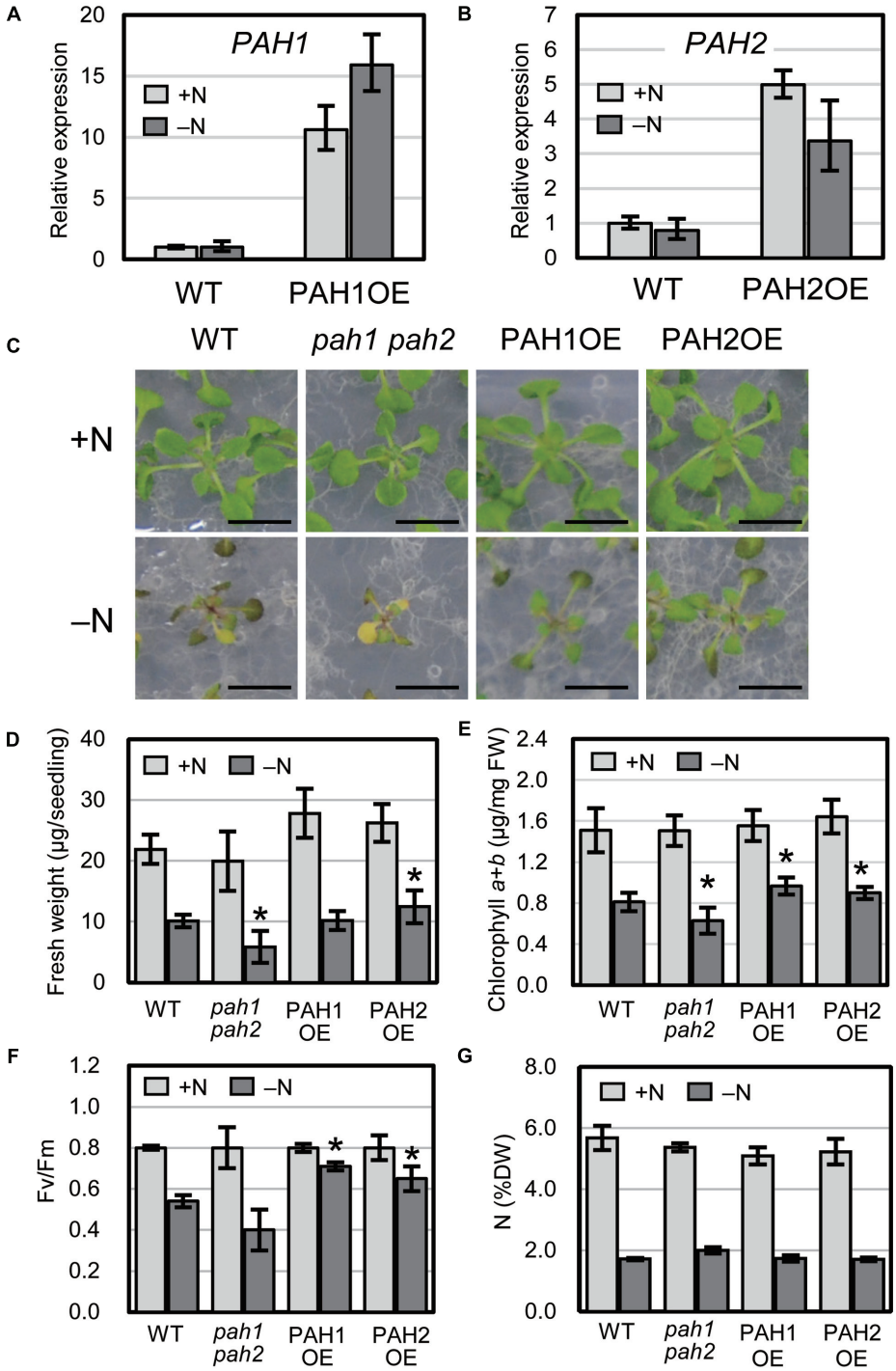

FIGURE 1 | Expression of *PAH1* and *PAH2* in the transgenic lines and the effect of N starvation on Arabidopsis growth. **(A)** Expression of *PAH1* in PAH1OE, **(B)** expression of *PAH2* in PAH2OE, **(C)** growth phenotypes, **(D)** shoot fresh weight, **(E)** chlorophyll content, **(F)** F_v/F_m, and **(G)** total N concentration in shoots. WT, *pah1 pah2*, PAH1OE, and PAH2OE were grown under N-sufficient (+N, light gray) and N-depleted (–N, dark gray) conditions. Scale bars: 1 cm. Data represent the mean ± SD from three independent experiments; $^*P < 0.05$ for a *t*-test versus WT under each condition. FW, fresh weight; DW, dry weight.

WT, respectively, under N starvation (–N) (**Figures 1A,B**). When we grew plants under N-depleted conditions, seedlings of the Arabidopsis double-knockout mutant *pah1 pah2* were significantly smaller than WT seedlings, whereas PAH1OE and PAH2OE seedlings were comparable to or larger than WT seedlings (**Figures 1C,D**). Under N-sufficient conditions,

the chlorophyll content in WT, *pah1 pah2*, PAH1OE, and PAH2OE did not differ significantly (**Figure 1E**). Under N-depleted conditions, however, the chlorophyll content in *pah1 pah2* was significantly lower than that in WT, whereas the content in PAH1OE and PAH2OE was similar to or greater than that in WT (**Figure 1E**). As for photosynthetic activity parameters under N-depleted conditions, both PAH1OE and PAH2OE showed significantly higher maximum quantum yield (F_v/F_m) as compared with those of WT and *pah1 pah2* (**Figure 1F**). The differences in sensitivity to N starvation among WT, *pah1 pah2*, PAH1OE, and PAH2OE could be due to the enhanced efficiency of N uptake during the first 10 days of growth under N-sufficient conditions. Therefore, we assessed total N concentration in seedlings of WT, *pah1 pah2*, PAH1OE, and PAH2OE; the N concentrations across these plants were comparable under both N-sufficient and N-depleted conditions (**Figure 1G**), suggesting that the growth defect in *pah1 pah2* during N starvation is not due to the lower N content in the seedlings as compared with the other plants.

Chloroplast Membrane Structure Was Severely Disrupted in *pah1 pah2* under N-Depleted Conditions

As a significant decrease in chlorophyll content was observed only in *pah1 pah2* grown under N starvation, we visualized the intracellular structure of plant leaves with electron microscopy and compared the structures among WT, *pah1 pah2*, and PAH1OE under N-sufficient and N-depleted conditions (**Figure 2** and **Supplementary Figure S2**). Under N-sufficient conditions, chloroplast membrane structures were similar among WT, *pah1 pah2* and PAH1OE (**Figures 2A–C**). Under N-depleted conditions, starch accumulation in chloroplasts was observed across all of the plants (**Figures 2D–F** and **Supplementary Figure S2**). The belt shaped-structures observed in starch granules have no biological phenotype but the technical reason of cutting the sample in the resin for microscopic analysis. As for the thylakoid membrane structures in the enlarged images, however, we could often observe grana-lamellae stacking structures in the thylakoid membrane of WT and PAH1OE but not in *pah1 pah2* under N-depleted conditions (**Figures 2G–I** and **Supplementary Figure S2**). Thus, it was clearly shown that the absence of PAH enhances breakdown of the chloroplast membrane structure, especially under N starvation and thus decreases chlorophyll content under N-depleted conditions as compared with WT (**Figure 1E**). We also observed the chloroplast membrane structure of PAH1OE. The membrane structure of PAH1OE was either comparable with WT or showed a slightly increased number of grana-lamellae stacking structures under N-depleted conditions (**Figures 2C,F,I** and **Supplementary Figure S2**). Although we could not assess these data statistically because the number of grana-lamellae stacking structures in *pah1 pah2* was markedly lower than that in WT and PAH1OE, the stacking repeat distance in thylakoids of *pah1 pah2* was wider than those in WT and PAH1OE (**Supplementary Figure S3**). Thus, our results showed that the absence of PAH affects the structure of photosynthetic membranes in chloroplasts, especially under N starvation.

The Mole Percent of Chloroplast Lipids Was Markedly Decreased in the *pah1 pah2* Mutant under N Starvation

Nitrogen starvation leads to a decrease in MGDG and a concomitant increase in DGDG in WT Arabidopsis (Gaude et al., 2007). In *pah1 pah2*, the mole percent of MGDG and DGDG in the total glycerolipids are smaller than in WT, even under N-sufficient conditions (Nakamura et al., 2009), which was also observed in our results (**Figure 3**). However, in *pah1 pah2*, the mole percent of MGDG decreased notably whereas that of DGDG only slightly increased during N starvation as compared with those in WT, PAH1OE, and PAH2OE (**Figure 3**). In PAH1OE and PAH2OE, the membrane lipid compositions were similar to one another, and changes in their mole percent during N starvation did not differ substantially from WT, except that the mole percent of MGDG in PAH1OE was slightly greater than that in WT under N-depleted conditions (**Figures 3A,C,D**). Given that PAH1 and PAH2 similarly complemented the *pah1 pah2* phenotype with respect to membrane glycerolipid composition (**Figures 3A,C,D**), PAH1 and PAH2 may have a redundant role in maintaining membrane lipid homeostasis of the ER and chloroplasts under both N-sufficient and N-depleted conditions. Moreover, these results clearly show that PAH1 and PAH2 play an important role in maintaining the mole percent of chloroplast membrane lipids to the extraplastidial membrane lipids, namely phospholipids, especially under N-depleted conditions. Given that the fatty acid compositions of MGDG and DGDG were similar among WT, *pah1 pah2*, PAH1OE and PAH2OE under both N conditions (**Supplementary Figure S4**), it was suggested that the prokaryotic pathway and the eukaryotic pathway equally contributed to the galactolipid synthesis. We also analyzed the TAG and DAG contents (**Figures 3E–G**). Under N-sufficient conditions, the amounts of TAG were comparable among plants (**Figure 3E**). However, under N-depleted conditions, the amount of TAG in *pah1 pah2* was lower and that in PAH1OE was slightly higher than that in WT (**Figure 3F**), suggesting that PAH1 is involved in the TAG accumulation in leaves under N starvation. PAH2OE showed a similar result to PAH1OE, but it was not significant. Given that the fatty acid compositions of TAG were similar among WT, *pah1 pah2*, PAH1OE and PAH2OE under both N conditions (**Supplementary Figures S5A–D**), it was suggested that PAH1 (and PAH2) might be only slightly involved in TAG synthesis under N starvation. The DAG contents also showed similar profile with the TAG contents (**Figure 3G**). Compared with WT, the lower amount of DAG in *pah1 pah2* under N-sufficient conditions and the higher amount of DAG in PAH1OE under N-depleted conditions were observed (**Figure 3G**). However, the fatty acid compositions of DAG were varied in *pah1 pah2*, PAH1OE and PAH2OE (**Supplementary Figures S5E–H**), suggesting that the lack or overexpression of PAH might destabilize the whole flow of DAG synthesis.

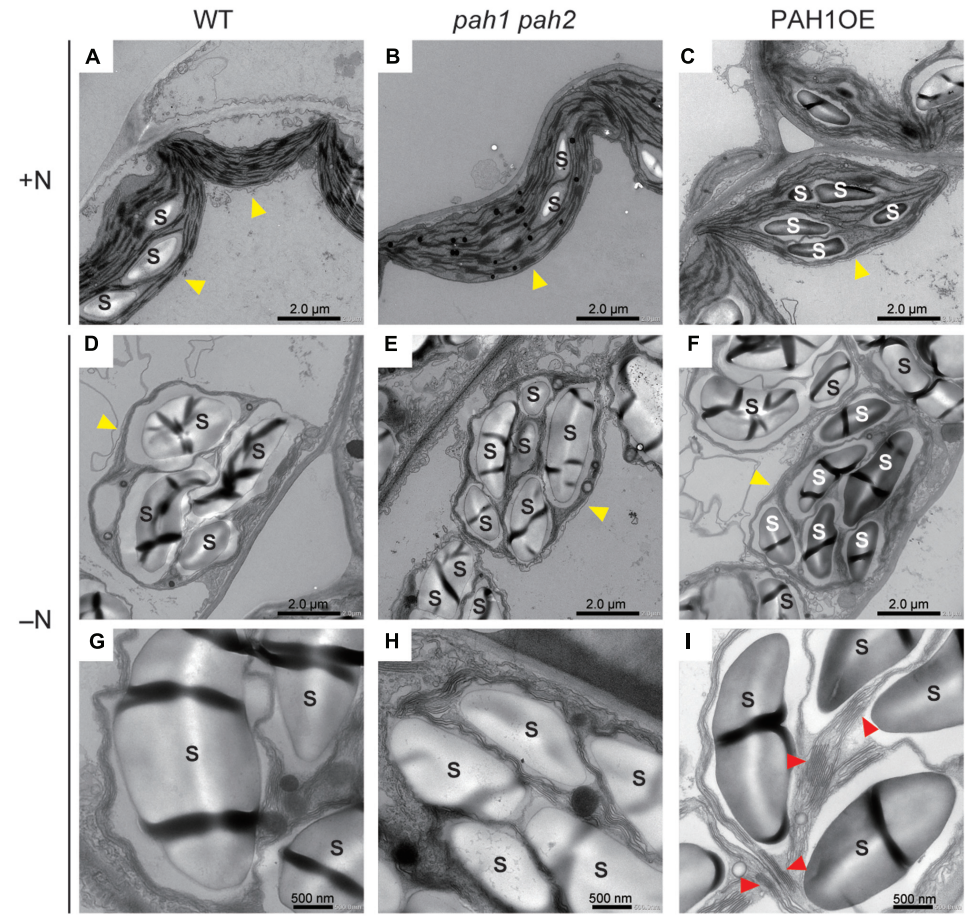

FIGURE 2 | Electron microscopy of chloroplast membrane structures in leaves. **(A)** WT, **(B)** *pah1 pah2*, and **(C)** PAH1OE under N-sufficient conditions (+N). **(D)** and **(G)** WT, **(E)** and **(H)** *pah1 pah2*, and **(F)** and **(I)** PAH1OE under N-depleted conditions (–N). Red arrowheads in **(I)** indicate grana-lamellae structures in thylakoid membranes. Yellow arrowheads indicate chloroplasts. S, starch granules.

Expression of the Genes for Fatty Acid Phytyl Ester Synthase in *pah1 pah2* Was Higher than in Other Plants under N Starvation

In plants grown under N-depleted conditions, the synthesis of fatty acid phytyl esters catalyzed by PES1 and PES2 is accelerated in chloroplasts to avoid the accumulation of free fatty acids and phytols derived from the degradation of thylakoid membrane lipids and chlorophyll, respectively (Lippold et al., 2012). Thus, we analyzed the expression of *PES1* and *PES2* under N-sufficient and N-depleted conditions (**Figures 4A,B**). In WT, the expression of *PES1* and *PES2* increased markedly under N-depleted conditions (Lippold et al., 2012) (**Figures 4A,B**). In *pah1 pah2*, the expression of *PES1* and *PES2* was significantly higher than that in WT under N-depleted conditions (**Figures 4A,B**), suggesting that the breakdown of MGDG and chlorophyll was enhanced in *pah1 pah2*, especially during N starvation, which is consistent with the results in **Figure 1**. In contrast, in PAH1OE and PAH2OE, the expression of *PES1* and *PES2* was comparable with that in WT under both N-sufficient and N-depleted conditions (**Figures 4A,B**).

Expression of MGDG Synthase Genes Was Comparable between WT and *pah1 pah2* but Was Upregulated in PAH1OE and PAH2OE Especially under N-Depleted Conditions

To clarify the effect of the absence or the overexpression of PAH on galactolipid synthesis, we analyzed the expression of MGDG synthesis genes (*MGD1*, *MGD2*, and *MGD3*, Awai et al., 2001) and DGDG synthesis genes (*DGD1* and *DGD2*, Dörmann et al., 1999; Kelly and Dörmann, 2002) and compared their expression levels among WT, *pah1 pah2*, PAH1OE, and PAH2OE under both N conditions (**Figures 4C–G**). In both WT and *pah1 pah2*, the expression of *MGD1* and *MGD2* was significantly decreased during N starvation, whereas it remained unchanged in PAH1OE and PAH2OE during N starvation (**Figures 4C,D**). In WT and *pah1 pah2*, *MGD3* expression remained unchanged or slightly increased during N

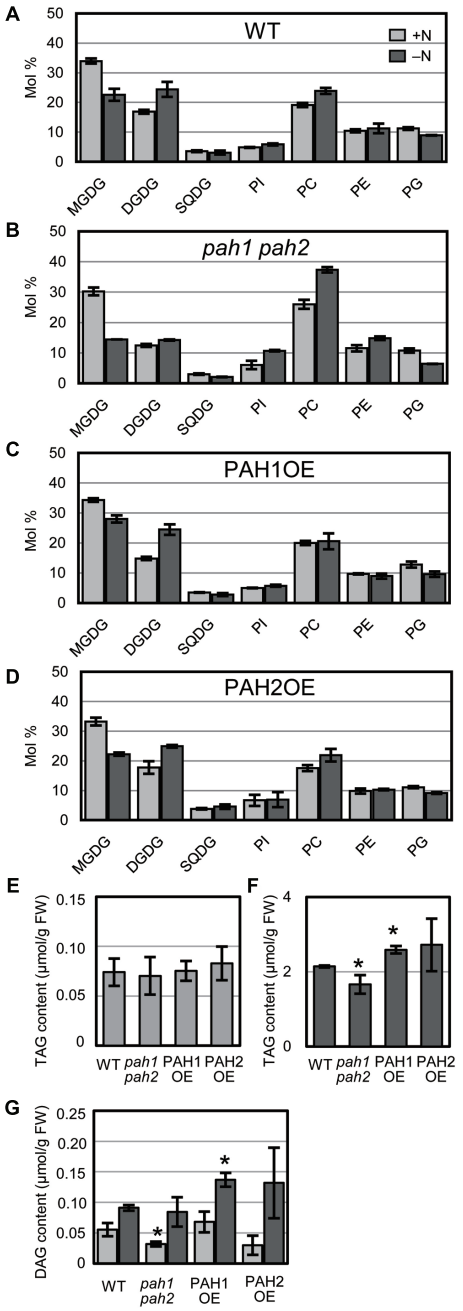

FIGURE 3 | Glycerolipid composition. Membrane glycerolipid composition of **(A)** WT, **(B)** *pah1 pah2*, **(C)** PAH1OE, and **(D)** PAH2OE. The TAG contents under N-sufficient conditions **(E)** and under N-depleted conditions **(F)**. **(G)** The DAG content. Results for N-sufficient (+N, light gray) and N-depleted (−N, dark gray) conditions are shown. SQDG, sulfoquinovosyldiacylglycerol; PI, phosphatidylinositol; PE, phosphatidylethanolamine; PG, phosphatidylglycerol; TAG, triacylglycerol; DAG, diacylglycerol. Values represent the mean ± SD of measurements made on samples from three different plants for each genotype. $^*P < 0.05$ for a *t*-test versus WT under each condition.

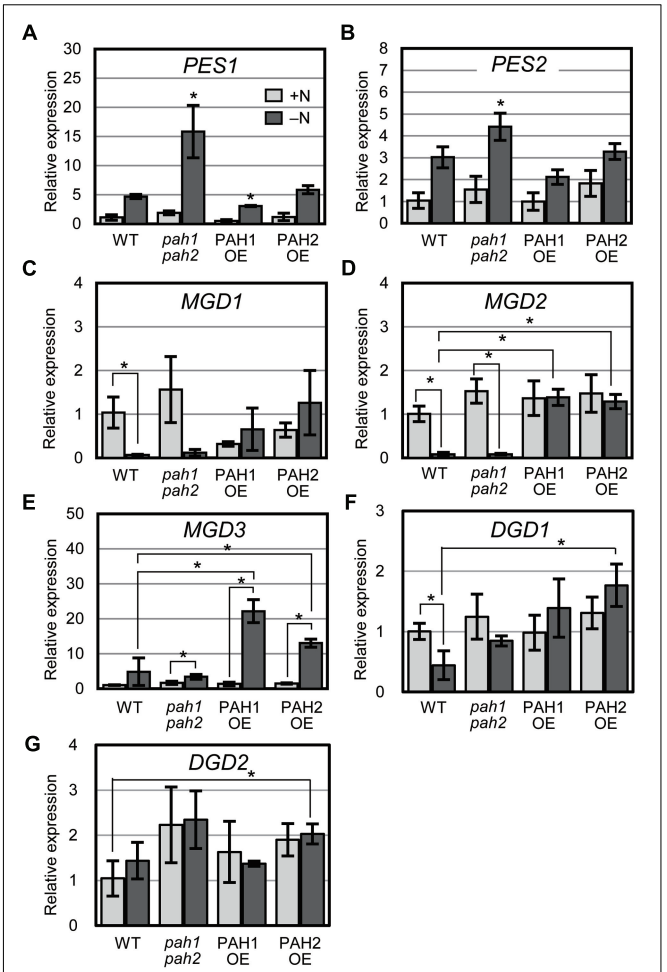

FIGURE 4 | Expression of genes encoding fatty acid phytyl ester synthase, MGDG synthase and DGDG synthase. Expression of **(A)** *PES1*, **(B)** *PES2*, **(C)** *MGD1*, **(D)** *MGD2*, **(E)** *MGD3*, **(F)** *DGD1* and **(G)** *DGD2* in plants of the indicated genotype relative to their corresponding levels in WT under N-sufficient conditions as assessed with quantitative reverse transcription-PCR. N-sufficient (+N, light gray) and N-depleted (−N, dark gray) conditions are shown. Values represent the mean ± SD of measurements made on samples from three different plants for each genotype. **(A,B)** $^*P < 0.05$ for a *t*-test versus WT under each condition. **(C–G)** $^*P < 0.05$ for a *t*-test between plants indicated by the brackets.

starvation, whereas its expression in PAH1OE and PAH2OE under N starvation was significantly higher than that under normal conditions (**Figure 4E**). Thus, although the three genes for MGDG synthesis showed mostly higher expression in PAH1OE and PAH2OE than in WT and *pah1 pah2* during N starvation, these expression levels were not remarkably different between WT and *pah1 pah2* under any N conditions. On the other hand, although the expression of *DGD1* in PAH1OE and PAH2OE under N-depleted conditions seemed higher than that in WT and *pah1 pah2* (**Figure 4F**), most of the expression was similar among plants under any conditions (**Figures 4F,G**). These results indicated that the absence of PAH has no effect on the expression of MGDG synthases under any N conditions, but the overexpression of PAH increases their expression levels, especially during N starvation.

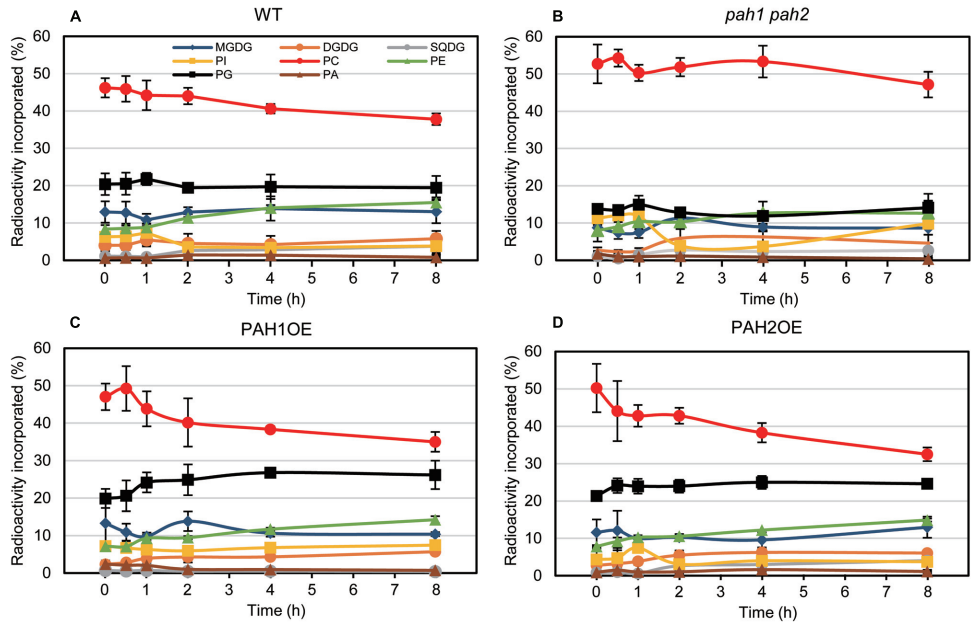

FIGURE 5 | *In vivo* pulse-chase labeling of membrane lipids during N starvation. [^{14}C]acetate labeling of fatty acids associated with individual lipids in **(A)** WT, **(B)** *pah1 pah2*, **(C)** PAH1OE, and **(D)** PAH2OE under N-depleted conditions was analyzed. Experiments were repeated three times, each with similar results. Values represent the mean ± SD of measurements made on samples from three different plants for each genotype.

Pulse-Chase Labeling of Membrane Lipids during N Starvation Indicated a Significant Decrease in the Labeling Percent of Chloroplast Lipids in *pah1 pah2*

In the case of [^{14}C]acetate labeling of Arabidopsis WT seedlings under normal growth conditions, the ^{14}C label is rapidly incorporated into PC and MGDG (Browse et al., 1986; Xu et al., 2003; Nakamura et al., 2009). Under N-depleted conditions, as well as under N-sufficient conditions, PC was the major ^{14}C-labeled lipid. However, the second most prevalent labeled lipid was PG in WT (**Figure 5A**). In *pah1 pah2*, the labeling percent of PC in the total labeled glycerolipids was markedly higher than that of WT (**Figure 5B**), which was plausibly caused by the enhanced PC synthesis in *pah1 pah2*, even under N starvation, or by the repression of PC breakdown and lipid trafficking from the ER to chloroplasts. Accordingly, in *pah1 pah2*, the relative amounts for labeled chloroplast lipids such as MGDG and PG in the total labeled glycerolipids were lower than in WT (**Figure 5B**). However, it is noteworthy that the percent of labeled phosphatidylinositol (PI) in *pah1 pah2* was about 2-fold higher than that in WT at the beginning and end of the time course (**Figures 5A,B**), which is consistent with the membrane glycerolipid compositions under N starvation in *pah1 pah2* (**Figure 3B**). In PAH1OE and PAH2OE, the profile of the labeled lipids, except PC and PG, were comparable with that in WT throughout the time course (**Figures 5A,C,D**). In PAH1OE and PAH2OE, the percent of the labeled PC was decreased by ∼8% during the initial 2 h, whereas the decrease was <5% in WT (**Figures 5A,C,D**). Moreover, the percent of the labeled PG increased by ∼5% over the time course, whereas that in WT and *pah1 pah2* remained unchanged (**Figure 5**). However, the percent of PC and PG in the membrane glycerolipids were not significantly different among WT, PAH1OE, and PAH2OE (**Figures 3A,C,D**). Thus, the exchange of the labeled fatty acids between PC and PG might occur in PAH1OE and PAH2OE under N starvation, but the amount is too small to affect the membrane glycerolipid composition.

DISCUSSION

We previously reported that PAH is involved in Pi-starvation tolerance, because the growth of *pah1 pah2* is severely impaired under Pi starvation (Nakamura et al., 2009). In the *pah1 pah2* mutant, the relative amount of galactolipids to phospholipids is lower than in WT under both Pi-sufficient and Pi-depleted conditions owing to an enhanced PC synthesis in the ER and a decreased supply rate of DAG from the ER to chloroplasts (Nakamura et al., 2009; Eastmond et al., 2010; Craddock et al., 2015, 2016). Thus, the negative effect on growth during Pi starvation can be explained simply as a decrease in the amount of Pi released from phospholipid degradation caused by the absence of PAH. However, here we found that PAH was also essential for growth under N starvation. PAH is involved in PC and phosphatidylethanolamine (PE) degradation because the substrate for PAH is PA produced from PC or PE by PLD. Thus, we first thought that N released from phospholipids could be essential for maintaining the N content in the cell and its growth under N starvation. However, compared with the amount of N in

chlorophyll and proteins, that in phospholipids such as PC, PE, and phosphatidylserine is too low to suggest that phospholipids function in N storage (Carrari et al., 2005; Gaude et al., 2007). Indeed, the N content in the seedlings was comparable between WT and *pah1 pah2* under either N condition. Thus, the severe phenotype of *pah1 pah2* under N starvation was not caused by a decrease in the N content, and the absence of PAH had no effect on the N content in the seedlings.

PA accumulates in *pah1 pah2* seedlings (Nakamura et al., 2009). As PA is a signaling molecule for some environmental stresses (Katagiri et al., 2001; Munnik, 2001; Sang et al., 2001; Jouhet et al., 2012), it is also possible that the accumulation of PA in *pah1 pah2* during N starvation affects the signaling cascade related to N starvation. However, overexpression of PLDε enhances N signaling and growth in Arabidopsis and *Brassica napus*, and PA produced by PLDε functions as a lipid messenger response to N starvation (Hong et al., 2009; Lu et al., 2016). In Arabidopsis, there are 12 PLDs that differ with respect to their localization and functions (Testerink and Munnik, 2011). It is not known which PLD is involved in the PA supply for PAH, but it is most likely that differences in the localization and the timing of PA accumulation result in the different effects on plant growth. Thus, to clarify the correlation between PA content as a signaling molecule and tolerance to N starvation in *pah1 pah2*, we will need to undertake additional experiments using transgenic plants—resulting from crosses between *pah1 pah2* mutants, PAH-overexpressing plants, PLD mutants or overexpressing plants—that have been modified with respect to PA content and to the subcellular localization of PA. Recently, the involvement of phosphatidylinositol–phospholipase C (PI-phospholipase C) in the N signaling pathway was shown in Arabidopsis (Riveras et al., 2015). PI-phospholipase C affects the amount of calcium ions in the cytosol, and the resulting increase in calcium ions activates the expression of N-responsive genes. PIphospholipase C produces DAG and inositol 1,4,5-triphosphate from PI. In *pah1 pah2* during N starvation, not only the mole percent of PC but also that of PI was remarkably higher than WT in the membrane glycerolipids, suggesting that the 1,4,5-triphosphate synthesis from PI might be affected as well as the synthesis of other phospholipids under N starvation.

In Arabidopsis WT seedlings, a marked decrease in the MGDG mole percent with an increase in the DGDG mole percent in the total glycerolipids occurs during N starvation (Gaude et al., 2007), which was also observed in our results. However, in *pah1 pah2*, the decrease in the MGDG mole percent was even greater during N starvation as compared with WT. As these results were based on the relative amount of the lipids, it seemed that the results might simply be explained by the enhancement of PC synthesis in *pah1 pah2* (Eastmond et al., 2010). However, the microscopic analysis clearly showed a difference in membrane structures between WT and *pah1 pah2*. The enhanced degradation of the thylakoid membranes was observed only in *pah1 pah2* grown under N starvation, indicating that PAH is involved in the maintenance of thylakoid membranes during N starvation. Indeed, in *pah1 pah2*, fatty acid phytyl ester synthesis was transcriptionally upregulated, especially under N starvation, suggesting that the degradation of MGDG is enhanced in *pah1 pah2* during N starvation. PAH was previously described as not being involved in lipid trafficking between the ER and chloroplast and as being involved only in phospholipid synthesis and its homeostasis in the ER under normal growth conditions (Eastmond et al., 2010). Under Pi-depleted conditions, however, we observed the involvement of PAH in lipid trafficking between the ER and chloroplast based on the difference in the fatty acid composition of MGDG, although its contribution to lipid trafficking seemed smaller than expected considering the severe phenotype of *pah1 pah2* under Pi starvation (Nakamura et al., 2009). Under N starvation, most of the lipid synthetic pathways except PC synthesis was markedly downregulated in *pah1 pah2* based on the results from our pulse-chase labeling experiments. Thus, it is unclear that PAH is involved in lipid trafficking between the ER and chloroplast under N starvation as well as under Pi starvation.

We previously produced *pah1 pah2* complementation lines (Nakamura et al., 2009), which overexpress PAH1 or PAH2 and were designated as PAH1OE or PAH2OE, respectively, in this study. PAH1OE and PAH2OE complemented the *pah1 pah2* phenotype, especially with respect to membrane lipid composition and growth under N-sufficient and N-depleted conditions. However, one of the photosynthetic parameters, F_v/F_m, and the chlorophyll content were significantly greater in both PAH1OE and PAH2OE as compared with WT, especially under N starvation. These results clearly showed that PAH affects the photosynthetic activity and the chlorophyll content during N starvation. Although the membrane glycerolipid composition of these two overexpressing lines was comparable with WT, enhancement of the DAG supply from the ER to chloroplasts might be a trigger for enhancement of membrane lipid turnover in chloroplasts, because DAG is a common substrate for the synthesis of the lipids MGDG, sulfoquinovosyldiacylglycerol, and PG. Indeed, in the pulse-chase experiments using [^{14}C]acetate during N starvation, the most remarkable finding was that PG was the second-most predominant labeled lipid during N starvation, which has not been observed under normal growth conditions. Moreover, the labeling percents were increased only in PAH1OE and PAH2OE throughout the time course. Thus, it may be that the plants are dying under N starvation but manage to maintain PG synthesis because PG is the essential lipid for photosynthesis (Hagio et al., 2002; Kobayashi et al., 2015, 2016; Lin et al., 2016). In *pah1 pah2*, the labeling percent of PG and the other chloroplast lipids was significantly lower than WT, possibly because of the enhanced PC synthesis in *pah1 pah2* and the decrease in PC breakdown even under N starvation. The enhanced incorporation of [^{14}C]acetate into PC might cause the reduced incorporation of [^{14}C]acetate into the chloroplast membrane lipids. In contrast, in PAH1OE and PAH2OE, the labeling percent of PG increased with a concomitant decrease in that of PC during N starvation, which was not observed in WT. Although PAH might have a crucial role for regulating lipid homeostasis between the ER and chloroplasts, the molecular mechanism was not clarified in this study. The yet unknown molecular mechanism might explain why the expression of *MGD2* and *MGD3* in PAH1OE and PAH2OE was markedly higher than in WT, especially under N starvation.

AUTHOR CONTRIBUTIONS

YY, KN, HO, and MS directed the study. YY and MS designed the experiments. YY, RS, YM, KI, MM, KS, and DS performed the experiments and analyzed the data. YY and MS wrote the manuscript.

FUNDING

This work was supported in part by a Grants-in-Aid for Scientific Research on Innovative Areas (Nos. 23119506, 25119708 and 17H06417); by a Grant-in-Aid for Scientific Research (C) (No. 15K07335) from the Ministry of Education, Culture, Sports, Science and Technology of Japan; and by Core Research for Evolutional Science and Technology programs of the Japanese Science and Technology Agency.

SUPPLEMENTARY MATERIAL

The Supplementary Material for this article can be found online at: https://www.frontiersin.org/articles/10.3389/fpls.2017.01847/full#supplementary-material

FIGURE S1 | Expression levels of *PAH1* and *PAH2* in WT, *pah1 pah2*, and the transgenic plants PAH1OE and PAH2OE under N-sufficient conditions. Expression of *PAH1* and *PAH2* relative to their corresponding levels in WT under N-sufficient conditions as assessed by quantitative reverse transcription–PCR. Values represent the mean ± SD of measurements made on samples from three different plants for each genotype.

FIGURE S2 | Electron microscopy of chloroplast membrane structures in leaves. **(A,D)** WT, **(B,E)** *pah1 pah2*, and **(C,F)** PAH1OE under N-depleted conditions. Red arrowheads indicate grana-lamellae stacking structures in thylakoid membranes. S, starch granules.

FIGURE S3 | Ultrastructural analysis of the stacking repeat distance in thylakoids of WT, *pah1 pah2*, and PAH1OE under N-depleted conditions. **(A)** WT, **(B)** *pah1 pah2*, **(C)** PAH1OE. The repeat distance of grana thylakoid membranes was analyzed from transmission electron microscopy images according to the method of Wang et al. (2014). **(A)** and **(C)**, $n = 100$ grana thylakoid membrane regions from 10 different chloroplasts, with 10 grana thylakoid membrane regions from each chloroplast; **(B)**, $n = 42$ grana thylakoid membrane regions from 10 different chloroplasts, with four or five grana thylakoid membrane regions from each chloroplast.

FIGURE S4 | Fatty acid compositions of MGDG and DGDG. MGDG in **(A)** WT, **(B)** *pah1 pah2*, **(C)** PAH1OE, and **(D)** PAH2OE. DGDG in **(E)** WT, **(F)** *pah1 pah2*, **(G)** PAH1OE, and **(H)** PAH2OE. Results for N-sufficient (+N, light gray) and N-depleted (−N, dark gray) conditions are shown. Values represent the mean ± SD of measurements made on samples from three different plants for each genotype.

FIGURE S5 | Fatty acid compositions of TAG and DAG. TAG in **(A)** WT, **(B)** *pah1 pah2*, **(C)** PAH1OE, and **(D)** PAH2OE. DAG in **(E)** WT, **(F)** *pah1 pah2*, **(G)** PAH1OE, and **(H)** PAH2OE. Results for N-sufficient (+N, light gray) and N-depleted (−N, dark gray) conditions are shown. Values represent the mean ± SD of measurements made on samples from three different plants for each genotype.

REFERENCES

Awai, K., Maréchal, E., Block, M. A., Brun, D., Masuda, T., Shimada, H., et al. (2001). Two types of MGDG synthase genes, found widely in both 16:3 and 18:3 plants, differentially mediate galactolipid syntheses in photosynthetic and nonphotosynthetic tissues in *Arabidopsis thaliana*. *Proc. Natl. Acad. Sci. U.S.A.* 98, 10960–10965. doi: 10.1073/pnas.181331498

Bligh, E. G., and Dyer, W. J. (1959). A rapid method of total lipid extraction and purification. *Can. J. Biochem. Physiol.* 37, 911–917. doi: 10.1139/o59-099

Block, M. A., Dorne, A. J., Joyard, J., and Douce, R. (1983). Preparation and characterization of membrane fractions enriched in outer and inner envelope membranes from spinach chloroplasts. II. Biochemical characterization. *J. Biol. Chem.* 258, 13281–13286.

Boussadia, O., Steppe, K., Zgallai, H., Ben El Hadj, S., Braham, M., Lemeur, R., et al. (2010). Effects of nitrogen deficiency on leaf photosynthesis, carbohydrate status biomass production in two olive cultivars "Meski" and "Koroneiki.". *Sci. Hortic.* 123, 336–342. doi: 10.1016/j.scienta.2009.09.023

Browse, J., McCourt, P., and Somerville, C. (1986). A mutant of *Arabidopsis* deficient in $C_{18:3}$ and $C_{16:3}$ leaf lipids. *Plant physiol.* 81, 859–864. doi: 10.1104/pp.81.3.859

Carrari, F., Coll-Garcia, D., Schauer, N., Lytovchenko, A., Palacios-Rojas, N., Balbo, I., et al. (2005). Deficiency of a plastidial adenylate kinase in Arabidopsis results in elevated photosynthetic amino acid biosynthesis and enhanced growth. *Plant Physiol.* 137, 70–82. doi: 10.1104/pp.104.056143

Craddock, C. P., Adams, N., Bryant, F. M., Kurup, S., and Eastmond, P. J. (2015). PHOSPHATIDIC ACID PHOSPHOHYDROLASE regulates phosphatidylcholine biosynthesis in *Arabidopsis* by phosphatidic acid-mediated activation of CTP:PHOSPHOCHOLINE CYTIDYLYLTRANSFERASE activity. *Plant Cell* 27, 1251–1264. doi: 10.1105/tpc.15.00037

Craddock, C. P., Adams, N., Kroon, J., Bryant, F. M., Hussey, P. J., Kurup, S., et al. (2016). Cyclin-dependent kinase activity enhances phosphatidylcholine biosynthesis in Arabidopsis by repressing phosphatidic acid phosphohydrolase activity. *Plant J.* 89, 3–14. doi: 10.1111/tpj.13321

Crawford, N. M., and Forde, B. G. (2002). Molecular and developmental biology of inorganic nitrogen nutrition. *Arabidopsis Book* 1:e0011. doi: 10.1199/tab.0011

Dörmann, P., Balbo, I., and Benning, C. (1999). *Arabidopsis* galactolipid biosynthesis and lipid trafficking mediated by DGD1. *Science* 284, 2181–2184. doi: 10.1126/science.284.5423.2181

Dörmann, P., and Benning, C. (2002). Galactolipids rule in seed plants. *Trends Plant Sci.* 7, 112–118. doi: 10.1016/S1360-1385(01)02216-6

Eastmond, P. J., Quettier, A.-L., Kroon, J. T. M., Craddock, C., Adams, N., and Slabas, A. R. (2010). Phosphatidic acid phosphohydrolase 1 and 2 regulate phospholipid synthesis at the endoplasmic reticulum in *Arabidopsis*. *Plant Cell* 22, 2796–2811. doi: 10.1105/tpc.109.071423

Estelle, M. A., and Somerville, C. (1987). Auxin-resistant mutants of *Arabidopsis thaliana* with an altered morphology. *Mol. Gen. Genet.* 206, 200–206. doi: 10.1007/BF00333575

Gaude, N., Bréhélin, C., Tischendorf, G., Kessler, F., and Dörmann, P. (2007). Nitrogen deficiency in Arabidopsis affects galactolipid composition and gene expression and results in accumulation of fatty acid phytyl esters. *Plant J.* 49, 729–739. doi: 10.1111/j.1365-313X.2006.02992.x

Guo, F. Q., Wang, R., Chen, M., and Crawford, N. M. (2001). The Arabidopsis dual-affinity nitrate transporter gene *AtNRT1.1* (*CHL1*) is activated and functions in nascent organ development during vegetative and reproductive growth. *Plant Cell* 13, 1761–1777. doi: 10.1105/tpc.13.8.1761

Hachiya, T., and Noguchi, K. (2008). Effect of growth temperature and total non-structural carbohydrate accumulation on growth coefficient in *Petunia x hybrida* petals. *Physiol. Plant.* 134, 293–302. doi: 10.1111/j.1399-3054.2008.01132.x

Hagio, M., Sakurai, I., Sato, S., Kato, T., Tabata, S., and Wada, H. (2002). Phosphatidylglycerol is essential for the development of thylakoid membranes in *Arabidopsis thaliana*. *Plant Cell Physiol.* 42, 1456–1464. doi: 10.1093/pcp/pcf185

Hanaoka, H., Noda, T., Shirano, Y., Kato, T., Hayashi, H., Shibata, D., et al. (2002). Leaf senescence and starvation-induced chlorosis are accelerated by the disruption of an Arabidopsis autophagy gene. *Plant Physiol.* 129, 1181–1193. doi: 10.1104/pp.011024

Härtel, H., and Benning, C. (2000). Can digalactosyldiacylglycerol substitute for phosphatidylcholine upon phosphate deprivation in leaves and roots of *Arabidopsis*? *Biochem. Soc. Trans.* 28, 729–732.

Hong, Y., Devaiah, S. P., Bahn, S. C., Thamasandra, B. N., Li, M., Welti, R., et al. (2009). Phospholipase Dε and phosphatidic acid enhance Arabidopsis nitrogen signaling and growth. *Plant J.* 58, 376–387. doi: 10.1111/j.1365-313X.2009.03788.x

Jouhet, J., Maréchal, E., and Block, M. A. (2012). Role of phosphatidic acid in plant galactolipid synthesis. *Biochimie* 94, 86–93. doi: 10.1016/j.biochi.2011.03.012

Katagiri, T., Takahashi, S., and Shinozaki, K. (2001). Involvement of a novel *Arabidopsis* phospholipase D, AtPLDδ, in dehydration-inducible accumulation of phosphatidic acid in stress signaling. *Plant J.* 26, 595–605. doi: 10.1046/j.1365-313x.2001.01060.x

Kelly, A. A., and Dörmann, P. (2002). DGD2, an arabidopsis gene encoding a UDP-galactose-dependent digalactosyldiacylglycerol synthase is expressed during growth under phosphate-limiting conditions. *J. Biol. Chem.* 277, 1166–1173. doi: 10.1074/jbc.M110066200

Kobayashi, K., Awai, K., Nakamura, M., Nagatani, A., Masuda, T., and Ohta, H. (2009). Type-B monogalactosyldiacylglycerol synthases are involved in phosphate starvation-induced lipid remodeling, and are crucial for low-phosphate adaptation. *Plant J.* 57, 322–331. doi: 10.1111/j.1365-313X.2008.03692.x

Kobayashi, K., Endo, K., and Wada, H. (2016). Multiple impacts of loss of plastidic phosphatidylglycerol biosynthesis on photosynthesis during seedling growth of Arabidopsis. *Front. Plant Sci.* 7:336. doi: 10.3389/fpls.2016.00336

Kobayashi, K., Fujii, S., Sato, M., Toyooka, K., and Wada, H. (2015). Specific role of phosphatidylglycerol and functional overlaps with other thylakoid lipids in Arabidopsis chloroplast biogenesis. *Plant Cell Rep.* 34, 631–642. doi: 10.1007/s00299-014-1719-z

Kobayashi, K., Kondo, M., Fukuda, H., Nishimura, M., and Ohta, H. (2007). Galactolipid synthesis in chloroplast inner envelope is essential for proper thylakoid biogenesis, photosynthesis, and embryogenesis. *Proc. Natl. Acad. Sci. U.S.A.* 104, 17216–17221. doi: 10.1073/pnas.0704680104

Kobayashi, K., Masuda, T., Takamiya, K.-I., and Ohta, H. (2006). Membrane lipid alteration during phosphate starvation is regulated by phosphate signaling and auxin/cytokinin cross-talk. *Plant J.* 47, 238–248. doi: 10.1111/j.1365-313X.2006.02778.x

Lin, Y. C., Kobayashi, K., Hung, C. H., Wada, H., and Nakamura, Y. (2016). Arabidopsis phosphatidylglycerophosphate phosphatase 1 involved in phosphatidylglycerol biosynthesis and photosynthetic function. *Plant J.* 88, 1022–1037. doi: 10.1111/tpj.13311

Lippold, F., vom Dorp, K., Abraham, M., Hölzl, G., Wewer, V., Yilmaz, J. L., et al. (2012). Fatty acid phytyl ester synthesis in chloroplasts of *Arabidopsis*. *Plant Cell* 24, 2001–2014. doi: 10.1105/tpc.112.095588

Little, D. Y., Rao, H., Oliva, S., Daniel-Vedele, F., Krapp, A., and Malamy, J. E. (2005). The putative high-affinity nitrate transporter NRT2.1 represses lateral root initiation in response to nutritional cues. *Proc. Natl. Acad. Sci. U.S.A.* 102, 13693–13698. doi: 10.1073/pnas.0504219102

Lu, S., Yao, S., Wang, G., Guo, L., Zhou, Y., Hong, Y., et al. (2016). Phospholipase Dε enhances *Braasca napus* growth and seed production in response to nitrogen availability. *Plant Biotechnol. J.* 14, 926–937. doi: 10.1111/pbi.12446

Maathuis, F. J. M. (2009). Physiological functions of mineral macronutrients. *Curr. Opin. Plant Biol.* 12, 250–258. doi: 10.1016/j.pbi.2009.04.003

Martin, T., Oswald, O., and Graham, I. A. (2002). Arabidopsis seedling growth, storage lipid mobilization, and photosynthetic gene expression are regulated by carbon:nitrogen availability. *Plant Physiol.* 128, 472–481. doi: 10.1104/pp.010475

Moran, R., and Porath, D. (1980). Chlorophyll determination in intact tissues using *N,N*-dimethylformamide. *Plant Physiol.* 65, 478–479. doi: 10.1104/pp.65.3.478

Munnik, T. (2001). Phosphatidic acid: an emerging plant lipid second messenger. *Trends Plant Sci.* 6, 227–233. doi: 10.1016/S1360-1385(01)01918-5

Murashige, T., and Skoog, F. (1962). A revised medium for rapid growth and bio assays with tobacco tissue cultures. *Physiol. Plant.* 15, 473–497. doi: 10.1111/j.1399-3054.1962.tb08052.x

Nakamura, Y. (2013). Phosphate starvation and membrane lipid remodeling in seed plants. *Prog. Lipid Res.* 52, 43–50. doi: 10.1016/j.plipres.2012.07.002

Nakamura, Y., Koizumi, R., Shui, G., Shimojima, M., Wenk, M. R., Ito, T., et al. (2009). *Arabidopsis* lipins mediate eukaryotic pathway of lipid metabolism and cope critically with phosphate starvation. *Proc. Natl. Acad. Sci. U.S.A.* 106, 20978–20983. doi: 10.1073/pnas.0907173106

Narasimhan, R., Wang, G., Li, M., Roth, M., Welti, R., and Wang, X. (2013). Differential changes in galactolipid and phospholipid species in soybean leaves and roots under nitrogen deficiency and after nodulation. *Phytochemistry* 96, 81–91. doi: 10.1016/j.phytochem.2013.09.026

Ono, K., Terashima, I., and Watanabe, A. (1996). Interaction between nitrogen deficit of a plant and nitrogen content in the old leaves. *Plant Cell Physiol.* 37, 1083–1089. doi: 10.1093/oxfordjournals.pcp.a029057

Orsel, M., Chopin, F., Leleu, O., Smith, S. J., Krapp, A., Daniel-Vedele, F., et al. (2006). Characterization of a two-component high-affinity nitrate uptake system in Arabidopsis. Physiology and protein-protein interaction. *Plant Physiol.* 142, 1304–1317. doi: 10.1104/pp.106.085209

Peng, M., Bi, Y.-M., Zhu, T., and Rothstein, S. J. (2007). Genome-wide analysis of *Arabidopsis* responsive transcriptome to nitrogen limitation and its regulation by the ubiquitin ligase gene *NLA*. *Plant Mol. Biol.* 65, 775–797. doi: 10.1007/s11103-007-9241-0

Raghothama, K. G. (1999). PHOSPHATE ACQUISITION. *Annu. Rev. Plant Physiol. Plant Mol. Biol.* 50, 665–693. doi: 10.1146/annurev.arplant.50.1.665

Remans, T., Nacry, P., Pervent, M., Girin, T., Tillard, P., Lepetit, M., et al. (2006). A central role for the nitrate transporter NRT2.1 in the integrated morphological and physiological responses of the root system to nitrogen limitation in Arabidopsis. *Plant Physiol.* 140, 909–921. doi: 10.1104/pp.105.075721

Riveras, E., Alvarez, J. M., Vidal, E. A., Oses, C., Vega, A., and Gutiérrez, R. A. (2015). The calcium ion is a second messenger in the nitrate signaling pathway of Arabidopsis. *Plant Physiol.* 169, 1397–1404. doi: 10.1104/pp.15.00961

Sang, Y., Cui, D., and Wang, X. (2001). Phospholipase D and phosphatidic acid-mediated generation of superoxide in Arabidopsis. *Plant Physiol.* 126, 1449–1458. doi: 10.1104/pp.126.4.1449

Shimojima, M., and Ohta, H. (2011). Critical regulation of galactolipid synthesis controls membrane differentiation and remodeling in distinct plant organs and following environmental changes. *Prog. Lipid Res.* 50, 258–266. doi: 10.1016/j.plipres.2011.03.001

Sun, C.-W., and Callis, J. (1997). Independent modulation of *Arabidopsis thaliana* polyubiquitin mRNAs in different organs and in response to environmental changes. *Plant J.* 11, 1017–1027. doi: 10.1046/j.1365-313X.1997.11051017.x

Testerink, C., and Munnik, T. (2011). Molecular, cellular, and physiological responses to phosphatidic acid formation in plants. *J. Exp. Bot.* 62, 2349–2361. doi: 10.1093/jxb/err079

Vidal, E. A., and Gutiérrez, R. A. (2008). A systems view of nitrogen nutrient and metabolite responses in Arabidopsis. *Curr. Opin. Plant Biol.* 11, 521–529. doi: 10.1016/j.pbi.2008.07.003

Wang, S., Uddin, M. I., Tanaka, K., Yin, L., Shi, Z., Qi, Y., et al. (2014). Maintenance of chloroplast structure and function by overexpression of the rice *MONOGALACTOSYLDIACYLGLYCEROL SYNTHASE* gene leads to enhanced salt tolerance in tobacco. *Plant Physiol.* 165, 1144–1155. doi: 10.1104/pp.114.238899

Xu, C., Fan, J., Riekhof, W., Froehlich, J. E., and Benning, C. (2003). A permease-like protein involved in ER to thylakoid lipid transfer in *Arabidopsis*. *EMBO J.* 22, 2370–2379. doi: 10.1093/emboj/cdg234

Yang, Y., Yu, X., Song, L., and An, C. (2011). ABI4 activates DGAT1 expression in *Arabidopsis* seedlings during nitrogen deficiency. *Plant Physiol.* 156, 873–883. doi: 10.1104/pp.111.175950

Conflict of Interest Statement: The authors declare that the research was conducted in the absence of any commercial or financial relationships that could be construed as a potential conflict of interest.

frontiers in Plant Science

ORIGINAL RESEARCH
published: 27 November 2017
doi: 10.3389/fpls.2017.02007

Mutations in the Arabidopsis *AtMRS2-11/AtMGT10/VAR5* Gene Cause Leaf Reticulation

*Shuang Liang†, Yafei Qi†, Jun Zhao, Yuanfeng Li, Rui Wang, Jingxia Shao, Xiayan Liu, Lijun An and Fei Yu**

State Key Laboratory of Crop Stress Biology for Arid Areas and College of Life Sciences, Northwest A&F University, Yangling, China

In higher plants, the development of functional chloroplasts is essential for photosynthesis and many other physiological processes. With a long-term goal of elucidating the genetic regulation of chloroplast development, we identified two allelic leaf variegation mutants, *variegated5-1* (*var5-1*) and *var5-2*. Both mutants showed a distinct leaf reticulation phenotype of yellow paraveinal regions and green interveinal regions, and the leaf reticulation phenotype correlated with photosynthetic defects. Through the identification of mutation sites in the two mutant alleles and the molecular complementation, we confirmed that *VAR5* encodes a CorA family of Mg^{2+} transporters also known as AtMRS2-11/AtMGT10. Using protoplast transient expression and biochemical fractionation assays, we demonstrated that AtMRS2-11/AtMGT10/VAR5 likely localizes to the chloroplast envelope. Moreover, we established that AtMRS2-11/AtMGT10/VAR5 forms large molecular weight complexes in the chloroplast and the sizes of these complexes clearly exceed those of their bacterial counterparts, suggesting the compositions of CorA Mg^{2+} transporter complex is different between the chloroplast and bacteria. Our findings indicate that AtMRS2-11/AtMGT10/VAR5 plays an important role in the tissue specific regulation of chloroplast development.

Keywords: AtMRS2-11/AtMGT10/VAR5, chloroplast development, leaf variegation, Mg^{2+} transporters, chloroplast envelope

OPEN ACCESS

Edited by:
Julian Eaton-Rye, University of Otago, New Zealand

Reviewed by:
Sheng Luan, University of California, Berkeley, United States
Jinpeng Gao, Washington State University, United States

****Correspondence:***
Fei Yu
flyfeiyu@gmail.com

†These authors have contributed equally to this work.

Specialty section:
This article was submitted to Plant Cell Biology, a section of the journal Frontiers in Plant Science

Received: *12 July 2017*
Accepted: *10 November 2017*
Published: *27 November 2017*

Citation:
Liang S, Qi Y, Zhao J, Li Y, Wang R, Shao J, Liu X, An L and Yu F (2017) Mutations in the Arabidopsis AtMRS2-11/AtMGT10/VAR5 Gene Cause Leaf Reticulation. Front. Plant Sci. 8:2007. doi: 10.3389/fpls.2017.02007

INTRODUCTION

Magnesium ion (Mg^{2+}) is one of the most abundant divalent cations in cells and is involved in myriads of essential metabolic processes (Maguire and Cowan, 2002). The electrically charged nature of Mg^{2+} necessitates the presence of membrane transporters to facilitate efficient Mg^{2+} trafficking across biological membranes. The functions and regulations of these transporters ensure the maintenance of Mg^{2+} homeostasis in different sub-cellular compartments in cells (Shaul, 2002).

Magnesium ion transport systems were most extensively studied in prokaryotes, and several types of putative Mg^{2+} transporters, including CorA, MgtE, and P-type ATPase Mgt, have been

Abbreviations: AtMGT, *Arabidopsis thaliana* Mg^{2+} transporters; AtMRS2, *Arabidopsis thaliana* mitochondrial RNA splicing2; CaMV, Cauliflower Mosaic Virus; CorA, Co^{2+} resistance A; GFP, green fluorescence protein; GMN, glycine–methionine–asparagine motif; L*er*, Landsberg *erecta*; PSI, photosystem I; PSII, photosystem II; UTR: untranslated region; *VAR5*, *Variegated5*.

identified in bacteria (Smith and Maguire, 1995; Moomaw and Maguire, 2008). In eukaryotic cells, the CorA family Mg^{2+} transporter was identified in yeast mitochondria as MRS2 and is involved in group II intron splicing (Bui et al., 1999). Typical CorA Mg^{2+} transporters contain two C-terminal transmembrane domains and in between a conserved GMN motif as a Mg^{2+} binding site (Lunin et al., 2006; Pfoh et al., 2012). Genes coding for putative Mg^{2+} transporters are also present in plant genomes and the most extensively studied Mg^{2+} transporters in plants are the CorA family of transporters (Gardner, 2003). In the model system *Arabidopsis thaliana*, there are at least 10 genes encoding putative CorA Mg^{2+} transporters and they have been designated as encoding AtMRS2 or magnesium transport (AtMGT) (Schock et al., 2000; Li et al., 2001). Functionally, Arabidopsis CorA Mg^{2+} transporters were able to complement bacterial or yeast mutants that are defective in Mg^{2+} transport, suggesting that they are bona fide Mg^{2+} transporters (Schock et al., 2000; Li et al., 2001, 2008; Drummond et al., 2006; Mao et al., 2008; Chen et al., 2009; Gebert et al., 2009). Consistent with the important roles of Mg^{2+} in biological systems, *AtMRS2*/*AtMGT* genes have been shown to be important for several cellular processes. For example, AtMRS2-6/AtMGT5 and AtMRS2-2/AtMGT9 have been shown to be involved in pollen development (Li et al., 2008; Chen et al., 2009). Moreover, attempts to obtain insertional knock-out mutants of several *AtMRS2*/*AtMGT* genes have not yielded homozygous mutants for several genes including *AtMRS2-2*/*AtMGT9*, *AtMRS2-6*/*AtMGT5*, and *AtMRS2-11*/*AtMGT10*, suggesting these genes may be essential genes in Arabidopsis (Li et al., 2008; Chen et al., 2009; Gebert et al., 2009). Consistent with their membrane protein identities, these transporters are targeted to different sub-cellular compartments and are presumably responsible for Mg^{2+} homeostasis in various organelles. For example, AtMRS2-10/AtMGT1 and AtMRS2-4/AtMGT6 are plasma membrane Mg^{2+} transporters (Li et al., 2001; Mao et al., 2014). AtMRS2-6/AtMGT5 was shown to be targeted to mitochondria (Li et al., 2008). AtMRS2-7/AtMGT7 has been suggested to be located in the endoplasmic reticulum (Gebert et al., 2009). AtMRS2-1/AtMGT2 and AtMRS2-5/AtMGT3 are targeted to the tonoplast and involved in Mg^{2+} partition in leaf mesophyll cell vacuoles (Conn et al., 2011). In addition to the CorA Mg^{2+} transporters, other types of putative Mg^{2+} transporters have also been identified in plants including the AtMHX H^+/Mg^{2+} transporter (Shaul et al., 1999; Shaul, 2002).

The chloroplast is the organelle for photosynthesis and many other essential processes in plants (Pogson and Albrecht, 2011). Mg^{2+} also plays critical roles in the chloroplast. For example, in the light reactions, Mg^{2+} is an integral part of photosynthetic pigment chlorophylls. In carbon reactions, it is known that Mg^{2+} can regulate the activities of ribulose 1,5-bisphosphate reductase/oxygenase (rubisco) and many other enzymes. Thus, it is not surprising that Mg^{2+} transporters are necessary in the chloroplast to facilitate the transport of the ion and to regulate chloroplast Mg^{2+} homeostasis. Of the AtMRS2/AtMGT family of Mg^{2+} transporters, AtMRS2-11/AtMGT10 is predicted to be targeted to the chloroplast based on the presence of a N-terminal chloroplast transit peptide (Drummond et al., 2006).

Plant variegation mutants generally refer to mutants that display differential leaf color in plant organs, especially in leaves (Yu et al., 2007). In variegation mutants defective in nuclear genes for chloroplast proteins, differential chlorophyll accumulation/chloroplast development can arise from a uniform mutant genetic background, and these mutants have long attracted attention because the mechanisms of variegation are instrumental in our understanding of chloroplast development. Among variegation mutants, one unique group of leaf variegation mutants is the reticulate mutants (Yu et al., 2007). These mutants usually show a differential chlorophyll accumulation/chloroplast development between paraveinal regions and interveinal regions, thus giving rise to a "net" like phenotype. Most of the reticulate mutants reported so far display green paraveinal regions and yellow interveinal regions and several reticulate mutants have been characterized at the molecular level (López-Juez et al., 1998; Yu et al., 2007). The mutation of *CHLOROPHYLL A/B BINDING PROTEIN* (*CAB*) *GENE UNDEREXPRESSED 1* (*CUE1*) in Arabidopsis leads to a reticulate phenotype (Streatfield et al., 1999). *CUE1* encodes a chloroplast envelope localized phosphoenolpyruvate (PEP)/phosphate translocator, which is responsible for transporting PEP into the chloroplast for the shikimate pathway and the synthesis of aromatic amino acids (Streatfield et al., 1999). The addition of aromatic amino acids can rescue the reticulate phenotype of *cue1* mutants, suggesting a role for aromatic amino acids in the regulation of mesophyll chloroplast development (Streatfield et al., 1999). *RETICULATA* (*RE*) is another Arabidopsis locus that leads to a reticulate phenotype when mutated and *RE* encodes a novel protein of unknown functions that is also known as LOW CELL DENSITY 1 (LCD1) (Barth and Conklin, 2003; González-Bayón et al., 2006). The Arabidopsis *differential development of vascular associated cells 1* (*dov1*) mutant defines another reticulate mutant with green paraveinal regions and yellow interveinal regions, and *DOV1* encodes glutamine phosphoribosyl pyrophosphate aminotransferase 2 (ATase2), the first enzyme in the purine nucleotide biosynthesis pathway (Kinsman and Pyke, 1998; Rosar et al., 2012). Additional Arabidopsis reticulate mutants include *venosa3* (*ven3*) and *ven6* that are defective in carbamoyl phosphate synthetase and arginine biosynthesis (reviewed in Yu et al., 2007; Mollá-Morales et al., 2011; Lundquist et al., 2014). It is interesting to note that most of the genes that are associated with the reticulate mutant phenotypes code for proteins involved in primary metabolism (Lundquist et al., 2014). In addition, reticulate mutants with yellow paraveinal regions and yellow interveinal regions are rare. The intriguing feature of these mutants implies that there are distinct tissue specific regulatory schemes controlling the differentiation of mesophyll and vascular chloroplasts.

In this work, building on our long-term efforts to identify and characterize leaf variegation mutants, we isolated two allelic *Arabidopsis thaliana* variegation mutants, designated *varigated5-1* (*var5-1*) and *var5-2*. Both mutant alleles showed a distinct reticulate leaf phenotype with yellow paraveinal regions and green interveinal regions. The molecular cloning of the

VAR5 locus revealed that *VAR5* encodes a putative magnesium transporter previously named as *AtMRS2-11/AtMGT10*. We confirmed that AtMRS2-11/AtMGT10/VAR5 is likely associated with the chloroplast envelope. In addition, blue native PAGE (BN-PAGE) analysis indicates that AtMRS2-11/AtMGT10/VAR5 forms large complexes in chloroplasts. Taken together, our data demonstrate that mutations in chloroplast Mg^{2+} transporter AtMRS2-11/AtMGT10/VAR5 can lead to a unique leaf reticulation phenotype and this intriguing tissue specific phenotype suggests that Mg^{2+} plays an important role in tissue specific regulation of chloroplast development.

MATERIALS AND METHODS

Plant Materials and Growth Conditions

Arabidopsis thaliana wild type, *var5-1* and *var5-2* mutants (all in Columbia-0 background) seeds were grown on commercial soil mix (Pindstrup, Denmark) or on Murashige and Skoog (MS) (Caisson Laboratories, Smithfield, UT, United States) containing 1% sucrose, and maintained under continuous light ($\sim$100 $\mu mol \cdot m^{-2}s^{-1}$) at 22°C in controlled growth rooms. The GABI T-DNA insertion line (TAIR stock number CS323329) was obtained from the TAIR.

Map-Based Cloning

To map the *VAR5* locus, *var5-1* was crossed with L*er* to generate the F2 mapping population. Bulked segregant analysis using a pool of DNAs from 96 F2 mapping plants with the *var5-1* phenotype and markers on all five Arabidopsis chromosomes placed *VAR5* between two molecular markers T29J13#1 and nga139 on chromosome 5. For fine mapping, 1,140 individual mapping plants were used to place the *VAR5* locus into a genomic region of 92 kb. In this region, genomic sequences of putative chloroplast genes were amplified by PCR and sequences and a point mutation in At5g22830 was detected. All primers used in this study are listed in Supplementary Table S1.

Chlorophyll Fluorescence Measurement and Starch Staining

The maximum quantum yield of PS II (F_V/F_M) was measured with the Open FluorCam FC800-O system (Photon Systems Instruments, Czechia) as described (Qi et al., 2016). To reveal the starch accumulation patterns in leaves, entire rosettes were boiled in 80% ethanol (v/v) until pigments were removed, then stained with fresh iodine solution (10 g/L KI and 1 g/L I_2) for 5 min, and de-stained in water for 1 h.

Light Microscopy Observation of Leaf Vein

The middle main vein section from the third or fourth true leaves of wild type and *var5-1* were hand cut and fixed in 4% (v/v) glutaraldehyde in 0.1 mM PBS buffer (pH 6.8) at 4°C overnight. After fixation, samples were dehydrated in a serial dilution of ethanol and embedded in Technovit 7100 resin (Kulzer, Wehrheim, Germany). Transverse semi-thin cross sections (3 μm) were prepared with Leica RM2265 microtome, placed on glass slides, stained with fresh iodine solution. Images of iodine stained leaf cross sections were obtained with a DM5000B microscope (Leica) equipped with a CCD camera.

Nucleic Acid Analysis and Arabidopsis Transformation

Arabidopsis DNA was isolated with the CTAB method (Yu et al., 2004). Total RNA was isolated with the TRIzol reagent according to the manufacturer's manual (Invitrogen, Carlsbad, CA, United States). cDNAs were synthesized with the Transcriptor First Strand cDNA synthesis kit (Roche, Switzerland) with random primers. For the complementation of the *var5-1* mutant, full-length At5g22830 cDNAs were amplified with TaKaRa PrimeSTAR polymerase using primers 22830F and 22830R and subsequently cloned into the binary vector pBI111L to generate P_{35S}*: At5g22830* (Yu et al., 2004). This construct was transformed in the *var5-1* mutant using the floral dip method (Clough and Bent, 1998), and transgenic plants were screened on 1/2 MS plates containing 50 mg/L kanamycin.

Bioinformatic Analysis

AtMRS2-11/AtMGT10/VAR5 homologous proteins in different species were identified using the BLASTP program of the National Center for Biotechnology Information. Multiple sequence alignment and phylogenetic analysis were performed using the MEGA6 software (Tamura et al., 2013). Gene structures were constructed based on gene sequences retrieved from the Phytozome resource[1] (Goodstein et al., 2012).

Protoplast Transient Expression Assay

To construct a transient expression vector P_{35S}:*VAR5-GFP*, full-length coding sequences of AtMRS2-11/AtMGT10/VAR5 were amplified with primers 22830GFPF and 22830GFPR and cloned into pUC18-GFP vector with the *GFP* coding sequences fused at its 3′ terminus, and the expression of VAR5-GFP was under the CaMV 35S promoter. The 35S promoter in P_{35S}:*VAR5-GFP* was replaced by a $\sim$1.9 kb promoter region of *VAR5* to generate P_{VAR5}:*VAR5-GFP*. These constructs, as well as the P_{35S}*:GFP* control vector, were transformed into protoplasts isolated from 4-week-old wild-type plants as described (Yoo et al., 2007). Chlorophyll fluorescence and GFP signals were examined by a Nikon A1 confocal microscope (Nikon, Japan).

Chloroplast Isolation, Fractionation, and BN-PAGE

Intact chloroplasts were isolated from 4-week-old Arabidopsis plants that were dark treated for 16 h (Kunst, 1998). To fractionate sub-chloroplast compartments, intact chloroplasts were broken by passing through a 24-gauge syringe in hypotonic buffer (10 mM Hepes-KOH pH7.6, 5 mM $MgCl_2$). The lysate was separated on sucrose gradients by ultracentrifugation with SW41 Ti rotor at 58,000 $\times$ *g* for 2 h (Beckman Coulter L100-XP),

[1] http://phytozome.jgi.doe.gov/

and fractions were collected as described (Qi et al., 2016). For BN-PAGE, chloroplast samples equivalent to 10 μg of total chlorophylls were solubilized in 25BTH20G buffer [25 mM Bis-Tris-HCl, pH 7.0, 20% (w/v) glycerol] containing 1.0% (w/v) of *n*-dodecyl-β-D-maltoside (β-DM) (Järvi et al., 2011). The solubilized chloroplast samples were resolved on 3–8% BN-PAGE with a constant voltage of 70 V at 4°C, and the first dimension gel strips were denatured and resolved on 10% SDS-PAGE. For immunoblot analysis, proteins separated by SDS-PAGE were transferred onto 0.2 μm PVDF membranes with the Trans-blot Semi-Dry Transfer Cell (Bio-Rad) following the manufacturer's manual. PVDF membranes were incubated with specific primary antibodies (Agrisera), followed by horseradish peroxidase-conjugated secondary antibodies. Signals were detected with chemiluminescence solutions and ChemiDoc Imaging System (Bio-Rad).

RESULTS

The Isolation of Two Reticulate Mutant Alleles *var5-1* and *var5-2*

During the characterization of an Arabidopsis SALK T-DNA insertion line, one unique reticulate ('net-like') leaf variegation mutant was recovered (**Figure 1A**; early stage of this work was carried out in the lab of Dr. Steve Rodermel at Iowa State University). A second and similar reticulate leaf variegation mutant was identified in our genetic screens for chloroplast development mutants (**Supplementary Figures S1A–D**, Qi et al., 2016). Genetic tests revealed that these two mutants were allelic and we thus designated the two mutants as *variegated5-1* (*var5-1*) and *variegated5-2* (*var5-2*), respectively, following the variegation mutant naming sequence (Martínez-Zapater, 1993; Yu et al., 2007) (**Supplementary Figures S1G,H**). Both mutant alleles showed a similar reticulate leaf variegation phenotype (**Figures 1A,B** and **Supplementary Figure S1A**). This unique leaf variegation phenotype is more pronounced in adult leaves than juvenile leaves, as the seventh true leaf of *var5-1* showed a clear reticulate phenotype, with overall yellow paraveinal regions and green interveinal regions (**Figure 1B**). Taken together, *var5-1* and *var5-2* represent two allelic mutants that display a unique leaf reticulation phenotype.

Tissue Specific Starch Accumulation Defects in the *var5-1* Mutant

The reticulate leaf color phenotype suggests that photosynthetic capacities are compromised in *var5-1* mutants. To correlate the visible leaf color phenotype with the photosynthetic status of the mutant, we measured parameters that indicate photosynthetic performance. For the light reactions, we measured the maximum quantum yield of PS II, also known as F_V/F_M, using a whole plant chlorophyll fluorescence imaging system. The average F_V/F_M of 15 min dark adapted wild-type whole plants was 0.82, while that of *var5-1* was 0.66, suggesting that photosynthesis is compromised in the mutant (**Figure 1C**). In addition, while a single leaf of wild-type plant showed a uniform distribution of F_V/F_M values, the F_V/F_M from *var5-1* also showed a 'net-like' pattern, with paraveinal regions showing higher value while interveinal regions having lower F_V/F_M (**Figure 1D**). We next examined the accumulation of starch in the wild type and *var5-1* plants as one indicator of photosynthetic productivities. Interestingly, the starch accumulation in the *var5-1* mutant shows clearly a reticulate pattern, clearly matching both the leaf reticulation and F_V/F_M patterns (**Figures 1E,F**). In addition, iodine stained leaf cross sections showed that chloroplasts in the palisade mesophyll cells on the top of vascular bundles in the *var5-1* mutant, were significantly less stained compared to that of wild type (**Supplementary Figures S2A–D**), suggesting the development of chloroplasts in the yellow paraveinal regions are compromised in the *var5-1* mutant. These data indicate that the mutation in *var5-1* leads to a unique expression of leaf reticulation and a pronounced reduction of photosynthetic capacities as indicated by PSII activities and starch accumulation in paraveinal regions than in interveinal regions.

The Molecular Cloning of *VAR5*

Genetic analysis revealed that the reticulate phenotype of *var5-1* was likely caused by a single nuclear recessive mutation, and map-based cloning procedures were used to clone the *VAR5* locus (**Figure 2**). Initial mapping with molecular markers on all five chromosomes and subsequent fine mapping using 1,140 mapping plants placed *VAR5* in a ∼92 kb genomic region between markers MDJ22#2 and MRN17#1 on chromosome 5 (**Figure 2A**). Based on the leaf color phenotype, genomic DNA sequences of nuclear genes for chloroplast proteins in this interval were examined. A single G to A transition mutation was identified in the first nucleotide of intron 9 in At5g22830 (**Figure 2A**). At the mRNA level, amplification products spanning the mutation site appeared longer in the mutant than in wild type, suggesting pre-mRNA splicing might be affected in *var5-1* (**Figure 2B**). Sequencing of the full-length At5g22830 cDNA in *var5-1* revealed the nature of pre-mRNA splicing defects in *var5-1*. The mutation in the intron 9 led to the retention of the entire intron 9 in the At5g22830 transcript (**Figure 2C**). Surprisingly, a partial segment of intron 6 (the first 17 bp of the 328 bp wild-type intron 6) was also retained (**Figure 2C**). The translation of this aberrant mRNA would in theory give rise to a protein with the first 262 amino acids of the annotated 459 amino acids of wild-type protein plus four additional amino acids before a premature stop codon (**Figure 2D**). In theory, this early stop codon would abolish the C-terminal transmembrane domains and the conserved GMN motif (**Figure 2E**). We also determined the mutation site in *var5-2* and identified a G to A mutation at the last nucleotide of intron 4, which also caused abnormal At5g22830 transcript in *var5-2* (**Supplementary Figures S1E,F**). This mutation led to the retention of the entire intron 4 (80 bp) in the At5g22830 transcript and a putative translation product with the first 208 amino acids of wild-type protein before a premature stop codon (**Supplementary Figures S1E,F**).

To confirm that the reticulate phenotype of *var5-1* was indeed caused by the mutation identified in At5g22830, a binary

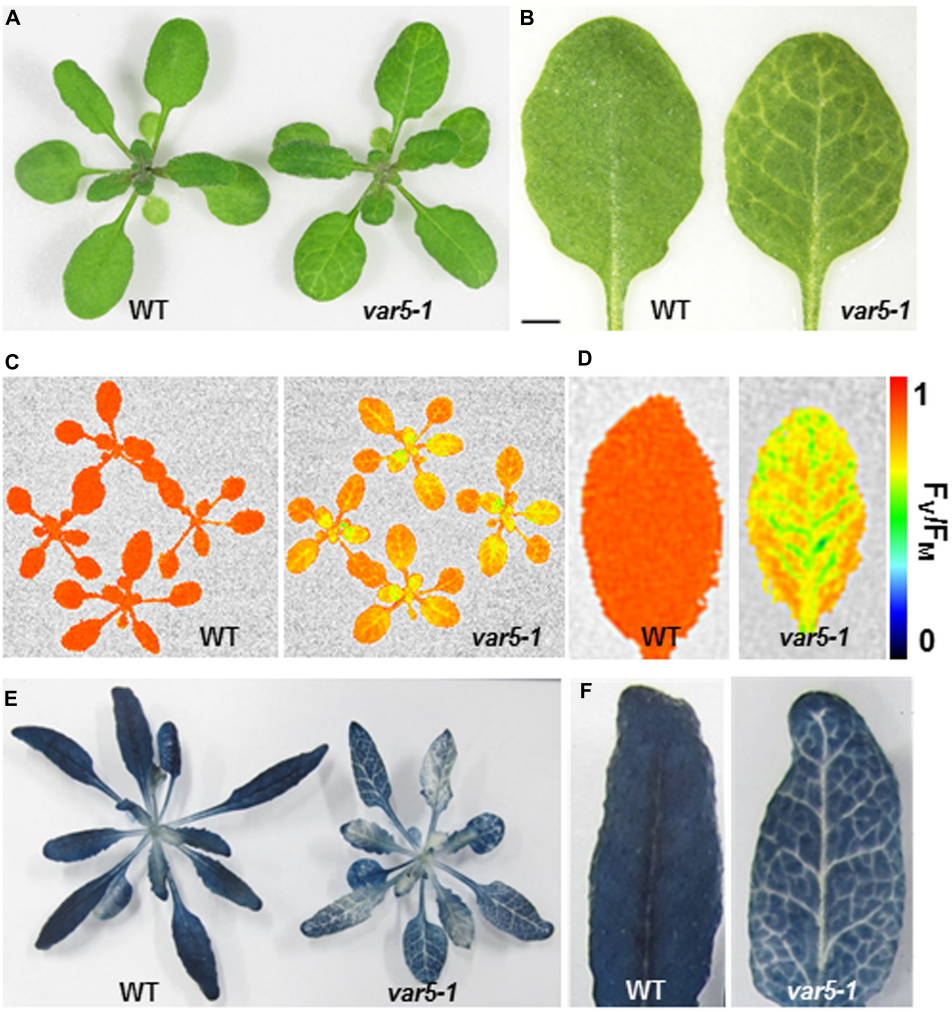

FIGURE 1 | Phenotypes of the *var5-1* mutant. **(A)**. Representative 3-week-old seedlings of wild type (WT) and the *var5-1* mutant. **(B)** Details of the third or fourth true leaf from 3-week-old WT and *var5-1* mutant. **(C,D)** F_V/F_M measurement of WT and the *var5-1* mutant (C for 3-week-old whole plants, and D for the detached seventh or eighth true leaves from 4-week-old plants). The color scale representing for the value of F_V/F_M is at the right of the figure. **(E,F)** Iodine staining with seedlings of 4-week-old WT and the *var5-1* mutant.

vector (P_{35S}: *At5g22830*) containing the wild-type At5g22830 cDNA under the control of the CaMV 35S promoter was constructed and transformed into *var5-1*. Multiple transgenic lines that showed completely green leaf color and the presence of wild-type cDNA amplification products were identified, indicating that the reticulate phenotype of *var5-1* can be rescued by the wild-type At5g22830 (**Figures 3A–D**). At the mRNA level, the complementation lines showed the presence of wild-type At5g22830 cDNA (**Figure 3E**). At the protein level, we generated polyclonal antibodies against amino acid residues from 61 to 263 of At5g22830 and Western blotting analyses detected the accumulation of At5g22830 protein in the wild type, but not in the *var5-1* mutant (**Figure 3F**). In contrast, At5g22830 protein accumulation was greatly enhanced in the *var5-1* P_{35S}:*At5g22830* complementation line (**Figure 3F**). Similar results were obtained with *var5-2* mutant (**Supplementary Figure S1G**). The identifications of mutations sites in *var5-1* and *var5-2*, the molecular complementation and the western data show that At5g22830 is *VAR5*.

VAR5/At5g22830 Encodes a Putative CorA Family Magnesium Transporter, *AtMRS2-11/AtMGT10*, in Arabidopsis

VAR5/*At5g22830* was previously reported to encode a putative CorA family Mg^{2+} transporter that is also known as *AtMRS2-11*/*AtMGT10* (Schock et al., 2000; Li et al., 2001; Drummond et al., 2006). At the protein level, AtMRS2-11/AtMGT10/VAR5 contains the characteristic features of CorA Mg^{2+} transporters, including the two C-terminal transmembrane domains and in between the Mg^{2+}-binding GMN motif (Lunin et al., 2006; Pfoh et al., 2012). There are at least 10 members of CorA family Mg^{2+} transporters in *Arabidopsis thaliana*, and some of them are

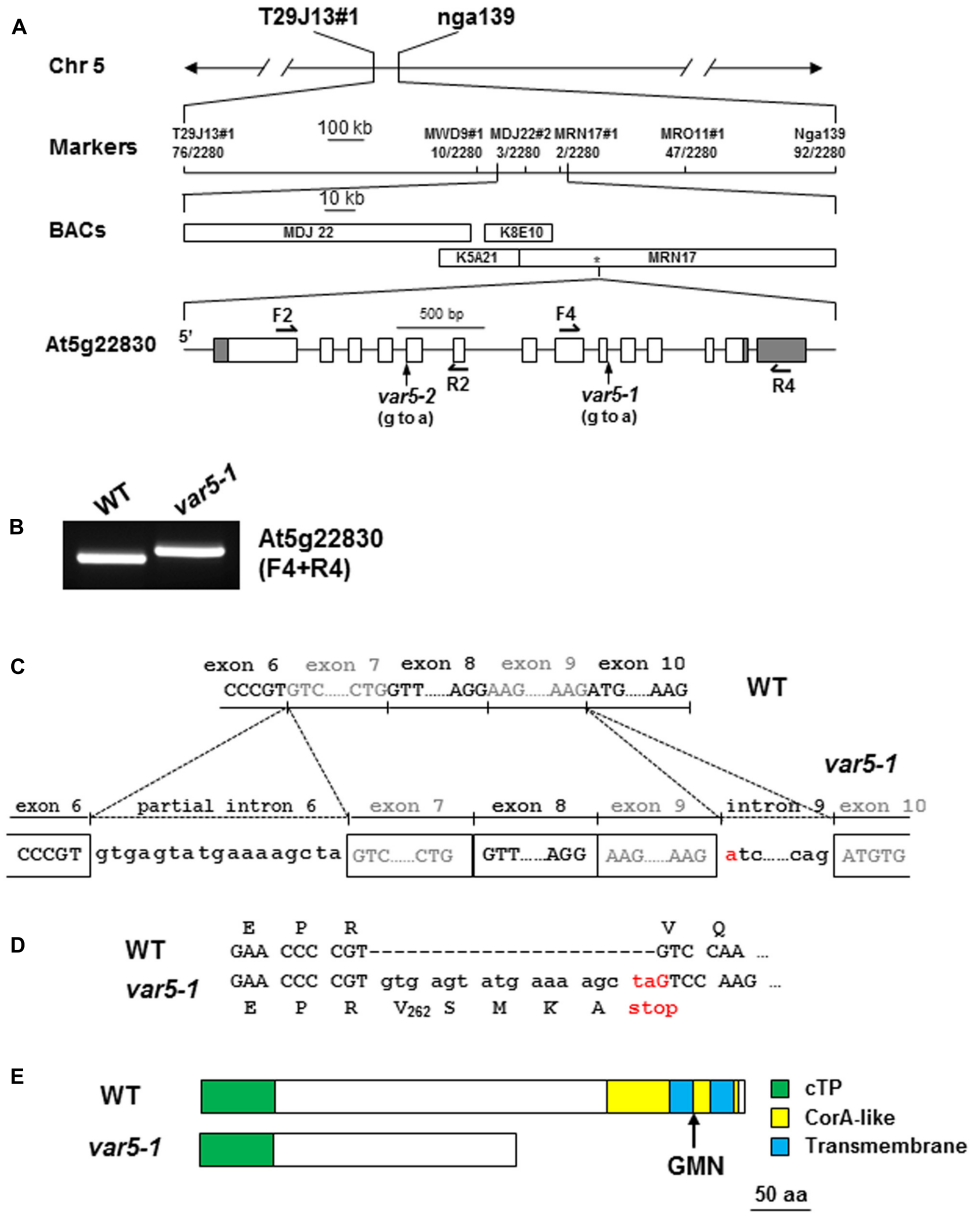

FIGURE 2 | The molecular cloning of *VAR5*. **(A)** The map based cloning of *VAR5*. The mutation of *var5-1* was linked to markers T29J13#1 and nga139 on chromosome 5. A total of 1,140 F2 individual plants (2,280 chromosomes) were used in fine mapping, and the numbers of recombinants are listed under each marker. The asterisk indicates the position of At5g22830. In At5g22830 gene model, gray boxes and white boxes represent UTR and exons, respectively, and solid lines indicate introns. The position of the G to A mutation in *var5-1* was shown. **(B)** RT-PCR analysis of At5g22830 transcripts in WT and *var5-1*. Primers used in the amplifications were indicated in the parentheses. **(C)** The molecular nature of mutations in *var5-1*. The G to A transition mutation was shown red in the first nucleotide of intron 9 in At5g22830. Intron 9 and partial intron 6 remain in the At5g22830 transcripts in *var5-1*. **(D)** The *var5-1* mutation leads to a premature stop codon at the end of partial intron 6. **(E)** Based on the sequences of abnormal mRNAs of At5g22830 in *var5-1*, the putative translation products of mutant mRNA of At5g22830 was indicated. Domains are indicated with colored boxes, and cTP for chloroplast transit peptide.

predicted to be targeted into organelles including the chloroplast and the mitochondrion (Gebert et al., 2009). We analyzed the relationship between AtMRS2-11/AtMGT10/VAR5 and its putative chloroplast-localized homologs from various eukaryotic photosynthetic organisms, as well as CorA homologs from bacteria (**Figure 4A**). Overall, AtMRS2-11/AtMGT10/VAR5 homologs from different organisms are highly conserved (**Figure 4A**). In addition, these proteins can be grouped into major clades including eudicot, monocot, algae and prokaryotic organisms (**Figure 4A**). The evolutionary relationship between these genes were also obvious at the DNA level as putative higher plant AtMRS2-11/AtMGT10/VAR5 related genes shared identical gene structures, suggesting these genes emerged before the divergence of eudicot and monocot plants (**Figure 4B**).

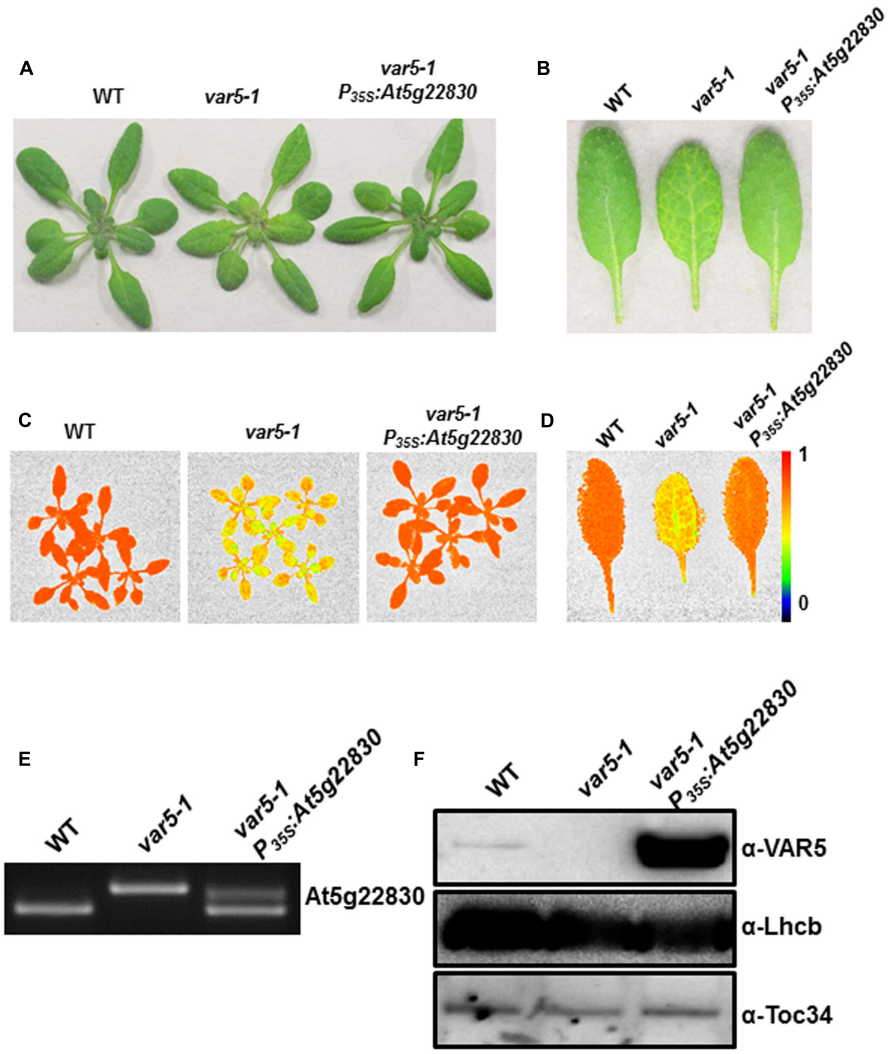

FIGURE 3 | Complementation of *var5-1*. **(A)** Representative 3-week-old WT, *var5-1*, and the *var5-1* complementation line (*var5-1* P_{35S}*:At5g22830*). **(B)** Representative individual leaves of WT, *var5-1*, and *var5-1* P_{35S}*:At5g22830*. **(C,D)** F_V/F_M measurement of WT, *var5-1* and *var5-1* P_{35S}*:At5g22830* (C for 18-day-old whole plants, and D for the detached third or fourth true leaves from 18-day-old plants). The color scale representing for the value of F_V/F_M is at the right of the figure. **(E)** At5g22830 transcript accumulations in WT, *var5-1*, and *var5-1* P_{35S}*:At5g22830*. Total leaf RNA was extracted, and subjected to reverse transcription PCR with primers F4 and R4. **(F)** At5g22830 protein accumulations in WT, *var5-1*, and *var5-1* P_{35S}*:At5g22830*. Membrane fractions were isolated from leaf tissues and proteins were separated with 10% SDS-PAGE. Immunoblots were probed with antibodies against At5g22830, Lhcb and Toc34.

In contrast, AtMRS2-11/AtMGT10/VAR5 homologs from green algae did not share conserved gene structures with their plant counterparts (**Figure 4B**). These data suggest that the CorA family Mg^{2+} transporter is prevalent and highly conserved, consistent with the critical roles Mg^{2+} plays in prokaryotic and eukaryotic cells.

AtMRS2-11/AtMGT10/VAR5 Localizes to the Chloroplast Envelope

AtMRS2-11/AtMGT10/VAR5 is predicted by the ChloroP program to contain a putative chloroplast transit peptide (Emanuelsson et al., 1999). Experimentally, it was shown to be localized on the periphery of chloroplasts (Drummond et al., 2006). We took two approaches to independently confirm the sub-cellular localization of AtMRS2-11/AtMGT10/VAR5. First, we used the protoplast transient expression assay to examine the localization of VAR5-GFP under the control of the 35S promoter (P_{35S}*:VAR5-GFP*) and the endogenous *VAR5* promoter (P_{VAR5}*:VAR5-GFP*), respectively (**Figure 5A**). Control vector (P_{35S}*:GFP*) gave GFP signals mainly in the cytosol and the nucleus (**Figure 5A**). In contrast, both P_{35S}*:VAR5-GFP* and P_{VAR5}*:VAR5-GFP* gave GFP signals that outlined the periphery of the chloroplast, as well as some puncta inside the chloroplast, suggesting both promoters can direct VAR5 to sub-chloroplast locations that likely correspond to the chloroplast envelope (**Figure 5A**). Next, we determined the AtMRS2-11/AtMGT10/VAR5 sub-chloroplast

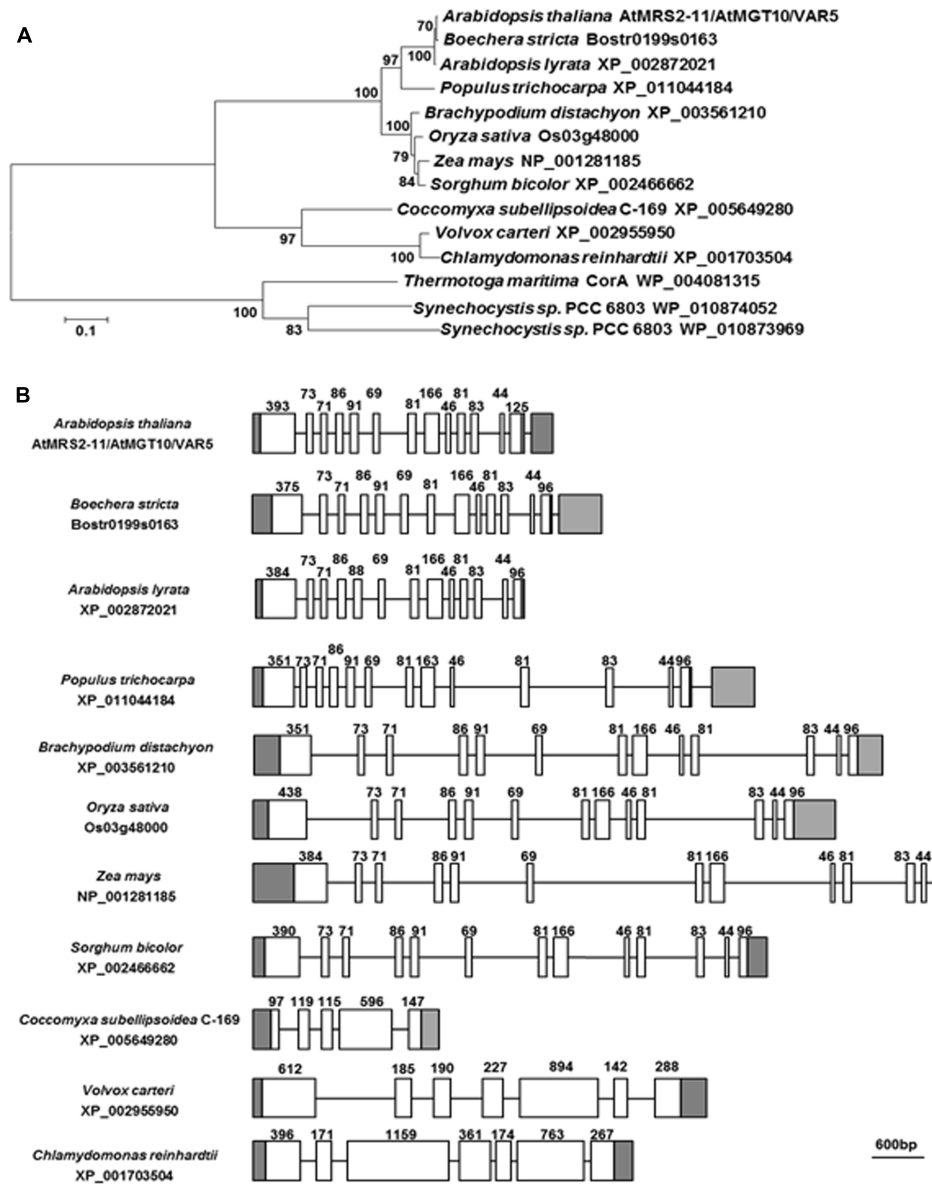

FIGURE 4 | The *AtMRS2-11/AtMGT10/VAR5* gene family. **(A)** Phylogenetic analysis of the AtMRS2-11/AtMGT10/VAR5 protein family. Full-length protein sequences of AtMRS2-11/AtMGT10/VAR5 homologous proteins from dicots *Arabidopsis thaliana*, *Boechera stricta*, *Arabidopsis lyrata*, *Populus trichocarpa*, monocots *Brachypodium distachyon*, *Oryza sativa*, *Zea mays*, *Sorghum bicolor*, green algae *Coccomyxa subellipsoidea*, *Volvox carteri*, *Chlamydomonas reinhardtii*, and prokaryotes *Thermotoga maritime* and *Synechocystis* sp. PCC6803 were obtained from NCBI. The phylogenetic tree was constructed with MEGA6 (Tamura et al., 2013). The accession numbers were included. **(B)** Gene Structures of *AtMRS2-11/AtMGT10/VAR5* homologous genes. Genomic DNA sequences were retrieved from the Phytozome (https://phytozome.jgi.doe.gov/pz/portal.html). In gene structures, white boxes and lines indicate exons and introns, respectively. Gray boxes indicate UTRs. Lengths of coding exons sequences were shown.

localization biochemically (**Figure 5B**). Intact chloroplasts were fractionated into the thylakoids (Thy), the stroma (Str), the envelope fraction 1 (Env1) and 2 (Env2) with sucrose gradient centrifugations (Qi et al., 2016). Using antibodies against chloroplast proteins with known sub-chloroplast localizations, we showed that RbcL (Rubisco large subunit) was enriched in the stroma fraction, and Lhcb (PSII light harvesting complex protein) was enriched in the thylakoids fraction as expected. The enrichment of chloroplast envelope membranes in the Env2 fraction was indicated by chloroplast envelope proteins Tic40 and Toc34 (components of the Translocon at the Inner/Outer Envelope Membrane of Chloroplasts, TIC/TOC) (**Figure 5B**; Nakai, 2015). Using VAR5 antibodies that we had generated, we found that the majority of AtMRS2-11/AtMGT10/VAR5 was present in the Env2 fraction, similar to the distribution patterns of TIC/TOC components, suggesting that it is likely a chloroplast envelope membrane protein (**Figure 5B**).

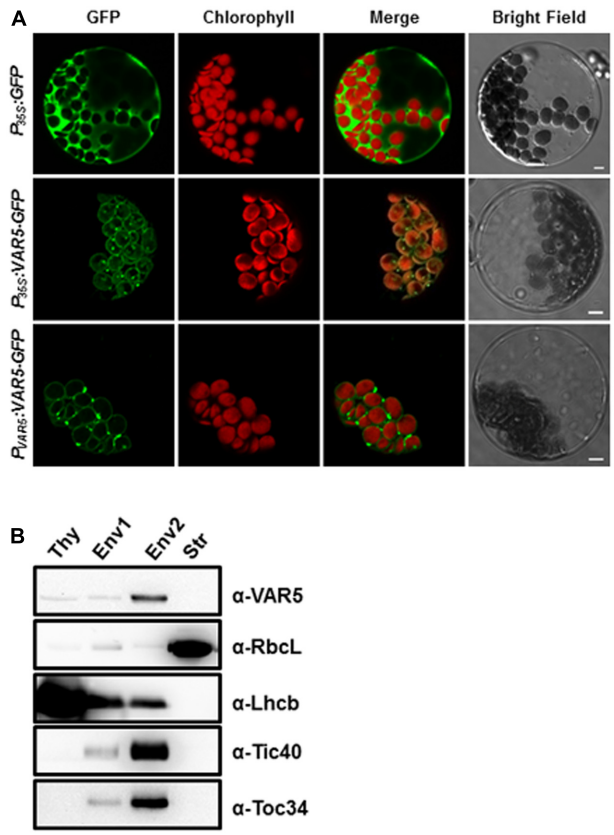

FIGURE 5 | Subcellular localization of AtMRS2-11/AtMGT10/VAR5. **(A)** Protoplasts from 3-week-old WT plants were transformed with vectors containing the full-length *VAR5* (P_{35S}*:VAR5-GFP* and P_{VAR5}*:VAR5-GFP*) and the GFP control (P_{35S}*:GFP*) and examined via confocal microcopy. Representative protoplasts with GFP fluorescence were shown. Chlorophyll is for chlorophyll fluorescence, and bars are 5 μm. **(B)** Fractions of thylakoid (Thy), Env1 (mixed envelope and thylakoids), Env2 (mainly envelope) and stroma (Str) were isolated from WT chloroplasts and subjected to immunoblot. Antibodies against RbcL (stroma control), Lhcb (thylakoid control), Tic40 and Toc34 (envelope control) were used to indicate different fractions.

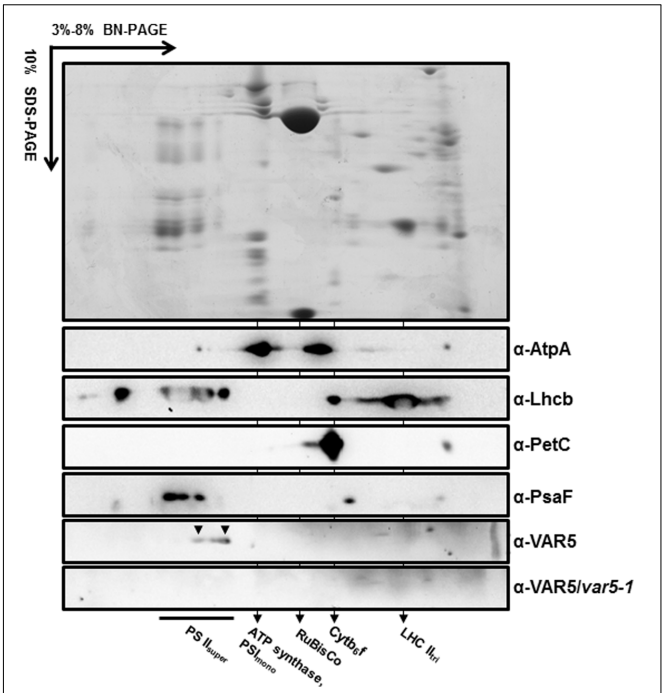

FIGURE 6 | AtMRS2-11/AtMGT10/VAR5 forms large molecular weight complexes. Intact chloroplasts were solubilized with 1.0% β-DM, and subjected to first dimension 3–8% blue native PAGE (BN-PAGE). The first dimension gel strips were cut, denatured and resolved in 10% SDS-PAGE for the second dimension. Antibodies against subunits of different photosynthetic complexes were used for immunoblotting. The immunoblotting of second dimension BN-PAGE of *var5-1* sample was used for a negative control.

AtMRS2-11/AtMGT10/VAR5 Forms Large Protein Complexes in the Chloroplast

The crystal structure of the thermophilic bacterium *Thermotoga maritima* CorA Mg^{2+} transporter indicates that it forms a homopentamer (Lunin et al., 2006). To determine whether AtMRS2-11/AtMGT10/VAR5 forms complexes in Arabidopsis, two-dimensional BN-PAGE was carried out (Järvi et al., 2011). BN-PAGE can effectively separate chloroplast membrane protein complexes, and the estimated sizes of the major photosynthetic protein complexes are known (**Figure 6**). For instance, the sizes of the four large PSII supercomplexes were estimated to be 880–1,400 kDa (Caffarri et al., 2009; Hou et al., 2015), while the PSI monomer and the rubisco holoenzyme migrate at approximately 600 and 540 kDa, respectively (Berghöfer and Klösgen, 1999; Järvi et al., 2011). Western blot analysis with second dimension gels using antibodies against AtpA (the α subunit of the chloroplast ATP synthase), Lhcb, PetC (a subunit of the cytochrome b_6f complex) and PsaF (a subunit of the PSI) clearly identified various photosynthetic complexes at expected sizes (**Figure 6**). Interestingly, AtMRS2-11/AtMGT10/VAR5 antibodies detected a streak of signals in the second dimension gels (**Figure 6**). Based on our results, it is clear that different forms of complexes containing AtMRS2-11/AtMGT10/VAR5 exist in the chloroplast, and the sizes of these complexes are clearly larger than the PSI monomer (~600 kDa) (**Figure 6**). The distribution of AtMRS2-11/AtMGT10/VAR5 complexes overlapped partially with the PSII supercomplexes, which suggest the complexes could reach over 800 kDa (**Figure 6**). This is in stark contrast to the CorA complexes in *Thermotoga maritime*, which have molecular weights around 210 kDa as homopentamers (Lunin et al., 2006; Matthies et al., 2016). We did not detect AtMRS2-11/AtMGT10/VAR5 signals in *var5-1* plants, agreeing with our one dimension SDS-PAGE results (**Figure 2**). These data suggest that AtMRS2-11/AtMGT10/VAR5 forms large complexes and the complex compositions are different in Arabidopsis from those in bacteria.

DISCUSSION

We are interested in the genetic regulation of chloroplast development and have characterized Arabidopsis leaf variegation

mutants that are results of mutations in nuclear genes (Yu et al., 2007; Liu et al., 2010; Putarjunan et al., 2013). These variegation mutants are intriguing because non-uniform leaf color phenotypes can arises from uniform genetic mutant backgrounds. Plant variegation mutants can be categorized based on their variegation patterns. The first type of variegation mutants shows apparently random distributions of chlorophyll accumulation and/or chloroplast development. Mutants in this category include *immutans* (*im*), *yellow variegated* (*var2*), and *thylakoid formation* (*thf*) (reviewed in Yu et al., 2007). The second type, the virescent mutant, displays differential chlorophyll accumulation and/or chloroplast development along the leaf proximal-distal axis, usually with the leaf base regions containing less chlorophylls and tip regions containing higher levels of chlorophylls (López-Juez et al., 1998). The third type displays differential chlorophyll accumulation and/or chloroplast development between paraveinal regions and interveinal regions, giving rise to a reticulate pattern. A number of reticulate mutants including *chlorophyll a/b binding protein (CAB) gene underexpressed 1* (*cue1*), *reticulata* (*re*; also known as *lower cell density 1*, *lcd1*), and *differential development of vascular associated cells 1*(*dov1*) have been reported and characterized (Kinsman and Pyke, 1998; Streatfield et al., 1999; Barth and Conklin, 2003; González-Bayón et al., 2006).

In this report, we identified two new allelic leaf variegation mutants in *Arabidopsis thaliana* that display a striking reticulate phenotype and designated these mutants as *var5-1* and *var5-2*. We cloned *VAR5* via map-based cloning procedures and identified mutations in At5g22830 in *var5-1* and *var5-2*, respectively. Both mutants contain mutations in the conserved sequences that form the plant intron borders and these mutations lead to the mis-splicing of pre-mRNA of At5g22830 (**Figure 2**; Lorković et al., 2000). It is worthy of noting that the mutation in intron 9 caused mis-splicing of intron 6 in *var5-1*, suggesting that downstream intron sequences can influence the splicing of upstream introns (Nesic and Maquat, 1994). Our data from two mutant alleles, the molecular cloning of *VAR5* and molecular complementation results clearly establish that the reticulate leaf phenotype of *var5-1* and *var5-2* is the result of mutations in At5g22830, which is also known as *AtMRS2-11*/*AtMGT10*.

AtMRS2-11/*AtMGT10*/*VAR5* encodes a CorA family of Mg^{2+} transporter in Arabidopsis. In bacteria, the canonical CorA is situated at the plasma membrane and regulates Mg^{2+} homeostasis inside the cell (Maguire, 2006). CorA family Mg^{2+} transporters are also present in higher plants (Schock et al., 2000; Li et al., 2001). In *Arabidopsis thaliana*, the 10 members of the CorA family of Mg^{2+} transporters are shown to be targeted into different sub-cellular compartments, with AtMRS2-11/AtMGT10/VAR5 as the sole member that is predicted to contain a chloroplast transit peptide (Gebert et al., 2009). Given the many processes Mg^{2+} is involved in the chloroplast, it is reasonable to assume that Mg^{2+} transporters need to be present in the chloroplast envelope to facilitate the transport of Mg^{2+}. Indeed, a previous report has shown that AtMRS2-11/AtMGT10/VAR5 is possibly located at the periphery of the chloroplast through fluorescent microscopy observations (Drummond et al., 2006). In this work, we demonstrated that AtMRS2-11/AtMGT10/VAR5 is likely located to the chloroplast envelope using two approaches. First, through protoplast transient expression and confocal microscopy, we showed that VAR5-GFP can be localized to sub-chloroplast compartments that likely correspond to the chloroplast envelope (**Figure 5**). We also confirmed the chloroplast envelope localization of VAR5 biochemically and found that VAR5 showed similar localization patterns with components of the TIC/TOC complexes at the chloroplast enveloped (**Figure 5**; Nakai, 2015). To our surprise, we did observe VAR5-GFP signals inside the chloroplast with both the 35S and the endogenous *VAR5* promoter driven VAR5-GFP, and we do not yet know the nature of this phenomenon. Consistent with the chloroplast localization of AtMRS2-11/AtMGT10/VAR5, the two *VAR5* mutant alleles we identified show clear defects of chloroplast development (**Figure 1**). The reticulate phenotype of both mutants indicates a tissue specific expression of mutant phenotype. There are several possible explanations for this intriguing phenotype. It is possible that the essential roles of vascular tissues for transporting may necessitate higher levels of AtMRS2-11/AtMGT10/VAR5 activities and the lack of the transporter in *var5-1* mutants would lead to more detrimental effects in these tissues. Alternatively, other types of Mg^{2+} channels, such as fast activating chloroplast cation channels (FACC), may also be present in the chloroplast envelope to transport Mg^{2+} (Pottosin and Dobrovinskaya, 2015). It is thus possible that they may compensate for the lack of AtMRS2-11/AtMGT10/VAR5 in the interveinal regions. It was shown that AtMRS2-11/AtMGT10/VAR5 displays tissue specific expression patterns (Drummond et al., 2006; Gebert et al., 2009). However, the tissue expression pattern does not correlate with the reticulate mutant phenotype. Because both alleles we identified contain point mutations that lead to mis-regulated splicings of *VAR5* pre-mRNA, we also sought to identify a T-DNA insertion line for *VAR5*. In a previous report, no homozygous mutant plant was recovered in a GABI T-DNA insertion line (TAIR stock number CS323329), which has a T-DNA insertion in the sixth intron, suggesting that the complete loss of *AtMRS2-11*/*AtMGT10*/*VAR5* might be lethal (Gebert et al., 2009). Characterizing the same T-DNA line, we identified the precise insertion site of the T-DNA in *VAR5* but also failed to obtain homozygous insertion plants (data not shown). It is possible that the null allele of *VAR5* is lethal at early stage of embryo development. However, we could not rule out the possibility that additional secondary mutations may contribute to this lethality, as reported for other cases (Gebert et al., 2009; Bergelson et al., 2016).

In this report, we clearly demonstrated that AtMRS2-11/AtMGT10/VAR5 forms large complexes and the estimates of the molecular weights of these complexes are exceeding 800 kDa (**Figure 6**). The formation of complexes for the CorA family of Mg^{2+} transporters is not unexpected as it has been shown in bacteria that CorA forms homopentamers with a molecular weight of ∼200 kDa (Lunin et al., 2006; Matthies et al., 2016). However, the sizes we observed for

AtMRS2-11/AtMGT10/VAR5 complexes are surprising and well beyond its bacterial counterparts. Although we don't know the precise nature of these AtMRS2-11/AtMGT10/VAR5-containing complexes, it does suggest that the formation and regulation of CorA transporter complexes are different in plants, at least in the chloroplast. It is possible that in Arabidopsis chloroplasts, AtMRS2-11/AtMGT10/VAR5 forms homo-oligomers that contain more than five subunits. Alternatively, AtMRS2-11/AtMGT10/VAR5 complexes in the chloroplast may contain additional components. Considering the importance roles Mg^{2+} plays in the chloroplast, it is reasonable to assume that addition subunits may be necessary to serve structural or regulatory functions. The future determination of the components of these complexes containing AtMRS2-11/AtMGT10/VAR5 would shine more light on the functions of CorA family Mg^{2+} transporters in the chloroplast and the roles it plays in chloroplast development and biomass production, especially under low-magnesium or plus-magnesium conditions.

AUTHOR CONTRIBUTIONS

FY conceived and coordinated the study. SL and YQ designed, performed, and analyzed the experiments shown in **Figures 1–3** and supplemental data. YQ and JZ designed, performed, and analyzed the experiments shown in **Figures 4**, **6**. YL and RW designed, performed, and analyzed the experiments shown in **Figure 5**. JS, LA, and XL provided technical assistance and contributed to the preparation of the figures. FY and YQ wrote the manuscript. All authors reviewed the results and approved the final version of the manuscript.

FUNDING

This work was supported by National Natural Science Foundation of China Grants 31400216 (to JZ), 31300988 (to YQ), and 31470290 (to LA), by Natural Science Foundation of Shaanxi Province Grants 2015JM3081 (to FY), and by Fundamental Research Funds for the Central Universities Grants QN2013034 (to JS), 2014YB036 (to LA), and 2452015215 (to XL).

SUPPLEMENTARY MATERIAL

The Supplementary Material for this article can be found online at: https://www.frontiersin.org/articles/10.3389/fpls.2017.02007/full#supplementary-material

FIGURE S1 | The molecular nature of *var5-2*. **(A)** Representative 3-week-old seedlings of wild type (WT) and the *var5-2* mutant. **(B)** Details of the third or fourth true leaf from 3-week-old WT and *var5-2* mutant. **(C,D)** F_V/F_M measurement of WT and the *var5-2* mutant (C for 3-week-old whole plants, and D for the detached third or fourth true leaves from 3-week-old plants). The color scale representing for the value of F_V/F_M is at the right of the figure. **(E)** The molecular nature of mutations in *var5-2*. Intron 4 remains in the At5g22830 transcripts in *var5-2*. **(F)** The *var5-2* mutation leads to a premature stop codon at the beginning of intron 4. Based on the sequences of abnormal mRNAs of At5g22830 in *var5-2*, the putative translation products of mutant mRNA of At5g22830 was indicated. Domains are indicated with colored boxes. H. The representative first or second true leaf from 3-week-old WT, *var5-1*, *var5-2*, and *var5-1 var5-2* F1 generation. **(G)** The accumulation of VAR5 in WT, *var5-1*, *var5-2* and *var5-1 var5-2* F1. TIC40 was used for the envelope protein control.

FIGURE S2 | Light microscopy of leaf sections. The middle main vein section from the third or fourth true leaves of 2-week-old WT and *var5-1* were fixed and observed with iodine staining. **(A)** WT; **(B)** *var5-1*. **(C,D)** The dash line areas from **A** and **B** were enlarged.

REFERENCES

Barth, C., and Conklin, P. L. (2003). The lower cell density of leaf parenchyma in the *Arabidopsis thaliana* mutant *lcd1-1* is associated with increased sensitivity to ozone and virulent *Pseudomonas syringae*. *Plant J.* 35, 206–218. doi: 10.1046/j.1365-313X.2003.01795.x

Bergelson, J., Buckler, E. S., Ecker, J. R., Nordborg, M., and Weigel, D. (2016). A proposal regarding best practices for validating the identity of genetic stocks and the effects of genetic variants. *Plant Cell* 28, 606–609. doi: 10.1105/tpc.15.00502

Berghöfer, J., and Klösgen, R. B. (1999). Two distinct translocation intermediates can be distinguished during protein transport by the TAT (Δph) pathway across the thylakoid membrane. *FEBS Lett.* 460, 328–332. doi: 10.1016/S0014-5793(99)01365-4

Bui, D. M., Gregan, J., Jarosch, E., Ragnini, A., and Schweyen, R. J. (1999). The bacterial magnesium transporter CorA can functionally substitute for its putative homologue Mrs2p in the yeast inner mitochondrial membrane. *J. Biol. Chem.* 274, 20438–20443. doi: 10.1074/jbc.274.29.20438

Caffarri, S., Kouril, R., Kereïche, S., Boekema, E. J., and Croce, R. (2009). Functional architecture of higher plant photosystem II supercomplexes. *EMBO J.* 28, 3052–3063. doi: 10.1038/emboj.2009.232

Chen, J., Li, L., Liu, Z., Yuan, Y., Guo, L., Mao, D., et al. (2009). Magnesium transporter AtMGT9 is essential for pollen development in *Arabidopsis*. *Cell Res.* 19, 887–898. doi: 10.1038/cr.2009.58

Clough, S. J., and Bent, A. F. (1998). Floral dip: a simplified method for Agrobacterium-mediated transformation of *Arabidopsis thaliana*. *Plant J.* 16, 735–743. doi: 10.1046/j.1365-313x.1998.00343.x

Conn, S. J., Conn, V., Tyerman, S. D., Kaier, B. N., Leigh, R. A., and Gilliham, M. (2011). Magnesium transporters, MGT2/MRS2-1 and MGT2/MRS2-5, are important for magnesium partitioning within *Arabidopsis thaliana* mesophyll vacuoles. *New Phytol.* 190, 583–594. doi: 10.1111/j.1469-8137.2010.03619.x

Drummond, R. S. M., Tutone, A., Li, Y., and Gardner, R. C. (2006). A putative magnesium transporter AtMRS2-11 is localized to the plant chloroplast envelope membrane system. *Plant Sci.* 170, 78–89. doi: 10.1016/j.plantsci.2005.08.018

Emanuelsson, O., Nielsen, H., and von Heijne, G. (1999). ChloroP, a neural network-based method for predicting chloroplast transit peptides and their cleavage sites. *Protein Sci.* 8, 978–984. doi: 10.1110/ps.8.5.978

Gardner, R. C. (2003). Genes for magnesium transport. *Curr. Opin. Plant Biol.* 6, 263–267. doi: 10.1016/S1369-5266(03)00032-3

Gebert, M., Meschenmoser, K., Svidová, S., Weghuber, J., Schweyen, R., Eifler, K., et al. (2009). A root-expressed magnesium transporter of the *MRS2*/*MGT* gene family in *Arabidopsis thaliana* allows for growth in low-Mg2+ environments. *Plant Cell* 21, 4018–4030. doi: 10.1105/tpc.109.070557

González-Bayón, R., Kinsman, E. A., Quesada, V., Vera, A., Robles, P., Ponce, M. R., et al. (2006). Mutations in the *RETICULATA* gene dramatically alter internal architecture but have little effect on overall organ shape in Arabidopsis leaves. *J. Exp. Bot.* 57, 3019–3031. doi: 10.1093/jxb/erl063

Goodstein, D. M., Shu, S., Howson, R., Neupane, R., Hayes, R. D., Fazo, J., et al. (2012). Phytozome: a comparative platform for green plant genomics. *Nucleic Acids Res.* 40, D1178–D1186. doi: 10.1093/nar/gkr944

Hou, X., Fu, A., Garcia, V. J., Buchanan, B. B., and Luan, S. (2015). PSB27: a thylakoid protein enabling Arabidopsis to adapt to changing light intensity. *Proc. Natl. Acad. Sci. U.S.A.* 112, 1613–1618. doi: 10.1073/pnas.1424040112

Järvi, S., Suorsa, M., Paakkarinen, V., and Aro, E. M. (2011). Optimized native gel systems for separation of thylakoid protein complexes: novel super- and mega-complexes. *Biochem. J.* 439, 207–214. doi: 10.1042/BJ20102155

Kinsman, E. A., and Pyke, K. A. (1998). Bundle sheath cells and cell-specific plastid development in *Arabidopsis* leaves. *Development* 125, 1815–1822.

Kunst, L. (1998). Preparation of physiologically active chloroplasts from Arabidopsis. *Methods Mol. Biol.* 82, 43–48. doi: 10.1385/0-89603-391-0:43

Li, L., Sokolov, L. N., Yang, Y., Li, D., Ting, J., Pandy, G. K., et al. (2008). A mitochondrial magnesium transporter functions in Arabidopsis pollen development. *Mol. Plant* 1, 675–685. doi: 10.1093/mp/ssn031

Li, L., Tutone, A. F., Drummond, R. S. M., Gardner, R. C., and Luan, S. (2001). A novel family of magnesium transport genes in *Arabidopsis*. *Plant Cell* 13, 2761–2775. doi: 10.1105/tpc.010352

Liu, X., Yu, F., and Rodermel, S. (2010). Arabidopsis chloroplast ftsH, *var2* and suppressors of *var2* leaf variegation: a review. *J. Integr. Plant Biol.* 52, 750–761. doi: 10.1111/j.1744-7909.2010.00980.x

López-Juez, E., Jarvis, R. P., Takeuchi, A., Page, A. M., and Chory, J. (1998). New Arabidopsis *cue* mutants suggest a close connection between plastid- and phytochrome regulation of nuclear gene expression. *Plant Physiol.* 118, 803–815. doi: 10.1104/pp.118.3.803

Lorković, Z. J., Wieczorek-Kirk, D. A., Lambermon, M. H., and Filipowicz, W. (2000). Pre-mRNA splicing in higher plants. *Trends Plant Sci.* 5, 160–167. doi: 10.1016/S1360-1385(00)01595-8

Lundquist, P. K., Rosar, C., Bräutigam, A., and Weber, A. P. M. (2014). Plastid signals and the bundle sheath: mesophyll development in reticulate mutants. *Mol. Plant* 7, 14–29. doi: 10.1093/mp/sst133

Lunin, V. V., Dobrovetsky, E., Khutoreskaya, G., Zhang, R., Joachimiak, A., Doyle, D. A., et al. (2006). Crystal structure of the CorA Mg2+ transporter. *Nature* 404, 833–837. doi: 10.1038/nature04642

Mao, D., Chen, J., Tian, L., Liu, Z., Yang, L., Tang, R., et al. (2014). *Arabidopsis* transporter MGT6 mediates magnesium uptake and is required for growth under magnesium limitation. *Plant Cell* 26, 2234–2248. doi: 10.1105/tpc.114.124628

Mao, D., Tian, L., Li, L., Chen, J., Deng, P., Li, D., et al. (2008). *AtMGT7*: an Arabidopsis gene encoding a low-affinity magnesium transporter. *J. Integr. Plant Biol.* 50, 1530–1538. doi: 10.1111/j.1744-7909.2008.00770.x

Maguire, M. E. (2006). The structure of CorA: a Mg2+-selective channel. *Curr. Opin. Struct. Biol.* 16, 432–438. doi: 10.1016/j.sbi.2006.06.006

Maguire, M. E., and Cowan, J. A. (2002). Magnesium chemistry and biochemistry. *Biometals* 15, 203–210. doi: 10.1023/A:1016058229972

Martínez-Zapater, J. M. (1993) Genetic analysis of variegated mutants in Arabidopsis. *J. Hered.* 84, 138–140. doi: 10.1093/oxfordjournals.jhered.a111298

Matthies, D., Dalmas, O., Borgnia, M. J., Dominik, P. K., Merk, A., Rao, P., et al. (2016). Cryo-EM structures of the magnesium channel CorA reveal symmetry break upon gating. *Cell* 164, 747–756. doi: 10.1016/j.cell.2015.12.055

Mollá-Morales, A., Sarmiento-Mañús, R., Robles, P., Quesada, V., Pérez-Pérez, J. M., González-Bayón, R., et al. (2011). Analysis of *ven3* and *ven6* reticulate mutants reveals the importance of arginine biosynthesis in Arabidopsis leaf development. *Plant J.* 65, 335–345. doi: 10.1111/j.1365-313X.2010.04425.x

Moomaw, A. S., and Maguire, M. E. (2008). The unique nature of Mg2+ channels. *Physiology* 23, 275–285. doi: 10.1152/physiol.00019.2008

Nakai, M. (2015). The TIC complex uncovered: the alternative view on the molecular mechanism of protein translocation across the inner envelope membrane of chloroplasts. *Biochim. Biophys. Acta* 1847, 957–967. doi: 10.1016/j.bbabio.2015.02.011

Nesic, D., and Maquat, L. E. (1994). Upstream introns influence the efficiency of final intron removal and RNA 3'-end formation. *Genes Dev.* 8, 363–375. doi: 10.1101/gad.8.3.363

Pfoh, R., Li, A., Chakrabarti, N., Payandeh, J., Pomes, R., and Pai, E. F. (2012). Structural asymmetry in the magnesium channel CorA points to sequential allosteric regulation. *Proc. Natl. Acad. Sci. U.S.A.* 109, 18809–18814. doi: 10.1073/pnas.1209018109

Pogson, B. J., and Albrecht, V. (2011). Genetic dissection of chloroplast biogenesis and development: an overview. *Plant Physiol.* 155, 1545–1551. doi: 10.1104/pp.110.170365

Pottosin, I., and Dobrovinskaya, O. (2015). Ion channels in native chloroplast membranes: challenges and potential for direct patch-clamp studies. *Front. Physiol.* 6:396. doi: 10.3389/fphys.2015.00396

Putarjunan, A., Liu, X., Nolan, T., Yu, F., and Rodermel, S. (2013). Understanding chloroplast biogenesis using second-site suppressors of *immutans* and *var2*. *Photosynth. Res.* 116, 437–453. doi: 10.1007/s11120-013-9855-9

Qi, Y., Liu, X., Liang, S., Wang, R., Li, Y., Zhao, J., et al. (2016). A putative chloroplast thylakoid metalloprotease VIRESCENT3 regulates chloroplast development in *Arabidopsis thaliana*. *J. Biol. Chem.* 291, 3319–3332. doi: 10.1074/jbc.M115.681601

Rosar, C., Kanonenberg, K., Nanda, A. M., Mielewczik, M., Bräutigam, A., Novák, O., et al. (2012). The leaf reticulate mutant *dov1* is impaired in the first step of purine metabolism. *Mol. Plant* 5, 1227–1241. doi: 10.1093/mp/sss045

Schock, I., Gregan, J., Steinhauser, S., Schweyen, R., Brennicke, A., and Knoop, V. (2000). A member of a novel *Arabidopsis thaliana* gene family candidate Mg2+ ion transporters complements a yeast mitochondrial group II intron-splicing mutant. *Plant J.* 24, 489–501. doi: 10.1111/j.1365-313X.2000.00895.x

Shaul, O. (2002). Magnesium transport and function in plants: the tip of the iceberg. *Biometals* 15, 309–323. doi: 10.1023/A:1016091118585

Shaul, O., Hilgemann, D. W., de-Almeida-Engler, J., Van Montagu, M., Inzé, D., and Galili, G. (1999). Cloning and characterization of a novel Mg2+/H+ exchanger. *EMBO J.* 18, 3973–3980. doi: 10.1093/emboj/18.14.3973

Smith, R. L., and Maguire, M. E. (1995). Distribution of the CorA Mg2+ transport system in gram-negative bacteria. *J. Bacteriol.* 177, 1638–1640. doi: 10.1128/jb.177.6.1638-1640.1995

Streatfield, S. J., Weber, A., Kinsman, E. A., Häusler, R. E., Li, J., Post-Beittenmiller, D., et al. (1999). The phosphoenolpyruvate/phosphate translocator is required for phenolic metabolism, palisade cell development, and plastid-dependent nuclear gene expression. *Plant Cell* 11, 1609–1621. doi: 10.1105/tpc.11.9.1609

Tamura, K., Stecher, G., Peterson, D., Filipski, A., and Kumar, S. (2013). MEGA6: Molecular Evolutionary Genetics Analysis version 6.0. *Mol. Biol. Evol.* 30, 2725–2729. doi: 10.1093/molbev/mst197

Yoo, S. D., Cho, Y. H., and Sheen, J. (2007). Arabidopsis mesophyll protoplasts: a versatile cell system for transient gene expression analysis. *Nat. Protoc.* 2, 1565–1572. doi: 10.1038/nprot.2007.199

Yu, F., Fu, A., Aluru, M., Park, S., Xu, Y., Liu, H., et al. (2007). Variegation mutants and mechanisms of chloroplast biogenesis. *Plant Cell Environ.* 30, 350–365. doi: 10.1111/j.1365-3040.2006.01630.x

Yu, F., Park, S., and Rodermel, S. R. (2004). The Arabidopsis FtsH metalloprotease gene family: interchangeability of subunits in chloroplast oligomeric complexes. *Plant J.* 37, 864–876. doi: 10.1111/j.1365-313X.2003.02014.x

Conflict of Interest Statement: The authors declare that the research was conducted in the absence of any commercial or financial relationships that could be construed as a potential conflict of interest.

frontiers in Plant Science

ORIGINAL RESEARCH
published: 07 December 2017
doi: 10.3389/fpls.2017.02095

AT2G21280 Only Has a Minor Role in Chloroplast Division

*Yiqiong Li[1], Lulu Wang[1], Guangshuai Wang[1], Yue Feng[2] and Xiaomin Liu[1]**

[1] College of Biological Sciences and Biotechnology, Beijing Forestry University, Beijing, China, [2] Beijing Key Lab of Bioprocess, College of Life Science and Technology, Beijing University of Chemical Technology, Beijing, China

Chloroplast division is an important cellular process, which involves complicated coordination of multiple proteins. In mutant plants with chloroplast division defects, chloroplasts are usually found to be with enlarged size and reduced numbers. Previous studies have shown that *AT2G21280*, which was named as *GC1* (*GIANT CHLOROPLAST 1*) or *AtSulA*, was an important chloroplast division gene, because either reduced expression or overexpression of the gene could result in an apparent chloroplast division phenotype (Maple et al., 2004; Raynaud et al., 2004). To further study the function of *AT2G21280*, we obtained mutants of this gene by CRISPR/Cas9-mediated gene editing and T-DNA insertion. Most of the chloroplasts in the mutants were similar to that of the wild type in size. Larger chloroplasts were rarely found in the mutants. Moreover, we obtained transgenic plants overexpressing *AT2G21280*, analyzed the chloroplast division phenotype, and found there were no significant differences between the wild type and various overexpressing plants. Phylogenetic analysis clearly indicated that AT2G21280 was not in the family of bacterial cell division protein SulA. Instead, BLAST analysis suggested that AT2G21280 is an NAD dependent epimerase/dehydratase family enzyme. Since the main results of the previous studies that *AT2G21280* is an important chloroplast division gene cannot be confirmed by our intensive study and large chloroplasts are rarely found in the mutants, we think the previous names of *AT2G21280* are inappropriate. Localization study results showed that AT2G21280 is a peripheral protein of the inner envelope of chloroplasts in the stroma side. AT2G21280 is well conserved in plants and cyanobacteria, suggesting its function is important, which can be revealed in the future study.

Keywords: chloroplast division, AT2G21280, GC1, AtSulA, phylogenetic analysis

OPEN ACCESS

Edited by:
Fei Yu,
Northwest A&F University, China

Reviewed by:
Yan Lu,
Western Michigan University, United States
Maryse Anne Block,
Centre National de la Recherche Scientifique (CNRS), France

****Correspondence:***
Xiaomin Liu
liuxiaomin@bjfu.edu.cn

Specialty section:
This article was submitted to Plant Cell Biology, a section of the journal Frontiers in Plant Science

Received: *01 October 2017*
Accepted: *24 November 2017*
Published: *07 December 2017*

Citation:
Li Y, Wang L, Wang G, Feng Y and Liu X (2017) AT2G21280 Only Has a Minor Role in Chloroplast Division. Front. Plant Sci. 8:2095. doi: 10.3389/fpls.2017.02095

INTRODUCTION

Chloroplasts originated from free-living cyanobacteria as endosymbionts in plant cells (Gould et al., 2008; Keeling, 2013). Like bacteria, chloroplasts are proliferated through binary division, which maintains the stability of the chloroplast number in the cell and is important for the photosynthesis of plants (Dutta et al., 2015). Chloroplast division is carried out by division machinery. Ultrastructural observation showed that there are two plastid dividing (PD) ring structures formed at the division site of chloroplasts: one on the cytosolic surface of the outer envelope membrane (OEM), and the other on the stromal surface of the inner envelope membrane (IEM) (Kuroiwa et al., 1998). The constriction process was suggested to be driven by four different ring-like protein complexes, two in the stroma, the filamenting temperature-sensitive Z (FtsZ) and

the inner PD rings, and two in the cytoplasm, the accumulation and replication of chloroplasts 5 (ARC5)/dynamin-related protein 5B (DRP5B) and the outer PD rings (Miyagishima, 2011). With the motive force provided by FtsZ ring and ARC5/DRP5B ring, a chloroplast is divided into two daughter chloroplasts (Yoshida et al., 2006, 2016; Erickson et al., 2010). Chloroplast division occurs in the middle of the organelle. As the first assembled component of division machinery, the localization of FtsZ ring determines the position of the entire division complex (Nakanishi et al., 2009). In *Arabidopsis*, the midplastid localization of FtsZ ring is controlled by the chloroplast Min system, including ARC3, MinD, MinE, and MCD1. The division process of chloroplasts involves a series of proteins, which are assembled into a division complex. Among these proteins, some are derived from cyanobacteria, such as FtsZ1, FtsZ2, ARC6, MinD, and MinE, (Osteryoung, 1995; Colletti et al., 2000; Itoh et al., 2001; Maple et al., 2002; Vitha et al., 2003), while others are of eukaryotic origin, such as ARC5, PDV1 (PLASTID DIVISION 1), and PDV2 (Gao et al., 2003; Miyagishima et al., 2006; Nakanishi et al., 2009). The mutation of chloroplast division genes could result in various chloroplast division phenotypes, such as enlarged dumbbell-shaped chloroplasts, which are due to the mutations in *ARC5*, *PDV1*, or *PDV2* (Pyke and Leech, 1994; Robertson et al., 1996; Gao et al., 2003; Miyagishima et al., 2006), and a few large chloroplasts in the cell, which are due to the mutations in *FtsZ1*, *FtsZ2,* or *ARC6* (Osteryoung et al., 1998; Vitha et al., 2003; Schmitz et al., 2009).

SulA is a member of the SOS regulon in *Escherichia coli*. It can partially interfere with cell division followed by a blocking of DNA replication after DNA damage (Huisman and D'Ari, 1981; Huisman et al., 1984). SulA inhibits bacterial cell division by directly interacting with FtsZ and interrupting its normal division activity (Lutkenhaus, 1983; Jones and Holland, 1985; Bi and Lutkenhaus, 1990; Chen et al., 2012; Nazir and Harinarayanan, 2016). This inhibition is reversible because SulA is very unstable and once DNA is repaired, SulA disappears and cell division activity is restored soon after (Mizusawa and Gottesman, 1983; Maguin et al., 1986). In a *lon* mutant, in which the degradation of SulA slows down, the inhibition of cell division by SulA is prolonged (Mizusawa and Gottesman, 1983). As a result, cell morphology is altered with prolonged filamentation (Gottesman et al., 1981).

Previous results suggested that *AT2G21280*, which was named as *GC1* (*GIANT CHLOROPLAST 1*) or *AtSulA*, is an important chloroplast division gene. The protein sequence of AT2G21280 was shown to have a 50% identity with slr1223 protein of *Synechocystis* (SSulA) and ∼65% similarity to All2390 protein of *Anabaena* sp. PCC7120, which were annotated as cell division-inhibitor SulA proteins (Maple et al., 2004; Raynaud et al., 2004). Raynaud et al. (2004) showed that the disruption of *SSulA* in *Synechocystis* caused cell division defect, which could lead to cell death. Then they further showed that in *Arabidopsis*, overexpression of *AtSulA* with a 35S promotor driving full length cDNA with a GFP fusion inhibited chloroplast division in different types of cells, including mesophyll cells, bundle sheath cells and root cells, but the effect of inhibition varied in different lines and even in the same plants. Moreover, it was shown that overexpression of *AtSulA* could restore chloroplast division defect caused by overexpression of *AtFtsZ1-1* or *AtFtsZ2-1* (Raynaud et al., 2004). Maple et al. (2004) found that a severe reduction, but not overexpression, of *GC1* transcripts by cosuppression could cause a strong chloroplast division defect with only a few giant chloroplasts in the cells, whereas the other transgenic plants with normal or elevated level of *GC1* transcripts displayed normal chloroplast division in mesophyll and hypocotyl cells. Therefore, these two studies suggested *AT2G21280* is an important chloroplast division gene but with some contradictions.

To clarify these contradictions and further study the function of *AT2G2180*, we analyzed the chloroplast division phenotype of the mutant and overexpression plants of this gene. In mutant plants, large chloroplasts were observed in rare cases, and the sizes of most of the chloroplasts were found to be similar to that of the wild type. There is no apparent difference of the chloroplast division phenotype between various overexpression plants and the wild-type plants. Furthermore, phylogenetic analysis and sequence analysis indicated that AT2G2180 and SulA are proteins from totally different families. Therefore, our results show that *AT2G2180* is not important for the division of chloroplasts.

RESULTS

Knockout of *AT2G21280* Have a Very Little Effect on Chloroplast Division

AT2G21280 in *Arabidopsis* has 12 exons and 11 introns (**Figure 1**). In order to investigate the function of this gene, we took the advantage of CRISPR/Cas9-mediated gene-editing technique. Four constructs were designed to target four different sites in the gene, respectively and transformed into the wild-type plants. As expected, in the T1 and T2 generation, a part of the transgenic plants were edited at the targeting sites, and sgRNA mutants, such as sgRNA5#7-14, sgRNA6#6-1, sgRNA2#62-5, sgRNA1#13-5 (**Figure 1**), which have mutations in the 8th, 9th, and 12th exons, were obtained (**Figure 2**).

Homozygous mutants were verified by DNA sequencing for further analysis (**Figure 2**). In sgRNA5#7-14, a single base pair was inserted, causing a frame shift from the 184th amino acid and premature termination of the protein soon after. Similarly, in sgRNA6#6-1, a single base pair insertion caused a frame shift from the 206th amino acid and a premature stop codon 46 amino acids downstream. In sgRNA2#62-5, five base pairs were missing, which resulted in a frame shift and premature stop of the protein. In sgRNA1#13-5, a single base pair insertion caused a frame shift and premature stop codon 6 amino acids after. BLAST analysis indicated that the protein sequence of AT2G21280 is well-conserved in plants with 347 amino acids, except the N-terminal region, which is a chloroplast transit peptide. So, the premature stop of the protein in these mutants should have a severe effect on the function of the gene. Even for sgRNA1#13-5, the mutation site is in the last exon and only 63 amino acids upstream of the stop codon, the function of the gene is also very likely to be affected (**Figure 2**).

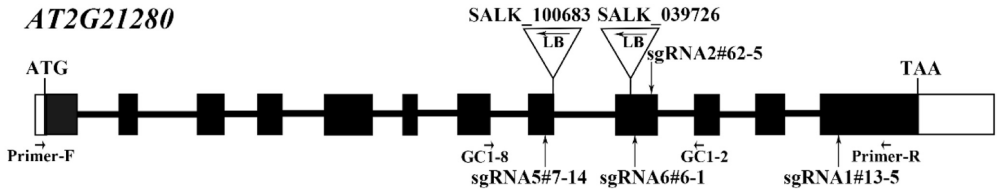

FIGURE 1 | Gene structure of *AT2G21280* and a diagram of T-DNA and sgRNA mutants. White boxes represent the 5′- and 3′-untranslated regions, black boxes represent exons, and black lines represent introns. Triangles and arrowheads in them mark the locations of T-DNA insertion of the SALK lines and indicate the directions of the T-DNA, respectively. Perpendicular arrows mark the targeting sites of sgRNAs. Positions of primers used for T-DNA insertion mutants identification in Supplementary Figure 1 and the RT-PCR analysis in Supplementary Figure 2 are marked with arrows.

FIGURE 2 | Sequencing analysis of four sgRNA mutants of *AT2G21280*. Asterisks indicate the sites of insertions or deletion in sgRNA mutants. Sequences of DNA and amino acids are compared between the wild type and mutants to show the mutations. Sequences changed are shown in red. Asterisks at the end of amino acid sequences represent stop codon. Numbers above DNA and protein sequences indicated the positions in the cDNA and proteins, respectively.

At first, we studied the chloroplast division phenotypes of the 3-week-old plants of these sgRNA mutants (**Figures 3A,B**). The results indicated that the chloroplast sizes of these mutants are similar to that of the wild type. Only in rare cases, slightly enlarged chloroplasts were found in sgRNA5#7-14 (4 out of more than 800 cells) and sgRNA2#62-5 (1 out of more than 800 cells) (**Figure 3A**). We also analyzed the chloroplast division phenotype of 5-week-old plants, which have larger cell and chloroplast sizes and may give a stronger chloroplast division phenotype. In these mutant plants, chloroplast sizes are also similar to that of the wild type (**Figures 3C,D**). Furthermore, statistical analysis of the numbers of chloroplasts per cell and cell area indicated that there was no obvious difference between the mutant and the wild type, both in 3- and 5-week-old plants (**Figures 3B,D**). This result is completely different from the previous reports that GC1 cosuppression lines contained giant chloroplasts (Maple et al., 2004).

To further explore this discrepancy, transfer DNA (T-DNA) insertional mutants (SALK_100683 and SALK_039726) were obtained for analysis. The homozygous SALK_100683 and SALK_039726, which contain T-DNA insertions in the 8th exon and the 9th exon, respectively, were verified by PCR (**Figure 1**

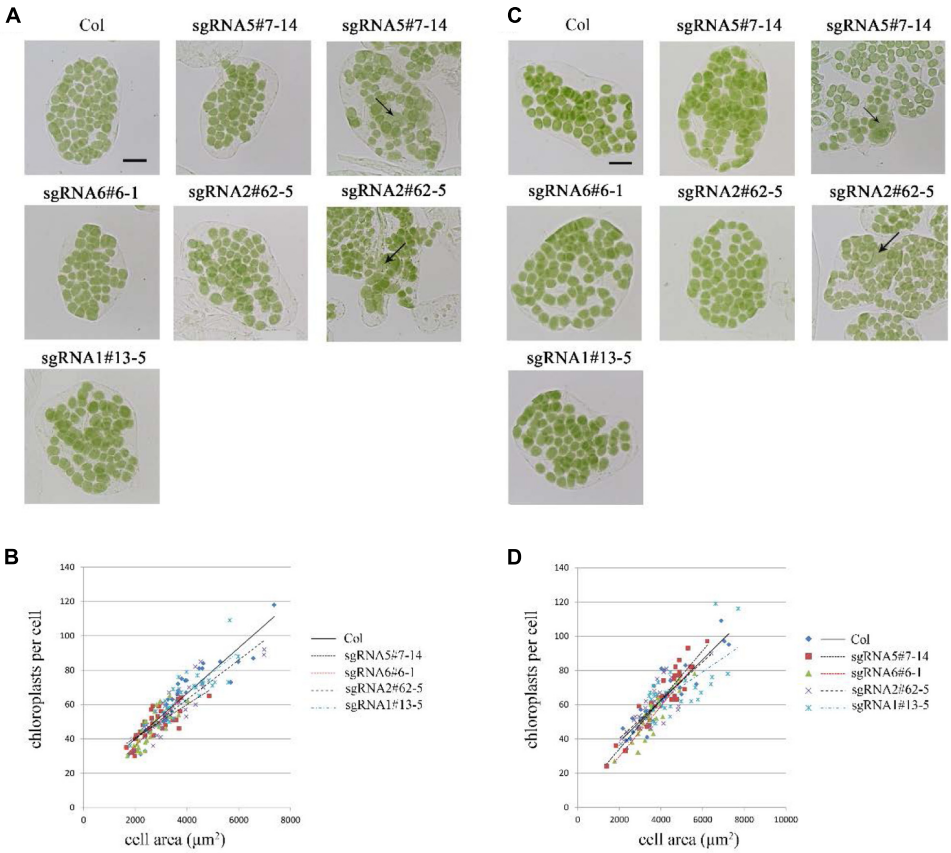

FIGURE 3 | Phenotype analysis of sgRNA mutants. **(A)** Chloroplast division phenotypes of 3-week-old plants. Arrow indicates the enlarged chloroplast. Bar = 20 μm. **(B)** Relationships between chloroplast number and mesophyll cell area in 3-week-old plants. The R^2 values of the best-fit lines are 0.8511, 0.5785, 0.6690, 0.7743, and 0.7173 in order. **(C)** Chloroplast division phenotypes of 5-week-old plants. Bar = 20 μm. **(D)** Relationships between chloroplast number and mesophyll cell area in 5-week-old plants. The R^2 values of the best-fit lines are 0.8274, 0.8586, 0.8003, 0.6238, and 0.4595 in order (n = 30).

and Supplementary Figure 1). Mutant plants of SALK_100683 and SALK_039726 at the stages of 3 and 5 weeks were analyzed for the chloroplast division phenotypes (**Figure 4**). We found that the sizes of most of the chloroplasts in the mutants are similar to that of the wild type, and only in rare cases (5 out of more than 800 cells), larger chloroplasts could be found (**Figures 4A,C**). Statistical analysis further indicated that the number of chloroplasts per cell of the mutants and the wild type are similar (**Figures 4B,D**). Thus, the results of T-DNA insertion mutants are similar to that of sgRNA mutants. At the same time, chloroplast division mutants *pdv2-3* and *arc6-6* were used as controls for comparison (Vitha et al., 2003; Miyagishima et al., 2006; Chang et al., 2017; Wang et al., 2017). These mutants contains only a few giant chloroplasts in the cell (**Figures 4A,C**).

The transcriptional level of *AT2G21280* in different sgRNA and T-DNA mutant lines was analyzed by semi-quantitative reverse transcription (RT) PCR (Supplementary Figure 2). The results showed that the levels of *AT2G21280* were reduced in all of these mutant lines. Especially, PCR product was undetectable in T-DNA insertion mutants.

To further analyze the protein levels in these mutant lines, we generated the antibodies of AT2G21280. As shown in **Figure 5**, a band of approximately 33 kD was detected in the wild type, which is close to the expected size of AT2G21280. While in all of these mutants, this band was missing. Moreover, no band smaller than this size was detected in these mutants. These results indicated that the protein of AT2G21280 was either not translated or degraded. Therefore, these sgRNA and T-DNA mutants are true knockout mutants.

Taken together, these results showed that *AT2G21280* only has a minor role in chloroplast division.

Overexpression of *AT2G21280* Has No Effect on Chloroplast Division

To test whether overexpression of *AT2G21280* can affect chloroplast division as reported before (Raynaud et al., 2004), we transformed *Arabidopsis* wild-type plants with constructs containing CaMV35S-driven full-length cDNA (c), or full-length genome DNA (g) individually. Moreover, we also obtained transgenic plants expressing 35S-g-YFP and 35S-g$^{\Delta H}$-YFP, respectively. The latter had a truncation of the last C-terminal 20 amino acids (for details see below) of the protein. The protein level of AT2G21280 in the transgenic plants with various constructs as mentioned above was analyzed by immuno-blot.

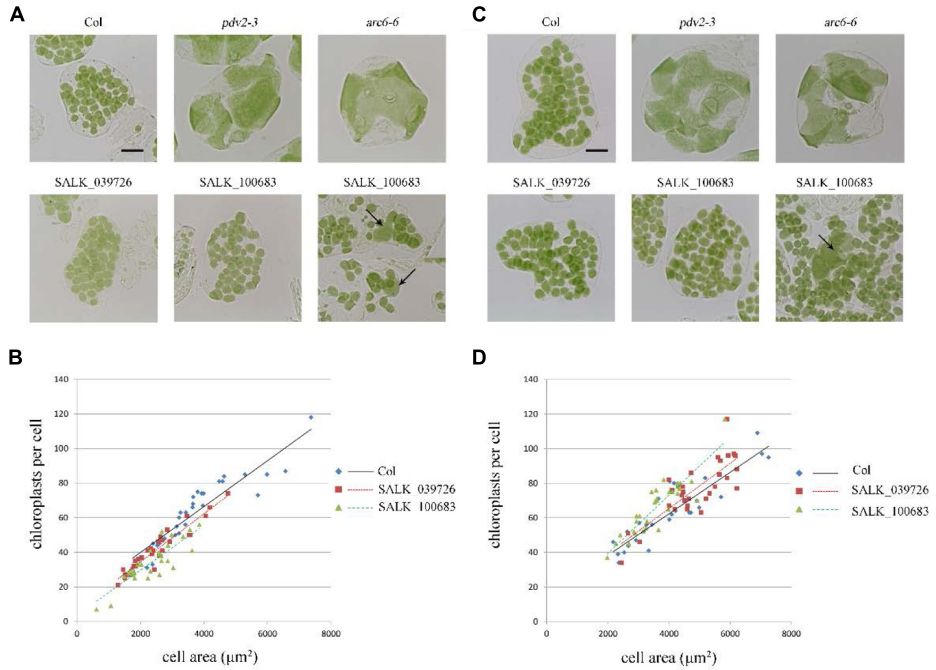

FIGURE 4 | Phenotype analysis of T-DNA mutants. **(A)** Chloroplast division phenotypes of 3-week-old plants of wild type (Col), *pdv2-3*, *arc6-6*, SALK_039726 and SALK_100683. Arrows indicate enlarged chloroplasts in the T-DNA mutants. Bar = 20 μm. **(B)** Relationships between chloroplast number and mesophyll cell area of 3-week-old plants. The R^2 values of the best-fit lines are 0.8511, 0.9017, and 0.7351 in order. **(C)** Chloroplast division phenotypes of 5-week-old plants of wild type (Col), *pdv2-3*, *arc6-6*, SALK_039726 and SALK_100683. Arrow indicates the enlarged chloroplast. Bar = 20 μm. **(D)** Relationships between chloroplast number and mesophyll cell area of 5-week-old plants. The R^2 values of the best-fit lines are 0.8274, 0.6584, and 0.798 in order (n = 30).

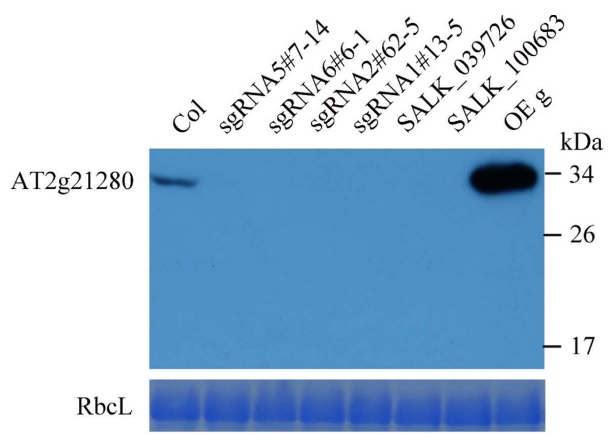

FIGURE 5 | Western blot analysis of AT2G21280. The specificity of the antibodies and the protein level of AT2G21280 in the Col wild type, sgRNA mutants, T-DNA mutants and overexpression plant were analyzed. Total proteins were extracted from leaves of 4-week-old plants, and loaded in each lane. RbcL was used as a loading control. The molecular weight of protein markers are labeled on the right.

Most of the transgenic plants have a protein level much higher than that of the wild type (**Figure 6C**). We chose the plants with a very high level of AT2G21280 for phenotypic analysis. The chloroplasts in these plants are very similar to those in the wild-type plants (**Figure 6A**). Then we analyzed chloroplast division phenotypes of these plants by statistical analysis and still found no obvious differences between these overexpression lines and the wild type (**Figure 6B**).

In addition, in some of the lines, the endogenous protein level of AT2G21280 was undetectable, possibly due to cosuppression. The chloroplast phenotype of these lines was also analyzed (Supplementary Figure 3). Phenotypic and statistical analysis results indicated that there was no significant difference between them and the wild type.

Thus, the previous report that overexpression of AtSulA could cause a chloroplast division defect (Raynaud et al., 2004) cannot be verified by us. Based on these results and the results shown above, we think the previous names of *AT2G21280*, *GC1* and *AtSulA*, are not appropriate.

AT2G21280 Is Localized to the Envelope of Chloroplasts

Previous study suggested that the nine amino acids at the C-terminal end is an amphipathic helix which may anchor AT2G21280 to the chloroplast inner envelope in tobacco leaf cells with a transiently expression of *35S-AT2G21280-YFP* fusion protein (Maple et al., 2004). We studied the subcellular localization of AT2G21280 with GFP fused to the full-length protein 35S-g-YFP (or AT2G21280-YFP), and a protein with a 20 amino acids truncation at the C-terminal end, 35S-g$^{\Delta H}$-YFP (or AT2G21280$^{\Delta H}$-YFP) in *Arabidopsis*. The results showed that, consistent with previous results, AT2G21280-YFP was indeed

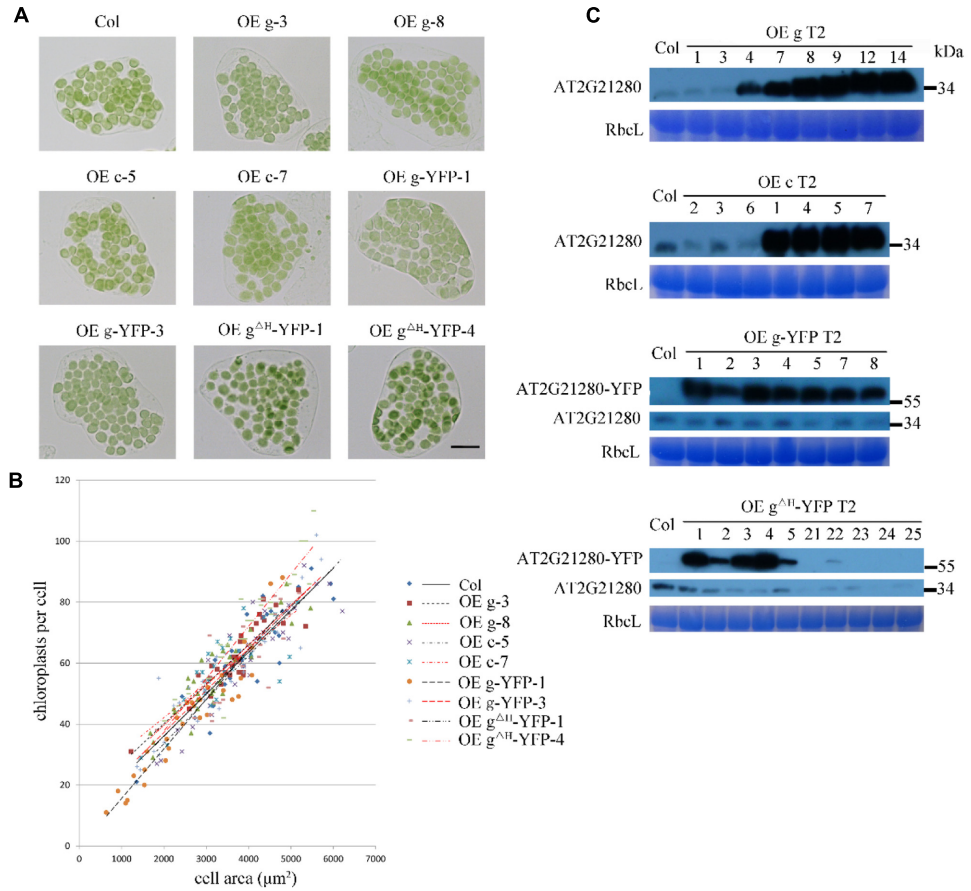

FIGURE 6 | Phenotype and protein level analysis of AT2G21280 overexpressing plants. **(A)** Chloroplast division phenotypes of different overexpression lines. "OE g" represents the overexpression of genomic DNA, "OE c" represents the overexpression of cDNA, "OE g-YFP" represents the overexpression of AT2G21280 fused with YFP, "OE $g^{\Delta H}$ -YFP" represents the overexpression of AT2G21280 lacking the last 20 amino acids with a C-terminal YFP fusion. Leaf tissues were sampled from 4-week-old plants. The scale bar is 20 μm. **(B)** Relationships between chloroplast number and mesophyll cell area of the wild type and different AT2G21280 overexpressing plants. The R^2 values of the best-fit lines are 0.7814, 0.8314, 0.6333, 0.8096, 0.8238, 0.9101, 0.8457, 0.6875, and 0.8840 in order (n = 30). **(C)** Immunoblot analysis of the protein level of AT2G21280 in different plants. Total proteins were extracted from leaves of 4-week-old plants, and loaded in each lane. RbcL served as a loading control. The molecular weight of protein markers are labeled on the right.

localized to the envelope of chloroplasts (**Figure 7**). However, we found that AT2G21280$^{\Delta H}$-YFP had two types of distribution, one is dot-like aggregation in the stroma as before (Maple et al., 2004), the other is a region near the chloroplast envelope, which is wider than and different from that of AT2G21280-YFP (**Figure 7**), suggesting when missing the last C-terminal 20 amino acids, AT2G21280 cannot bind well to the envelop membrane. The latter localization result is different from the previous study (Maple et al., 2004).

Phylogenetic Analysis of AT2G21280 and SulA

Previous results suggest that AT2G21280 is similar to slr1223 protein of *Synechocystis* (SSulA) and All2390 protein of *Anabaena* sp. PCC7120, which were annotated as SulA homologs in *Cyanobacteria* (Maple et al., 2004; Raynaud et al., 2004). These proteins are well-conserved in *Cyanobacteria* and plants. However, a BLAST search with the real SulA protein of *E. coli* found no homologs in *Cyanobacteria* and plants. Moreover, BLAST searches with AT2G21280, slr1223, All2390, or their homologs all suggest these proteins are NAD dependent epimerase/dehydratase family enzymes, which is totally different from SulA.

To resolve this problem, we retrieved homologous sequences of SulA in bacteria and AT2G21280 in bacteria and plants based on BLAST search results and carried out a phylogenetic analysis. The result clearly indicated that SulA and AT2G21280 are proteins of distinct families (**Figure 8**). AT2G21280 belongs to a family widely distributed in bacteria and plants, while SulA belongs to a family in *E. coli* in its close relatives. Therefore, it is a mistake to name AT2G21280 as AtSulA.

DISCUSSION

An optimized number and size of chloroplasts is important for the normal physiological function of chloroplasts *in vivo* (Dutta

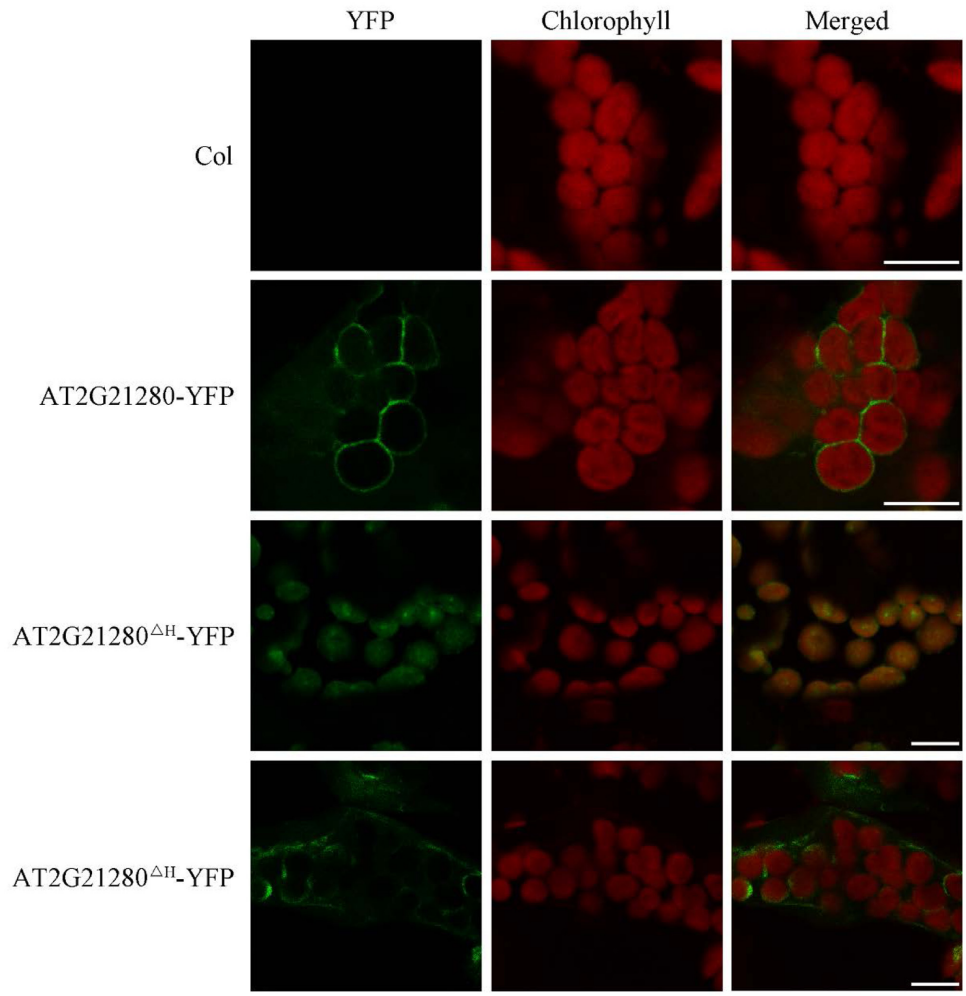

FIGURE 7 | Subcellular localization study of AT2G21280-YFP and AT2G21280$^{\Delta H}$-YFP. The full length of AT2G21280 or a truncation of the last 20 AA at C-terminal end (AT2G21280$^{\Delta H}$) with a YFP fusion were used to study the subcellular localization of the protein in *Arabidopsis*. Col wild type was used as a control. Green fluorescence signals indicate AT2G21280-YFP or AT2G21280$^{\Delta H}$-YFP, and red signals indicate the autofluorescence of chlorophyll. Bar = 10 μm.

et al., 2015). Therefore, plant cells must maintain an appropriate division of chloroplasts. Chloroplast division is completed by a protein complex composed of many components. If one protein of the complex is severely affected by mutation or other types of interference, it can cause abnormal chloroplast division, and result in a reduction of chloroplast number and an enlargement of chloroplast size (Osteryoung et al., 1998; Miyagishima et al., 2006) (**Figure 4A**). In this study, we analyzed the role of *AT2G21280*, a gene previously reported as a chloroplast division gene, in chloroplast division. By observing and statistically analyzing the chloroplast division phenotype of *at2g21280* mutants and *AT2G21280* overexpressing plants, we found that *AT2G21280* is not important for chloroplast division. Moreover, bioinformatic analysis suggested that there is no relationship between AT2G21280 and bacterial cell division-related protein SulA.

Previous studies reported that AT2G21280 is a chloroplast division protein. Maple et al. (2004) found that AT2G21280 was localized to the stromal side of chloroplast inner envelope by the C-terminal amphipathic helix. They also obtained AT2G21280 transgenic *Arabidopsis* plants with a CaMV35S-driven full-length cDNA in the sense orientation. They reported that a greatly reduction of *AT2G21280* transcript level could result in a reduction of the number of chloroplasts and the occurrence of giant chloroplasts in the mesophyll cells of the cosuppression lines, while a great increase of *AT2G21280* transcript level had no effect on chloroplast division. Furthermore, cosuppression of *AT2G21280* produced homogenously giant chloroplasts in mesophyll cells but chloroplasts with heterogeneous sizes in hypocotyl cells, especially in the cells closed to the hypocotyl base (Maple et al., 2004). Raynaud et al. (2004) reported loss of function mutation of *SSulA* in *Synechocystis* by gene disruption affected cell division. Furtherly, they constructed *AT2G21280-GFP* with full length cDNA of *AT2G21280* under control of the 35S promotor in sense orientation. They screened transgenic plants through observing GFP fluorescence

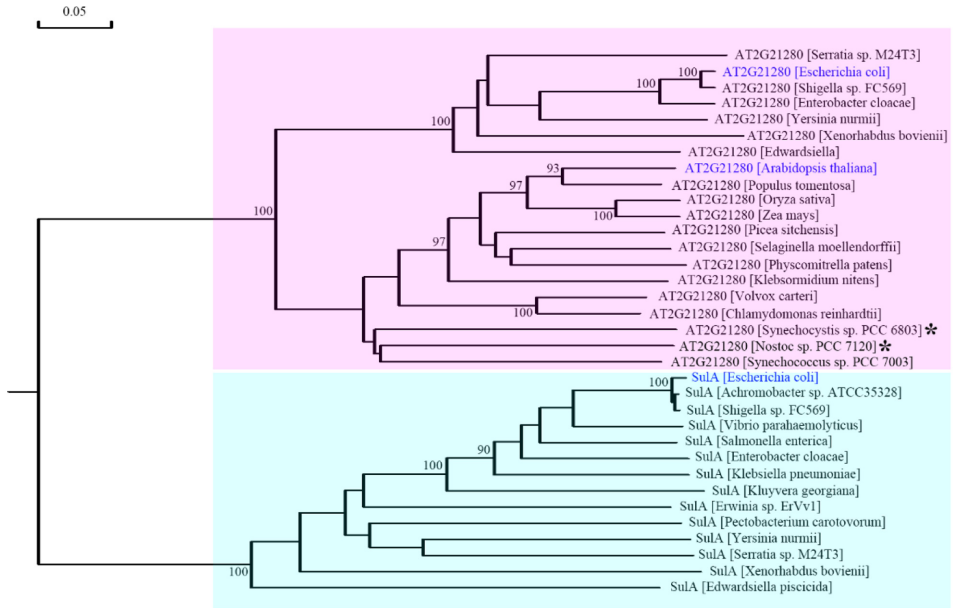

FIGURE 8 | Phylogenetic analysis of AT2G21280 and SulA. A phylogenetic tree of the protein sequences of AT2G21280 and SulA and their homologs in different species. Asterisks indicated the species whose sequences were used to search homologous proteins in *Arabidopsis* and found AT2G21280 in previous studies. Anabeana was later renamed as Nostoc. AT2G21280 in *Arabidopsis*, its homologs in *E. coli*, and SulA in *E. coli* are shown with blue color. AT2G21280 and SulA families are highlighted with pink and cyan colors, respectively. Bootstrap values ≥ 90% are shown at the corresponding nodes based on 1000 bootstrapping replicates.

in root cells. Their analysis suggested that overexpression of *AT2G21280* could cause an obvious chloroplast division defect in some cells and the phenotype was heterogeneous even in the same plant. They suggested the inhibition of plastid division was due to the high levels of AT2G21280-GFP (Raynaud et al., 2004). In contrast, Maple et al. (2004) found increased level of *AT2G21280* had no effect on chloroplast division in *Arabidopsis*. That is, these studies have some contradictions.

In our study, we analyzed the role of AT2G21280 in chloroplast division with several knockout mutants, including RNA-guided CRISPR/Cas9 mutants, T-DNA insertion mutants and possible AT2G21280 cosuppression lines in *Arabidopsis*. In addition, we obtained various overexpression lines, including overexpression the full length genomic DNA or cDNA of *AT2G21280*, and *YFP* fusion genes. Our Western Blot results also showed the protein levels in the mutant or transgenic plants have undetectable or very high levels of AT2G21280. This kind of experiments are more convincing but were not carried out in the previous studies (Maple et al., 2004; Raynaud et al., 2004). Nevertheless, our genetic and phenotypic analysis studies with multiple lines of evidences showed that enlarged chloroplasts in the mutant can only be found in rare cases, and overexpression of AT2G21280 doesn't affect chloroplast division. These results are generally quite different from the previous reports.

AT2G21280 in *Arabidopsis* was found by searching the homologous proteins of the bacterial cell division-inhibitor protein SulA. It shared ∼65% similarity to with the *Anabaena* sp. PCC 7120 All2390 (Maple et al., 2004). But our experimental results do not support the conclusion that AT2G21280 is a chloroplast division protein. Therefore, is the *Anabaena* sp. PCC 7120 All2390 a real SulA protein? What is the relationship between AT2G21280 in *Arabidopsis* and SulA in *E. coli*. A phylogenetic analysis of AT2G21280-related proteins and SulA-related proteins was carried out to resolve these questions. Our analysis clearly shows that AT2G21280 and SulA are from different families (**Figure 8**). Therefore, they should have different functions in chloroplasts or bacterial cells.

Subcellular localization in both previous study and our analysis showed that AT2G21280 was localized to the inner envelope of chloroplasts. Then, what is the real function of AT2G21280? BLAST search result suggested that AT2G21280 is mostly composed of a conserved domain of NAD (P)-dependent epimerase or an atypical short-chain dehydrogenase, which use nucleotide-sugar substrates for a variety of chemical reactions. Sugar epimerase is widely found in animals, plants and microorganisms. It is initially isolated from *E. coli*, catalyzing an epimerization reaction through the transient reduction of NAD^+ (Arabshahi et al., 1988; Somers et al., 1998). Once an epimerase gene of bacteria is mutated, it can cause reduced infection, decreased pathogenicity, and high sensitivity to antibiotics (Coleman and Leive, 1979; Vaara, 1993; Yamashita et al., 1999). Based on these facts, we speculate that AT2G21280 may modify and regulate the carbohydrates attached to the surface of the membrane of chloroplast inner envelope in the stromal side.

MATERIALS AND METHODS

Plant Materials and Growth Conditions

All *Arabidopsis* plants used in this study are in Col ecotype background. T-DNA insertion mutants of *AT2G21280*, SALK_039726 and SALK_100683, were obtained from ABRC (Arabidopsis Biological Resource Center, United States). Seeds were sterilized and sowed on 1/2MS (Murashige and Skoog) solid medium containing 0.8% agar and 1% sucrose. After being placed in a refrigerator at 4°C for 2 days, plates were moved to a growth chamber at 22°C with 16-h-light/8-h-dark cycles. Ten days later, seedlings were transferred into soil and grown in the same growth chamber.

Chloroplast Phenotype and Fluorescence Microscopy Analysis

Leaf fixation and chloroplast phenotype analysis were performed as described previously (Gao et al., 2013; Chang et al., 2017). Briefly, a piece of 4-week-old leaf was immersed into a tube containing 1 mL 3.5% glutaraldehyde for 1 h in the dark. Then the fixative solution was replaced with 0.1 M Na_2EDTA (pH9.0) and the tube was incubated in water bath at 55°C for 2 h. Chloroplast phenotype was observed with an Olympus CX21 microscope (Olympus, Tokyo, Japan) equipped with a USB 2.0 digital camera (Changheng, Beijing, China). Statistical analysis of chloroplast phenotypes was done as before (Gao et al., 2013). Fluorescence images of YFP and chlorophyll were obtained with a TCS SP8 confocal laser scanning microscope (Leica Microsystems, Germany).

Plasmid Construction

A series of constructs were made based on the CRISPR/CAS9 plasmid, pHEE401E (Wang et al., 2015), in order to edit *AT2G21280*. Targeting sites were chosen with the tools at the website CRISPRscan[1] and CAS-OFFinder[2]. Primers used for targeting four different sites of *AT2G21280* (sgRNA5, sgRNA6, sgRNA2, and sgRNA1) were shown in Supplementary Table 1.

For constructs overexpressing *AT2G21280*, OE g (genomic DNA) and OE c (cDNA), the full length genomic DNA and cDNA were amplified by PCR with primers 2g21280-5 and 2g21280-6 (Supplementary Table 1), digested with *Nco*I and *Mlu*I, and cloned into 3302Y2 vector, respectively.

To construct 35S-g-YFP and 35S-$g^{\Delta H}$-YFP, full length genomic DNA (g) of *AT2G21280* and *AT2G21280* lacking of the last 20 amino acids at the C terminus were amplified using primers GC1-5 and GC1-6 and GC1-5 and GC1-7 (Supplementary Table 1). The PCR products digested with *Mlu*I were cloned into pCAMBIA 3302Y3 vector.

Generation of Transgenic Plants

Overexpressing constructs were introduced into *Agrobacterium tumefaciens* and then transformed into *Arabidopsis* by floral dipping method (Feldmann and Marks, 1987; Clough and Bent, 1998; Bent, 2006). Transgenic plants of T1 generation were screened with Basta. T2 plants were used for the analysis.

Transgenic plants of *AT2G21280* sgRNA were obtained as described above. The T1 transgenic plants were screened on 1/2 MS medium containing 20 μg/mL hygromycin and 10 μg/mL carbenicillin. The plates were placed in the dark for 3∼4 days and then moved to the light. One week later, seedlings selected by the antibiotic were transferred into soil and grown in a growth chamber.

Identification of sgRNA Mutants and T-DNA Insertion Mutants

For *AT2G21280* sgRNA mutants, sgRNA5#7-14, sgRNA6#6-1, and sgRNA2#62-5 were identified by amplifying genomic DNA sequences using primers GC1-8 and GC1-2 and analyzing the sequencing results of the PCR products (Supplementary Table 1). For sgRNA1#13-5, primers GC1-9 and GC1-3 were used instead (Supplementary Table 1).

The sequences flanking the insertion sites of T-DNA mutants, SALK_039726 and SALK_100683, were amplified by PCR with primers GC1-8 and LBC1. The accurate insertion sites were deduced by DNA sequencing. The genomic DNA sequence spanning the insertion sites in the two T-DNA mutants was amplified by primers GC1-8 and GC1-2 (Supplementary Table 1 and **Figure 1**).

RNA Extraction and RT-PCR Analysis

RNA was isolated from the leaves of 4-week-old plants grown in soil under white light, using an RNApure Total RNA Isolation Kit (Aidlab, Beijing, China). The RNA samples (3 μg each) were used as templates for first-strand cDNA synthesis (Thermo Fisher Scientific, United States). Semi-quantitative RT-PCR analysis was performed according to Pan et al. (2013). *AT2G21280* were amplified with specific primers GC1-5 and GC1-7. The *PP2AA3* gene was taken as a control and amplified with primers PP2AA3-1 and PP2AA3-2.

Immunoblot Analysis

To generate AT2G21280 antibodies, a fragment of AT2G21280, which is from the 46th amino acid to the end, was expressed in *E. coli* and purified as antigen. Antibodies were produced in rabbit and purified. For immunoblot analysis, proteins from 5 mg of leaves were separated by SDS–PAGE and transferred to PVDF membrane (Bio-rad). After being blocked with 5% milk for 2 h, the PVDF membrane was incubated with anti-AT2G21280 polyclonal antibodies at a dilution of 1:1000 in 3% milk for 1 h, then washed with 3% milk for four times, and incubated with HRP-labeled goat anti-mouse IgG secondary antibody at a dilution of 1:10,000. Finally, an eECL Western Blot kit (Beijing ComWin Biotech Company, China) were used for the film development.

Phylogenetic Analysis

Homologous sequences of AT2G21280 and SulA in various species were searched with NCBI BLAST[3] and downloaded

[1]http://www.crisprscan.org/?page=sequence

[2]http://www.rgenome.net/cas-offinder/

[3]https://blast.ncbi.nlm.nih.gov/Blast.cgi

(Supplementary Table 2). Phylogenetic analysis of AT2G21280, SulA and their relatives was carried out by DNAman software (Version 7, Lynnon Biosoft Inc., United States).

AUTHOR CONTRIBUTIONS

XL conceived the project and designed the experiments. YL, LW, and GW performed most of the experiments. YF participated in the preparation of AT2G21280 antibodies. XL and YL wrote the manuscript. All authors read and approved the final manuscript.

FUNDING

This work was supported by grants from the National Natural Science Foundation of China (31501090).

SUPPLEMENTARY MATERIAL

The Supplementary Material for this article can be found online at: https://www.frontiersin.org/articles/10.3389/fpls.2017.02095/full#supplementary-material

REFERENCES

Arabshahi, A., Flentke, G., and Frey, P. (1988). Uridine diphosphate galactose 4-epimerase. pH dependence of the reduction of NAD+ by a substrate analog. *J. Biol. Chem.* 263, 2638–2643.

Bent, A. (2006). *Arabidopsis thaliana* floral dip transformation method. *Methods Mol. Biol.* 343, 87–103. doi: 10.1385/1-59745-130-4:87

Bi, E., and Lutkenhaus, J. (1990). Analysis of *ftsZ* mutations that confer resistance to the cell division inhibitor SulA (SfiA). *J. Bacteriol.* 172, 5602–5609. doi: 10.1128/jb.172.10.5602-5609.1990

Chang, N., Sun, Q., Li, Y., Mu, Y., Hu, J., Feng, Y., et al. (2017). PDV2 has a dosage effect on chloroplast division in *Arabidopsis*. *Plant Cell Rep.* 36, 471–480. doi: 10.1007/s00299-016-2096-6

Chen, Y., Milam, S. L., and Erickson, H. P. (2012). SulA inhibits assembly of FtsZ by a simple sequestration mechanism. *Biochemistry* 51, 3100–3109. doi: 10.1021/bi201669d

Clough, S. J., and Bent, A. F. (1998). Floral dip: a simplified method for *Agrobacterium*-mediated transformation of *Arabidopsis thaliana*. *Plant J.* 16, 735–743. doi: 10.1046/j.1365-313x.1998.00343.x

Coleman, W., and Leive, L. (1979). Two mutations which affect the barrier function of the *Escherichia coli* K-12 outer membrane. *J. Bacteriol.* 139, 899–910.

Colletti, K. S., Tattersall, E. A., Pyke, K. A., Froelich, J. E., Stokes, K. D., and Osteryoung, K. W. (2000). A homologue of the bacterial cell division site-determining factor MinD mediates placement of the chloroplast division apparatus. *Curr. Biol.* 10, 507–516. doi: 10.1016/S0960-9822(00)00466-8

Dutta, S., Cruz, J. A., Jiao, Y., Chen, J., Kramer, D. M., and Osteryoung, K. W. (2015). Non-invasive, whole-plant imaging of chloroplast movement and chlorophyll fluorescence reveals photosynthetic phenotypes independent of chloroplast photorelocation defects in chloroplast division mutants. *Plant J.* 84, 428–442. doi: 10.1111/tpj.13009

Erickson, H. P., Anderson, D. E., and Osawa, M. (2010). FtsZ in bacterial cytokinesis: cytoskeleton and force generator all in one. *Microbiol. Mol. Biol. Rev.* 74, 504–528. doi: 10.1128/MMBR.00021-10

Feldmann, K. A., and Marks, M. D. (1987). *Agrobacterium*-mediated transformation of germinating seeds of *Arabidopsis thaliana*: a non-tissue culture approach. *Mol. Gen. Genet.* 208, 1–9. doi: 10.1007/BF00330414

Gao, H., Kadirjan-Kalbach, D., Froehlich, J. E., and Osteryoung, K. W. (2003). ARC5, a cytosolic dynamin-like protein from plants, is part of the chloroplast division machinery. *Proc. Natl. Acad. Sci. U.S.A.* 100, 4328–4333. doi: 10.1073/pnas.0530206100

Gao, Y., Liu, H., An, C., Shi, Y., Liu, X., Yuan, W., et al. (2013). *Arabidopsis* FRS4/CPD25 and FHY3/CPD45 work cooperatively to promote the expression of the chloroplast division gene *ARC5* and chloroplast division. *Plant J.* 75, 795–807. doi: 10.1111/tpj.12240

Gottesman, S., Halpern, E., and Trisler, P. (1981). Role of *sulA* and *sulB* in filamentation by lon mutants of *Escherichia coli* K-12. *J. Bacteriol.* 148, 265–273.

Gould, S. B., Waller, R. F., and Mcfadden, G. I. (2008). Plastid evolution. *Annu. Rev. Plant Biol.* 59, 491–517. doi: 10.1146/annurev.arplant.59.032607.092915

Huisman, O., and D'Ari, R. (1981). An inducible DNA replication–cell division coupling mechanism in *E. coli*. *Nature* 290, 797–799. doi: 10.1038/290797a0

Huisman, O., D'ari, R., and Gottesman, S. (1984). Cell-division control in *Escherichia coli*: specific induction of the SOS function SfiA protein is sufficient to block septation. *Proc. Natl. Acad. Sci. U.S.A.* 81, 4490–4494. doi: 10.1073/pnas.81.14.4490

Itoh, R., Fujiwara, M., Nagata, N., and Yoshida, S. (2001). A chloroplast protein homologous to the eubacterial topological specificity factor MinE plays a role in chloroplast division. *Plant Physiol.* 127, 1644–1655. doi: 10.1104/pp.010386

Jones, C., and Holland, I. B. (1985). Role of the SulB (FtsZ) protein in division inhibition during the SOS response in *Escherichia coli*: FtsZ stabilizes the inhibitor SulA in maxicells. *Proc. Natl. Acad. Sci. U.S.A.* 82, 6045–6049. doi: 10.1073/pnas.82.18.6045

Keeling, P. J. (2013). The number, speed, and impact of plastid endosymbioses in eukaryotic evolution. *Annu. Rev. Plant Biol.* 64, 583–607. doi: 10.1146/annurev-arplant-050312-120144

Kuroiwa, T., Kuroiwa, H., Sakai, A., Takahashi, H., Toda, K., and Itoh, R. (1998). The division apparatus of plastids and mitochondria. *Int. Rev. Cytol.* 181, 1–41. doi: 10.1016/S0074-7696(08)60415-5

Lutkenhaus, J. F. (1983). Coupling of DNA replication and cell division: *sulB* is an allele of *ftsZ*. *J. Bacteriol.* 154, 1339–1346.

Maguin, E., Lutkenhaus, J., and D'ari, R. (1986). Reversibility of SOS-associated division inhibition in *Escherichia coli*. *J. Bacteriol.* 166, 733–738. doi: 10.1128/jb.166.3.733-738.1986

Maple, J., Chua, N. H., and Møller, S. G. (2002). The topological specificity factor AtMinE1 is essential for correct plastid division site placement in *Arabidopsis*. *Plant J.* 31, 269–277. doi: 10.1046/j.1365-313X.2002.01358.x

Maple, J., Fujiwara, M. T., Kitahata, N., Lawson, T., Baker, N. R., Yoshida, S., et al. (2004). GIANT CHLOROPLAST 1 is essential for correct plastid division in *Arabidopsis*. *Curr. Biol.* 14, 776–781. doi: 10.1016/j.cub.2004.04.031

Miyagishima, S.-Y. (2011). Mechanism of plastid division: from a bacterium to an organelle. *Plant Physiol.* 155, 1533–1544. doi: 10.1104/pp.110.170688

Miyagishima, S.-Y., Froehlich, J. E., and Osteryoung, K. W. (2006). PDV1 and PDV2 mediate recruitment of the dynamin-related protein ARC5 to the plastid division site. *Plant Cell* 18, 2517–2530. doi: 10.1105/tpc.106.045484

Mizusawa, S., and Gottesman, S. (1983). Protein degradation in *Escherichia coli*: the lon gene controls the stability of sulA protein. *Proc. Natl. Acad. Sci. U.S.A.* 80, 358–362. doi: 10.1073/pnas.80.2.358

Nakanishi, H., Suzuki, K., Kabeya, Y., and Miyagishima, S.-Y. (2009). Plant-specific protein MCD1 determines the site of chloroplast division in concert with bacteria-derived MinD. *Curr. Biol.* 19, 151–156. doi: 10.1016/j.cub.2008.12.018

Nazir, A., and Harinarayanan, R. (2016). Inactivation of cell division protein FtsZ by SulA makes Lon indispensable for the viability of a ppGpp0 strain of *Escherichia coli*. *J. Bacteriol.* 198, 688–700. doi: 10.1128/JB.00693-15

Osteryoung, K. W. (1995). Conserved cell and organelle division. *Nature* 376, 473–474. doi: 10.1038/376473b0

Osteryoung, K. W., Stokes, K. D., Rutherford, S. M., Percival, A. L., and Lee, W. Y. (1998). Chloroplast division in higher plants requires members of two functionally divergent gene families with homology to bacterial *ftsZ*. *Plant Cell* 10, 1991–2004. doi: 10.1105/tpc.10.12.1991

Pan, D., Shi, Y., Liu, X., Gao, Y., Liu, Z., and Gao, H. (2013). Genetic mapping and isolation of two *arc3* alleles in *Arabidopsis*. *Plant Cell Rep.* 32, 173–182. doi: 10.1007/s00299-012-1352-7

Pyke, K. A., and Leech, R. M. (1994). A genetic analysis of chloroplast division and expansion in *Arabidopsis thaliana*. *Plant Physiol.* 104, 201–207. doi: 10.1104/pp.104.1.201

Raynaud, C., Cassier-Chauvat, C., Perennes, C., and Bergounioux, C. (2004). An *Arabidopsis* homolog of the bacterial cell division inhibitor SulA is involved in plastid division. *Plant Cell* 16, 1801–1811. doi: 10.1105/tpc.022335

Robertson, E. J., Rutherford, S. M., and Leech, R. M. (1996). Characterization of chloroplast division using the *Arabidopsis* mutant *arc5*. *Plant Physiol.* 112, 149–159. doi: 10.1104/pp.112.1.149

Schmitz, A. J., Glynn, J. M., Olson, B. J., Stokes, K. D., and Osteryoung, K. W. (2009). *Arabidopsis* FtsZ2-1 and FtsZ2-2 are functionally redundant, but FtsZ-based plastid division is not essential for chloroplast partitioning or plant growth and development. *Mol. Plant* 2, 1211–1222. doi: 10.1093/mp/ssp077

Somers, W. S., Stahl, M. L., and Sullivan, F. X. (1998). GDP-fucose synthetase from *Escherichia coli*: structure of a unique member of the short-chain dehydrogenase/reductase family that catalyzes two distinct reactions at the same active site. *Structure* 6, 1601–1612. doi: 10.1016/S0969-2126(98)00157-9

Vaara, M. (1993). Outer membrane permeability barrier to azithromycin, clarithromycin, and roxithromycin in gram-negative enteric bacteria. *Antimicrob. Agents Chemother.* 37, 354–356. doi: 10.1128/AAC.37.2.354

Vitha, S., Froehlich, J. E., Koksharova, O., Pyke, K. A., Van Erp, H., and Osteryoung, K. W. (2003). ARC6 is a J-domain plastid division protein and an evolutionary descendant of the cyanobacterial cell division protein Ftn2. *Plant Cell* 15, 1918–1933. doi: 10.1105/tpc.013292

Wang, W., Li, J., Sun, Q., Yu, X., Zhang, W., Jia, N., et al. (2017). Structural insights into the coordination of plastid division by the ARC6-PDV2 complex. *Nat Plants* 3:17011. doi: 10.1038/nplants.2017.11

Wang, Z. P., Xing, H. L., Dong, L., Zhang, H. Y., Han, C. Y., Wang, X. C., et al. (2015). Egg cell-specific promoter-controlled CRISPR/Cas9 efficiently generates homozygous mutants for multiple target genes in *Arabidopsis* in a single generation. *Genome Biol.* 16:144. doi: 10.1186/s13059-015-0715-0

Yamashita, Y., Tomihisa, K., Nakano, Y., Shimazaki, Y., Oho, T., and Koga, T. (1999). Recombination between *gtfB* and *gtfC* is required for survival of a dTDP-rhamnose synthesis-deficient mutant of *Streptococcus mutans* in the presence of sucrose. *Infect. Immun.* 67, 3693–3697.

Yoshida, Y., Kuroiwa, H., Misumi, O., Nishida, K., Yagisawa, F., Fujiwara, T., et al. (2006). Isolated chloroplast division machinery can actively constrict after stretching. *Science* 313, 1435–1438. doi: 10.1126/science.1129689

Yoshida, Y., Mogi, Y., Terbush, A. D., and Osteryoung, K. W. (2016). Chloroplast FtsZ assembles into a contractible ring via tubulin-like heteropolymerization. *Nat. Plants* 2:16095. doi: 10.1038/nplants.2016.95

Conflict of Interest Statement: The authors declare that the research was conducted in the absence of any commercial or financial relationships that could be construed as a potential conflict of interest.

frontiers in Plant Science

ORIGINAL RESEARCH
published: 15 December 2017
doi: 10.3389/fpls.2017.02154

Deletion of CGLD1 Impairs PSII and Increases Singlet Oxygen Tolerance of Green Alga *Chlamydomonas reinhardtii*

*Jiale Xing[1,2], Peng Liu[1,2], Lei Zhao[1] and Fang Huang[1]**

[1] Key Laboratory of Photobiology, Institute of Botany, Chinese Academy of Sciences, Beijing, China, [2] University of Chinese Academy of Sciences, Beijing, China

The green alga *Chlamydomonas reinhardtii* is a key model organism for studying photosynthesis and oxidative stress in unicellular eukaryotes. Using a forward genetics approach, we have identified and characterized a mutant *x32*, which lacks a predicted protein named CGLD1 (Conserved in Green Lineage and Diatom 1) in GreenCut2, under normal and stress conditions. We show that loss of CGLD1 resulted in minimal photoautotrophic growth and PSII activity in the organism. We observed reduced amount of PSII complex and core subunits in the *x32* mutant based on blue-native (BN)/PAGE and immunoblot analysis. Moreover, *x32* exhibited increased sensitivity to high-light stress and altered tolerance to different reactive oxygenic species (ROS) stress treatments, i.e., decreased resistance to H_2O_2/or tert-Butyl hydroperoxide (t-BOOH) and increased tolerance to neutral red (NR) and rose bengal (RB) that induce the formation of singlet oxygen, respectively. Further analysis via quantitative real-time PCR (qRT-PCR) indicated that the increased singlet-oxygen tolerance of *x32* was largely correlated with up-regulated gene expression of glutathione-*S*-transferases (GST). The phenotypical and physiological implications revealed from our experiments highlight the important roles of CGLD1 in maintaining structure and function of PSII as well as in protection of Chlamydomonas under photo-oxidative stress conditions.

Keywords: *C. reinhardtii*, *x32* mutant, PSII, photo-oxidative stress, singlet oxygen

OPEN ACCESS

Edited by:
Hongbo Gao,
Beijing Forestry University, China

Reviewed by:
Deqiang Duanmu,
Huazhong Agricultural University, China
Wei Huang,
Kunming Institute of Botany (CAS), China

****Correspondence:***
Fang Huang
fhuang@ibcas.ac.cn

Specialty section:
This article was submitted to Plant Physiology, a section of the journal Frontiers in Plant Science

Received: *28 September 2017*
Accepted: *05 December 2017*
Published: *15 December 2017*

Citation:
Xing J, Liu P, Zhao L and Huang F (2017) Deletion of CGLD1 Impairs PSII and Increases Singlet Oxygen Tolerance of Green Alga Chlamydomonas reinhardtii. Front. Plant Sci. 8:2154. doi: 10.3389/fpls.2017.02154

INTRODUCTION

Microalgae are major source of sustainable biofuel feedstock and CO_2 sinks for the future (Brennan and Owende, 2010; Scranton et al., 2015). Compared to higher plants, microalgae have advantages in developing such kind of future because these organisms can be cultivated with CO_2 supply toward reducing greenhouse gas emissions in non-arable areas (Pulz and Gross, 2004; Oey et al., 2013). However, there are limitations in available wild-type strains, including low efficiency of photosynthetic light utilization and high sensitivity to photo-oxidative stress, that impact the algal resource being economically competitive (Wijffels and Barbosa, 2010; Gimpel et al., 2013). To overcome these limitations, generation and characterization of novel mutant strains with desired phenotype is essential.

Chlamydomonas reinhardtii (henceforth referred to as Chlamydomonas) is one of the dominant model organisms for studying photosynthesis and oxidative stress in unicellular eukaryotes (Harris et al., 1989; Dent et al., 2015). This is virtually due to its advances in availability of genetic tools for transformation and selection, fully annotated genome (Merchant et al., 2007) that facilitates molecular genetics and 'omics' studies toward understanding of fundamental biological processes such as photosynthesis and stress responses (Fischer et al., 2005; Gonzalez-Ballester et al., 2010; Blaby et al., 2013, 2015; Heinnickel and Grossman, 2013; Wu et al., 2015), as well as the processes with biofuel significance including H_2 photoproduction (Matthew et al., 2009; Chen et al., 2010; Toepel et al., 2013). Also, the organism is haploid capable of heterotrophic growth in the dark and highly sensitive to light, which makes Chlamydomonas extremely ideal for efficient generation and identification of photo-oxidative mutants such as *sor1* and *sak1* (Dent et al., 2001; Fischer et al., 2012; Wakao et al., 2014). The findings based on the studies of the mutants have improved our understanding of cell response in Chlamydomonas to oxidative stress substantially.

Recent advances in phylogenomics have established the GreenCut2 database which reveals 597 nucleus-encoded proteins conserved in plants and algae (Karpowicz et al., 2011). These proteins are presumed to be central to photosynthetic process (Dent et al., 2015). However, functional significance for more than half of these proteins including CGLD (Conserved in the Green Lineage and Diatom) remains to be experimentally determined (Karpowicz et al., 2011). Using forward genetic approach, we have isolated a number of Chlamydomonas mutants with reduced photosynthetic activity, including *msf1* (Zhao et al., 2017) and *x32* which lacks a predicted protein named CGLD1 encoded by Cre02.g084350. Most recent work from *Arabidopsis thaliana* and *Synechocystis* sp. Strain PCC 6803 showed that the homolog proteins of CGLD1 were presumably involved in efficient uptake of Mn^{2+} to thylakoids (Schneider et al., 2016) or homeostasis of Ca^{2+} or Mn^{2+} in Arabidopsis (Wang et al., 2016) or cyanobacterial cells (Brandenburg et al., 2017; Gandini et al., 2017). In contrast, phenotypic and physiological characterization of *cgld1* mutant in Chlamydomonas, which is a key model system for photosynthesis research with great potential in synthetic biology and application (Scharff and Bock, 2014), is still limited (Dent et al., 2015; Schneider et al., 2016). No sufficient information is available regarding functional significance of CGLD1 in Chlamydomonas under various adverse conditions.

Here, we have investigated phenotypic and physiological characteristics of *x32* mutant under normal and photo-oxidative stress conditions. We show that loss of CGLD1 resulted in minimal photoautotrophic growth and PSII activity in Chlamydomonas. We also show that the amount of PSII core proteins and PSII complex was drastically reduced in *x32*. Furthermore, we found that *x32* mutant exhibits increased photoinhibition and altered tolerance to different reactive oxygen species (ROS) treatments. The increased tolerance to singlet oxygen could be largely attributed to up-regulated gene expression of glutathione-*S*-transferases (GST) in the mutant under such conditions.

MATERIALS AND METHODS

Strains, Culture Conditions, and Stress Treatments

Chlamydomonas reinhardtii wild-type strains CC400 (mt−), 137c (mt+), CC4051 (mt+) and *cgld1* mutant (strain CAL029_02_05) was obtained from the Chlamydomonas Genetics Center[1]. The *x32* mutant was isolated from an insertion mutant library constructed in our laboratory (Zhao et al., 2017) described in more detail below. The algal cells were cultured in TAP (Gorman and Levine, 1965) or in high-salt minimal (HSM) medium under continuous cool-white fluorescent light (60 μmol photons m^{-2} s^{-1}) at 25°C. For all experiments, cells were grown to mid-exponential phase and harvested by centrifugation followed by adjusting the cell density to 2–4 × 10^6 cells ml^{-1}. High-light stress treatment (1,300 μmol photons m^{-2} s^{-1}) was performed according to (Zhao et al., 2013) except that the culture was transferred to flasks (25 ml) and the cell density was adjusted to 2 × 10^6 cells ml^{-1}. ROS stress treatments were done as described (Chen et al., 2016). For mRNA and protein analysis, cells were harvested by centrifugation at 2500 *g* (4°C) for 5 min. After washing once with 0.01 M sodium phosphate buffer (pH 7.4), the cell pellets were stored at −70°C.

Mutant Library Construction and Mutant Isolation with Chlorophyll Fluorescence

The insertion mutant library construction and photosynthetic mutants screen were described (Zhao et al., 2017). Briefly, the wild-type strain (CC400) was used and the mutant library was constructed by transforming this strain via the glass bead method with K*pn*I linearized plasmid pSI103 containing the *aphVIII* gene conferring paromomycin resistance (Kindle, 1990). Transformants that grew on TAP plates with 10 μg ml^{-1} paromomycin (Sigma) were isolated for photosynthetic mutants screening. Mutant screening was based on chlorophyll *a* fluorescence measurements. Sample preparation was done as previously (Zhao et al., 2013) and the measurements were taken with a chlorophyll fluorometer (Maxi-Imaging PAM; Walz, Effeltrich, Germany) by following the manufacturer's instructions. Among the mutants with both the lowest F_v/F_m and Y(II) values, *x32* was chosen for subsequent characterization.

Oxygen Evolution Rate, 77K Fluorescence Emission Spectra and P700 Absorbance Measurements

Oxygen evolution rate of Chlamydomonas was measured as previously described (Sun et al., 2013) with a Chlorolab-2 oxygen electrode (Hansatech, Norfolk, United Kingdom). 77K fluorescence emission spectra were measured with a fluorescence spectrophotometer (F-2500; Hitachi, Japan) as described (Yang

[1]http://www.chlamycollection.org

et al., 2014) with minor changes (Zhao et al., 2017). An excitation wavelength of 435 nm (5 nm bandwidth) was used to induce chlorophyll *a* fluorescence. The emission spectra were recorded (600–750 nm) and normalized at 716 nm. Light-induced redox changes of P700 were monitored by measuring absorbance at 820 nm using PAM101 fluorometer equipped with a dual-wavelength P700 unit (ED800T). Sample preparation was done according to Berry et al. (2011). A far-red light illumination (FR, 720 nm, 24 μmol photons m^{-2} s^{-1}) was provided for 45 s to enable oxidation of P700 to a steady state then turned off to monitor the initial rate of $P700^{+}$ dark reduction according to Klughammer and Schreiber (1998).

Genetic Analysis and Complementation

Genetic analysis and complementation was done as described (Zhao et al., 2017) with minor modifications. For DNA blot analysis, genomic DNA was isolated from wild-type (CC400) and *x32* mutant using the Plant Genomic DNA Kit by following the manufacturer's instructions (Tiangen Biotech; Beijing, China). About 10 μg of genomic DNA was digested overnight with the restriction endonucleases *Kpn*I and *Hind* III (New England Biolabs). The fragments resulting from the digestion were separated by 0.8% agarose gel electrophoresis followed by blotting onto nitrocellulose membranes and hybridizing with the DIG high prime DNA labeling and detection starter kit II from Roche (Catalog NO. 11585614910). The detection was achieved using a chemiluminescent substrate CSPD (Disodium 3-(4-methoxyspiro {l,2-dioxetane-3,2′-(5′-chloro)tricyclo[3.3.1.1^{3,7}]decan}-4-yl) phenyl phosphate) (Catalog NO. 11 755 633 001).

For gene mapping, genomic DNA flanking the *aphVIII* gene was isolated using high efficiency TAIL-PCR with the specific primers listed in Supplementary Table 1 according to (Liu and Chen, 2007) with slight modifications. The primary amplification reactions (20 μL) was composed of 2 μL of PCR buffer (Takara Bio Inc, Otsu, Shiga; Japan), 200 μM of dNTPs (TransGen Biotech; Beijing, China), 1 μM of any of the LAD primers, 0.3 μM of SP0, 0.5 μL of LA Taq (Takara Bio Inc, Otsu, Shiga; Japan) and 20–30 ng of DNA. Each 25-μL secondary reaction contained 2.5 μL of PCR buffer, 200 μM each of dNTPs, 0.3 μM of AC1 and SP1, 0.5 μl of LA Taq, and 1 μL of 50-fold diluted primary product. The amplified products from the secondary reactions were analyzed by agarose gel electrophoresis and were purified prior to sequencing. Sequencing reactions were performed by Sunbiotech (Beijing Sunbiotech; China) and the data were used to search the Chlamydomonas genome.

For tetrad analysis, genetic crosses between *x32* and the wild-type (137c, mt+) and zygote dissection were performed accordingly to (Harris et al., 1989). The mutant was backcrossed twice and four progeny from distinct zygotes of the second generation (T2-*x32*) were obtained. To complement the *x32* mutant, the gene was amplified from wild-type (CC400) with primers listed in Supplementary Table 1. The amplification product was digested with *Nde*I and *Eco*RI and subcloned into similarly treated vector pDble (Fischer and Rochaix, 2001). The constructed plasmids were introduced into *x32* mutant by transformation. The transformants were then analyzed by chlorophyll fluorescence measurements. Colonies that displayed a wild-type phenotype were also analyzed for the integration of *x32* by PCR with the specific primers listed in Supplementary Table 1.

Production of Antiserum against Recombinant CGLD1 Protein

Cloning and heterologous expression were performed as previously described (Chen et al., 2010). Total RNA isolation/purification and reverse transcription reactions were done as described (Sun et al., 2013). Briefly, the coding region of the *CGLD1* gene without transmembrane sequence was amplified by PCR with PrimeSTAR HS DNA Polymerase (Takara, Ohtsu, Japan) using specific primers Pet28-CGLD1-F/R (Supplementary Table 1). The amplified fragment was cloned directly into p*Easy*-blunt vector (Beijing TransGen Biotech, China), which was then transformed into competent *Escherichia coli* DH5α cells. Positive clones containing the recombinant plasmid were selected and sequenced to ensure the authenticity of the ORFs (Beijing Sunbiotech, China). Extraction and purification of *E. coli* proteins were done as described (Zhou et al., 2008). A rabbit serum was produced by MBL (MBL, Nagoya, Japan) using the purified recombinant CGLD1 protein as immunogen. Specificity of the antibody was verified by immunoblotting using proteins extracted from the *E. coli* and Chlamydomonas cells, respectively.

Protein Extraction, BN-PAGE, SDS-PAGE, and Immunoblot Analysis

Cells breakage, isolation of membrane proteins for blue-native (BN)/SDS-PAGE and SDS-PAGE were done as described (Chen et al., 2016). BN gel was prepared and electrophoresis was performed at 4°C with the running program previously reported (Yang et al., 2014) and immunoblot analysis were done according to (Zhao et al., 2013, 2017). The antibodies against D1, D2, CP43, CP47, $Cytb_6f$, and AtpB were from Agrisera and those against PsaB, Lhcb4, and LhcII were from J.-D. Rochaix (University of Geneva). The dilutions for the specific antibodies used in this study were: anti-CGLD1 (1:1000), anti-CP43 and CP47 (1:3000), anti-AtpB (1:4000), anti-D1 and D2 (1:5000), anti-PsaB, $Cytb_6$, LhcII and Lhcb4 (1:10000). The immuno-signal was detected using the Pro-light HRP ECL detection system (Tiangen Biotech; Beijing, China). The blots were scanned using a UMAX Power-Look 2100XL scanner (Willich, Germany). Protein content was determined according to Peterson (1977) using BSA as standard.

qRT-PCR Analysis and Enzyme Activity Assay

Quantitative real-time reverse transcription-PCR (qRT-PCR) was done as described (Zhao et al., 2013) using *CBLP* as the internal control. Gene-specific PCR primer pairs for *psbA* and *psbC* were designed using the online program Primer3[2]. The primer pairs previously reported for *APX1, CAT1, GSTS1*, *GSTS2,* and *GPXH* (Fischer et al., 2012; Pokora et al., 2017) were used and listed in

[2]http://frodo.wi.mit.edu/

Supplementary Table 1. Relative abundance was expressed as the fold change in expression level relative to the reference, calculated as $2^{-\Delta\Delta C_T}$.

For enzyme activity assay, crude extracts preparation and determination of SOD and CAT activity was done as described (Chen et al., 2016).

RESULTS

Phenotypic and Photosynthetic Characteristics of *x32* Mutant

The *x32* mutant was isolated during a genetic screen for Chlamydomonas insertion mutants with decreased photosynthetic activity as described previously (for details see Zhao et al., 2017). **Figure 1** shows that, compared to wild-type, growth of *x32* in TAP and high salt minimal (HSM) medium (**Figure 1A**) was severely repressed, suggesting impaired photosynthesis in the mutant. This was confirmed by the measurements of *in vivo* chlorophyll *a* fluorescence (Imaging PAM, Heinz Walz, Germany). The maximal and effective quantum yield of PSII, F_v/F_m and Y(II), was reduced to the minimal (6.6 and 3.0% of the wild-type level, respectively) (**Figure 1B**). In line with these, the rate of photosynthetic oxygen evolution in *x32* mutant was undetectable (**Figure 1C**). To obtain further functional insights of photosystems in *x32*, low temperature fluorescence (77K) emission spectra of *x32* and wild-type cells were then compared (**Figure 1D**). A differential reduction of the fluorescence emission peak at 686 nm, which is characteristic for PSII mutants (Össenbuhl et al., 2004), was observed in *x32* (**Figure 1D**). This indicates the level of functional PSII in the mutant was significantly lower than wild-type. Since no difference in the light-induced redox kinetics of PSI was revealed between wild-type and the mutant (**Figure 1E**), we conclude that only PSII is affected in the Chlamydomonas mutant *x32*.

The *x32* Mutant Is Deficient in CGLD1 Protein

DNA blot analysis revealed a single insertion of the paromomycin resistance cassette in the genome of *x32* (**Figure 2A**). The insertion site was mapped on the genome of Chlamydomonas via sequencing the flanking regions of the insert through thermal asymmetric interlaced PCR (Liu and Chen, 2007). Analysis of this genomic region in *x32* revealed a DNA rearrangement that resulted in the deletion of five genes, i.e., Cre02.g084250, Cre02.g084300, Cre02.g084350, Cre02.g084400, and Cre02.g084450 (**Figure 2B**). Prediction by PredAlgo software[3] shows that only the gene Cre02.g084350 encoding CGLD1 in the GreenCut2 (Karpowicz et al., 2011) is localized in the chloroplast. We therefore introduced the gene into *x32* for complementation. The *x32* mutant phenotype could be fully rescued in the complemented strains (C15, C19) based on growth, F_v/F_m and Y(II) values (**Figure 1A**). Analysis of genetic crosses between *x32* mutant and wild-type was in agreement with these data (Supplementary Figures 1A,B). The photosynthetic defect of *x32* co-segregated with paromomycin resistance in six complete tetrads analyzed, suggesting that the phenotype is linked to this genetic disruption.

To further confirm the candidate gene, we compared the phenotype of *x32* and another *cgld1* mutant obtained from the Chlamydomonas Resource Center[4], which was derived from wild-type strain CC4051 with an insertion in exon2 of the *CGLD1* gene (Dent et al., 2015; Schneider et al., 2016), in the presence of additional manganese (Mn^{2+}) and calcium (Ca^{2+}) (Supplementary Figure 1C). The similar results of growth profiles and F_v/F_m values of the two *cgld1* mutants (Schneider et al., 2016; Supplementary Figure 1C) verify that disruption of *CGLD1* is the cause of the phenotype observed in *x32*.

In the genome of Chlamydomonas, CGLD1 is annotated as a predicted protein (Phytozome v12.1[5]). To determine the expression of CGLD1 protein in wild-type Chlamydomonas and verify the lack of CGLD1 in *x32*, we generated an antibody against recombinant CGLD1 protein and verified its specificity by immunoblotting using protein extracts from the wild-type Chlamydomonas (**Figure 2C**). Heterologous expression and purification of the recombinant CGLD1 protein was performed as previously reported (Zhou et al., 2008; Sun et al., 2013; Zhao et al., 2017). As shown in **Figure 2C**, the *E. coli* Transetta (DE3) cells produced a substantial amount of the expected recombinant protein possessing an estimated molecular mass of 15 kDa. This corresponds to the molecular mass calculated from the coding region of Chlamydomonas *CGLD1* gene without the transmembrane sequences (**Figure 2C**, left panel). Total proteins extracted from the *E. coli* cells and Chlamydomonas cells were analyzed by immunoblotting with the antibody. A single band at 28 and 15 kDa was detected in wild-type Chlamydomonas and *E. coli* expressing the recombinant CGLD1 protein (**Figure 2C**, right panel), respectively. The former corresponds to the molecular mass that was calculated from the coding sequence of *CGLD1* gene in Chlamydomonas. Since no band was detected in *x32* mutant (**Figure 2C**, right panel), this antibody was therefore used for quantification of CGLD1 in wild-type, *x32* and the complemented (C15, C19) strains (**Figure 2D**).

Reduced Accumulation of PSII in *x32* Mutant

The decreased PSII activity of *x32* could be due to reduced accumulation of thylakoid membrane proteins. To clarify this, we analyzed membrane protein complexes of *x32* and wild-type cells by blue-native (BN)/SDS-PAGE using a slightly modified protocol (Yang et al., 2014) as described (Chen et al., 2016). As shown in **Figure 3A**, the overall BN-gel profile of thylakoid membranes isolated from wild-type was similar to earlier reported (Dewez et al., 2009; Chen et al., 2016), demonstrating high technical reproducibility of the BN-PAGE from different experiments. Comparision of the BN-PAGE gel pattern between wild-type and *x32* revealed a clear reduction of the band

[3]https://giavap-genomes.ibpc.fr/cgi-bin/predalgodb.perl?page=main

[4]http://www.chlamycollection.org

[5]https://phytozome.jgi.doe.gov

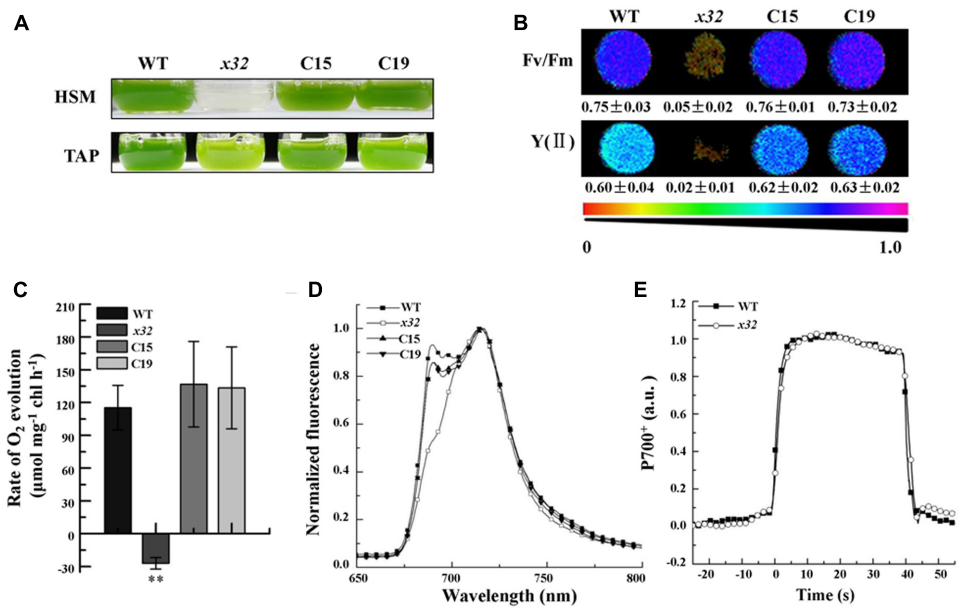

FIGURE 1 | Growth and photosynthetic characters of wild-type (WT), *x32* and the complemented strains (C15 and C19). **(A)** Growth in HSM and TAP medium with an irradiance of 60 μmol photons m^{-2} s^{-1} for 6 and 3 days, respectively. **(B)** Maximal (F_v/F_m) and effective quantum yield of PSII (YII) of the indicated strains. Standard deviations were estimated from three biological replicates. All experiments were repeated twice with similar results. **(C)** Rate of O_2 evolution in different strains. Standard deviations were estimated from three biological replicates. All experiments were repeated twice with similar results. $^{**}p$-value < 0.01 in Student's *t*-test. **(D)** 77K fluorescence emission spectra of the indicated strains. The spectra were normalized at 716 nm. All experiments were repeated twice with similar results. **(E)** Light-induced redox kinetics of P700 in wild-type (WT) and *x32* mutant. All experiments were repeated twice with similar results.

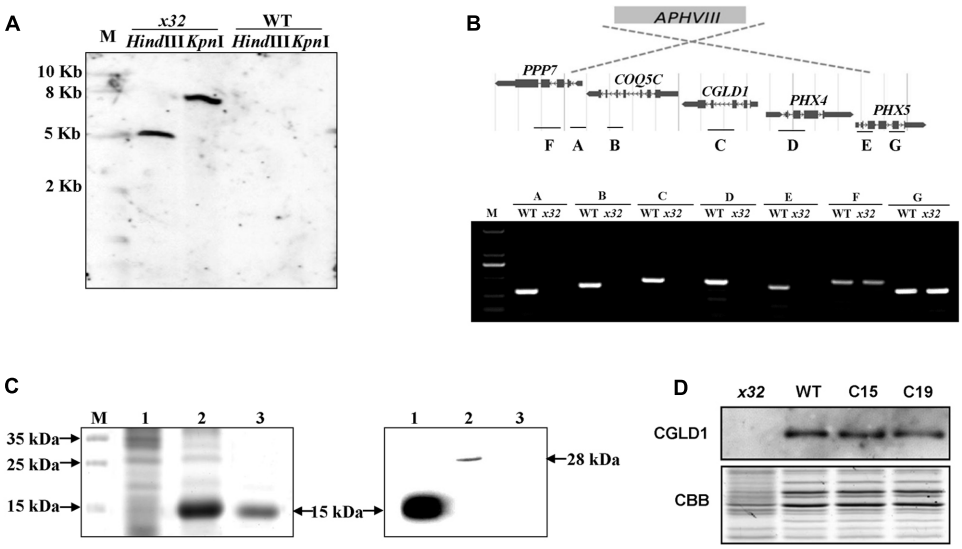

FIGURE 2 | Genetic analysis of the *x32* mutant. **(A)** DNA blot analysis of wild-type and *x32*. Genomic DNA was digested with *Hind*III and *Kpn*I, fractionated by agarose gel electrophoresis and hybridized with a DNA probe of 407bp of *APHVIII* gene. **(B)** Mapping of the deletion in *x32* caused by insertion of the paromomycin resistance cassette (*APHVIII*) by comparative analysis of wild-type and *x32* DNA using PCR specific primer pairs. **(C)** Heterologous expression of recombinant CGLD1 protein and specificity of CGLD1 antibody. Coomassie-stained SDS-PAGE gel separating proteins extracted from *Escherichia coli* cells (left panel). M, protein molecular mass marker. 1 and 2, total proteins without or with isopropyl β-D-1-thiogalactopyranoside (IPTG) induction, respectively. 3, recombinant CGLD1 purified using Ni-NTA column. Specificity detection of the CGLD1 antibody by immunoblotting (right panel). Lane 1, purified recombinant CGLD1 protein (0.02 μg). Lanes 2 and 3, proteins (20 μg) extracted from wild-type and *x32*, respectively. **(D)** Immunoblot detection of CGLD1 in wild-type, *x32* and the complemented strains C15 and C19. Membrane proteins (20 μg per lane) were separated by SDS-PAGE (16%) followed by immunoblotting with the CGLD1 antibody.

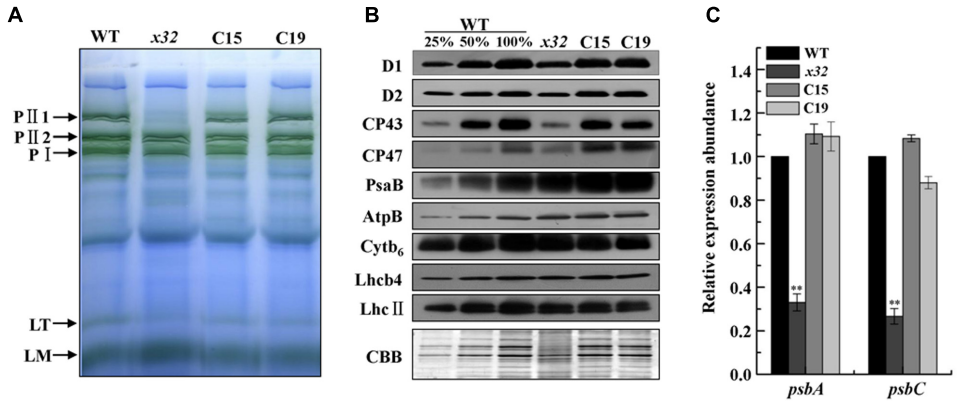

FIGURE 3 | Abundance of photosynthetic proteins and complexes in thylakoid membranes of WT, *x32* and the complemented strains (C15 and C19). **(A)** BN-PAGE of the thylakoid membranes. DM-solubilized membrane proteins (25 μg per lane) were separated by BN-PAGE. PII1, PII2, PSII supercomplexes; PI, PSI-LHCI complex; LT, LHCII trimer; LM, LHCII monomer. Similar results were obtained in two independent experiments. **(B)** Immunoblot detection of various photosynthetic proteins. Membrane proteins (10 μg per lane) were separated by 12% SDS-PAGE followed by immunoblot detection of indicated proteins. A dilution series of wild-type protein extract was used to quantify the amount of proteins in *x32*. Similar results were obtained in at least three independent experiments. **(C)** qRT-PCR analysis of mRNA levels of *psbA* and *psbC* in the indicated strains. Standard deviations were estimated from three biological replicates. Similar results were obtained in three independent experiments. *CBLP* gene was used as a control. $^{**}p$-value < 0.01 in Student's *t*-test.

corresponding to a PSII supercomplex, PII1 containing core subunits of PSII (D1, D2, CP43, CP47) (Rexroth et al., 2003; Dewez et al., 2009), in the mutant (**Figure 3A**). This was further confirmed by immunoblotting using the antibodies specific for key proteins of photosynthetic apparatus (**Figure 3B**). The levels of core subunits of PSII (D1, D2, CP43, and CP47) in *x32* were 30% or less of that in wild-type whereas the levels of the key subunits of PSI (PsaB), Cytb_6f (Cytb_6), and ATP synthase (AtpB) as well as the LHCII proteins (LhcII and Lhcb4) remained unchanged in *x32* (**Figure 3B**). To test whether the reduced levels of the core PSII proteins in *x32* was due to limited transcription, we then compared the *psbA* and *psbC* mRNA levels between wild-type and *x32* by quantitative real-time PCR (qRT-PCR) analysis. The transcript level of both genes was decreased 67.2% (*psbA*) and 68.3% (*psbC*) in relation to the wild-type (**Figure 3C**). Thus, these experimental data demonstrate a significant and specific impact of CGLD1 on PSII at both mRNA and protein level in Chlamydomonas.

Increased Sensitivity to High-Light and Peroxide Stress in *x32*

To determine potential physiological roles of CGLD1 protein in Chlamydomonas under adverse condition, we performed various stress experiments. Because high-light is the most common stress condition occurring to photosynthetic organisms and Chlamydomonas is a key model system for studying photo-oxidative stress in unicellular eukaryotes, we compared CGLD1 levels of wild-type cells after treatments with high-light (1,300 μmol photons m^{-2} s^{-1}) and different ROS, i.e., H_2O_2, neutral red (NR) and rose bengal (RB). The stress treatments were done as described (Zhao et al., 2013; Chen et al., 2016) and the CGLD1 protein was monitored using immunoblot analyses. As shown in **Figure 4A**, the amount of CGLD1 was in most cases increased after these stress treatments, indicating that this protein is also involved in photoinhibition/photoprotection against photo-oxidative stress in the organism. To confirm these, we then investigated the sensitivity of *x32* to high-light stress treatment (**Figure 4B**). As expected, cell growth of *x32* was significantly repressed during high-light stress treatment (1,300 μmol photons m^{-2} s^{-1}) compared to wild-type (**Figure 4B**). The remarkable reduction of cell growth was observed upon exposure of *x32* to high light for 40 min. This was more apparent based on F_v/F_m values (**Figure 4B**, right panel), suggesting increased photoinhibition in the mutant.

To determine whether the tolerance of *x32* mutant to oxidative stress was changed due to loss of CGLD1, we also compared the sensitivity of *x32* and wild- type cells to different ROS treatments. Similar results were obtained with wild-type strain in the present (**Figure 4B**) and earlier investigations (Chen et al., 2016). However, the *x32* mutant was more sensitive to H_2O_2 and tert-Butyl hydroperoxide (t-BOOH) than wild-type (**Figure 4C**, upper panel). Correlated with this, both gene expression of ascorbate peroxidase 1 (*APX1*) and catalase 1 (*CAT1*) (Supplementary Figure 2), which are known to be H_2O_2-responsive marker genes (Wakao et al., 2014), as well as the increase of activity of superoxide dismutases (SOD) and catalases (CAT), which are the dominant ROS scavenging enzymes known to be present in the chloroplasts, was less pronounced in *x32* mutant than in wild-type (Supplementary Figure 3). Interestingly, our experimental data shows that *x32* was more resistant to neutral red (NR) and rose bengal (RB) than wild-type (**Figure 4B**, lower panel). These observations raise the possibility that anti-singlet oxygen response is enhanced in *x32* mutant under such stress conditions.

Up-Regulated *GSTS* Expression in *x32* Mutant

To test the possibility mentioned above, we measured the mRNA levels of several key genes encoding glutathione-*S*-transferases

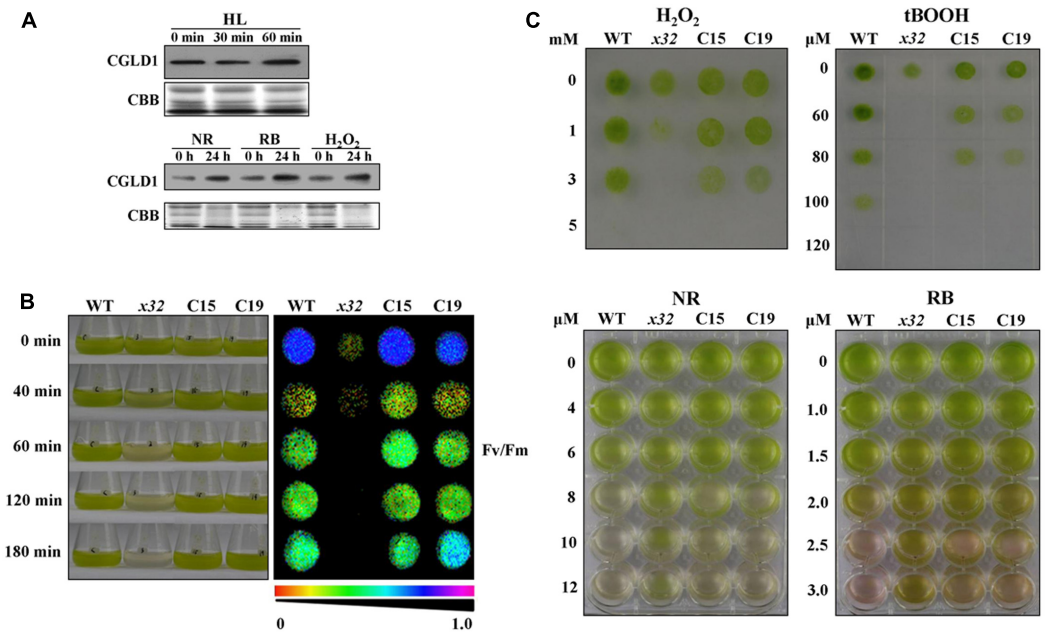

FIGURE 4 | High-light and ROS-stress tolerance of WT, *x32* and the complemented strains (C15 and C19). **(A)** Immunoblot analyses of CGLD1 amounts in Chlamydomonas under high-light (HL; 1,300 μmol photons m^{-2} s^{-1}) and ROS-stress conditions. Membrane proteins (10 μg per lane) were separated by SDS-PAGE (16%) followed by immunoblotting with the CGLD1 antibody. Similar results were obtained in three independent experiments. **(B)** Growth and quantum yield of PSII (F_v/F_m) of the indicated strains under high-light treatment (1,300 μmol photons m^{-2} s^{-1}). Similar results were obtained in at least three independent experiments. **(C)** ROS tolerance of the indicated strains. Growth recovery after treatment with H_2O_2, t-BOOH (tert-Butyl hydroperoxide) followed by spotting on TAP plates for 3 days (upper). Growth after treatment with NR (neutral red) and RB (rose bengal). Similar results were obtained in at least three independent experiments.

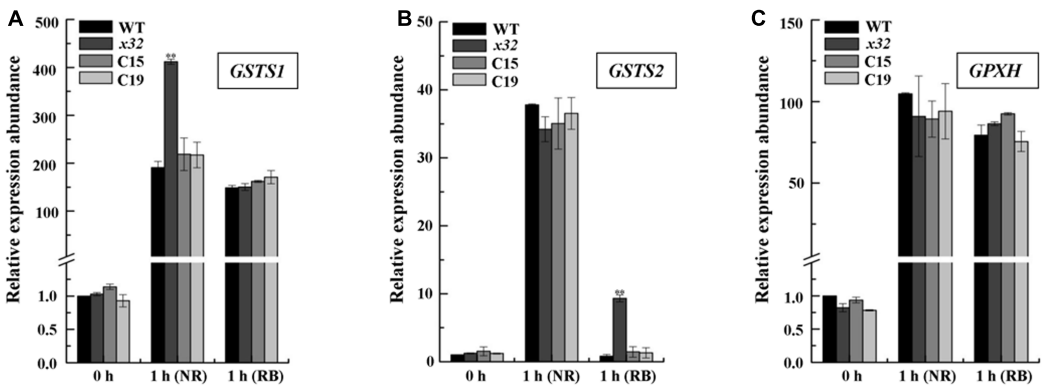

FIGURE 5 | Up-regulated *GSTS* expression in *x32* mutant under singlet oxygen stress. qRT-PCR analysis of expression of *GSTS1* **(A)**, *GSTS2* **(B)**, and *GPXH* **(C)** in WT, *x32* and the complemented strains (C15 and C19) treated with NR and RB, respectively. Standard deviations were estimated from three biological replicates. Similar results were obtained in at least three independent experiments. *CBLP* gene was used as a control. *p-values < 0.05, **$p < 0.01$ in Student's t-test, respectively.

and thioredoxin peroxidase, i.e., *GSTS* and *GPXH*, that are known to be involved in singlet oxygen-induced acclimation process in Chlamydomonas (Leisinger et al., 2001; Fischer et al., 2005, 2009; Ledford et al., 2007) using qRT-PCR. Total mRNA isolated from different strains treated with NR or RB was subjected for the analysis. **Figure 5** shows that expression of these genes was in most cases increased in all strains. The fold-increase of expression in wild-type was similar to the earlier report (Fischer et al., 2005). In *x32*, a differential increase pattern of expression was observed compared to that in wild-type (**Figures 5A–C**). Higher expression of *GSTS1* and *GSTS2* in *x32* was most remarkable under NR (2.3-fold) and RB (8.9-fold) treatment, respectively. Based on these experimental results, we conclude that the singlet-oxygen resistance observed in the mutant could be largely attributed to the up-regulated expression of *GST* genes.

DISCUSSION

In this work, we have isolated and characterized *x32* mutant lacking CGLD1, a predicted protein belongs to the GreenCut2 superfamily, in Chlamydomonas. We have provided direct experimental evidence of CGLD1 in maintaining structure and function of PSII as well as in protecting Chlamydomonas against photo-oxidative stress. New insights revealed in this work are discussed below.

In the genome of Chlamydomonas. CGLD1 is annotated as a predicted protein with unknown function (Phytozome v12.1[6]). Using a forward genetics approach, we have determined its important and specific role in PSII functionality of this organism (**Figures 1**, **3**). This finding is somewhat different from that reported in Arabidopsis and Synechocystis, showing that not only PSII supercomplex but also PSI complex was significantly reduced (Schneider et al., 2016; Gandini et al., 2017). Indeed, functional and structural analysis of the photosystems, i.e., low temperature fluorescence (77K) emission spectra and light-induced redox kinetics of P700, BN-PAGE and immunoblot quantifications (**Figures 1**, **3**), allows us to propose a crucial role of CGLD1 for maintaining PSII in Chlamydomonas. Also, based on the genomic information, we have generated a specific antibody against CGLD1 and verified the expression of *CGLD1* in wild-type Chlamydomonas (**Figure 2**). These are novel and direct experimental evidence of presence and major function of CGLD1 protein in Chlamydomonas.

Similar to the observations in Arabidopsis and the original *cgld1* mutant (Schneider et al., 2016), which was derived from a different wild-type Chlamydomonas strain (Dent et al., 2015), supplementation of excess Mn^{2+} rather than Ca^{2+} could largely restored the photosynthetic activity (F_v/F_m) in *x32* mutant (Supplementary Figure 1). These consistent results obtained from different Chlamydomonas strains as well as the cyanobacterium Synechocystis (Brandenburg et al., 2017; Gandini et al., 2017), strongly support the suggestion that CGLD1 is involved in uptake/maintenance of Mn^{2+} homeostasis in photosynthetic organisms. Nevertheless, how this is exactly elicited in chloroplast and cyanobacteria remains an open question. Although direct experimental evidences are currently lacking it is presumed that in Arabidopsis the homolog of CGLD1 (PAM71) functions in Mn^{2+} uptake into thylakoids for optimal PSII performance (Schneider et al., 2016). In Chlamydomonas, it is not fully understood how deletion of CGLD1 impaires PSII under normal growth condition. Based on the similar photosynthetic phenotype of Chlamydomonas and Arabidopsis in response to excess Mn^{2+} (Supplementary Figure 1; Schneider et al., 2016), it could be postulated that CGLD1 protein in Chlamydomonas functions in the similar way that proposed for its homolog in Arabidopsis (Schneider et al., 2016) under normal growth condition.

No information is available so far characterizing the expression of CGLD1 protein under adverse conditions including high-light irradiation and oxidative stress. Our finding of elevated level of CGLD1 protein in wild-type Chlamydomonas cells after these treatments (**Figure 4**) implicates its putative function in photo-oxidative responses. Physiological significance of CGLD1 under these stress conditions was demonstrated by the distinct phenotype of wild-type and *x32* (**Figure 4**). Based on the increased sensitivity of the mutant to high-light and peroxide stress, we propose that CGLD1 is also involved in photoinhibition or photodamage/repair of PSII. Since D1 protein is widely accepted as the primary target damaged during photoinhibition *in vivo* (Mulo et al., 2012) and a repair mechanism which involves an intricate and multi-step process operates in all photosynthetic organisms (Nixon et al., 2010; Nickelsen and Rengstl, 2013), we could speculate that deletion of CGLD1 may impact efficient PSII repair (including D1 synthesis) in the organism. Further research is directed toward in-depth understanding of the underlying molecular mechanisms.

Interestingly, we found different response patterns of *x32* to photo-oxidative stress in comparison with wild-type Chlamydomonas. While higher sensitivity of the mutant to high-light and peroxide stress, as frequently reported for PSII mutants as well as the reduced SOD and CAT activity in *x32* treated with H_2O_2 (Supplementary Figure 3), was expected, the increased tolerance to singlet-oxygen stress was for the first time revealed in a Chlamydomonas mutant lacking CGLD1 (**Figure 4**). The reason for this novel phenotype of *x32* is currently unclear. In *sor1* mutant, which lacks a basic leucine zipper transcription factor, the singlet-oxygen resistance has been mainly attributed to up-regulated expression of the stress responsive genes *GSTS* and *GPXH* in Chlamydomonas (Fischer et al., 2012). Our finding of up-regulated *GSTS* expression in *x32* under singlet oxygen stress (**Figure 5**) is of indication that the detoxifying system described in *sor1* is also reinforced in this mutant under such stress conditions. Moreover, it has been previously reported that non-photochemical quenching (NPQ) was increased compared to the wild-type (Dent et al., 2015). Considering that NPQ is one of the efficient modules in photoprotection, we would presume that the NPQ mechanism is also enhanced in *x32* mutant lacking CGLD1 and contributes at least partially to its increased resistance to singlet oxygen stress.

In summary, the present work determined expression and functional significance of CGLD1 in Chlamydomonas. Loss of CGLD1 leads to minimal photoautotrophic growth and PSII activity in *x32* mutant. Biochemical analysis of *x32* revealed that the steady levels of PSII supercomplex and core proteins was dramatically reduced compared to wild-type. Furthermore, we found that *x32* was, due to loss of CGLD1, more tolerant to singlet oxygen stress than wild-type. Correlated with this, up-regulated *GSTS* expression was found increased more in *x32*. The phenotypical and physiological implications revealed from this study provide important information for in-depth studies toward understanding structure and function of CGLD1 in Chlamydomonas as well as a valuable alga strain with increased resistance to singlet oxygen stress for potential applications.

[6]https://phytozome.jgi.doe.gov

AUTHOR CONTRIBUTIONS

JX and FH conceived the research and designed the experiments. JX, PL, and LZ performed the experiments. JX and FH analyzed data and wrote the manuscript.

FUNDING

This study was supported by grants from the National Natural Science Foundation of China (Nos. 31670239, 31470340), National Basic Research Program of China (973 Program, No. 2015CB150100) and the funding from the Strategic Priority Research Program (Nos. XDB17000000; KGCX2-YW-373) of Chinese Academy of Sciences.

SUPPLEMENTARY MATERIAL

The Supplementary Material for this article can be found online at: https://www.frontiersin.org/articles/10.3389/fpls.2017.02154/full#supplementary-material

REFERENCES

Berry, L. L., Brzezowski, P., and Wilson, K. E. (2011). Inactivation of the STT7 gene protects PsaF-deficient *Chlamydomonas reinhardtii* cells from oxidative stress under high light. *Physiol. Plant.* 141, 188–196. doi: 10.1111/j.1399-3054.2010.01421.x

Blaby, I. K., Blaby-Haas, C. E., Perez-Perez, M. E., Schmollinger, S., Fitz-Gibbon, S., Lemaire, S. D., et al. (2015). Genome-wide analysis on *Chlamydomonas reinhardtii* reveals the impact of hydrogen peroxide on protein stress responses and overlap with other stress transcriptomes. *Plant J.* 84, 974–988. doi: 10.1111/tpj.13053

Blaby, I. K., Glaesener, A. G., Mettler, T., Fitz-Gibbon, S. T., Gallaher, S. D., Liu, B., et al. (2013). Systems-level analysis of nitrogen starvation–induced modifications of carbon metabolism in a *Chlamydomonas reinhardtii* starchless mutant. *Plant Cell* 25, 4305–4323. doi: 10.1105/tpc.113.117580

Brandenburg, F., Schoffman, H., Kurz, S., Kramer, U., Keren, N., Weber, A. P. M., et al. (2017). The *Synechocystis* manganese exporter Mnx is essential for manganese homeostasis in Cyanobacteria. *Plant Physiol.* 173, 1798–1810. doi: 10.1104/pp.16.01895

Brennan, L., and Owende, P. (2010). Biofuels from microalgae-a review of technologies for production, processing, and extractions of biofuels and co-products. *Renew. Sustain. Energy Rev.* 14, 557–577. doi: 10.1016/j.rser.2009.10.009

Chen, M., Zhang, J., Zhao, L., Xing, J., Peng, L., Kuang, T., et al. (2016). Loss of algal proton gradient regulation 5 increases reactive oxygen species scavenging and H2 evolution. *J. Integr. Plant Biol.* 58, 943–946. doi: 10.1111/jipb.12502

Chen, M., Zhao, K., Sun, Y. L., Cui, S. X., Zhang, L. F., Yang, B., et al. (2010). Proteomic analysis of hydrogen photoproduction in sulfur-deprived *Chlamydomonas* cells. *J. Proteome Res.* 9, 3854–3866. doi: 10.1021/pr100076c

Dent, R. M., Han, M., and Niyogi, K. K. (2001). Functional genomics of plant photosynthesis in the fast lane using *Chlamydomonas reinhardtii*. *Trends Plant Sci.* 6, 364–371. doi: 10.1016/S1360-1385(01)02018-0

Dent, R. M., Sharifi, M. N., Malnoe, A., Haglund, C., Calderon, R. H., Wakao, S., et al. (2015). Large-scale insertional mutagenesis of *Chlamydomonas* supports phylogenomic functional prediction of photosynthetic genes and analysis of classical acetate-requiring mutants. *Plant J.* 82, 337–351. doi: 10.1111/tpj.12806

Dewez, D., Park, S., Garcia-Cerdan, J. G., Lindberg, P., and Melis, A. (2009). Mechanism of REP27 protein action in the D1 protein turnover and photosystem II repair from photodamage. *Plant Physiol.* 151, 88–99. doi: 10.1104/pp.109.140798

Fischer, B. B., Dayer, R., Schwarzenbach, Y., Lemaire, S. D., Behra, R., Liedtke, A., et al. (2009). Function and regulation of the glutathione peroxidase homologous gene GPXH/GPX5 in *Chlamydomonas reinhardtii*. *Plant Mol. Biol.* 71, 569–583. doi: 10.1007/s11103-009-9540-8

Fischer, B. B., Krieger-Liszkay, A., and Eggen, R. I. L. (2005). Oxidative stress induced by the photosensitizers neutral red (type I) or rose Bengal (type II) in the light causes different molecular responses in *Chlamydomonas reinhardtii*. *Plant Sci.* 168, 747–759. doi: 10.1016/j.plantsci.2004.10.008

Fischer, B. B., Ledford, H. K., Wakao, S., Huang, S. G., Casero, D., Pellegrini, M., et al. (2012). SINGLET OXYGEN RESISTANT 1 links reactive electrophile signaling to singlet oxygen acclimation in *Chlamydomonas reinhardtii*. *Proc. Natl. Acad. Sci. U.S.A.* 109, E1302–E1311. doi: 10.1073/pnas.1116843109

Fischer, N., and Rochaix, J. D. (2001). The flanking regions of PsaD drive efficient gene expression in the nucleus of the green alga *Chlamydomonas reinhardtii*. *Mol. Genet. Genomics* 265, 888–894. doi: 10.1007/s004380100485

Gandini, C., Schmidt, S. B., Husted, S., Schneider, A., and Leister, D. (2017). The transporter SynPAM71 is located in the plasma membrane and thylakoids, and mediates manganese tolerance in *Synechocystis* PCC6803. *New Phytol.* 215, 256–268. doi: 10.1111/nph.14526

Gimpel, J. A., Specht, E. A., Georgianna, D. R., and Mayfield, S. P. (2013). Advances in microalgae engineering and synthetic biology applications for biofuel production. *Curr. Opin. Chem. Biol.* 17, 489–495. doi: 10.1016/j.cbpa.2013.03.038

Gonzalez-Ballester, D., Casero, D., Cokus, S., Pellegrini, M., Merchant, S. S., and Grossman, A. R. (2010). RNA-Seq analysis of sulfur-deprived *Chlamydomonas* cells reveals aspects of acclimation critical for cell survival. *Plant Cell* 22, 2058–2084. doi: 10.1105/tpc.109.071167

Gorman, D. S., and Levine, R. P. (1965). Cytochrome F and plastocyanin - their sequence in photosynthetic electron transport chain of *Chlamydomonas reinhardtii*. *Proc. Natl. Acad. Sci. U.S.A.* 54, 1665–1669. doi: 10.1073/pnas.54.6.1665

Harris, E. H., Burkhart, B. D., Gillham, N. W., and Boynton, J. E. (1989). Antibiotic-resistance mutations in the chloroplast 16s and 23s rRNA genes of *Chlamydomonas reinhardtii*: correlation of genetic and physical maps of the chloroplast genome. *Genetics* 123, 281–292.

Heinnickel, M. L., and Grossman, A. R. (2013). The GreenCut: re-evaluation of physiological role of previously studied proteins and potential novel protein functions. *Photosynth. Res.* 116, 427–436. doi: 10.1007/s11120-013-9882-6

Karpowicz, S. J., Prochnik, S. E., Grossman, A. R., and Merchant, S. S. (2011). The GreenCut2 resource, a phylogenomically derived inventory of proteins specific to the plant lineage. *J. Biol. Chem.* 286, 21427–21439. doi: 10.1074/jbc.M111.233734

Kindle, K. L. (1990). High-frequency nuclear transformation of *Chlamydomonas reinhardtii*. *Proc. Natl. Acad. Sci. U.S.A.* 87, 1228–1232. doi: 10.1073/pnas.87.3.1228

Klughammer, C., and Schreiber, U. (1998). Measuring P700 absorbance changes in the near infrared spectral region with a dual wavelength pulse modulation system. *Photosynth. Mech. Effects* I–V, 4357–4360. doi: 10.1007/978-94-011-3953-3_1008

Ledford, H. K., Chin, B. L., and Niyogi, K. K. (2007). Acclimation to singlet oxygen stress in *Chlamydomonas reinhardtii*. *Eukaryot. Cell* 6, 919–930. doi: 10.1128/Ec.00207-06

Leisinger, U., Rufenacht, K., Fischer, B., Pesaro, M., Spengler, A., Zehnder, A. J. B., et al. (2001). The glutathione peroxidase homologous gene from *Chlamydomonas reinhardtii* is transcriptionally up-regulated by singlet oxygen. *Plant Mol. Biol.* 46, 395–408. doi: 10.1023/A:1010601424452

Liu, Y. G., and Chen, Y. (2007). High-efficiency thermal asymmetric interlaced PCR for amplification of unknown flanking sequences. *Biotechniques* 43, 649–656. doi: 10.2144/000112601

Matthew, T., Zhou, W. X., Rupprecht, J., Lim, L., Thomas-Hall, S. R., Doebbe, A., et al. (2009). The metabolome of *Chlamydomonas reinhardtii* following induction of anaerobic H_2 production by sulfur depletion. *J. Biol. Chem.* 284, 23415–23425. doi: 10.1074/jbc.M109.003541

Merchant, S. S., Prochnik, S. E., Vallon, O., Harris, E. H., Karpowicz, S. J., Witman, G. B., et al. (2007). The *Chlamydomonas* genome reveals the evolution of key animal and plant functions. *Science* 318, 245–251. doi: 10.1126/science.1143609

Mulo, P., Sakurai, I., and Aro, E.-M. (2012). Strategies for psbA gene expression in cyanobacteria, green algae and higher plants: from transcription to PSII repair. *Biochim. Biophys. Acta* 1817, 247–257. doi: 10.1016/j.bbabio.2011.04.011

Nickelsen, J., and Rengstl, B. (2013). Photosystem II assembly: from cyanobacteria to plants. *Annu. Rev. Plant Biol.* 64, 609–635. doi: 10.1146/annurev-arplant-050312-120124

Nixon, P. J., Michoux, F., Yu, J. F., Boehm, M., and Komenda, J. (2010). Recent advances in understanding the assembly and repair of photosystem II. *Ann. Bot.* 106, 1–16. doi: 10.1093/aob/mcq059

Oey, M., Ross, I. L., Stephens, E., Steinbeck, J., Wolf, J., Radzun, K. A., et al. (2013). RNAi Knock-Down of LHCBM1, 2 and 3 increases photosynthetic H2 production efficiency of the green alga *Chlamydomonas reinhardtii*. *PLOS ONE* 8:e61375. doi: 10.1371/journal.pone.0061375

Össenbuhl, F., Gohre, V., Meurer, J., Krieger-Liszkay, A., Rochaix, J. D., and Eichacker, L. A. (2004). Efficient assembly of photosystem II in *Chlamydomonas reinhardtii* requires Alb3.1p, a homolog of Arabidopsis ALBINO3. *Plant Cell* 16, 1790–1800. doi: 10.1105/tpc.023226

Peterson, G. L. (1977). A simplification of the protein assay method of Lowry et al. which is more generally applicable. *Anal. Biochem.* 83, 346–356. doi: 10.1016/0003-2697(77)90043-4

Pokora, W., Aksmann, A., Bascik-Remisiewicz, A., Dettlaff-Pokora, A., Rykaczewski, M., Gappa, M., et al. (2017). Changes in nitric oxide/hydrogen peroxide content and cell cycle progression: study with synchronized cultures of green alga *Chlamydomonas reinhardtii*. *J. Plant Physiol.* 208, 84–93. doi: 10.1016/j.jplph.2016.10.008

Pulz, O., and Gross, W. (2004). Valuable products from biotechnology of microalgae. *Appl. Microbiol. Biotechnol.* 65, 635–648. doi: 10.1007/s00253-004-1647-x

Rexroth, S., Meyer, J. M. W., Tittingdorf, Z., Frank Krause, F., Dencher, N. A., and Seelert, H. (2003). Thylakoid membrane at altered metabolic state: challenging the forgotten realms of the proteome. *Electrophoresis* 24, 2814–2823. doi: 10.1002/elps.200305543

Scharff, L. B., and Bock, R. (2014). Synthetic biology in plastids. *Plant J.* 78, 783–798. doi: 10.1111/tpj.12356

Schneider, A., Steinberger, I., Herdean, A., Gandini, C., Eisenhut, M., Kurz, S., et al. (2016). The evolutionarily conserved protein PHOTOSYNTHESIS AFFECTED MUTANT71 is required for efficient manganese uptake at the thylakoid membrane in Arabidopsis. *Plant Cell* 28, 892–910. doi: 10.1105/tpc.15.00812

Scranton, M. A., Ostrand, J. T., Fields, F. J., and Mayfield, S. P. (2015). *Chlamydomonas* as a model for biofuels and bio-products production. *Plant J.* 82, 523–531. doi: 10.1111/tpj.12780

Sun, Y. L., Chen, M., Yang, H. M., Zhang, J., Kuang, T. Y., and Huang, F. (2013). Enhanced H_2 photoproduction by down-regulation of ferredoxin-$NADP^+$ reductase (FNR) in the green alga *Chlamydomonas reinhardtii*. *Int. J. Hydrogen Energy* 38, 16029–16037. doi: 10.1016/j.ijhydene.2013.10.011

Toepel, J., Illmer-Kephalides, M., Jaenicke, S., Straube, J., May, P., Goesmann, A., et al. (2013). New insights into *Chlamydomonas reinhardtii* hydrogen production processes by combined microarray/RNA-seq transcriptomics. *Plant Biotechnol. J.* 11, 717–733. doi: 10.1111/pbi.12062

Wakao, S., Chin, B. L., Ledford, H. K., Dent, R. M., Casero, D., Pellegrini, M., et al. (2014). Phosphoprotein SAK1 is a regulator of acclimation to singlet oxygen in *Chlamydomonas reinhardtii*. *eLife* 3:e02286. doi: 10.7554/eLife.02286

Wang, C., Xu, W. T., Jin, H. L., Zhang, T. J., Lai, J. B., Zhou, X., et al. (2016). A putative chloroplast-localized Ca^{2+}/H^+ antiporter CCHA1 is involved in calcium and pH homeostasis and required for PSII function in *Arabidopsis*. *Mol. Plant* 9, 1183–1196. doi: 10.1016/j.molp.2016.05.015

Wijffels, R. H., and Barbosa, M. J. (2010). An outlook on microalgal biofuels. *Science* 330, 796–799. doi: 10.1126/science.1189003

Wu, G. X., Hufnagel, D. E., Denton, A. K., and Shiu, S. H. (2015). Retained duplicate genes in green alga *Chlamydomonas reinhardtii* tend to be stress responsive and experience frequent response gains. *BMC Genomics* 16:149. doi: 10.1186/S12864-015-1335-5

Yang, H. M., Liao, L. B., Bo, T. T., Zhao, L., Sun, X. W., Lu, X. F., et al. (2014). Slr0151 in *Synechocystis* sp PCC 6803 is required for efficient repair of photosystem II under high-light condition. *J. Integr. Plant Biol.* 56, 1136–1150. doi: 10.1111/jipb.12275

Zhao, L., Chen, M., Cheng, D. M., Yang, H. M., Sun, Y. L., Zhou, H. Y., et al. (2013). Different B-type methionine sulfoxide reductases in *Chlamydomonas* may protect the alga against high-light, sulfur-depletion, or oxidative stress. *J. Integr. Plant Biol.* 55, 1054–1068. doi: 10.1111/jipb.12104

Zhao, L., Cheng, D. M., Huang, X. H., Chen, M., Dall'Osto, L., Xing, J. L., et al. (2017). A light harvesting complex- like protein in maintenance of photosynthetic components in *Chlamydomonas*. *Plant Physiol.* 174, 2419–2433. doi: 10.1104/pp.16.01465

Zhou, J. X., Zhou, J., Yang, H. M., Chen, M., and Huang, F. (2008). Characterization of two glutaminases from the filamentous cyanobacterium *Anabaena* sp PCC 7120. *FEMS Microbiol. Lett.* 289, 241–249. doi: 10.1111/j.1574-6968.2008.01395.x

Conflict of Interest Statement: The authors declare that the research was conducted in the absence of any commercial or financial relationships that could be construed as a potential conflict of interest.

frontiers in Plant Science

ORIGINAL RESEARCH
published: 19 December 2017
doi: 10.3389/fpls.2017.02140

At5g19540 Encodes a Novel Protein That Affects Pigment Metabolism and Chloroplast Development in *Arabidopsis thaliana*

*Xing-Qi Huang, Lei Zhao, Jin-Di Rui, Chang-Fang Zhou, Zhong Zhuang and Shan Lu**

State Key Laboratory of Pharmaceutical Biotechnology, School of Life Sciences, Nanjing University, Nanjing, China

Chlorophylls and carotenoids not only function in photosynthesis and photoprotection but are also involved in the assembly of thylakoid membranes and the stabilization of apoproteins in photosystems. In this study, we identified a nuclear gene required for chlorophyll and carotenoid metabolism, namely, *DWARF AND YELLOW 1* (*DY1*). Growth of the loss-of-function *dy1* mutant was severely retarded, and the seedlings of this mutant accumulated significantly less amounts of both chlorophylls and carotenoids in cotyledons and rosette leaves, although genes related to pigment metabolism did not show corresponding fluctuation at the transcriptional level. In chloroplasts of the *dy1* leaves, thylakoids were loosely packed into grana. The *dy1* mutant also possessed severely impaired photosynthetic and photoprotective abilities. *DY1* encodes a chloroplast stroma protein that is highly conserved in vascular plants. Our results demonstrated that after the full-length DY1 (53 kDa) was imported into the chloroplast and its N-terminal transit peptide was processed, the C-terminal end of this premature DY1 (42 kDa) was also removed during the maturation of rosette leaves, resulting in a 24-kDa mature peptide. Our blue native PAGE and Western blot analyses showed the presence of both premature and mature forms of DY1 in protein complexes. The involvement of DY1 in chloroplast development is discussed.

Keywords: ***Arabidopsis thaliana*, chloroplast, development, pigments, Dwarf and Yellow 1 (DY1), RABE1b**

OPEN ACCESS

Edited by:
Fei Yu,
Northwest A&F University, China

Reviewed by:
Fabrice Franck,
University of Liège, Belgium
Chanhong Kim,
Shanghai Center for Plant Stress Biology, Shanghai Institutes for Biological Sciences (CAS), China

****Correspondence:***
Shan Lu
shanlu@nju.edu.cn

Specialty section:
This article was submitted to Plant Physiology, a section of the journal Frontiers in Plant Science

Received: *02 September 2017*
Accepted: *04 December 2017*
Published: *19 December 2017*

Citation:
Huang X-Q, Zhao L, Rui J-D, Zhou C-F, Zhuang Z and Lu S (2017) At5g19540 Encodes a Novel Protein That Affects Pigment Metabolism and Chloroplast Development in Arabidopsis thaliana. Front. Plant Sci. 8:2140. doi: 10.3389/fpls.2017.02140

INTRODUCTION

Chloroplast development is a key event for plant growth and adaptation. It involves different processes, including the expression of nuclear and plastid genes, the biosynthesis and accumulation of chlorophylls and carotenoids, and the assembly of membrane systems, that are highly coordinated in a spatiotemporal context (Mullet, 1988; Pfalz and Pfannschmidt, 2013; Andriankaja et al., 2014). Different mechanisms of regulating chloroplast development through pigment biosynthesis have been reported. For example, members of the PHYTOCHROME-INTERACTING FACTOR (PIF) family interact with DELLA to regulate the expression of light-dependent genes, especially those genes for chlorophyll and carotenoid metabolism (Cheminant et al., 2011). The expression of the gene for phytoene synthase (PSY), a key enzyme for carotenoid biosynthesis, is also directly repressed by PIFs (Toledo-Ortiz et al., 2010). Moreover, genes involved in the assembly of thylakoid membranes and in plastid-encoded RNA polymerase (PEP)-dependent transcription, such as the DnaJ-like zinc finger domain protein PSA2 and the heat shock

protein HSP21, were also reported to modulate chloroplast development and to affect acclimation to high-light stress (Zhong et al., 2013; Fristedt et al., 2014; Wang et al., 2016).

It has been demonstrated that pigment mutants with albino, yellow or variegated cotyledons or true leaves are a good system for the discovery of novel regulating components. For example, the well-studied *immutans* (*im*) and *variegated* (*var*) mutants were found to encode a plastid terminal oxidase and FtsH, respectively (Aluru et al., 2001; Sakamoto, 2003; Yu et al., 2007). Studies of *snowy cotyledon* mutants also identified the involvement of chloroplast elongation factor G (SCO1), zinc-finger domain protein (SCO2), microtubule and peroxisome-associated protein (SCO3) and proteinase (SCO4) in chloroplast development (Albrecht et al., 2006, 2008, 2010; Albrecht-Borth et al., 2013). These studies illustrated that different mechanisms at metabolic, transcriptional, and translational levels are involved in the regulation of pigment metabolism, chloroplast development, or both.

In this work, by screening a pool of *Arabidopsis thaliana* T-DNA insertion mutants for seedlings with abnormal pigment accumulation, we identified a novel gene, *Dwarf and Yellow 1* (*DY1*/*At5g19540*) that regulates both pigment metabolism and thylakoid membrane assembly.

MATERIALS AND METHODS

Plant Materials and Growth Conditions

The *Arabidopsis thaliana* T-DNA insertion mutant pool (CS76508) was purchased from the Arabidopsis Biological Resource Center (ABRC, Ohio State University, Columbus, OH, United States). All *A. thaliana* plants used in this study were in Col-0 wild-type (WT) background. After 3 days stratification at 4°C in the dark, seeds were germinated on Murashige-Skoog (MS) plates containing 2% sucrose at 22°C under a light intensity of 120 μmol photons m^{-2} s^{-1} with a 16 h/8 h light/dark photoperiod. Two-week-old seedlings were moved to grow in soil (a mixture of peat moss, vermiculite and perlite at 1:1:1) under the same conditions (Wang et al., 2016).

Mutants were screened on MS plates containing 25 mg/L kanamycin. Seedlings with albino, yellowish, or pale green cotyledons were moved to grow in soil, and their seeds were individually collected.

Molecular Manipulation and Plant Transformation

Genomic DNA was extracted from rosette leaves using the CTAB method (Green and Sambrook, 2012). For identifying T-DNA insertion position of each mutant, genome walking was performed using a Genome Walking Kit (TaKaRa, Shiga, Japan) following the manufacturer's manual. Homozygous progenies of the mutants were screened according to the SIGnAL iSect tool[1]. All primers used in this study are listed in **Supplementary Table S1**.

[1]http://signal.salk.edu/tdnaprimers.2.html

RNA was isolated using RNAiso Plus Reagent (TaKaRa) according to manufacturer's instruction. Total RNA (1 μg) was reverse transcribed using a PrimeScript 1st Strand cDNA synthesis Kit (TaKaRa). Transcript abundance of each gene studied was determined by quantitative real-time PCR (qPCR) in a Thermal Cycler Dice Real Time System TP800 (TaKaRa) using SYBR Premix ExTaq II (TaKaRa), following the manufacturer's manuals, and calculated using the comparative C_T method (Schmittgen and Livak, 2008). *ACT 2* (*At3g18780*) was used as a reference. At least three biological replicates, each with three repeats, were analyzed for each sample.

For genetic complementation, a 4332 bp genomic DNA fragment of *DY1* (*At5g19540*), ranging from −2044 bp upstream of the translation initiation codon (ATG) to 290 bp downstream of the stop codon, was amplified using primers DY1-GF and DY1-GR, and cloned into the *Bam*H I site of pCAMBIA1300 (CAMBIA, Canberra, ACT, Australia) to generate the construct *DY1:DY1*. For subcellular localization study, full-length open reading frame (ORF) of *DY1* or *At4g20360* was amplified from the 1st strand cDNA pool using primers DY1-HF and DY1-ER for *DY1*, or RABE1b-HF and RABE1b-ER for *At4g20360*, and subsequently cloned into the *Bam*H I site of pA7-eYFP to generate the construct *35S:DY1-eYFP* or *35S:At4g20360-eYFP*. To generate the construct for expressing DY1 with dual fluorescent proteins, the coding sequences for the chloroplast transit peptide (cTP) of DY1 (cTP^{DY1}) (using primer pair DY1-cTP-HF and DY1-cTP-ER), eYFP (eYFP-HF and eYFP-ER), DY1 without cTP ($DY1^{\Delta cTP}$) (DY1-ΔcTP-HF and DY1-ΔcTP-ER) and mCherry (mCherry-HF and mCherry-ER), were separately amplified and joined together into the *Bam*H I and *Sac* I sites of pA7-eYFP using In-Fusion technique (TaKaRa). The entire fragment encoding the cTP^{DY1}-eYFP-$DY1^{\Delta cTP}$-mCherry fusion protein was further amplified (DY1-mature-HF and DY1-mature-ER) and then subcloned into the *Nco* I site of pCAMBIA1300-RTL2 using In-Fusion technique for transient expression in tobacco leaves and genetic transformation of Arabidopsis. *A. thaliana* was transformed by the floral dip method (Clough and Bent, 1998).

For transient transformation, protoplasts were isolated from rosette leaves according to Yoo et al. (2007). About 20 μg of purified plasmid DNA was applied for each transformation. The protoplasts were incubated in the dark at 22°C overnight before microscopy observation.

For all PCR amplifications, high-fidelity PrimeSTAR DNA polymerase (TaKaRa) was used according to the manufacturer's instruction.

Sequence Analysis

Subcellular localization of DY1 were predicted using online programs ChloroP and TargetP (Emanuelsson et al., 1999; Emanuelsson et al., 2007). Deduced amino acid sequence of DY1 was used as a query to search its homologs in different plant species of which full genomes have been sequenced in GenBank using the BlastP algorithm. Sequences were aligned using the ClustalX program and a maximum-likelihood phylogenetic tree was constructed using MEGA 6 with a bootstrap replication value of 1,000 (Chenna et al., 2003; Tamura et al., 2013).

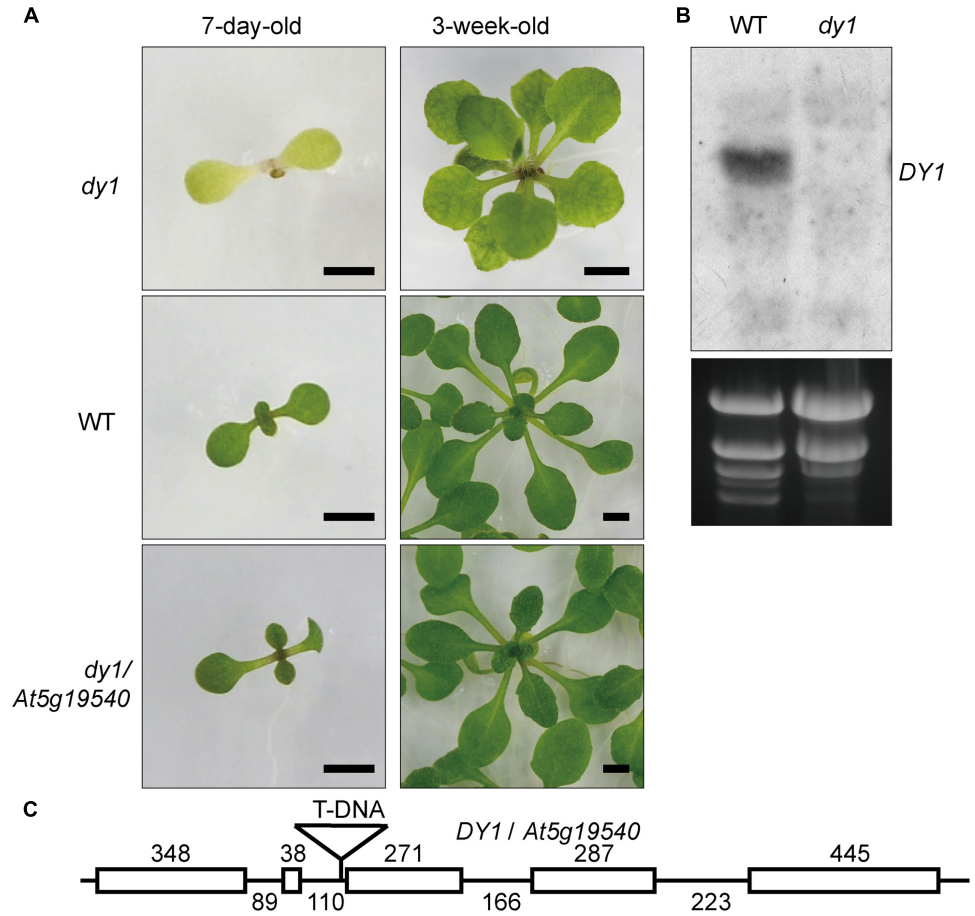

FIGURE 1 | Phenotype and characterization of the *dy1* mutant plant. **(A)** *dy1*, WT and *At5g19540* transformed *dy1* plants grown on MS plates. Bars = 2 mm. **(B)** Northern blot showing the silence of *At5g19540* in the *dy1* mutant. **(C)** T-DNA insertion position of *dy1*. The insertion is 3 bp upstream the third exon of *At5g19540*. Sizes of each intron and exon are labeled.

Northern Blot

To perform Northern blot, total RNA was extracted from leaves of 3-week-old *dy1* mutant and WT plants. Ten microgram of total RNA was loaded for each lane and separated on 1.5% agarose gel. After separation, the RNA was blotted onto a positively charged nylon membrane (GE Healthcare, Pittsburgh, PA, United States). The probe for detecting *DY1* transcripts was amplified using primer pair DY1-Probe-F and DY1-Probe-R, with *DY1* cDNA as a template, and then labeled using DIG DNA Labeling Mix (Roche, Basel, Switzerland). Probing, washing, and detection of *DY1* were performed according to the DIG High Prime DNA Labeling and Detection Starter Kit II user's manual (Roche).

Protein Extraction and Western Blot Analysis

Total protein was extracted from rosette leaves using the trichloroacetic acid (TCA) precipitation method. Approximately 1 g of rosette leaves was homogenized in liquid nitrogen. Ten milliliter of cold 10% TCA in acetone was then added and mixed well by vortex and sonication. The mixture was incubated at −20°C for at least 4 h and then centrifuged at 4°C, 15,000 *g* for 20 min. The pellet was washed several times with cold acetone, air dried briefly, and solubilized in 9 M urea (in 100 mM phosphate buffered saline, 1 mM DTT) with sonication. The precipitation was repeated once, and the pelleted protein was finally dissolved in 9 M urea solution for direct use or storage.

Protein samples were mixed with equal amounts of 2 × SDS loading buffer (Green and Sambrook, 2012), heated at 65°C for 10 min, separated on 12 % SDS–polyacrylamide gel and subsequently blotted onto nitrocellulose membrane (GE Healthcare) for immunodetection. A peptide (WSIRNPTDLETSSY) was synthesized based on deduced amino acid sequence of DY1 and used as an antigen to immune rabbits by GenScript (Nanjing, China). Antiserum was purified from blots according to Harlow and Lane (1988). Antibody against Actin 11 was purchased from Agrisera (Vännäs, Sweden). Horseradish peroxidase (HRP)-conjugated secondary antibody against rabbit IgG was from Promega (Madison, WI, United States). Common protocols (Green and Sambrook, 2012) and the manufacturers' manuals for electrophoresis, semi-dry

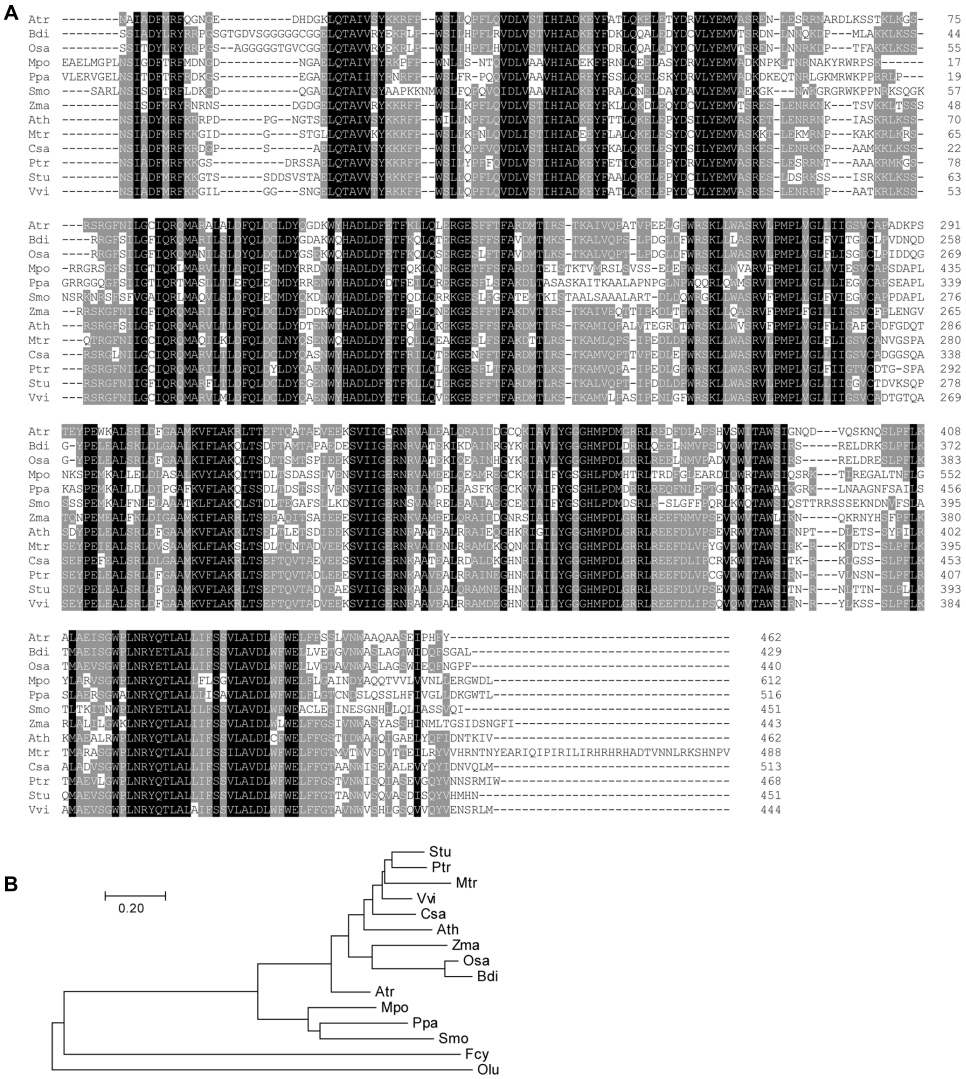

FIGURE 2 | Multiple sequence alignment **(A)** and phylogenetic analysis **(B)** of DY1 homologs. Sequences are from plant species for which full genomes have been sequenced, including *Amborella trichopoda* (Atr, XP_006833290.3), *Arabidopsis thaliana* (Ath, OAO95398.1), *Brachypodium distachyon* (Bdi, XP_003574414.1), *Cucumis sativus* (Csa, XP_004150055.2), *Marchantia polymorpha* (Mpo, OAE23078.1), *Medicago truncatula* (Mtr, AFK48173.1), *Oryza sativa* (Osa, XP_015650923.1), *Physcomitrella patens* (Ppa, XP_001768011.1), *Populus trichocarpa* (Ptr, XP_002324991.1), *Selaginella moellendorffii* (Smo, XP_002961080.1), *Solanum tuberosum* (Stu, XP_006353458.1), *Vitis vinifera* (Vvi, XP_002280972.1), *Zostera marina* (Zma, KMZ73824.1). Sequences from the green alga *Ostreococcus lucimarinus* (Olu, XP_001420303.1) and the diatom *Fragilariopsis cylindrus* (Fcy, OEU12403.1) which showed similarities with DY1 were incorporated in the phylogenetic tree. The scale bar corresponds to 20% amino acid sequence divergence.

blotting and Western detection using the ECL Western Blotting Substrate (Promega, Madison, WI, United States) were followed.

Microscopy

A FluoView FV1000 (Olympus, Tokyo, Japan) laser scanning confocal microscopy system was used for fluorescence observation. The eYFP fluorescent was excited with 488 nm laser and the emitted light was recorded from 500 to 530 nm. The mCherry fluorescent was excited with 543 nm laser, recorded from 580 to 620 nm. 543 nm laser excitation and 680 to 720 nm recording range were used for chlorophyll auto-fluorescence observation.

For transmission electron microscopy (TEM) analysis, leaves from 3-week-old seedlings were fixed, embedded and sectioned according to Faso et al. (2009). A Hitachi-7700 transmission electron microscope (Hitachi, Tokyo, Japan) was used for observation and image capturing.

Chloroplast Isolation, Fractionation and Blue Native (BN)-PAGE

About 10 g of rosette leaves were homogenized briefly in cold chloroplast isolation buffer (0.3 M sorbitol, 5 mM $MgCl_2$, 5 mM EGTA, 5 mM EDTA, 20 mM HEPES, 10 mM $NaHCO_3$, pH 8.0) and then filtered through two layers of

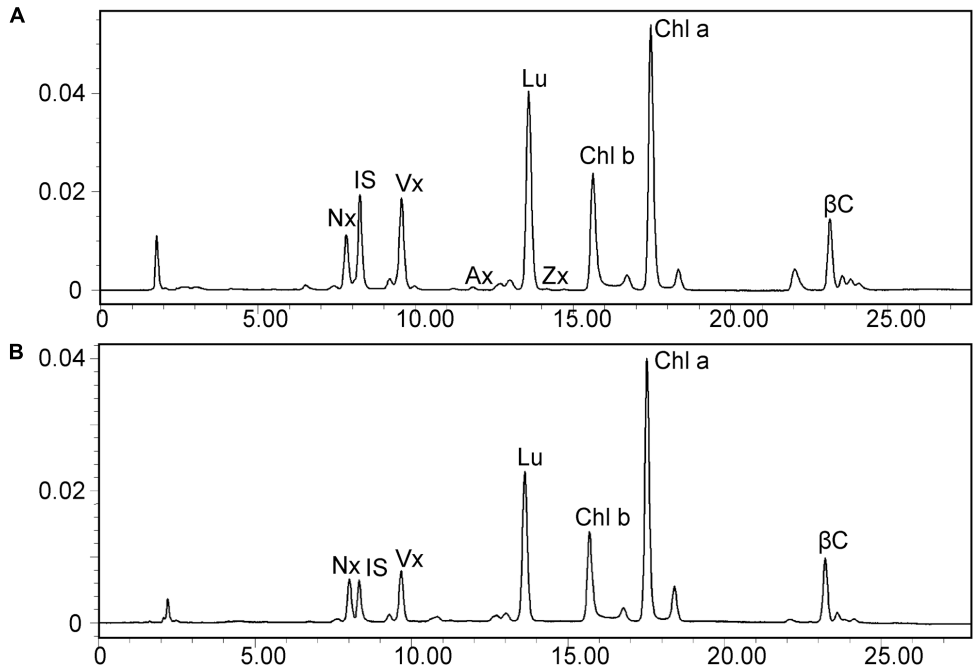

FIGURE 3 | High-performance liquid chromatography (HPLC) separation of pigments in 3-week-old rosette leaves of the *dy1* mutant **(A)** and the wild-type **(B)** plants. Peaks are neoxanthin (Nx), internal standard (IS), violaxanthin (Vx), antheraxanthin (Ax), lutein (Lu), zeaxanthin (Zx), β-carotene (βC), and chlorophyll *a* and *b* (Chl *a* and Chl *b*).

miracloth (EMD Millipore, Billerica, MA, United States). Crude chloroplasts were collected by centrifugation for 5 min at 4°C, 1,000 *g*. After the separation of crude chloroplasts on a 2-layer Percoll gradient (40 and 80%), intact chloroplasts were obtained from the interface between two layers. Purified chloroplasts were further lysed in TE solution (10 mM Tris–HCl, 1 mM EDTA, pH 7.5) for 30 min on ice, followed by a centrifugation for 5 min at 3,000 *g* to collect thylakoid membranes.

For BN-PAGE, intact chloroplasts were solubilized in Solubilization Buffer (50 mM Bis–Tris, pH 7.0, 0.5 M aminocaproic acid, 10% glycerol, 1% *n*-dodecyl β-D-maltoside and 1 mM PMSF) on ice for 10 min before separation on a 4% ∼ 14% gradient gel. After the first dimension electrophoresis, the gel was either directly blotted onto a PVDF membrane (Millipore) or further separated by SDS–PAGE for a second dimension (Zhou et al., 2017).

Pigment Quantification

Chlorophylls and carotenoids were isolated from rosette leaves according to Pogson et al. (1996). One hundred milligram of leaves was ground in liquid nitrogen into fine powder and mixed thoroughly with 250 μl 80% acetone containing 10 μg deuteroporphyrin IX dimethyl ester (Sigma–Aldrich, St. Louis, MO, United States) as an internal standard. The extract was then mixed with 250 μl ethyl acetate, followed by 200 μl of water. After a centrifugation at 4°C, 15,000 *g* for 10 min, the upper organic phase was collected and dried under a stream of nitrogen. The pigment was re-dissolved in Solvent A (acetonitrile:water:trimethylamine = 9:1:0.01) for high-performance liquid chromatography (HPLC) analysis. All steps were carried out under dim light.

Total pigment samples were analyzed by HPLC (Waters 2695 separation module) with a Waters ODS2 C18 analytical column (5 μm, 4.6 mm × 250 mm) and 2998 photodiode array detector (Waters, Milford, MA, United States) according to Wang et al. (2016).

Chlorophyll Fluorescence Analysis

Chlorophyll fluorescence of 3-week-old *dy1* mutant and WT plants were measured by a MINI-PAM fluorometer (Walz, Effeltrich, Germany) according to Wang et al. (2016). For

TABLE 1 | Leaf pigment profile of the *Arabidopsis thaliana* wild-type (WT) and *dy1* mutant plants (μg/g fresh weight).

Pigment	WT	*dy1*	Ratio (*dy1*/WT)
Chl *a*	835.03 ± 6.82	289.55 ± 21.61**	34.6%
Chl *b*	325.91 ± 14.33	128.98 ± 0.20**	39.6%
Lutein	208.06 ± 0.21	77.46 ± 3.06**	37.0%
β-Carotene	76.31 ± 2.56	24.86 ± 2.06**	32.6%
Neoxanthin	51.61 ± 2.80	17.85 ± 0.11**	34.5%
Violaxanthin	60.62 ± 0.45	34.18 ± 0.99**	56.4%
Antheraxanthin	–	0.98 ± 0.08**	
Zeaxanthin	–	0.711 ± 0.04**	

*Data represent means ± SD (Student's t-test; n = 6; **P < 0.01).*

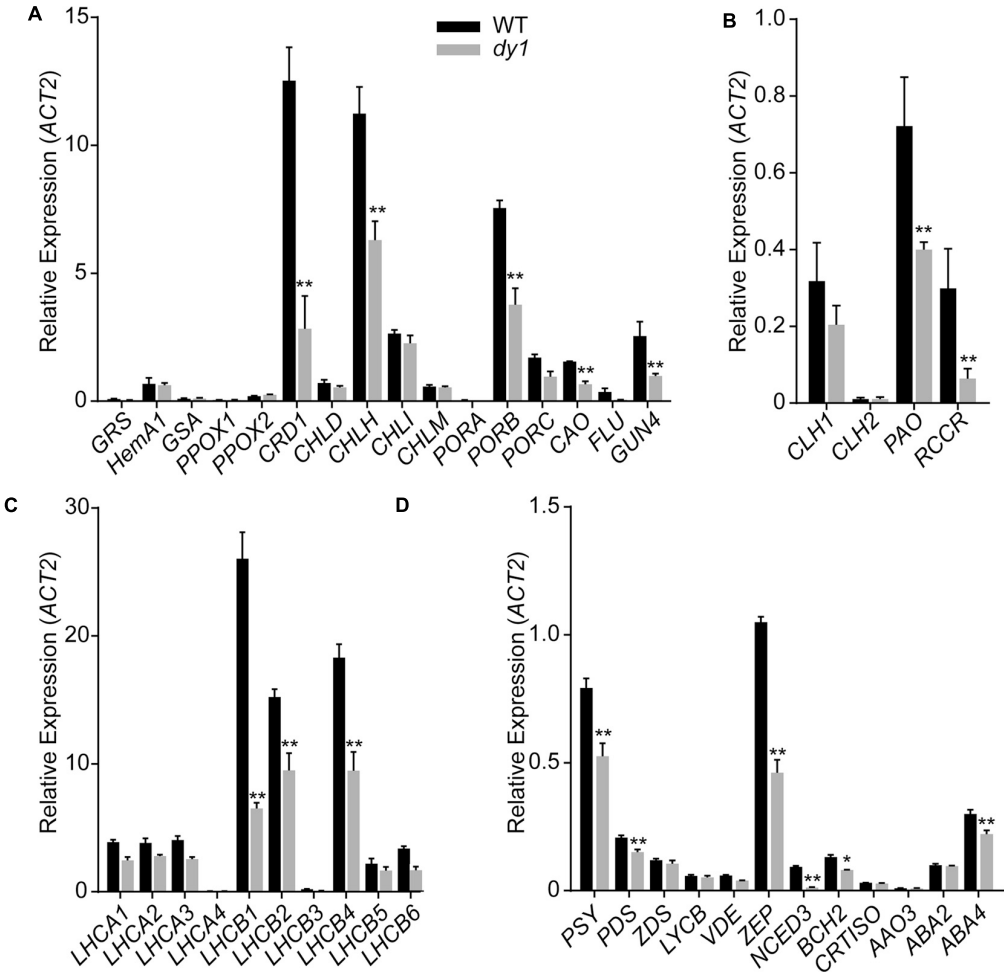

FIGURE 4 | Expression of the genes encoding enzymes for chlorophyll biosynthesis **(A)** and turnover **(B)**, chlorophyll-binding proteins **(C)** and enzymes for carotenoid metabolism **(D)** in rosette leaves of the 3-week-old *dy1* and wild-type (WT) seedlings. Transcript abundance of each gene was determined by quantitative real-time PCR and are normalized against the level of *ACT2* (*At3g18780*). Data represent means ± SD (Student's *t*-test; $n = 3$; $^{*}P < 0.05$; $^{**}P < 0.01$).

light-response curves of PSII quantum yield (ΦPSII) and non-photochemical quenching (NPQ), dark-adapted plants were illuminated at a series of photosynthetically active photon flux densities (PPFD) (3, 19, 43, 145, 300, 387, 611, 1,006, and 1,312 μmol photons m^{-2} s^{-1}). The minimal yield of fluorescence (F_0) under 650 nm was measured at 0.8 μmol photons m^{-2} s^{-1}. To estimate the maximum fluorescence yield (F_m), a saturating pulse (0.8 s, 5,000 μmol photons m^{-2} s^{-1}) was applied.

TABLE 2 | Chlorophyll fluorescence parameters in the leaves of the *dy1* mutant and the wild-type (WT) plants grown under 100 μmol m^{-2} s^{-1}.

	WT	*dy1*
F_0	199.30 ± 3.60	245.80 ± 17.00**
F_m	1156.50 ± 32.00	905.40 ± 126.00**
F_v/F_m	0.8273 ± 0.0061	0.7256 ± 0.0209**

*Data represent means ± SD (Student's t-test; n = 6; **P < 0.01).*

Yeast Two-Hybrid Screening

The yeast two-hybrid screening was performed largely according to the Matchmaker™ GAL4 Two-Hybrid System 3 & Libraries User Manual (TaKaRa). Full length ORF of *DY1* was cloned into pDEST32 (Invitrogen, Carlsbad, CA, United States) and then transformed into the yeast (*Saccharomyces cerevisiae*) strain AH109. *A. thaliana* cDNA library constructed in pDEST22 (Invitrogen) was maintained in the yeast strain Y187. After mating, diploid yeast cells were screened on SD/-Leu/-Trp/-His triple dropout medium. From positive colonies, cDNA insertions encoding the prey proteins were amplified by PCR and sequenced. Candidate genes were further tested for pair-wise interaction using a pGAD-T7/pGBK-T7 system (TaKaRa). Briefly, the coding sequences of *DY1* and candidate genes were cloned into pGAD-T7 and pGBK-T7, respectively. Plasmids were co-transformed into yeast strain AH109 and selected on SD/-Leu/-Trp double drop out plates. Colonies were serial diluted and further tested on SD/-Leu/-Trp/-His/-Ade quadruple dropout plates for detecting protein–protein interactions.

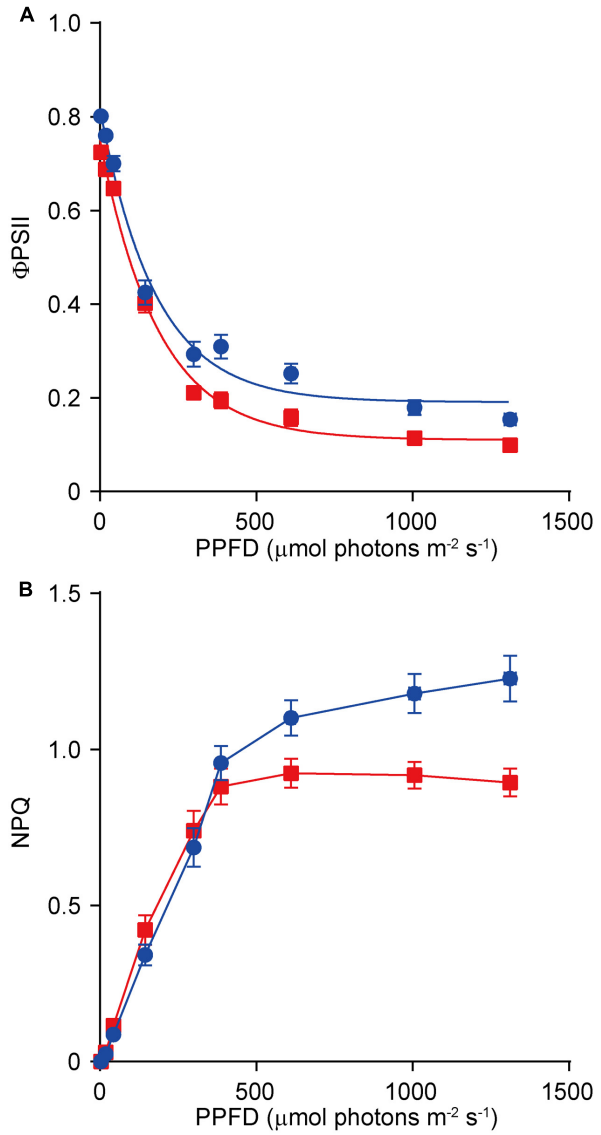

FIGURE 5 | Light-response curves of PSII quantum yield (ΦPSII) **(A)** and non-photochemical quenching (NPQ) **(B)** in the wild-type (WT, in blue) and the *dy1* mutant (in red) seedlings. The measurements were taken at photosynthetic active photon flux densities (PPFD) of 3, 19, 43, 145, 300, 387, 611, 1,006, and 1,312 μmol m^{-2} s^{-1}. Data represent means ± SD (n = 6).

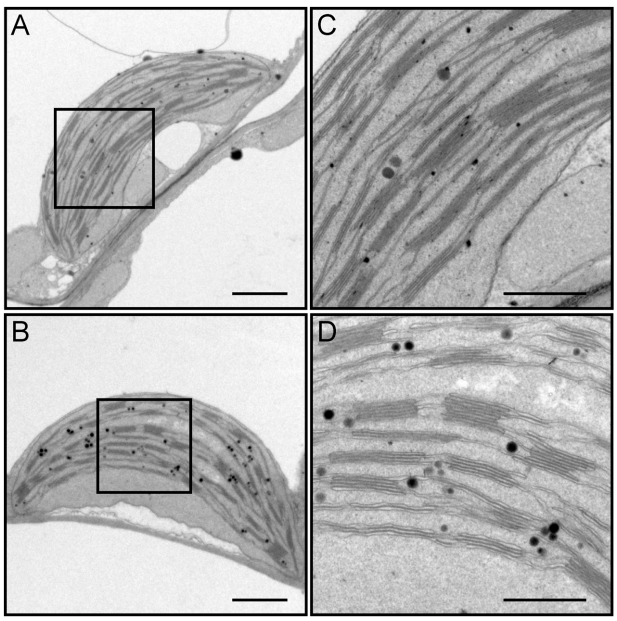

FIGURE 6 | Transmission electron microscopy (TEM) observation of chloroplasts from leaves of the wild-type (WT) **(A,C)** and the *dy1* mutant seedlings **(B,D)**. Bars = 1 μm (in **A,B**) or 500 nm (in **C,D**). **(C,D)** Are magnified views of the boxed regions in **(A,B)**, respectively.

Statistical Analysis

Statistical significance was tested using GraphPad Prism6 (GraphPad Software). Data are shown as the means ± SD of at least three replications.

RESULTS

Characterization of the *dy1* Mutant

We screened 10,000 individuals of the T-DNA insertion mutant library. At least 20 lines showed pale green, yellowish or completely albino cotyledons. The T-DNA insertion positions of these lines were identified by genome walking. One of these lines that showed dwarfed growth and yellowish cotyledons (**Figure 1A**) was proved to harbor a T-DNA insertion in front of the third exon of *At5g19540* (**Figure 1C**). We named this uncharacterized gene *Dwarf and Yellow 1* (*DY1*). Northern blot (**Figure 1B**) and genomic complementation (**Figure 1A**) experiments confirmed that *At5g19540* is responsible for the corresponding phenotypes. *DY1* encodes a 53-kDa protein with a predicted N-terminal transit peptide (cTP), which was predicted to target DY1 to chloroplasts (**Supplementary Figure S1**). The *dy1* mutant seedlings were defective in de-etiolation, i.e., their cotyledons stayed yellow after illumination. Vegetative growth of the *dy1* seedlings was severely retarded. Juvenile true leaves of the *dy1* mutant also had defects in their pigmentation, whereas mature leaves of the mutant were greener (**Figure 1A**).

DY1 Is Highly Conserved in Plants

We did not find functional characterization reports nor annotation for *DY1*, and therefore, we searched GenBank for homologs of *DY1*. In each plant species for which a full genome has been sequenced, only one copy of a *DY1* homolog gene was found. We did not find any close homologs of *DY1* in cyanobacteria, green algae or diatoms, although there are some sequences in certain organisms with weak similarities to *DY1* (**Figure 2**).

Comparisons of the deduced amino acid sequences of DY1 homologs identified highly conserved regions spanning the entire sequence beyond the homologs' cTPs (**Figure 2A**). Overall sequence identity among DY1 homologs is higher than 40%, and

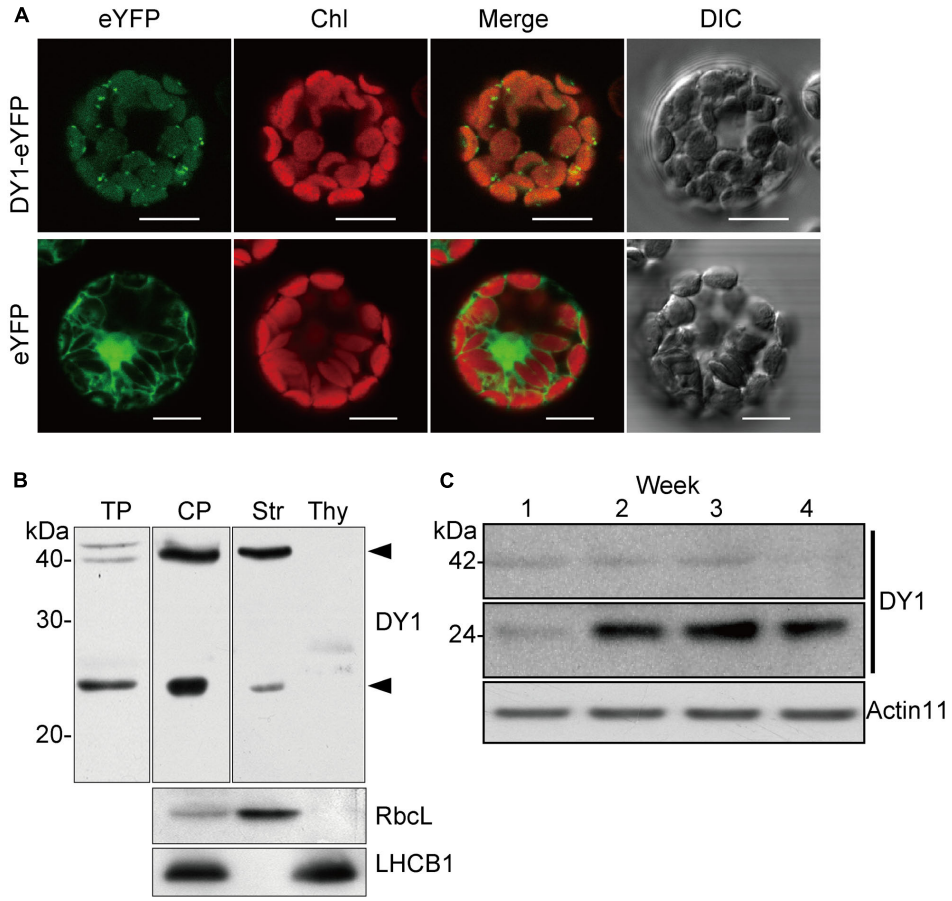

FIGURE 7 | DY1 is a chloroplast stroma protein. **(A)** Subcellular localization of DY1 in chloroplast. Protoplasts transformed with pA7-eYFP-DY1 were observed under a FLUOVIEW FV1000 Laser Confocal Microscopy System (Olympus) (Bars = 20 μm). **(B)** Western blot analysis demonstrating the stroma localization of DY1. Purified chloroplast were sub-fractionated into the stroma and thylakoid membrane fractions, separated by SDS–PAGE, blotting and probed with the antiserum against DY1. LHCB1 and RbcL were probed as controls. The bands of processed and mature forms of DY1 at 42 and 24 kDa, respectively, are indicated. TP, plant total protein; CP, intact chloroplast protein; Str, stroma fraction; Thy, thylakoid membrane fraction. **(C)** Western blot analysis of the accumulation of the 24 kDa form of DY1 during leaf development. The numbers above each lane indicate the growth stages in weeks.

it is over 60% if we exclude the most variable cTP regions. On a phylogenetic tree, DY1 homologs formed two major clades, one of which was composed of members from angiosperms and the other of which consisted of homologs from the remaining land plants, including gymnosperms and bryophytes. The angiosperm clade can be further divided into 2 sub-clades, one each for dicots and monocots (**Figure 2B**).

The *dy1* Mutant Is Impaired in Pigment Biosynthesis and Light Acclimation

Leaves of the *dy1* mutant showed a distinctly lighter color compared to those of the WT plants. Therefore, we postulated that the *dy1* mutant might accumulate lower amounts of pigments. In our quantification of the pigments in 3-week-old seedlings, both chlorophyll *a* and *b* contents in the *dy1* mutant were significantly lower than in the WT plants. For carotenoids, *dy1* leaves also accumulated less neoxanthin, violaxanthin, lutein and β-carotene compared with the WT plants. However, under normal growth conditions, two xanthophylls, antheraxanthin and zeaxanthin, were found to accumulate in *dy1* leaves, although at trace amounts (**Figure 3**). The quantities of all pigment contents are listed in **Table 1**.

We then quantified transcript abundances of genes for chlorophyll and carotenoid biosynthesis. In 3-week-old *dy1* leaves, the expression of most of the genes for chlorophyll biosynthesis, e.g., *CRD1*, *CHLH*, *PORB*, *GUN4* and *CAO*, were down-regulated (**Figure 4A**). Interestingly, genes for chlorophyll turnover, including *PAO* and *RCCR*, were also down-regulated in *dy1* (**Figure 4B**). Moreover, the expression of most of the genes for chlorophyll *a*/*b*-binding proteins (*CABs*) was also down-regulated in *dy1* (**Figure 4C**). Most of the genes for carotenoid biosynthesis and catabolism were down-regulated in *dy1* as well (**Figure 4D**). In brief, no genes for pigment metabolism were up-regulated in *dy1* in our determination.

Because *dy1* had lower amounts of leaf pigments, we postulated that it might also have lower photosynthetic capacity. This was confirmed by measurements of chlorophyll fluorescence parameters. In our study, F_v/F_m, which reflects the efficiency of

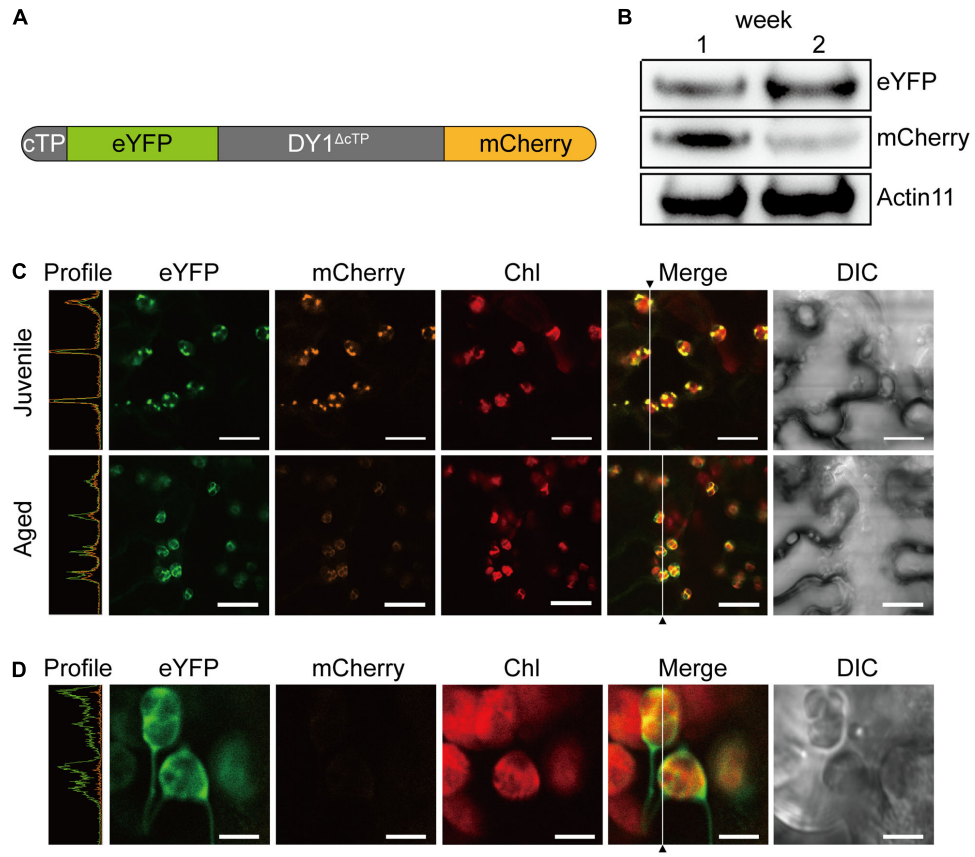

FIGURE 8 | Mature form of DY1 is further processed during the development of leaves. **(A)** A diagram showing the pre-protein structure of the DY1 protein labeled with dual fluorescent proteins. **(B)** Western blot analysis of the quantities of both ends of DY1 labeled with dual fluorescent proteins. Total proteins were extracted from 1- and 2-week-old transgenic Arabidopsis seedlings. **(C)** Transient expression of the eYFP-DY1-mCherry fusion protein in tobacco leaves demonstrating a possible cleavage of the C-terminus of DY1 during leaf development. Bars = 10 μm. **(D)** Fluorescent observation of 2-week-old Arabidopsis seedlings showing the lack of mCherry signals. Bars = 5 μm. In **(C)** and **(D)**, the Profile panels (green line, eYFP signal; orange line, mCherry signal) demonstrate the signal intensity profiles along the vertical lines indicated in the Merge panels.

PSII photochemistry, was reduced from 0.83 in the WT plants to 0.73 in *dy1* (**Table 2**). We also measured light-responsive curves to assess ΦPSII and NPQ of both *dy1* and WT plants under a series of light intensities. WT plants had higher ΦPSII than did *dy1* plants under all of the light intensities that we measured (**Figure 5A**). However, *dy1* had a higher NPQ than did the WT plants when light intensity was lower than 300 μmol photons m^{-2} s^{-1} ($P < 0.05$ at 43 and 145 μmol photons m^{-2} s^{-1}) (**Figure 5B**).

DY1 Affects Thylakoid Membrane Assembly

We dissected true leaves of 3-week-old *dy1* mutant and WT plants for TEM observations. The *dy1* mutant generally showed normal chloroplast shape and thylakoid formation. However, in the *dy1* mutant, thylakoid membranes were loosely packed into grana (with an average thickness of each grana thylakoid layer at 21.3 ± 1.9 nm, comparing with the WT level of 14.3 ± 1.4 nm) and possessed more plastoglobules (**Figure 6**).

DY1 Is a Chloroplast Protein That Undergoes Post-translational Regulation

DY1 encodes a protein with 462 amino acids. Both online programs ChloroP and TargetP predicted chloroplast localization. To confirm chloroplast localization, full-length DY1 protein with an enhanced yellow fluorescent protein (eYFP) fused to its C-terminus was transiently expressed in Arabidopsis protoplasts. The fluorescence of DY1-eYFP strictly overlapped with chlorophyll auto-fluorescence, indicating chloroplast localization (**Figure 7A**). From the amino acid sequence of DY1, we identified a twin-arginine ($R^{84}R^{85}$) motif (**Supplementary Figure S1**), which indicates that DY1 is probably imported into chloroplasts through the ΔpH-dependent pathway (Robinson and Bolhuis, 2001). It was reported that, for proteins imported through this pathway, their C-terminal fragments prior to the twin-arginine motif are to be cleaved after importing (Williams et al., 2000; Robinson and Bolhuis, 2001). Therefore, we isolated intact chloroplasts from WT leaves, sub-fractioned them into stroma and thylakoid fractions, and performed SDS–PAGE and Western blot analyses. From our immunoblots probed with a

specific antibody raised against DY1, a band at 42 kDa was found in the total-chloroplast protein sample and the stromal fraction (**Figure 7B**). This finding agreed with the calculated size of DY1 after the cleavage ($DY1^{\Delta cTP}$) and proved the stroma localization of DY1.

To our surprise, an additional smaller band of 24 kDa was frequently detected in the stroma fractions of the WT plants (**Figure 7B**). We found that the protein level of $DY1^{\Delta cTP}$ was more stable throughout developmental stages, while the content of the smaller form tended to accumulate over time (**Figure 7C**). Thus, we postulated that after being imported into chloroplasts, DY1 might be further processed during the maturation of leaves. To test this visually, we fused eYFP immediately after the cTP and mCherry at the end of the C-terminus of DY1 (**Figure 8A**), and we expressed this fusion protein with dual fluorescent tags in tobacco and Arabidopsis. In tobacco, we performed transient expression in juvenile leaves that were close to the apical shoot and in mature leaves from the bottom of the plant. After 3 days, signals of both eYFP and mCherry could be clearly observed within chloroplasts in juvenile leaves. However, in mature leaves, most observed chloroplasts had similar strengths of the eYFP signal but their mCherry signals were much weaker (**Figure 8C**). In Arabidopsis plants that were genetically transformed to express this fusion protein, it was clear that only eYFP signal could be detected in mature leaves (**Figure 8D**). When we probed the protein samples of 1- and 2-week-old transgenic Arabidopsis seedlings, antibody against eYFP could detect the DY1 fusion protein in both samples, whereas that against mCherry showed only a faint band on the blot, suggesting a removal of the C-terminus from DY1 (**Figure 8B**). These results demonstrated that DY1 matures with leaf development.

To determine the distributions of the two forms of DY1 in chloroplasts, we performed BN-PAGE to separate different protein complexes in chloroplasts (**Figure 9A**), followed by SDS–PAGE as a second dimension (**Figure 9B**). After electrophoresis, gels of each dimension were blotted and then probed with an antibody against DY1. Our Western blot clearly showed that both the 42- and 24-kDa forms of DY1 could be found at the position of about 300-kDa, which is around the PSII core + Cyt b_6f complex (Timperio et al., 2007; Chen et al., 2010), and the 42-kDa form could also be probed at the position of approximately 100 kDa (**Figure 9B**).

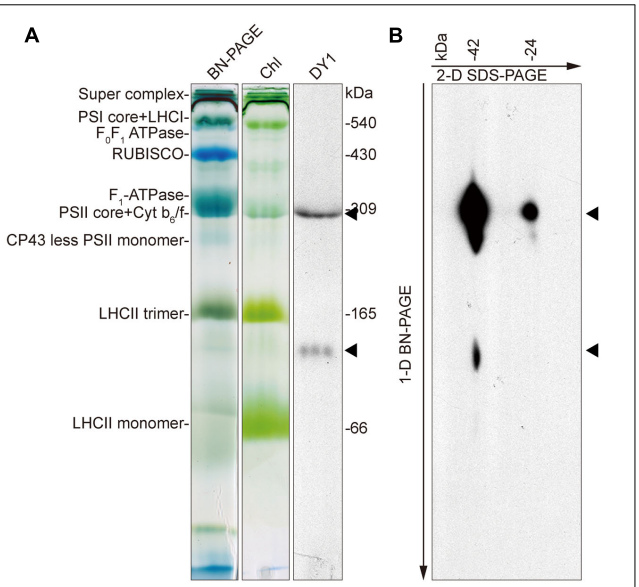

FIGURE 9 | Blue-native PAGE and Western blot showing that DY1 exists in different protein complexes in chloroplast. Protein samples of intact chloroplasts from 3-week-old wild-type Arabidopsis plants were separated by BN-PAGE as the first dimension **(A)**. Chl, gel after blotting which contains chlorophylls only. The gel was either directly blotted and probed with the anti-DY1 antibody or further separated by SDS–PAGE as the second dimension and then blotted and probed with the same antibody **(B)**. Positions of DY1 protein probed by its antibody were indicated by triangles.

DISCUSSION

In this study, by screening a pool of T-DNA insertion mutants of Arabidopsis, we identified a novel protein encoded by *At5g19540*, DY1, that is essential for the biosynthesis of both chlorophylls and carotenoids and is involved in the assembly of grana thylakoids. The fact that we failed to obtain close homologs from cyanobacteria, green algae and diatoms indicated that *DY1* was probably acquired by only the ancestor of vascular plants. The presence of only one copy of *DY1* in the genome of each plant species and the high sequence identity among its homologs suggested its critical function.

A distinct phenotype of the *dy1* mutant is its lower amounts of both chlorophylls and carotenoids. Based on our quantification of genes encoding enzymes for chlorophyll and carotenoid metabolism, both involved in biosynthesis and catabolism, and for the chlorophyll-binding proteins, it seems that the expression of all of these genes was down-regulated by the silencing of *DY1*. However, from our HPLC analysis, we found an abnormal accumulation of two xanthophylls, antheraxanthin and zeaxanthin, in *dy1* leaves under growth light. Both antheraxanthin and zeaxanthin are members of a non-photochemical, energy-quenching mechanism utilized by higher plants under high-light stress, termed the xanthophyll cycle (Demmig-Adams and Adams, 1996; Johnson et al., 2008). These pigments are absent in WT plants adapted to normal growth light, but they accumulate when there is a defect in photosystem functionality or the plants are suffering from high-light damage. Interestingly, in our analysis of chlorophyll fluorescence, the *dy1* mutant leaves showed an increase in minimal fluorescence yield (F_0), together with a decreased level of the maximum fluorescence yield (F_m) and the resulting maximum quantum yield of PSII ($F_v/F_m = [F_m - F_0]/F_m$). This indicated either a defect in electron transfer within PSII and/or a partial disconnection of the LHCII antenna, similar to the *hhl1* and *pam71* mutants (Jin et al., 2014; Schneider et al., 2016). This was supported by our determination of ΦPSII and NPQ, which were all lower in *dy1* plants compared with the WT plants. However, the *dy1* plants had a higher NPQ, comparing with the WT plants, when light intensity was lower than 300 μmol

photons m^{-2} s^{-1}. It is probably because of the accumulation of both zeaxanthin and antheraxanthin in *dy1* plants. Taken together, our results demonstrated the stressed condition of *dy1* PSII. This might provide an explanation of the lower amounts of total chlorophylls and carotenoids and the retarded growth of *dy1*.

The involvement of DY1 in the function of chloroplasts is further supported by our TEM observation, together with the BN-PAGE and Western blot analyses. It has been reported that grana stacking is critical for xanthophyll cycle-dependent NPQ (Goss et al., 2007). Although chloroplasts of the *dy1* mutants retained the normal shape of the WT ones, it was clear that thylakoids were loosely stacked into grana in *dy1* chloroplasts. Our Western blots showing that DY1 exists in a protein complex co-migrates with the PSII core + Cyt b_6f complex suggest the possible involvement of DY1 in PSII.

A special feature of DY1 is its maturation. From our Western blot and observation of subcellular localization of the fusion protein with dual fluorescent tags, it is clear that the DY1 peptide is processed twice after translation. It is common for a chloroplast protein encoded by a nuclear gene to have its transit peptide removed after the pre-protein is imported into chloroplasts. But, the C-terminal end of DY1 was further cleaved during the maturation of leaves. It is unclear whether this mature form of DY1 is needed for or is simply a result of leaf maturation. Moreover, although DY1 was only found in the stroma fraction of chloroplasts, our Western blot of the BN-PAGE separated samples also demonstrated its existence in two different protein complexes, suggesting its possible interactions with different protein partners. In a yeast two-hybrid screening, we identified that DY1 interacts with RABE1b, a GTP-binding elongation factor (**Supplementary Figure S2A**). Our protoplast transient expression also confirmed chloroplast localization of RABE1b (**Supplementary Figure S2B**), indicating spatial co-localization of these two proteins. In depth analysis of the protein–protein interaction between DY1 and RABE1b might help to decipher novel machinery that regulates pigment metabolism and chloroplast functions during plant development.

AUTHOR CONTRIBUTIONS

X-QH, LZ, and SL conceived and designed the experiments. X-QH, LZ, J-DR, C-FZ, and ZZ performed the experiments. X-QH, LZ, C-FZ, and SL analyzed the data. SL wrote the paper.

FUNDING

This work was supported by the State Key Basic Research and Development Plan of China (973, No. 2013CB127004), and the National Natural Science Foundation of China (NSFC, Nos. 31770331 and 90817002).

ACKNOWLEDGMENT

The authors thank ABRC for the Arabidopsis T-DNA insertion mutant pool.

SUPPLEMENTARY MATERIAL

The Supplementary Material for this article can be found online at: https://www.frontiersin.org/articles/10.3389/fpls.2017.02140/full#supplementary-material

FIGURE S1 | Nucleotide and deduced amino acid sequence of DY1. Predicted cleavage site after the chloroplast transit peptide is indicated by a black arrow. Peptide fragment used for raising antiserum against DY1 is underlined.

FIGURE S2 | DY1 interacts with a RAB GTPase homolog protein At4g20360. **(A)** Yeast two-hybrid analysis of the interaction between DY1 and At4g20360. *DY1* and *At4g20360* were cloned into pDEST32 and pDEST22, respectively. Yeast AH109 cells were co-transformed with a combination of these plasmids, and plated onto non-selective (SD/-Leu/-Trp, DDO) and selective (SD/-Leu/-Trp/-His/-Ade, QDO) plates in series dilution. **(B)** At4g20360 also localizes in chloroplasts.

TABLE S1 | Primers used in this study.

REFERENCES

Albrecht, V., Ingenfeld, A., and Apel, K. (2006). Characterization of the *snowy cotyledon 1* mutant of *Arabidopsis thaliana*: the impact of chloroplast elongation factor G on chloroplast development and plant vitality. *Plant Mol. Biol.* 60, 507–518. doi: 10.1007/s11103-005-4921-0

Albrecht, V., Ingenfeld, A., and Apel, K. (2008). *Snowy cotyledon 2*: the identification of a zinc finger domain protein essential for chloroplast development in cotyledons but not in true leaves. *Plant Mol. Biol.* 66, 599–608. doi: 10.1007/s11103-008-9291-y

Albrecht, V., Simkova, K., Carrie, C., Delannoy, E., Giraud, E., Whelan, J., et al. (2010). The cytoskeleton and the peroxisomal-targeted SNOWY COTYLEDON3 protein are required for chloroplast development in *Arabidopsis*. *Plant Cell* 22, 3423–3438. doi: 10.1105/tpc.110.074781

Albrecht-Borth, V., Kauss, D., Fan, D., Hu, Y., Collinge, D., Marri, S., et al. (2013). A novel proteinase, SNOWY COTYLEDON4, is required for photosynthetic acclimation to higher light intensities in Arabidopsis. *Plant Physiol.* 163, 732–745. doi: 10.1104/pp.113.216036

Aluru, M. R., Bae, H., Wu, D., and Rodermel, S. R. (2001). The Arabidopsis *immutans* mutation affects plastid differentiation and the morphogenesis of white and green sectors in variegated plants. *Plant Physiol.* 127, 67–77. doi: 10.1104/pp.127.1.67

Andriankaja, M. E., Danisman, S., Mignolet-Spruyt, L. F., Claeys, H., Kochanke, I., Vermeersch, M., et al. (2014). Transcriptional coordination between leaf cell differentiation and chloroplast development established by TCP20 and the subgroup Ib bHLH transcription factors. *Plant Mol. Biol.* 85, 233–245. doi: 10.1007/s11103-014-0180-2

Cheminant, S., Wild, M., Bouvier, F., Pelletier, S., Renou, J. P., Erhardt, M., et al. (2011). DELLAs regulate chlorophyll and carotenoid biosynthesis to prevent photooxidative damage during seedling deetiolation in Arabidopsis. *Plant Cell* 23, 1849–1860. doi: 10.1105/tpc.111.085233

Chen, K.-M., Holmström, M., Raksajit, W., Suorsa, M., Piippo, M., and Aro, E.-M. (2010). Small chloroplast-targeted DnaJ proteins are involved in optimization of photosynthetic reactions in *Arabidopsis thaliana*. *BMC Plant Biol.* 10:43. doi: 10.1186/1471-2229-10-43

Chenna, R., Sugawara, H., Koike, T., Lopez, R., Gibson, T. J., Higgins, D. G., et al. (2003). Multiple sequence alignment with the clustal

series of programs. *Nucleic Acids Res.* 31, 3497–3500. doi: 10.1093/nar/gkg500

Clough, S. J., and Bent, A. F. (1998). Floral dip: a simplified method for *Agrobacterium*-mediated transformation of *Arabidopsis thaliana*. *Plant J.* 16, 735–743. doi: 10.1046/j.1365-313x.1998.00343.x

Demmig-Adams, B., and Adams, W. W. III. (1996). The role of xanthophyll cycle carotenoids in the protection of photosynthesis. *Trends Plant Sci.* 1, 21–26. doi: 10.1016/S1360-1385(96)80019-7

Emanuelsson, O., Brunak, S., Von Heijne, G., and Nielsen, H. (2007). Locating proteins in the cell using TargetP, SignalP and related tools. *Nat. Protoc.* 2, 953–971. doi: 10.1038/nprot.2007.131

Emanuelsson, O., Nielsen, H., and Von Heijne, G. (1999). ChloroP, a neural network-based method for predicting chloroplast transit peptides and their cleavage sites. *Protein Sci.* 8, 978–984. doi: 10.1110/ps.8.5.978

Faso, C., Chen, Y. N., Tamura, K., Held, M., Zemelis, S., Marti, L., et al. (2009). A missense mutation in the *Arabidopsis* COPII coat protein Sec24A induces the formation of clusters of the endoplasmic reticulum and Golgi apparatus. *Plant Cell* 21, 3655–3671. doi: 10.1105/tpc.109.068262

Fristedt, R., Williams-Carrier, R., Merchant, S. S., and Barkan, A. (2014). A thylakoid membrane protein harboring a DnaJ-type zinc finger domain is required for photosystem I accumulation in plants. *J. Biol. Chem.* 289, 30657–30667. doi: 10.1074/jbc.M114.587758

Goss, R., Oroszi, S., and Wilhelm, C. (2007). The importance of grana stacking for xanthophyll cycle-dependent NPQ in the thylakoid membranes of higher plants. *Physiol. Plant.* 131, 496–507. doi: 10.1111/j.1399-3054.2007.00964.x

Green, M. R., and Sambrook, J. (2012). *Molecular Cloning: A Laboratory Manual*. Cold Springer Harbor, NY: Cold Spring Harbor Laboratory Press.

Harlow, E., and Lane, D. (1988). *Antibodies: A Laboratory Manual*. Cold Spring Harbor, NY: Cold Spring Harbor Laboratory Press.

Jin, H., Liu, B., Luo, L., Feng, D., Wang, P., Liu, J., et al. (2014). HYPERSENSITIVE TO HIGH LIGHT1 interacts with LOW QUANTUM YIELD OF PHOTOSYSTEM II1 and functions in protection of photosystem II from photodamage in *Arabidopsis*. *Plant Cell* 26, 1213–1229. doi: 10.1105/tpc.113.122424

Johnson, M. P., Davison, P. A., Ruban, A. V., and Horton, P. (2008). The xanthophyll cycle pool size controls the kinetics of non-photochemical quenching in *Arabidopsis thaliana*. *FEBS Lett.* 582, 262–266. doi: 10.1016/j.febslet.2007.12.016

Mullet, J. E. (1988). Chloroplast development and gene expression. *Annu. Rev. Plant Physiol. Plant Mol. Biol.* 39, 475–502. doi: 10.1146/annurev.pp.39.060188.002355

Pfalz, J., and Pfannschmidt, T. (2013). Essential nucleoid proteins in early chloroplast development. *Trends Plant Sci.* 18, 186–194. doi: 10.1016/j.tplants.2012.11.003

Pogson, B., McDonald, K. A., Truong, M., Britton, G., and DellaPenna, D. (1996). Arabidopsis carotenoid mutants demonstrate that lutein is not essential for photosynthesis in higher plants. *Plant Cell* 8, 1627–1639. doi: 10.1105/tpc.8.9.1627

Robinson, C., and Bolhuis, A. (2001). Protein targeting by the twin-arginine translocation pathway. *Nat. Rev. Mol. Cell Biol.* 2, 350–356. doi: 10.1038/35073038

Sakamoto, W. (2003). Leaf-variegated mutations and their responsible genes in *Arabidopsis thaliana*. *Genes Genet. Syst.* 78, 1–9. doi: 10.1266/ggs.78.1

Schmittgen, T. D., and Livak, K. J. (2008). Analyzing real-time PCR data by the comparative C_T method. *Nat. Protoc.* 3, 1101–1108. doi: 10.1038/nprot.2008.73

Schneider, A., Steinberger, I., Herdean, A., Gandini, C., Eisenhut, M., Kurz, S., et al. (2016). The evolutionarily conserved protein PHOTOSYNTHESIS AFFECTED MUTANT71 is required for efficient manganese uptake at the thylakoid membrane in Arabidopsis. *Plant Cell* 28, 892–910. doi: 10.1105/tpc.15.00812

Tamura, K., Stecher, G., Peterson, D., Filipski, A., and Kumar, S. (2013). MEGA6: molecular evolutionary genetics analysis version 6.0. *Mol. Biol. Evol.* 30, 2725–2729. doi: 10.1093/molbev/mst197

Timperio, A. M., D'Amici, G. M., Barta, C., Loreto, F., and Zolla, L. (2007). Proteomics, pigment composition, and organization of thylakoid membranes in iron-deficient spinach leaves. *J. Exp. Bot.* 58, 3695–3710. doi: 10.1093/jxb/erm219

Toledo-Ortiz, G., Huq, E., and Rodríguez-Concepción, M. (2010). Direct regulation of phytoene synthase gene expression and carotenoid biosynthesis by phytochrome-interacting factors. *Proc. Natl. Acad. Sci. U.S.A.* 107, 11626–11631. doi: 10.1073/pnas.0914428107

Wang, Y. W., Chen, S. M., Wang, W. J., Huang, X. Q., Zhou, C. F., Zhuang, Z., et al. (2016). The DnaJ-like zinc finger domain protein PSA2 affects light acclimation and chloroplast development in *Arabidopsis thaliana*. *Front. Plant Sci.* 7:360. doi: 10.3389/fpls.2016.00360

Williams, D. C., Wildung, M. R., Jin, A. Q., Dalal, D., Oliver, J. S., Coates, R. M., et al. (2000). Heterologous expression and characterization of a "Pseudomature" form of taxadiene synthase involved in paclitaxel (Taxol) biosynthesis and evaluation of a potential intermediate and inhibitors of the multistep diterpene cyclization reaction. *Arch. Biochem. Biophys.* 379, 137–146. doi: 10.1006/abbi.2000.1865

Yoo, S. D., Cho, Y. H., and Sheen, J. (2007). *Arabidopsis* mesophyll protoplasts: a versatile cell system for transient gene expression analysis. *Nat. Protoc.* 2, 1565–1572. doi: 10.1038/nprot.2007.199

Yu, F., Fu, A., Aluru, M., Park, S., Xu, Y., Liu, H., et al. (2007). Variegation mutants and mechanisms of chloroplast biogenesis. *Plant Cell Environ.* 30, 350–365. doi: 10.1111/j.1365-3040.2006.01630.x

Zhong, L., Zhou, W., Wang, H., Ding, S., Lu, Q., Wen, X., et al. (2013). Chloroplast small heat shock protein HSP21 interacts with plastid nucleoid protein pTAC5 and is essential for chloroplast development in *Arabidopsis* under heat stress. *Plant Cell* 25, 2925–2943. doi: 10.1105/tpc.113.111229

Zhou, F., Wang, C. Y., Gutensohn, M., Jiang, L., Zhang, P., Zhang, D., et al. (2017). A recruiting protein of geranylgeranyl diphosphate synthase controls metabolic flux toward chlorophyll biosynthesis in rice. *Proc. Natl. Acad. Sci. U.S.A.* 114, 6866–6871. doi: 10.1073/pnas.1705689114

Conflict of Interest Statement: The authors declare that the research was conducted in the absence of any commercial or financial relationships that could be construed as a potential conflict of interest.

frontiers in Plant Science

ORIGINAL RESEARCH
published: 17 January 2018
doi: 10.3389/fpls.2017.02183

NDH-1 Is Important for Photosystem I Function of *Synechocystis* sp. Strain PCC 6803 under Environmental Stress Conditions

Jiaohong Zhao[1], *Fudan Gao*[1], *Da-Yong Fan*[2,3], *Wah Soon Chow*[3] *and Weimin Ma*[1]*

[1] Department of Biology, College of Life and Environment Sciences, Shanghai Normal University, Shanghai, China, [2] State Key Laboratory of Vegetation and Environmental Change, Institute of Botany, Chinese Academy of Sciences, Beijing, China, [3] Division of Plant Sciences, Research School of Biology, Australian National University, Canberra, ACT, Australia

OPEN ACCESS

Edited by:
Hongbo Gao,
Beijing Forestry University, China

Reviewed by:
Hualing Mi,
Shanghai Institutes for Biological Sciences, Chinese Academy of Science, China
Fang Huang,
Key Laboratory of Photosynthesis and Environmental Molecular Physiology, Institute of Botany, (CAS), China
Qiang Wang,
Institute of Hydrobiology (CAS), China
Stefano Santabarbara,
Consiglio Nazionale Delle Ricerche (CNR), Italy

***Correspondence:**
Weimin Ma
wma@shnu.edu.cn

Specialty section:
This article was submitted to Plant Physiology, a section of the journal Frontiers in Plant Science

Received: *12 May 2017*
Accepted: *12 December 2017*
Published: *17 January 2018*

Citation:
Zhao J, Gao F, Fan D-Y, Chow WS and Ma W (2018) NDH-1 Is Important for Photosystem I Function of Synechocystis sp. Strain PCC 6803 under Environmental Stress Conditions. Front. Plant Sci. 8:2183. doi: 10.3389/fpls.2017.02183

Cyanobacterial NDH-1 interacts with photosystem I (PSI) to form an NDH-1-PSI supercomplex. Here, we observed that absence of NDH-1 had little, if any, effect on the functional fractions of PSI under growth conditions, but significantly reduced the functional fractions of PSI when cells of *Synechocystis* sp. strain PCC 6803 were moved to conditions of multiple stresses. The significant reduction in NDH-1-dependent functional fraction of PSI was initiated after PSII activity was impaired. This finding is consistent with our observation that the functional fraction of PSI under growth conditions was rapidly and significantly decreased with increasing concentrations of DCMU, which rapidly and significantly suppressed PSII activity by blocking the transfer of electrons from Q_A to Q_B in the PSII reaction center. Furthermore, absence of NDH-1 resulted in the PSI limitation at the functionality of PSI itself but not its donor-side and acceptor-side under conditions of multiple stresses. This was supported by the result of a significant destabilization of the PSI complex in the absence of NDH-1 but the presence of multiple stresses. Based on the above results, we propose that NDH-1 is important for PSI function of *Synechocystis* sp. strain PCC 6803 mainly via maintaining stabilization of PSI under conditions of environmental stresses.

Keywords: NDH-1, NDH-1-PSI, PSI function, environmental stress, *Synechocystis* sp. strain PCC 6803

INTRODUCTION

Cyanobacterial NDH-1 is predominantly, if not totally, located in the thylakoid membrane (Ohkawa et al., 2001, 2002; Zhang et al., 2004; Xu et al., 2008; Battchikova et al., 2011), and participates in a variety of bioenergetic reactions, including respiration, cyclic electron transport around PSI, and CO_2 acquisition (Ogawa, 1991; Mi et al., 1992; Ohkawa et al., 2000). The function of NDH-1 is usually minor under normal growth conditions and becomes important under conditions of environmental stresses. In line with this, absence of NDH-1 has little, if any, effect on cell growth under normal conditions but retards cell growth and even causes cell death under conditions of environmental stresses, such as high light (Battchikova et al., 2011; Dai et al., 2013; Zhang et al., 2014; Zhao et al., 2014b, 2015; Gao et al., 2016a; Wang et al., 2016) and high temperature (Zhao et al., 2014a; Gao et al., 2016b). Therefore, cyanobacterial NDH-1 plays an important role in coping with various environmental stresses.

When cyanobacterial cells are transferred from normal growth conditions to multiple stressful environments, the amount of NDH-1 and its activity, for example, NDH-1-dependent cyclic electron transport around PSI (NDH-CET), are significantly increased under conditions of high temperature (Rowland et al., 2010; Zhao et al., 2014a), high salt (Hibino et al., 1996; Tanaka et al., 1997), high light (Mi et al., 2001), and low CO_2 (Deng et al., 2003). Such an increase is assumed to be important in repairing the photodamaged PSII, optimizing photosynthesis by increasing the proton gradient across the thylakoid membrane and supplying additional ATP (Allakhverdiev et al., 2005). However, the effect of cyanobacterial NDH-1 on PSI remains elusive.

Recently, cyanobacterial NDH-1 was found to interact with PSI to form an NDH-1-PSI supercomplex via CpcG2-phycobilisome, a PSI-specific antenna (Kondo et al., 2007; Gao et al., 2016a). Further, the supercomplex was found to be involved in NDH-CET but not respiration and CO_2 uptake (Gao et al., 2016a). Here, our results demonstrate that NDH-1 is important for PSI function of *Synechocystis* sp. strain PCC 6803 (hereafter *Synechocystis* 6803) under conditions of multiple stresses. We further found that NDH-1-dependent PSI function was initiated after PSII was impaired and its impairment is mostly the result of destabilization of PSI. The contribution of NDH-1-PSI supercomplex to PSI function is discussed.

MATERIALS AND METHODS

Culture Conditions

A glucose tolerant strain of wild-type (WT) *Synechocystis* 6803 and its mutants, Δ*ndhB* (M55) (Ogawa, 1991), M55+NdhB and Δ*pgr5* were cultured at 30°C in BG-11 medium (Allen, 1968) buffered with Tris-HCl (5 mM, pH 8.0) by bubbling with 2% (*v*/*v*) CO_2 in air. Continuous illumination was provided by fluorescence lamps at 40 μmol photons $m^{-2}s^{-1}$. The mutant strains were grown in the presence of appropriate antibiotics.

Construction of Δ*pgr5* Mutant

The Δ*pgr5* mutant was constructed as follows. The upstream and downstream regions of *ssr2016* (*pgr5*) were amplified by PCR, creating appropriate restriction sites. A DNA fragment encoding a kanamycin resistance (Kam^R) cassette was also amplified by PCR, creating *Sal*I and *Xba*I sites using appropriate PCR primers, *pgr5*-C and *pgr5*-D (Supplementary Table S1). These three PCR products were ligated into the multiple cloning site of pUC19 (**Figure 5A**) and used to transform the WT cells of *Synechocystis* 6803 to generate the Δ*pgr5* mutant. The transformants were spread on agar plates containing BG-11 medium and kanamycin (10 μg mL^{-1}) buffered at pH 8.0, and the plates were incubated in 2% (*v*/*v*) CO_2 in air under illumination by fluorescent lamps at 40 μmol photons m^{-2} s^{-1} as described previously (Williams and Szalay, 1983; Long et al., 2011). The mutated *pgr5* in the transformants was segregated to homogeneity (by successive streak purification) as determined by PCR amplification and reverse transcription (RT)-PCR analysis (**Figures 5B,C**).

Construction of M55 Complementation Strain

The M55 complementation strain was constructed as follows. A DNA fragment containing the *ndhB* gene was amplified by PCR and then inserted into *Nde*I site of P*psbAII* expression vector (Jiang et al., 2012) to form the P*psbAII-ndhB* expression plasmid (Supplementary Figure S1A; primers are shown in Supplementary Table S1), which was used to transform the M55 mutant of *Synechocystis* 6803 to generate the M55 complementation strain. The transformants were spread on agar plates containing BG-11 medium, spectinomycin (10 μg mL^{-1}) and kanamycin (10 μg mL^{-1}) buffered at pH 8.0, and the plates were incubated in 2% (*v*/*v*) CO_2 in air under illumination by fluorescent lamps at 40 μmol photons m^{-2} s^{-1} as described previously (Williams and Szalay, 1983; Long et al., 2011). Complete segregation of the transformants was confirmed by PCR (Supplementary Figure S1B) and the expression level of *ndhB* in the transformants was estimated by RT-PCR (Supplementary Figure S1C).

RNA Extraction and RT-PCR Analysis

Total RNA was isolated and analyzed as described previously (McGinn et al., 2003). RT-PCR was performed using the Access RT-PCR system (Promega) to generate products corresponding to *pgr5* and *16S rRNA*, with 0.5 μg of DNase-treated total RNA as starting material. RT-PCR conditions were 95°C for 5 min followed by cycles of 95, 62, and 72°C for 30 s each. The reactions were stopped after 25 cycles for *16S rRNA* and after 35 cycles for *ndhB* and *pgr5*. The primers used are summarized in Supplementary Table S1.

Chlorophyll Fluorescence

The yield of chlorophyll (Chl) fluorescence at the steady state of electron transport was measured using a Dual-PAM-100 monitoring system (Walz, Effeltrich, Germany) equipped with an ED-101US/MD unit (Schreiber et al., 1986; Ma et al., 2008), as shown in Supplementary Figure S2. Minimal fluorescence corresponding to open PSII centers in the dark-adapted state (F_o) and in the far-red (FR) light-adapted state (F_o') was excited by a weak measuring light (650 nm) at a PFD of 0.05–0.15 μmol photons $m^{-2}s^{-1}$. A saturation pulse of red light (100 ms, 10,000 μmol photons $m^{-2}s^{-1}$) was applied to determine the maximal fluorescence at closed PSII centers in the dark-adapted state (F_m) and in the red actinic light (AL)-adapted state (F_m') as described previously (Klughammer and Schreiber, 2008a). Subsequently, red AL was applied to monitor fluorescence under the steady-state condition (F_s). F_v/F_m and *q*P were calculated as $(F_m-F_o)/F_m$ (Kitajima and Butler, 1975) and $(F_m'-F_s)/(F_m'-F_o')$ (van Kooten and Snel, 1990), respectively.

Abbreviations: BN-PAGE, blue-native-PAGE; CBB, Coomassie Brilliant Blue; Chl, chlorophyll; DCMU, 3-(3,4-dichlorophenyl)-1,1-dimethylurea; F_v/F_m, maximal quantum yield of PSII; HL, high light; HS, high salt; M55, Δ*ndhB*; NDH-CET, NDH-1-dependent cyclic electron transport around PSI; MV, methyl viologen; PRG5, PROTON GRADIENT REGULATION 5; P_m, the maximal P700 change; *q*P, the ratio of the oxidized PQ pool; *Synechocystis* 6803, *Synechocystis* sp. strain PCC 6803; WT, wild-type.

The P700$^+$ Signal Monitored as an 830 nm Absorbance Change

With the Dual-PAM-100, P700$^+$ was monitored as the absorption difference between 830 and 875 nm in transmission mode. The quantum yields of PSI were determined using the saturation pulse method as described previously (Klughammer and Schreiber, 1994, 2008b; Supplementary Figure S3). The level of maximal P700$^+$ signal observed upon full oxidation, P_m, was determined by application of a saturation pulse of red light (100 ms; 10,000 μmol photons $m^{-2}s^{-1}$) in the presence of far-red light (about 0.3 μmol photons $m^{-2}s^{-1}$) at 720 nm.

Photosynthetic Oxygen Evolution

Oxygen evolution by photosynthesis was measured at 30°C in the presence of 10 mM $NaHCO_3$ with a Clark-type oxygen electrode (Hansatech, Hertfordshire, UK) according to the method described by Ma and Mi (2005). Cells were suspended in fresh BG-11 medium at a Chl *a* concentration of 5 μg mL^{-1} and, different concentrations of 3-(3,4-dichlorophenyl)-1,1-dimethylurea (DCMU) were added to the cell suspension cultures prior to measurement. The intensity of AL used for the measurement of photosynthetic oxygen evolution was 800 μmol photons m^{-2} s^{-1}.

Isolation of Crude Thylakoid Membranes

Cell in cultured medium (800 mL) were harvested at the logarithmic phase of growth and washed twice by suspending in 50 mL of fresh BG-11 medium, and the thylakoid membranes were isolated according to Gombos et al. (1994) with some modifications as follows. The cells suspended in 5 mL of disruption buffer (10 mM HEPES-NaOH, 5 mM sodium phosphate, pH 7.5, 10 mM $MgCl_2$, 10 mM NaCl, and 25% [*v*/*v*]

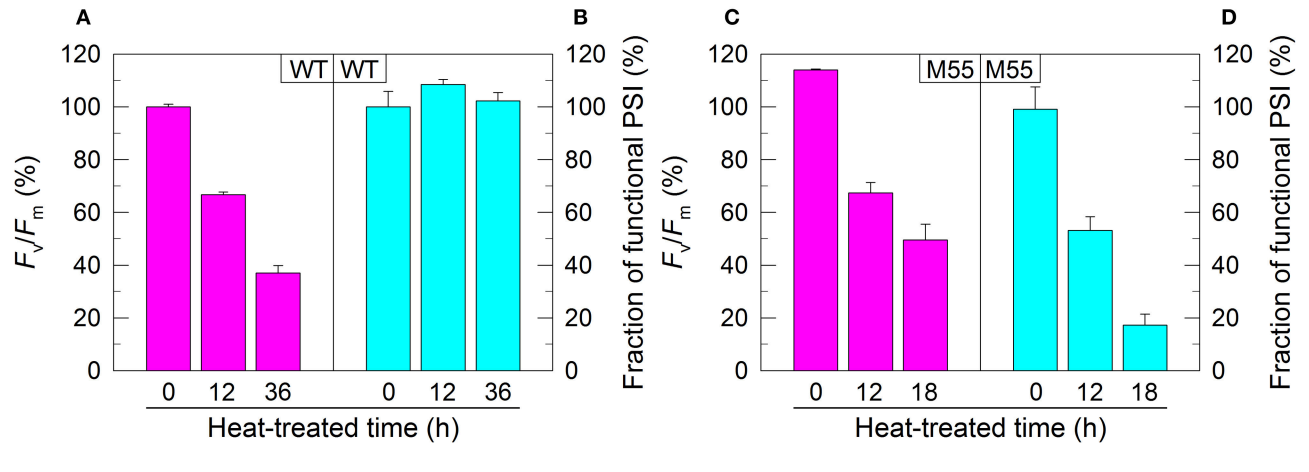

FIGURE 1 | PSII activity and PSI functional fraction of WT **(A,B)** and M55 **(C,D)** under high temperature conditions. Cells were grown at 30°C for 24 h and were transferred to 45°C for different periods. Prior to the measurements, the Chl *a* concentration was adjusted to 20 μg mL^{-1}. PSII activity and PSI functionality were determined by the F_v/F_m and P_m parameters, respectively, expressed as percentage of the WT (100%). The F_v/F_m and P_m values that correspond to 100% are 0.46 ± 0.02 and 0.58 ± 0.02, respectively. Values are means ± *SD* ($n = 5$).

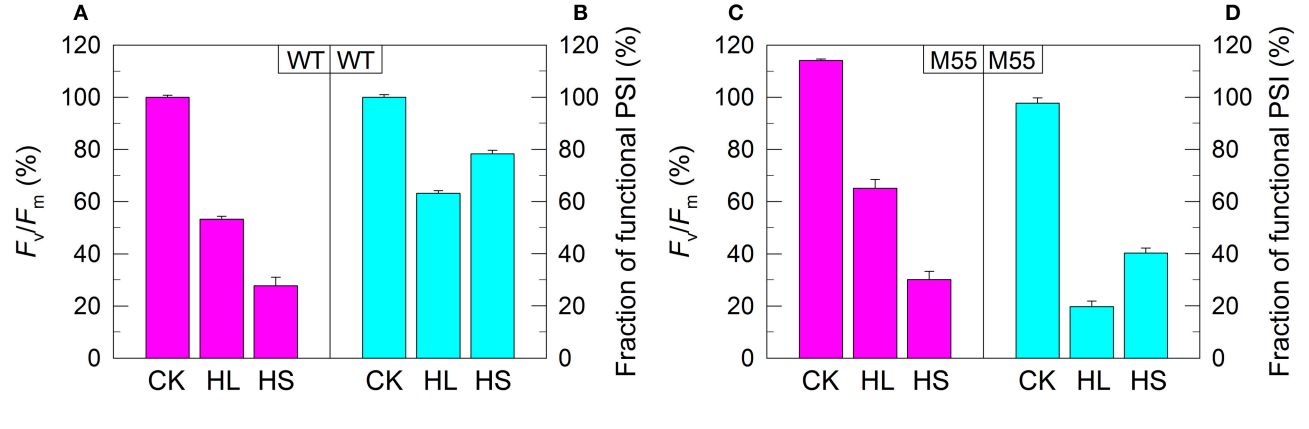

FIGURE 2 | PSII activity and PSI functional fraction of WT **(A,B)** and M55 **(C,D)** under conditions of high light and high salt. Cells were grown under normal salt conditions at 40 μmol photons m^{-2} s^{-1} for 24 h and were transferred to 300 μmol photons m^{-2} s^{-1} for 36 h or to 0.8 M NaCl for 12 h. Prior to the measurements, the Chl *a* concentration was adjusted to 20 μg mL^{-1}. PSII activity and PSI functionality were determined by the F_v/F_m and P_m parameters, respectively, expressed as percentage of the WT (100%). The F_v/F_m and P_m values that correspond to 100% are shown in the legend of **Figure 1**. Values are means ± *SD* ($n = 5$). CK, control check; HL, high light; HS, high salt.

glycerol) were supplemented by zirconia/silica beads and broken by vortexing 20 times at the highest speed for 30 s at 4°C with 5 min of cooling on ice between the runs. The crude extract was centrifuged at 5,000×*g* for 5 min to remove the glass beads and unbroken cells. By further centrifugation at 20,000×*g* for 30 min, we obtained crude thylakoid membranes as precipitates.

Electrophoresis

Blue-native (BN)-PAGE of *Synechocystis* 6803 membranes was performed as described previously (Kügler et al., 1997) with slight modifications (Battchikova et al., 2011; Dai et al., 2013; Zhang et al., 2014; Zhao et al., 2014a, 2015; Gao et al., 2016a,b; Wang et al., 2016). Isolated membranes were prepared for BN-PAGE as follows. Membranes were washed with 330 mM sorbitol, 50 mM Bis-Tris (pH 7.0), and 0.5 mM phenylmethylsulfonyl fluoride (PMSF; Sigma) and resuspended in 20% (*w*/*v*) glycerol, 25 mM Bis-Tris (pH 7.0), 10 mM $MgCl_2$, 0.1 units of RNase-free DNase RQ1 (Promega) at a Chl *a* concentration of 0.25 mg mL^{-1}, and 0.5 mM PMSF. The samples were incubated on ice for 10 min, and an equal volume of 3% DM was added. Solubilization was performed for 40 min on ice. Insoluble components were removed by centrifugation at 18,000×*g* for 15 min. The collected supernatant was mixed with one-tenth volume of sample buffer, 5% Serva Blue G, 100 mM Bis-Tris (pH 7.0), 30% (*w*/*v*) sucrose, 500 mM ε-amino-*n*-caproic acid, and 10 mM EDTA. Solubilized membranes were then applied to a 0.75-mm-thick, 5–12.5% acrylamide gradient gel (Hoefer Mighty Small mini-vertical unit). Samples were loaded on an equal Chl *a* basis per lane. Electrophoresis was performed at 4°C by increasing the voltage gradually from 50 up to 200 V during the 5.5-h run.

RESULTS

NDH-1 Is Important for PSI Function under Conditions of Multiple Stresses

In *Synechocystis* 6803, NDH-1 interacts with PSI to form an NDH-1-PSI supercomplex (Gao et al., 2016a). To test whether the absence of NDH-1 affected the function of PSI under conditions of growth and environmental stress, we monitored the fractions of functional PSI when cells of WT and Δ*ndhB* (M55), which lacks all functional NDH-1 complexes (Zhang et al., 2004), were incubated under high temperature conditions for different periods. The fractions of functional PSI of WT and M55 were similar under conditions of growth temperature (30°C), as deduced from the maximal P700 change (P_m) level (0 h in **Figures 1B,D**). When cells were moved to conditions of high temperature (45°C) for different periods, however, we observed some expected and unexpected results. As expected, the activity of PSII in WT and M55 was gradually decreased (**Figures 1A,C**) whereas the fraction of functional PSI in WT was always maintained at a high level (**Figure 1B**) with the extension of heating time. Unexpectedly, the fraction of functional PSI in M55 was gradually and drastically decreased with the increase in heat incubation (**Figure 1D**).

We also measured the fractions of functional PSI upon exposure of WT and M55 cells to conditions of high light and high salt. As expected, the remaining functional fraction of PSI in M55 was about 20% of that in the WT under high light and was about 40% of that in the WT under high salt (**Figures 2B,D**). It is worthy of note that these decreased fractions of functional PSI in M55 under conditions of heat, high light, and high salt could be recovered in its complementation strain M55+NdhB to the levels of WT (Supplementary Figures S1D–F). Taking all these results together, we can conclude that NDH-1 is important for the function of PSI under conditions of environmental stresses but not under growth conditions.

NDH-1-Dependent PSI Function Is Initiated after PSII Activity Is Impaired

Under conditions of normal growth, WT and M55 cells had a similar activity of PSII (measured as the maximal quantum yield of PSII, F_v/F_m) and had also a similar functional activity of PSI (0 h in **Figures 1A–D**). When cells of WT and M55 were transferred to conditions of multiple stresses and the activity of PSII was significantly suppressed in both strains, the functional fraction of PSI was significantly decreased in M55 mutant but not (**Figure 1B**) or to a lesser extent (**Figure 2B**) in the WT. It appears plausible that the decrease in PSII activity is a prerequisite for initiating the NDH-1-depenent PSI function.

To confirm this possibility, we measured the fractions of functional PSI in WT and M55 cells without or with different concentrations of DCMU, which blocks the transfer of electrons from Q_A to Q_B in the PSII reaction center (Trebst, 1980). As expected, with the increase in DCMU concentration, the activity of PSII (measured as oxygen evolution) was rapidly and similarly suppressed in WT and M55 (**Figure 3**). By contrast, the fractions of functional PSI were rapidly and significantly decreased in M55 but much less in the WT with the increase in DCMU concentration (**Figure 4A**), although both strains had a similar

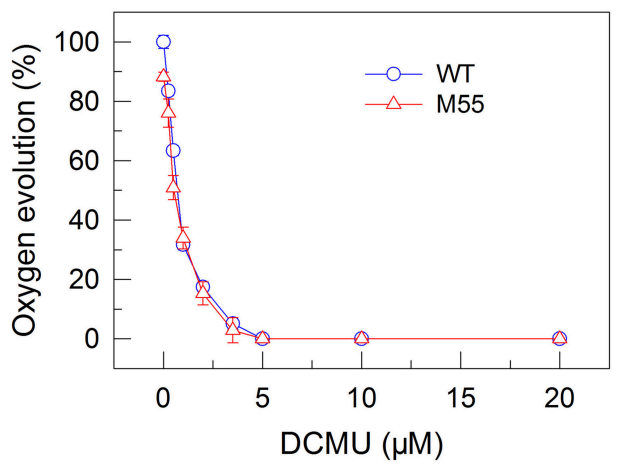

FIGURE 3 | Effects of DCMU treatment at different concentrations on the PSII activity in WT and M55 strains. PSII activity was assessed by the light-saturated photosynthetic oxygen evolution rate in the presence of DCMU and $NaHCO_3$, expressed as percentage of the WT (100%). The rate of photosynthetic oxygen evolution that corresponds to 100% is 128.2 ± 8.6 μmol O_2 mg^{-1} Chl *a* h^{-1}. Values are means ± *SD* ($n = 5$).

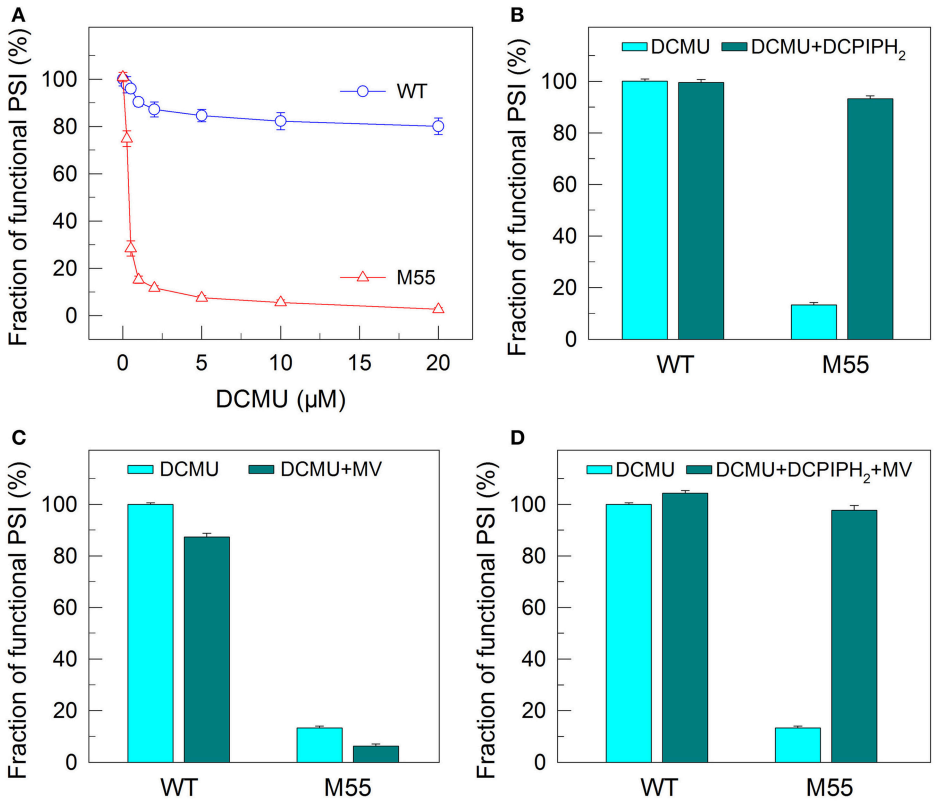

FIGURE 4 | Functional fractions of PSI in WT and M55 with or without PSII electron transport inhibitor and/or PSI electron donor and acceptor. Cells were grown under 2% CO_2 at 40 μmol photons m^{-2} s^{-1} and were collected during their logarithmic growth phase. The Chl *a* concentration of WT and M55 cells was adjusted to 20 μg mL^{-1}. Prior to the P_m measurements, DCMU of different concentrations **(A)** or 10 μM **(B–D)** was added to the cell suspension **(A)**, to the cell suspension containing 200 μM 2,6-dichlorophenol-indophenol and 5 mM sodium ascorbate **(B)**, to the cell suspension containing 200 μM methyl viologen **(C),** and to the cell suspension containing 200 μM 2,6-dichlorophenol-indophenol, 5 mM sodium ascorbate, and 200 μM methyl viologen **(D)**. The functionality of PSI reaction centers was determined by the P_m parameter, expressed as a percentage of the WT (100%). The P_m value that corresponds to 100% is shown in the legend of **Figure 1**. Values are means ± *SD* ($n = 5$).

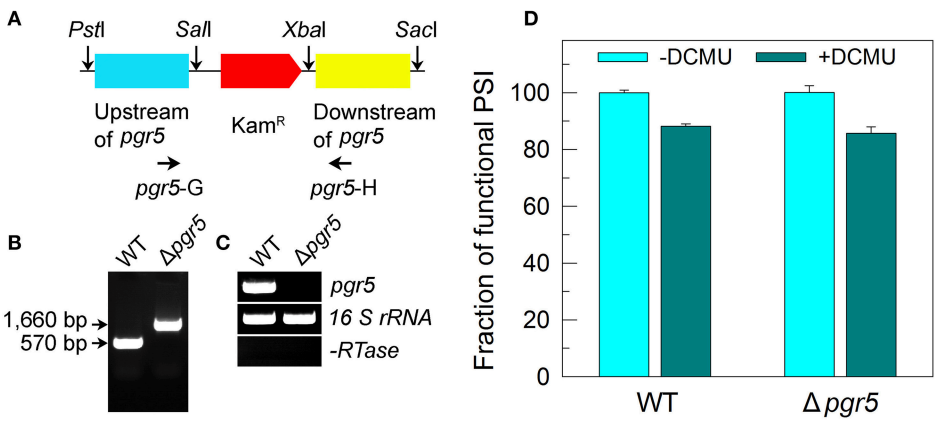

FIGURE 5 | Deletion of *pgr5* and its effect on P_m in the presence of DCMU. **(A)** Construction of the plasmid used to generate the *pgr5* deletion mutant (Δ*pgr5*). **(B)** PCR segregation analysis of the Δ*pgr5* mutant using the *pgr5*-G and *pgr5*-H primer sequences (Supplementary Table S1). **(C)** Transcript levels of *pgr5* in the WT and Δ*pgr5* strains. The transcript level of *16 S rRNA* in each sample is shown as a control. The absence of DNA contamination was confirmed by PCR without reverse transcriptase reaction. **(D)** Cells were grown under 2% CO_2 at 40 μmol photons m^{-2} s^{-1} and were collected during their logarithmic growth phase. The Chl *a* concentration of WT and Δ*pgr5* cells was adjusted to 20 μg mL^{-1}. Prior to the P_m measurements, DCMU (10 μM; final concentration) was added to the cell suspension. The functionality of PSI reaction centers was determined by the P_m parameter, expressed as a percentage of the WT (100%). The P_m value that corresponds to 100% is shown in the legend of **Figure 1**. Values are means ± *SD* ($n = 5$).

function of PSI in the absence of DCMU (0 μM in **Figure 4A**). Under conditions of DCMU addition, however, these changes in PSI function in the absence of NDH-1 were not observed in the absence of PROTON GRADIENT REGULATION 5 (PGR5) (**Figures 5A–D**), an alternative to NDH-1 in cyclic electron transport around PSI (Yeremenko et al., 2005). Based on the above results, we can conclude that NDH-1-depenent PSI function is specifically initiated after PSII activity is impaired but PGR5 is not involved in this process.

Functionality of PSI Itself Is Impaired in the Background of NDH-1 Absence and Multiple Stresses

To test how NDH-1 affected PSI function under conditions of multiple stresses, we measured the PSI limitation at donor-side and acceptor-side as well as the functionality of PSI itself in WT and M55 strains. The reduced fractions of functional PSI under conditions of high temperature, high light and high salt were

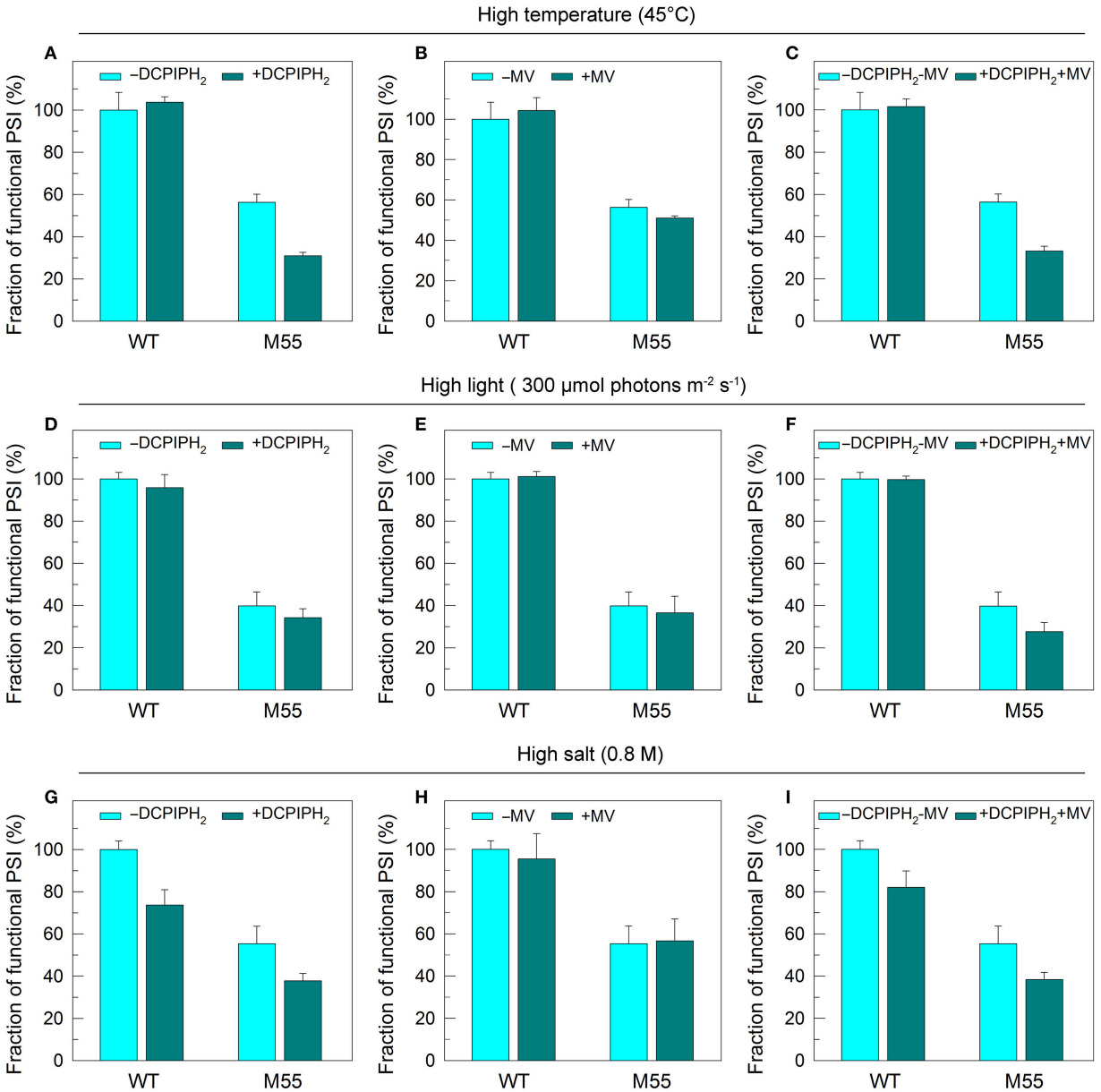

FIGURE 6 | PSI functional fractions of WT and M55 under multiple stresses with PSI electron donor and/or acceptor**.** Cells were grown under normal salt conditions at 30°C and 40 μmol photons m^{-2} s^{-1} for 24 h and were transferred to 45°C for 12 h, 300 μmol photons m^{-2} s^{-1} for 36 h, or to 0.8 M NaCl for 12 h. The Chl *a* concentration of WT and M55 cells was adjusted to 20 μg mL^{-1}. Prior to the P_m measurements, 200 μM 2,6-dichlorophenol-indophenol and 5 mM sodium ascorbate and/or 200 μM methyl viologen were added to the cell suspension, as shown in **(A–I)**. The functionality of PSI reaction centers was determined by the P_m parameter, expressed as a percentage of the WT (100%). The P_m value that corresponds to 100% is shown in the legend of **Figure 1**. Values are means ± *SD* ($n = 5$).

not recovered in M55 and were even slightly decreased by the addition of an exogenous PSI electron donor and/or acceptor to the cell suspension cultures of M55 (**Figures 6A–I**). Here, 2,6-dichlorophenolindophenol together with ascorbate ($DCPIPH_2$) and methyl viologen (MV) were used as an exogenous electron donor (Mi et al., 1995) and acceptor (Takahashi and Katoh, 1984) for the PSI complex, respectively. Taking all these results together, we suggest that the impairment of PSI function in the absence of NDH-1 but the presence of multiple stresses is a result of impaired functionality of PSI itself.

DCMU addition and multiple stress treatments have a similar damage effect on PSI function in the absence of NDH-1 (see **Figures 1**, **2**, **4**) possibly because of suppressed PSII activity (**Figures 1–3**). To see whether the impairment of PSI function in DCMU-treated M55 cells also resulted from impaired functionality of PSI itself, we monitored the fractions of functional PSI in DCMU-treated cells of WT and M55 with or without $DCPIPH_2$ and/or MV. Unexpectedly, the reduced fractions of functional PSI were completely recovered in M55 by the addition of $DCPIPH_2$ with or without MV to the cell suspension cultures of M55 (**Figures 4B,D**), although they were still not recovered in M55 by the addition of only MV to the cell suspension cultures of M55 (**Figure 4C**). Therefore, the impairment of PSI function in the absence of NDH-1 but the presence of DCMU is a result of donor-side limitation of PSI. Based on the above results, we suggest that DCMU addition and multiple stress treatments have a similar damage effect on PSI function in the absence of NDH-1 but their impaired targets are different.

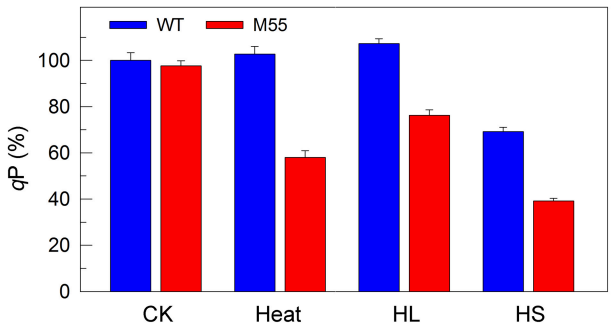

FIGURE 7 | The ratio of the oxidized PQ pool (*q*P) of WT and M55 under multiple stresses. Cells were grown under normal salt conditions at 30°C and 40 μmol photons m^{-2} s^{-1} for 24 h and were transferred to 45°C for 12 h, 300 μmol photons m^{-2} s^{-1} for 36 h, or to 0.8 M NaCl for 12 h. Prior to the *q*P measurements, the Chl *a* concentration of WT and M55 cells was adjusted to 20 μg mL^{-1}. The ratio of the oxidized PQ pool was determined by the *q*P parameter, expressed as a percentage of the WT (100%). The *q*P value that corresponds to 100% is 0.81 ± 0.03. Values are means ± *SD* ($n = 5$).

To obtain insights into the reason why DCMU addition and multiple stress treatments have different impaired targets in PSI, we measured the redox state of plastoquinone (PQ) pool in WT and M55 grown under conditions of multiple stresses. The fluorescence parameter *q*P can reflect the redox state of the PQ pool and its decrease is closely linked with reduction of the PQ pool (Misumi et al., 2016). Under conditions of high temperature, high light or high salt, the reduction level of the PQ pool in M55 was higher than that in WT as deduced from the *q*P values (**Figure 7**, right), regardless of similar redox state of the PQ pool under conditions of growth temperature (**Figure 7**, left). In addition, it is known that DCMU addition results in oxidation of the PQ pool via blocking the transfer of electrons from Q_A to Q_B in PSII (Trebst, 1980) and in the presence of DCMU, the oxidation level of the PQ pool in M55 might be higher than that in WT, because of absence of NDH-1-dependent cyclic and respiratory flows in M55 (Mi et al., 1992). Taking all these results together, we propose that multiple stresses and DCMU addition

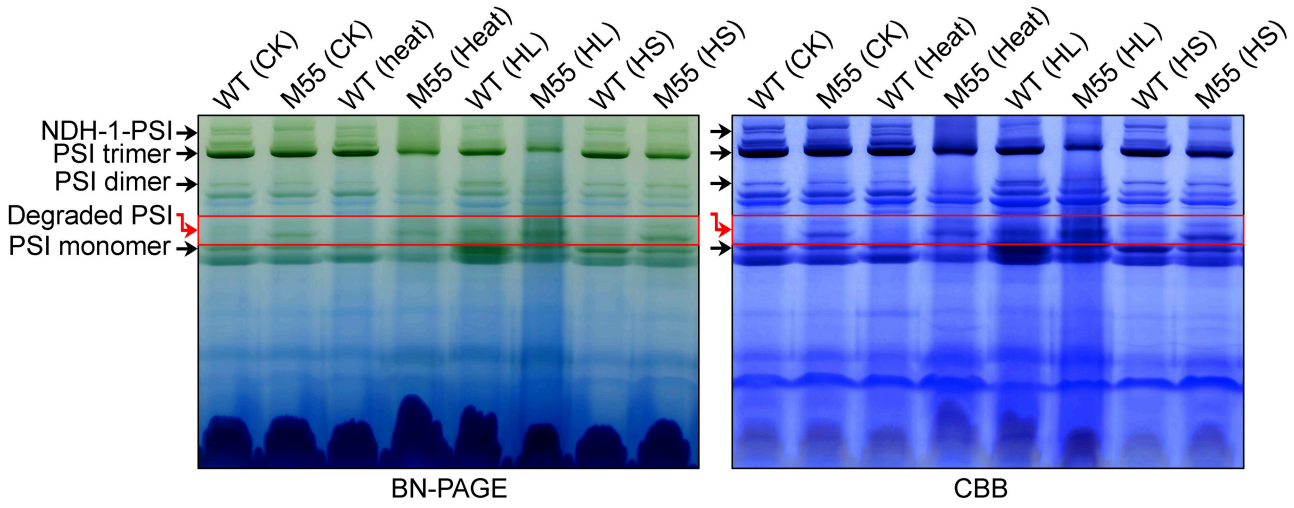

FIGURE 8 | Accumulation of various PSI types under conditions of multiple stresses. Various PSI types isolated from the thylakoid membrane of WT and M55 cells were separated by BN-PAGE **(left)** and were stained by Coomassie Brilliant Blue (CBB; **right**). Black, and red arrows represent various PSI types and degraded PSI, respectively.

cause an opposite change in the redox state of the PQ pool, which may give a clue to the reason why they have different impaired targets in PSI.

Absence of NDH-1 Destabilizes the PSI Complex under Multiple Stresses

To understand why the functionality of PSI itself is impaired under conditions of high temperature, high light and high salt, we examined various types of PSI complexes in WT and M55 cells grown under these stress conditions. Under normal growth conditions, the absence of NDH-1 in M55 resulted in a slight destabilization of the PSI complexes compared to the WT (see red box in **Figure 8**; left), just like the results of previous studies (Gao et al., 2016a). Such destabilization became more evident under conditions of multiple stresses, as reflected by the relative contents of the PSI trimer, dimer and monomer (**Figure 8**; left); these differences between WT and M55 were clearer after staining with Coomassie Brilliant Blue (**Figure 8**; right). These results strongly suggest that absence of NDH-1 destabilized the PSI complex, specifically under multiple stresses, and consequently impaired the functionality of PSI itself.

DISCUSSION

Over the past decades, a significant achievement has been made in identifying the important role of cyanobacterial NDH-1 in protecting photosynthesis against environmental stresses, including protecting PSII and optimizing carbon assimilation via producing additional ATP and improving the ATP/NADPH ratio (Battchikova et al., 2011; Dai et al., 2013; Zhang et al., 2014; Zhao et al., 2014a,b, 2015; Gao et al., 2016a,b; Wang et al., 2016). The results of this study further indicate that cyanobacterial NDH-1 is important in maintaining the functionality of PSI itself (**Figure 6**), thereby guaranteeing a high level of PSI function under multiple stress conditions (**Figures 1**, **2**). To our knowledge, this is the first study that reveals the contribution of NDH-1 to maintaining PSI functionality in cyanobacteria.

Recently, an NDH-1-PSI supercomplex was identified in the cyanobacterium *Synechocystis* 6803 (Gao et al., 2016a). We further found that absence of NDH-1 collapsed the supercomplex and resulted in a slight destabilization of the PSI complex, as deduced from the results of this study (**Figure 8**) and a previous study (Gao et al., 2016a) and that such destabilization became more evident under conditions of environmental stresses, as deduced from the results of this study (**Figure 8**) and a previous study (Zhao et al., 2014a). This finding may (1) explain why multiple stress treatments impairs the functionality of PSI itself, and (2) indicate that formation of the NDH-1-PSI supercomplex is important to keep a high level of PSI function under various stressful conditions.

Although the NDH-1-PSI supercomplex was also identified in angiosperms (Peng et al., 2008, 2009; Kouřil et al., 2014), the linker protein between NDH-1 and PSI as well as the component and function of NDH-1 were altered during evolution from cyanobacteria to higher plants. Stable formation of the supercomplex in higher plants needs two light-harvesting complex I (LHCI) proteins, Lhca5 and Lhca6, and in cyanobacteria needs a PSI-specific peripheral antenna, CpcG2-phycobilisome, but their homologs lack in each other (Peng et al., 2009; Gao et al., 2016a). In addition, NDH-1 included in the NDH-1-PSI supercomplex of cyanobacteria and higher plants has a similar L-shaped skeleton. Despite their similarity, a large number of NDH-1 subunits in higher plants, including ferredoxin-binding subcomplex subunits NdhT and NdhU and all the subunits of subcomplex B and lumen subcomplex, are absent in the cyanobacterial NDH-1 (for review, see Ma and Ogawa, 2015).

It is known that the NDH-1-PSI supercomplex mainly participates in NDH-CET (Peng et al., 2008, 2012; Gao et al., 2016a). NDH-CET can produce ATP via building a proton gradient across the thylakoid membrane, which is important for running the Calvin-Benson cycle under conditions of environmental stress; consequently, the presence of NDH-1 keeps a high PSI functional activity. In Arabidopsis, NDH-CET had no effect on PSI function even under conditions of fluctuating light, regardless of an important protecting role of PGR5-CET in PSI function under fluctuating light (Suorsa et al., 2012; Kono et al., 2014). Unexpectedly, in rice, NDH-CET plays an important contribution on PSI function, although the contribution is still minor compared with the PGR5-CET (Yamori et al., 2016). What's even more amazing is that NDH-1 seems to aid the antimycin A-sensitive PGR5-CET in Arabidopsis (Kou et al., 2015). By contrast, in *Synechocystis* 6803, NDH-CET is found to be important for PSI function under conditions of multiple stresses (**Figures 1**, **2**) but PGR5-CET had little, if any, effect on PSI function even in the presence of DCMU (**Figure 5**). Based on the above results, we propose that the role of NDH-1 on PSI function has been altered during evolution from cyanobacteria to higher plants.

AUTHOR CONTRIBUTIONS

WM: designed and supervised the experiments; JZ and FG: performed the experiments and analyzed the data; D-YF, WC, and WM: analyzed and interpreted the data and wrote the article.

ACKNOWLEDGMENTS

We thank Professors Teruo Ogawa (Nagoya University) and Bao-Sheng Qiu (Central China Normal University) for kindly providing the M55 mutant and the P*psbAII* expression vector, respectively. This work was supported by the National Natural Science Foundation of China (grant nos. 31370270, 31570235, 31770259, and 31700205), China Postdoctoral Science Foundation (grant nos. 2015M581643 and 2017T100304), Shanghai Science and Technology Committee (grant no. 17070502900) and Project of Shanghai Normal University (grant no. SK201705).

SUPPLEMENTARY MATERIAL

The Supplementary Material for this article can be found online at: https://www.frontiersin.org/articles/10.3389/fpls.2017.02183/full#supplementary-material

REFERENCES

Allakhverdiev, S. I., Nishiyama, Y., Takahashi, S., Miyairi, S., Suzuki, I., and Murata, N. (2005). Systematic analysis of the relation of electron transport and ATP synthesis to the photodamage and repair of photosystem II in *Synechocystis*. *Plant Physiol.* 137, 263–273. doi: 10.1104/pp.104.054478

Allen, M. M. (1968). Simple conditions for growth of unicellular blue-green algae on plates. *J. Phycol*. 4, 1–4. doi: 10.1111/j.1529-8817.1968.tb04667.x

Battchikova, N., Wei, L., Du, L., Bersanini, L., Aro, E. M., and Ma, W. (2011). Identification of novel Ssl0352 protein (NdhS), essential for efficient operation of cyclic electron transport around photosystem I, in NADPH: plastoquinone oxidoreductase (NDH-1) complexes of *Synechocystis* sp. PCC 6803. *J. Biol. Chem*. 286, 36992–37001. doi: 10.1074/jbc.M111.263780

Dai, H., Zhang, L., Zhang, J., Mi, H., Ogawa, T., and Ma, W. (2013). Identification of a cyanobacterial CRR6 protein, Slr1097, required for efficient assembly of NDH-1 complexes in *Synechocystis* sp. PCC 6803. *Plant J*. 75, 858–866. doi: 10.1111/tpj.12251

Deng, Y., Ye, J., and Mi, H. (2003). Effects of low CO_2 on NAD(P)H dehydrogenase, a mediator of cyclic electron transport around photosystem I in the cyanobacterium *Synechocystis* PCC6803. *Plant Cell Physiol*. 44, 534–540. doi: 10.1093/pcp/pcg067

Gao, F., Zhao, J., Chen, L., Battchikova, N., Ran, Z., Aro, E. M., et al. (2016a). The NDH-1L-PSI supercomplex is important for efficient cyclic electron transport in cyanobacteria. *Plant Physiol.* 172, 1451–1464. doi: 10.1104/pp.16.00585

Gao, F., Zhao, J., Wang, X., Qin, S., Wei, L., and Ma, W. (2016b). NdhV is a subunit of NADPH dehydrogenase essential for cyclic electron transport in *Synechocystis* sp. strain PCC 6803. *Plant Physiol*. 170, 752–760. doi: 10.1104/pp.15.01430

Gombos, Z., Wada, H., and Murata, N. (1994). The recovery of photosynthesis from low-temperature photoinhibition is accelerated by the unsaturation of membrane lipids: a mechanism of chilling tolerance. *Proc. Natl. Acad. Sci. U.S.A*. 91, 8787–8791. doi: 10.1073/pnas.91.19.8787

Hibino, T., Lee, B. H., Rai, A., Ishikawa, H., Kojima, H., Tawada, M., et al. (1996). Salt enhances photosystem I content and cyclic electron flow via NAD(P)H dehydrogenase in the halotolerant cyanobacterium *Aphanothece halophytica*. *Aust. J. Plant Physiol.* 23, 321–330. doi: 10.1071/PP9960321

Jiang, H. B., Lou, W. J., Du, H. Y., Price, N. M., and Qiu, B. S. (2012). Sll1263, a unique cation diffusion facilitator protein that promotes iron uptake in the cyanobacterium *Synechocystis* sp. strain PCC 6803. *Plant Cell Physiol.* 53, 1404–1417. doi: 10.1093/pcp/pcs086

Kitajima, M., and Butler, W. (1975). Quenching of chlorophyll fluorescence and primary photochemistry in chloroplasts by dibromothymoquinone. *Biochim. Biophys. Acta* 376, 105–115. doi: 10.1016/0005-2728(75)90209-1

Klughammer, C., and Schreiber, U. (1994). An improved method, using saturating light pulses, for the determination of photosystem I quantum yield via $P700^+$-absorbance changes at 830 nm. *Planta* 192, 261–268. doi: 10.1007/BF01089043

Klughammer, C., and Schreiber, U. (2008a). Complementary PS II quantum yields calculated from simple fluorescence parameters measured by PAM fluorometry and the Saturation Pulse method. *PAM Appl. Notes* 1, 27–35. Available online at: http://walz.asia/downloads/pan/PAN078007.pdf

Klughammer, C., and Schreiber, U. (2008b). Saturation pulse method for assessment of energy conversion in PS I. *PAM Appl. Notes* 1, 11–14. Available online at: http://www.photosynthesissystem.com/downloads/pan/PAN07002.pdf

Kondo, K., Ochiai, Y., Katayama, M., and Ikeuchi, M. (2007). The membrane-associated CpcG2-phycobilisome in *Synechocystis*: a new photosystem I antenna. *Plant Physiol*. 144, 1200–1210. doi: 10.1104/pp.107.099267

Kono, M., Noguchi, K., and Terashima, I. (2014). Roles of the cyclic electron flow around PSI (CEF-PSI) and O_2-dependent alternative pathways in regulation of the photosynthetic electron flow in short-term fluctuating light in *Arabidopsis thaliana*. *Plant Cell Physiol.* 55, 990–1004. doi: 10.1093/pcp/pcu033

Kou, J., Takahashi, S., Fan, D. Y., Badger, M. R., and Chow, W. S. (2015). Partially dissecting the steady-state electron fluxes in photosystem I in wild-type and *pgr5* and *ndh* mutants of Arabidopsis. *Front. Plant Sci.* 6:758. doi: 10.3389/fpls.2015.00758

Kouřil, R., Strouhal, O., Nosek, L., Lenobel, R., Chamrád, I., Boekema, E. J., et al. (2014). Structural characterization of a plant photosystem I and NAD(P)H dehydrogenase supercomplex. *Plant J*. 77, 568–576. doi: 10.1111/tpj.12402

Kügler, M., Jänsch, L., Kruft, V., Schmitz, U. K., and Braun, H.-P. (1997). Analysis of the chloroplast protein complexes by blue-native polyacrylamide gel electrophoresis (BN-PAGE). *Photosyn. Res.* 53, 35–44. doi: 10.1023/A:1005882406718

Long, Z., Zhao, J., Zhang, J., Wei, L., Wang, Q., and Ma, W. (2011). Effects of different light treatments on the natural transformation of *Synechocystis* sp. strain PCC 6803. *Afr. J. Microbiol. Res*. 5, 3603–3610. doi: 10.5897/AJMR10.123

Ma, W., and Mi, H. (2005). Expression and activity of type 1 NAD(P)H dehydrogenase at different growth phases of the cyanobacterium, *Synechocystis* PCC 6803. *Physiol. Plant*. 125, 135–140. doi: 10.1111/j.1399-3054.2005.00555.x

Ma, W., and Ogawa, T. (2015). Oxygenic photosynthesis-specific subunits of cyanobacterial NADPH dehydrogenases. *IUBMB Life* 67, 3–8. doi: 10.1002/iub.1341

Ma, W., Wei, L., and Wang, Q. (2008). The response of electron transport mediated by active NADPH dehydrogenase complexes to heat stress in the cyanobacterium *Synechocystis* 6803. *Sci. China C Life Sci*. 51, 1082–1087. doi: 10.1007/s11427-008-0139-0

McGinn, P. J., Price, G. D., Maleszka, R., and Badger, M. R. (2003). Inorganic carbon limitation and light control the expression of transcripts related to the CO_2-concentrating mechanism in the cyanobacterium *Synechocystis* sp. strain PCC6803. *Plant Physiol*. 132, 218–229. doi: 10.1104/pp.019349

Mi, H., Deng, Y., Tanaka, Y., Hibino, T., and Takabe, T. (2001). Photo-induction of an NADPH dehydrogenase which functions as a mediator of electron transport to the intersystem chain in the cyanobacterium *Synechocystis* PCC6803. *Photosyn. Res*. 70, 167–173. doi: 10.1023/A:1017946524199

Mi, H., Endo, T., Ogawa, T., and Asada, K. (1995). Thylakoid membrane-bound, NADPH-specific pyridine nucleotide dehydrogenase complex mediated cyclic electron transport in the cyanobacterium *Synechocystis* sp. PCC 6803. *Plant Cell Physiol.* 36, 661–668. doi: 10.1093/oxfordjournals.pcp.a078807

Mi, H., Endo, T., Schreiber, U., Ogawa, T., and Asada, K. (1992). Electron donation from cyclic and respiratory flows to the photosynthetic intersystem chain is mediated by pyridine nucleotide dehydrogenase in the cyanobacterium *Synechocystis* PCC 6803. *Plant Cell Physiol.* 33, 1233–1237. doi: 10.1093/oxfordjournals.pcp.a078378

Misumi, M., Katoh, H., Tomo, T., and Sonoike, K. (2016). Relationship between photochemical quenching and non-photochemical quenching in six species of cyanobacteria reveals species difference in redox state and species commonality in energy dissipation. *Plant Cell Physiol.* 57, 1510–1517. doi: 10.1093/pcp/pcv185

Ogawa, T. (1991). A gene homologous to the subunit-2 gene of NADH dehydrogenase is essential to inorganic carbon transport of *Synechocystis* PCC6803. *Proc. Natl. Acad. Sci. U.S.A*. 88, 4275–4279. doi: 10.1073/pnas.88.10.4275

Ohkawa, H., Pakrasi, H. B., and Ogawa, T. (2000). Two types of functionally distinct NAD(P)H dehydrogenases in *Synechocystis* sp. strain PCC6803. *J. Biol. Chem.* 275, 31630–31634. doi: 10.1074/jbc.M003706200

Ohkawa, H., Sonoda, M., Hagino, N., Shibata, M., Pakrasi, H. B., and Ogawa, T. (2002). Functionally distinct NAD(P)H dehydrogenases and their membrane localization in *Synechocystis* sp. PCC6803. *Funct. Plant Biol*. 29, 195–200. doi: 10.1071/PP01180

Ohkawa, H., Sonoda, M., Shibata, M., and Ogawa, T. (2001). Localization of NAD(P)H dehydrogenase in the cyanobacterium *Synechocystis* sp. strain PCC 6803. *J. Bacteriol.* 183, 4938–4939. doi: 10.1128/JB.183.16.4938-4939.2001

Peng, L., Fukao, Y., Fujiwara, M., and Shikanai, T. (2012). Multistep assembly of chloroplast NADH dehydrogenase-like subcomplex A requires several nucleus-encoded proteins, including CRR41 and CRR42, in Arabidopsis. *Plant Cell* 24, 202–214. doi: 10.1105/tpc.111.090597

Peng, L., Fukao, Y., Fujiwara, M., Takami, T., and Shikanai, T. (2009). Efficient operation of NAD(P)H dehydrogenase requires supercomplex formation with photosystem I via minor LHCI in Arabidopsis. *Plant Cell* 21, 3623–3640. doi: 10.1105/tpc.109.068791

Peng, L., Shimizu, H., and Shikanai, T. (2008). The chloroplast NAD(P)H dehydrogenase complex interacts with photosystem I in Arabidopsis. *J. Biol. Chem.* 283, 34873–34879. doi: 10.1074/jbc.M803207200

Rowland, J. G., Simon, W. J., Nishiyama, Y., and Slabas, A. R. (2010). Differential proteomic analysis using iTRAQ reveals changes in thylakoids associated with Photosystem II-acquired thermotolerance in *Synechocystis* sp. PCC 6803. *Proteomics* 10, 1917–1929. doi: 10.1002/pmic.200900337

Schreiber, U., Schliwa, U., and Bilger, W. (1986). Continuous recording of photochemical and non-photochemical chlorophyll fluorescence quenching with a new type of modulation fluorometer. *Photosyn. Res.* 10, 51–62. doi: 10.1007/BF00024185

Suorsa, M., Järvi, S., Grieco, M., Nurmi, M., Pietrzykowska, M., Rantala, M., et al. (2012). PROTON GRADIENT REGULATION5 is essential for proper acclimation of Arabidopsis photosystem I to naturally and artificially fluctuating light conditions. *Plant Cell* 24, 2934–2948. doi: 10.1105/tpc.112.097162

Takahashi, Y., and Katoh, S. (1984). Triplet states in a photosystem I reaction center complex. Inhibition of radical pair recombination by bipyridinium dyes and naphthoquinones. *Plant Cell Physiol.* 25, 785–794. doi: 10.1093/oxfordjournals.pcp.a076773

Tanaka, Y., Katada, S., Ishikawa, H., Ogawa, T., and Takabe, T. (1997). Electron flow from NAD(P)H dehydrogenase to photosystem I is required for adaptation to salt shock in the cyanobacterium *Synechocystis* sp. PCC 6803. *Plant Cell Physiol.* 38, 1311–1318. doi: 10.1093/oxfordjournals.pcp.a029123

Trebst, A. (1980). Inhibitors in electron flow: tools for the functional and structural localization of carriers and energy conservation sites. *Methods Enzymol.* 69, 675–715. doi: 10.1016/S0076-6879(80)69067-3

van Kooten, O., and Snel, J. F. (1990). The use of chlorophyll fluorescence nomenclature in plant stress physiology. *Photosyn. Res.* 25, 147–150. doi: 10.1007/BF00033156

Wang, X., Gao, F., Zhang, J., Zhao, J., Ogawa, T., and Ma, W. (2016). A cytoplasmic protein Ssl3829 is important for NDH-1 hydrophilic arm assembly in *Synechocystis* sp. strain PCC 6803. *Plant Physiol.* 171, 864–877. doi: 10.1104/pp.15.01796

Williams, J. G., and Szalay, A. A. (1983). Stable integration of foreign DNA into the chromosome of the cyanobacterium *Synechococcus* R2. *Gene* 24, 37–51 doi: 10.1016/0378-1119(83)90129-4

Xu, M., Ogawa, T., Pakrasi, H. B., and Mi, H. (2008). Identification and localization of the CupB protein involved in constitutive CO_2 uptake in the cyanobacterium, *Synechocystis* sp. strain PCC 6803. *Plant Cell Physiol.* 49, 994–997. doi: 10.1093/pcp/pcn074

Yamori, W., Makino, A., and Shikanai, T. (2016). A physiological role of cyclic electron transport around photosystem I in sustaining photosynthesis under fluctuating light in rice. *Sci. Rep.* 6:20147. doi: 10.1038/srep20147

Yeremenko, N., Jeanjean, R., Prommeenate, P., Krasikov, V., Nixon, P. J., Vermaas, W. F., et al. (2005). Open reading frame *ssr2016* is required for antimycin A-sensitive photosystem I-driven cyclic electron flow in the cyanobacterium *Synechocystis* sp. PCC 6803. *Plant Cell Physiol.* 46, 1433–1436. doi: 10.1093/pcp/pci147

Zhang, J., Gao, F., Zhao, J., Ogawa, T., Wang, Q., and Ma, W. (2014). NdhP is an exclusive subunit of large complex of NADPH dehydrogenase essential to stabilize the complex in *Synechocystis* sp. strain PCC 6803. *J. Biol. Chem.* 289, 18770–18781. doi: 10.1074/jbc.M114.553404

Zhang, P., Battchikova, N., Jansen, T., Appel, J., Ogawa, T., and Aro, E.-M. (2004). Expression and functional roles of the two distinct NDH-1 complexes and the carbon acquisition complex NdhD3/NdhF3/CupA/Sll1735 in *Synechocystis* sp. PCC 6803. *Plant Cell* 16, 3326–3340. doi: 10.1105/tpc.104.026526

Zhao, J., Gao, F., Qiu, Z., Wang, Q., and Ma, W. (2014a). Deletion of an electron donor-binding subunit of the NDH-1 complex, NdhS, results in a heat-sensitive growth phenotype in *Synechocystis* sp. PCC 6803. *Chin. Sci. Bull.* 59, 4484–4490. doi: 10.1007/s11434-014-0596-8

Zhao, J., Gao, F., Zhang, J., Ogawa, T., and Ma, W. (2014b). NdhO, a subunit of NADPH dehydrogenase, destabilizes medium size complex of the enzyme in *Synechocystis* sp. Strain PCC 6803. *J. Biol. Chem.* 289, 26669–26676. doi: 10.1074/jbc.M114.553925

Zhao, J., Rong, W., Gao, F., Ogawa, T., and Ma, W. (2015). Subunit Q is required to stabilize the large complex of NADPH dehydrogenase in *Synechocystis* sp. strain PCC 6803. *Plant Physiol.* 168, 443–451. doi: 10.1104/pp.15.00503

Conflict of Interest Statement: The authors declare that the research was conducted in the absence of any commercial or financial relationships that could be construed as a potential conflict of interest.

frontiers in Plant Science

ORIGINAL RESEARCH
published: 26 January 2018
doi: 10.3389/fpls.2018.00034

Transcriptomic and Functional Analyses Reveal That *PpGLK1* Regulates Chloroplast Development in Peach (*Prunus persica*)

Min Chen[1,2†], *Xiao Liu*[1,2†], *Shenghui Jiang*[1,2], *Binbin Wen*[1,2], *Chao Yang*[1,2], *Wei Xiao*[1,2], *Xiling Fu*[1,2], *Dongmei Li*[1,2], *Xiude Chen*[1,2], *Dongsheng Gao*[1,2*] and *Ling Li*[1,2*]

[1] College of Horticulture Science and Engineering, Shandong Agricultural University, Tai'an, China, [2] State Key Laboratory of Crop Biology, Shandong Agricultural University, Tai'an, China

Peach is an ideal species for fruit tree research because of its small, fully sequenced genome. Chloroplast development is dependent on the tight cooperation between the nuclear and plastid genomes, and is regulated by GLK transcription factors. In this work, the pigment content was monitored and the chloroplast-to-chromoplast conversion during the fruit ripening was visualized by transmission electron microscopy. Localization and expression analyses showed that PpGLK1 was located in the nucleus and expressed mainly in the leaves and fruit skin. A transcriptome analysis showed that *PpGLK1* and its target genes were significantly differentially expressed in ripening peach fruit skin. *PpGLK1* silencing affected chlorophyll accumulation in peach leaves and fruits. Overexpression of *PpGLK1* rescued the phenotypes of the *Arabidopsis Atglk1Atglk2* double mutant and the tomato *uniform ripening* mutant. The results of a yeast two-hybrid analysis showed that PpGLK1 is autoactivated and that PpGLK1 (301-542 a.a.) interacted with PpARF5. Together, our results indicate that *PpGLK1* regulates chloroplast development in green tissues in peach. Therefore, it may be a promising target gene for improving the production and quality of peach by genetic engineering and breeding approaches.

Keywords: chloroplast development, chlorophyll, GLK transcription factor, peach, PpARF5

OPEN ACCESS

Edited by:
Rebecca L. Roston, University of Nebraska-Lincoln, United States

Reviewed by:
Shan Lu, Nanjing University, China
Maria Valeria Lara, Universidad Nacional de Rosario (CONICET), Argentina

***Correspondence:**
Dongsheng Gao
dsgao@sdau.edu.cn
Ling Li
lilingsdau@163.com

† These authors have contributed equally to this work.

Specialty section:
This article was submitted to Plant Cell Biology, a section of the journal Frontiers in Plant Science

Received: *19 October 2017*
Accepted: *09 January 2018*
Published: *26 January 2018*

Citation:
Chen M, Liu X, Jiang S, Wen B, Yang C, Xiao W, Fu X, Li D, Chen X, Gao D and Li L (2018) Transcriptomic and Functional Analyses Reveal That PpGLK1 Regulates Chloroplast Development in Peach (Prunus persica). Front. Plant Sci. 9:34. doi: 10.3389/fpls.2018.00034

INTRODUCTION

Peach (*Prunus persica*), an economically important diploid tree crop that originated in China, is one of the most highly genetically characterized deciduous trees in fruit and forest tree research (Verde et al., 2013). Photosynthesis converts light energy into electrochemical energy, and is the source of all organic molecules in plants (Alric and Johnson, 2017); therefore, photosynthesis is a target to increase crop productivity. Leaves are the main photosynthetic organ in plants, but most fruits have partially photosynthetic metabolism before they undergo the transition to truly heterotrophic metabolism. Pavel and Dejong (1993) showed that developing peach fruit provide 5–9% of the fruit photosynthate. Chloroplast development and chlorophyll content can affect the photosynthetic capacity of green tissues (Nadakuduti et al., 2014).

Many studies have been reported in peach. For example, *PpYUC11*, which participates in auxin biosynthesis, was identified as a candidate gene involved in the regulation of the stony hard

phenotype in peach (Pan et al., 2015). Zhou et al. (2015) demonstrated that *PpNAC1* can activate *PpMYB10.1*, a key gene in blood-flesh peach. Cao et al. (2016) described 12 key agronomic traits including flesh color and non-acid fruit in peach. Su et al. (2012) documented the distinctive physiological characteristics of red and green peel during fruit maturation, and Karagiannis et al. (2016) studied the effect of altitude on peach skin quality traits using comparative physiological and proteomic analyses. However, chloroplast development and photosynthesis in green tissues of peach are not fully understood.

Regulating chloroplast development and increasing the photosynthetic capacity are alternative strategies to improve the production and quality of plants. Chloroplasts are not only the sites for photosynthesis but also play important roles in the biosynthesis of many metabolites (Lopez-Juez and Pyke, 2005). In recent years, there has been increasing interest in the genetic analysis of photosynthetic processes and chloroplast development. In tomato, a ripening-related transcription factor *ARABIDOPSIS PSEUDO RESPONSE REGULATOR 2-LIKE* (*SlAPRR2-LIKE*), was shown to influence pigmentation, and the overexpression of *SlAPPR2-Like* produced a more intense green color (Pan et al., 2013). The down-regulation of *SlARF4* causes a dark-green fruit phenotype at the pre-ripening stage (Sagar et al., 2013). The *high-pigment* mutants (*hp1*, *hp2*) had higher chlorophyll level in immature fruits than wild-type (Galpaz et al., 2008). The *Curl* (*Cu*) mutant, a dominant gain-of-function mutation of *TKN2*, showed elevated chlorophyll level and increased chloroplast numbers across the entire fruit surface (Nadakuduti et al., 2014). Cytokinin has been shown to affect chloroplast function via modulating photosynthetic performance (Cortleven and Schmülling, 2015) and activating chloroplast-related genes (Cortleven et al., 2016). In addition, inactivation of the Golden 2-like transcription factor *SlGLK2* during breeding selection affected fruit chloroplast development, resulting in light green tomato fruit with reduced sugars (Powell et al., 2012).

The GLK transcription factors were first identified in maize, and were subsequently found in *Arabidopsis*, maize, rice, sorghum, and the moss *Physcomitrella patens*. To date, land plants have been found contain 1-4 GLKs but no GLK has been found in algal genomes (Wang et al., 2013). The GLK genes contain two conserved domains: a specific GLK/C-terminal box (GCT-box) only in the GLKs of land plants; and a DNA-binding domain (DBD) (Rossini et al., 2001). In *Arabidopsis*, the two GLKs act redundantly and the double mutant *Atglk1Atglk2* exhibited a pale-green phenotype (Rossini et al., 2001; Fitter et al., 2002). In tomato, the two GLKs are functionally equivalent and only *SlGLK2* is expressed in fruit, mainly in the green shoulder region. A truncated *SlGLK2* caused the loss of the green shoulder (Powell et al., 2012). Overexpression of either *SlGLK1* or *SlGLK2* led to uniform ripening, resulting in darker green immature fruit, and improved quality of mature fruit (Cheng and Lai, 2013; Nguyen et al., 2014). In pepper, *CaGLK2* was shown to regulate chloroplast development throughout the entire fruit (Brand et al., 2014). Kobayashi et al. (2012) demonstrated that the auxin signaling pathway can regulate chloroplast development via GLKs in fruit and roots. *BZR1-1D* transgenic lines produced fruits with a dark-green shoulder region and asynchronous ripening (the *Uniform ripening* (*U*) phenotype) and up-regulated expression of *SlGLK2* (Liu et al., 2014). Using chromatin immunoprecipitation analyses, Waters et al. (2009) showed that nuclear photosynthetic genes including *Lhcb3*, *PpLhcb5*, *Lhcb4.2*, *Lhcb6*, *Lhcb2.2*, *Lhca1*, *Lhca2*, *Lhca3*, *PORA*, *CHLM*, *CHLH*, *PsaK*, *PsaD*, and *GUN4* are potential target genes of GLK in *Arabidopsis*. However, little is known about the roles of GLK in peach.

In this study, the chloroplast-to-chromoplast conversion in ripening peach fruits was observed by transmission electron microscopy (TEM). A transcriptome analysis of the immature to mature epicarp showed that *PpGLK1* and its target genes were significantly differentially expressed during fruit ripening. We tested the role of *PpGLK1* by virus-induced gene silencing (VIGS) in peach and overexpression in *Arabidopsis* and tomato. Finally, we confirmed that PpGLK1 interacts with PpARF5 in peach. In conclusion, these results confirm that *PpGLK1* regulates chloroplast development in peach. Thus, it is a candidate target gene for improving photosynthesis via genetic engineering or breeding strategies.

MATERIALS AND METHODS

Plant Material

Peach trees (*Prunus persica* L.cv LuYou Tao1) were grown in a greenhouse at Shandong Agriculture University, Tai'an, China. Ten peach fruits from eight different trees were sampled from 19 to 68 DAFB (days after full bloom). They were sampled at approximately 7-day intervals at 10:00 to 11:00. The exocarp was collected, and immediately frozen in liquid N_2, and then stored at −80°C. Part of the exocarp was directly used for TEM analysis.

Pigment Determination

The chlorophyll and total carotenoid contents in peach fruit skin were measured each week during ripening and were calculated as described previously (Lichtenthaler, 1987). To measure the anthocyanin content, 0.5 g fruit skin was ground into a powder in liquid N_2, mixed with 5 mL cold methanol containing 0.1% HCl, and then kept at 4°C for 24 h in the dark. After this, a two-buffer assay system was used to determine anthocyanin content (Jin et al., 2016).

Electron Microscopy

Samples including fruit skin, leaves, and siliques were used for the microscopic analyses. All samples were fixed in 3.5% glutaraldehyde and washed with 0.1 M phosphate buffered saline (PBS). The samples were briefly post-fixed in 1% osmium tetroxide and dehydrated in an ascending ethanol series (10–70% ethanol). After this, the samples were subjected to endosmosis, and then imbedded and polymerized in Epon812 resin. Ultra-thin sections were cut using an LKB-V ultramicrotome and stained with uranium acetate and lead citrate. Finally, ultrastructure was examined under a JEOL-1200EX TEM (JEOL, Tokyo, Japan).

Subcellular Localization Analyses

The full coding sequence of PpGLK1 without the stop codon was PCR-amplified and inserted into the pPZP211 vector. The primer was shown in **Table S1**. The plasmids harboring the PpGLK1-GFP and the control GFP were transformed into *Agrobacterium tumefaciens* strains GV3101 and LBA4404. *A. tumefaciens* LBA4404 was used to infect onion epidermal cells (Wang et al., 2017). Equal volumes of *A. tumefaciens* GV3101 and P19 were mixed together and used to infiltrate young tobacco leaves (Jiang et al., 2017). GFP fluorescence was detected under a Zeiss LSM880 microscope (Carl Zeiss, Oberkochen, Germany) and the pictures were analyzed using ZEN lite software (https://www.zeiss.de/corporate/home.html). The subcellular localization assays were repeated more than three times with similar results.

RNA-Seq Data Analysis

The *P. persica* genome annotations, downloaded from the Phytozome database (https://phytozome.jgi.doe.gov/pz/portal.html), were used as a reference. Bowtie2 v2.2.3 (Langmead and Salzberg, 2012) was used to build the genome index, and clean data were mapped to the reference genome using TopHat v2.0.12. The number of reads for each gene in the samples was counted by HTSeq v0.6.0. The expression levels of the genes in each sample were estimated as Reads Per Kilobase Million Mapped Reads. DEGseq v1.14.0 software was used to identify the DEGs between two biological replicate samples using a model based on negative binomial distribution (Wang et al., 2010). A *P*-value was assigned to each gene and adjusted by the Benjamini and Hochberg approach to control the false discovery rate. Genes with $q \leq 0.05$ and $|\log2\_ratio| \geq 1$ were identified as DEGs.

Isolation of RNA and qRT-PCR Analysis

Total RNA was isolated from 1 g fruit skin using an RNeasy Plus Mini Kit (Qiagen) as the manufacturer's instructions and extracted three times for each sample. Three duplicates of three total RNA were reverse-transcribed for qRT-PCR first-strand cDNA synthesis using the SuperScript III First-Strand Synthesis System (Invitrogen) in a total volume of 20 μL. The qRT-PCR mixture consisted of 10 μL SYBR Premix Ex Taq (TaKaRa Biotechnology, Dalian, China),

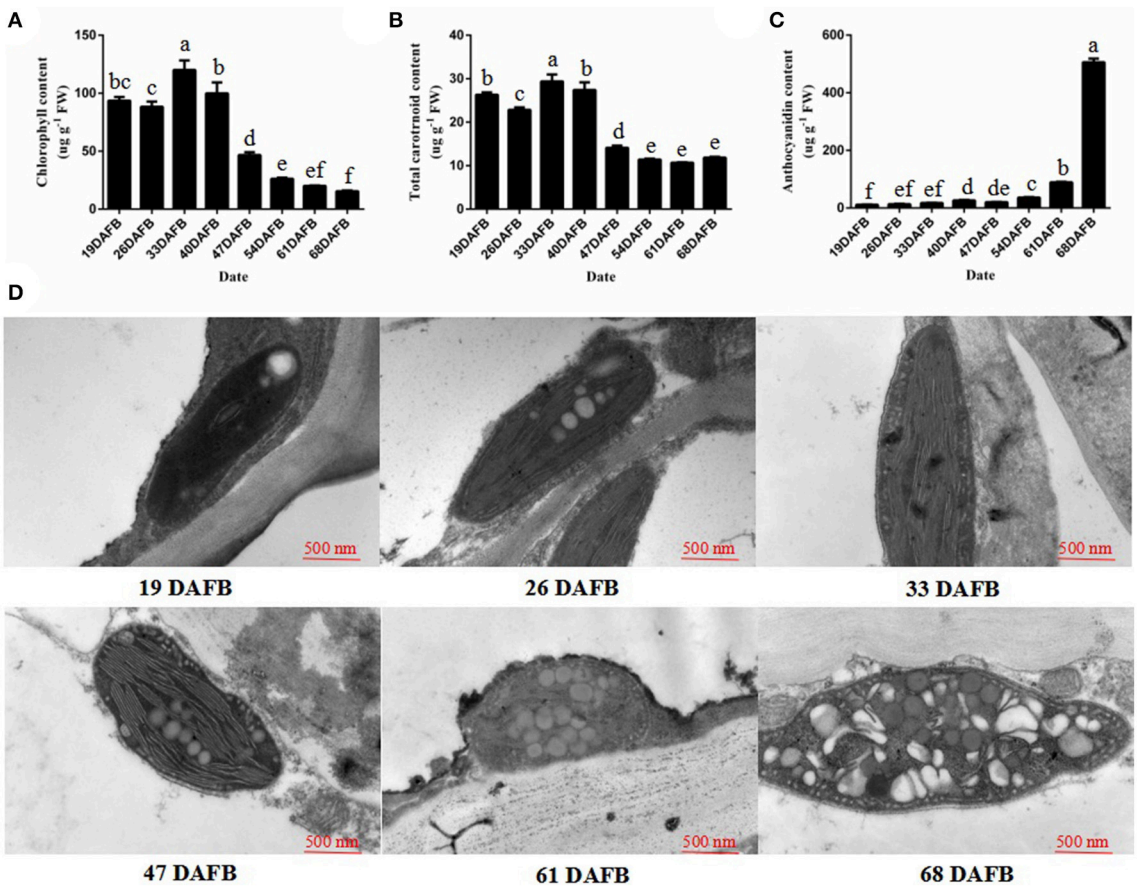

FIGURE 1 | Chlorophyll, the total carotrnoid, anthocyanin contents, and chloroplast development during fruit ripening. **(A)** Chlorophyll content in peach skin during fruit development. **(B)** Total carotenoid content in peach skin during fruit development. **(C)** Anthocyanin content in peach skin during fruit development. **(D)** Transmission electron micrographs of chloroplast development in peach skin during fruit ripening. Data is presented as the means ± SD, $n = 3$. Different letters above bars denote statistical significance according to one-way ANOVA and Duncan's test ($P < 0.05$).

1 μL cDNA, and 1 μL each primer pair. The qRT-PCR conditions followed the manufacturer's instructions. The primers were designed using Beacon Designer 7 software, and produced 120–200 bp amplicons (see **Table S1**). The thermal cycling protocol was 10 min at 95°C, 40 cycles of 95°C for 15 s, and 1 min at 58°C for annealing and extension. The specificity was assessed by a melting curve analysis and size estimation of the amplified product. The relative expression levels of DEGs were calculated using the $2^{-\Delta\Delta t}$ method. All statistic analysis were performed using DPSv7.05.The *Actin* reference genes Prupe.6G163400 and Prupe. 3G205200 were used to normalize the assayed genes; Prupe.6G163400 was selected because of its stable expression during fruit development (**Figure S1**). The results shown are the average of three independent biological replicates repeated three times.

Virus-Induced Gene Silencing of *PpGLK1* in Peach

A specific cDNA fragment of *PpGLK1* was amplified and inserted into pTRV2. pTRV2-PpGLK1, pTRV2, and pTRV1 were individually transformed into *A. tumefaciens* strain GV3101 for the VIGS experiments. The primer was shown in **Table S1**. The *A. tumefaciens* GV3101 lines containing pTRV2-PpGLK1, pTRV2, and pTRV1 were selected, incubated, resuspended to an OD_{600} of 0.8 in infiltration buffer (10 mM $MgCl_2$, 10 mM MES, 150 μM acetosyringone), and then kept at room temperature

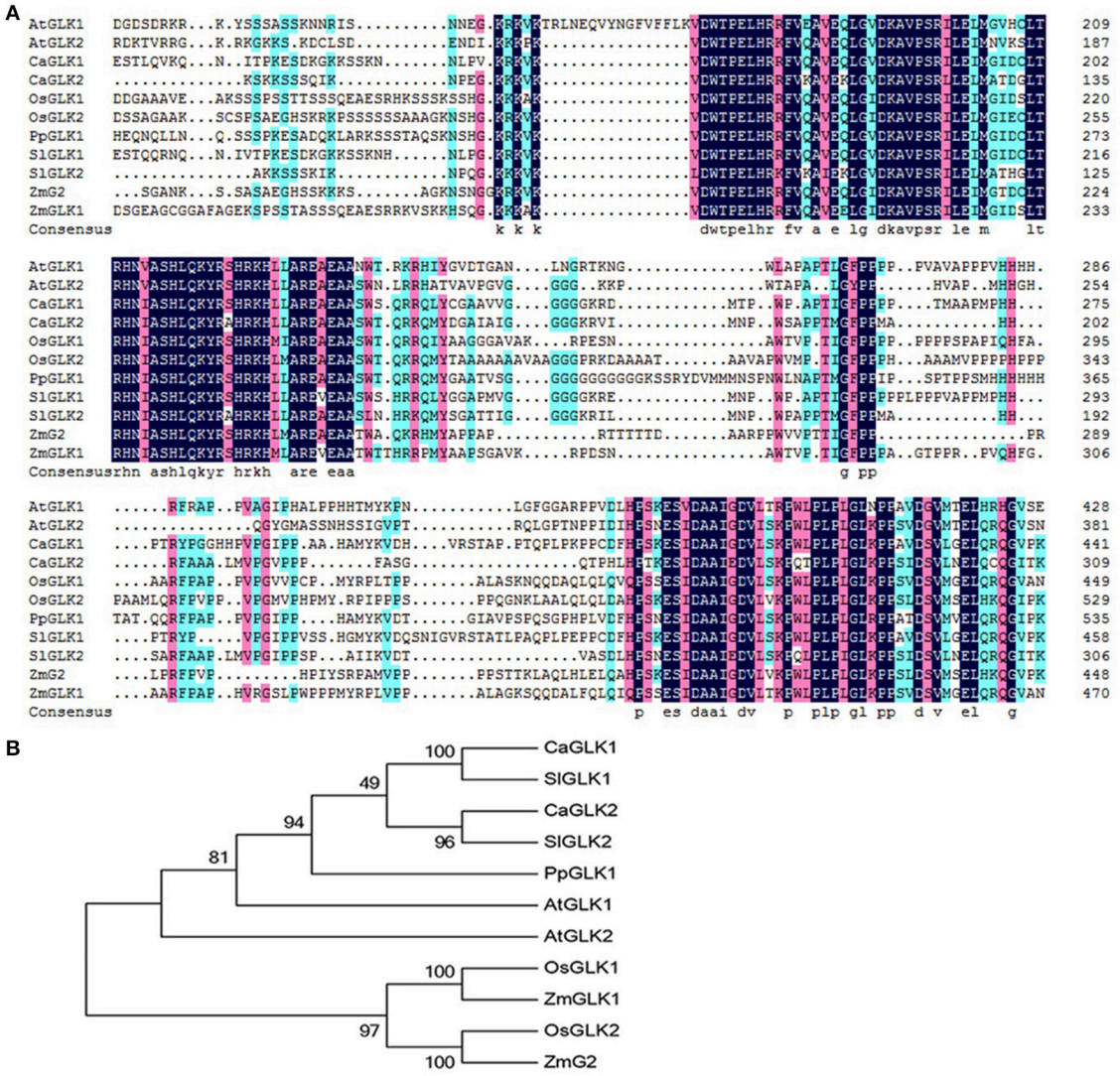

FIGURE 2 | Analysis of GLKs in different species including *Arabidopsis*, tomato, pepper, rice, maize, and peach. **(A)** Multiple alignment of GLK amino acid sequences from *Arabidopsis*, tomato, pepper, rice, maize, and peach. (AtGLK1: AT2G20570; AtGLK2: AT5G44190; SlGLK1: Solyc07g053630.2.1; SlGLK2: Solyc10g008160.2.1; CaGLK1: LOC107878377; CaGLK2: LOC107845460; OsGLK1: LOC4340977; OsGLK2: LOC4326363; ZmGLK1: GRMZM2G026833; ZmG2: GRMZM2G087804; PpGLK1: Prupe.3G127700). **(B)** Phylogenetic tree analysis of GLKs from *Arabidopsis*, tomato, pepper, rice, maize, and peach. Phylogenetic tree was built using MEGA5.1 with the neighbor-joining method. Data of sequences used for phylogenetic analysis is provided in **Table S4**.

without shaking for 2 h. Considering the firmness of immature peach (63 DAFB), the pTRV2-PpGLK1 mixture (pTRV1:pTRV2-PpGLK1=1:1, v/v) and the control mixture (pTRV1:pTRV2=1:1, v/v) were gently vacuum-infiltrated into peach leaves and fruits for 30 min and 1 h, respectively. The infiltrated leaves were kept in the dark at 21°C overnight and then transferred to a light growth chamber. Peach leaves and fruits were sampled and photographed at 3 and 7 d after infiltration, respectively.

Over-Expression of *PpGLK1* in Arabidopsis and Tomato

PpGLK1 was introduced into the pRI101-AN vector containing a GFP tag sequence to form 35S:: PpGLK1-GFP (Wang et al., 2017). The recombinant plasmid was transformed into *A. tumefaciens* LBA4404 and GV3101. The *A. tumefaciens* cells were then used to transform the vector into *Arabidopsis* (GV3101) and tomato cotyledons (LBA4404) (Fillatti et al., 1987). In *Arabidopsis,* T1 transgenic seedlings were isolated by selection on MS solid medium containing kanamycin and then grown in a light incubator. Seeds of the T3 generation were collected for later use. Transgenic tomato plants were selected on MS solid medium containing kanamycin. Tomato seedlings were grown in a light growth chamber (16-h light/8-h dark, 27°C/19°C). Three lines were verified as transgenic plants. Fruits of the selected plants were used for further analyses.

Y2H Assay

A Yeast Two-Hybrid Library was constructed using peach fruit skin. Cloning and testing bait for autoactivation and toxicity, and two-hybrid screening using yeast mating were performed according to the Matchmaker® Gold Yeast Two-Hybrid System User Manual (Clontech, Palo Alto, CA, USA). The domain-deleted form (301-542 a.a.) of PpGLK1, recombined into the pGBKT7 vector, was used for screening and the Y2H assay. The CDS of PpARF5 was cloned into the pGADT7 vector (Clontech). These two recombinant plasmids were co-transformed into Y2H Gold yeast cells, and then the cells cultured on selective medium lacking Trp and Leu (-T/-L) at 30°C. The putative transformants were transferred to selective medium lacking Trp, Leu, His, and adenine (-Leu/-Trp/-His/-Ade) with or without X-α-gal.

BiFC Assay

The CDS without stop codon of PpGLK1 was cloned to the 35S-pSPYNE-YFP vector and the CDS without stop codon of PpARF5 was cloned to the 35S-pSPYCE-YFP vector. These two recombinant plasmids were co-transformed into *A.*

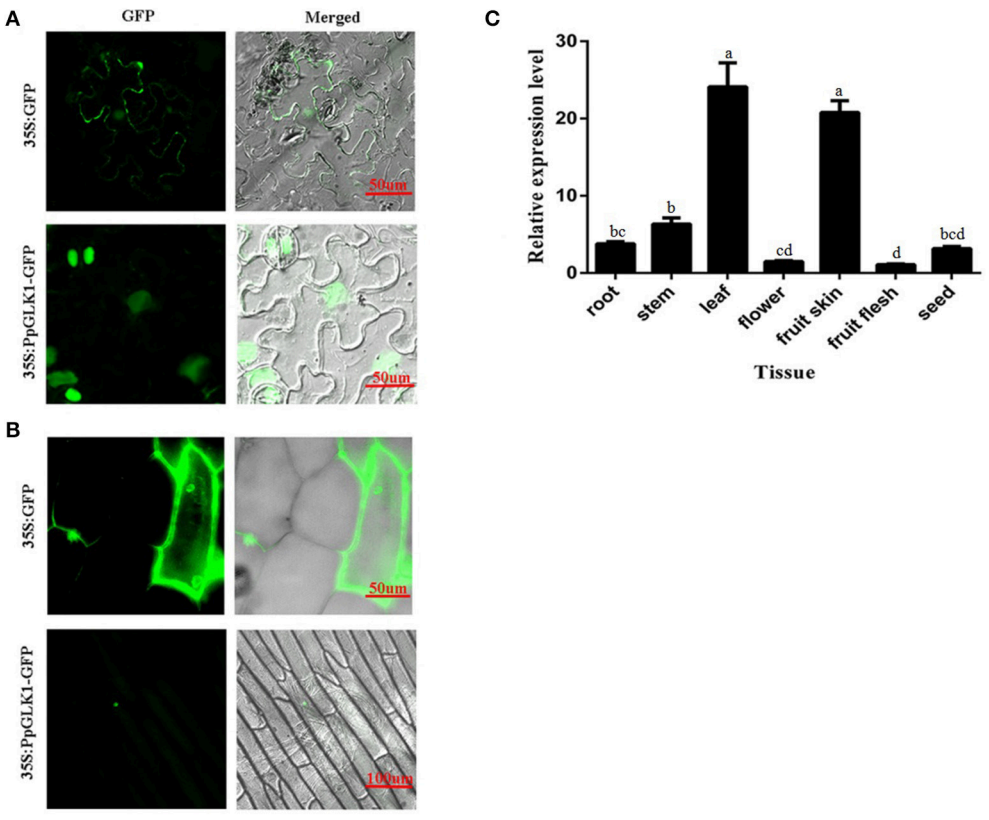

FIGURE 3 | Subcellular localization and tissue-specific expression of PpGLK1. **(A)** Subcellular localization of *PpGLK1* in tobacco lower epidermal cells. Fluorescence, and merged images are shown (left to right). **(B)** Subcellular localization of PpGLK1 in onion epidermal cells. **(C)** Expression patterns of *PpGLK1* in different tissues including root, stem, leaf, flower, fruit skin, flesh, seed. Data is presented as the means ± SD, $n = 3$. Different letters above bars denote statistical significance according to one-way ANOVA and Duncan's test ($P < 0.05$).

tumefaciens LBA4404. The mixture (35S-PpGLK1-pSPYNE:35S-PpARF5-pSPYCE=1:1, v/v) and the control (35S-pSPYNE:35S-pSPYCE=1:1, v/v) were used to infect onion epidermal cells for 25–30 min. Then, the onion epidermal cells were cultured on MS solid medium for 24–48 h at 28°C. Finally, YFP fluorescence was detected at an excitation wavelength of 488 nm under a confocal laser scanning microscope (Carl Zeiss, Oberkochen, Germany).

Pull-Down Assay

The pull-down assay was conducted as described by Wang et al. (2017). The PpGLK1 coding sequence was combined into the pET-32a (+) vector (Novagen, Madison, WI, USA) for His-tag fusion, and PpARF5 was cloned into the pGEX-4T-1 vector containing a GST-tag sequence. Then, both recombinant plasmids were individually transformed into *Escherichia coli* BL21 (DE3) to induce tag proteins. Subsequently, His-PpGLK1 was incubated with GST-PpARF5 or GST. After immunoprecipitation with an anti-His column, the pellet fraction was detected via immunoblotting using an anti-GST antibody.

RESULTS

Pigment Contents and Ultrastructure Analysis of Peach Fruit Skin

The fruit skin of peach fruits was analyzed at eight stages of growth to monitor the changes in pigment during fruit development. During fruit development, the chlorophyll and total carotenoid concentration decreased from 40 days after full bloom (DAFB) (**Figures 1A,B**). However, the anthocyanin

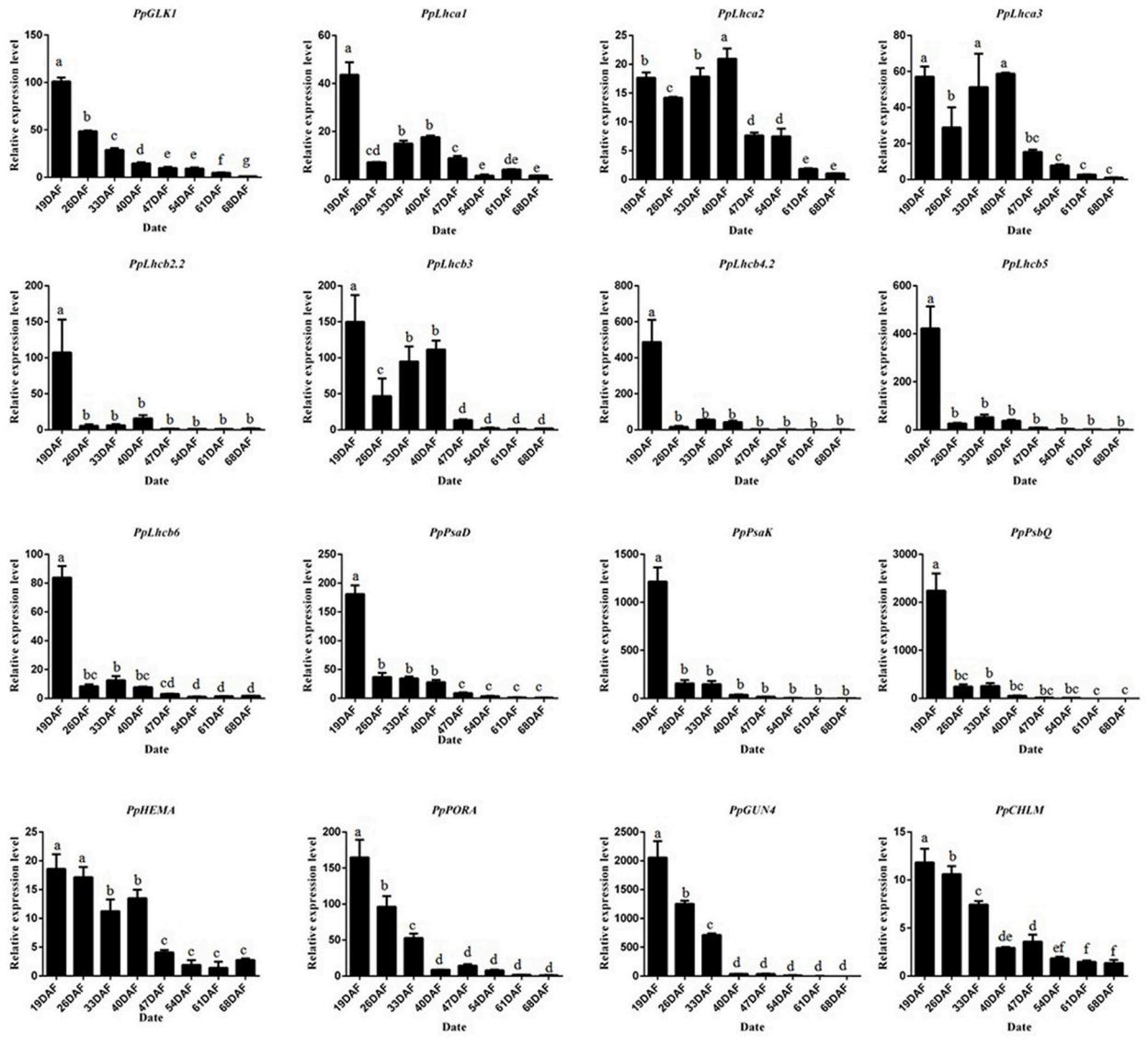

FIGURE 4 | Expression analysis of *PpGLK1* and its target genes in fruit skin of 19–68 DAFB. Data is presented as the means ± SD, $n = 3$. Different letters above bars denote statistical significance according to one-way ANOVA and Duncan's test ($P < 0.05$).

content significantly increased, and was especially rapid from 61 DAFB onwards (**Figure 1C**). Then, we observed the plastids in peach fruit skin by transmission electron microscopy (TEM) at 19, 26, 33, 47, 61, and 68 DAFB. The chloroplasts in the fruit skin changed into chromoplasts as the fruit color changed (**Figure 1D**). Elongated chloroplasts with a clear inner structure were present in peach fruit skin at 19, 26, and 33 DAFB. Generally, these chloroplasts showed a typical arrangement of grana layers, starch grains, and parallel stromal thylakoids. Fruit coloration in peach occurred at 47 DAFB, and the chloroplast-to-chromoplast conversion caused ultrastructural changes because of the appearance of an elliptical plastid with disordered parallel stromal thylakoids and disrupted granal thylakoids. The plastoglobules were obsedved and the chloroplasts had changed into chromoplasts at 68 DAFB. Together, these results illustrated the conversion of chloroplasts into chromoplasts during peach fruit development.

Isolation and Analysis of PpGLK1

The peach genome contains only one GLK gene, so we named it PpGLK1. Sequence analysis showed that PpGLK1 contained 542 amino acids with a putative molecular weight of 59.17 kDa and a theoretical isoelectric point of 6.06. A multiple sequence alignment analysis demonstrated that PpGLK1 had a TEA DNA-binding domain and specific GCT-box at the C-terminal (**Figure 2A**).

We constructed a phylogenetic tree using the GLK amino acid sequences of *Arabidopsis thaliana*, *Oryza sativa*, *Capsicum annuum*, *Solanum lycopersicum*, and *Zea mays* (**Figure 2B**). In the phylogenetic tree, PpGLK1 was most closely related to AtGLK1 and SlGLK2. Generally, orthologs that cluster together are likely to have similar functions (Tatusov et al., 1997).

Subcellular Localization and Tissue-Specific Expression of *PpGLK1*

The subcellular localization of PpGLK1 was predicted as the nucleus by WoLFPSORT (http://www.genscript.com/tools/wolf-psort). To verify the accuracy of this prediction, a fusion protein PpGLK1-GFP and a control protein GFP driven by the CaMV 35S promoter were generated and then transiently expressed in tobacco leaves and onion epidermal cells. Confocal imaging showed that the fluorescence of the control was diffuse throughout the whole cell in the tobacco leaves (**Figure 3A**)

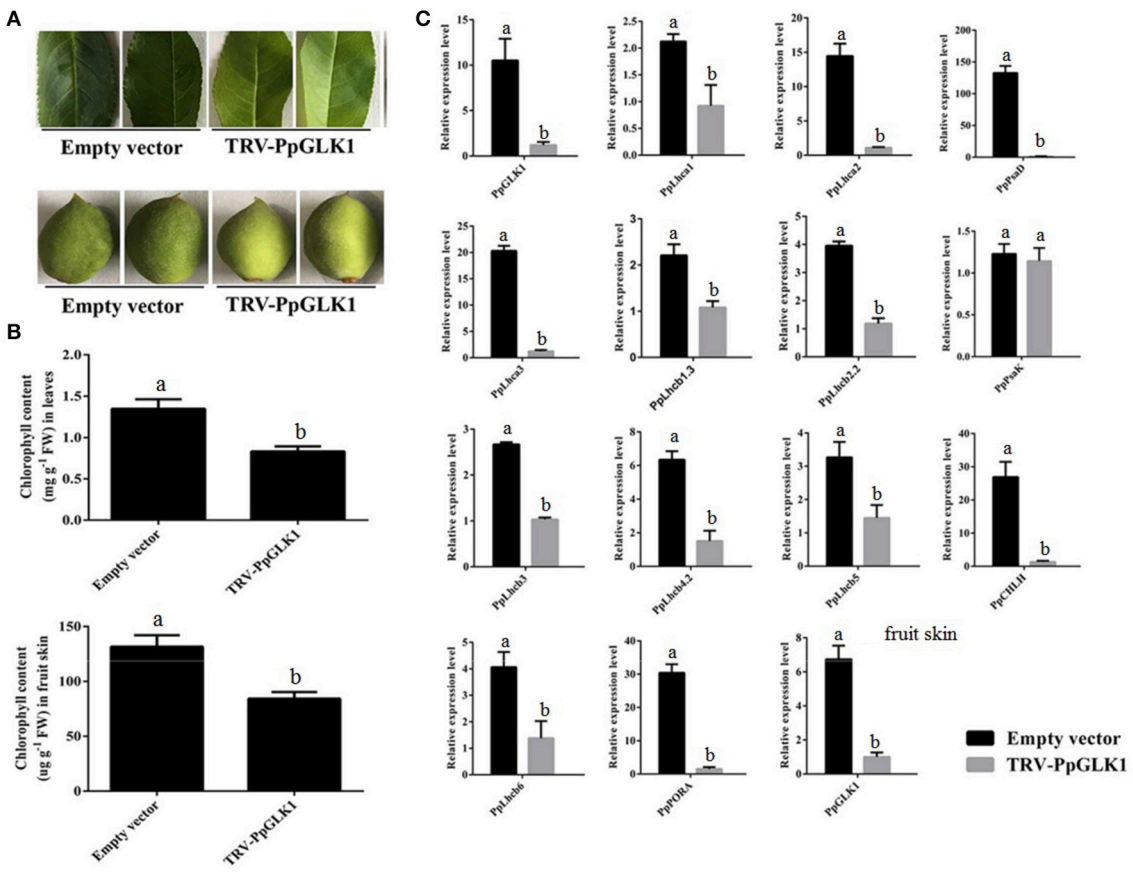

FIGURE 5 | Pale-green phenotype of peach after *PpGLK1* silencing. **(A)** Phenotypes of leaves and fruits of *PpGLK1*-silenced peach. **(B)** Chlorophyll contents in leaves and fruits of *PpGLK1*-silenced and control peach. **(C)** Transcript levels of *PpGLK1* and its target genes in leaves and fruits of *PpGLK1*-silenced and control peach. Data is presented as the means ± SD, $n = 3$. Different letters above bars denote statistical significance according to one-way ANOVA and Duncan's test ($P < 0.05$).

and the onion epidermal cells (**Figure 3B**). The fluorescence of PpGLK1-GFP was detected exclusively in the nucleus (**Figures 3A,B**), confirming the nuclear localization of PpGLK1. Next, the transcript levels of *PpGLK1* were measured in various tissues (root, stem, flower, leaf, fruit skin, fruit flesh, and seed) by qRT-PCR. There were high transcript levels of *PpGLK1* in the leaf and fruit skin, similar to the pattern of *SlGLK1* expression (**Figure 3C**).

Transcriptome Analysis

To study the molecular basis of chloroplast development in peach fruit skin, we performed a transcriptome analysis of the epicarp at immature to mature stages. Six cDNA libraries were constructed using mRNA from 19 DAFB and 68 DAFB fruit skin samples, with three biological replicates (GenBank Accession number: SRX3469636 and SRX3469635). Significant differentially expressed genes (DEGs) were identified based on their $|\log_2\text{Ratio}| \geq 1$ and $q < 0.05$ threshold. A Gene Ontology (GO) term analysis showed that large proportions DEGs were related to photosynthesis, light harvesting, chloroplast, and chlorophyll binding (**Table S2**). Importantly, the GLK transcription factor and its target genes such as *PpLhcb1.3*, *PpLhcb2.2*, *PpLhca3*, *PpHEMA*, *PpGUN4* all showed significant differences in expression during ripening, consistent with the changes in chlorophyll content. When gene transcript levels were determined using an alternative methodology, qRT-PCR, the results were consistent with those of the transcriptome analysis (**Figure 4**). The transcript levels of *PpGLK1* and its target genes decreased during fruit development. Based on these results, we concluded that *PpGLK1* may play an important role in chlorophyll biosynthesis and chloroplast development.

Virus-Induced Gene Silencing of *PpGLK1* Influences Its Target Genes and Chlorophyll Content in Peach

Next, we used VIGS to eliminate *PpGLK1* expression in peach. We selected a specific cDNA fragment of the *PpGLK1* gene

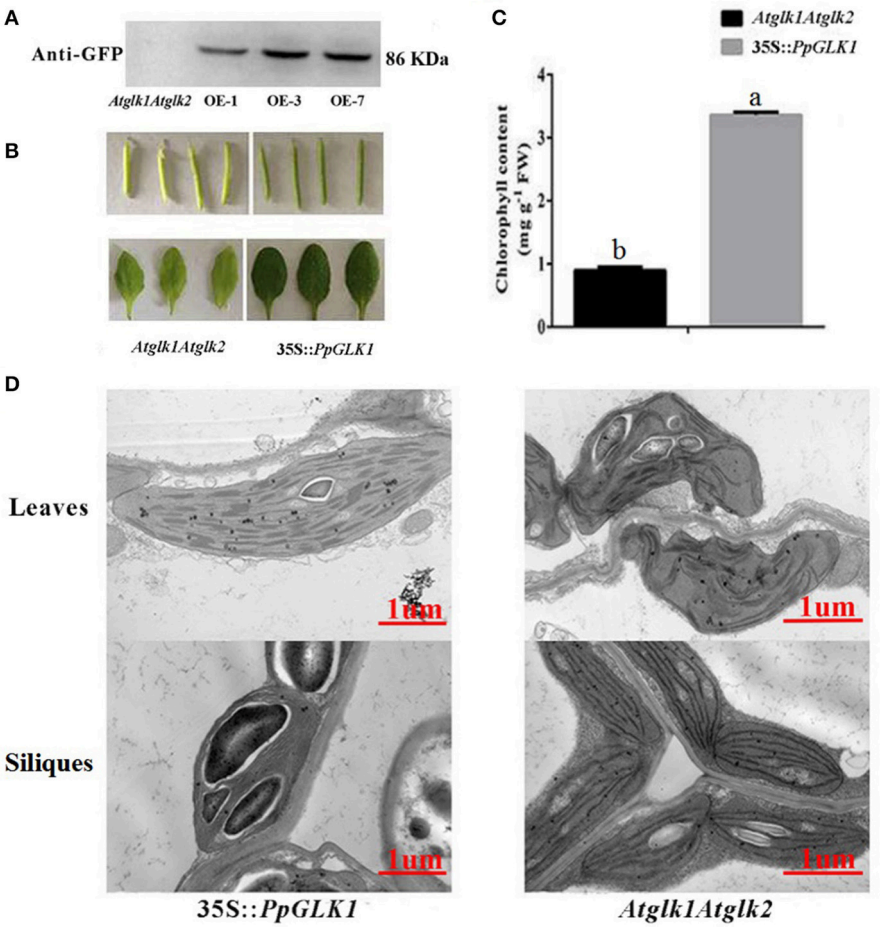

FIGURE 6 | Overexpression of *PpGLK1* in *Arabidopsis* double mutant *Atglk1Atglk2*. **(A)** Western blot analysis confirming *PpGLK1* overexpression in *Atglk1Atglk2*. **(B)** Phenotype of *PpGLK1*-overexpressing *Atglk1Atglk2*. **(C)** Chlorophyll contents in *Atglk1Atglk2* overexpressing *PpGLK1* and *Atglk1Atglk2*. **(D)** Chloroplast development in siliques and leaves observed by TEM in *Atglk1Atglk2* overexpressing *PpGLK1* and *Atglk1Atglk2*. Data is presented as the means ± SD, $n = 3$. Different letters above bars denote statistical significance according to one-way ANOVA and Duncan's test ($P < 0.05$).

and introduced it into the pTRV2 vector to produce pTRV2-PpGLK1. pTRV2 was used as the control. Both vectors were infiltrated into peach fruit and leaves along with pTRV1 for VIGS. Mature leaves and immature fruit of peach were selected to validate the effect of *PpGLK1* silencing. In mature leaves, the infiltration sites on the leaves became pale green by 3 days after transformation with pTRV1 and pTRV2-PpGLK1, whereas no clear phenotype was observed after transformation with the control vector (**Figure 5A**). Further analyses showed that chlorophyll content at the infiltration sites of pTRV1 and pTRV2-PpGLK1 was 0.73 mg g^{-1}, much lower than that at sites infiltrated with the control vector (1.41 mg g^{-1}; **Figure 5B**). The chlorophyll content was 1.52 mg g^{-1} at non-infiltrated sites. At 3 days after transformation, the transcript level of *PpGLK1* at sites infiltrated with pTRV1 and pTRV2-PpGLK1 was 91.20% lower than that at non-infiltrated sites (**Figure 5C**).

Waters et al. (2009) demonstrated that GLK can bind to the promoter of many nuclear photosynthetic genes including *Lhcb3, Lhcb5*, *Lhcb4.2*, *PpLhcb6*, *Lhcb2.2*, *Lhcb1.3, Lhca1*, *Lhca2*, *Lhca3*, *PORA*, *CHLM*, *CHLH*, *PsaK*, *PsaD*, and *GUN4*. The transcript levels of these target genes were clearly decreased at sites infiltrated with pTRV1 and pTRV2-PpGLK1 (**Figure 5C**). There were no significant differences in the transcript levels of each of these genes between sites infiltrated with the control vector and uninfected leaves. In the immature fruit, infiltration sites were paler than the control by 7 days after transformation with pTRV1 and pTRV2-PpGLK1 (**Figure 5A**) and the expression of *PpGLK1* and its target genes were down-regulated at the infiltrated sites (**Figure S2**). Measurements of chlorophyll content in peach fruit peel confirmed a decrease in chlorophyll content around the infiltrated sites (**Figure 5B**). Thus, silencing of *PpGLK1* affected the expression of its target genes and chlorophyll content in peach. Together, these results showed that *PpGLK1*

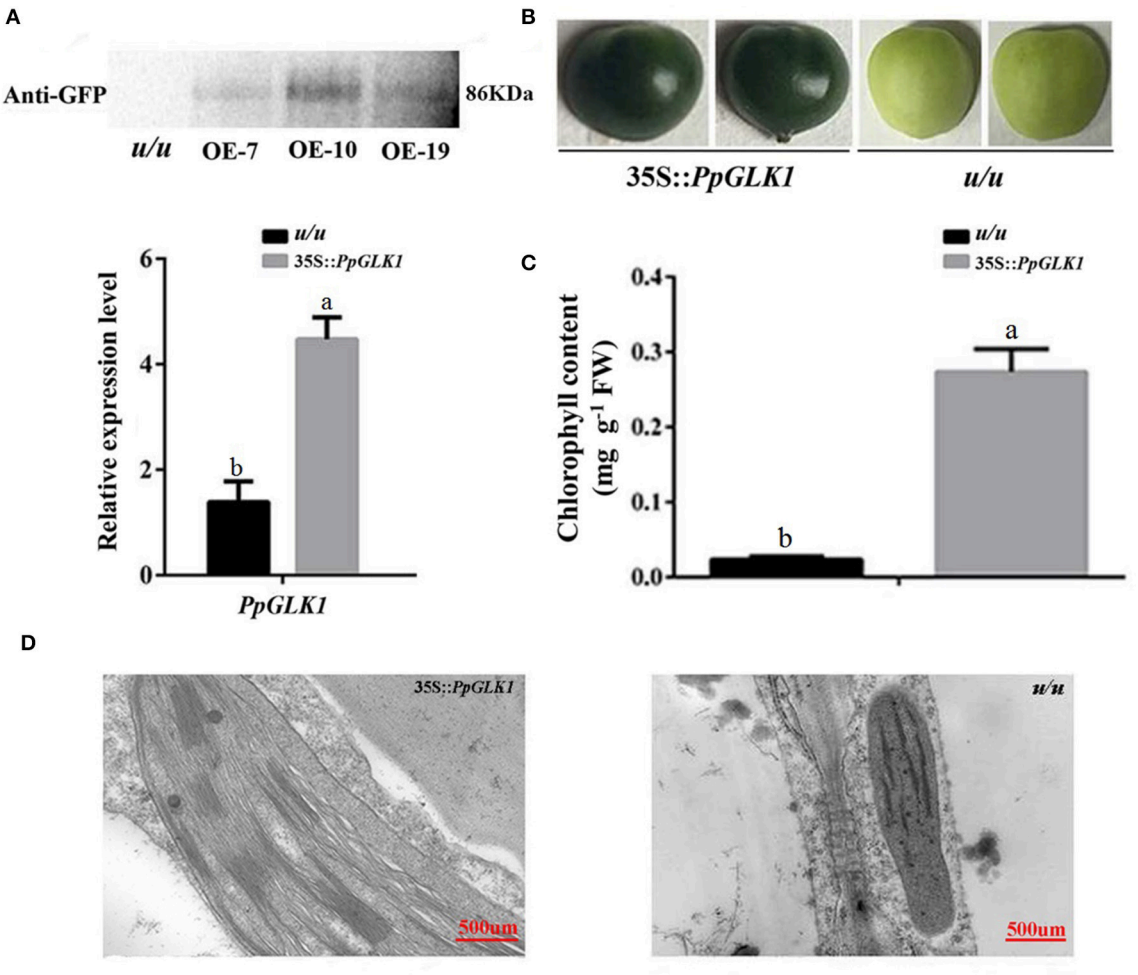

FIGURE 7 | Overexpression of *PpGLK1* in *u/u* tomato. **(A)** qRT-PCR and western blot analysis confirming *PpGLK1* overexpression in *u/u* tomato. **(B)** Phenotype of *PpGLK1*-overexpressing *u/u* tomato. **(C)** Chlorophyll contents in *u/u* tomato and *PpGLK1*-overexpressing *u/u* tomato. **(D)** Chloroplast development in fruit observed by TEM in *PpGLK1*-overexpressing *u/u* tomato fruit and *u/u* tomato fruit. Data is presented as the means ± SD, $n = 3$. Different letters above bars denote statistical significance according to one-way ANOVA and Duncan's test ($P < 0.05$).

can positively regulate chlorophyll accumulation in peach fruit peel.

Phenotypic Characterization of *PpGLK1-OE* Lines in *Arabidopsis thaliana* and Tomato

The GLK transcription factors have been shown to regulate chloroplast development and formation of the photosynthetic apparatus in *Arabidopsis* (Waters et al., 2009). To further verify the function of *PpGLK1*, a CaMV-35S promoter (35S::*PpGLK1*) vector was constructed and heterologously transformed into the *Arabidopsis glk1glk2* double mutant. Transgenic plants were identified by western blotting with GFP antibody (**Figure 6A**). Introduction of 35S::*PpGLK1* recovered the *glk1glk2* double mutant pale-green phenotype (**Figure 6B**); the chlorophyll content in 35S::*PpGLK1 Arabidopsis* was approximately 3.5 times that in *glk1glk2* (**Figure 6C**). The TEM analyses showed that there was a general increase in the number of granal thylakoids (8.9) in *PpGLK1-OE* lines, compared with *glk1glk2* leaves (1.5). The starch grains in the chloroplasts of *PpGLK1-OE* siliques were significantly larger than those of *Arabidopsis glk1glk2* mutant (**Figure 6D**). These results proved that *PpGLK1* could complement the chlorophyll biosynthesis phenotype of the

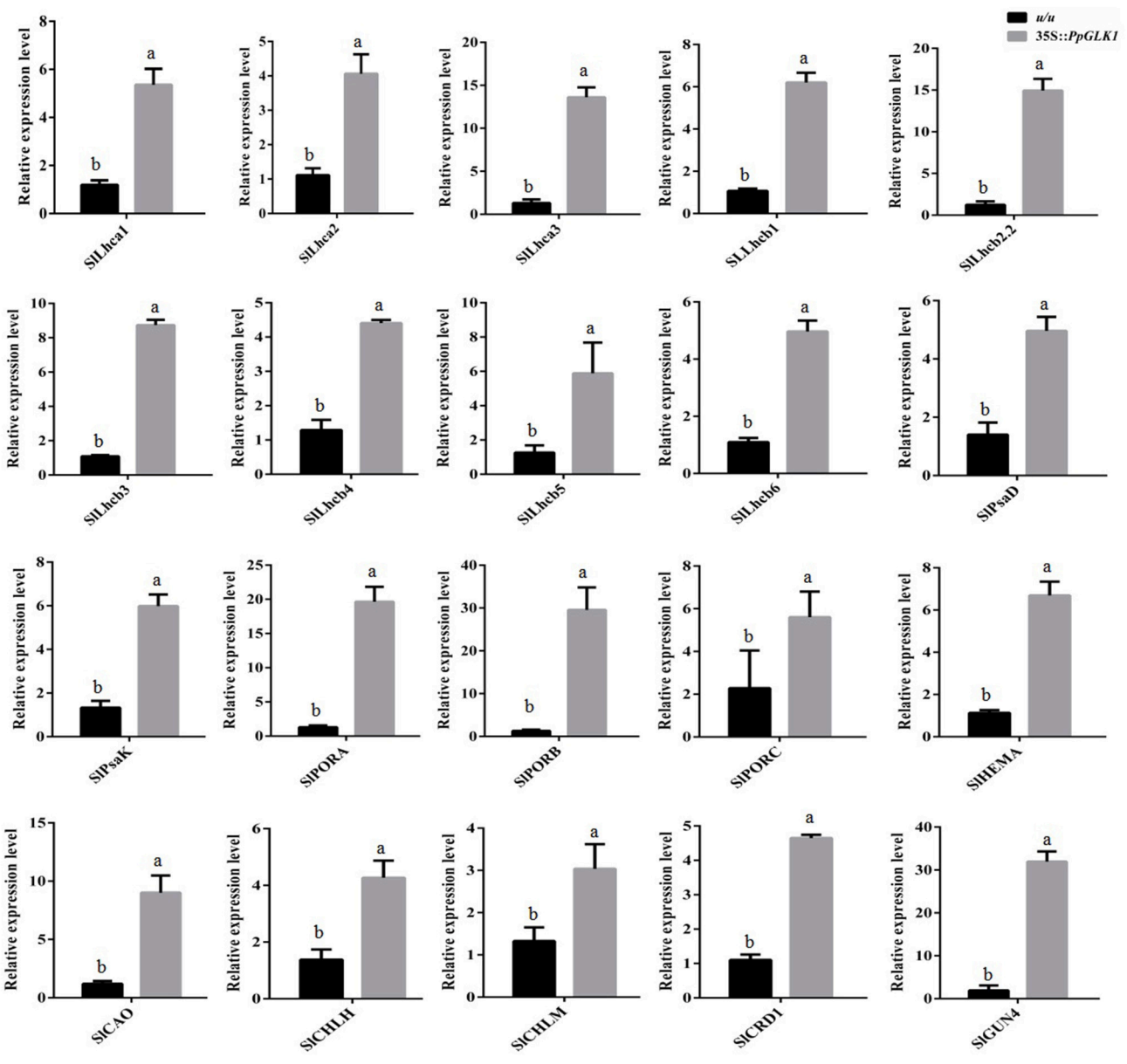

FIGURE 8 | Expression patterns of *PpGLK1* target genes in *PpGLK1*-overexpressing *u/u* tomato fruit. Data is presented as the means ± SD, $n = 3$. Different letters above bars denote statistical significance according to one-way ANOVA and Duncan's test ($P < 0.05$).

glk1glk2 double mutant. This complementary analysis showed that *PpGLK1* maintains its function to control chloroplast development in *Arabidopsis*, like in peach.

As reported by Powell et al. (2012), *uniform ripening* (*u*) encodes a truncated *Slglk2* that affects fruit chloroplast development in tomato. Micro-Tom, which is homozygous for the *u* mutation (*u/u*), was selected for further experiments (Nadakuduti et al., 2014). Similar to *PpGLK1-OE* in *Arabidopsis*, Micro-Tom lines overexpressing *PpGLK1-OE* were selected by qRT-PCR and western analysis (**Figure 7A**). The Micro-Tom *PpGLK1-OE* lines produced uniform dark-green unripe fruit (**Figure 7B**). Chlorophyll content was elevated by 135-fold (**Figure 7C**) compared with that in untransformed Micro-Tom (*u/u*). The number and size of chloroplasts were increased and the number of thylakoids per granum was also greater in Micro-Tom *PpGLK1-OE* fruit than in *u/u* fruit (**Figure 7D**). Interestingly, the transcript levels of GLK target genes were also up-regulated in Micro-Tom *PpGLK1-OE* (**Figure 8**). Thus, the phenotypic characterization of *PpGLK1-OE* in *u/u* tomato revealed that *PpGLK1* is associated with chloroplast development and chlorophyll biosynthesis in tomato, like in peach.

PpGLK1 Can Interact with PpARF5

To test bait for autoactivation and toxicity, the full-length PpGLK1 coding region fused to pGBKT7 was generated and transformed into competent Y2HGold cells; pGBKT7-53 served as the positive control. After selection on SD/-Trp, SD/-Trp/X-a-Gal and SD/-Trp/X-a-Gal/AbA medium, we found that the expression of our bait protein was not toxic in yeast and that the PpGLK1 protein autoactivated (**Figure 9A** and **Figure S3**). To select the fragment for yeast two-hybrid (Y2H) screening, the PpGLK1 protein was cut into two fragments: 1-300 a.a. and 301-542 a.a. The 301-542 a.a. fragment did not autoactivate and was used as bait for Y2H screening (**Figure 9A**). In the Y2H screening, several positive colonies harbored the PpARF5 protein, which is homolog of AtARF5. In a Y2H assay, PpGLK1 (301–542) interacted with the full-length PpARF5 protein (**Figure 9B** and **Figure S3**). When this interaction was tested in a bimolecular fluorescence complementation (BiFC) analysis, PpGLK1 interacted with the full-length PpARF5 protein *in vivo* (**Figure 9C**). A pull-down assay confirmed the interaction between PpGLK1 and PpARF5 *in vitro* (**Figure 9D**).

DISCUSSION

Although many genes have been reported to regulate chloroplast development, only GLKs control a large number of photosynthesis-related genes (Waters et al., 2009). Thus, it is critical to elucidate the function and effects of *PpGLK1* in peach. In this study, our results showed that *PpGLK1* regulates chloroplast development in peach, leading to chlorophyll accumulation. These results indicate that *PpGLK1* is a good target for improvements in fruit quality and production via breeding or transgenic approaches.

The transition from chloroplasts into chromoplasts has been documented for ripening goji berries (Hempel et al., 2017), and was shown to be induced by fruit shading in grapefruit (Lado et al., 2015). Yang et al. (2015) demonstrated that chlorophyll content was significantly lower in a rubescent leaf color mutant of *Anthurium andraeanum* than in the wild type, and analyses of the micro- and ultra-structures in the chloroplasts showed that a chloroplast-to-chromoplast transition occurred in the leaf color mutants (Cheung et al., 1993; Yang et al., 2015). A comparative proteomic analysis showed that the proteins involved in the light

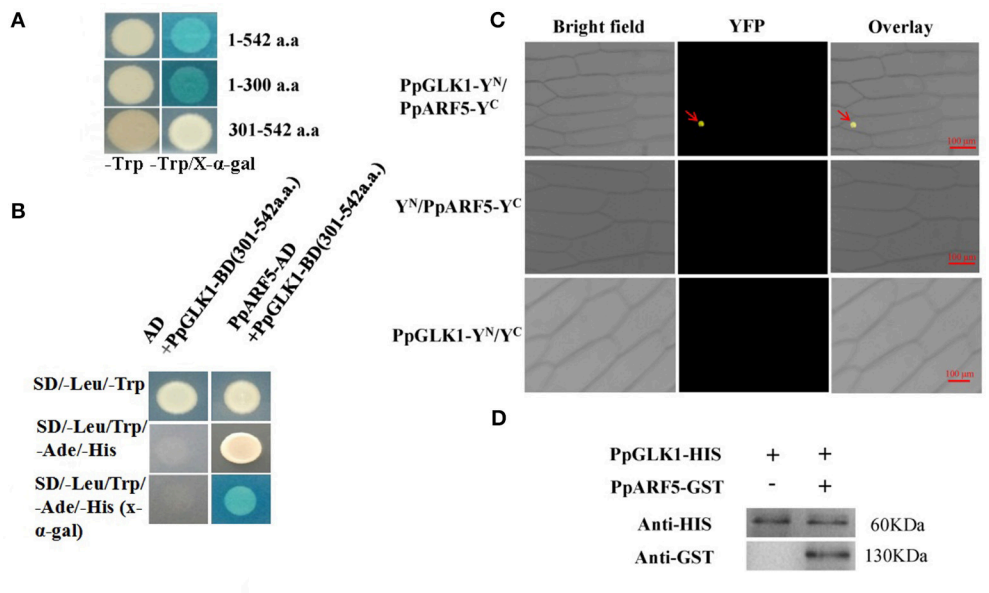

FIGURE 9 | Interaction between PpGLK1 and PpARF5. **(A)** Autoactivation of PpGLK1 in yeast cells. **(B)** Interaction between PpGLK1 and PpARF5 in Y2H assay. **(C)** Interaction between PpGLK1 and PpARF5 in BiFC assay. **(D)** Interaction between PpGLK1 and PpARF5 *in Vitro* in pull-down assay.

reactions of photosynthesis decreased in abundance during the chloroplast-to-chromoplast transition in tomato (Barsan et al., 2012). In our study, the chlorophyll and the total carotrnoid content decreased during fruit development and analyses of ultra-structural changes in chloroplasts revealed the details of the chloroplast-to-chromoplast transition. This transition has also been documented in tomato (Harris and Spurr, 1969) and bell pepper (Spurr and Harris, 1968).

Transcriptomic profiling can reveal the patterns of gene expression over time and in different parts of the plant (Wang et al., 2009). In the present study, we added a transcriptome analysis to reveal the molecular foundation of the chloroplast-to-chromoplast transition. Interestingly, the transcript levels of *PpGLK1* and its target genes decreased during the fruit ripening in peach. In *Arabidopsis* and tomato, homologs of *PpGLK1* have been shown play an important role in chloroplast development (Waters et al., 2009; Powell et al., 2012). In addition, mutants of GLK target genes (including *CAO* and *CHLM*) exhibited pale-green phenotypes. However, whether *PpGLK1* also functions in chloroplast development in peach was yet to be confirmed. The *GLK* genes are members of the GARP family (Riechmann et al., 2000) which contains 35 genes in peach. Rossini et al. (2001) demonstrated that *GLK* genes contain two highly conserved domains. Based on these two conserved domains, we searched for and found only one *GLK* gene in peach. One explanation for this result may be that ancestral triplicated blocks are fragmentary and a recent whole-genome duplication event has not occurred in peach (Verde et al., 2013). In the phylogenetic analysis, PpGLK1 was most closely related to AtGLK1 and SlGLK2 (**Figure 2B**) and the multiple sequence alignment showed that they have the same functional domains (**Figure 2A**). All these results suggested that *PpGLK1* may have the same function in peach, tomato, and *Arabidopsis*. Overexpression of *PpGLK1* complemented the double mutant *Atglk1Atglk2 (Arabidopsis)* and *u/u* (tomato) (**Figures 6B**, **7B**). In addition, the *PpGLK1*-complemented mutants showed increased expression of chlorophyll-related genes and increased chlorophyll content. These results provided further evidence *PpGLK1* has the same function as *AtGLK1* and *SlGLK2,* which are known to be involved in chloroplast development and chlorophyll biosynthesis. Improving the photosynthetic capacity can lead to increased carbohydrate and carotenoids contents in mature fruit (Powell et al., 2012).

The VIGS system, which is composed of TRV1 and TRV2, is a powerful tool for gene functional characterization *in vivo* (Sun et al., 2016). It has been successfully used to investigate gene function in the leaves and fruits of *Pyrus betulaefolia* (Li et al., 2017), apple (Hu et al., 2016; Jiang et al., 2017), pear (Zhai et al., 2016), and peach (Zhou et al., 2015). The *Arabidopsis* double mutant *Atglk1Atglk2* exhibited a pale-green phenotype and the tomato double mutant *u/u* produced uniformly light-green unripe fruit. In peach, silencing of *PpGLK1* decreased the chlorophyll content and led to pale-green fruit and leaves (**Figures 5A,B**) suggesting that GLK regulates chloroplast development in peach leaves and fruits. On the basis of our results, we concluded that PpGLK1 is positive regulator of chloroplast development like GLKs in other species.

Complex hormonal signals activate the transcription factors that regulate chloroplast development-related genes (Nakamura et al., 2009). Brassinosteroids regulate plant growth and development through *BES1* and *BZR1* transcription factors. The *bes1-D* mutant exhibited a pale-green color and exhibited a reduced chlorophyll content. Another *BES1* mutant with repressed *GLK1* and *GLK2* expression showed inhibited chloroplast development (Yu et al., 2011). Chloroplast biogenesis in greening roots was shown to depend on the combination of *HY5* and *GLKs,* which function downstream of light and auxin/cytokinin signaling pathways (Kobayashi et al., 2012). GLK proteins need partners to bind DNA (Waters et al., 2009).Tamai et al. (2002) demonstrated that AtGLK1 and AtGLK2 transactivate transcription in yeast and can interact with GBF1. In addition, AtGLK1 was shown to interact with GBF3. Our results showed that PpGLK1 can autoactivate, like AtGLK1 and AtGLK2 (**Figure 9A**). The results of the Y2H, pull-down, and BiFC assays all confirmed the interaction between PpGLK1 and PpARF5 (**Figures 9B–D**). The coordinated actions of ARF and Aux/IAA transcriptional repressors play a foremost role in auxin action. Sagar et al. (2013) showed that auxin can repress the expression of *GLK2,* and that down-regulation of *SlARF4* resulted in a dark-green fruit phenotype. It is noteworthy that the promoter of *PpGLK1* contained an auxin-responsive element, the AACGAC box (**Table S3**). The coordinated action of ARF and Aux/IAA transcriptional repressors play a major role in auxin action. ARF5/MP broadly regulates the expression of *Aux/IAA* genes in distinct subclades and is under negative feedback control by *Aux/IAA* genes (Krogan et al., 2014). Together, the results of this study provide further evidence for a link between auxin signaling and chloroplast development.

AUTHOR CONTRIBUTIONS

MC, DG, and LL designed the research. MC and XL performed the experiments. MC, SJ, and XL analyzed the data. LL, DL, XC, DG, and XF contributed new models. MC, SJ wrote the manuscript. LL, CY revised the intellectual content of this manuscript. All authors read and approved the final manuscript.

FUNDING

This study was funded by the National Natural Science Foundation of China (Grant number 31372050 and 31672137) and Funds of Shandong "Double Tops" Program.

SUPPLEMENTARY MATERIAL

The Supplementary Material for this article can be found online at: https://www.frontiersin.org/articles/10.3389/fpls.2018.00034/full#supplementary-material

Figure S1 | The Cq of the *Actin* genes (Prupe.6G163400 and Prupe. 3G205200).

Figure S2 | Transcript levels of PpGLK1 target genes in fruit skin of *PpGLK1*-silenced and control peach.

Figure S3 | The original figures of **Figures 9A,B**.

Table S1 | The primers used in this article.

Table S2 | GO term enrichment analysis of DEGs.

Table S3 | The analysis of *PpGLK1* promoter.

Table S4 | Data of sequences used for phylogenetic analysis.

REFERENCES

Alric, J., and Johnson, X. (2017). Alternative electron transport pathways in photosynthesis: a confluence of regulation. *Curr. Opin. Plant Biol.* 37, 78–86. doi: 10.1016/j.pbi.2017.03.014

Barsan, C., Zouine, M., Maza, E., Bian, W., Egea, I., Rossignol, M., et al. (2012). Proteomic analysis of chloroplast-to-chromoplast transition in tomato reveals metabolic shifts coupled with disrupted thylakoid biogenesis machinery and elevated energy-production components. *Plant Physiol.* 160, 708–725. doi: 10.1104/pp.112.203679

Brand, A., Borovsky, Y., Hill, T., Rahman, K. A. A., Bellalou, A., Deynze, A. V., et al. (2014). CaGLK2 regulates natural variation of chlorophyll content and fruit color in pepper fruit. *Theor. Appl. Genet.* 127, 2139–2148. doi: 10.1007/s00122-014-2367-y

Cao, K., Zhou, Z., Wang, Q., Guo, J., Zhao, P., Zhu, G., et al. (2016). Genome-wide association study of 12 agronomic traits in peach. *Nat. Commun.* 7:13246. doi: 10.1038/ncomms13246

Cheng, L., and Lai, K. (2013). *Golden2- Like (GLK2) Transcription Factor: Developmental Control of Tomato Fruit Photosynthesis and Its Contribution to Ripe Fruit Characteristics*. M.S. thesis, University of California, Davis, CA.

Cheung, A. Y., McNellis, T., and Piekos, B. (1993). Maintenance of chloroplast components during chromoplast differentiation in the tomato mutant Green Flesh. *Plant Physiol.* 101, 1223–1229. doi: 10.1104/pp.101.4.1223

Cortleven, A., Marg, I., Yamburenko, M. V., Schlicke, H., Hill, K., Grimm, B., et al. (2016). Cytokinin regulates the etioplast-chloroplast transition through the two-component signaling system and activation of chloroplast-related genes. *Plant Physiol.* 172, 464–478. doi: 10.1104/pp.16.00640

Cortleven, A., and Schmülling, T. (2015). Regulation of chloroplast development and function by cytokinin. *J. Exp. Bot.* 66, 4999–5013. doi: 10.1093/jxb/erv132

Fillatti, J., Kiser, J., Rose, R., and Comai, L. (1987). Efficient transfer of a glyphosate tolerance gene into tomato using a binary *Agrobacterium tumefaciens* vector. *Nat. Biotechnol.* 5, 726–730. doi: 10.1038/nbt0787-726

Fitter, D. W., Martin, D. J., Copley, M. J., Scotland, R. W., and Langdale, J. A. (2002). GLK gene pairs regulate chloroplast development in diverse plant species. *Plant J.* 31, 713–727. doi: 10.1046/j.1365-313X.2002.01390.x

Galpaz, N., Wang, Q., Menda, N., Zamir, D., and Hirschberg, J. (2008). Abscisic acid deficiency in the tomato mutant high-pigment 3 leading to increased plastid number and higher fruit lycopene content. *Plant J.* 53, 717–730. doi: 10.1111/j.1365-313X.2007.03362.x

Harris, W. M., and Spurr, A. R. (1969). Chromoplasts of tomato fruit. II. the red tomato. *Am. J. Bot.* 56, 380–389. doi: 10.2307/2440813

Hempel, J., Schädle, C. N., Sprenger, J., Heller, A., Carle, R., and Schweiggert, R. M. (2017). Ultrastructural deposition forms and bioaccessibility of carotenoids and carotenoid esters from goji berries (*Lycium barbarum* L.). *Food Chem.* 218, 525–533. doi: 10.1016/j.foodchem.2016.09.065

Hu, D. G., Sun, C. H., Zhang, Q. Y., An, J. P., You, C. X., and Hao, Y. J. (2016). Glucose sensor MdHXK1 phosphorylates and stabilizes MdbHLH3 to promote anthocyanin biosynthesis in apple. *PLoS Genet.* 12:e1006273. doi: 10.1371/journal.pgen.1006273

Jiang, Y., Liu, C., Yan, D., Wen, X., Liu, Y., Wang, H., et al. (2017). MdHB1 down-regulation activates anthocyanin biosynthesis in the white-fleshed apple cultivar 'Granny Smith'. *J. Exp. Bot.* 68, 1055–1069. doi: 10.1093/jxb/erx029

Jin, W., Wang, H., Li, M., Wang, J., Yang, Y., Zhang, X., et al. (2016). The R2R3 MYB transcription factor PavMYB10.1 involves in anthocyanin biosynthesis and determines fruit skin colour in sweet cherry (*Prunus avium* L.). *Plant Biotechnol. J.* 14, 2120–2133. doi: 10.1111/pbi.12568

Karagiannis, E., Tanou, G., Samiotaki, M., Michailidis, M., Diamantidis, G. S., Minas, I., et al. (2016). Comparative physiological and proteomic analysis reveal distinct regulation of peach skin quality traits by altitude. *Front. Plant Sci.* 7:1689. doi: 10.3389/fpls.2016.01689

Kobayashi, K., Baba, S., Obayashi, T., Sato, M., Toyooka, K., Keränen, M., et al. (2012). Regulation of root greening by light and auxin/cytokinin signaling in Arabidopsis. *Plant Cell* 24, 1081–1095. doi: 10.1105/tpc.111.092254

Krogan, N. T., Yin, X., Ckurshumova, W., and Berleth, T. (2014). Distinct subclades of *Aux/IAA* genes are direct targets of ARF5/MP transcriptional regulation. *New Phytol.* 204, 474–483. doi: 10.1111/nph.12994

Lado, J., Cronje, P., Alquézar, B., Page, A., Manzi, M., Gómez-Cadenas, A., et al. (2015). Fruit shading enhances peel color, carotenes accumulation and chromoplast differentiation in red grapefruit. *Physiol. Plant.* 154, 469–484. doi: 10.1111/ppl.12332

Langmead, B., and Salzberg, S. L. (2012). Fast gapped-read alignment with Bowtie 2. *Nat. Methods* 9, 357–359. doi: 10.1038/nmeth.1923

Li, K., Xing, C., Yao, Z., and Huang, X. (2017). PbrMYB21, a novel MYB protein of *Pyrus betulaefolia*, functions in drought tolerance and modulates polyamine levels by regulating arginine decarboxylase gene. *Plant Biotechnol. J.* 15, 1186–1203. doi: 10.1111/pbi.12708

Lichtenthaler, H. K. (1987). Chlorophylls and carotenoids: pigments of photosynthetic biomembranes. *Method Enzymol* 148, 350–382. doi: 10.1016/0076-6879(87)48036-1

Liu, L., Jia, C., Zhang, M., Chen, D., Chen, S., Guo, R., et al. (2014). Ectopic expression of a BZR1-1D transcription factor in brassinosteroid signalling enhances carotenoid accumulation and fruit quality attributes in tomato. *Plant Biotechnol. J.* 12, 105–115. doi: 10.1111/pbi.12121

Lopez-Juez, E., and Pyke, K. A. (2005). Plastids unleashed: their development and their integration in plant development. *Int. J. Dev. Biol.* 49, 557–577. doi: 10.1387/ijdb.051997el

Nadakuduti, S. S., Holdsworth, W. L., Klein, C. L., and Barry, C. S. (2014). KNOX genes influence a gradient of fruit chloroplast development through regulation of GOLDEN2-LIKE expression in tomato. *Plant J.* 78, 1022–1033. doi: 10.1111/tpj.12529

Nakamura, H., Hakata, M., Ueno, O., Nagamura, Y., Hirochika, H., Takano, M., et al. (2009). Ectopic overexpression of the transcription factor OsGLK1 induces chloroplast development in non-green rice cells. *Plant Cell Physiol.* 50, 1933–1949. doi: 10.1093/pcp/pcp138

Nguyen, C. V., Vrebalov, J. T., Gapper, N. E., Zheng, Y., Zhong, S., Fei, Z., et al. (2014). Tomato GOLDEN2-LIKE transcription factors reveal molecular gradients that function during fruit development and ripening. *Plant Cell* 26, 585–601. doi: 10.1105/tpc.113.118794

Pan, L., Zeng, W., Niu, L., Lu, Z., Lu, H., Cui, G., et al. (2015). PpYUC11, a strong candidate gene for the stony hard phenotype in peach (*Prunus persica* L. batsch), participates in IAA biosynthesis during fruit ripening. *J. Exp. Bot.* 66, 7031–7044. doi: 10.1093/jxb/erv400

Pan, Y., Bradley, G., Pyke, K., Ball, G., Lu, C., Fray, R., et al. (2013). Network inference analysis identifies an APRR2-Like gene linked to pigment accumulation in tomato and pepper fruits. *Plant Physiol.* 161, 1476–1485. doi: 10.1104/pp.112.212654

Pavel, E. W., and Dejong, T. M. (1993). Source-and sink-limited growth periods of developing peach fruits indicated by relative growth rate analysis. *J. Am. Soc. Hortic. Sci.* 6, 820–824.

Powell, A. L., Nguyen, C. V., Hill, T., Cheng, K. L., Figueroa-Balderas, R., Aktas, H., et al. (2012). Uniform ripening encodes a Golden2-like transcription factor regulating tomato fruit chloroplast development. *Science* 336, 1711–1715. doi: 10.1126/science.1222218

Riechmann, J. L., Heard, J., Martin, G., Reuber, L., Jiang, C., Keddie, J., et al. (2000). Arabidopsis transcription factors: genome-wide comparative analysis among eukaryotes. *Science* 290, 2105–2110. doi: 10.1126/science.290.5499.2105

Rossini, L., Cribb, L., Martin, D. J., and Langdale, J. A. (2001). The maize Golden2 gene defines a novel class of transcriptional regulators in plants. *Plant Cell* 13, 1231–1244. doi: 10.1105/tpc.13.5.1231

Sagar, M., Chervin, C., Mila, I., Hao, Y., Roustan, J. P., Benichou, M., et al. (2013). SlARF4, an auxin response factor involved in the control of sugar

metabolism during tomato fruit development. *Plant Physiol.* 161, 1362–1374. doi: 10.1104/pp.113.213843

Spurr, A. R., and Harris, W. M. (1968). Ultrastructure of chloroplasts and chromoplasts in *Capsicum annuum*. I. thylakoid membrane changes during fruit ripening. *Am. J. Bot*. 55, 1210–1224. doi: 10.2307/2440743

Su, M., Chen, K., Ye, Z., Zhang, B., Guo, J., Xu, C., et al. (2012). Physical changes and physiological characteristics of red and green peel during nectarine (cv. Hu018) maturation. *J. Sci. Food Agric.* 92, 1448–1454. doi: 10.1002/jsfa.4724

Sun, D., Nandety, R. S., Zhang, Y., Reid, M. S., Niu, L., and Jiang, C. Z. (2016). A petunia ethylene-responsive element binding factor, PhERF2, plays an important role in antiviral RNA silencing. *J. Exp. Bot.* 67, 3353–3365. doi: 10.1093/jxb/erw155

Tamai, H., Iwabuchi,M., and Meshi,T. (2002). Arabidopsis GARP transcriptional activators interact with the pro-rich activation domain shared by G-box-binding bZIP factors. *Plant Cell Physiol*. 43, 99–107. doi: 10.1093/pcp/pcf011

Tatusov, R. L., Koonin, E. V., and Lipman, D. J. (1997). A genomic perspective on protein families. *Science* 278, 631–637.

Verde, I., Abbott, A. G., Scalabrin, S., Jung, S., Shu, S., Marroni, F., et al. (2013). The high-quality draft genome of peach (*Prunus persica*) identifies unique patterns of genetic diversity, domestication and genome evolution. *Nat. Genet*. 45, 487–494. doi: 10.1038/ng.2586

Wang, L., Feng, Z., Wang, X., Wang, X., and Zhang, X. (2010). DEGseq: an R package for identifying differentially expressed genes from RNA-seq data. *Bioinformatics* 26, 136–138. doi: 10.1093/bioinformatics/btp612

Wang, N., Xu, H., Jiang, S., Zhang, Z., Lu, N., Qiu, H., et al. (2017). MYB12 and MYB22 play essential roles in proanthocyanidin and flavonol synthesis in red-fleshed apple (*Malus sieversii* f. niedzwetzkyana*). Plant J*. 90, 276–292. doi: 10.1111/tpj.13487

Wang, P., Fouracre, J., Kelly, S., Karki, S., Gowik, U., Aubry, S., et al. (2013). Evolution of GOLDEN2-LIKE gene function in C3 and C4 plants. *Planta* 237, 481–495. doi: 10.1007/s00425-012-1754-3

Wang, Z., Gerstein, M., and Snyder, M. (2009). RNA-Seq: a revolutionary tool for transcriptomics. *Nat. Rev. Genet*. 10, 57–63. doi: 10.1038/nrg2484

Waters, M. T., Wang, P., Korkaric, M., Capper, R. G., Saunders, N. J., and Langdale, J. A. (2009). GLK transcription factors coordinate expression of the photosynthetic apparatus in Arabidopsis. *Plant Cell* 21, 1109–1128. doi: 10.1105/tpc.108.065250

Yang, Y., Chen, X., Xu, B., Li, Y., Ma, Y., and Wang, G. (2015). Phenotype and transcriptome analysis reveals chloroplast development and pigment biosynthesis together influenced the leaf color formation in mutants of *Anthurium andraeanum* 'Sonate'. *Front. Plant Sci*. 6:139. doi: 10.3389/fpls.2015.00139

Yu, X., Li, L., Zola, J., Aluru, M., Ye, H., Foudree, A., et al. (2011). A brassinosteroid transcriptional network revealed by genome-wide identification of BESI target genes in *Arabidopsis thaliana*. *Plant J*. 65, 634–646. doi: 10.1111/j.1365-313X.2010.04449.x

Zhai, R., Wang, Z., Zhang, S., Meng, G., Song, L., Wang, Z., et al. (2016). Two MYB transcription factors regulate flavonoid biosynthesis in pear fruit (*Pyrus bretschneideri* Rehd.). *J. Exp. Bot*. 67, 1275–1284. doi: 10.1093/jxb/erv524

Zhou, H., Wang, K., Wang, H., Gu, C., Dare, A. P., Espley, R. V., et al. (2015). Molecular genetics of blood-fleshed peach reveals activation of anthocyanin biosynthesis by NAC transcription factors. *Plant J*. 82, 105–121. doi: 10.1111/tpj.12792

Conflict of Interest Statement: The authors declare that the research was conducted in the absence of any commercial or financial relationships that could be construed as a potential conflict of interest.

frontiers in Plant Science

ORIGINAL RESEARCH
published: 20 February 2018
doi: 10.3389/fpls.2018.00179

SKL1 Is Essential for Chloroplast Development in Arabidopsis

Huimin Xu[1,2,3†], Liwen Zhang[1,2†], Ruili Li[1,2†], Xinwei Wang[2], Shuai Liu[1,2], Xiaomin Liu[1,2], Yanping Jing[1,2] and Jianwei Xiao[1,2]*

[1] Beijing Advanced Innovation Center for Tree Breeding by Molecular Design, Beijing Forestry University, Beijing, China, [2] College of Biological Sciences and Biotechnology, Beijing Forestry University, Beijing, China, [3] College of Life Sciences, Peking University, Beijing, China

The Arabidopsis *shikimate kinase-like 1* (*skl1-8*) mutant is characterized by a pigment-defective phenotype. Although the related phenotypical defect mainly has been attributed to the blocking of chloroplast development, the molecular functions of SKL1 remain largely unknown. In this study, we combined multiple approaches to investigate the potential functions of SKL1. Results showed that the *skl1-8* mutant exhibited an albino phenotype and had dramatically reduced chlorophyll content as a consequence of a single nuclear recessive gene mutation. Chemical complementation analysis indicated that SKL1 does not function as SK enzyme in the shikimate pathway. In addition, by chlorophyll fluorescence parameters and immunoblot analysis, the levels of photosynthetic proteins are substantially reduced. Moreover, by transcriptome analysis, specific groups of nuclear genes involved in photosynthesis, such as light-harvesting complex, pigment metabolism, carbon metabolism, and chloroplast gene expression, were down-regulated, whereas several defense and oxidative stress responsive genes were up-regulated in the *skl1-8* mutant compared with the wide type. Furthermore, we found the expression of genes related to auxin transport and response was repressed in the *skl1-8* mutant, probable suggesting that SKL1 is involved in auxin-related pathways during chloroplast development. Together, these results provide a useful reference for characterization of SKL1 function during chloroplast biogenesis and development.

Keywords: SKL1, chloroplast, development, Arabidopsis, gene expression

OPEN ACCESS

Edited by:
Fei Yu,
Northwest A&F University, China

Reviewed by:
Yue Wu,
Massachusetts General Hospital, Harvard Medical School, United States
Yan Lu,
Western Michigan University, United States

***Correspondence:**
Jianwei Xiao
xiaojianwei@bjfu.edu.cn

† These authors have contributed equally to this work.

Specialty section:
This article was submitted to Plant Physiology, a section of the journal Frontiers in Plant Science

Received: *18 September 2017*
Accepted: *31 January 2018*
Published: *20 February 2018*

Citation:
Xu H, Zhang L, Li R, Wang X, Liu S, Liu X, Jing Y and Xiao J (2018) SKL1 Is Essential for Chloroplast Development in Arabidopsis. Front. Plant Sci. 9:179. doi: 10.3389/fpls.2018.00179

INTRODUCTION

Chloroplasts are organelles, specialized subunits, in plant and algal cells. The most important role of chloroplast is to conduct photosynthesis and related productions are critical for plant growth (Abdallah et al., 2000; Peltier et al., 2006). As the main site of photosynthesis, chloroplasts rely on the energy captured by photosynthetic pigment chlorophyll to fix carbon dioxide (Waters and Langdale, 2009), and numerous important biosynthetic pathways are carried out in the chloroplast, including tetrapyrroles, terpenoids, fatty acid biosynthesis, amino acids biosynthesis, hormones, and the immune response in plants (Givan and Stumpf, 1971; Kusumi et al., 2004; Seay et al., 2009; Hou et al., 2016).

Chloroplasts, which originated from cyanobacterial ancestors, are semiautonomous organelles with their own genome in higher plants (Martin et al., 2002; Hanaoka et al., 2003). The most photosynthetic proteins are nuclear encoded, synthesized in cytoplasm as precursor proteins and being imported into the chloroplast (Inaba and Schnell, 2008), it is has been confirmed that the

disruption on nuclear-encoded and chloroplast-localized proteins can specifically disrupts the chloroplast biogenesis by alternative biological functions, such as chloroplast gene expression, protein import, complexes assembly, lipid biosynthesis and so on (Gutiérrez-Nava et al., 2004; van Wijk, 2015; Zheng et al., 2016; Wang et al., 2017; Zhang Z. et al., 2017). Therefore, studies on such mutants would be further elucidating the regulatory mechanisms of chloroplast biogenesis and development. By investigating the SeedGenes database, a total of 119 chloroplast proteins encoded by nuclear genes were found to participate in embryo development in Arabidopsis (Tzafrir et al., 2004). Then reported proteins can be roughly classified into three groups based on their potential roles: (i) proteins required for the localization and modification of chloroplast proteins; (ii) enzymes are necessary for the biosynthesis of vitamins, amino acids, fatty acids and nucleotides; and (iii) regulated factors participated in the plastid genes expression (Bryant et al., 2011).

Among the nuclear-encoded factors that are involved in chloroplast and embryo development, the *shikimate kinase-like 1-8* (*skl1-8*) mutant was first described by characterization of an albino phenotype of a T-DNA-inserted allele of *AtSKL1*, and it was reported that SKL1 is essential for chloroplast development (Fucile et al., 2008). The *SKL1* gene evolved from Shikimate kinase (SK) gene duplicates more than 400 million years ago and can be found in all major extant angiosperm lineages (Fucile et al., 2008; Maeda and Dudareva, 2012). The SK proteins are involved in the intermediate step of the shikimate pathway, which is closely linked with produced processes of the aromatic amino acids (Herrmann, 1995). Considerable studies have been carried on the shikimate pathway because the three aromatic amino acids cannot be produced by some livestock and humans (Tzin and Galili, 2010). It has been estimated that 20% of the carbon fixed by plants can be directed toward the shikimate pathway (Herrmann, 1995), and this pathway is usually confined in chloroplast (Mustafa and Verpoorte, 2005). As the ancient homologous protein to SK, the recombinant SKL1 is purified in the same manner and showed a similar stable level as the active AtSK1, but SKL1 does not possess SK enzyme activity *in vitro* (Fucile et al., 2008).

SKL1 has been implicated in plastid biogenesis in Arabidopsis, however, a number of questions still remain unresolved, such as the exact function in chloroplast development and plastid biogenesis. In this study, we address these questions by combining a phenotypic and transcriptome analysis to further our understanding in the mechanism of SKL1 in the chloroplast development.

MATERIALS AND METHODS

Plant Materials and Growth Conditions

Surface-sterilized wild type and *skl1-8* mutant seeds were sown on 1/2 Murashige and Skoog (MS) agar Petri plates, and placed in the dark at 4°C for 48 h to imbibe. After germination, the plants moved to a growth chamber maintained at 22°C under long day conditions (16 h light, 8 h dark). For chemical complementation analysis, we resuspended shikimate 3-phosphate (Sigma, St. Louis, MO, United States) and chorismate (Sigma, St. Louis, MO, United States) in water at a concentration of 50 mM and next added it to the MS medium at a final working concentration of 50 μM.

Complementation of the *skl1-8* Mutant

To complement the *skl1-8* mutant, we amplified a full-length cDNA fragment encoding SKL1 by reverse transcription polymerase chain reaction (RT-PCR) using the specific primers from wild type. The primers sequences are list in the **Supplementary Table S1**. The PCR product was digested and subcloned into the pSN1301 vector by controlling of the cauliflower mosaic virus 35S promoter. Through the floral dip method, the construct was introduced into heterozygous *skl1-8* plant (Clough and Bent, 1998). The transgenic Arabidopsis was selected using 50 mg L^{-1} hygromycin medium and successful complementation was confirmed by PCR analysis.

Measurement of Chlorophyll

To measure the chlorophyll content, the whole Arabidopsis leaves were collected from three individual WT and *skl1-8* seedlings, respectively. We extracted the chlorophyll in 80% acetone and brief centrifugation (12000 *g*) at 4°C and quantified using a UV2800 spectrophotometer (Unico, Dayton, NJ, United States). We calculated the chlorophyll content from the absorbance following the method of Arnon (1949).

Total Protein Preparations and Immunoblot Analysis

In immunoblot analysis, total proteins were extracted from Arabidopsis leaves and separated by SDS–polyacrylamide gel electrophoresis (PAGE), and then were transferred to nitrocellulose membranes. The membranes were incubated with specific primary antibodies, and signals from secondary conjugated antibodies were visualized using the enhanced chemiluminescence method. We scanned X-ray films using an AlphaImager 2200 documentation and analysis system (Alpha Innotech Corporation, San Leandro, CA, United States). The antibodies referred in this analysis according to Zhang J. et al. (2017).

Chlorophyll Fluorescence Measurements

We measured the chlorophyll fluorescence by using a CF Imager (Technologica, Essex, United Kingdom) and operated it as described by Xiao et al. (2012). In briefly, the leaves were first dark adapted for 10 min before each measurement and the minimum fluorescence yield (F_o) was measured with a measuring light intensity of 0.8 mmol m^{-2} s^{-1}. For measuring the maximum fluorescence yield (F_m), we applied a saturating pulse of white light to the plants for 1 s, and the light intensity is 3000 mmol m^{-2} s^{-1}. We calculated the maximal photochemical efficiency of PSII by the ratio of F_v ($F_m - F_o$) to F_m. In image analysis, the corresponding data measured in the plants were normalized to a false-color scale with assigned extreme highest value with 0.8 (red) and lowest value with 0.1 (blue), respectively.

RNA Isolation, cDNA Library Preparation, and Transcriptome Sequencing

The method used in the transcripome analysis according to Xue et al. (2017). In general, sequencing libraries were generated using the NEBNext® Ultra™ RNA Library Prep Kit for an Illumina® device (NEB, Ipswich, MA, United States). Three cDNA libraries each for *skl1-8* mutant and wild type were constructed and sequencing by using the Illumina HiSeq 2500 platform. We pooled the clean reads of the three libraries for *de novo* assembly of the global transcriptome using Trinity (Grabherr et al., 2011). We cross-checked all of the assembled unigenes against the NR database using the Basic Logic Alignment Search Tool algorithm with an *E*-value cut-off of 10^{-5} (Korf et al., 2003).

Differentially expressed genes (DEGs) were identified in *skl1-8* and wild type according to the $|\log_2 (\text{fold-change})| \geq 1$ with the p-value < 0.05. The expression level for each unigene was calculated and normalized using the RPKM (reads per kb per million reads; Mortazavi et al., 2008). In addition, Gene Ontology Enrichment Analysis Software Toolkit were used to multi-GO enrichment analyses of DEGs (Zheng and Wang, 2008).

Quantitative Real-Time PCR

We synthesized first-strand cDNA using Transcript One-Step gDNA Removal and cDNA Synthesis SuperMix (TianGen Biotech, Beijing, China) following the instructions of manufacturer. Three samples were obtained from the wild-type and *skl1-8* mutant leaves, respectively. We conducted real-time PCR reactions containing 2 μL of first-strand cDNA in a total volume of 20 μL. Relative quantities of expression levels of the genes were calculated using the $2^{-\Delta\Delta Ct}$ method (Livak and Schmittgen, 2001) and the *Actin* gene used as internal control. We using a LineGene 9600 detection system to measure the quantity of amplified DNA by the fluorescence produced in the end of PCR reaction (BIOER, Hangzhou, China). The measurement for each sample was repeated in three times and the primer pairs used in this analysis listed in **Supplementary Table S1**.

RESULTS

Phenotype of *skl1-8* Mutant

The *skl1-8* mutant was first characterized by Fucile et al. (2008), and we got this mutant from Arabidopsis Biological Resource Center. The *skl1-8* mutant exhibited an albino phenotype and was obviously smaller in size relative to the wild type (**Figure 1A**). To confirm whether the phenotype of the *skl1-8* mutant was due to the disruption in *SKL1*, we transformed the full-length coding region of *SKL1* gene into the *skl1-8* mutant. After 14 days of

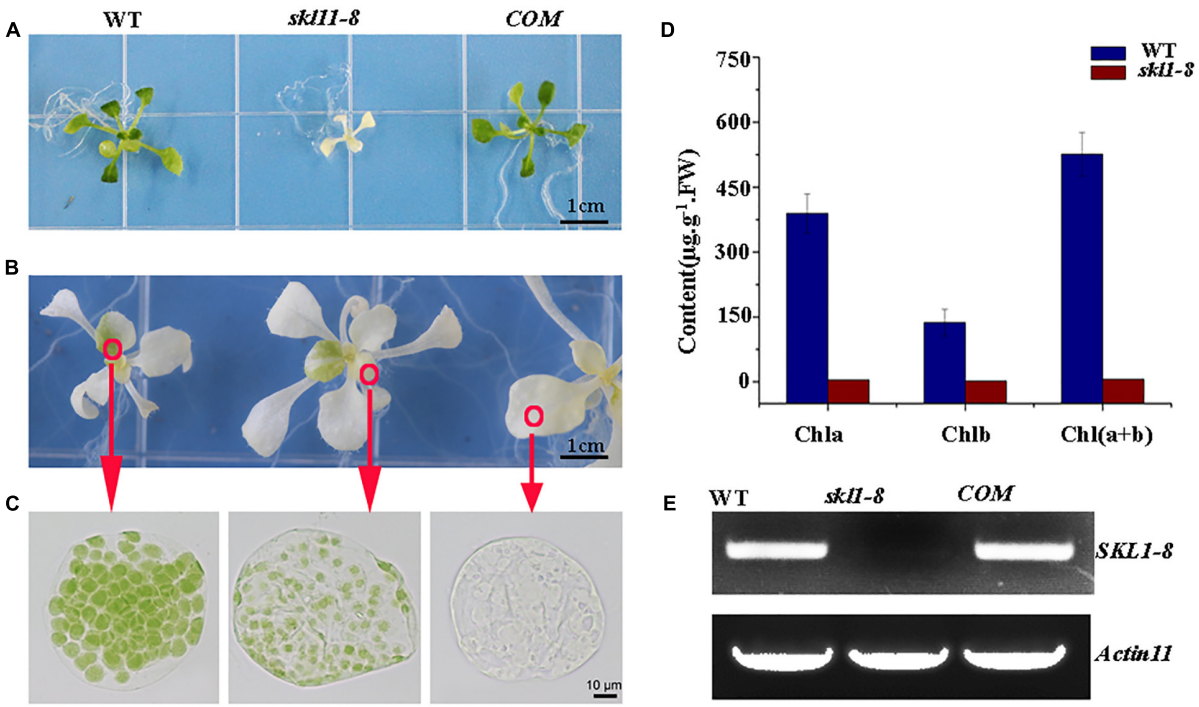

FIGURE 1 | Identification of the *skl1-8* mutant. **(A)** Identification and complementation of the *skl1-8* mutant. The cDNA of the wild-type *SKL1* with the flag sequence was cloned into a binary plant transformation vector and used for complementation of the *skl1-8* mutant (*COM*). WT, wild type. 14-day-old plants, including WT, *skl1-8*, and *COM*, were grown on sucrose-supplemented medium. Scale bar: 3 mm. **(B)** Different yellow-green phenotype in *skl1-8* mutant. **(C)** Chloroplast phenotypes of mesophyll cells in *skl1-8* mutant with different yellow–green phenotype. **(D)** Reverse transcription (RT)-PCR analysis. RT-PCR was performed using specific primers for *SKL1* or *ACTIN11*. **(E)** Mean values of chlorophyll contents (Chla and Chlb) in WT and *skl1-8* mutant seedlings. Leaf tissue was sampled from 14-day-old plants and data are mean values of three measurements ± SD.

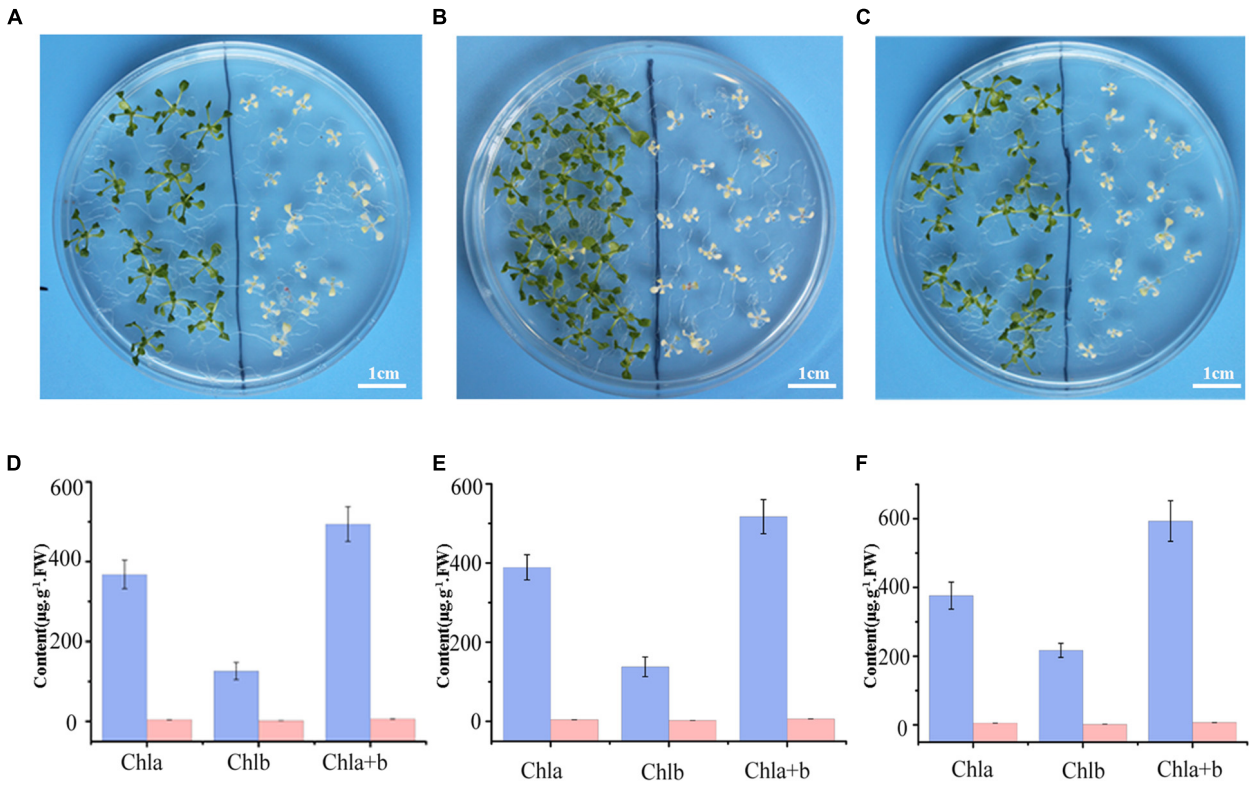

FIGURE 2 | Complement analysis of compound intermediates in the shikimate pathway. Phenotype of wild-type (left), and *skl1-8* seedlings (right) grown in **(A)** the regular MS medium, **(B)** the presence of chorismate, and **(C)** shikimate 3-phosphate. The chlorophyll contents in Arabidopsis seedlings were showed in **(D–F)**, respectively, and the data are mean values of three measurements ± SD.

growth, we observed *COM* transgenic plant showing similar leave color and plant size to the wild type (**Figure 1A**). When cultivated in sucrose-supplemented medium for 4 weeks, some white parts of the leaf in *skl1-8* mutant developed to different shades of yellow and green patches (**Figure 1B**). In addition, we also observed chloroplast phenotypes of different sections of the mesophyll cells with varied green parts in the *skl1-8* mutant (**Figure 1C**), showing that the chloroplast was more seriously affected in the white part than in the green part. Furthermore, we measured the chlorophyll content in 4-week-old *skl1-8* mutant and exhibited dramatically reduced levels compared with wild type (**Figure 1D**). Eventually, *COM* plants accumulated substantial quantities of chlorophyll, almost reaching the wild-type levels. RT-PCR analysis showed that the transcript of the *SKL1* gene was barely detected in *skl1-8* mutant, whereas obvious signals were obtained from *COM* and wild-type plants (**Figure 1E**). These results indicating that *skl1-8* mutant is null and *SKL1* gene was responsible for the phenotype of the *skl1-8*.

Homozygous *skl1-8* Mutant Cannot Be Rescued by Intermediates in Shikimate Pathway

Previous research suggested SKL1 to be an ancient homologous protein with SK proteins (Fucile et al., 2008), leading us to investigate whether SKL1 plays a similar role as SK in the shikimate pathway. We analyzed the phenotype of young seedlings of *skl1-8* mutant by growth in a complement of compound intermediates in the shikimate pathway. We first germinated *skl1-8* and wild-type plants on regular MS medium and then transferred them to MS medium supplemented with either chorismate or shikimate 3-phosphate. The materials transferred to regular MS medium were used as control. After cultivated for 2 weeks and compared with the control, the albino phenotype of *skl1-8* mutant showed no visible changes whatever grown on chorismate or shikimate 3-phosphate containing medium (**Figures 2A–C**).

Meanwhile, the pigment profiles of wild-type plant and *skl1-8* mutant are similar to the corresponding parts grown on regular MS medium (**Figures 2D–F**). This result indicates that the phenotype of *skl1-8* cannot be recovered when grows in the presence of chorismate or shikimate 3-phosphate. Thus, the combination of phenotypic and chlorophyll analysis excludes the fact that SKL1 function as SK proteins in the shikimate pathway.

Immunoblot Analysis of Chloroplast Proteins in *skl1-8* Mutant

Our previous studies have shown that the reduced content of chlorophyll is always coupled with defective accumulation of photosynthetic protein complexes (Zhang J. et al., 2017). To test this possibility, we analyzed the protein profile to

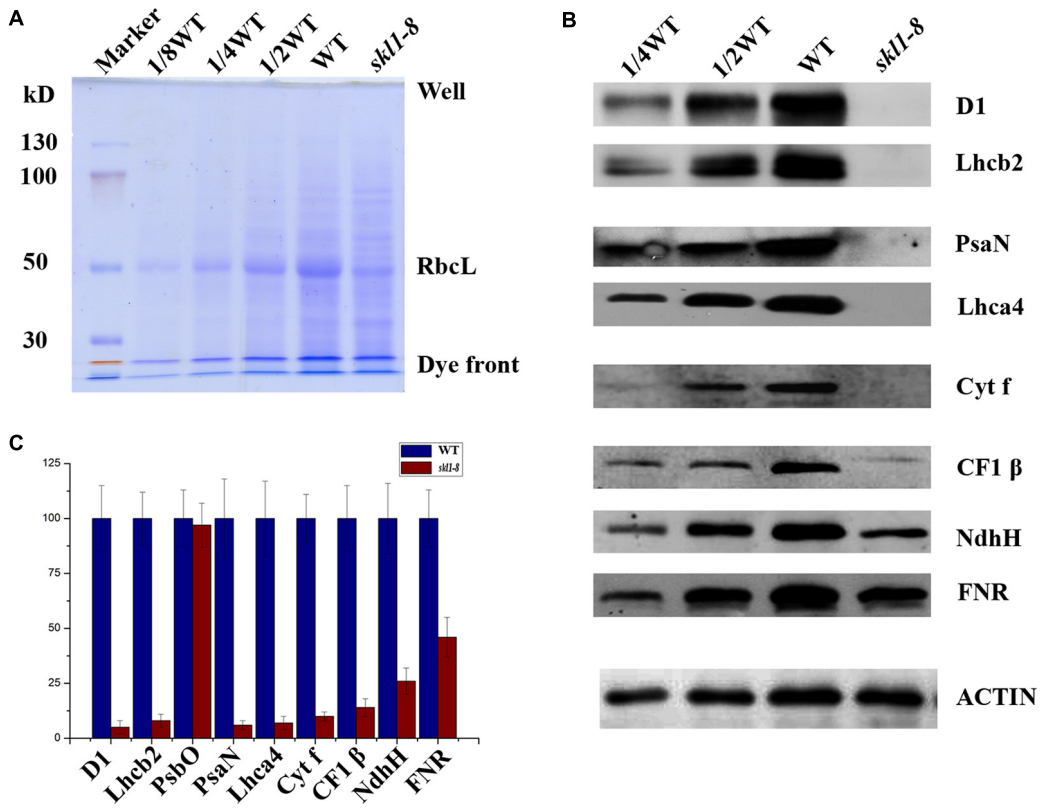

FIGURE 3 | Accumulation of chloroplast proteins. **(A)** Coomassie brilliant blue staining of total proteins. Total protein resolved by SDS/PAGE from WT and *skl1-8* and the major band of RbcL was indicated. **(B)** Western blot analysis of D1, Lhcb2, PsaN, Lhca4, Cyt f, CF1β, NdhH, FNR, and ACTIN in the total protein extract from wild-type and *skl1-8* plants. These experiments were repeated three times independently, and similar results were obtained each time. Results from a representative experiment are shown. **(C)** The average signal intensities for each protein were quantified by the ImageJ software for three independent times, expressed level relative to the WT* (=100), and are indicated on the left.

further investigate the stable level of photosynthetic proteins in *skl1-8* mutant. By coomassie brilliant blue staining, we observed a significant reduction in the content of the large subunit of ribulose bisphosphate carboxylase (RbcL) in *skl1-8* mutant (**Figure 3A**). We also performed western blot experiment to analyze the proteins involved in photosynthesis, including core subunit of photosystem II, D1; N subunit of photosystem I, PsaN; the light-harvesting chlorophyll binding protein2, Lhcb2; β subunit of the ATP synthase, CF1 β; H subunit of Ndh complex, NdhH; and major subunit of Cyt b6/f complex, Cyt f. D1, Lhcb2, PsaN, Lhca4, and Cyt f were all barely detectable in *skl1-8* mutant, and CF1 β and NdhH were dramatically reduced (**Figures 3B,C**). A component of photosynthetic electron transport chain, FNR, was reduced about 50% of the wild type (**Figures 3B,C**). The significant reduction in representative subunits of photosynthetic complexes was detected by western blot analysis revealed that the thylakoid membrane was very likely disrupted and resulted in albino phenotype in *skl1-8* mutant.

Chlorophyll Fluorescence Analysis

As a non-invasive signature of photosynthesis, chlorophyll fluorescence was usually used to measure the functional status of the photosynthetic apparatus (Mohammed et al., 1995). Therefore, the fluorescence parameters F_o, F_m, F_v/F_m, quantum yield of photosystem II (Yield), photochemical quenching (qP), and electron transport rate (ETR) were recorded by a pulse amplitude modulation fluorometer (PAM-2100; Heinz Walz GmbH, Effeltrich, Germany). We measured the chlorophyll fluorescence in wild type, *skl1-8*, and *COM* grown on MS medium for 4 weeks and studied their photosynthetic photochemical image (**Figure 4A**). Compared with that of wild type, the Yield, F_m, and $F_m^{'}$ in *skl1-8* mutant decreased by 99, 60, and 63%, respectively (**Figure 4B**). Photochemical quenching (qP) measures the fraction of active PSII reaction centers. In *skl1-8* mutant, qP values were close to zero, and qP increased pronouncedly in *COM* plants nearly about to wild-type level (**Figure 4B**). In addition, the ETR of *skl1-8* mutant also decreased dramatically compared with the wild type (**Figure 4C**). The F_v/F_m ratio reflects the maximum capacity of absorbed quanta in PSII reaction centers, and in *skl1-8* mutant, compared with the wild type, the F_v/F_m ratio decreased by 98%, but in *COM* plants almost recovered to normal level (**Figure 4D**), suggesting that the photosynthetic efficiency was severely affected in *skl1*-8 mutant.

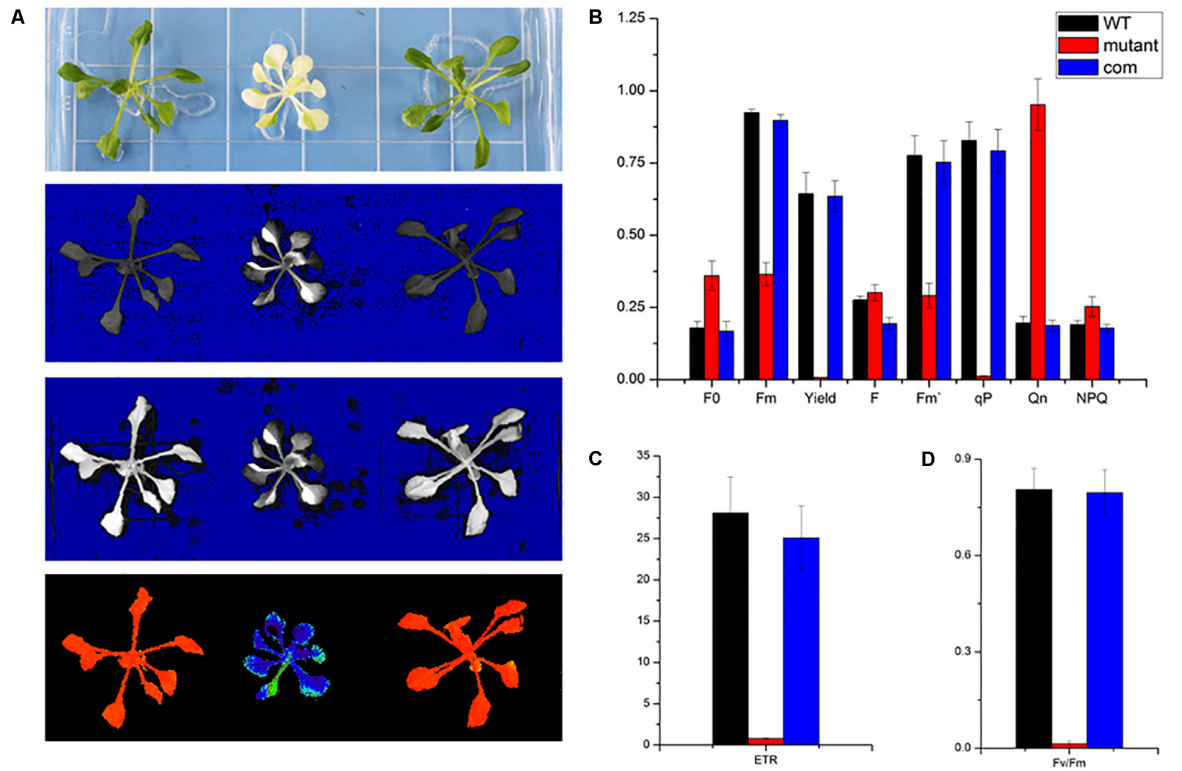

FIGURE 4 | Photosynthetic fluorescence parameters of WT, *skl1-8* mutant, and *COM*. **(A)** Fluorescence images of WT, *skl1* mutant, and *COM*. **(B)** The values of minimum fluorescence (F_o), maximum fluorescence (F_m), and F_o/F_m; effective quantum yields of PS (Yield); photochemical quenching (qP); and quantum yield of regulated energy dissipation (NPQ). **(C)** Relative electron transport rates (ETRs). **(D)** F_v/F_m ratios. The above experiments were repeated three times independently.

Transcriptome Analysis of *skl1-8* Mutant Revealed Concerted Changes in Gene Expression

From the previously described chemical and physiological features (Zhang J. et al., 2017), we proposed that the expression pattern of genes responsible for photosynthesis and chloroplast development may have been altered in *skl1-8* mutant. To test this hypothesis, we subjected cDNA libraries from wild-type Arabidopsis and *skl1-8* mutant to Illumina sequencing. After removing invalid reads and data cleaning, we obtained 53101230, 70398388, 51095958 and 52035280, 51115882, 45617702 clean reads from three constructed libraries of *skl1-8* and wild type, respectively. The proportion of nucleotides with quality values larger than 20 in reads (the Q20 percentages) were 97.34 and 97.45, and the guanine and cytosine (GC) percentages were 46.07 and 45.73% (**Table 1**).

We identified a total of 1180 significant DEGs, consisting of 557 upregulated genes and 623 downregulated genes according to the RPKM calculation (**Figure 5A** and **Supplementary Table S2**). We classified all the functional DEGs and unigenes based on the gene ontology (GO) database through Blast2GO suite. We classified the DEGs into three different groups: biological process, molecular function and cellular component (**Figure 5B**). Importantly, we found that the oxidation-reduction process (123 genes) and the single-organism metabolic process (228 genes) involved in the biological process were significantly different, as well as the oxidoreductase activity (136 genes) involved in the molecular processes (**Supplementary Table S2**).

Photosynthesis-Related Genes Expression Affected in *skl1-8* Mutant

In higher land plants, photosynthesis is a complex process involving a highly coordinated gene expression between nuclear and chloroplast genome. Identification and characterization of the DEGs within chloroplast-related mutants would be helpful in elucidating the mechanism of photosynthetic development and sustained autotrophic growth.

Our study showed that four protein subunits of LHCII proteins surrounding the PSII core were all significantly suppressed in *skl1-8* mutant, including *LHCB4-2*, *LHCB2-4*, *LHCB2-2,* and *LHCB2-1*, as well as *RBCS-2B* (gene encoded small subunit of RUBISCO; **Figure 6A**). By contrast, several of the genes involved in oxidative and other stress, such as some heat-shock proteins (i.e., *HSP70*) and *CPN60B2*, were highly activated in *skl1-8* mutant (**Figure 6B**). In addition, a high transcript level of *ELIP2* (*AT4G14690*), and the WRKY family transcription factors was observed in *skl1-8* mutant (**Figure 6B**). Furthermore, it is worth noting that a large number of key genes related to photosynthetic regulation in *skl1-8* mutant, such as

TABLE 1 | Summary for transcriptome data of wild-type *Arabidopsis thaliana* and *skl1*-8 mutant.

Sample name	Raw reads	Clean reads	clean bases	Error rate (%)	Q20 (%)	Q30 (%)	GC content (%)
WT_1	53101230	53101230	7.97G	0.01	97.81	94.2	45.86
WT_2	70398388	70398388	10.56G	0.01	97.7	93.96	46.06
WT_3	51138598	51095958	7.66G	0.02	96.52	90.99	46.31
*skl1*_1	52035280	52035280	7.81G	0.01	97.86	94.32	45.45
*skl1*_2	51115882	51115882	7.67G	0.01	97.81	94.21	45.43
*skl1*_3	45655910	45617702	6.84G	0.02	96.69	91.3	46.33

GLK1, *GLK2*, *CCL*, *PHOT1*, and *NPH3* were downregulated (**Figure 6C** and **Supplementary Table S2**), conversely, *TIC20-IV* and *CAH1*, are involved in the nuclear-encoded proteins import into chloroplast, are activated in *skl1-8* mutant (**Figure 6C** and **Supplementary Table S2**). As expected, the level of *SKL1* (*AT3G26900*) transcripts was greatly reduced about 3.53-fold in *skl1-8* mutant compared with wild type (**Figure 6C** and **Supplementary Table S2**).

In the present study, genes related to pigment biosynthesis, such as light-dependent protochlorophyllide reductase (*PORA, PORB,* and *PORC*), *ATCHL2*, Tocopherol *O*-methyltransferase (*G-TMT*) and carotenoid oxygenase (*NCED4*) were all suppressed (**Figures 6D,E** and **Supplementary Table S2**), which was consistent with the albino leaf phenotype of *skl1-8*. Altogether, the result of the transcriptome analysis indicated that the reduced level of photosynthesis-related genes were responsible for defective chloroplast in *skl1-8* mutant, and meanwhile to modulate the expression of corresponding genes to deal with insufficient energy supply.

Expression Patterns of Genes Response to Biosynthesis of Secondary Metabolites and Plant Hormones

We analyzed the DEGs in biosynthesis of secondary metabolites (**Figure 7A**), including Fatty acid desaturase (*ADS1*), Fatty acid hydroxylase (*CER1*) and Pyridoxal phosphate-dependent transferase (*ACS5*) appeared to be repressed in *skl1-8* mutant. The expression of *ACS5* in *skl1-8* mutant had an obvious 4.8-fold change compared with wild type (**Figure 7A** and **Supplementary Table S2**). Some genes associated with cell wall biosynthesis response to secondary metabolites were also downregulated, such as xyloglucan endotransglucosylase (*ATXTH19*, *ATXTH17*), UDP-glucosyltransferase (*AtUGT85A5*), Terpenoid cyclases (*LUP1*). Conversely, components of the secondary metabolites signaling pathway, glycoside hydrolase (*BGLU11*) and thiamine pyrophosphate enzyme, were obviously upregulated in *skl1-8* mutant (**Figure 7A** and **Supplementary Table S2**).

By transcriptome analysis, we found that the hormone signal transduction pathways were altered in *skl1*-8 mutant (**Figure 7B** and **Supplementary Table S2**). Strikingly, most auxin-related genes, such as *IAA1*, *IAA2*, *IAA19*, and *IAA29*, showed an especially lower level of transcripts in *skl1-8* mutant (**Supplementary Table S2**), and similarly, the auxin efflux carrier, including *PIN3* and *PIN4*, were downregulated (**Figure 7B** and **Supplementary Table S2**). The altered expression patterns of genes related secondary metabolites and plant hormones provided a clue for elucidation for the mechanism of SKL1 involved in chloroplast development.

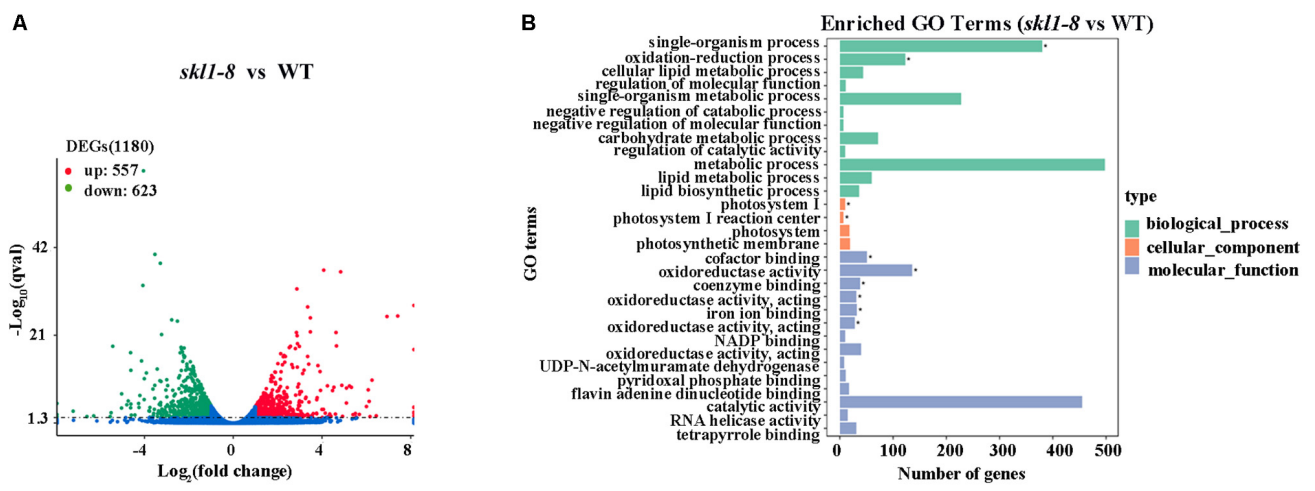

FIGURE 5 | Differential expression analysis. **(A)** Diagram showing the number of significantly differentially expressed genes (*P*-value < 0.05, FC >= 1) in *skl1-8* and WT. **(B)** differentially expressed genes GO enriched pathway.

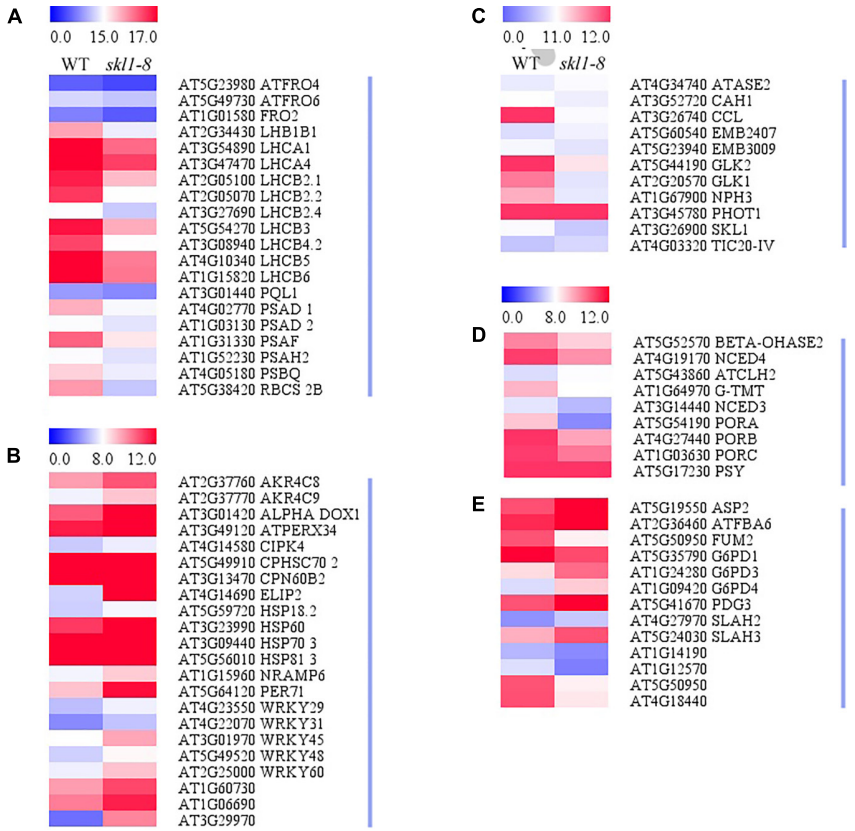

FIGURE 6 | Heat map of DEGs in WT and *skl1-8*. **(A)** The genes related to photosynthesis and light-harvesting complex. **(B)** The response of genes to stress. **(C)** Genes related to photosynthetic regulation. **(D)** Pigment metabolism. **(E)** Carbon metabolism. The bar represents the scale of the expression levels for each gene (log_2 FPKM) in WT and *skl1-8* as indicated by red/blue rectangles. Red indicates upregulation [log_2 (fold change) ≥ 1.0, p-value < 0.05], green indicates downregulation [log_2 (fold change) ≤ -1.0, p-value < 0.05] as compared with the wild type. The details of each gene are presented in **Supplementary Table S2**.

Gene Expression Profiles Confirmed by qRT-PCR

We performed the real-time RT-PCR analysis to confirmed the transcriptome result about *SKL1* mutation on photosynthetic gene expression. We first analyzed the transcript levels of nucleus-encoded photosynthetic genes, containing *LHCB2.4*, *LHCB2.1*, and *LHCB2.2*, which were light-harvesting complex II proteins and were downregulated in the *skl1-8* mutant compared with the wild type (**Figure 8**). Furthermore, *HSP70-3* and *ELIP2*, were upregulated, and the other genes, such as *NCED4*, *IAA29*, *IAA19*, *PIN3*, *PIN4*, and *IAA1* were all repressed in the *skl1-8* mutant (**Figure 8**). In total, we selected 11 genes as candidates for qRT-PCR analysis, in agreement with the transcriptome analysis.

DISCUSSION

We investigated the role of the SKL1, an ortholog of SK protein located in Arabidopsis chloroplast, which was shown to be responsible for early chloroplast development and plant growth (Fucile et al., 2008). In this study, we found the phenotype and chlorophyll content were dramatically affected in *skl1-8* mutant, a feature that highlighted the critical role of SKL1 during early plant development. Our current result demonstrated that SKL1 is required for the accumulation of four complexes related the photosynthesis. By inactivation of *SKL1* in Arabidopsis, we confirmed that SKL1 leads to a considerable decrease in photosynthetic performance.

The shikimate pathway is widely found in plants and bacteria and it is crucial for the biological synthesis of the aromatic amino acids required for the synthesis of other compounds in secondary metabolic pathways (Herrmann, 1995). In the shikimate pathway, SK is the key enzyme which can phosphorylate shikimate into shikimate 3-phosphate (Herrmann, 1995). As a homolog of SK proteins, SKL1, probably possesses the similar enzyme activity and affects the compounds' biosynthesis in chloroplast. By complementation analysis, our result consisted with previous findings and confirmed that SKL1 does not perform a SK enzyme activity in Arabidopsis. It has been reported that SKL1 possesses a phosphoglycerate mutase-like (PGML) domain which conserved in phosphoglycerate mutase (PGAM) amino sequence (Fucile et al., 2008). In the glycolysis pathway, PGAM is a critical enzyme, and catalyses the interconversion of the phosphate group from 3 to 2-PGA. Andriotis et al. (2010) reported that total six genes, including *At1g22170*, *At3g08590*, *At1g09780*, *At1g78050*, *At3g30840*, and *At4g09520*, encode putative PGAM proteins,

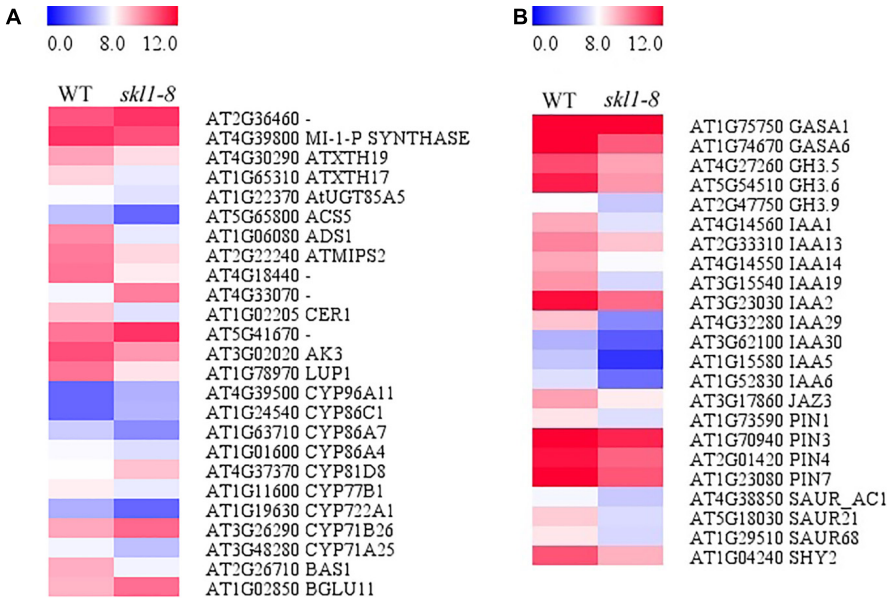

FIGURE 7 | Analysis of DEGs in **(A)** biosynthesis of secondary metabolites and **(B)** plant hormone signal transduction. Red indicates upregulation [$\log_2$ (fold change) $\geq$ 1.0, p-value $<$ 0.05], and green indicates downregulation [$\log_2$ (fold change) $\leq$ −1.0, p-value $<$ 0.05] as compared with the wild type. The details of each gene are presented in **Supplementary Table S2**.

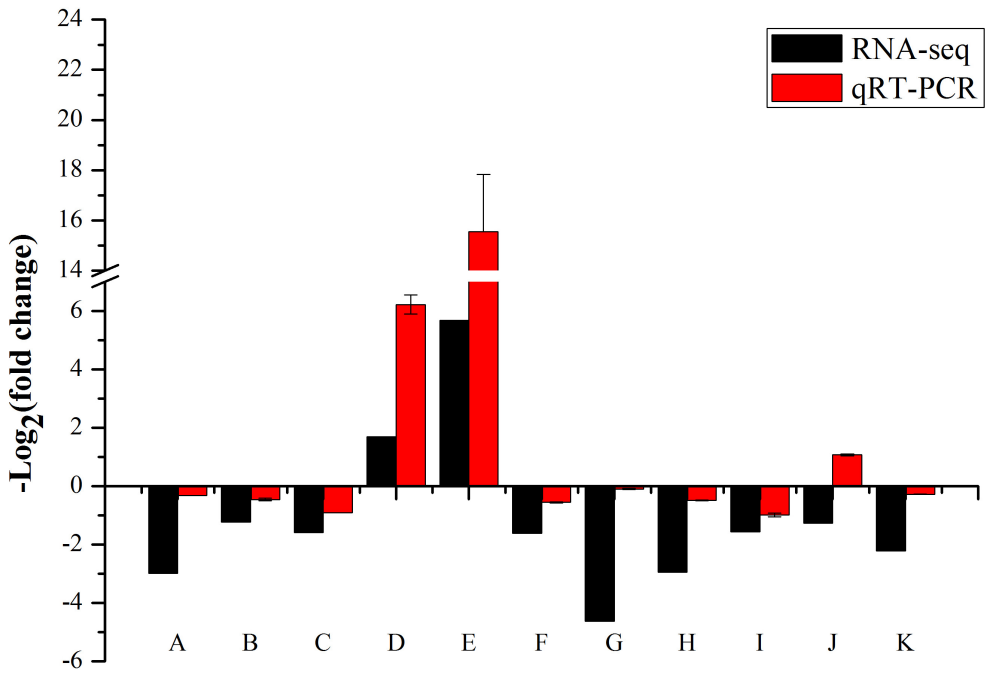

FIGURE 8 | Validation of RNA-seq results by RT-qPCR. The 19 points (A–K) from left to right on the x-axis represent genes encoding *LHCB2.4* (*AT3G27690*), *LHCB2.1* (*AT2G05100*), *LHCB2.2* (*AT2G05070*), *HSP70-3* (*AT3G09440*), *ELIP2* (*AT4G14690*), *NCED4* (*AT4G19170*), *IAA29* (AT4G32280), *IAA19* (*AT3G15540*), *PIN3* (*AT1G70940*), *PIN4* (*AT2G01420*), *IAA1* (*AT4G14560*). The measurement for each sample was repeated in three times.

and proteins At1g22170 and At3g08590 were confirmed to be localized in chloroplast (Andriotis et al., 2010). Followed studies indicated that none of the single mutant of *At1g09780*, *At1g22170*, or *At3g08590* showed any visible morphological phenotypes compared with wild-type plants (Andriotis et al., 2010; Zhao and Assmann, 2011). Although we cannot exclude the possibility that SKL1 functions as PGAM in the chloroplast by present data, and according to above researches, it is hardly to attributed the serious

phenotype in *skl1-8* mutant as a result of dysfunctional PGAM enzyme activity.

The reduced transcript level in photosynthetic genes always closely linked with albino phenotype in Arabidopsis (Zhang J. et al., 2017). Thus, we performed transcriptome analysis and identified a total of 1180 DEGs in *skl1-8* mutant, including 557 upregulated genes and 623 downregulated genes. Consistent with our original prediction, *skl1-8* mutant showed a differential transcript level of genes related to photosynthetic performance, such as gene expression (*GLK1*, *GLK2,* and *ATASE2*), protein transport (*TIC20-IV* and *CAH1*), chlorophyll biosynthesis (*PORA*, *PORB,* and *PORC*), and pigment biosynthesis (*PSY* and *NCED4*). In agreement with the notion that the defective chloroplast affects the transcription of nuclear-encoded chloroplast proteins via retrograde signaling (Chi et al., 2013), and in our results, dozens of nuclear genes that are relate to chloroplast development and photosynthesis are suppressed in *skl1-8* mutant. Thus, disrupted expression of related genes has potential responsiblity for the decreasing photosynthetic capability and abnormal growth of *skl-8* mutant.

Of most importance, by interacted with assistant proteins, chlorophyll pigments can be assembled into the light harvesting complexes, which capture light energy and transfer it to centers of PSII and PSI (Liu et al., 2004). On the basis of the transcriptome database, we found that LHC-encoding genes (*LHCB4.2*, *LHCB2.4*, *LHCB2.1*, and *LHCB2.2*) and *RBCS-2B* were classified into DEGs, showing reduced expression levels in *skl1-8* mutant compared with the wild type. We assume that the expression of nucleus-encoded but chloroplast-located proteins, is controlled by the anterograde and retrograde signals conveyed between the chloroplasts and the nucleus (Leister, 2005; Chi et al., 2013; Ng et al., 2014). Therefore, relative reduction in transcripts of nuclear-encoded genes in *skl1-8* is closely resembled to those of *embs* mutants, which can alter signaling level from chloroplast to nuclear and subsequently repress the expression of *RBCS* and *LHCBs* (Mochizuki et al., 2001; Rodermel, 2001; Strand et al., 2003; Chi et al., 2013). Previously, the two GLK transcription factors, AtGLK1 and AtGLK2 have been considered as positive regulators which can modulate the photosynthetic capacity by combining to the promoter, and the transcript levels of *GLK* genes can be affected by the state of plastid development (Kakizaki et al., 2009; Waters et al., 2009). In our results, we found that both *GLK1* and *GLK2* transcript levels were significantly reduced in the *skl1-8* mutant. This result coincided with previous study and suggested that *GLK* genes may perform as regulators in the expression of nuclear photosynthetic genes to cope with varying developmental and environmental conditions (Waters et al., 2009).

Most of induced genes can be classified as detoxification- and stress-related genes, including *peroxidase*, *WRKY* and *HSPs*. Presumably, the phenotype of *skl1-8* mutant is partially as result of side effects of photo-oxidative stress, and thus these genes may be induced for cell defense and survival under unfitted environmental conditions. Previous studies have indicated that HSPs and CPN play critical roles in the folding and protecting of enhanced *de novo* proteins from varied stresses (Zhang and Glaser, 2002). Interestingly, similar downregulated expression of photosynthetic genes had been reported under varied stress conditions (Bilgin et al., 2010), suggesting that the main defense response in plants is to depress photosynthesis capability in adverse environment to cope with the damages by oxidative molecular produced in plant cells.

In the *skl1-8* mutant, the chlorophyll and the carotenoid biosynthesis pathway related genes, such as *ATCLH2*, *PORs*, *BGL1*, *BETA-OHASE 2*, and *NCED4,* which also involved in the biosynthesis of secondary metabolites were downregulated. Similarly, the expression of genes involved in the related auxin pathways, such as *IAAs* and *PINs*, were significantly suppressed in *skl1-8* mutant. Previous research has revealed that auxin is a key regulator controlling bilateral symmetry and establishing embryo patterning in the process of embryogenesis (Liu et al., 1993). The altered expression of genes related to hormone signaling and secondary metabolites probably provided an explanation to the growth defects in *skl1-8* mutant.

AUTHOR CONTRIBUTIONS

JX designed the study. HX, LZ, RL, XW, SL, and XL performed the research. HX and JX analyzed the data and wrote the paper. YJ discussed the results and made comments on the manuscript.

FUNDING

This work was funded by the National Natural Science Foundation of China (No. 31400210 and 31670182), the Fundamental Research Funds for the Central Universities (No. 2017ZY10) and the State '13.5' Key Research Program of China (No. 2016YFD0600102).

ACKNOWLEDGMENTS

We are grateful to the Arabidopsis Biological Resource Center for the *skl1-8* mutant line and LetPub (www.letpub.com) for kindly providing its assistance to linguistic modification. RNA-seq data generated in this research has been submitted to the Sequence Read Archive database in NCBI under the accession number SRP131832.

SUPPLEMENTARY MATERIAL

The Supplementary Material for this article can be found online at: https://www.frontiersin.org/articles/10.3389/fpls.2018.00179/full#supplementary-material

TABLE S1 | List of primers used in this study.

TABLE S2 | Analysis of differentially expressed genes involved in the photosynthesis, pigment metabolism, carbon metabolism, biosynthesis of secondary metabolites, and plant hormone signal transduction.

REFERENCES

Abdallah, F., Salamini, F., and Leister, D. (2000). A prediction of the size and evolutionary origin of the proteome of chloroplasts of *Arabidopsis*. *Trends Plant Sci.* 5, 141–142. doi: 10.1016/S1360-1385(00)01574-0

Andriotis, V. M., Kruger, N. J., Pike, M. J., and Smith, A. M. (2010). Plastidial glycolysis in developing Arabidopsis embryos. *New Phytol.* 185, 649–662. doi: 10.1111/j.1469-8137.2009.03113.x

Arnon, D. I. (1949). Copper enzymes in isolated chloroplasts: polyphenoloxidase in *Beta vulgaris*. *Plant Physiol.* 24, 1–15. doi: 10.1104/pp.24.1.1

Bilgin, D. D., Zavala, J. A., Zhu, J., Clough, S. J., Ort, D. R., and DeLucia, E. H. (2010). Biotic stress globally downregulates photosynthesis genes. *Plant Cell Environ.* 33, 1597–1613. doi: 10.1111/j.1365-3040.2010.02167.x

Bryant, N., Lloyd, J., Sweeney, C., Myouga, F., and Meinke, D. (2011). Identification of nuclear genes encoding chloroplast-localized proteins required for embryo development in *Arabidopsis*. *Plant Physiol.* 155, 1678–1689. doi: 10.1104/pp.110.168120

Chi, W., Sun, X., and Zhang, L. (2013). Intracellular signaling from plastid to nucleus. *Annu. Rev. Plant Biol.* 64, 559–582. doi: 10.1146/annurev-arplant-050312-120147

Clough, S. J., and Bent, A. F. (1998). Floral dip: a simplified method for *Agrobacterium*-mediated transformation of *Arabidopsis thaliana*. *Plant J.* 16, 735–743. doi: 10.1046/j.1365-313x.1998.00343.x

Fucile, G., Falconer, S., and Christendat, D. (2008). Evolutionary diversification of plant shikimate kinase gene duplicates. *PLoS Genet.* 4:e1000292. doi: 10.1371/journal.pgen.1000292

Givan, C. V., and Stumpf, P. K. (1971). Fat metabolism in higher plants: some factors regulating fatty acid synthesis by isolated spinach chloroplasts. *Plant Physiol.* 47, 510–515. doi: 10.1104/pp.47.4.510

Grabherr, M. G., Haas, B. J., Yassour, M., Levin, J. Z., Thompson, D. A., Amit, I., et al. (2011). Full-length transcriptome assembly from RNA-Seq data without a reference genome. *Nat. Biotechnol.* 29, 644–652. doi: 10.1038/nbt.1883

Gutiérrez-Nava, M., Gillmor, C. S., Jiménez, L. F., Guevara-García, A., and León, P. (2004). *CHLOROPLAST BIOGENESIS* genes act cell and noncell autonomously in early chloroplast development. *Plant Physiol.* 135, 471–482. doi: 10.1104/pp.103.036996

Hanaoka, M., Kanamaru, K., Takahashi, H., and Tanaka, K. (2003). Molecular genetic analysis of chloroplast gene promoters dependent on SIG2, a nucleus-encoded sigma factor for the plastid-encoded RNA polymerase, in *Arabidopsis thaliana*. *Nucleic Acids Res.* 31, 7090–7098. doi: 10.1093/nar/gkg935

Herrmann, K. M. (1995). The shikimate pathway: early steps in the biosynthesis of aromatic compounds. *Plant Cell* 7, 907–919. doi: 10.1105/tpc.7.7.907

Hou, X., Rivers, J., León, P., Mcquinn, R. P., and Pogson, B. J. (2016). Synthesis and function of apocarotenoid signals in plants. *Trends Plant Sci.* 21, 792–803. doi: 10.1016/j.tplants.2016.06.001

Inaba, T., and Schnell, D. J. (2008). Protein trafficking to plastids: one theme, many variations. *Biochem. J.* 413, 15–28. doi: 10.1042/BJ20080490

Kakizaki, T., Matsumura, H., Nakayama, K., Che, F. S., Terauchi, R., and Inaba, T. (2009). Coordination of plastid protein import and nuclear gene expression by plastid-to-nucleus retrograde signaling. *Plant Physiol.* 151, 1339–1353. doi: 10.1104/pp.109.145987

Korf, I., Yandell, M., and Bedell, J. (2003). *BLAST*. Sebastopol, CA: O'Reilly & Associates Inc.

Kusumi, K., Yara, A., Mitsui, N., Tozawa, Y., and Iba, K. (2004). Characterization of a rice nuclear-encoded plastid RNA polymerase gene OsRpoTp. *Plant Cell Physiol.* 45, 1194–1201. doi: 10.1093/pcp/pch133

Leister, D. (2005). Genomics-based dissection of the cross-talk of chloroplasts with the nucleus and mitochondria in *Arabidopsis*. *Gene* 354, 110–116. doi: 10.1016/j.gene.2005.03.039

Liu, C. M., Xu, Z. H., and Chua, N. (1993). Auxin polar transport is essential for the establishment of bilateral symmetry during early plant embryogenesis. *Plant Cell* 5, 621–630. doi: 10.1105/tpc.5.6.621

Liu, Z., Yan, H., Wang, K., Kuang, T. Y., Zhang, J. P., Gui, L. L., et al. (2004). Crystal structure of spinach major light-harvesting complex at 2.72 angstrom resolution. *Nature* 428, 287–292. doi: 10.1038/nature02373

Livak, K. J., and Schmittgen, T. D. (2001). Analysis of relative gene expression data using real-time quantitative PCR and the $2^{-\Delta\Delta C_T}$ method. *Methods* 25, 402–408. doi: 10.1006/meth.2001.1262

Maeda, H., and Dudareva, N. (2012). The shikimate pathway and aromatic amino acid biosynthesis in plants. *Annu. Rev. Plant Biol.* 63, 73–105. doi: 10.1146/annurev-arplant-042811-105439

Martin, W., Rujan, T., Richly, E., Hansen, A., Cornelsen, S., Lins, T., et al. (2002). Evolutionary analysis of *Arabidopsis*, cyanobacterial, and chloroplast genomes reveals plastid phylogeny and thousands of cyanobacterial genes in the nucleus. *Proc. Natl. Acad. Sci. U.S.A.* 99, 12246–12251. doi: 10.1073/pnas.182432999

Mochizuki, N., Brusslan, J. A., Larkin, R., Nagatani, A., and Chory, J. (2001). *Arabidopsis genomes uncoupled 5 (GUN5)* mutant reveals the involvement of Mg-chelatase H subunit in plastid-to-nucleus signal transduction. *Proc. Natl. Acad. Sci. U.S.A.* 98, 2053–2058. doi: 10.1073/pnas.98.4.2053

Mohammed, G. H., Binder, W. D., and Gillies, S. L. (1995). Chlorophyll fluorescence: a review of its practical forestry applications and instrumentation. *Scand. J. For. Res.* 10, 383–410. doi: 10.1080/02827589509382904

Mortazavi, A., Williams, B. A., McCue, K., Schaeffer, L., and Wold, B. (2008). Mapping and quantifying mammalian transcriptomes by RNA-Seq. *Nat. Methods* 5, 621–628. doi: 10.1038/nmeth.1226

Mustafa, N. R., and Verpoorte, R. (2005). Chorismate derived c6c1 compounds in plants. *Planta* 222, 1–5. doi: 10.1007/s00425-005-1554-0

Ng, S., de Clercq, I., van Aken, O., Law, S. R., and Ivanova, A. (2014). Anterograde and retrograde regulation of nuclear genes encoding mitochondrial proteins during growth, development, and stress. *Mol. Plant* 7, 1075–1093. doi: 10.1093/mp/ssu037

Peltier, J. B., Cai, Y., Sun, Q., Zabrouskov, V., and Giacomelli, L. (2006). The oligomeric stromal proteome of *Arabidopsis thaliana* chloroplasts. *Mol. Cell. Proteomics* 5, 114–133. doi: 10.1074/mcp.M500180-MCP200

Rodermel, S. (2001). Pathways of plastid-to-nucleus signaling. *Trends Plant Sci.* 6, 471–478. doi: 10.1016/S1360-1385(01)02085-4

Seay, M., Hayward, A. P., Tsao, J., and Dinesh-Kumar, S. P. (2009). Something old, something new: plant innate immunity and autophagy. *Curr. Top. Microbiol. Immunol.* 335, 287–306. doi: 10.1007/978-3-642-00302-8_14

Strand, A., Asami, T., Alonso, J., Ecker, J. R., and Chory, J. (2003). Chloroplast to nucleus communication triggered by accumulation of Mg-protoporphyrinIX. *Nature* 421, 79–83. doi: 10.1038/nature01204

Tzafrir, I., Pena-Muralla, R., Dickerman, A., Berg, M., Rogers, R., Hutchens, S., et al. (2004). Identification of genes required for embryo development in Arabidopsis. *Plant Physiol.* 135, 1206–1220. doi: 10.1104/pp.104.045179

Tzin, V., and Galili, G. (2010). New insights into the shikimate and aromatic amino acids biosynthesis pathways in plants. *Mol. Plant* 3, 956–972. doi: 10.1093/mp/ssq048

van Wijk, K. J. (2015). Protein maturation and proteolysis in plant plastids, mitochondria, and peroxisomes. *Annu. Rev. Plant Biol.* 66, 75–111. doi: 10.1146/annurev-arplant-043014-115547

Wang, R., Zhao, J., Jia, M., Xu, N., Liang, S., Shao, J., et al. (2017). Balance between cytosolic and chloroplast translation affects leaf variegation. *Plant Physiol.* 176, 804–818. doi: 10.1104/pp.17.00673

Waters, M. T., and Langdale, J. A. (2009). The making of a chloroplast. *EMBO J.* 28, 2861–2873. doi: 10.1038/emboj.2009.264

Waters, M. T., Wang, P., Korkaric, M., Capper, R. G., Saunders, N. J., and Langdale, J. A. (2009). GLK transcription factors coordinate expression of the photosynthetic apparatus in *Arabidopsis*. *Plant Cell* 21, 1109–1128. doi: 10.1105/tpc.108.065250

Xiao, J., Li, J., Ouyang, M., Yun, T., He, B., Ji, D., et al. (2012). DAC is involved in the accumulation of the cytochrome b_6/f complex in Arabidopsis. *Plant Physiol.* 160, 1911–1922. doi: 10.1104/pp.112.204891

Xue, X., Wang, Q., Qu, Y. L., Wu, H. Y., Dong, F. Q., Cao, H. Y., et al. (2017). Development of the photosynthetic apparatus of *Cunninghamia lanceolata* in light and darkness. *New Phytol.* 213, 300–313. doi: 10.1111/nph.14096

Zhang, J., Xiao, J., Li, Y., Su, B., Xu, H., Shan, X., et al. (2017). PDM3, a pentatricopeptide repeat-containing protein, affects chloroplast development. *J. Exp. Bot.* 68, 5615–5627. doi: 10.1093/jxb/erq033

Zhang, X. P., and Glaser, E. (2002). Interaction of plant mitochondrial and chloroplast signal peptides with the Hsp70 molecular chaperone. *Trends Plant Sci.* 7, 14–21. doi: 10.1016/S1360-1385(01)02180-X

Zhang, Z., Cui, X., Wang, Y., Wu, J., Gu, X., and Lu, T. (2017). The RNA editing factor WSP1 is essential for chloroplast development in rice. *Mol. Plant* 10, 86–98. doi: 10.1016/j.molp.2016.08.009

Zhao, Z., and Assmann, S. M. (2011). The glycolytic enzyme, phosphoglycerate mutase, has critical roles in stomatal movement, vegetative growth, and pollen production in *Arabidopsis thaliana*. *J. Exp. Bot.* 62, 5179–5189. doi: 10.1093/jxb/err223

Zheng, M., Liu, X., Liang, S., Fu, S., Qi, Y., Zhao, J., et al. (2016). Chloroplast translation initiation factors regulate leaf variegation and development. *Plant Physiol.* 172, 1117–1130. doi: 10.1104/pp.15.02040

Zheng, Q., and Wang, X. J. (2008). GOEAST: a web-based software toolkit for Gene Ontology enrichment analysis. *Nucleic Acids Res.* 36, 358–363. doi: 10.1093/nar/gkn276

Conflict of Interest Statement: The authors declare that the research was conducted in the absence of any commercial or financial relationships that could be construed as a potential conflict of interest.

frontiers in Plant Science

ORIGINAL RESEARCH
published: 27 March 2018
doi: 10.3389/fpls.2018.00370

Alterations of Membrane Lipid Content Correlated With Chloroplast and Mitochondria Development in *Euglena gracilis*

*Shiori Shibata[1], Shin-ichi Arimura[2,3], Takahiro Ishikawa[4,5] and Koichiro Awai[1,5,6]**

[1] Graduate School of Integrated Science and Technology, Shizuoka University, Shizuoka, Japan, [2] Graduate School of Agricultural and Life Sciences, The University of Tokyo, Tokyo, Japan, [3] Precursory Research for Embryonic Science and Technology, Japan Science and Technology Agency, Saitama, Japan, [4] Department of Life Science and Biotechnology, Faculty of Life and Environmental Science, Shimane University, Matsue, Japan, [5] Core Research for Evolutional Science and Technology, Japan Science and Technology Agency, Tokyo, Japan, [6] Research Institute of Electronics, Shizuoka University, Hamamatsu, Japan

Euglenoids are unique protists that can grow photoautotrophically, photomixotrophically, and heterotrophically. Here we grew *Euglena gracilis* under these different growth conditions and determined cellular contents of seven membrane lipids and one storage lipid (triacylglycerol), which account for more than 94 mol% of total membrane lipids. We also describe the relationship among chloroplast and mitochondria developments with lipid contents, protein contents, and oxygen evolution/consumption rates. In photoautotrophic growth conditions, *E. gracilis* cells accumulated chlorophyll, photosynthetic proteins, and glycolipids typical to thylakoid membranes. The same occurred for the cells grown under photomixotrophic conditions with higher respiration rates. In heterotrophic conditions, *E. gracilis* cells had higher respiration rates compared to cells grown in other conditions with the accumulation of pyruvate: NADP+ oxidoreductase, a mitochondrial protein and phospholipid common in mitochondria. Cells were also observed using a confocal laser scanning microscope and found to show more chlorophyll autofluorescence when grown photoautotrophically and photomixotrophycally, and fluorescence of MitoTracker when grown photomixotrophically and heterotrophically. These results suggest that under illumination, *E. gracilis* develops functional thylakoid membranes with membrane lipids and proteins for photosynthesis. In the medium with glucose, the cells develop mitochondria with phospholipids and proteins for respiration. Possible application based on lipid analysis for the enhancement of wax ester or alkene synthesis is discussed.

Keywords: *Euglena gracilis*, membrane lipids, photosynthesis, respiration, thylakoid membranes, MitoTracker, confocal laser scanning microscopy

OPEN ACCESS

Edited by:
Rebecca L. Roston, University of Nebraska–Lincoln, United States

Reviewed by:
Yonghua Li-Beisson, Commissariat à l'Energie Atomique et aux Energies Alternatives (CEA), France
Wayne Riekhof, University of Nebraska–Lincoln, United States

***Correspondence:**
Koichiro Awai
awai.koichiro@shizuoka.ac.jp

Specialty section:
This article was submitted to Plant Cell Biology, a section of the journal Frontiers in Plant Science

Received: *30 November 2017*
Accepted: *06 March 2018*
Published: *27 March 2018*

Citation:
Shibata S, Arimura S-i, Ishikawa T and Awai K (2018) Alterations of Membrane Lipid Content Correlated With Chloroplast and Mitochondria Development in Euglena gracilis. Front. Plant Sci. 9:370. doi: 10.3389/fpls.2018.00370

INTRODUCTION

Euglenoids are unicellular photosynthetic protists mostly found in freshwater, such as lakes, ponds, and rivers. Euglenoids are believed to acquire chloroplasts by secondary endosymbiosis with the alga that shares a common ancestor with current green algae (Gibbs, 1978; McFadden, 2001). Euglenoids are uniquely able to grow photoautotrophically, photomixotrophically, and

heterotrophically. According to this feature, these organisms have been used for analysis of chloroplast development, especially in the model euglenoid *Euglena gracilis*. Since *E. gracilis* can grow heterotrophically, chloroplast development has been analyzed by illuminating dark-grown cells. When the *E. gracilis* cells transform from dark-heterotrophic to light-photoautotrophic growth, the cells start developing chloroplasts. *E. gracilis* cells are known to accumulate a storage carbohydrate, paramylon (β-1,3-glucose polymer) under heterotrophic growth conditions (Schwartzbach et al., 1975; Inui et al., 1982), and they utilize it during chloroplast development for synthesis of proteins, nucleic acids, and membrane lipids (Rosenberg and Pecker, 1964; Schiff and Schwartzbach, 1982; Osafune et al., 1990; Sumida et al., 2007). Light-grown cells have also been placed in the dark and analyzed for degradation of chloroplasts (Scheer and Parthier, 1982; Ferroni et al., 2009). These studies report the morphology of chloroplasts; content of photosynthetic proteins, pigments, and membrane lipids; and degradation of paramylon. However, there are few reports describing the relationship between membrane lipid composition and cell specialization in *E. gracilis*.

In *E. gracilis*, a wax ester, a type of storage lipid, is well analyzed for potential use as a biofuel (Inui et al., 1982, 1984, 2017). This wax ester is mainly composed of C14:0 saturated fatty acid, myristic acid, and myristyl alcohol (Hulanicka et al., 1964). It is known to accumulate especially under hypoxic conditions by consuming the paramylon to obtain energy without respiration (Inui et al., 1982). Both wax ester and membrane lipids are made from fatty acids, there are not much information on membrane lipids of *E. gracilis*. Early reports described the lipid metabolism (Hulanicka et al., 1964) and the effect of light intensity on lipid composition (Constantopoulos and Bloch, 1967), but these reports mainly analyzed fatty acid composition and only described membrane lipids as the sums of polar lipids or phospholipids. Some reports describe the membrane lipid composition of *E. gracilis*, especially thylakoid glycolipids monogalactosyldiacylglycerol (MGDG), digalactosyldiacylglycerol (DGDG) and sulfoquinovosyldiacylglycerol (SQDG) (Rosenberg, 1963; Rosenberg and Pecker, 1964; Rosenberg et al., 1966). More recently, comprehensive analyses of membrane lipids were done with classical (Regnault et al., 1995) or more advanced techniques (LC-MS/MS) (Ogawa et al., 2014). The former one reports only five membrane lipids including MGDG, DGDG, phosphatidylglycerol (PG), phosphatidylcholine (PC), and phosphatidylethanolamine (PE). The latter one showed unusual lipid contents (lacking DGDG and SQDG with a very high content of sphingomyelin). Phosophatidylinositol (PI) is also described as a minor component in some reports (Calvayrac and Douce, 1970; Fujita et al., 1995). Therefore, more detailed analyses of lipid compositions of *E. gracilis* are needed.

In this article, we present comprehensive analysis of lipids in *E. gracilis* by a combination of traditional TLC-based methods with LC-MS/MS. Based on this, we analyzed the relationship between membrane lipid contents and chloroplast/mitochondria developments with oxygen evolution/consumption rates, quantum efficiency of photosystem II (PSII), amounts of chloroplastic/mitochondrial proteins, and a confocal laser scanning microscopy.

MATERIALS AND METHODS

Growth Conditions

Euglena gracilis Z was cultured in 200-ml flasks containing 100 ml of Cramer–Myers (CM) medium (Cramer and Myers, 1952) for photoautotrophic growth at 26°C under continuous light (100 μmol·photons m^{-2}·s^{-1}) with rotary shaking at 120 rpm. For photomixotrophic growth, CM medium with 0.6% (w/v) glucose (CM+Glc) was used under the same conditions. For the heterotrophic growth, cells were cultured in CM+Glc medium in the same condition, but the flasks were completely wrapped with aluminum foil. To obtain growth curves, algal cultures were diluted with fresh medium at an initial cell number of 3.0×10^3, and the cell number was counted using the Cellometer (Auto T4, Nexcelom, United States) every 24 h.

Chlorophyll Contents, Oxygen Evolution Rates, and Chlorophyll Fluorescence

Chlorophyll content was measured as described (Arnon, 1949). The oxygen evolution rate of intact cells was measured with a Clark-type oxygen electrode (Hansatech Instruments Ltd.) and a LED lamp (CCS Inc., Kyoto, Japan). Chlorophyll fluorescence measurements were performed with a Dual-PAM system (Heinz Walz GmbH). PSII quantum efficiency was measured as (Fm-Fo)/Fm, where Fm is the maximum PSII fluorescence obtained with a red saturating pulse (635 nm, 300 ms duration, 20,000 μmol photons m^{-2} s^{-1}) and Fo is the minimum fluorescence obtained after 10 min of far red light (intensity setting 20) to ensure a state 1 transition.

Protein Extraction, SDS-PAGE, and Western Blot Analysis

For protein extraction, 2 ml of culture (∼1×10^6 cells) was centrifuged at 16,000 × *g*, and the precipitated cells were frozen with liquid nitrogen. These cells were lysed five times by a homogenizer (Micro Smash MS-100R, TOMY) at 2,000 rpm for 20 s. Then the powdered cells were suspended in 200 μl of the resuspend buffer [50 mM HEPES (pH 7.0), 25 mM $CaCl_2$, 5 mM $MgCl_2$, 10% (v/v) glycerol, 1 mM PMSF, and 5 mM 6-aminocaproic acid] (Barthel et al., 2013) and used for Western blot analysis. For protein content analysis, aliquots of the suspended cells were mixed with the same volume of detergent solution [60 mM Tris-HCl (pH6.8), 2% SDS (w/v)]. A BCA Protein Assay Kit (Thermo Fischer Scientific) was used with BSA as a standard.

Laemmli SDS-PAGE (Laemmli, 1970) was performed using polyacrylamide gels containing 10% (w/v) acrylamide. Proteins from the same number of cells (∼5×10^4 cells) were applied to each lane. Samples were mixed with loading buffer with 175 mM DTT and not heat-denatured to avoid aggregation of membrane proteins. The gels were stained with Coomassie

Brilliant Blue R-250 (CBB). Pre-stained Protein Markers (Broad Range) for SDS-PAGE (Nacalai Tesque) were used to calibrate the gels.

For immunodetection, rabbit antibodies against PsbC (AS111787, CP43), PsbO (AS06-142-33), and RbcL (AS03037) (Agrisera) were used at a 1:3,000 dilution. Polyclonal antibodies against spinach PsbA/D (a gift from Dr. Masahiko Ikeuchi at The University of Tokyo) and Euglena pyruvate: NADP+ oxidoreductase (PNO, a gift from Dr. Masami Nakazawa at Osaka Prefecture University) were used at the same dilution. These antibodies were detected with an anti-rabbit horseradish peroxidase-coupled antibody (ab97051, Abcam) at a dilution of 1:10,000 using Can Get Signal Immunoreaction Enhancer Solution (Toyobo) followed by development with Western Lightning Plus-ECL (Perkin Elmer).

Fluorescence Microscopy

Fluorescence microscopy was carried out as described (Nagaoka et al., 2017). Briefly, Euglena cells were stained with MitoTracker Orange CMTMRos (Life Technologies) for 30 min and washed five times with CM medium before observations by a fluorescent microscope (Nikon, ECLIPSE Ti) equipped with a confocal laser scanning microscope system (Nikon, C1Si).

Lipid Analysis

Lipids were extracted as described (Bligh and Dyer, 1959) and separated by TLC. For membrane lipid analysis, a solvent system of chloroform: methanol: petroleum ether: acetone: acetic acid: H_2O (20: 15: 10: 5: 1.3: 1, v/v) (Suzuki et al., 2016) was used for initial separation. Then, detected spots were further separated by the solvent systems hexane: tetrahydrofuran: 2-propanol: H_2O (50: 0.5: 35: 3, v/v) (Hölzl et al., 2005), chloroform: methanol: acetic acid: H_2O (34: 5: 5: 0.8, v/v) (Nichols and James, 1964), or chloroform: methanol: H_2O (65: 25: 4, v/v) (Allen et al., 1966). For neutral lipid analysis, a solvent system of hexane: diethyl ether: acetic acid (80: 20: 1 or 90: 15: 1, v/v) (Kalscheuer and Steinbuchel, 2003) was used.

Separated lipids were determined by TLC co-chromatographed with standard lipids and liquid chromatography-mass spectrometry (LC-MS, Shimadzu LCMS-2010A system) as described (Okazaki et al., 2013).

For quantitative and qualitative analysis of fatty acids attached to lipids, each separated spot was scraped off and fatty acid methyl esters (FAMEs) were prepared. FAMEs were then analyzed by gas chromatography (GC) equipped with a flame ionization detector (FID) for quantitative analysis, and GC-mass spectrometry (MS) for qualitative analysis. GC-FID was carried out as described (Awai et al., 2014) with slight modification. Shimadzu GC-2014 equipped with a FID on a capillary column (BPX90, 60 m × 0.25 mm, SGE Analytical Science) was used. The column temperature was gradually increased from 140°C to 240°C at a rate of 5°C/min. The injector and detector temperature were both 250°C. The linear velocity of carrier gas (He) was 25 cm/min. GC-MS was carried out using a Shimadzu GCMS-QP2010SE under the same condition as GC-FID. The ion source temperature was set to 200°C and both the injection port and interface temperature were 250°C.

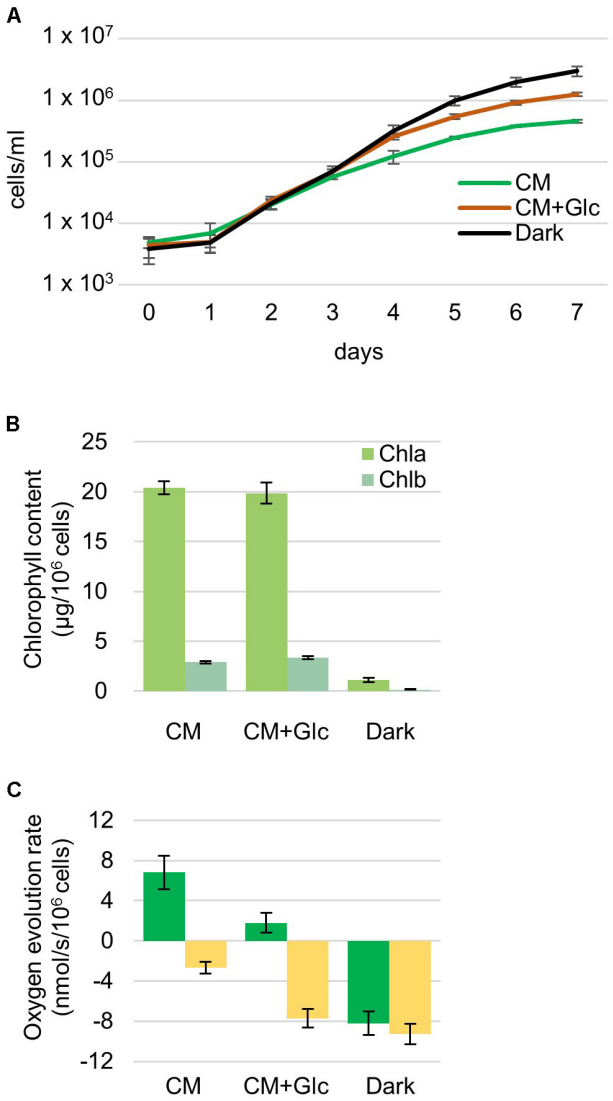

FIGURE 1 | Properties of Euglena cells grown under photoautotrophic, photomixotrophic and heterotrophic conditions. **(A)** Growth curve of the cells. Algal cultures were diluted with fresh medium at an initial cell number approximately 4,000 and grown for 7 days. Error bars indicate the SE based on six independent experiments. **(B)** Chlorophyll contents per 10^6 cells. Error bars indicate the SE based on at least twelve independent experiments. **(C)** Oxygen evolution and consumption rates. Oxygen evolution rates were measured under the growth light intensity (105 μmol photons $m^{-2} \cdot s^{-1}$). Green bar: oxygen evolution rate, yellow bar: oxygen consumption rate. Error bars indicate the SE based on at least three independent experiments.

RESULTS

Growth and Photosynthetic Activity of *E. gracilis* Under Different Growth Conditions

Euglena gracilis cells were grown under different growth conditions, namely photoautotrophic (CM: CM medium, 100 μmol photons m^{-2} s^{-1}), photomixotrophic (CM+Glc:

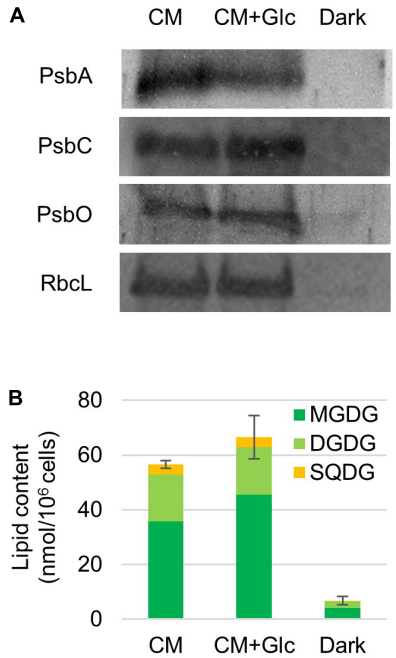

FIGURE 2 | Photosynthetic protein and thylakoid glycolipid levels in cells grown under photoautotrophic, photomixotrophic and heterotrophic conditions. **(A)** Western blot analysis of photosynthetic proteins. Antibodies used are indicated on the left. **(B)** Thylakoid glycolipid content. Error bar shows SE (n = 3) of the total amount of glycolipids.

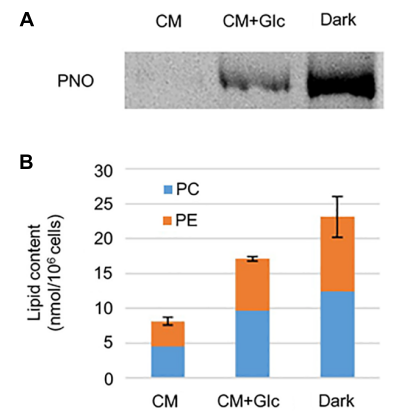

FIGURE 3 | Mitochondrial protein and phospholipid levels in cells grown under photoautotrophic, photomixotrophic and heterotrophic conditions. **(A)** Western blot analysis of a mitochondrion protein, PNO. **(B)** Phospholipid content. Error bar shows SE (n = 3) of total amount of two extraplastidic phospholipids, PC and PE.

CM medium with 0.6% glucose, 100 μmol photons m^{-2} s^{-1}) and heterotrophic (Dark: CM medium with 0.6% glucose, dark) conditions. First, growth rates of *E. gracilis* cells in each condition were compared. As shown in **Figure 1A**, the cells grew at similar rates under all conditions and the Dark condition showed the highest cell number compared with the others. Chlorophyll content was almost the same among cells grown in CM and

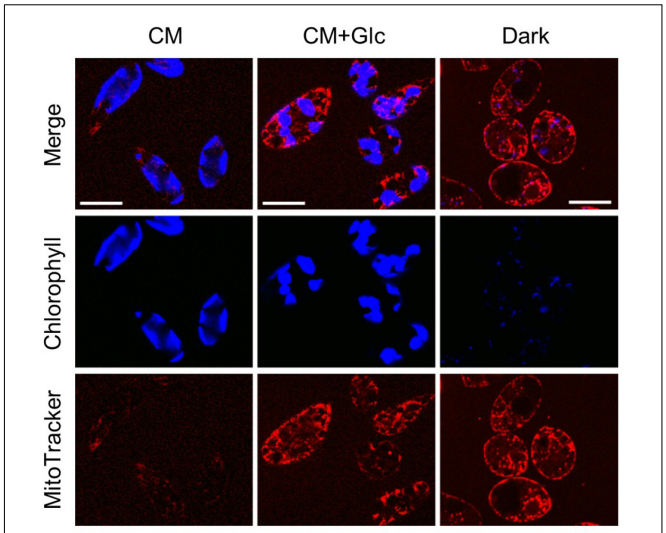

FIGURE 4 | Confocal laser scan microscopy of the cells grown under photoautotrophic, photomixotrophic, and heterotrophic conditions. Typical images of the cells grown in each culture were shown. Bar = 20 μm.

CM+Glc media [chlorophyll (Chl) a + b per 10^6 cells ± SE, $n \geq 12$: CM, 23.30 ± 0.75 μg Chl; CM+Glc, 23.22 ± 1.20 μg Chl] (**Figure 1B**). On the other hand, in Dark conditions, chlorophyll content was much lower than in the cells illuminated by light (1.25 ± 0.28 μg Chl). We next analyzed oxygen evolution rate in the cells. As expected from the lower Chl contents, oxygen consumption was observed in the cells cultured in Dark conditions even under light (**Figure 1C**). This consumption rate was slightly lower than the oxygen consumption rate measured under dark conditions (respiration), indicating that the dark-grown cells still have a weak photosynthetic activity. Cells grown under CM conditions showed a higher oxygen evolution rate compared with the cells grown under CM+Glc conditions. This can be explained by a higher rate of oxygen consumption in the cells of CM+Glc conditions (**Figure 1C**). In fact, the total amount of oxygen evolution/consumption was almost the same in the cells grown in CM and CM+Glc conditions (CM, 9.48 nmol/s/10^6 cells; CM+Glc, 9.53 nmol/s/10^6 cells). These results suggest that cells grown under light have similar photosynthetic activities, but addition of glucose stimulated respiration activity in the cells grown in CM+Glc conditions. The protein content of the cells was also analyzed (protein per 10^6 cells ± SE, n = 3: CM, 269.63 ± 17.87 μg Protein; CM+Glc, 253.06 ± 9.93 μg Protein; Dark, 200.61 ± 11.13 μg Protein). Dark-grown cells had less proteins than others but still to the same extent. Compositional changes in the protein profile were shown using a CBB-stained acrylamide gel (**Supplementary Figure S1**).

Chloroplast Development in Illuminated *E. gracilis* Cells

It was expected from the above-mentioned results that chloroplasts are developed under light regardless of the

carbon source (CO_2 or CO_2 + Glc). To confirm this finding, we analyzed protein levels of photosynthetic complexes and thylakoid lipids. First, photosynthetic proteins, namely proteins from PSII [PsbA/D (D1/D2), PsbC (CP43) and PsbO] and the Rubisco large subunit were analyzed. As shown in **Figure 2**, these proteins were abundant in the cells grown under light (CM and CM+Glc conditions). On the other hand, these proteins were less abundant in the cells grown under Dark conditions.

We then analyzed the amount of thylakoid lipids in the cells grown under each condition. The major lipids in the thylakoid membranes are MGDG, DGDG, SQDG, and PG (Kobayashi et al., 2016). However, PG is also found in other membrane system such as the ER and mitochondria. We analyzed the amount of the glycolipids, namely MGDG, DGDG, and SQDG. Galactolipids MGDG and DGDG accumulated to high levels in the cells grown in both CM and CM+Glc conditions. Together with SQDG, the total amounts of glycolipids were 56.58 ± 1.36 nmol/10^6 cells in CM conditions and 66.55 ± 7.89 nmol/10^6 cells in CM+Glc conditions. In contrast, in Dark conditions, the amount of glycolipids was about ten times lower (6.80 ± 1.48 nmol/10^6 cells), indicating that the thylakoid membrane was not developed well in dark-grown cells. We also analyzed the quantum efficiency of PSII, yet this could not be detected in the cells grown in Dark conditions. This is probably because there are not enough PSII proteins, such as PsbA/D, PsbC, and PsbO (**Figure 2A**). Conversely, the cells grown under light showed similar efficiencies regardless of carbon source (CM condition, 0.66 ± 0.01; CM+Glc conditions, 0.62 ± 0.02). These results suggest that *E. gracilis* grown under light accumulated proteins of photosynthetic complexes and thylakoid glycolipids to construct active thylakoid membranes.

Mitochondria Development in *E. gracilis* Under Heterotrophic Conditions

As shown in **Figure 2**, respiration rate increased under heterotrophic conditions. To monitor whether the *E. gracilis* cells developed mitochondria in those conditions, we analyzed mitochondrial protein content. We used an antibody against pyruvate: NADP+ oxidoreductase (PNO) which is involved in the formation of acetyl-CoA and localizes in mitochondria

TABLE 1 | Glycerolipid content of *E. gracilis* cells grown under photoautotrophic, photomixotrophic and heterotrophic conditions.

	CM	CM+Glc	Dark
MGDG	35.73 ± 2.11	45.46 ± 6.93	4.11 ± 0.99
DGDG	17.22 ± 0.69	17.38 ± 1.27	2.33 ± 0.41
SQDG	3.63 ± 0.11	3.71 ± 0.42	0.35 ± 0.09
PG	2.94 ± 0.10	2.67 ± 0.08	0.47 ± 0.15
PC	4.54 ± 0.34	9.64 ± 0.52	12.40 ± 0.80
PE	3.58 ± 0.32	7.44 ± 0.39	10.71 ± 2.14
PI	0.37 ± 0.04	0.61 ± 0.07	0.40 ± 0.08
others	2.83 ± 0.33	3.25 ± 0.23	1.95 ± 0.29
TAG	0.39 ± 0.06	1.58 ± 0.65	2.85 ± 0.53

Values are nmol/10^6 cells ± SE (n = 3).

TABLE 2 | Fatty acid composition of membrane lipids from *E. gracilis* cultured under CM conditions.

	14:0	15:0	16:0	16:1	16:2	16:3	16:4	17:3	18:0	18:1(9)	18:1(11)	18:2	18:3 (*n*-6)	18:3 (*n*-3)	18:4	20:2	20:3 (*n*-6)	20:4	20:5	22:2
MGDG	0.18 ± 0.03	0.09 ± 0.03	0.35 ± 0.07	2.22 ± 0.34	15.46 ± 3.58	1.32 ± 0.29	24.09 ± 6.28	8.08 ± 2.09	0.04 ± 0.03	0.15 ± 0.03	0.26 ± 0.01	11.66 ± 3.33	0.16 ± 0.04	30.73 ± 8.22	ND	0.02 ± 0.01	0.42 ± 0.03	0.74 ± 0.08	1.39 ± 0.10	2.65 ± 0.17
DGDG	0.26 ± 0.02	0.06 ± 0.06	5.13 ± 0.35	3.52 ± 0.43	23.83 ± 0.38	0.29 ± 0.01	7.48 ± 0.48	12.61 ± 0.19	0.85 ± 0.39	0.17 ± 0.00	2.17 ± 0.49	18.57 ± 0.45	0.20 ± 0.02	22.06 ± 0.92	0.01 ± 0.01	0.04 ± 0.02	0.30 ± 0.04	0.47 ± 0.05	0.51 ± 0.03	1.45 ± 0.21
SQDG	2.90 ± 0.34	ND	59.38 ± 1.57	2.41 ± 0.28	2.88 ± 0.11	ND	0.66 ± 0.11	1.16 ± 0.10	1.60 ± 0.62	ND	2.94 ± 0.12	9.69 ± 0.39	0.20 ± 0.13	14.53 ± 1.30	ND	ND	0.18 ± 0.09	0.16 ± 0.08	0.28 ± 0.14	1.02 ± 0.08
PG	1.02 ± 0.34	ND	4.60 ± 0.71	50.09 ± 2.58	1.28 ± 0.21	ND	0.85 ± 0.22	0.13 ± 0.13	1.72 ± 1.09	ND	2.30 ± 0.09	26.98 ± 0.15	0.77 ± 0.08	10.04 ± 0.72	ND	ND	0.06 ± 0.06	ND	ND	0.16 ± 0.09
PC	9.84 ± 0.62	0.41 ± 0.27	17.95 ± 0.90	0.41 ± 0.13	0.06 ± 0.06	ND	ND	ND	1.32 ± 0.30	ND	8.75 ± 0.35	1.05 ± 0.31	0.15 ± 0.08	0.38 ± 0.38	ND	4.91 ± 0.13	5.31 ± 0.18	20.42 ± 0.38	17.73 ± 0.43	11.3 ± 0.53
PE	4.31 ± 0.32	0.32 ± 0.32	26.16 ± 1.47	3.23 ± 0.15	1.02 ± 0.18	ND	0.17 ± 0.17	0.20 ± 0.11	1.05 ± 0.19	ND	34.25 ± 0.63	3.34 ± 0.37	ND	1.02 ± 0.32	0.06 ± 0.06	1.82 ± 0.23	0.86 ± 0.04	17.09 ± 0.52	4.05 ± 0.14	1.06 ± 0.05
PI	8.32 ± 2.07	1.39 ± 1.39	57.51 ± 1.57	ND	ND	ND	ND	ND	4.12 ± 2.08	ND	ND	ND	ND	0.70 ± 0.70	ND	12.39 ± 2.66	ND	12.72 ± 2.51	2.87 ± 1.53	ND
others	12.54 ± 2.39	0.70 ± 0.36	47.62 ± 0.31	2.31 ± 0.51	1.39 ± 0.34	ND	ND	0.18 ± 0.18	11.84 ± 5.51	ND	6.64 ± 0.98	3.12 ± 0.33	ND	0.86 ± 0.17	ND	1.53 ± 0.76	ND	2.71 ± 0.70	8.40 ± 0.99	0.16 ± 0.16

Each value is represented as mol%. SE is based on three independent experiments. ND, not detected (<0.01 mol%).

TABLE 3 | Fatty acid composition of membrane lipids from *E. gracilis* cultured under CM+Glc conditions.

	14:0	15:0	16:0	16:1	16:2	16:3	16:4	17:3	18:0	18:1(9)	18:1(11)	18:2	18:3 (*n*-6)	18:3 (*n*-3)	18:4	20:2	20:3 (*n*-6)	20:4	20:5	22:2
MGDG	0.26 ± 0.05	0.10 ± 0.01	0.71 ± 0.04	2.28 ± 0.24	13.64 ± 2.00	0.59 ± 0.02	22.42 ± 1.81	11.61 ± 0.63	0.09 ± 0.02	0.19 ± 0.02	0.96 ± 0.27	11.91 ± 1.47	0.26 ± 0.04	33.87 ± 1.94	ND	0.03 ± 0.01	0.10 ± 0.03	0.29 ± 0.05	0.41 ± 0.09	0.26 ± 0.08
DGDG	0.30 ± 0.05	0.12 ± 0.05	6.17 ± 0.43	3.02 ± 0.58	19.51 ± 2.67	0.06 ± 0.02	3.89 ± 0.41	19.55 ± 2.13	0.10 ± 0.02	0.23 ± 0.03	4.56 ± 0.97	15.11 ± 2.80	0.30 ± 0.06	26.51 ± 4.20	ND	0.02 ± 0.01	0.07 ± 0.02	0.19 ± 0.02	0.13 ± 0.02	0.17 ± 0.04
SQDG	2.42 ± 0.24	0.43 ± 0.18	55.65 ± 1.20	1.93 ± 0.37	2.68 ± 0.48	ND	0.29 ± 0.11	1.77 ± 0.35	1.59 ± 0.07	ND	6.95 ± 0.56	9.92 ± 1.28	0.16 ± 0.11	15.87 ± 2.13	0.03 ± 0.03	ND	0.03 ± 0.03	0.03 ± 0.03	0.05 ± 0.05	0.17 ± 0.06
PG	1.12 ± 0.29	0.05 ± 0.05	5.66 ± 1.40	40.26 ± 4.58	4.41 ± 0.93	0.14 ± 0.14	8.18 ± 4.71	3.40 ± 1.77	0.41 ± 0.15	0.06 ± 0.06	2.77 ± 0.43	20.34 ± 3.08	1.66 ± 0.83	11.17 ± 0.55	ND	ND	0.12 ± 0.11	0.06 ± 0.06	0.07 ± 0.04	0.11 ± 0.11
PC	9.75 ± 1.74	1.56 ± 0.42	16.37 ± 1.86	1.20 ± 0.17	0.09 ± 0.06	0.02 ± 0.02	0.08 ± 0.03	ND	1.14 ± 0.41	0.11 ± 0.11	7.40 ± 0.43	1.88 ± 0.13	0.47 ± 0.06	0.89 ± 0.34	0.11 ± 0.04	6.02 ± 1.11	11.31 ± 3.40	18.38 ± 1.03	14.29 ± 1.49	8.93 ± 2.95
PE	5.35 ± 0.71	1.96 ± 0.88	23.09 ± 1.52	6.87 ± 0.32	3.69 ± 1.29	ND	0.20 ± 0.03	0.13 ± 0.08	0.66 ± 0.05	ND	25.51 ± 1.76	7.42 ± 0.58	0.03 ± 0.03	0.69 ± 0.20	0.04 ± 0.02	1.61 ± 0.28	1.30 ± 0.09	17.82 ± 0.62	3.20 ± 0.30	0.42 ± 0.06
PI	7.93 ± 1.35	1.74 ± 0.90	53.53 ± 0.99	1.71 ± 0.72	ND	ND	ND	ND	3.62 ± 0.77	ND	0.38 ± 0.22	0.21 ± 0.21	ND	ND	ND	8.73 ± 1.53	1.08 ± 0.64	16.85 ± 1.76	4.22 ± 0.59	ND
others	12.26 ± 0.12	0.90 ± 0.18	36.35 ± 1.39	3.70 ± 0.47	1.41 ± 0.66	ND	0.05 ± 0.05	0.07 ± 0.07	8.85 ± 3.46	ND	5.85 ± 1.32	1.57 ± 0.29	0.43 ± 0.34	0.28 ± 0.20	0.17 ± 0.17	4.19 ± 1.21	0.37 ± 0.22	3.75 ± 1.21	19.46 ± 1.50	0.32 ± 0.18

Each value is represented as mol%. SE is based on four independent experiments. ND, not detected (<0.01 mol%).

TABLE 4 | Fatty acid composition of membrane lipids from *E. gracilis* cultured under Dark conditions.

	14:0	15:0	16:0	16:1	16:2	16:3	16:4	17:3	18:0	18:1(9)	18:1(11)	18:2	18:3 (*n*-6)	18:3 (*n*-3)	18:4	20:2	20:3 (*n*-6)	20:4	20:5	22:2
MGDG	1.66 ± 0.92	0.49 ± 0.52	3.66 ± 2.13	7.37 ± 4.86	19.23 ± 12.38	0.08 ± 0.00	2.70 ± 1.79	19.01 ± 9.23	0.69 ± 0.37	1.77 ± 2.93	4.66 ± 3.84	13.96 ± 8.88	0.06 ± 0.00	21.67 ± 10.45	ND	0.07 ± 0.00	0.24 ± 0.21	2.09 ± 1.43	0.59 ± 0.43	ND
DGDG	1.57 ± 0.12	ND	7.12 ± 0.27	4.77 ± 0.45	14.63 ± 0.51	ND	0.34 ± 0.17	25.24 ± 0.93	0.84 ± 0.13	ND	7.52 ± 0.80	11.89 ± 1.10	ND	25.28 ± 1.83	ND	0.07 ± 0.07	ND	0.67 ± 0.14	0.07 ± 0.07	ND
SQDG	12.29 ± 1.20	ND	59.78 ± 3.07	1.97 ± 1.00	4.15 ± 0.38	ND	ND	1.68 ± 0.92	4.50 ± 0.28	ND	5.80 ± 1.62	4.76 ± 0.78	ND	5.06 ± 0.08	ND	ND	ND	ND	ND	ND
PG	9.78 ± 2.02	ND	13.14 ± 2.10	10.06 ± 2.60	1.34 ± 0.71	ND	ND	ND	4.97 ± 1.21	ND	ND	17.00 ± 17.00	34.67 ± 17.33	ND	ND	ND	3.79 ± 0.91	3.57 ± 0.40	ND	1.67 ± 1.67
PC	12.69 ± 0.91	0.39 ± 0.09	16.54 ± 0.40	1.95 ± 0.09	0.07 ± 0.02	0.03 ± 0.03	0.09 ± 0.00	0.03 ± 0.03	0.81 ± 0.11	ND	5.25 ± 0.36	2.85 ± 0.20	0.53 ± 0.09	0.84 ± 0.09	0.32 ± 0.01	6.74 ± 1.03	12.95 ± 1.58	29.72 ± 1.09	6.24 ± 0.27	1.95 ± 0.12
PE	8.48 ± 1.52	0.44 ± 0.07	28.12 ± 0.92	10.82 ± 1.08	0.31 ± 0.03	ND	0.12 ± 0.01	0.02 ± 0.02	0.71 ± 0.16	ND	16.80 ± 2.11	4.93 ± 0.11	0.10 ± 0.10	0.30 ± 0.10	0.07 ± 0.00	2.17 ± 0.70	1.85 ± 0.11	22.43 ± 0.77	2.14 ± 0.19	0.20 ± 0.00
PI	11.96 ± 1.18	0.63 ± 0.63	58.11 ± 1.61	ND	ND	ND	ND	ND	6.14 ± 0.42	ND	ND	ND	ND	ND	ND	4.98 ± 0.17	0.42 ± 0.42	16.31 ± 0.39	1.44 ± 0.72	ND
Others	15.75 ± 1.19	0.42 ± 0.42	25.30 ± 1.40	2.01 ± 0.70	0.34 ± 0.20	ND	0.16 ± 0.16	ND	6.71 ± 0.31	ND	2.65 ± 1.07	0.90 ± 0.09	0.16 ± 0.16	1.05 ± 0.65	ND	5.85 ± 1.51	1.86 ± 0.61	10.16 ± 1.11	26.24 ± 1.77	0.43 ± 0.21

Each value is represented as mol%. SE is based on three independent experiments. ND, not detected (<0.01 mol%).

TABLE 5 | Fatty acid composition of TAG from *E. gracilis* cultured under CM, CM+Glc and Dark conditions.

	12:0	13:0	14:0	15:0	16:0	16:1	16:2	16:4	17:3	18:0	18:1(11)	18:2	18:3 (n-6)	18:3 (n-3)	20:2	20:3 (n-6)	20:4	20:5	22:2
CM	5.30 ± 0.26	4.93 ± 0.99	18.52 ± 0.56	7.17 ± 0.17	27.43 ± 3.78	0.90 ± 0.90	0.43 ± 0.43	0.41 ± 0.41	ND	6.86 ± 2.14	7.03 ± 1.05	0.52 ± 0.27	ND	ND	1.86 ± 0.98	0.86 ± 0.44	9.39 ± 1.60	6.17 ± 1.53	2.2 ± 0.19
CM+Glc	4.81 ± 0.59	5.99 ± 0.68	21.77 ± 2.14	4.24 ± 1.07	14.09 ± 1.93	2.11 ± 0.59	2.38 ± 0.58	3.08 ± 1.73	1.04 ± 0.64	2.38 ± 0.25	4.83 ± 0.57	2.48 ± 0.69	ND	2.63 ± 1.46	4.56 ± 0.50	2.53 ± 0.59	14.53 ± 1.72	5.35 ± 0.56	1.2 ± 0.46
Dark	15.14 ± 1.50	4.07 ± 0.65	39.15 ± 2.65	1.54 ± 0.79	18.68 ± 0.70	5.67 ± 1.01	ND	ND	ND	2.13 ± 0.74	5.81 ± 2.79	1.33 ± 0.51	0.07 ± 0.07	ND	1.60 ± 0.33	0.89 ± 0.57	3.74 ± 1.61	0.19 ± 0.19	ND

Each value is represented as mol%. SE is based on three independent experiments. ND, not detected (<0.01 mol%).

(Nakazawa et al., 2017). As expected, under heterotrophic conditions, *E. gracilis* cells accumulated PNO compared to the cells grown under CM conditions (**Figure 3A**). We also detected PNO in the cells grown under CM+Glc conditions, but it was less than that of the Dark conditions.

We next analyzed content of phospholipids, PC, and PE, which are typical membrane lipids in mitochondria. As shown in **Figure 3B**, the amounts of these lipids were highest in the cells grown under Dark conditions (23.12 ± 2.93 nmol/10^6 cells). The cells grown under CM+Glc conditions had fewer lipids (17.08 ± 0.36 nmol/10^6 cells) than the cells grown in the dark, but still more than twice as much as the cells grown under CM conditions (8.12 ± 0.56 nmol/10^6 cells). Together with the respiration rate and amount of PNO, these results suggest that mitochondria are well developed when a carbon source is added to the medium.

To confirm these phenomena, we observed the cells grown under each condition using a confocal laser scanning microscope. As shown in **Figure 4**, auto-fluorescence of chlorophyll (indicated by blue) was seen clearly in the cells grown under light (CM and CM+Glc conditions). The cells grown in Dark conditions showed faint signal of chlorophyll, correlate with the chlorophyll content of the cells (**Figure 1B**). Mitochondria were stained using MitoTracker and indicated by pink. The cells grown with glucose (CM+Glc and Dark conditions) showed strong signals of MitoTracker compared with the cells grown under CM conditions, which also correlate with the respiration activity; contents of PNO and phospholipids. These results agree with the idea that lipid contents correlated with chloroplasts and mitochondria development.

Revisiting Lipid and Fatty Acid Contents of *E. gracilis*

Lipid content of *E. gracilis* is summarized in **Table 1**. We detected seven membrane lipids as major constituents, including three glycolipids (MGDG, DGDG, and SQDG) and four phospholipids (PC, PE, PG, and PI). This composition is very similar to the lipid content of other eukaryotic phototrophs, such as the model dicot *Arabidopsis thaliana* (Browse et al., 1986). According to the fatty acid base calculation, we succeeded in detecting more than 94 mol% of membrane lipids in *E. gracilis*. The other 6 mol% of membrane lipids (others in **Table 1**) could not be determined because they did not co-migrate with the available standards, such as sphingomyelin or phosphatidylserine and were difficult to analyze by LC-MS/MS because of their low abundancies.

Fatty acid contents of each membrane lipid in the different growth conditions are described in **Tables 2–4**. The fatty acid content was similar regardless of growth conditions, except for PG. PG in the cells grown under Dark condition had much more γ-linolenic acid [18:3(n-6)] compared to the cells grown under CM or CM+Glc conditions [more α-linolenic acid: 18:3(n-3)]. Thylakoid galactolipids, namely MGDG and DGDG, were found to have more hexadeca-4,7,10,13-tetraenoic acid (16:4). Phospholipids such as PC and PE contained more of the long chain fatty acid, eicosatetraenoic acid (20:4).

TABLE 6 | List of genes encoding homologs of thylakoid glycolipid synthases found in RNAseq data.

Genes	Function	Comp number in the RNAseq data
MGD1	Galactosyltransferase for MGDG synthesis (plant type)	comp33364_c0_seq1
		comp31220_c0_seq1
DGD1	Galactosyltransferase for DGDG synthesis (plant type)	comp33692_c1_seq1
		comp27690_c0_seq1
SQD2	Sulfoquinovosyltransferase for SQDG synthesis	comp34481_c0_seq2
		comp21910_c0_seq1

The sequence data are available at the DDBJ Sequence Read Archive (DRA) with accession number SRP060591.

We also analyzed the abundancy of triacylglycerol (TAG) (**Table 1**), which is another storage lipid. The amount of TAG per cell increased when Glc was added to the medium, and TAG was highest in the cells grown under Dark conditions. This TAG had short chain saturated fatty acids, such as lauric acid 12:0, 14:0, and 16:0 as the major components (**Table 5**). On the other hand, the cells grown under CM or CM+Glc conditions had fewer short chain saturated fatty acids and more long chain fatty acids (20:4).

DISCUSSION

E. gracilis Uses Plant-Type Pathways for Galactolipid Synthesis

Euglenoids are believed to acquire chloroplasts through secondary endosymbiosis. We found that, under illumination, *E. gracilis* cells accumulated thylakoid glycolipids, especially two galactolipids, MGDG and DGDG. These galactolipids can be found in all oxygenic phototrophs and are known to be synthesized by two pathways, the plant-type pathway and cyanobacteria-type pathway (Awai, 2016). Some algae, such as primitive red algae and glaucophytes, are known to have the plant-type enzyme for MGDG synthesis and the cyanobacteria-type enzyme for DGDG synthesis (Awai et al., 2007; Sakurai et al., 2007; Hori et al., 2016; Maida and Awai, 2016; Sato and Awai, 2016). We analyzed whether the chloroplast glycolipids in *E. gracilis* are synthesized by the plant-type enzymes using EST data (Yoshida et al., 2016). As expected, the genes encoding plant-type enzymes for galactolipid synthesis were found (**Table 6**), as green algae utilize plant-type enzymes for both MGDG and DGDG synthesis. The SQDG synthetic pathway is basically conserved from cyanobacteria to plants, and *E. gracilis* was found to use the same system. We also tried to analyze the synthetic pathways for phospholipids determined by our analysis, but it was too complicated to be analyzed since euglenoids seem to have pathways from both the host cell and engulfed cell of the secondary symbiosis. Genomic sequencing analysis will be required to solve whole lipid synthetic pathway in *E. gracilis*.

Possible Application for Bioengineering by Controlling Flow of Fatty Acid Metabolism

The production of biofuel for sustainable energy is highly anticipated as a next generation energy source for ecological and economic reasons (Chisti, 2007; Kraan, 2013). *E. gracilis* is a strong candidate for the production of such energy because of its ability to produce wax ester, which can exceed 40% of its dry weight (Inui et al., 1983). Wax ester in *E. gracilis* is synthesized from fatty acid and fatty alcohol mainly by WSD-type wax synthase (Tomiyama et al., 2017). This wax ester is suitable for bioenergy, because of their relatively short chained (C14) fatty acids and alcohols. Since the synthesis of membrane lipids and TAG also require fatty acids, it is important to know how the fatty acid flow and channel for synthesis of wax ester or glycerolipids. Our study described here provides details on how much glyceorolipids are synthesized in *E. gracilis* grown in photoautotrophic, photomixotrophic, and heterotrophic conditions. These data will inform the manipulation of fatty acid flow between glycerolipids and wax ester. We observed the accumulation of short chain fatty acid, especially 14:0 in TAG from cells grown under heterotrophic conditions. The major fatty acid of wax ester in *E. gracilis* is also 14:0, and TAG will be a target to enhance wax ester accumulation.

Recently, a photoenzyme which converts fatty acids to hydrocarbons was found in green algae (Sorigue et al., 2017). Using the amino acid sequence of this enzyme as a bait, we did a BLAST search of an Euglena EST database and found its homologs belonging to the GMC oxidoreductase super family (comp29747_c0_seq1: Expect = 6e-80 and comp30342_c0_seq1: Expect = 5e-40). However, enzymes of this family more closely resemble bacterial choline dehydrogenase, not the hydrocarbon synthase of green algae, implying that *E. gracilis* do not possess such enzymes for alkane synthesis. *E. gracilis* has the capacity to accumulate wax ester, and it is likely that it can be switch to synthesize alkene. Recently, a method for introduction of transgenes has been established in *E. gracilis* (Ogawa et al., 2015). It will be interesting to see if we can introduce this photoenzyme to *E. gracilis* with regulated fatty acid flow for another type of biofuel production in *E. gracilis*.

AUTHOR CONTRIBUTIONS

SS, TI, and KA conceived the research. SS and S-iA conducted the experiments. SS, S-iA, TI, and KA performed the data analysis and wrote the manuscript.

FUNDING

This work was supported in part by grants, Precursory Research for Embryonic Science and Technology, from the Japan Science

and Technology Agency to S-iA, and Core Research for Evolutional Science and Technology, from the Japan Science and Technology Agency to TI and KA.

ACKNOWLEDGMENTS

The authors are grateful to Dr. Masahiko Ikeuchi and Dr. Masami Nakazawa for their gift of anti-PsbA and anti-PNO antibodies, respectively.

SUPPLEMENTARY MATERIAL

The Supplementary Material for this article can be found online at: https://www.frontiersin.org/articles/10.3389/fpls.2018.00370/full#supplementary-material

FIGURE S1 | SDS-PAGE of *E. gracilis* proteins. Proteins were extracted from cells grown under photoautotrophic, photomixotrophic and heterotrophic conditions and subjected to SDS-PAGE followed by CBB staining. Lane 1, CM conditions; lane 2, CM+Glc conditions; lane 3, Dark conditions. M: molecular weight marker (Nacalai Tesque, Inc.).

REFERENCES

Allen, C. F., Good, P., Davis, H. F., Chisum, P., and Fowler, S. D. (1966). Methodology for the separation o plant lipids and application to spinach leaf and chloroplast lamellae. *J. Am. Oil Chem. Soc.* 43, 223–231. doi: 10.1007/bf02641091

Arnon, D. I. (1949). Copper enzymes in isolated chloroplasts. Polyphenoloxidase in *Beta vulgaris*. *Plant Physiol.* 24, 1–15. doi: 10.1104/pp.24.1.1

Awai, K. (2016). Thylakoid development and galactolipid synthesis in cyanobacteria. *Subcell. Biochem.* 86, 85–101. doi: 10.1007/978-3-319-25979-6_4

Awai, K., Ohta, H., and Sato, N. (2014). Oxygenic photosynthesis without galactolipids. *Proc. Natl. Acad. Sci. U.S.A.* 111, 13571–13575. doi: 10.1073/pnas.1403708111

Awai, K., Watanabe, H., Benning, C., and Nishida, I. (2007). Digalactosyldiacylglycerol is required for better photosynthetic growth of *Synechocystis* sp. PCC6803 under phosphate limitation. *Plant Cell Physiol.* 48, 1517–1523. doi: 10.1093/pcp/pcm134

Barthel, S., Bernat, G., Seidel, T., Rupprecht, E., Kahmann, U., and Schneider, D. (2013). Thylakoid membrane maturation and PSII activation are linked in greening *Synechocystis* sp. PCC 6803 cells. *Plant Physiol.* 163, 1037–1046. doi: 10.1104/pp.113.224428

Bligh, E. G., and Dyer, W. J. (1959). A rapid method of total lipid extraction and purification. *Can. J. Biochem. Physiol.* 37, 911–917. doi: 10.1139/y59-099

Browse, J., Warwick, N., Somerville, C. R., and Slack, C. R. (1986). Fluxes through the prokaryotic and eukaryotic pathways of lipid synthesis in the '16:3' plant *Arabidopsis thaliana*. *Biochem. J.* 235, 25–31. doi: 10.1042/bj2350025

Calvayrac, R., and Douce, R. (1970). Les polyglycerophospholipides d'*Euglena gracilis*. *FEBS Lett.* 7, 259–262. doi: 10.1016/0014-5793(70)80175-2

Chisti, Y. (2007). Biodiesel from microalgae. *Biotechnol. Adv.* 25, 294–306. doi: 10.1016/j.biotechadv.2007.02.001

Constantopoulos, G., and Bloch, K. (1967). Effect of light intensity on the lipid composition of *Euglena gracilis*. *J. Biol. Chem.* 242, 3538–3542.

Cramer, M., and Myers, J. (1952). Growth and photosynthetic characteristics of *Euglena gracilis*. *Arch. Mikrobiol.* 17, 384–402. doi: 10.1007/bf00410835

Ferroni, L., Baldisserotto, C., Pantaleoni, L., Fasulo, M. P., Fagioli, P., and Pancaldi, S. (2009). Degreening of the unicellular alga *Euglena gracilis*: thylakoid composition, room temperature fluorescence spectra and chloroplast morphology. *Plant Biol.* 11, 631–641. doi: 10.1111/j.1438-8677.2008.00152.x

Fujita, T., Matsuda, H., Sato, T., Iwasaki, T., and Takafuji, S. I. (1995). Phospholipid composition and phospholipase activity of Euglena. *J. Japan Oil Chem. Soc.* 44, 197–202. doi: 10.5650/jos1956.44.197

Gibbs, S. P. (1978). The chloroplasts of *Euglena* may have evolved from symbiotic green algae. *Can. J. Bot.* 56, 2883–2889. doi: 10.1139/b78-345

Hölzl, G., Zahringer, U., Warnecke, D., and Heinz, E. (2005). Glycoengineering of cyanobacterial thylakoid membranes for future studies on the role of glycolipids in photosynthesis. *Plant Cell Physiol.* 46, 1766–1778. doi: 10.1093/pcp/pci189

Hori, K., Nobusawa, T., Watanabe, T., Madoka, Y., Suzuki, H., Shibata, D., et al. (2016). Tangled evolutionary processes with commonality and diversity in plastidial glycolipid synthesis in photosynthetic organisms. *Biochim. Biophys. Acta* 1861, 1294–1308. doi: 10.1016/j.bbalip.2016.04.015

Hulanicka, D., Erwin, J., and Bloch, K. (1964). Lipid metabolism of *Euglena gracilis*. *J. Biol. Chem.* 239, 2778–2787.

Inui, H., Ishikawa, T., and Tamoi, M. (2017). Wax ester fermentation and its application for biofuel production. *Adv. Exp. Med. Biol.* 979, 269–283. doi: 10.1007/978-3-319-54910-1_13

Inui, H., Miyatake, K., Nakano, Y., and Kitaoka, S. (1982). Wax ester fermentation in *Euglena gracilis*. *FEBS Lett.* 150, 89–93. doi: 10.1016/0014-5793(82)81310-0

Inui, H., Miyatake, K., Nakano, Y., and Kitaoka, S. (1983). Production and composition of wax esters by fermentation of *Euglena gracilis*. *Agric. Biol. Chem.* 47, 2669–2671. doi: 10.1080/00021369.1983.10866013

Inui, H., Miyatake, K., Nakano, Y., and Kitaoka, S. (1984). Fatty acid synthesis in mitochondria of *Euglena gracilis*. *Eur. J. Biochem.* 142, 121–126. doi: 10.1111/j.1432-1033.1984.tb08258.x

Kalscheuer, R., and Steinbuchel, A. (2003). A novel bifunctional wax ester synthase/acyl-CoA:diacylglycerol acyltransferase mediates wax ester and triacylglycerol biosynthesis in *Acinetobacter calcoaceticus* ADP1. *J. Biol. Chem.* 278, 8075–8082. doi: 10.1074/jbc.M210533200

Kobayashi, K., Endo, K., and Wada, H. (2016). "Roles of lipids in photosynthesis," in *Lipids in Plant and Algae Development*, eds Y. Nakamura and Y. Li-Beisson (Cham: Springer International Publishing), 21–49.

Kraan, S. (2013). Mass-cultivation of carbohydrate rich macroalgae, a possible solution for sustainable biofuel production. *Mitig. Adapt. Strateg. Glob. Change* 18, 27–46. doi: 10.1007/s11027-010-9275-5

Laemmli, U. K. (1970). Cleavage of structural proteins during the assembly of the head of bacteriophage T4. *Nature* 227, 680–685. doi: 10.1038/227680a0

Maida, E., and Awai, K. (2016). Digalactosyldiacylglycerol is essential in *Synechococcus elongatus* PCC 7942, but its function does not depend on its biosynthetic pathway. *Biochim. Biophys. Acta* 1861(9 Pt B), 1309–1314. doi: 10.1016/j.bbalip.2016.03.011

McFadden, G. I. (2001). Primary and secondary endosymbiosis and the origin of plastids. *J. Phycol.* 37, 951–959. doi: 10.1046/j.1529-8817.2001.01126.x

Nagaoka, N., Yamashita, A., Kurisu, R., Watari, Y., Ishizuna, F., Tsutsumi, N., et al. (2017). DRP3 and ELM1 are required for mitochondrial fission in the liverwort *Marchantia polymorpha*. *Sci. Rep.* 7:4600. doi: 10.1038/s41598-017-04886-0

Nakazawa, M., Hayashi, R., Takenaka, S., Inui, H., Ishikawa, T., Ueda, M., et al. (2017). Physiological functions of pyruvate:NADP+ oxidoreductase and 2-oxoglutarate decarboxylase in *Euglena gracilis* under aerobic and anaerobic conditions. *Biosci. Biotechnol. Biochem.* 81, 1386–1393. doi: 10.1080/09168451.2017.1318696

Nichols, B. W., and James, A. T. (1964). The lipids of plant storage tissue. *Fette Seifen Anstrichmittel* 66, 1003–1006. doi: 10.1002/lipi.19640661207

Ogawa, T., Furuhashi, T., Okazawa, A., Nakai, R., Nakazawa, M., Kind, T., et al. (2014). Exploration of polar lipid accumulation profiles in *Euglena gracilis* using LipidBlast, an MS/MS spectral library constructed in *silico*. *Biosci. Biotechnol. Biochem.* 78, 14–18. doi: 10.1080/09168451.2014.877826

Ogawa, T., Tamoi, M., Kimura, A., Mine, A., Sakuyama, H., Yoshida, E., et al. (2015). Enhancement of photosynthetic capacity in *Euglena gracilis* by expression of cyanobacterial fructose-1,6-/sedoheptulose-1,7-bisphosphatase leads to increases in biomass and wax ester production. *Biotechnol. Biofuels* 8:80. doi: 10.1186/s13068-015-0264-5

Okazaki, Y., Kamide, Y., Hirai, M. Y., and Saito, K. (2013). Plant lipidomics based on hydrophilic interaction chromatography coupled to ion trap time-of-flight mass spectrometry. *Metabolomics* 9(Suppl. 1), 121–131. doi: 10.1007/s11306-011-0318-z

Osafune, T., Sumida, S., Ehara, T., Ueno, N., Hase, E., and Schiff, J. A. (1990). Lipid (wax) and Paramylum as Sources of Carbon and Energy for the Early

Development of Proplastids in Dark-Grown *Euglena gracilis* Cells Transferred to an Inorganic Medium. *J. Electron Microsc.* 39, 372–381. doi: 10.1093/oxfordjournals.jmicro.a050821

Regnault, A., Chervin, D., Chammai, A., Piton, F., Calvayrac, R., and Mazliak, P. (1995). Lipid composition of *Euglena gracilis* in relation to carbon-nitrogen balance. *Phytochemistry* 40, 725–733. doi: 10.1016/0031-9422(95)00268-C

Rosenberg, A. (1963). A comparison of lipid patterns in photosynthesizing and nonphotosynthesizing cells of *Euglena gracilis*. *Biochemistry* 2, 1148–1154. doi: 10.1021/bi00905a042

Rosenberg, A., Gouaux, J., and Milch, P. (1966). Monogalactosyl and digalactosyl diglycerides from heterotrophic, hetero-autotrophic, and photobiotic *Euglena gracilis*. *J. Lipid Res.* 7, 733–738.

Rosenberg, A., and Pecker, M. (1964). Lipid alterations in *Euglena gracilis* cells during light-induced greening. *Biochemistry* 3, 254–258. doi: 10.1021/bi00890a019

Sakurai, I., Mizusawa, N., Wada, H., and Sato, N. (2007). Digalactosyldiacylglycerol is required for stabilization of the oxygen-evolving complex in photosystem II. *Plant Physiol.* 145, 1361–1370. doi: 10.1104/pp.107.106781

Sato, N., and Awai, K. (2016). Diversity in biosynthetic pathways of galactolipids in the light of endosymbiotic origin of chloroplasts. *Front. Plant Sci.* 7:117. doi: 10.3389/fpls.2016.00117

Scheer, A., and Parthier, B. (1982). Dark-induced chloroplast dedifferentiation in *Euglena gracilis*. *Planta* 156, 274–281. doi: 10.1007/BF00393736

Schiff, J. A., and Schwartzbach, S. D. (1982). "Photocontrol of chloroplast development in euglena," in *The Biology of Euglena Physiology,* Vol. 3, D. E. Buetow (Cambridge, MA: Academic Press), 313–352.

Schwartzbach, S. D., Schiff, J. A., and Goldstein, N. H. (1975). Events surrounding the early development of *Euglena* chloroplasts. *Plant Physiol.* 63, 908–915.

Sorigue, D., Legeret, B., Cuine, S., Blangy, S., Moulin, S., Billon, E., et al. (2017). An algal photoenzyme converts fatty acids to hydrocarbons. *Science* 357, 903–907. doi: 10.1126/science.aan6349

Sumida, S., Lyman, H., Kiyohara, N., and Osafune, T. (2007). Mechanism of conversion from heterotrophy to autotrophy in *Euglena gracilis*. *Cytologia* 72, 447–457. doi: 10.1508/cytologia.72.447

Suzuki, S., Awai, K., Ishihara, A., and Yamauchi, K. (2016). Cold temperature blocks thyroid hormone-induced changes in lipid and energy metabolism in the liver of *Lithobates catesbeianus* tadpoles. *Cell Biosci.* 6:19. doi: 10.1186/s13578-016-0087-5

Tomiyama, T., Kurihara, K., Ogawa, T., Maruta, T., Ogawa, T., Ohta, D., et al. (2017). Wax ester synthase/diacylglycerol acyltransferase isoenzymes play a pivotal role in wax ester biosynthesis in *Euglena gracilis*. *Sci. Rep.* 7:13504. doi: 10.1038/s41598-017-14077-6

Yoshida, Y., Tomiyama, T., Maruta, T., Tomita, M., Ishikawa, T., and Arakawa, K. (2016). De novo assembly and comparative transcriptome analysis of *Euglena gracilis* in response to anaerobic conditions. *BMC Genomics* 17:182. doi: 10.1186/s12864-016-2540-6

Conflict of Interest Statement: The authors declare that the research was conducted in the absence of any commercial or financial relationships that could be construed as a potential conflict of interest.

The reviewer WR and handling Editor declared their shared affiliation.

frontiers in Plant Science

ORIGINAL RESEARCH
published: 23 May 2018
doi: 10.3389/fpls.2018.00676

Characterization of Ferredoxin-Dependent Biliverdin Reductase PCYA1 Reveals the Dual Function in Retrograde Bilin Biosynthesis and Interaction With Light-Dependent Protochlorophyllide Oxidoreductase LPOR in *Chlamydomonas reinhardtii*

*Weiqing Zhang[1], Huan Zhong[1], Hui Lu[1], Yuxiang Zhang[1], Xuan Deng[2], Kaiyao Huang[2] and Deqiang Duanmu[1]**

[1] State Key Laboratory of Agricultural Microbiology, College of Life Science and Technology, Huazhong Agricultural University, Wuhan, China, [2] Key Laboratory of Algal Biology, Institute of Hydrobiology, Chinese Academy of Sciences, Wuhan, China

OPEN ACCESS

Edited by:
Hongbo Gao,
Beijing Forestry University, China

Reviewed by:
Wenqiang Yang,
Key Laboratory of Photobiology, Institute of Botany (CAS), China
Shih-Long Tu,
Institute of Plant and Microbial Biology, Academia Sinica, Taiwan
Ru Zhang,
Donald Danforth Plant Science Center, United States

***Correspondence:**
Deqiang Duanmu
duanmu@mail.hzau.edu.cn

Specialty section:
This article was submitted to Plant Physiology, a section of the journal Frontiers in Plant Science

Received: 28 November 2017
Accepted: 03 May 2018
Published: 23 May 2018

Citation:
Zhang W, Zhong H, Lu H, Zhang Y, Deng X, Huang K and Duanmu D (2018) Characterization of Ferredoxin-Dependent Biliverdin Reductase PCYA1 Reveals the Dual Function in Retrograde Bilin Biosynthesis and Interaction With Light-Dependent Protochlorophyllide Oxidoreductase LPOR in Chlamydomonas reinhardtii. Front. Plant Sci. 9:676. doi: 10.3389/fpls.2018.00676

Bilins are linear tetrapyrroles commonly used as chromophores of phycobiliproteins and phytochromes for light-harvesting or light-sensing in photosynthetic organisms. Many eukaryotic algae lack both phycobiliproteins and phytochromes, but retain the bilin biosynthetic enzymes including heme oxygenase (HO/HMOX) and ferredoxin-dependent biliverdin reductase (FDBR). Previous studies on *Chlamydomonas reinhardtii* heme oxygenase mutant (*hmox1*) have shown that bilins are not only essential retrograde signals to mitigate oxidative stress during diurnal dark-to-light transitions, they are also required for chlorophyll accumulation and maintenance of a functional photosynthetic apparatus in the light. However, the underlying mechanism of bilin-mediated regulation of chlorophyll biosynthesis is unclear. In this study, Chlamydomonas phycocyanobilin:ferredoxin oxidoreductase PCYA1 FDBR domain was found to specifically interact with the rate-limiting chlorophyll biosynthetic enzyme LPOR (light-dependent protochlorophyllide oxidoreductase). PCYA1 is partially associated with chloroplast envelope membrane, consistent with the observed export of bilin from chloroplast to cytosol by cytosolic expression of a bilin-binding reporter protein in Chlamydomonas. Both the *pcya1-1* mutant with the carboxyl-terminal extension of PCYA1 eliminated and efficient knockdown of *PCYA1* expression by artificial microRNA exhibited no significant impact on algal phototrophic growth and photosynthetic proteins accumulation, indicating that the conserved FDBR domain is sufficient and minimally required for bilin biosynthesis and functioning. Taken together, these studies provide novel insights into the regulatory role of PCYA1 in chlorophyll biosynthesis via interaction with key Chl biosynthetic enzyme.

Keywords: PCYA1, bilin, POR, chlorophyll biosynthesis, algae, photoacclimation

INTRODUCTION

Evolutionary origin of higher plants and eukaryotic algal chloroplast can be traced back to approximately 1.5 billion years ago during the primary endosymbiotic event, namely a eukaryotic cell engulfing a free-living cyanobacterium and the endosymbiont gradually evolving into modern-day photosynthetic organelle (Keeling, 2010; de Vries and Archibald, 2017). As a semi-autonomous essential organelle present in all extant eukaryotic oxygenic photosynthetic organisms, chloroplast contains the photosynthetic machinery and also serves as the factory of numerous biosynthetic pathways to provide intermediate biomolecules or end products essential for plant development and physiological functions (Joyard et al., 2009). Additionally, to sense extracellular environmental cues and integrate intracellular signals, a functional chloroplast is critical for biogenic and stress responses, which requires the coordinated expression between chloroplast and nucleus genomes (Fernández and Strand, 2008; Xiao et al., 2013). The bilateral communication is largely facilitated by anterograde and retrograde signaling pathways (Woodson and Chory, 2008; Bobik and Burch-Smith, 2015).

In the past three decades, many different retrograde signaling pathways in photosynthetic species are discovered and well characterized by using model organisms such as *Arabidopsis thaliana* and *Chlamydomonas reinhardtii* (Arabidopsis and Chlamydomonas thereafter) (Chi et al., 2013, 2015; Börner, 2017). Briefly, these retrograde signals can be cataloged into at least five distinct groups based on the sources of origin: tetrapyrrole intermediates (Terry and Smith, 2013), reactive oxygen species (ROS) (Wakao et al., 2014), plastid redox status (Bräutigam et al., 2009), plastid gene expression (Leister et al., 2017), and other chloroplast-derived metabolites such as 3′-phosphoadenosine 5′-phosphate (PAP), methylerythritol cyclodiphosphate (MEcPP) (Xiao et al., 2012; Chan et al., 2016).

Tetrapyrroles, including chlorophyll, siroheme and heme, are mainly produced in chloroplasts and share a common biosynthetic pathway starting from the precursor 5-aminolevulinic acid (ALA) (Tanaka and Tanaka, 2007; Tanaka et al., 2011). Tetrapyrroles play significant roles in many physiological processes such as photosynthesis and drought acclimation (Nagahatenna et al., 2015). Over-accumulated tetrapyrrole intermediates are highly phototoxic and can induce oxidative stress upon light illumination. Therefore, a precise regulation of tetrapyrrole biosynthesis is vital to avoid oxidative stress caused by mis-accumulation of phototoxic tetrapyrrole intermediates (Mochizuki et al., 2010; Busch and Montgomery, 2015). Tetrapyrrole intermediates are also reported to control the nuclear gene expression both positively and negatively as retrograde signals (Larkin, 2014; Brzezowski et al., 2015). Previous studies have shown that the accumulated Mg-Protoporphyrin IX (MgPPIX) acts as a retrograde signal emitting from plastid to negatively regulate photosynthetic gene expression (Strand et al., 2003; Ankele et al., 2007; Zhang et al., 2011). In contrast, a ferrochelatase 1 (FC1)-overexpression mutant in Arabidopsis (*gun 6-1D*) implied that the specific heme pool produced by FC1 was accountable for upregulation of several photosynthesis associated nuclear genes (PhANGs) expression (Woodson et al., 2011).

Heme oxygenase (HO) and ferredoxin-dependent biliverdin reductase (FDBR) could further convert heme to open-chain tetrapyrroles, i.e., biliverdin IXα (BV IXα) and bilins, respectively (Dammeyer and Frankenberg-Dinkel, 2008). Distinct FDBRs with different regiospecificities are found in photosynthetic organisms from cyanobacteria, eukaryotic algae to land plants to yield various types of bilins, such as phycocyanobilin (PCB), phytochromobilin (PΦB), phycoerythrobilin (PEB) and phycourobilin (PUB) (Rockwell et al., 2014b; Rockwell and Lagarias, 2017). These bilins usually act as cofactors of phycobiliproteins for light-harvesting in cyanobacteria and some eukaryotic algae (Singh et al., 2015), or as the chromophores of phytochromes for light sensing in many photosynthetic organisms (Falklöf and Durbeej, 2016). It is thus surprising that although some green algae lack phycobiliproteins and phytochromes, all of them contain the bilin biosynthetic enzymes including HO and certain form of FDBR (Duanmu et al., 2014). Based on characterization of the Chlamydomonas *hmox1* mutant, two recent reports proposed a more ancient and possibly widely conserved function of bilins as biogenic retrograde signals essential for photoacclimation and functional chloroplast maintenance during diurnal transition from dark to light (Duanmu et al., 2013, 2017). It was also hypothesized that chlorochrome, a putative bilin-dependent blue-light photoreceptor residing in the chloroplast, is involved in regulation of the chlorophyll (Chl) biosynthesis and photosystem I (PSI) and light-harvesting complex I (LHCI) protein accumulation (Wittkopp et al., 2017).

However, the biochemical evidence of bilin transportation and the underlying mechanism of bilin-mediated regulation of Chl biosynthesis is still unclear. In this study, we provided evidences that Chlamydomonas PCYA1 protein directly interacts with the key Chl biosynthetic enzyme LPOR (light-dependent protochlorophyllide oxidoreductase), and this interaction is specific to Chlamydomonas since the Arabidopsis homologous proteins do not interact with each other. PCYA1 is also partially associated with the chloroplast envelope and absent from thylakoid membrane. Heterologous expression of a bilin-binding reporter protein in the cytosol of Chlamydomonas confirmed that the bilin molecule could be exported from chloroplast to cytosol, an essential character of chloroplast retrograde signals. Furthermore, analysis of an insertional mutant *pcya1-1* and knockdown mutants of *PCYA1* by artificial microRNA demonstrated that loss of carboxyl-terminal extension (CTE) and reduced accumulation of PCYA1 have no significant impact on phototrophic growth and PSI related proteins accumulation in Chlamydomonas. These results provide further insights into direct regulation of Chl biosynthesis by bilin biosynthetic enzyme and putative bilin transport in photosynthetic eukaryotes.

MATERIALS AND METHODS

Chlamydomonas Strains and Growth Conditions

Chlamydomonas reinhardtii wild-type strain 4A+ and *hmox1* mutant were described previously (Duanmu et al., 2013). CC400 was obtained from the Chlamydomonas Stock Center, University of Minnesota, St. Paul, United States. The *pcya1-1* mutant and its parental strain HS211 were obtained from Institute of Hydrobiology, Chinese Academy of Sciences, Wuhan, China (Cheng et al., 2017). All strains were maintained on TAP (Tris-acetate-phosphate) agar plates with a revised mineral element recipe (Kropat et al., 2011), at 22∼24°C and under cool-white fluorescent light (10∼20 μmol photons $m^{-2}s^{-1}$). For phototrophic phenotype comparison, cells were resuspended in TP (Tris-phosphate without acetate) medium, spotted on TAP or TP agar plates and maintained under dark, low light (∼60 μmol photons $m^{-2}s^{-1}$), elevated light (∼700 μmol photons $m^{-2}s^{-1}$) or dark/light (12 h dark/12 h light) diurnal conditions. For photosystem I (PSI) related protein accumulation analyses, cells were grown under similar light conditions as described previously (Wittkopp et al., 2017). Briefly, all strains were grown in TAP medium under ∼30 μmol photons $m^{-2}s^{-1}$ until reaching the mid logarithmic phase, then cells were diluted in TAP medium to a density around ∼1 × 10^6 cells/mL. Half of the cell cultures were grown in the dark for 24 h, while the other half were grown in the dark for 12 h and then exposed to light (∼160 μmol photons $m^{-2}s^{-1}$) for 12 h. Cells were harvested and used for protein extraction.

FDBRs Sequence Alignments

FDBRs protein sequences of *C. reinhardtii* (Cre13.g587100), *Volvox carteri* (Vocar.0001s0011), *A. thaliana* (AT3G09150), *Physcomitrella patens* (Pp3c13_10580V3), *Micromonas pusilla* CCMP1545 (58884) were obtained from Phytozome 12[1]. FDBRs sequences from *Synechococcus* sp. PCC 7002 (GI: 169886494), *Synechocystis* sp. PCC 6803 (GI: 499176294), *Paulinella micropora* (APP88044.1), *Cyanidioschyzon merolae* strain 10D (GI: 544211022), *Gloeochaete wittrockiana* SAG46.84 were based on previous paper (Rockwell et al., 2017). CLUSTAL X[2] and DNAMAN[3] were used for multiple sequence alignments.

Yeast Two-Hybrid Analyses of Protein–Protein Interaction

For autoactivation activity test and cDNA library screening, we followed the instruction of "HybriZAP-2.1 Two-Hybrid Libraries" system (Agilent). Coding regions of CrPCYA1ΔTP (amino acids 56–556), CrPCYA1-NTE (amino acids 56–174), CrPCYA1-FDBR (amino acids 175–451), CrPCYA1-CTE (amino acids 449–556) were amplified by PCR (see **Supplementary Table S1** for primers details) from a Chlamydomonas cDNA library described previously (Wang and Spalding, 2006) and cloned into pBD-GAL4 vector. Transformed YRG2 yeast cells containing respective recombinant constructs were maintained on synthetic dropout plates lacking tryptophan (SD-Trp) or lacking both tryptophan and histidine (SD-Trp-His) for autoactivation test. For cDNA library screening, the bait construct (pBD-CrPCYA1-FDBR) and cDNA plasmids library were sequentially transformed into YRG2 cells. The transformed yeast cells were spreaded on selective SD plates without tryptophan, leucine and histidine (SD-Trp-Leu-His) and incubated at 28°C for 2–4 days until colonies appeared, which were selected as potential interacting candidates.

To confirm the interaction between the bait and putative prey proteins, we used the Matchmaker Gold Yeast Two-Hybrid System (Clontech) following the recommended instruction manual. The coding regions of FDBR (amino acids 175–451) and LPOR (amino acids 35-397) were amplified from pBD-CrPCYA1-FDBR vector and a Chlamydomonas cDNA library, respectively. Coding regions of CHLB/CHLL/CHLN (full length of each gene) were amplified from wild-type 4A+ genomic DNA. An Arabidopsis cDNA library was used to amplify AtHY2ΔTP (amino acids 46–329), AtPORAΔTP (amino acids 54–405), AtPORBΔTP (amino acids 44–401) and AtPORCΔTP (amino acids 67–401). The bait sequences, FDBR and AtHY2ΔTP, were cloned into pGBKT7 vector and introduced into Y2H Gold yeast strain. The prey sequences were cloned into pGADT7 vector and introduced into Y187 yeast cells. To verify the bait-prey interaction, equal amount of Y2H Gold and Y187 cells were mated before spotting on SD/-Trp-Leu, SD/-Trp-Leu-Ade-His and SD/-Trp-Leu plates supplemented with 80 μg/ml β-X-gal (BIOSHARP) and incubated at 28°C for 2–3 days. Interactions of P53 with SV40, and Lam with SV40, were respectively used as positive and negative controls.

Pull-Down Assay

Ferredoxin-dependent biliverdin reductase coding region was PCR-amplified from pGBKT7-FDBR and cloned into pGEX-6P-1 (GE Healthcare Life Sciences) to generate pGEX-6P-FDBR for GST-FDBR fusion protein expression. Similarly, coding region of LPOR was obtained from pGADT7-LPOR by PCR and cloned into vector pMAL-C2X (New England Biolabs) to produce pMAL-C2X-LPOR for expressing MBP-LPOR recombinant protein. These constructs were introduced into *Escherichia coli* BL21 for protein induction with 0.3 mM IPTG (isopropyl β-D-1-thiogalactopyranoside) at 28°C for 4 h. Cells were harvested, rinsed with 1 × PBS (135 mM NaCl, 2.7 mM KCl, 2 mM NaH_2PO_4, and 10 mM Na_2HPO_4, pH 7.4) buffer and disrupted by high pressure homogenization (D-3L; PhD Technology International, MN, United States). Cells were clarified by centrifuging at 10,000 × *g*, 10 min at 4°C and supernatants containing fusion proteins were collected. Equal volume of supernatant containing GST-FDBR or MBP-LPOR were mixed and incubated with MBP beads (New England Biolabs) at 4°C for 1–2 h. After incubation, MBP beads were collected and washed ten times with 1 × PBS buffer to remove unbound proteins, and then boiled with 1 × SDS loading buffer [50 mM Tris–HCl, pH 6.8, 2% (w/v) SDS, 0.1% (w/v) bromophenol blue, 10% (v/v) Glycerol, 1%

[1]https://phytozome.jgi.doe.gov/pz/portal.html

[2]http://www.clustal.org/clustal2/

[3]http://www.lynnon.com/dnaman.html

(v/v) β-mercaptoethanol] for 10 min. The supernatant was then subjected to immunoblot analysis using GST and MBP antibodies.

Split-Luciferase Complementation

The split-luciferase complementation assay was performed based on the previous paper (Chen et al., 2008). Briefly, coding regions of PCYA1 (full-length), FDBR and AtHY2ΔTP were cloned into JW772-cLUC vector, whereas the coding regions of LPOR, CHLB, CHLL, CHLN, AtPORAΔTP, AtPORBΔTP, and AtPORCΔTP were ligated into JW771-nLUC vector. These constructs were introduced into Agrobacterium strain GV3101 by electroporation. Logarithmic phase cells of GV3101 containing respective plasmids were centrifuged at 10,000 × *g* for 5 min, washed twice with ddH_2O, and then resuspended in infiltration buffer (10 mM MES, pH 5.8; 10 mM $MgCl_2$, 150 μM acetosyringone). After 2 h incubation at room temperature, equal amounts of Agrobacteria cells containing JW771- or JW772- vectors were mixed and co-infiltrated into *Nicotiana benthamiana* leaves. After 48 h, tobacco leaves infiltrated with bacteria were sprayed with 1 mM luciferin substrate (Gold Bio) and luminescence signals were acquired by a CCD imaging apparatus (Lumazone Pylon2048B).

Subcellular Fractionation

The cell wall-deficient Chlamydomonas strain CC400 was used to isolate chloroplast soluble fraction, chloroplast envelope and thylakoid membrane. Cells were grown under synchronous condition (12 h light: 12 h dark) in minimal medium until reaching cell density around ∼5 × 10^6 cells/ml. At 4th hour in the light phase, cells were harvested and centrifuged at 4,000 × *g*, 10 min and intact chloroplasts were isolated following the protocol described previously (Mason et al., 2006). Sucrose buffer A (50 mM HEPES-KOH, pH 7.5; 2 mM $MgCl_2$) and sucrose buffer B (50 mM HEPES-KOH, pH 7.5; 10 mM EDTA) were prepared before the following fractionation procedures. The intact chloroplast was resuspended in sucrose buffer A at chlorophyll concentration around 500 mM. The complete lysis was monitored under microscope. Chloroplast suspension was applied on top of a gradient of sucrose buffer A (10 ml of 0.9 M sucrose and 5 ml of 0.6 M sucrose) and centrifuged at 100, 000 × *g* (SW41 Ti rotor) for 1 h. Soluble chloroplast proteins are in the sample zone (top layer, no sucrose). Chloroplast envelope membranes could be recovered as a yellow band at the interface between two sucrose layers, whereas thylakoid membranes became a pellet. Envelope membranes were collected with a Pasteur pipette, diluted with sucrose buffer A and centrifuged at 100,000 × *g* (Ti60 rotor) for 1 h. The chloroplast soluble fraction was further centrifuged at 100,000 × *g* (Ti60 rotor) for 1 h to get rid of any pellet contamination and only kept the supernatant. Thylakoid membranes were resuspended in 1.8 M sucrose buffer B. Layered on top are 1.3, 0.9, and 0.6 M of sucrose buffer B. After centrifuge at 100,000 × *g* (SW41 Ti rotor) for 1 h, purified thylakoid membranes are collected from the interface of 1.8 and 1.3 M sucrose layers. Equal volume of 0 M sucrose buffer B is added to the collected thylakoid membranes and centrifuge at 100,000 × *g* (Ti60 rotor) for 1 h to yield pellet of purified thylakoid membranes. Pelleted envelope membrane and thylakoid membrane were dissolved in SDS sample buffer [50 mM Tris–HCl, pH 6.8; 2% (w/v) SDS]. Chloroplast soluble fraction were precipitated using SDS-methanol-chloroform method as described previously (Duanmu et al., 2013).

DtenPHY1 Expression and Protein Purification

The photosensory core module (PCM) region of *Dolichomastix tenuilepis* phytochrome DtenPHY1 was amplified from pBAD-DtPHYΔL (Duanmu et al., 2014) and ligated into an engineered vector containing the PSAD promoter and a Twin-Strep-tag. The PSAD-DtenPHY1 construct was linearized by KpnI/BamHI double digestion before glass bead transformation into Chlamydomonas wild-type strain CC400. Transgenic cells with highest DtenPHY1 protein expression were cultured in 2 L TAP medium until reaching a density of ∼5 × 10^6 cells/mL under 60 μmol photons $m^{-2}s^{-1}$ fluorescent white light. Cells were centrifuged at 4,000 × *g* for 10 min at 4°C and resuspended in 20 mL lysis buffer (100 mM Tris–HCl, pH 8.0, 150 mM NaCl, 1 mM PMSF, 10 mM β-mercaptoethanol, 1% (v/v) Triton X-100 and 1 mM EDTA). Cells were disrupted by high pressure homogenization (D-3L; Ph.D. Technology International, MN, United States) and then clarified by centrifuge at 4,000 × *g* for 10 min at 4°C. The supernatant was collected and incubated with strep-tag resin (IBA Lifesciences) at 4°C for 2 h. Subsequently, the resin with bound proteins was washed five times with washing buffer (100 mM Tris–HCl, pH 8.0; 150 mM NaCl, 1 mM EDTA). The target protein was eluted from the resin by elution buffer (2.5 mM desthiobiotin in washing buffer) and dialyzed overnight [10% (v/v) glycerol in 1 × PBS buffer]. The purified DtenPHY1 protein was concentrated with Amicon Ultra 15 mL Centrifugal Filters (30,000 MWCO; Millipore). DtenPHY1 protein expressed in *Escherichia coli* LMG194/pPL-PCB was purified as described previously (Duanmu et al., 2014).

Zinc-Dependent Fluorescence Assay

Purified DtenPHY1 protein from Chlamydomonas CC400 cells was incubated with assembly reaction buffer [20 mM TES, pH 8.0; 0.5 mM EDTA, 1 mM TCEP, 20 mM PCB, 20 mM KCl, 8% (v/v) Glycerol] at room temperature for ∼2 h in the darkness. The mixture was added with SDS loading buffer (no boiling), separated by SDS–PAGE and proteins were transferred to PVDF membrane. PVDF membrane was incubated with 1.3 M zinc acetate for at least 1 h at room temperature. Membrane was washed with ddH_2O repeatedly and fluorescence signal was visualized by an Odyssey CLx Infrared Imaging System with 700 nm fluorescence channel (LI-COR). Two-fold serial dilutions of DtenPHY1 protein purified from *E. coli* LMG194/pPL-PCB cells were used as positive controls.

Artificial microRNA-Mediated Gene Silencing

We exploited artificial microRNAs (amiRNAs) to knock-down *PCYA1* gene expression based on previous publications

(Molnar et al., 2009). One amiRNA targeting the first exon of *PCYA1* gene was designed by WMD3[4], with the following sequences: 5′-TCAATTGATTTGGGGATGCTA-3′. Primers for this amiRNA (5′-ctagtTAGCATCCCCAAATCGGTTGAtctcgct gatcggcaccatgggggtggtggtgatcagcgctaTCAATTGATTTGGGGAT GCTAg-3′ and 5′-ctagcTAGCATCCCCAAATCAATTGAtagcgct gatcaccaccacccccatggtgccgatcagcgagaTCAACCGATTTGGGGAT GCTAa-3′) were annealed by boiling at 100°C and cooled gradually overnight, and then cloned into pChlamiRNA3int vector predigested by SpeI to generate the final construct pChlamiRNA3int-CrPCYA1. The linearized plasmid by KpnI and NotI double digestion was transformed into wild-type strain 4A+ via electroporation (BTX Gemini X2 System, 800 V voltage, 1575 Ω resistance and 50 μF capacitance, 10.0 s pulses interval) and transgenic colonies were selected on TAP agar plates supplemented with 20 μg/mL paromomycin under constant low light (∼30 μmol photons $m^{-2}s^{-1}$).

Protein Extraction and Immunoblot Analysis

Total protein extraction and immunoblot analyses were performed as described previously (Duanmu et al., 2013). Antibodies against GST-tag (66001-I-1g, anti-mouse, 1:2000 dilution) and MBP-tag (66003-I-1g anti-mouse, 1:2000 dilution) were purchased from Proteintech. Antibodies against CrPCYA1 and CrHMOX1 (anti-rabbit, 1:1000 dilution) were generated previously (Duanmu et al., 2013). Antibodies against LHCA1 (AS01 005, anti-rabbit, 1:10000 dilution), PSAD (AS09 461, anti-rabbit, 1:5000 dilution) and PsaA (AS06 172, anti-rabbit, 1:5000 dilution) were purchased from Agrisera. Strep tag antibody (A00626-40, anti-rabbit, 1:4000 dilution) was purchased from GenScript. Antibodies against Actin and Tic40 were from Professor Steven M. Theg (Plant Biology Department, University of California Davis, Davis, CA, United States). The secondary antibody conjugated to horseradish peroxidase (CWBio, CW0102S, goat anti-mouse IgG; or CW0103S, goat anti-rabbit IgG) was used (1:10000 dilution) with the enhanced chemiluminescence detection kit (Bio-Rad, Clarity Western ECL Substrate) for signal acquisition.

Total RNA Isolation and 3′ RACE

Total RNA from *pcya1-1* was extracted using TransZol plant kit (ET121, Transgen) following the instruction of the kit. RACE (rapid amplification of cDNA ends) was used to amplify the 3′ end cDNA of *pcya1-1* mutant to verify the reading frame of the truncated PCYA1 in *pcya1-1* (Scotto-Lavino et al., 2006). The reverse transcription reaction consisted of 2 μL 5 × reverse transcriptase M-MLV buffer, 0.5 μL reverse transcriptase M-MLV (SD4040, Takara), 0.5 μL Qt primer, 0.5 μL 2.5 mM dNTPs, 0.1 μL RNase inhibitor (SD0316, Takara) and 6.4 μL ddH_2O (RNase-free) in a total volume of 10 μL. The reaction was incubated at 42°C for 1 h, and the reverse transcriptase M-MLV was inactivated at 75°C for 10 min. The product of reverse transcription reaction was used as template for the first-round amplification using Qo and PCYA1-GSP1 primer pairs. The product of the first-round amplification was subsequently used as template for the second-round amplification using Qi and PCYA1-GSP2 primer pairs. The final product was sequenced using PCYA1-GSP2.

[4]http://wmd3.weigelworld.org

RESULTS

Chlamydomonas PCYA1 Contains Unique N-Terminal and C-Terminal Extensions That Exhibit Autoactivation Activity in Yeast Two-Hybrid System

CrPCYA1 is a key enzyme involved in bilin biosynthesis in Chlamydomonas (Duanmu et al., 2013). Besides the putative chloroplast transit peptide (TP) and the conserved ferredoxin-dependent biliverdin reductase (FDBR) domain, Chlamydomonas CrPCYA1 contains additional N-terminal extension (NTE) and C-terminal extension (CTE), approximately 120 and 108 amino acids, respectively (**Figure 1A**). It has been well established that FDBR is essential for bilin production in oxygenic photosynthetic organisms (Dammeyer and Frankenberg-Dinkel, 2008). However, there are no reports about the function of additional domains besides FDBR. Compared to homologous sequences of other species including plants, prasinophyte, rhodophyte, glaucophyte and cyanobacteria, the NTE and CTE domains are only found in another chlorophyte alga *V. carteri*, the closest relative of Chlamydomonas. Interestingly, another prasinophyte alga *Micromonas pusilla* CCMP1545 only possesses the CTE domain (**Supplementary Figure S1**). Notably, both NTE and CTE domains of CrPCYA1 exhibited autoactivation activity in yeast, whereas the FDBR domain cannot activate His gene expression (**Figure 1B**).

Chlamydomonas PCYA1 FDBR Interacts With LPOR but Not DPOR

To identify putative PCYA1-interacting proteins, FDBR domain was used as the bait to screen a Chlamydomonas cDNA library and a potential FDBR-interacting protein. Light-dependent NADPH:protochlorophyllide oxidoreductase (LPOR, Cre01.g015350) was thus identified (**Figure 2A**). LPOR is responsible for catalyzing the reaction of protochlorophyllide (PChlide) to chlorophyllide (Chlide), an essential step of chlorophyll biosynthesis (Gabruk and Mysliwa-Kurdziel, 2015). To further verify the interaction between FDBR and LPOR, pull down assay was performed by respective expression of the two proteins as GST-FDBR and MBP-LPOR fusion proteins in *E. coli*. MBP resin was used to capture the MBP tag and associated proteins. We observed that GST-FDBR, but not GST tag, was captured by MBP-LPOR, suggesting the interaction between FDBR and LPOR *in vitro* (**Figure 2B**). Moreover, split luciferase complementation assay identified strong luminescence from *Nicotiana benthamiana* leaves inoculated simultaneously with cLUC-PCYA1 and nLUC-LPOR (**Figure 2C**).

Distinct from higher plants, Chlamydomonas also contains a dark-operative protochlorophyllide oxidoreductase (DPOR) that consists of three chloroplast genes: *ChlB*, *ChlL* and *ChlN*

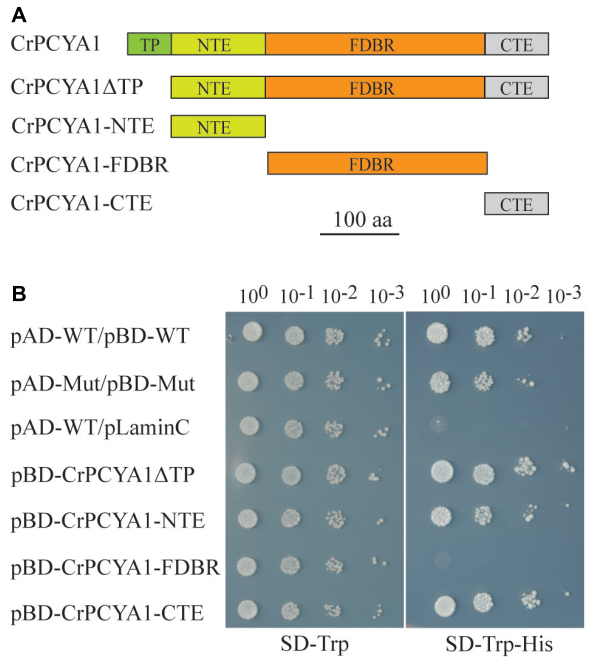

FIGURE 1 | Autoactivation activity test of Chlamydomonas CrPCYA1 protein in yeast. **(A)** Illustration of CrPCYA1 domains and CrPCYA1 truncated proteins used as baits for yeast two hybrid experiment. TP, putative chloroplast transit peptide; NTE, N-terminal extension; FDBR, ferredoxin-dependent biliverdin reductase; CTE, C-terminal extension. **(B)** Growth of yeast cells on synthetic dropout (SD) plates. The coding regions of CrPCYA1 truncated proteins were ligated into pBD-GAL4 vector and transformed into YRG2 yeast strain. Yeast cells were spotted onto SD-Trp and SD-Trp-His agar plates with 10-fold serial dilutions. pAD-WT/pBD-WT and pAD-Mut/pBD-Mut were used as positive controls, and pAD-WT/pLaminC was used as a negative control. WT, Wild-type fragment C of lambda cI repressor (aa 132–236); Mut, E233K mutated fragment of lambda cI repressor (aa 132–236); LaminC, human lamin C (aa 67–230).

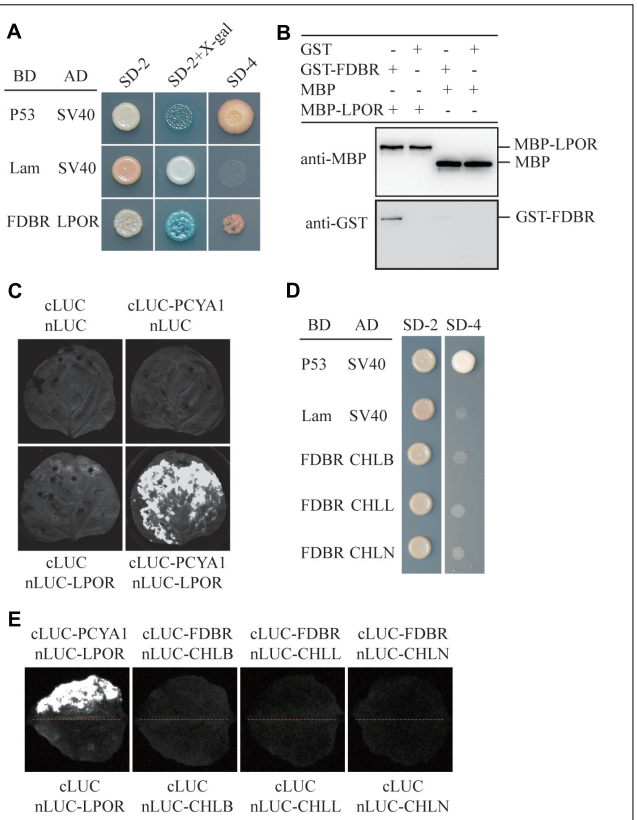

FIGURE 2 | CrPCYA1 FDBR domain interacts with LPOR, but not with DPOR *in vitro* and *in planta*. **(A)** Yeast two-hybrid assay of the interaction between FDBR and LPOR. P53 and SV40 were used as a pair of positive control. Lam and SV40 were used as a negative control. SD-2, SD-Trp-Leu; SD-2+X-gal, SD-Trp-Leu medium supplemented with X-β-gal (80 μg/ml); SD-4, SD-Trp-Leu-His-Ade. **(B)** Pull-down assay for the interaction of FDBR with LPOR *in vitro*. MBP-fusion protein and GST-fusion protein were co-incubated with MBP resin. After washing, proteins captured by MBP resin were analyzed. Antibodies against GST-tag and MBP-tag were used for immunoblotting analysis. **(C)** Split-luciferase assay by co-expression of cLUC-PCYA1 and nLUC-LPOR in tobacco leaves. cLUC and nLUC were used as a negative control. Images were taken at 48 h after infiltration. The strong luminescence signal indicates interaction between PCYA1 and LPOR *in planta*. **(D)** Yeast two-hybrid assay of the interaction between FDBR and three subunits of DPOR: CHLB, CHLL and CHLN. **(E)** Split-luciferase assay for the interaction of FDBR with CHLB, CHLL and CHLN. Co-expression of cLUC and nLUC, cLUC-FDBR and nLUC, cLUC and nLUC-CHLB/L/N in tobacco leaves were used as negative controls. Co-expression of cLUC-PCYA1 and nLUC-LPOR was used as a positive control.

(Gabruk and Mysliwa-Kurdziel, 2015). To investigate whether FDBR interacts with DPOR, we cloned the three subunit genes into pGADT7- or nLuc- vectors. Both yeast two-hybrid and split luciferase complementation assay were unable to detect interaction between FDBR and CHLB, CHLL or CHLN (**Figures 2D,E**). These data suggest that PCYA1 may specifically regulate the biosynthesis of Chl by interacting with LPOR, but not DPOR in Chlamydomonas.

Arabidopsis FDBR Homologous Protein HY2 Does Not Interact With PORs

To evaluate whether the interaction between FDBR and LPOR is unique in Chlamydomonas or conserved also in higher plants, we analyzed their homologous proteins in Arabidopsis. As reported previously, the FDBR in Arabidopsis is encoded by the *HY2* locus and responsible for phytochromobilin biosynthesis from biliverdin IXα (Kohchi et al., 2001). Unlike Chlamydomonas, Arabidopsis lacks DPOR but contains three POR isoenzymes encoded by nuclear genes *PORA*, *PORB,* and *PORC,* respectively (Gabruk and Mysliwa-Kurdziel, 2015). Chloroplast transit peptides of these four proteins were removed and AtHY2 with AtPORA, AtPORB or AtPORC were co-expressed in yeast cells or tobacco leaves. Our data from Y2H and split luciferase assay indicate no interactions between HY2 and PORs in Arabidopsis (**Figures 3A,B**), further underscoring the specific interaction between FDBR and LPOR in Chlamydomonas.

PCYA1 Is Partially Associated With Chloroplast Envelope Membrane

Previous research has shown that both HMOX1 and PCYA1 are localized to chloroplast. HMOX1 is a soluble protein,

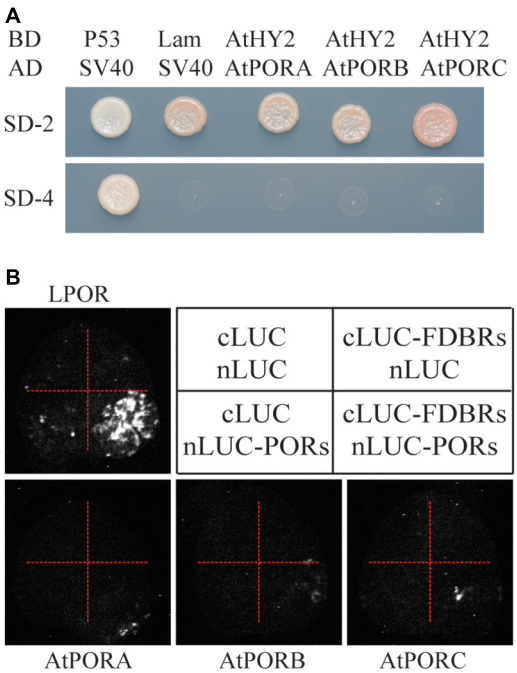

FIGURE 3 | Arabidopsis FDBR protein AtHY2 does not interact with Arabidopsis PORs. **(A)** Yeast two-hybrid assay for the interaction of AtHY2 with AtPORA, AtPORB and AtPORC. Putative chloroplast transit peptides of these chloroplast-localized proteins were removed. **(B)** Split-luciferase assay for the interaction of AtHY2 with AtPORA, AtPORB, and AtPORC (lower three images). Co-expression of cLUC and nLUC, cLUC-AtHY2 and nLUC, cLUC and nLUC-AtPORA/AtPORB/AtPORC in tobacco leaves were used as negative controls. Co-expression of cLUC-PCYA1 and nLUC-LPOR was used as a positive control (upper image).

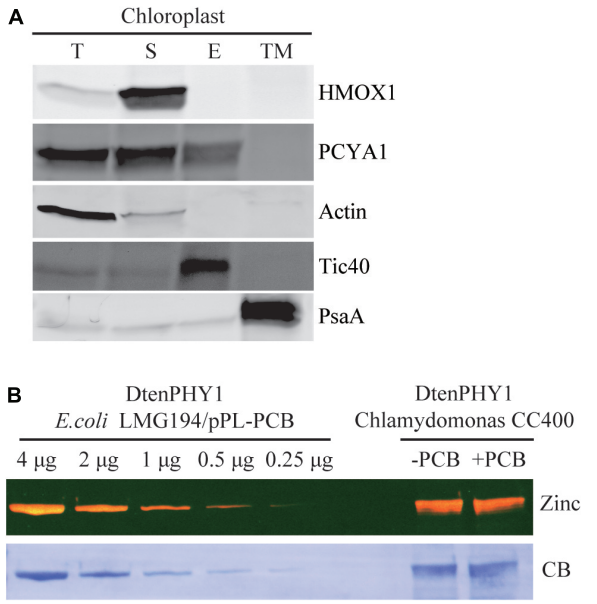

FIGURE 4 | Subcellular distribution of CrPCYA1 in chloroplast and the export of phycocyanobilin to cytosol. **(A)** Biochemical fractionation of chloroplast components. Antibodies against compartmental marker proteins distributed in different chloroplast fractions were employed to distinguish the presence of CrPCYA1 via immunoblot analysis of total proteins (T), soluble fraction (S), envelope membrane (E) and thylakoid membrane (TM) from isolated chloroplast. Tic40, chloroplast envelope marker; PsaA, thylakoid membrane marker. **(B)** Zinc-dependent fluorescence assay. Photosensory core module (PCM) region of the prasinophyte algal DtenPHY1 purified from Chlamydomonas CC400 covalently binds phycocyanobilin (PCB). Upper panel, zinc blot; lower panel, Coomassie blue stain (CB). The two-fold serial dilutions of *E. coli* LMG194/pPL-PCB expressed and purified DtenPHY1 were used as positive controls. –PCB, without addition of PCB; +PCB, assembly with PCB in *vitro*.

whereas PCYA1 is partially associated with membrane fraction (Duanmu et al., 2013). To determine with which specific membrane fraction PCYA1 is associated, intact chloroplasts of Chlamydomonas cell wall deficient strain CC400 were isolated and further separated into soluble fraction, chloroplast envelope and thylakoid membrane. Immunoblot analyses using envelope membrane marker protein Tic40 and thylakoid membrane marker PsaA indicate the high quality and free of cross-contamination of these two membrane fractions (**Figure 4A**). Consistent with previous observations, HMOX1 was totally soluble and absent from the membrane fractions and majority of PCYA1 was enriched in stromal fraction (Duanmu et al., 2013). However, a small fraction of PCYA1 was also found in chloroplast envelope but none was associated with thylakoid membrane. These data suggest that PCYA1 is dually localized in chloroplast stroma as well as the envelope membrane (**Figure 4A**).

Phycocyanobilin Is Exported to the Cytosol in Chlamydomonas

Biosynthesis of phycocyanobilin (PCB) in Chlamydomonas has been well established by expression and purification of a cyanobacterial GAF (cGMP-specific phosphodiesterases, adenylyl cyclases and formate hydrogen lyase) domain as the bilin-binding reporter (Duanmu et al., 2013). Since translocation out of the chloroplast is an essential character of *bona fide* chloroplast retrograde signaling molecules, we expressed another bilin-binding protein, the photosensory core module (PCM) of a phytochrome from the marine alga *Dolichomastix tenuilepis* (DtenPHY1) as described previously (Duanmu et al., 2014), in the cytosol of Chlamydomonas wild-type strain CC400. The purified protein exhibits strong fluorescence signal by zinc-dependent assay, comparable to the DtenPHY1 purified from *E. coli* LMG194 engineered to produce PCB cofactor, indicating presence of the covalently bound bilin chromophore of the heterologously expressed protein (**Figure 4B**). Thus, PCB is able to be exported to the cytosol in Chlamydomonas.

CTE Domain of PCYA1 Is Dispensable for Phototrophic Growth and Photosynthetic Proteins Accumulation

Previous results have shown that blocking of bilin biosynthesis in the *hmox1* mutant, or diverging of bilin biosynthesis by chloroplast expression of a mammalian biliverdin reductase both resulted in phototrophic growth deficiency under

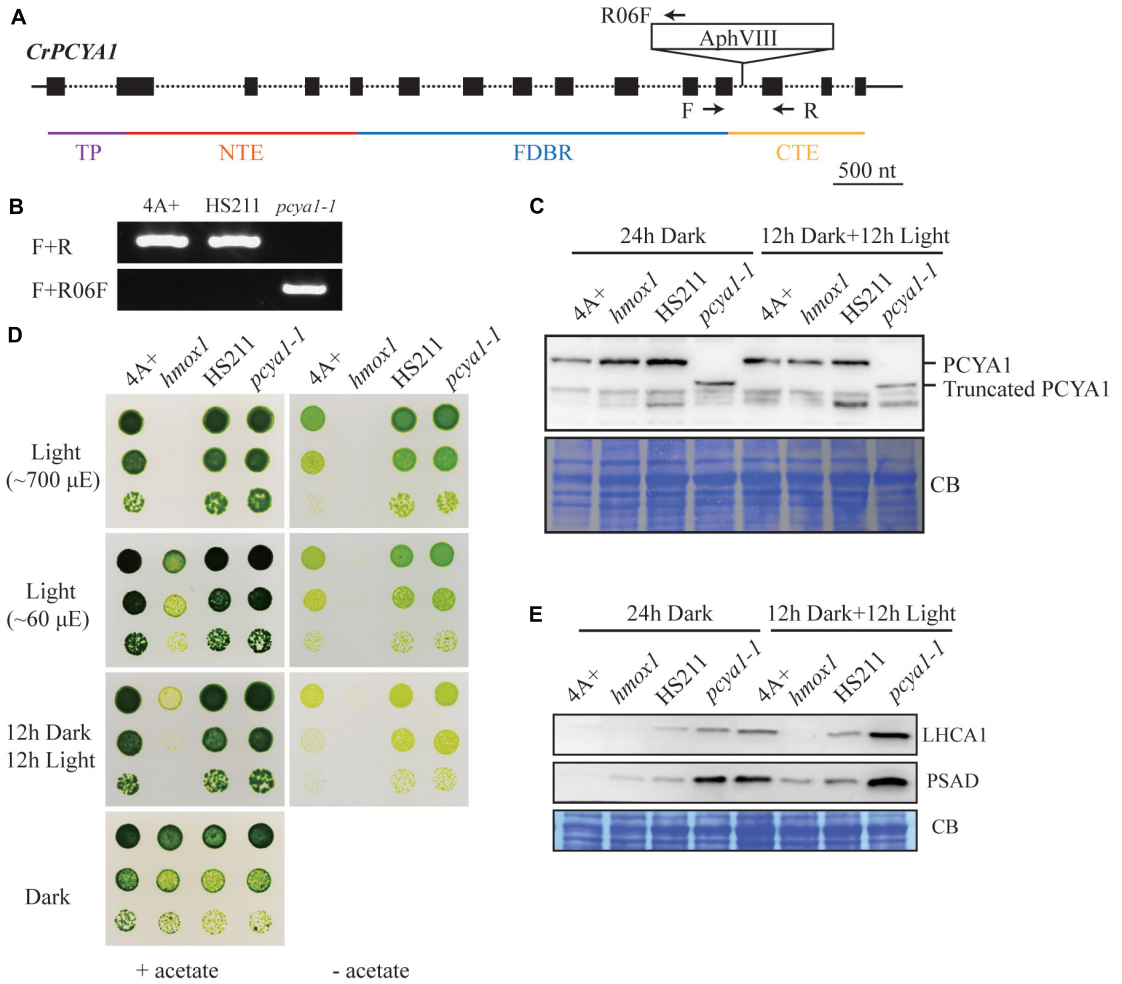

FIGURE 5 | Characterization of the CTE-disrupted *pcya1-1* mutant. **(A)** Schematic diagram of an AphVIII insertion cassette into the *PCYA1* locus in the *pcya1-1* mutant. Black solid line represents 5′UTR and 3′UTR; black dotted line symbolizes intron; black box stands for exon and black arrows indicate the targeting sites of PCR primers. Purple, red, blue, and orange solid lines represent TP, NTE, FDBR and CTE regions of PCYA1, respectively. **(B)** PCR confirmation of the AphVIII insertion in *pcya1-1*. Genomic DNA was extracted from 4A+, HS211 and *pcya1-1*, respectively. PCR were performed using primers depicted in **(A)**. HS211, the parental strain of *pcya1-1*. **(C)** Detection of CrPCYA1 expression in the dark or under light (~160 μmol photons $m^{-2}s^{-1}$). Upper, immunoblot analysis of CrPCYA1 protein accumulation using antibody against CrPCYA1 mature protein; lower, Coomassie blue stain as an equal loading control. **(D)** Comparison of phototrophic growth phenotypes of *pcya1-1* with 4A+, *hmox1* and HS211 under constant low light (~60 μmol photons $m^{-2}s^{-1}$), high light (~700 μmol photons $m^{-2}s^{-1}$) and 12 h dark/12 h light cycle. **(E)** Accumulation of the photosystem I related proteins in *pcya1-1*, 4A+, HS211 and *hmox1* in the dark or under light (~160 μmol photons $m^{-2}s^{-1}$). Immunoblot analyses were performed with LHCA1 and PSAD antibodies. Coomassie blue stain (CB) as an equal loading control. Approximately 30 μg total proteins were loaded in each lane.

light (Duanmu et al., 2013). One recently published paper further suggests that accumulation of photosynthetic proteins, especially PSI and LHCI, are drastically affected in the *hmox1* mutant (Wittkopp et al., 2017). Since HMOX1 and PCYA1 are involved in sequential conversion of heme to BV, and then to bilin, we attempted to isolate *PCYA1* mutants and characterize their phenotype. Indeed, we found 2 putative *pcya1* insertional mutants in the Chlamydomonas Stock Center (LMJ.SG0182.002607 and LMJ.RY0402.076336). However, immunoblot analyses indicate none of them have the *PCYA1* disrupted (data not shown). Instead, we obtained an insertional mutant of *PCYA1*, marked as *pcya1-1* from a recently released mutant library containing ~150,000 insertional mutants (Cheng et al., 2017). The AphVIII insertion cassette in *pcya1-1* mutant is in the 12th intron of *PCYA1* locus (**Figure 5A**) and this insertion was confirmed by genomic DNA extraction and PCR using gene and plasmid insert specific primers (**Figure 5B**). Immunoblotting analysis demonstrates that *pcya1-1* harbors a truncated PCYA1 protein as a result of the eliminated CTE domain (**Figure 5C**). 3′RACE and sequencing results further confirmed the modified reading frame of the truncated PCYA1 protein with CTE disrupted in *pcya1-1* mutant (**Supplementary Table S2**).

To assess the photosynthetic phenotype of *pcya1-1*, we examined the photoautotrophic growth of this mutant under constant low light (~60 μmol photons $m^{-2}s^{-1}$), constant high

light (~700 μmol photons $m^{-2}s^{-1}$) and light/dark diurnal cycle conditions. In all experimental settings, phototrophic growth of *pcya1-1* is similar to its parental strain HS211 and the wild-type 4A+, whereas *hmox1* mutant exhibits a photosynthetic deficiency phenotype as reported before (**Figure 5D**) (Duanmu et al., 2013; Wittkopp et al., 2017). Consistently, the Chl *a/b* ratios of *pcya1-1* mutant were similar as its parental strain HS211, whereas the Chl *a/b* ratio of *hmox1* was dramatically decreased under photoautotrophic growth conditions (**Supplementary Figure S2**).

As recently reported, the *hmox1* mutant displays a reduced PSI activity, due to the dramatically reduced or no accumulation of PSI related proteins such as PSAD and LHCA1 during dark to light transitions (Wittkopp et al., 2017). To evaluate the accumulation of these marker proteins, 4A+, HS211, *hmox1* and *pcya1-1* cells were cultured under similar conditions (24 h Dark or 12 h dark followed by 12 h illumination under ~160 μmol photons $m^{-2}s^{-1}$) as described previously (Wittkopp et al., 2017). Total proteins of all strains from above cultures were extracted and subjected to immunoblot analyses. Consistent with previous observations, the LHCA1 protein accumulation in *hmox1* is undetectable and PSAD is drastically reduced relative to 4A+. Compared to the lower-level accumulation of LHCA1 and PSAD in 4A+, HS211 and *pcya1* after 24 h dark acclimation, the illuminated cells demonstrate an obviously increased abundance of these two proteins (**Figure 5E**). Moreover, *pcya1-1* exhibits a higher-level of these PSI marker proteins than HS211 or 4A+ under those two conditions (**Figure 5E**). These results indicate that the CTE domain of PCYA1 is not required for accumulation of representative photosynthetic proteins and phototrophic growth of Chlamydomonas.

Efficient *PCYA1* Knockdown by Artificial microRNA Does Not Impact Algal Phototrophic Growth

Artificial microRNA-mediated gene silencing has been successfully used to inhibit gene expression and for functional analysis in Chlamydomonas (Vidal-Meireles et al., 2017). Since we have not been able to identify loss-of-function mutants of *PCYA1* based on several available mutant libraries, we attempted to generate *PCYA1* knockdown mutants by the artificial microRNA methodology (Molnar et al., 2009). AmiRNAs for *PCYA1* were designed based on WMD3 tool[5]. One appropriate amiRNA targeting first exon of *PCYA1* gene was selected, constructed into the amiRNA vector and used to transform the wild-type strain 4A+.

Several transgenic lines with significantly reduced PCYA1 protein accumulation were isolated, with the protein abundance ranging ~30–40% of WT level in lines 14, 21, and 46, compared to the near WT level of lines 34 and 35 that were included as controls (**Figure 6A**). Photoautotrophic growth of lines 14, 21, and 46 under different light conditions is indistinguishable from 4A+ WT cells (**Figure 6B**). Examination of LHCA1 and PSAD accumulation also indicates no decrease of these proteins in the amiRNAi lines (**Figure 6C**). The observed higher abundance of LHCA1 and PSAD proteins in line 14 may result from unknown mutations due to the random insertion of the construct. Nonetheless, these results reveal that residual amount of PCYA1 protein is still sufficient to support the photosynthetic proteins accumulation and phototrophic growth of Chlamydomonas.

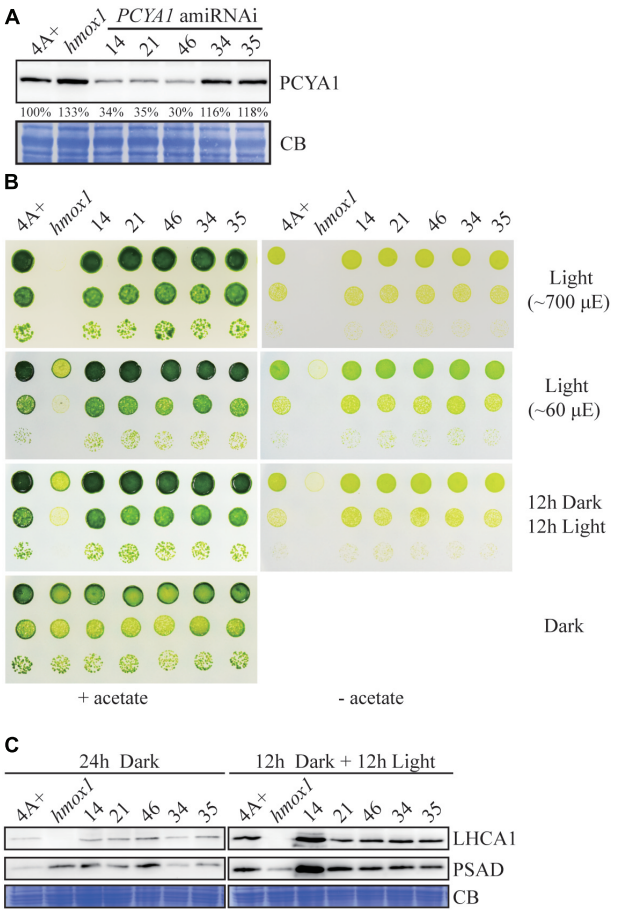

FIGURE 6 | *PCYA1* knockdown by artificial microRNA. **(A)** Analysis of CrPCYA1 protein accumulation in artificial microRNA-mediated *PCYA1* knockdown lines. **(B)** Phototrophic growth of *PCYA1* knockdown mutants were compared with 4A+ and *hmox1* under constant low light, high light and dark/light cycle. Low light, ~60 μmol photons $m^{-2}s^{-1}$; High light, ~700 μmol photons $m^{-2}s^{-1}$. **(C)** Accumulation of representative photosystem I related proteins in *PCYA1* knockdown mutants, 4A+ and *hmox1* in the dark or under light (~160 μmol photons $m^{-2}s^{-1}$). LHCA1 and PSAD antibodies were used for immunoblotting analyses. Around 30 μg total proteins were loaded in each lane.

DISCUSSION

Chlorophyll biosynthesis is under elaborate control to minimize accumulation of highly phototoxic porphyrin intermediates (Bröcker et al., 2012; Wang and Grimm, 2015). One rate-limiting step of Chl branch is the conversion from PChlide to Chlide that

[5]http://wmd3.weigelworld.org/cgi-bin/webapp.cgi

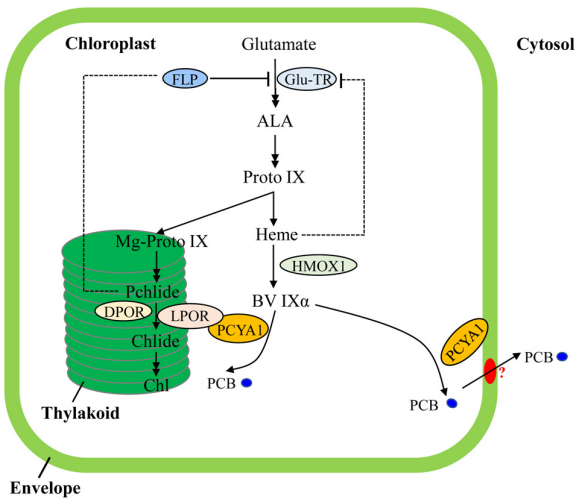

FIGURE 7 | Schematic illustration of tetrapyrrole pathway and regulatory mechanisms of tetrapyrrole biosynthesis in *C. reinhardtii*. FLP is a negative regulator of Glu-TR activity. Heme may also feedback inhibit Glu-TR activity, but to a lesser extent. PCYA1 is likely involved in regulation of Chl biosynthesis by direct interaction with LPOR. Additionally, the PCB molecule is exported from chloroplast to cytosol, via yet-to-be identified bilin transporter (red oval). ALA, 5-Aminolevulinic acid; Proto IX, protoporphyrin IX; Mg-Proto IX, magnesium-protoporphyrin IX; Pchlide, protochlorophyllide; Chlide, chlorophyllide; Chl, chlorophyll; BV IXα, biliverdin IXα; PCB, phycocyanobilin; Glu-TR, Glutamyl-tRNA reductase; HMOX1, heme oxygenase 1; PCYA1, phycocyanobilin ferredoxin-dependent biliverdin oxidoreductase; LPOR, light-dependent protochlorophyllide oxidoreductase; DPOR, light-independent protochlorophyllide oxidoreductase.

is catalyzed by PORs (Reinbothe et al., 2010). Two types of PORs, namely LPOR and DPOR with distinct evolutionary origin, are found in photosynthetic organisms (Hunsperger et al., 2015). LPOR is light-inducible and present in oxygenic phototrophs, whereas the dark-operative and light-inhibitory DPOR is oxygen-sensitive and encoded by chloroplast genome, and arises from anoxygenic phototrophs (Gabruk and Mysliwa-Kurdziel, 2015; Hunsperger et al., 2015). Apparently DPOR is gradually lost during evolution, since all flowering angiosperm plants do not contain the homologs and thus cannot synthesize Chl in the dark (Hunsperger et al., 2015). In this study, the observed interaction of Chlamydomonas PCYA1 with LPOR, but not with DPOR, is consistent with the hypothesized function of bilin biosynthesis in the regulation of Chl biosynthesis under light, but not in the dark, since the *hmox1* mutant or BVR overexpression lines do not exhibit Chl deficiency phenotype in the dark (Duanmu et al., 2013; Wittkopp et al., 2017).

Transcriptional regulation of PORs is mainly mediated by phytohormones (ethylene, gibberellin) and light in plants (Masuda and Takamiya, 2004; Gabruk and Mysliwa-Kurdziel, 2015). Chl biosynthesis could be also feedback regulated by heme in Arabidopsis (Terry and Smith, 2013). In contrast, transcriptomic analyses of Chlamydomonas bilin biosynthesis deficient *hmox1* mutant and *in vitro* BV feeding have shown that LPOR transcript abundance remains unchanged and heme inhibition is not the main cause for Chl deficiency (**Figure 7**), indicating distinct types of tetrapyrrole/chlorophyll biosynthesis regulation in chlorophyte algae compared with land plants (Duanmu et al., 2013; Rochaix, 2013; Wittkopp et al., 2017).

Notably, Arabidopsis employs FLU and Chlamydomonas employs FLP (FLU-like protein) as negative feedback regulators to inhibit enzymatic activity of glutamyl-tRNA reductase (GluTR), which is essential for the synthesis of the committed precursor ALA (Meskauskiene et al., 2001; Falciatore et al., 2005). In Arabidopsis, the FLU protein complex containing CHL27 and two PORs isoenzymes (PORB and PORC) can interact with GluTR after PChlide binding to PORs in the dark, resulting in inhibition of Chl biosynthesis (Kauss et al., 2012). Similarly, Chlamydomonas FLP protein also interacts with GluTR and represses Chl biosynthesis (Falciatore et al., 2005). It has not been investigated whether or not Chlamydomonas FLP interacts with LPOR. Since the dark-adapted Chlamydomonas cells should theoretically contain much lower level of PChlide due to a functional DPOR, it is reasonable to hypothesize that the observed PCYA1-LPOR interaction may contribute significantly to the regulation of Chl biosynthesis in the light, or during diurnal transition from dark to light. However, further research should be conducted to investigate whether the PCYA1-LPOR interaction and the bilin or PChlide molecules are also involved in FLP-dependent regulation of GluTR activity in Chlamydomonas. Additionally, it was proposed that LPOR adopts a structure to quench singlet oxygen and the triplet states of PChlide (Reinbothe et al., 2010). It would thus be interesting to test if PCYA1 and bilins are involved in this reaction.

As one of the few enzymes that require light for activation, largely due to the need for its substrate PChlide to absorb light and induce catalytic activity of the POR enzyme, the quantum yields of red light has been shown to be 3∼7 times more effective than blue light in the photoconversion of Pchlide to Chlide for plant POR enzymes (Hanf et al., 2012; Gabruk and Mysliwa-Kurdziel, 2015). Since the longer wavelength light, i.e., red light, is significantly attenuated in water column, more abundant blue or even shorter wavelength light could be more efficiently perceived by aquatic algae for light sensing and photoacclimation (Duanmu et al., 2014; Rockwell et al., 2014a; Wittkopp et al., 2017). In this regard, bilin-dependent blue light-regulated photosensory systems were proposed to regulate photosystem cofactors biosynthesis (i.e., Chl and naphthoquinone) and PSI/LHCI protein accumulation in Chlamydomonas (Wittkopp et al., 2017). PCYA1 with the associated enzymatic product, PCB, may also constitute an essential part of these systems and can significantly enhance LPOR activity under blue light (**Figure 7**). The transcriptional control is essential for long-term regulation of tetrapyrrole/Chl biosynthetic genes. In contrast, this type of post-translational regulatory mechanisms could enable a rapid response during dark/light transitions that accurately balance the enzymatic activities and orchestrate the flow of metabolites for photoacclimation (Czarnecki and Grimm, 2012; Duanmu et al., 2017).

Bilins have been hypothesized to play at least two types of complementary functions in Chlamydomonas, i.e., as

chromophore cofactor of putative chlorochrome in the chloroplast to sustain a robust photosynthesis and as retrograde signals to detoxify ROS during dark-to-light transition (Duanmu et al., 2017). The observed subcellular distribution pattern of bilin biosynthetic enzyme PCYA1 is consistent with the dual functions of bilins in Chlamydomonas. Chloroplast envelope associated PCYA1 may support efficient translocation of PCB to the cytosol by interacting with unknown bilin-transporters (Duanmu et al., 2017). Previous studies of oat seedlings also observed the association of FDBR with membrane fraction, congruent with the necessity of bilin export to the cytosol and assembly with apo-phytochromes in plants (McDowell and Lagarias, 2001). Since Chlamydomonas PCYA1 contains unique NTE and CTE that are absent from plant homologs, the NTE and CTE domains may thus not be essential for membrane association. Chl accumulation and phototrophic growth of the *pcya1-1* mutant with CTE disrupted is indistinguishable from wild-type strain, further calling into question the biological functions of this extra domain in Chlamydomonas.

Both the CTE-disrupted *pcya1-1* mutant and knock-down RNAi lines exhibit no obvious defects on phototrophic growth and photosynthetic proteins accumulation. An explanation for the indistinguishable phenotypes of these mutants is that the core FDBR domain in *pcya1-1* mutant and the residual amount of PCYA1 protein in RNAi lines are still sufficient to sustain bilin biosynthesis and maintain the biological functions. The inability to obtain a *pcya1* null mutant may underscore the indispensable roles of this enzyme in Chlamydomonas. Indeed, investigations of *PCYA* in cyanobacterium *Synechococcus sp*. strain PCC 7002 demonstrated that this gene was unable to be inactivated in wild-type cells, but could be easily disrupted after introducing the Arabidopsis phytochromobilin synthase HY2 into the cell, indicating the requirements of PCYA and/or the bilins for cell survival (Alvey et al., 2011).

CONCLUSION

In conclusion, the discovery reported in this study has provided novel insights into the multifaceted biological functions of bilins and bilin biosynthetic enzyme in Chlamydomonas. However, many questions still remain to be answered. Are the interactions between PCYA1 and LPOR dynamically regulated in the dark versus under light? What are the biological roles of bilins and PChlide in fine-tuning this interaction and regulating LPOR activity, and whether or not this type of post-translational regulation of Chl biosynthesis is conserved in all DPOR-containing or phytochrome-less phototrophs, including eukaryotic green/red algae and gymnosperms? Construction and characterization of *pcya1* mutants with NTE deletion or the whole gene disrupted by either random mutagenesis or by recently established CRISPR technology in Chlamydomonas (Ferenczi et al., 2017; Greiner et al., 2017) should be able to greatly deepen our understanding of the bilin-mediated tetrapyrrole/Chl biosynthetic regulation and photoacclimation in chlorophyte algae and other photosynthetic organisms.

AUTHOR CONTRIBUTIONS

WZ and DD designed the research and analyzed the results. WZ, HZ, and HL performed the experiments. XD and KH constructed and analyzed the mutant library. WZ, HZ, and DD wrote the paper. All the authors read and approved the manuscript.

FUNDING

Research in the Duanmu laboratory was supported by the National Natural Science Foundation of China (Grant No. 31570233), Huazhong Agricultural University Scientific and Technological Self-innovation Foundation (Program No. 2014RC018), and the Fundamental Research Funds for the Central Universities (Program No. 2662015PY171).

ACKNOWLEDGMENTS

Chlamydomonas *pcya1-1* mutant was obtained from Professor Kaiyao Huang (Institute of Hydrobiology, Chinese Academy of Sciences). Arabidopsis cDNA library was obtained from Dr. Lili Wang and split-luc experiment was performed with the help of Dr. Lili Wang (College of Life Science and Technology, Huazhong Agricultural University). Antibodies against Actin and Tic40 were gifts from Professor Steven M. Theg (Plant Biology Department, University of California Davis). We also thank Professor J. Clark Lagarias (University of California Davis) for technical comments of the experiments involved in this study.

SUPPLEMENTARY MATERIAL

The Supplementary Material for this article can be found online at: https://www.frontiersin.org/articles/10.3389/fpls.2018.00676/full#supplementary-material

FIGURE S1 | Multiple sequence alignments of FDBRs. CLUSTAL X and DNAMAN tools were used for the alignments. Consensus sequences were marked as lowercase letters. The black, pink and cyan bars indicate 100%, ≥ 75% and ≥ 50% sequence similarity, respectively. The overline regions with purple, red, blue and green solid lines represent TP, NTE, FDBR, and CTE domains of PCYA1 in Chlamydomonas, respectively. Cre, *C. reinhardtii*; Vca, *V. carteri*; Ath, *A. thaliana*; Ppa, *Physcomitrella patens*; Syn7002, *Synechococcus sp.* PCC 7002; Syn6803, *Synechocystis sp.* PCC 6803; Pmi, *Paulinella micropora;* Mpu, *Micromonas pusilla* CCMP1545; Cme, *Cyanidioschyzon merolae* strain 10D; Glo, *Gloeochaete wittrockiana* SAG46.84.

FIGURE S2 | Comparisons of Chl *a/b* ratios in 4A+, *hmox1*, HS211 and *pcya1-1*. These strains were grown under constant light (∼160 μE) with (black bar) or without acetate (gray bar). Data show means of three biological replicates ± SD.

TABLE S1 | Primers used in this study.

TABLE S2 | The amino acid sequences of PCYA1 in wild-type Chlamydomonas and *pcya1-1* mutant. Yellow letters represent the putative chloroplast transit peptide (TP); Red letters, the N-terminal extension (NTE); Cyan letters, the FDBR domain; Green letters, C-terminal extension (CTE). The mutated amino acid sequence of CTE in *pcya1-1* mutant was marked as gray letters.

REFERENCES

Alvey, R. M., Biswas, A., Schluchter, W. M., and Bryant, D. A. (2011). Effects of modified phycobilin biosynthesis in the cyanobacterium *Synechococcus* sp. strain PCC 7002. *J. Bacteriol.* 193, 1663–1671. doi: 10.1128/JB.01392-10

Ankele, E., Kindgren, P., Pesquet, E., and Strand, Å (2007). In vivo visualization of Mg-protoporphyrin IX, a coordinator of photosynthetic gene expression in the nucleus and the chloroplast. *Plant Cell* 19, 1964–1979. doi: 10.1105/tpc.106.048744

Bobik, K., and Burch-Smith, T. M. (2015). Chloroplast signaling within, between and beyond cells. *Front. Plant Sci.* 6:781. doi: 10.3389/fpls.2015.00781

Börner, T. (2017). The discovery of plastid-to-nucleus retrograde signaling-a personal perspective. *Protoplasma* 254, 1845–1855. doi: 10.1007/s00709-017-1104-1

Bräutigam, K., Dietzel, L., Kleine, T., Ströher, E., Wormuth, D., Dietz, K. J., et al. (2009). Dynamic plastid redox signals integrate gene expression and metabolism to induce distinct metabolic states in photosynthetic acclimation in *Arabidopsis*. *Plant Cell* 21, 2715–2732. doi: 10.1105/tpc.108.062018

Bröcker, M. J., Jahn, D., and Moser, J. (2012). "94 key enzymes of chlorophyll biosynthesis," in *Handbook of Porphyrin Science*, eds K. M. Kadish, K. M. Smith, and R Guilard (Singapore: World Scientific Publishing Company), 1–43.

Brzezowski, P., Richter, A. S., and Grimm, B. (2015). Regulation and function of tetrapyrrole biosynthesis in plants and algae. *Biochim. Biophys. Acta* 1847, 968–985. doi: 10.1016/j.bbabio.2015.05.007

Busch, A. W., and Montgomery, B. L. (2015). Interdependence of tetrapyrrole metabolism, the generation of oxidative stress and the mitigative oxidative stress response. *Redox Biol.* 4, 260–271. doi: 10.1016/j.redox.2015.01.010

Chan, K. X., Mabbitt, P. D., Phua, S. Y., Mueller, J. W., Nisar, N., Gigolashvili, T., et al. (2016). Sensing and signaling of oxidative stress in chloroplasts by inactivation of the SAL1 phosphoadenosine phosphatase. *Proc. Natl. Acad. Sci. U.S.A.* 113, E4567–E4576. doi: 10.1073/pnas.1604936113

Chen, H., Zou, Y., Shang, Y., Lin, H., Wang, Y., Cai, R., et al. (2008). Firefly luciferase complementation imaging assay for protein-protein interactions in plants. *Plant Physiol.* 146, 368–376. doi: 10.1104/pp.107.111740

Cheng, X., Liu, G., Ke, W., Zhao, L., Lv, B., Ma, X., et al. (2017). Building a multipurpose insertional mutant library for forward and reverse genetics in *Chlamydomonas*. *Plant Methods* 13:36. doi: 10.1186/s13007-017-0183-5

Chi, W., Feng, P., Ma, J., and Zhang, L. (2015). Metabolites and chloroplast retrograde signaling. *Curr. Opin. Plant Biol.* 25, 32–38. doi: 10.1016/j.pbi.2015.04.006

Chi, W., Sun, X., and Zhang, L. (2013). Intracellular signaling from plastid to nucleus. *Annu. Rev. Plant Biol.* 64, 559–582. doi: 10.1146/annurev-arplant-050312-120147

Czarnecki, O., and Grimm, B. (2012). Post-translational control of tetrapyrrole biosynthesis in plants, algae, and cyanobacteria. *J. Exp. Bot.* 63, 1675–1687. doi: 10.1093/jxb/err437

Dammeyer, T., and Frankenberg-Dinkel, N. (2008). Function and distribution of bilin biosynthesis enzymes in photosynthetic organisms. *Photochem. Photobiol. Sci.* 7, 1121–1130. doi: 10.1039/b807209b

de Vries, J., and Archibald, J. M. (2017). Endosymbiosis: Did plastids evolve from a freshwater cyanobacterium? *Curr. Biol.* 27, R103–R105. doi: 10.1016/j.cub.2016.12.006

Duanmu, D., Bachy, C., Sudek, S., Wong, C. H., Jiménez, V., Rockwell, N. C., et al. (2014). Marine algae and land plants share conserved phytochrome signaling systems. *Proc. Natl. Acad. Sci. U.S.A.* 111, 15827–15832. doi: 10.1073/pnas.1416751111

Duanmu, D., Casero, D., Dent, R. M., Gallaher, S., Yang, W., Rockwell, N. C., et al. (2013). Retrograde bilin signaling enables *Chlamydomonas* greening and phototrophic survival. *Proc. Natl. Acad. Sci. U.S.A.* 110, 3621–3626. doi: 10.1073/pnas.1222375110

Duanmu, D., Rockwell, N. C., and Lagarias, J. C. (2017). Algal light sensing and photoacclimation in aquatic environments. *Plant Cell Environ.* 40, 2558–2570. doi: 10.1111/pce.12943

Falciatore, A., Merendino, L., Barneche, F., Ceol, M., Meskauskiene, R., Apel, K., et al. (2005). The FLP proteins act as regulators of chlorophyll synthesis in response to light and plastid signals in *Chlamydomonas*. *Genes Dev.* 19, 176–187. doi: 10.1101/gad.321305

Falklöf, O., and Durbeej, B. (2016). Steric effects govern the photoactivation of phytochromes. *Chemphyschem* 17, 954–957. doi: 10.1002/cphc.201501080

Ferenczi, A., Pyott, D. E., Xipnitou, A., and Molnar, A. (2017). Efficient targeted DNA editing and replacement in *Chlamydomonas reinhardtii* using Cpf1 ribonucleoproteins and single-stranded DNA. *Proc. Natl. Acad. Sci. U.S.A.* 114, 13567–13572. doi: 10.1073/pnas.1710597114

Fernández, A. P., and Strand, A. (2008). Retrograde signaling and plant stress: plastid signals initiate cellular stress responses. *Curr. Opin. Plant Biol.* 11, 509–513. doi: 10.1016/j.pbi.2008.06.002

Gabruk, M., and Mysliwa-Kurdziel, B. (2015). Light-Dependent protochlorophyllide oxidoreductase: phylogeny, regulation, and catalytic properties. *Biochemistry* 54, 5255–5262. doi: 10.1021/acs.biochem.5b00704

Greiner, A., Kelterborn, S., Evers, H., Kreimer, G., Sizova, I., and Hegemann, P. (2017). Targeting of photoreceptor genes in *Chlamydomonas reinhardtii* via zinc-finger nucleases and CRISPR/Cas9. *Plant Cell* 29, 2498–2518. doi: 10.1105/tpc.17.00659

Hanf, R., Fey, S., Schmitt, M., Hermann, G., Dietzek, B., and Popp, J. (2012). Catalytic efficiency of a photoenzyme–an adaptation to natural light conditions. *Chemphyschem* 13, 2013–2015. doi: 10.1002/cphc.201200194

Hunsperger, H. M., Randhawa, T., and Cattolico, R. A. (2015). Extensive horizontal gene transfer, duplication, and loss of chlorophyll synthesis genes in the algae. *BMC Evol. Biol.* 15:16. doi: 10.1186/s12862-015-0286-4

Joyard, J., Ferro, M., Masselon, C., Seigneurin-Berny, D., Salvi, D., Garin, J., et al. (2009). Chloroplast proteomics and the compartmentation of plastidial isoprenoid biosynthetic pathways. *Mol. Plant* 2, 1154–1180. doi: 10.1093/mp/ssp088

Kauss, D., Bischof, S., Steiner, S., Apel, K., and Meskauskiene, R. (2012). FLU, a negative feedback regulator of tetrapyrrole biosynthesis, is physically linked to the final steps of the Mg^{++}-branch of this pathway. *FEBS Lett.* 586, 211–216. doi: 10.1016/j.febslet.2011.12.029

Keeling, P. J. (2010). The endosymbiotic origin, diversification and fate of plastids. *Philos. Trans. R. Soc. Lond. B Biol. Sci.* 365, 729–748. doi: 10.1098/rstb.2009.0103

Kohchi, T., Mukougawa, K., Frankenberg, N., Masuda, M., Yokota, A., and Lagarias, J. C. (2001). The Arabidopsis *HY2* gene encodes phytochromobilin synthase, a ferredoxin-dependent biliverdin reductase. *Plant Cell* 13, 425–436.

Kropat, J., Hong-Hermesdorf, A., Casero, D., Ent, P., Castruita, M., Pellegrini, M., et al. (2011). A revised mineral nutrient supplement increases biomass and growth rate in *Chlamydomonas reinhardtii*. *Plant J.* 66, 770–780. doi: 10.1111/j.1365-313X.2011.04537.x

Larkin, R. M. (2014). Influence of plastids on light signalling and development. *Philos. Trans. R. Soc. Lond. B Biol. Sci.* 369, 20130232. doi: 10.1098/rstb.2013.0232

Leister, D., Wang, L., and Kleine, T. (2017). Organellar gene expression and acclimation of plants to environmental stress. *Front. Plant Sci.* 8:387. doi: 10.3389/fpls.2017.00387

Mason, C. B., Bricker, T. M., and Moroney, J. V. (2006). A rapid method for chloroplast isolation from the green alga *Chlamydomonas reinhardtii*. *Nat. Protoc.* 1, 2227–2230. doi: 10.1038/nprot.2006.348

Masuda, T., and Takamiya, K. (2004). novel insights into the enzymology, regulation and physiological functions of light-dependent protochlorophyllide oxidoreductase in angiosperms. *Photosynth. Res.* 81, 1–29. doi: 10.1023/B:PRES.0000028392.80354.7c

McDowell, M. T., and Lagarias, J. C. (2001). Purification and biochemical properties of phytochromobilin synthase from etiolated oat seedlings. *Plant Physiol.* 126, 1546–1554.

Meskauskiene, R., Nater, M., Goslings, D., Kessler, F., Op Den Camp, R., and Apel, K. (2001). FLU: a negative regulator of chlorophyll biosynthesis in *Arabidopsis thaliana*. *Proc. Natl. Acad. Sci. U.S.A.* 98, 12826–12831. doi: 10.1073/pnas.221252798

Mochizuki, N., Tanaka, R., Grimm, B., Masuda, T., Moulin, M., Smith, A. G., et al. (2010). The cell biology of tetrapyrroles: a life and death struggle. *Trends Plant Sci.* 15, 488–498. doi: 10.1016/j.tplants.2010.05.012

Molnar, A., Bassett, A., Thuenemann, E., Schwach, F., Karkare, S., Ossowski, S., et al. (2009). Highly specific gene silencing by artificial microRNAs in the unicellular alga *Chlamydomonas reinhardtii*. *Plant J.* 58, 165–174. doi: 10.1111/j.1365-313X.2008.03767.x

Nagahatenna, D. S., Langridge, P., and Whitford, R. (2015). Tetrapyrrole-based drought stress signalling. *Plant Biotechnol. J.* 13, 447–459. doi: 10.1111/pbi.12356

Reinbothe, C., El Bakkouri, M., Buhr, F., Muraki, N., Nomata, J., Kurisu, G., et al. (2010). Chlorophyll biosynthesis: spotlight on protochlorophyllide reduction. *Trends Plant Sci.* 15, 614–624. doi: 10.1016/j.tplants.2010.07.002

Rochaix, J. D. (2013). Surprising roles for bilins in a green alga. *Proc. Natl. Acad. Sci. U.S.A.* 110, 3218–3219. doi: 10.1073/pnas.1300399110

Rockwell, N. C., Duanmu, D., Martin, S. S., Bachy, C., Price, D. C., Bhattacharya, D., et al. (2014a). Eukaryotic algal phytochromes span the visible spectrum. *Proc. Natl. Acad. Sci. U.S.A.* 111, 3871–3876. doi: 10.1073/pnas.1401871111

Rockwell, N. C., and Lagarias, J. C. (2017). Ferredoxin-dependent bilin reductases in eukaryotic algae: ubiquity and diversity. *J. Plant Physiol.* 217, 57–67. doi: 10.1016/j.jplph.2017.05.022

Rockwell, N. C., Lagarias, J. C., and Bhattacharya, D. (2014b). Primary endosymbiosis and the evolution of light and oxygen sensing in photosynthetic eukaryotes. *Front. Ecol. Evol.* 2:66. doi: 10.3389/fevo.2014.00066

Rockwell, N. C., Martin, S. S., Li, F. W., Mathews, S., and Lagarias, J. C. (2017). The phycocyanobilin chromophore of streptophyte algal phytochromes is synthesized by HY2. *New Phytol.* 214, 1145–1157. doi: 10.1111/nph.14422

Scotto-Lavino, E., Du, G., and Frohman, M. A. (2006). 3' end cDNA amplification using classic RACE. *Nat. Protoc.* 1, 2742–2745. doi: 10.1038/nprot.2006.481

Singh, N. K., Sonani, R. R., Rastogi, R. P., and Madamwar, D. (2015). The phycobilisomes: an early requisite for efficient photosynthesis in cyanobacteria. *EXCLI J.* 14, 268–289. doi: 10.17179/excli2014-723

Strand, A., Asami, T., Alonso, J., Ecker, J. R., and Chory, J. (2003). Chloroplast to nucleus communication triggered by accumulation of Mg-protoporphyrinIX. *Nature* 421, 79–83. doi: 10.1038/nature01204

Tanaka, R., Kobayashi, K., and Masuda, T. (2011). Tetrapyrrole metabolism in *Arabidopsis thaliana*. *Arabidopsis Book* 9:e0145. doi: 10.1199/tab.0145

Tanaka, R., and Tanaka, A. (2007). Tetrapyrrole biosynthesis in higher plants. *Annu. Rev. Plant Biol.* 58, 321–346. doi: 10.1146/annurev.arplant.57.032905.105448

Terry, M. J., and Smith, A. G. (2013). A model for tetrapyrrole synthesis as the primary mechanism for plastid-to-nucleus signaling during chloroplast biogenesis. *Front. Plant Sci.* 4:14. doi: 10.3389/fpls.2013.00014

Vidal-Meireles, A., Neupert, J., Zsigmond, L., Rosado-Souza, L., Kovács, L., Nagy, V., et al. (2017). Regulation of ascorbate biosynthesis in green algae has evolved to enable rapid stress-induced response via the VTC2 gene encoding GDP-l-galactose phosphorylase. *New Phytol.* 214, 668–681. doi: 10.1111/nph.14425

Wakao, S., Chin, B. L., Ledford, H. K., Dent, R. M., Casero, D., Pellegrini, M., et al. (2014). Phosphoprotein SAK1 is a regulator of acclimation to singlet oxygen in *Chlamydomonas reinhardtii*. *eLife* 3:e02286. doi: 10.7554/eLife.02286

Wang, P., and Grimm, B. (2015). Organization of chlorophyll biosynthesis and insertion of chlorophyll into the chlorophyll-binding proteins in chloroplasts. *Photosynth. Res.* 126, 189–202. doi: 10.1007/s11120-015-0154-5

Wang, Y., and Spalding, M. H. (2006). An inorganic carbon transport system responsible for acclimation specific to air levels of CO_2 in *Chlamydomonas reinhardtii*. *Proc. Natl. Acad. Sci. U.S.A.* 103, 10110–10115. doi: 10.1073/pnas.0603402103

Wittkopp, T. M., Schmollinger, S., Saroussi, S. I., Hu, W., Zhang, W., Fan, Q., et al. (2017). Bilin-dependent photoacclimation in *Chlamydomonas reinhardtii*. *Plant Cell* 29, 2711–2726. doi: 10.1105/tpc.17.00149

Woodson, J. D., and Chory, J. (2008). Coordination of gene expression between organellar and nuclear genomes. *Nat. Rev. Genet.* 9, 383–395. doi: 10.1038/nrg2348

Woodson, J. D., Perez-Ruiz, J. M., and Chory, J. (2011). Heme synthesis by plastid ferrochelatase I regulates nuclear gene expression in plants. *Curr. Biol.* 21, 897–903. doi: 10.1016/j.cub.2011.04.004

Xiao, Y., Savchenko, T., Baidoo, E. E., Chehab, W. E., Hayden, D. M., Tolstikov, V., et al. (2012). Retrograde signaling by the plastidial metabolite MEcPP regulates expression of nuclear stress-response genes. *Cell* 149, 1525–1535. doi: 10.1016/j.cell.2012.04.038

Xiao, Y., Wang, J., and Dehesh, K. (2013). Review of stress specific organelles-to-nucleus metabolic signal molecules in plants. *Plant Sci.* 212, 102–107. doi: 10.1016/j.plantsci.2013.08.003

Zhang, Z.W., Yuan, S., Feng, H., Xu, F., Cheng, J., Shang, J., et al. (2011). Transient accumulation of Mg-protoporphyrin IX regulates expression of PhANGs - New evidence for the signaling role of tetrapyrroles in mature Arabidopsis plants. *J Plant Physiol* 168, 714-721. doi: 10.1016/j.jplph.2010.10.016.

Conflict of Interest Statement: The authors declare that the research was conducted in the absence of any commercial or financial relationships that could be construed as a potential conflict of interest.

frontiers in Plant Science

ORIGINAL RESEARCH
published: 19 June 2018
doi: 10.3389/fpls.2018.00720

Molecular Characterization of Magnesium Chelatase in Soybean [*Glycine max* (L.) Merr.]

Dan Zhang, Enjie Chang, Xiaoxia Yu, Yonghuan Chen, Qinshuai Yang, Yanting Cao, Xiukun Li, Yuhua Wang, Aigen Fu and Min Xu**

Chinese Education Ministry's Key Laboratory of Western Resources and Modern Biotechnology, Key Laboratory of Biotechnology Shaanxi Province, College of Life Sciences, Northwest University, Xi'an, China

Soybean (*Glycine max*) seed yields rely on the efficiency of photosynthesis, which is poorly understood in soybean. Chlorophyll, the major light harvesting pigment, is crucial for chloroplast biogenesis and photosynthesis. Magnesium chelatase catalyzes the insertion of Mg^{2+} into protoporphyrin IX in the first committed and key regulatory step of chlorophyll biosynthesis. It consists of three types of subunits, ChlI, ChlD, and ChlH. To gain a better knowledge of chlorophyll biosynthesis in soybean, we analyzed soybean Mg-chelatase subunits and their encoding genes. Soybean genome harbors 4 *GmChlI* genes, 2 *GmChlD* genes, and 3 *GmChlH* genes, likely evolved from two rounds of gene duplication events. The qRT-PCR analysis revealed that *GmChlI, GmChlD,* and *GmChlH* genes predominantly expressed in photosynthetic tissues, but the expression levels among paralogs are different. In silicon promoter analyses revealed these genes harbor different *cis*-regulatory elements in their promoter regions, suggesting they could differentially respond to various environmental and developmental signals. Subcellular localization analyses illustrated that GmChlI, GmChlD, and GmChlH isoforms are all localized in chloroplast, consistent with their functions. Yeast two hybrid and bimolecular fluorescence complementation (BiFC) assays showed each isoform has a potential to be assembled into the Mg-chelatase holocomplex. We expressed each GmChlI, GmChlD, and GmChlH isoform in *Arabidopsis* corresponding mutants, and results showed that 4 GmChlI and 2 GmChlD isoforms and GmChlH1 could rescue the severe phenotype of *Arabidopsis* mutants, indicating that they maintain normal biochemical functions *in vivo*. However, GmChlH2 and GmChlH3 could not completely rescue the chlorotic phenotype of *Arabidopsis gun5-2* mutant, suggesting that the functions of these two proteins could be different from GmChlH1. Considering the differences shown on primary sequences, biochemical functions, and gene expression profiles, we conclude that the paralogs of each soybean Mg-chelatase subunit have diverged more or less during evolution. Soybean could have developed a complex regulatory mechanism to control chlorophyll content to adapt to different developmental and environmental situations.

Keywords: *Glycine max*, soybean, chlorophyll synthesis, magnesium chelatase, GmChlI, GmChlD, GmChlH

OPEN ACCESS

Edited by:
Fei Yu,
Northwest A&F University, China

Reviewed by:
Yue Wu,
Massachusetts General Hospital, Harvard Medical School, United States
Zhong-Nan Yang,
Shanghai Normal University, China

****Correspondence:***
Aigen Fu
aigenfu@nwu.edu.cn
Min Xu
xumin@nwu.edu.cn

Specialty section:
This article was submitted to Plant Physiology, a section of the journal Frontiers in Plant Science

Received: *04 December 2017*
Accepted: *14 May 2018*
Published: *19 June 2018*

Citation:
Zhang D, Chang E, Yu X, Chen Y, Yang Q, Cao Y, Li X, Wang Y, Fu A and Xu M (2018) Molecular Characterization of Magnesium Chelatase in Soybean [Glycine max (L.) Merr.]. Front. Plant Sci. 9:720. doi: 10.3389/fpls.2018.00720

INTRODUCTION

Soybean [*Glycine max* (L.) Merr.] is one of the most economically important crops as the main sources of plant protein and vegetable oil (Dornbos and Mullen, 1992; Ainsworth et al., 2012). Global soybean yield has been steadily increased over the past century attributed to improved cultivars and agronomy management, but average soybean yield is still away from reaching a plateau (Egli, 2008; Masuda and Goldsmith, 2009). In order to meet the growing need resulting from a fast expanding population and limited agricultural land, soybean yield and quality must improve at a higher speed than before. Multiple agricultural approaches can be exploited to achieve this goal, such as improving photosynthetic efficiency, optimizing utilization of carbon, increasing the efficiency of nitrogen fixation, and adjusting developmental process (Ainsworth et al., 2012; Natarajan et al., 2013; Koester et al., 2014).

Previous reports have shown that soybean seed yields are positively correlated to the increase in light interception, energy conversion, and partitioning efficiencies (Zhu et al., 2010; Koester et al., 2014), suggesting that improving photosynthetic efficiency could be a promising method to raise soybean production in the future. However, little is known about the molecular base of photosynthesis in soybean up to date, because soybean is not an ideal material to perform plant physiology study at molecular biology level. Soybean is a diploid ($2n = 40$) crop evolved from a recent tetraploid ancestor, possessing a 1.1-gigabase genome with approximate 50,000 genes, in which 75% are duplicated (Shoemaker et al., 2006; Schlueter et al., 2007). The complexity of genome and shortage of molecular biology tools are big obstacles to dissect soybean photosynthesis in detail.

Chlorophyll content of plant leaves is the major limiting factor for the efficiency of photosynthesis (Chen and Blankenship, 2011). Chlorophyll is the main light harvesting and energy converting pigment for photosynthesis (Croce and van Amerongen, 2014). It is composed of a chlorophyllide moiety and an isoprenoid phytol tail, which are generated through the tetrapyrrole biosynthetic pathway and methylerythritol phosphate (MEP) metabolic pathway, respectively (Masuda and Fujita, 2008; Kim et al., 2013; Croce and van Amerongen, 2014). The genes and corresponding enzymes involved in the chlorophyll biosynthesis pathway have been well-characterized in model photosynthetic organisms; however, the regulatory mechanisms of the pathway are only recently studied and not fully understood (Masuda and Fujita, 2008; Brzezowski et al., 2015).

In the first committed step of chlorophyll biosynthesis, magnesium chelatase (E.C.6.6.1.1, Mg-chelatase) inserts a magnesium ion (Mg^{2+}) into protoporphyrin IX to generate Mg-protoporphyrin IX (Masuda, 2008). Mg-chelatase is a highly conserved polymeric enzyme composed of 3 distinct subunits, ChlI, ChlD, and ChlH, with an approximate molecular weight of 40, 70, and 140 kDa, respectively (Walker and Willows, 1997; Sirijovski et al., 2006). The ChlI subunit belongs to the large AAA^+ family (ATPase Associated with various cellular Activities), contains typical ATP-binding motifs in sequence like Walker A and Walker B, and is responsible for ATP hydrolysis (Hansson et al., 2002; Lake et al., 2004). The ChlD subunit has an AAA^+ module at its N-terminus, an integrin I domain at the C-terminus, and an acidic proline-rich region in between; however, no ATPase activity is detected in ChlD (Gräfe et al., 1999; Fodje et al., 2001). The ChlH subunit is the porphyrin binding and catalytic subunit responsible for the insertion of Mg^{2+} into protoporphyrin IX (Jensen et al., 1998; Karger et al., 2001). It is composed of six domains (I–VI), and an internal Proto-binding pocket is located at the interface between domain III and V possibly functioning in engulfing a tetrapyrrole ligand (Chen et al., 2015).

The magnesium chelation reaction has been postulated to proceed in two steps. During initial activation step, 6 ChlI and 6 ChlD subunits are assembled into a two-tiered hexameric ring in the presence of ATP, and meanwhile ChlH are activated by binding Mg^{2+} and protoporphyrin IX. Next, the activated ChlH docks to the ATP-I-D complex to form Mg-chelatase holoenzyme, catalyzing Mg^{2+} chelation into protoporphyrin IX in an ATP hydrolysis-dependent manner (Sirijovski et al., 2006; Zhang et al., 2006; Masuda, 2008).

The Chlorophyll biosynthesis has to be tightly controlled to fit the requirement of chloroplast biogenesis, or to maintain proper function of photosynthetic machineries. Most of chlorophyll intermediates are strong photosensitizers, and they will accumulate and further produce reactive oxygen species to damage cells if the regulation of chlorophyll biogenesis is impaired (Masuda and Fujita, 2008; Stephenson and Terry, 2008). Magnesium chelation, the branch point between the heme and chlorophyll biosynthetic pathways, is the major regulatory point of the chlorophyll biosynthesis pathway. It is well-known that Mg-chelatase is tightly controlled by the light signaling pathway at transcriptional level during thylakoid biogenesis in young chloroplasts, and is also regulated by a diurnal cycle and photosynthetic electron transport at both transcriptional and post-transcriptional levels in mature chloroplasts (Masuda, 2008).

Several Mg-chelatase impaired mutant plants have been identified in soybean, and they showed chlorophyll deficient in heterozygous and homozygous mutant plants (Palmer et al., 1989; Campbell et al., 2015). In one Mg-chelatase impaired mutant, the chlorophyll amount of heterozygous plants reduces to 50% of the wild-type level, however the yield remains a similar level compared to wild-type plants (Slattery et al., 2017; Walker et al., 2017), or even is higher than wild-type plants (Pettigrew et al., 1989). It suggests a possibility to improve photosynthesis capacity and seed yield in soybean by means of manipulating chlorophyll content. As a key enzyme and major regulatory point of chlorophyll biogenesis, Mg-chelatase might be a primary target to engineer at molecular level.

One hurdle to regulate the activity of Mg-chelatase with molecular biology tools is that its molecular features and regulatory mechanisms are not well-understood in soybean. The complete genome sequence of soybean was released in 2010 (Schmutz et al., 2010). Along with improved gene transformation tools in soybean, it provides an opportunity to dissect the photosynthesis process in detail, and further to manipulate some key components to improve photosynthesis efficiency. To gain a

better knowledge of chlorophyll biogenesis in soybean, we take advantage of soybean genome data and molecular biology tools to examine all Mg-chelatase subunits at genomic, transcriptional, and protein levels. We think this knowledge will help us to better understand this key enzyme in soybean chlorophyll biosynthesis pathway; and it could lay a foundation to manipulate soybean Mg-chelatase for further improving photosynthesis efficiency.

MATERIALS AND METHODS

Primers

All the primers used in present study are listed in Supplementary Table S1.

Plant Materials and Growth Conditions

Soybean cultivar Williams 82 (Wm82) and *Nicotiana benthamiana* plants were grown in green house at 26°C with a photoperiod of 16 h light/8 h dark cycle at a photosynthetic flux of 140 $\mu mol \cdot m^{-2} \cdot s^{-1}$.

Five *Arabidopsis thaliana* lines were used in this study, including wild-type Columbia (Col-0), Lansberg *erecta* (L*er-0*), and three T-DNA insertion mutant lines, *chli1* (Sail_230_D11, L*er-0* background), *chld-2* (009D11, Col-0 background), and *gun5-2* (CS806665, Col-0 background). The *chli1*, *chld-2*, and *gun5-2* mutants were obtained from Hsou-min Li (Institute of Molecular Biology, Academia Sinica, Taipei), GABI-Kat (https://www.gabi-kat.de), and Fang-Qing Guo (Institute of Plant Physiology & Ecology, Shanghai, China), respectively. All these T-DNA insertion lines were confirmed with the primers listed in Supplementary Table S1.

Arabidopsis plants were grown in soil or on half-strength Murashige and Skoog (1/2 MS) medium (PhytoTech, USA) containing 1% sucrose at 23°C under a 16 h light/8 h dark cycle with an illumination of 100 $\mu mol \cdot m^{-2} \cdot s^{-1}$.

Sequence Retrieval and Bioinformatics Analysis

A search for soybean genes encoding Mg-chelatase I subunit (GmChlI), D subunit (GmChlD), and H subunit (GmChlH) was performed by using the BLASTN program against the soybean genome (https://soybase.org) with the coding sequences (CDSs) of *Arabidopsis* Mg-chelatase subunits I1 (AtChlI1), D (AtChlD), and H (AtChlH) (Mochizuki et al., 2001; Huang and Li, 2009; Du et al., 2012). The cDNA fragments of retrieved *GmChlI*s, *GmChlD*s, and *GmChlH*s were amplified by RT-PCR and further sequenced. A primary comparison between the deduced amino acid sequences of each subunit and their corresponding homologs from *Arabidopsis* and *Synechocystis* sp. PCC6803 (Ssp. PCC6803) was conducted with multiple sequence alignment program ClusterW2.

A further phylogenetic analysis was performed to elucidate the evolutionary history of GmChlI, GmChlD, and GmChlH. The amino acid sequences of ChlI, ChlD, and ChlH from 11 species in addition to soybean were obtained from NCBI database (https://www.ncbi.nlm.nih.gov), including 2 legume species (*Phaseolus vulgaris* and *Cajanus cajan*), 4 dicots other than legumes (*A. thaliana*, *Gossypium arboreum*, *Populus trichocarpa*, and *Vitis vinifera*), 4 monocots (*Oryza sativa*, *Zea mays, Brachypodium distachyon*, and *Sorghom bicolor*), and 1 cyanobacterium (Ssp. PCC6803). Sequences were aligned with the ClustalW2 program, and phylogenetic trees were constructed by MEGA version 6.0 (Tamura et al., 2013) based on the Neighbor-Joining method.

To investigate the potential regulation of gene expression, 1,500 bp sequences immediately upstream of the translation start codon of *GmChlI*, *GmChlD*, and *GmChlH* were subject to the analysis of putative *cis*-acting regulatory elements by using the PlantCARE online program (http://bioinformatics.psb.ugent.be/webtools/plantcare/html/, Lescot et al., 2002).

RNA Extraction, RT-PCR, and Real-Time qRT-PCR

Total RNA was extracted from desired soybean tissues by RNAPrep pure plant kit (TIANGEN, China) following the manufacturer's instruction. For regular RT-PCR, RNA from leaf tissue was used. For qRT-PCR analysis, RNAs were extracted from tissues at different developmental stages. The roots and cotyledons were harvested from 1-week old seedlings. The stems, young trifoliate leaves, and flowers were sampled from flowering plants at R2 stage (∼45-day old). Young pods (∼4 cm long) and immature seeds (∼1 cm in length) from 4 cm long pods were sampled from plants at R5 stage (65∼70-day old).

Total RNA was treated with Turbo DNA-free kit (Invitrogen, USA) to remove genomic DNA contamination before reverse transcription. One microgram of DNA-free RNA was reverse transcribed to 1st strand cDNA using the PrimeScript II 1st strand cDNA Synthesis Kit (Takara, Japan) according to the manufacturer's protocol. The full-length coding sequences of *GmChlI*s, *GmChlD*s, and *GmChlH*s were amplified from Wm82 leave cDNA by PCR with PrimerSTAR Max DNA polymerase (Takara, Japan). PCR was run with an initial pre-denaturation of 98°C for 30 s, followed by 30 cycles of 98°C for 15 s, 60°C for 15 s, and 72°C for 2 min. The PCR products were cloned into pMD18T vector (Takara, Japan) for sequencing.

For qRT-PCR analysis, the 1st strand cDNA was diluted 20 times, and 1 μl was used in each real time quantitative PCR. Quantitative PCR was performed on BioRad CFX96 with 2x SYBR Green qPCR Master Mix (Roche, Switzerland) in 20 μl reaction. PCR was run with the following program: 10 min in 95°C, followed by 40 cycles of 10 s at 95°C and 30 s at 63°C, then increasing up to 95°C at an increment of 0.5°C degree per min. The cycle threshold value was calculated by the CFX Manager Software version 3.0 (Bio-Rad, USA). Relative gene expression level was calculated by using the $2^{-\Delta Ct}$ method. All data were normalized against the expression level of the soybean *actin* gene (*Glyma18g290800*). For each sample, three replicates were performed.

Subcellular Localization and Bimolecular Fluorescence Complementation (BiFC)

Vectors pSPYNE and pSPYCE (Waadt et al., 2008) carrying the CaMV 35S promoter-driven N- and C-terminal half of YFP, respectively, were used for BiFC assay. Vector pSPY-GFP for localization is generated by replacing YFP_N in pSPYNE with *GFP*

gene. Coding sequences of *GmChlI*s, *GmChlD*s, and *GmChlH*s were cloned into pSPY-GFP, pSPYNE, and pSPYCE, in-frame fused to the N-terminus of the corresponding tags.

For subcellular localization, *Agrobacterium tumefaciens* (GV3101) carrying vectors expressing GmChlI-GFP, GmChlD-GFP, and GmChlH-GFP were co-infiltrated with the p19 strain into *N. benthamiana* leaves for transient expression as described in Waadt et al. (2008). Similarly, for BiFC, pairs of YFP_N and YFP_C fusion proteins were transiently co-expressed in the leaves of *N. benthamiana*. GFP and reconstructed YFP fluorescence were observed and imaged 2–3 days after infiltration using the Olympus Fluoview FV1000 confocal laser scanning microscope (Olympus, Japan).

Yeast Two Hybrid Assay

The yeast two-hybrid (Y2H) analysis was performed using the Matchmaker GAL4 Two-Hybrid System 3 according to the supplier's instruction (Clontech, USA). Coding sequences for mature peptides of GmChlIs, GmChlDs, and GmChlHs were cloned into both the bait vector pGBKT7 and the prey vector pGADT7, downstream in frame to the GAL4 DNA binding domain (BD) and the GAL4 activation domain (AD), respectively. Pairs of the resulting BD and AD constructs were co-transformed into yeast strain AH109 according to the manufacturer's instruction. Yeast cells were first grown on synthetic dropout medium missing Leu and Trp, and then the colonies were tested for growth on selective medium lacking Leu, Trp, His, and Ade.

Gene Transformation in *Arabidopsis* and Transgenic Plant Screening

Full length CDSs of *GmChlI*s, *GmChlD*s, and *GmChlH*s tagged with *HA* at C-terminus were cloned into pSPYCE by replacing the YFP_C fragment, and transformed into the corresponding *Arabidopsis* mutants, heterozygous *chli1*/+, *chld-2*/+, and homozygous *gun5-2*, through *Agrobacterium* mediated transformation (Clough and Bent, 1998). Transgenic lines were screened on MS plates against kanamycin. The genotypes at *chli1* or *chld-2* loci were evaluated by PCR in *GmChlI-HA* and *GmChlD-HA* transformants. Genomic DNA for PCR analysis was extracted from leaves using NuClean PlantGen DNA Kit (CWBIO, China). Transgenic plants with homozygous mutant background would be advanced to next generation for further analysis. Three-week old T_3 plants derived from three independent T_1 transgenic lines were surveyed for phenotypes and photographed. The lines that did not show a full complementation by the transgene were subject to further examinations of protein and chlorophyll content. The protein level of these transgenic lines was examined by western-blot analysis with HA monoclonal antibody (H9658, Sigma-Aldrich, USA).

Chlorophyll (Chl) Content Measurement

The chlorophyll was extracted from leaves by immersing in a 4.5: 4.5: 1 (v/v) mixture of acetone, ethanol, and distilled water for 12 h under dark condition. After extraction, the absorbance was measured at 663 and 645 nm with UV-VIS Double Beam Spectrophotometer (HALO DB-30, Dynamica, UK). Chlorophyll contents (mg per gram of fresh weight tissue, mg/g) were calculated using the following equations (Deng et al., 2014):

Chl_a (mg/g) $=[(9.978OD_{663}\text{-}0.99OD_{645})$ x V(ml)]/(tissue weight (g) x1000)

Chl_b (mg/g) $=[(21.426OD_{645}\text{-}4.65OD_{663})$ x V(ml)]/(tissue weight (g) x1000)

Total Chl (mg/g) $=Chl_a$ (mg/g) + Chl_b (mg/g)

The experimental result for each line was expressed as mean ± standard deviation (sd) of three replicates. Statistical significance of differences between transgenic lines and corresponding wild type or mutant lines were tested using the two-tailed Student's *t*-test algorithm. P-value < 0.05 was regarded as significant.

Accession Number

We deposited all the soybean chelatase genes in this article to the GenBank/EMBL databases under the following accession numbers: *GmChlI1a* (MG679388), *GmChlI1b* (MG696843), *GmChlI2a* (MG696844), *GmChlI2b* (MG696845), *GmChlD1* (MG696846), *GmChlD2* (MG696847), *GmChlH1* (MG696848), *GmChlH2* (MG696849), and *GmChlH3* (MG696850).

RESULTS AND DISCUSSION

Identification of the Mg-Chelatase Subunits in Soybean

We took the first step to undermine genes encoding Mg-chelatase subunits in the soybean genome using *Arabidopsis* Mg-chelatase subunits (AtChlI1, AtChlD, and AtChlH) as query references. After a genome-wide database searching in the soybean genome (https://soybase.org), we found 4 GmChlI, 2 GmChlD, and 3 GmChlH encoding genes. Gene names were assigned to respective loci as following: Glyma13g232500 (*GmChlI1a*), Glyma15g080200 (*GmChlI1b*), Glyma7g204300 (*GmChlI2a*), Glyma13g171800 (*GmChlI2b*), Glyma11g016000 (*GmChlD1*), Glyma1g226700 (*GmChlD2*), Glyma13g13700 (*GmChlH1*), Glyma19g139300 (*GmChlH2*), and Glyma10g097800 (*GmChlH3*). Out of these 9 genes, *GmChlI1a, GmChlI1b,* and *GmChlH1* have been reported previously (Nakayama et al., 1995, 1998; Campbell et al., 2015).

The cDNA of each gene was amplified by RT-PCR from Wm82 leaf tissue and sequenced to determine the right splicing forms. According to the sequencing results, *GmChlI1a*, *GmChlI1b*, and *GmChlI2b* encode a ∼40 kDa polypeptide with 433 amino acid (aa), while *GmChlI2a* encodes a 415-aa polypeptide. Proteins encoded by *GmChlID1* and *GmChlD2* are 751-aa long with molecular weight of ∼70 kDa. *GmChlH1* and *GmChlH3* both encode 1385-aa polypeptides with molecular weight of ∼140 kDa, while *GmChlH2* encodes a 1384-aa polypeptide. All soybean ChlI, ChlD, and ChlH subunits are similar in molecular mass to their corresponding homologs identified in other species (Figure S1) (Jensen et al., 1996; Sawers et al., 2006; Zhang et al., 2006; Du et al., 2012; Muller et al., 2014).

According to the prediction by TargetP, each soybean Mg-chelatase subunit contains a chloroplastic transit peptide (CTP) at the N-terminus as expected. Sequence comparison of GmChlIs, GmChlDs, and GmChlHs to their orthologs from

A. thaliana and Ssp. PCC6803 revealed that they are all well-conserved (Figures S1–S3). Four GmChlIs are highly similar, sharing at least 90% amino acid identity, and each of them contains the full set of characteristic motifs in ChlI, including Walker A, Walker B, Sensor I, Arginine fingers (R finger), and Sensor II (Figure S1). GmChlID1 and GmChlD2 share 97% identity on amino acid sequence (Figure S2). All three structural domains of ChlD are highly conserved in GmChlD proteins, including an AAA^+ like module at the N-terminus, a proline-rich linker region, and an integrin I domain at the C-terminus (Figure S2). GmChlH1 and GmChlH2 share 99% identity on amino acid sequence and both of them share 97% sequence identity with GmChlH3 (Figure S3). The sequences of three GmChlHs are conserved in all six functional domains, especially in domains III, V, and VI that constitute the putative active center (Chen et al., 2015). The residues surrounding the putative tetrapyrrole-binding pocket are invariant compared to SspChlH. Together, the primary structure information indicates that all isoforms of GmChlI, GmChlD, and GmChlH are likely functional *in vivo*.

Phylogenetic Analysis of Mg-Chelatase Subunits in Soybean

To investigate the evolution history of Mg-chelatase, protein sequences of GmChlI, GmChlD, and GmChlH were subjected to phylogenic analysis along with their orthologs from 11 species including 6 dicotyledons (*P. vulgaris*, *C. cajan*, *V. vinifera*, *G. arboreum*, *P. trichocarpa*, *A. thaliana*), 4 monocotyledons (*B. distachyon*, *Z. mays*, *S. bicolor*, *O. sativa*), and 1 cyanobacterium (Ssp. PCC6803). The sequences of ChlIs, ChlDs, and ChlHs are clustered into dicot and monocot clades along with Ssp. PCC6803 as an out-group, and subsequently diverged by family, showing that all the homologs from legume family are sub-grouped together (**Figure 1**). In legumes, most of species encode 2 ChlIs, 1 ChlD, and 2 ChlHs, in which the ChlI and ChlH subunits are further sub-divided into two clusters, indicating that these two subunits experienced a duplication at the origin of the legumes. Comparatively, soybean genome encodes 4 GmChlIs, 2 GmChlDs, and 3 GmChlHs, indicating that Mg-chelatase genes went through a second round of duplication at the origin of soybean. Therefore, four GmChlIs are separated into two groups, each belonging to one of the legume ChlI clusters. One group contains GmChlI1a and GmChlI1b while the other one contains GmChlI2a and GmChlI2b (**Figure 1A**). Similarly, three isoforms of GmChlH are divided into two groups as well, with GmChlH1 and GmChlH2 as one group and GmChlH3 as the other group (**Figure 1C**). The twin copy of *GmChlH3* gene is likely lost after the gene duplication event.

In addition, an interesting history is observed in the evolution of ChlI subunit (**Figure 1A**). Most dicotyledons encode 2 ChlI isoforms whereas monocotyledons and Ssp. PCC6803 only have 1 ChlI. It is logical to postulate that a duplication event of ChlI would happen near the origin of the dicots. However, the phylogenetic tree shows that ChlIs from the same dicotyledon species or family tend to cluster together indicating that various independent duplications of ChlI subunit happened during the evolution of dicots (**Figure 1A**).

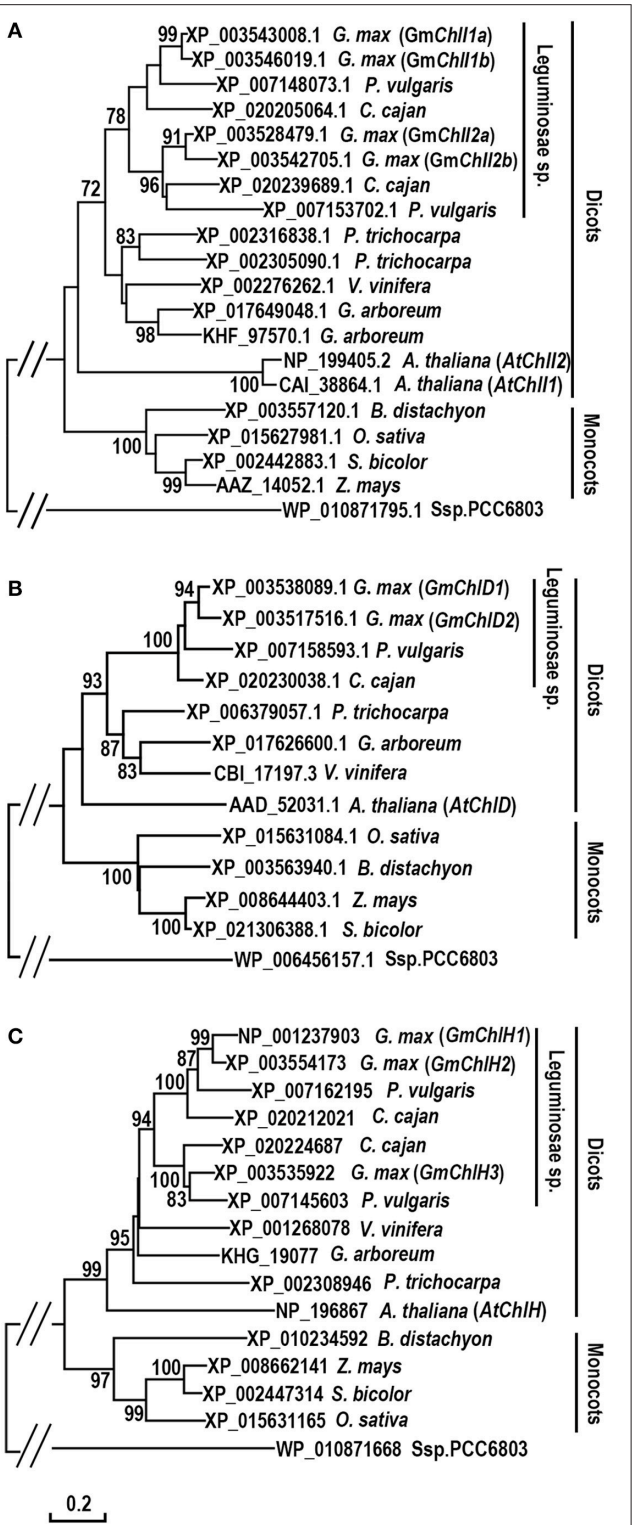

FIGURE 1 | Phylogenetic analysis of ChlI, ChlD, and ChlH subunits of Mg-chelatase**. (A)** Evolutionary relationships of ChlI subunits; **(B)** Evolutionary relationships of ChlD subunits; **(C)** Evolutionary relationships of ChlH subunits. Sequences were taken from *G. max* and 11 species from *cyanobacterium*,monocots, and dicots, of which the sequences of ChlI, ChlD, *(Continued)*

FIGURE 1 | and ChlH subunits from *A. thaliana* (Du et al., 2012), *O. sativa* (Zhang et al., 2006; Muller et al., 2014), Ssp. PCC6803 (Jensen et al., 1996), and the ChlI subunit from *Z. mays* (Sawers et al., 2006) were published previously. The unrooted phylogenetic trees were constructed using the Neighbor-Joining method and a 1,000 bootstrap resampling value. The bootstrap values >70% are shown next to the branches. The evolutionary distances were computed using the Poisson correction method and are in the units of the number of amino acid substitutions per site. Positions containing gaps and missing data were eliminated. Evolutionary analyses were conducted in MEGA6.

Tissue Specific Expression Profiles of *GmChlI*s, *GmChlD*s, and *GmChlH*s

To illustrate whether the paralogs of *GmChlI*, *GmChlD*, and *GmChlH* genes are diverged in biological function, we analyzed the tissue specific expression profile of each Mg-chelatase gene through real-time quantitative RT-PCR. The transcription levels of *GmChlI*s, *GmChlD*s, and *GmChlH*s were investigated in various tissues, including roots, stems, cotyledons, leaves, flowers, pods, and immature seeds. The results revealed that the tissue expression patterns of all the genes are generally similar, with the highest level in leaves followed by cotyledons, a relative lower level in stems, flowers, and pods, and an almost negligible level in roots.

The expression levels between paralogs are different, but the differences between closely related paralogs are smaller compared to distantly related ones (**Figures 1**, **2**). For example, *GmChlI1a* and *GmChlI1b* express much higher than *GmChlI2a* and *GmChlI2b*, which are barely expressed in all examined tissues (**Figure 2A**). Meanwhile, the expression levels of *GmChlI1a* and *GmChlI2a* are about 2-fold higher compared to *GmChlI1b* and *GmChlI2b*, respectively, in most of the tissues. These data imply that GmChlI1a and GmChlI1b are the major functional Mg-chelatase I subunit in soybean. The expression levels of two *GmChlD* genes were comparable in all tissues, but *GmChlD2* is expressed at a slightly higher level (less than 2 fold) compared to *GmChlD1* (**Figure 2B**), suggesting both of GmChlD paralogs function in soybean. Among three *GmChlH* genes, the expression of *GmChlH3* is generally lower than the other two especially in leaves and cotyledons, and no significant difference was detected between *GmChlH1* and *GmChlH2* (**Figure 2C**). Taken together, the transcription levels of *GmChlIs*, *GmChlDs*, and *GmChlHs* show a positive correlation with the tissue photosynthetic activity, which is consistent to the enzyme function. However, the functions of the paralogs of each subunit are likely diverged with respect to their different expression levels.

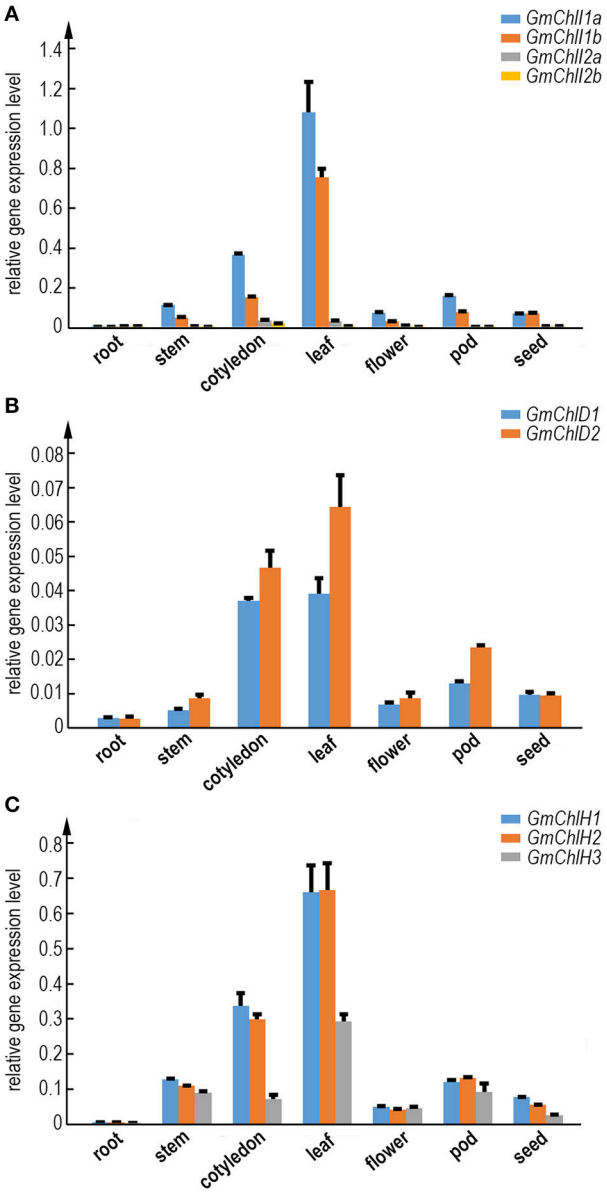

FIGURE 2 | Expression analysis of GmChlIs, GmChlDs, and GmChlHs in various tissues at different growth stage of soybean**.** Expression profiles of four *GmChlI* genes **(A)**, two *GmChlD* genes **(B)**, and three *GmChlH* genes **(C)** in different tissues are obtained by quantitative RT-PCR. The names of tissues are indicated below the chart. Root and cotyledon were taken from 7-day old seedlings. Stem, trifoliolate leaves, and flowers were taken from ~45-day-old flowering plants. Pods (~4 cm long) and immature seeds (~1 cm in length) were sampled from 65~70-day old plants. Expression level of each gene is normalized to those of actin. Error bars indicate standard deviation (sd) from three technical replicates.

Promoter Analyses of *GmChlI*s, *GmChlD*s and *GmChlH*s

We next carried out a promoter motif analyses to further study the potential regulatory mechanisms of *GmChlIs*, *GmChlDs*, and *GmChlHs*. The 1,500 bp region immediately upstream of start codon ATG of each gene was analyzed with the online program PlantCARE (Lescot et al., 2002). Multiple CAAT boxes and various *cis*-acting regulatory motifs were predicted from the promoter regions of these genes, including light responsive elements (LREs), circadian regulatory elements (CREs), hormone responsive elements (HREs), and defense and stress responsive elements (DSREs) (**Tables 1**, **2**).

The CAAT box is a proximal promoter element recognized by CAAT-box binding transcription factors and is important for the

TABLE 1 | Predicted CAAT boxes and *cis*-elements response to light and circadian in the promoter regions of *GmChlIs*, *GmChlDs,* and *GmChlHs* genes.

Motifs	Sequence	*GmChlI1a*	*GmChlI1b*	*GmChlI2a*	*GmChlI2b*	*GmChlD1*	*GmChlD2*	*GmChlH1*	*GmChlH2*	*GmChlH3*
CAAT box[a]	CAAT/CCAAT	−98,−164 −179,−203 −261,−296	−39,−93 −166,−181 −282	−216	−55,−104 −394	−88,−30 −178,−242	−28,−91 −147,−227 −273,−278 −315	−35,−54 −62, −85 −112,−240 −353	−52,−80 −100,−251 −295,−371	−359
Subtotal		**6**	**5**	**1**	**3**	**4**	**7**	**7**	**6**	**1**
Light response[b]										
AAAC-motif	CAACAAAAACCT	–	–	–	–	–	−579	−386	–	–
ACE	GACACGTATG	−850	−859	–	–	–	–	–	−751	−1150
AE-box	AGAAACAT	−53	−48	−17	−1017	–	−602	−335	−910, −1572	–
AT1-motif	AATTATTTTTTATT	–	−578	–	−695	–	–	–	–	–
ATCT-motif	AATCTGATCG	–	–	–	–	−58	55	−524	−541	–
Box 4	ATTAAT	−184, −682	−186, −540 −589,−908	–	−297,−685 −982, −1433	−507,−1034 −1453	−595,−1144 −1477	–	–	−68, −891 −1307
Box I	TTTCAAA	−771	−1129	−345,−375 −509	–	–	–	−173, −94	−109,−184 −1405	−63, −1302
Box II	CCACGTGGC	–	–	–	–	–	−203	−834	–	−335
CATT–motif	GCATTC	–	–	–	−1441	−748,−752 −1242	–	–	–	–
GAG-motif	AGAGAGT	–	–	−173	–	–	–	–	−435	–
GA-motif	AAGGAAGA	–	–	−22,−131	−161	–	–	–	−77	–
GATA-motif	AAGGATAAGG	−964	−611	−121	–	–	–	–	−73	–
G-box	CACGTG	−428	−84	−65	−391	−1321,−1374	−192,−201	−832	−343	−333
GT1-motif	GGTTAA	−538,−854	–	−272	−702	–	−100,−1058	−978	−938	–
Gap-box	AAATGGAGA	–	–	–	–	−1209	–	–	–	–
I-box	GATAAGATA	−964	−995	−123	–	−57	−554	−500, −1418	−517,−1467	−86
MNF1	GTGCCC	–	–	–	–	–	−1248	–	–	–
Sp1	CC(G/A)CCC	−106,−968 −1284	−101	−825,−860	−1389	–	−536	–	−124	−514
TCCC-motif	TCTCCCT	–	–	–	–	–	–	−566	–	–
TCT-motif	TCTTAC	–	−619	–	−630,−1145	−707,−1416	–	−46,−738	–	−681,−1180
chs-CMA1a	TTACTTAA	–	–	–	−634	–	–	–	–	–
Subtotal		**13**	**13**	**13**	**14**	**13**	**14**	**13**	**15**	**12**
Circadian response [b]										
Circadian	CAAAGATATC	–	−1308	–	–	−921	−1208	−688	−708	−69,−1282

The positions of the cis-elements with respect to the translation initiation site (+1) are list in the table.

[a]*CAAT boxes are predicted from 400 bp upstream promoter region of GmChls.*

[b]*These cis-elements are predicted from 1.5 kb upstream promoter region of GmChls.*

TABLE 2 | Predicted *cis*-elements response to hormones, stresses, and specific tissues in the 1.5 kb promoter regions of *GmChlIs*, *GmChlDs,* and *GmChlHs* genes.

Motifs	Sequence	*GmChlI1a*	*GmChlI1b*	*GmChlI2a*	*GmChlI2b*	*GmChlD1*	*GmChlD2*	*GmChlH1*	*GmChlH2*	*GmChlH3*
HORMONE AND STRESS RESPONSE										
AuxRR-core (auxin, growth)	GGTCCAT	–	–	–	−266	–	–	−1120	−168	–
TGA-element (auxin, growth)	AACGAC	–	–	−259	–	−15	–	–	−1158	–
GARE-motif (GA, growth)	(A/C)AACAGA	–	–	−1213	−411,−934	–	–	−488, −1443	−505	−58
P-box (GA, growth)	CCTTTTG	−636	−736, −855	−925, −1250	–	–	–	–	–	–
ABRE (ABA, stress)	CACGTG	−428	–	−65	–	−1377	−203	−334	−343	−335
ERE (ethylene,stress)	ATTTCAAA	–	–	−376, −509	–	–	–	–	–	–
TCA-element (SA, stress)	GAGAAGAATA	−145	−627	−1380	−88, −258	−1172	–	−1062	−1021	−48, −820, −910
CGTCA-motif (MeJA, stress)	CGTCA	–	−82	–	–	–	−613	–	–	–
HSE (heat)	AAAAAATTTC	–	−492, −900, −1155	−341, −381, −516, −1010	−288, −584	−863	−189	−619, −944, −1409	−636	−651, −1197
LTR (low temperature)	CCGAAA	–	–	–	–	−1388	–	−546	−563	−497, −947
MBS (drought)	TAACTG	−1276, −1303	–	−1205	−903,−1158, −1308	−807	–	−914	−873	−175, −310, −1262
TC-rich repeats (Pathogen)	ATTTTCTTCA	−594	−623, −868, −897, −1087	−343, −802	−741	–	–	−63, −990	−410, −950, −1189, −1211	−681
Subtotal		**6**	**11**	**15**	**11**	**6**	**3**	**12**	**12**	**13**
TISSUE SPECIFIC										
GCN_motif (Endosperm)	TGTGTCA	−1073	–	–	–	–	–	–	−1165	−358, −865
Skn-1_motif (Endosperm)	GTCAT	−400, −483	−1186, −1220	–	−242, −393, −761, −851	−636, −621, −716, −930, −997	−1191, −1460	−398, −798, −1084, −1305	−450, −744	−238, −349, −884, −866
CAT-box (Meristem)	GCCACT	−1096, −1202	–	–	–	−1343, −1354	–	–	–	–
HD-Zip1 (leaf)	CAATGATTGCCAG	–	–	–	–	–	−279	–	–	–
Subtotal		**5**	**2**	**–**	**4**	**7**	**3**	**4**	**3**	**6**

The positions of the cis-elements with respect to the translation initiation site (+1) are list in the table.

sufficient transcription of the downstream gene (Bi et al., 1997). We counted the predicted CAAT boxes in the 400 bp region upstream of Mg-chelatase genes, revealing a consistency with their transcription levels detected by qRT-PCR. The paralogs with more CAAT boxes generally show a higher expression compared to the ones with less CAAT boxes in most of tissues (**Figure 2** and **Table 1**).

Among *cis*-acting regulatory motifs, it is not surprised that LREs are the most abundant motifs in promoter regions of *GmChlI*s, *GmChlD*s, and *GmChlH*s (**Table 1**). Light is the main environmental factor regulating chlorophyll biosynthesis; it is required for massive expression of Mg-chelatase genes (Papenbrock et al., 1999; Winter et al., 2007; Stephenson and Terry, 2008). The total number of LREs is similar among 9 promoters, ranged from 12 to 15, in which G-box is commonly present (**Table 1**). G-box is the bind site of many transcription factors in light signaling pathway, such as ELONGATED HYPOCOTYL5 (HY5) and PHYTOCHROME INTERACTING FACTOR proteins (PIFs) (Toledo-Ortiz et al., 2014). Other than G-box, light responsive motifs are different across promoters, suggesting there is a difference in fine regulation of soybean Mg-chelatase genes responsive to light.

Several reports show that the expression of *ChlH* exhibits a diurnal oscillation pattern when plants are grown in light-dark regime whereas the expression of *ChlI* and *ChlD* displays less or no variation under the same situation (Gibson et al., 1996; Jensen et al., 1996; Papenbrock et al., 1999).

In soybean, the circadian regulatory element *circadian* is ubiquitously present in the promoter regions close to three *GmChlH*s; on the other hand, it is either absent in the 1,500 bp promoter regions of *GmChlIs* and *GmChlDs*, or present in the upstream regions far away from the genes (**Table 1**). These results indicate that the expression patterns of Mg-chelatase genes in soybean are similar to those in other species.

Another major type of elements in the promoters of *GmChl* genes is the hormone responsive element (HRE). It is well-known that phytohormones play important roles in chlorophyll biosynthesis pathway. For example, the greening process of seedlings is orchestrated through a complex network of interactions between auxin, gibberellic acids (GA), cytokinins (CK), ethylene, and light signal transduction pathways (Liu et al., 2017). Here, we can find auxin responsive elements, GA responsive elements, or both of them in *GmChl* promoters except for *pGmChlD2* (the promoter of *GmChlD2*), suggesting that the expression of most of *GmChl* genes can

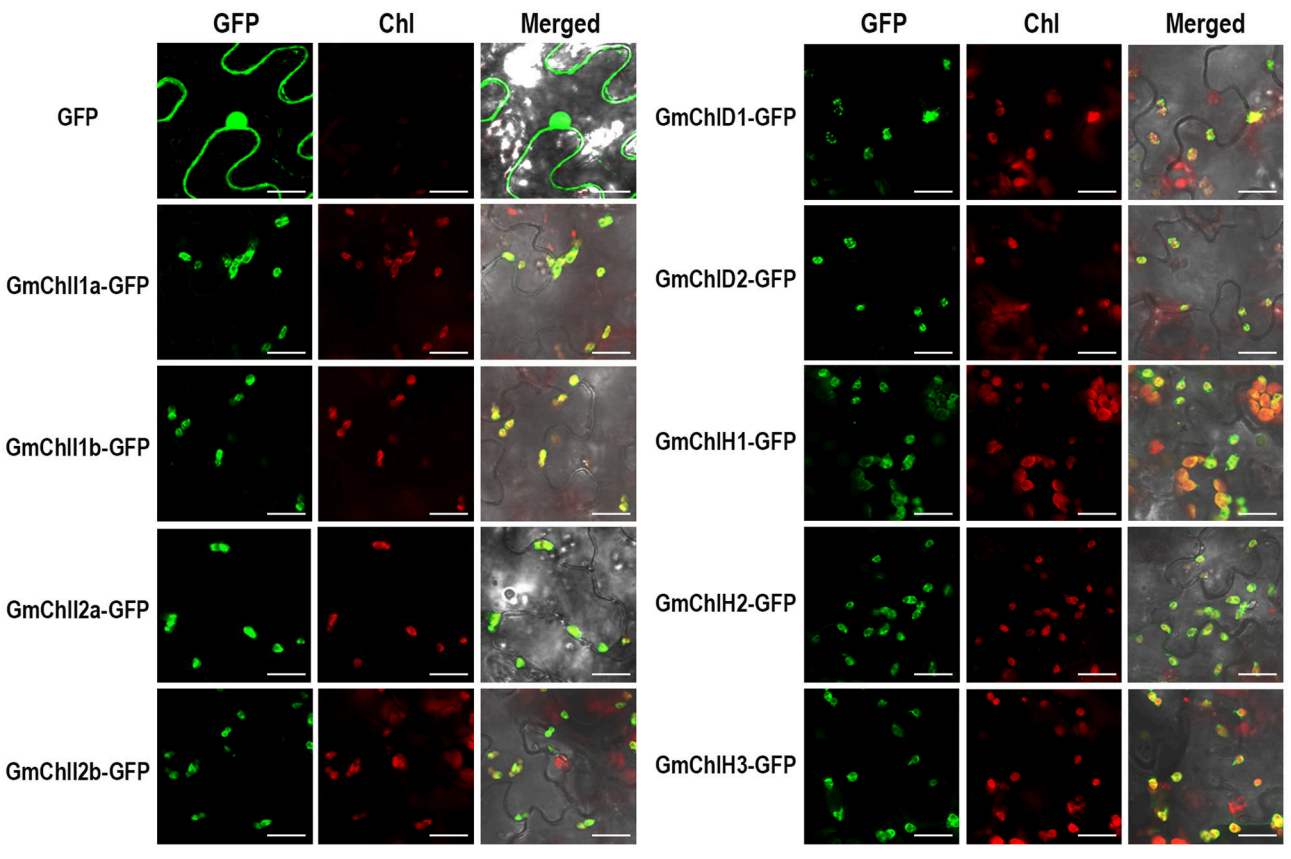

FIGURE 3 | Subcellular localization of GmChlIs, GmChlDs, and GmChlHs. Free GFP and GmChlIs, GmChlDs, and GmChlHs tagged with a C-terminal GFP were transiently expressed under the control of 35S promoter in *N. benthamina* leaves and observed by confocal microscopy. In each case, images of GFP fluorescence (GFP), chlorophyll autofluorescence (Chl), and merged GFP and chlorophyll fluorescence with bright-field (Merged) are shown. Scale bar = 20 μm.

be directly regulated by the components in auxin or/and GA signaling pathway. By contrast, no CK response element is detected in any of the promoters and ethylene responsive element is only observed in *pGmChlI2a*, suggesting CK and ethylene probably indirectly regulate the transcription of *GmChlI*s, G*mChlD*s, and G*mChlH*s via interacting with other signal transduction pathways. Previous report showed that the cytokinin-mediated *Arabidopsis* root greening is dependent on transcription factor HY5 (Kobayashi et al., 2012). ETHYLENE INSENSITIVE 3 (EIN3) can active PIFs to regulate the expression of Mg-chelatase genes (Zhong et al., 2014).

Comparatively, abscisic acid (ABA) mainly functions as an inhibitor of chlorophyll biosynthesis. ABSCISIC ACID INSENSITIVE 5 (ABI5) in *Arabidopsis* represses the cotyledon greening during seed germination under light through ABA-mediated pathway (Guan et al., 2014). Defect in transcription factor ABSCISIC ACID INSENSITIVE 3 (ABI3) leads *Arabidopsis* plants producing stay-green embryos (Delmas et al., 2013). Consistently, ABA response element (ABRE) is present in most of *GmChl* promoters, except for *pGmChlI1b* and *pGmChlI2b*, showing that chlorophyll synthesis is highly controlled by ABA in soybean.

Salicylic acid (SA) and jasmonates (JA) are important signal molecules in the regulation of plant response to biotic and abiotic stress conditions, such as pathogen attacks, extreme temperatures, salts, and oxidative conditions (Khan et al., 2010; Ahmad et al., 2012; Wasternack and Hause, 2013). Chlorophyll contents usually are reduced under stress conditions (Ramachandra Reddy et al., 2004). The elements responsive to SA, including TCA-element motifs and TC-rich repeats, are relatively abundant in *pGmChlI*s and *pGmChlH*s, but rare in *pGmChlD*s, while JA response element is only found in *pGmChlI1b* and *pGmChlD2* (**Table 2**). It indicates that the regulations of soybean Mg-chelatase genes are different in responsive to SA and JA signals. In addition, several abiotic stress responsive elements are found in the promoters of *GmChl*s, including HSE, LTR, and MBS motifs, which are responsive to heat, low temperature, and drought, respectively (**Table 2**). HSE and MBS are relatively common in the promoters of 9 *GmChl* genes, and LTR only presents in *pGmChlD1* and *pGmChlHs* with a low copy number, implying the expression of *GmChls* is likely more sensitive to heat and drought.

Moreover, there are some tissue specific *cis*-elements present in the promoters of all *GmChl* genes except *GmChlI2a* (**Table 2**). Interestingly, GCN and skn-1 motifs related to endosperm specific expression are common and abundant in *GmChl* genes, indicating Mg-chelatase in endosperm are likely functionally important. Additionally, two copies of CAT-box motifs related to root meristem development are found in *pGmChlI1a* and *pGmChlD1*, and one copy of HD-Zip1 related to leaf development is found in *GmChlD2* (**Table 2**).

Collectively, regulatory *cis*-elements response to environmental and growth conditions are diverse among the promoters of different Mg-chelatase genes, indicating that the expression of soybean Mg-chelatase genes are complicated and differentially regulated by various factors.

Subcellular Localization of GmChlIs, GmChlDs, and GmChlHs

Sequence alignment analysis showed that GmChlIs, GmChlDs, and GmChlHs all contain potential CTP at the N-terminus similar to AtChlI1, AtChlD, and AtChlH (Figures S1–S3). To confirm their subcellular localizations, we generated GFP fusion proteins by fusing *GFP* to the C termini of full-length *GmChlI*s, *GmChlD*s, and *GmChlH*s, respectively. Nine fusion proteins were

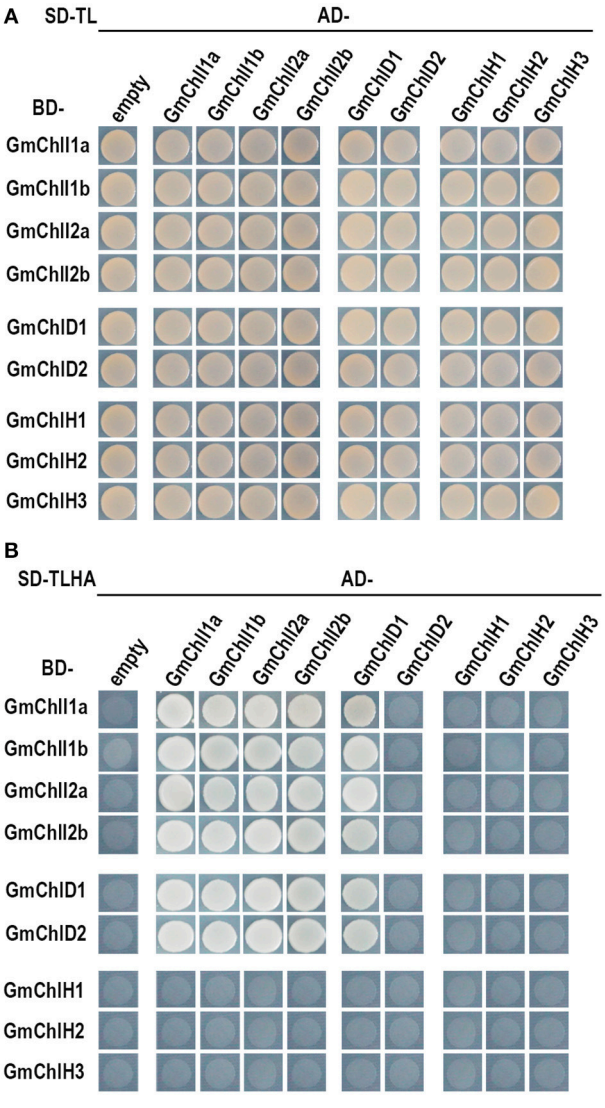

FIGURE 4 | Yeast two hybrid assay between GmChlIs, GmChlDs, and GmChlHs**.** pGBKT7 vectors expressing BD-fused GmChlIs, GmChlDs, and GmChlHs were co-transformed with pGADT7 empty vector or the ones expressing AD-fused GmChlIs, GmChlDs, and GmChlHs into the yeast strain AH109. The transformants were grown **(A)** on the synthetic dextrose medium (SD) lack of Trp and Leu (SD-TL) or **(B)** on the SD medium missing Trp, Leu, His, and Ade (SD-TLHA).

transiently expressed in the leaf tissue of *N. benthamiana* through agro-infiltration, and observed under confocal microscope 2 days after inoculation. The results clearly demonstrated that GFP-fused GmChlI, GmChlD, and GmChlH subunits were expressed and localized in the chloroplasts, as shown by the co-localization of GFP signal and chlorophyll autofluorescence (**Figure 3**), supporting that GmChlIs, GmChlDs, and GmChlHs are chloroplastic proteins, in agreement with their expected functions.

Interactions Among GmChlIs, GmChlDs, and GmChlHs

It has been established that ChlI, ChlD, and ChlH are assembled together to form an active Mg-chelatase holo-complex (Adhikari et al., 2011). We performed Y2H and BiFC assay to test these interactions among GmChlIs, GmChlDs, and GmChlHs.

The Y2H assays revealed that each GmChlI isoform can interact with itself and the other paralogs (**Figure 4**), suggesting that four GmChlIs are able to form homo- and hetero- hexameric ring. Similarly, they also interact with GmChlD1, indicating that they can form the oligomer with GmChlD1 protein. Meanwhile, GmChlD1 could interact with itself, which suggesting GmChlD1 can form the hexameric ring like GmChlIs. Notably, when GmChlD2 was fused with Gal4 activation domain, it did not interact with GmChlI or GmChlD proteins; but the interactions between them could be observed when GmChlD2 was fused with Gal4 DNA-binding domain (**Figure 4**), indicating that Gal4 activation domain could interfere the interaction of GmChlD2. In addition, no interaction was detected between a GmChlH isoform and any soybean Mg-chelatase subunit through Y2H method (**Figure 4**).

During BiFC experiments, obvious reconstructed YFP fluorescence was observed in chloroplasts coexpressing GmChlIs-YFP_N with GmChlIs-YFPc, GmChlDs-YFPc, or GmChlHs-YFPc (Figure S4). It confirmed the interactions between GmChlIs and GmChlDs detected in Y2H, and suggested that 4 GmChlIs could interact with all the GmChlH isoforms. Similar results were obtained by coexpression of GmChlDs-YFP_N with GmChlIs-YFPc, GmChlDs-YFPc, or GmChlHs-YFPc, verifying GmChlDs could interact with GmChlIs and GmChlDs, and implying the interactions between GmChlDs and GmChlHs as well (Figure S5). In addition, the interactions between GmChlHs and GmChlIs or GmChlDs were observed when GmChlHs-YFP_N was co-expressed with GmChlIs-YFPc or GmChlDs-YFPc in leaves (Figure S6). The interactions between GmChlH and other subunits were not observed in Y2H experiment possibly because GmChlH protein can only interact with GmChlI or GmChlD proteins in the two-tiered ring complex but not to the single GmChlI or GmChlD hexameric ring. As the negative control, no YFP signal was detected in the

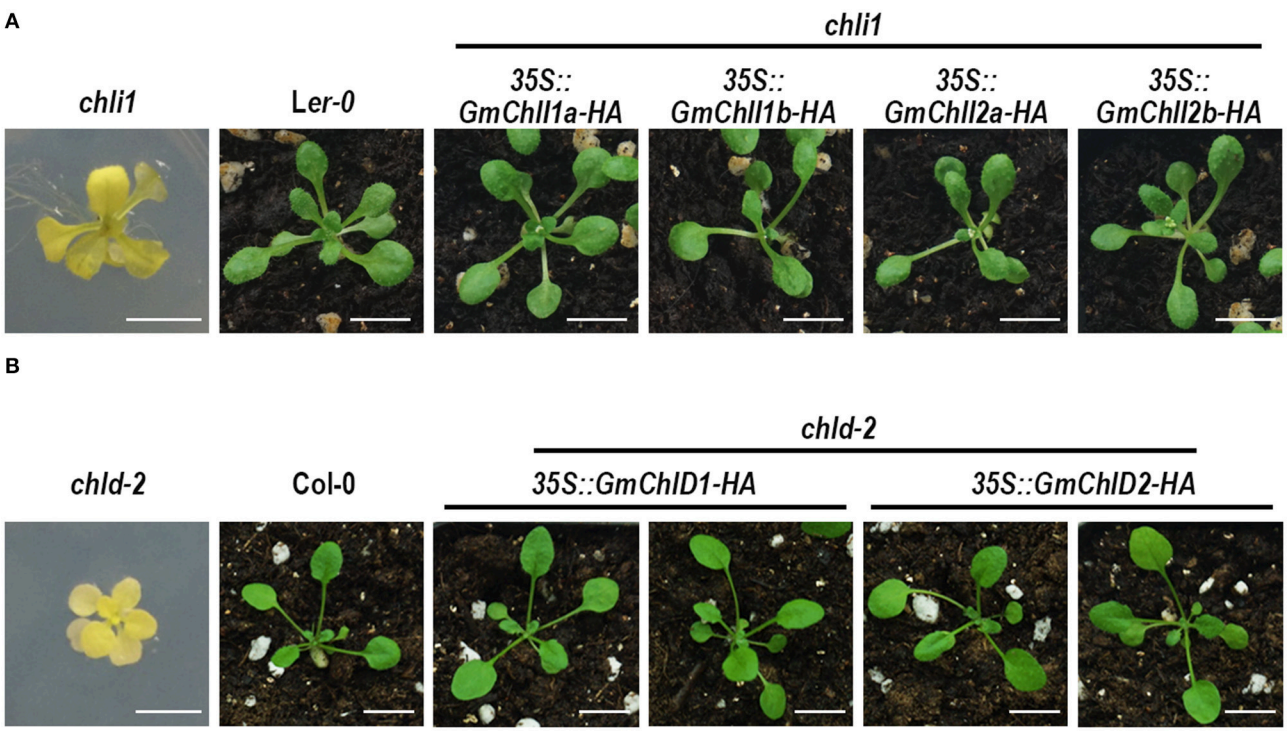

FIGURE 5 | Phenotypes of *Arabidopsis chli1* and *chld-2* mutants carrying *GmChlI* and *GmChlD* genes**. (A)** 3-week old plants of *chli1* mutant (*Ler-0* background), *Ler-0*, and transgenic *chli1* mutants carrying 35S-driven C-terminal *HA* fused *GmChlI1a*, *GmChlI1b*, *GmChlI2a*, or*GmChlI2b*; **(B)** 3-week old plants of *chld-2* mutant (Col-0 background), Col-0, and transgenic *chld-2* mutants carrying 35S-driven C-terminal *HA* fused *GmChlD1* or *GmChlD2*. All transgenic genes fully complement the mutant phenotypes. Scale bars = 5 mm.

leaves co-transformed with a GmChlI-YFP$_N$, GmChlD-YFP$_N$, or GmChlH-YFP$_N$ construct in combination with an empty YFP$_C$ vector. Taken together, these results suggest that all of GmChlIs, GmChlDs, and GmChlHs are likely involved in Mg-chelatase activity by physically interacting with each other.

Ecotopic Expression of *GmChlIs*, *GmChlDs,* and *GmChlHs* in *Arabidopsis* Corresponding Mutants

Evidences above imply that GmChlIs, GmChlDs, and GmChlHs are likely functional Mg-chelatase subunits. For further verification, we performed a complementation test by ectopically expressing *GmChlI*, *GmChlD*, and *GmChlH* genes in *Arabidopsis* corresponding mutants, *chli1*, *chld-2*, and *gun5-2*. *chli1* and *chld-2* are T-DNA insertional knockout and knockdown mutants respectively, Figure S7), showing seedling-lethal phenotypes (**Figure 5**). Therefore, all *35S::GmChlI-HA* and *35S::GmChlD-HA* constructs were transformed into corresponding heterozygous mutants, and the transgenic plants in homozygous mutant background were identified by PCR afterwards. At the T_3 generation, we found that homozygous *chli1* mutants carrying *35S::GmChlI1a-HA*, *GmChlI1b-HA*, *GmChlI2a-HA*, or *GmChlI2b-HA* showed wild-type green phenotype (**Figure 5A**). Similar wild-type phenotype was observed in homozygous *chld-2* mutants carrying *35S::GmChlD1-HA* or *GmChlD2-HA* (**Figure 5B**). These results demonstrated that all GmChlI and GmChlD isoforms could play a full functional role in the Mg-chelatase holoenzyme.

Arabidopsis gun5-2 mutant, an *AtChlH* knock-down mutant, harbors a T-DNA insertion at the promoter region of *AtChlH*

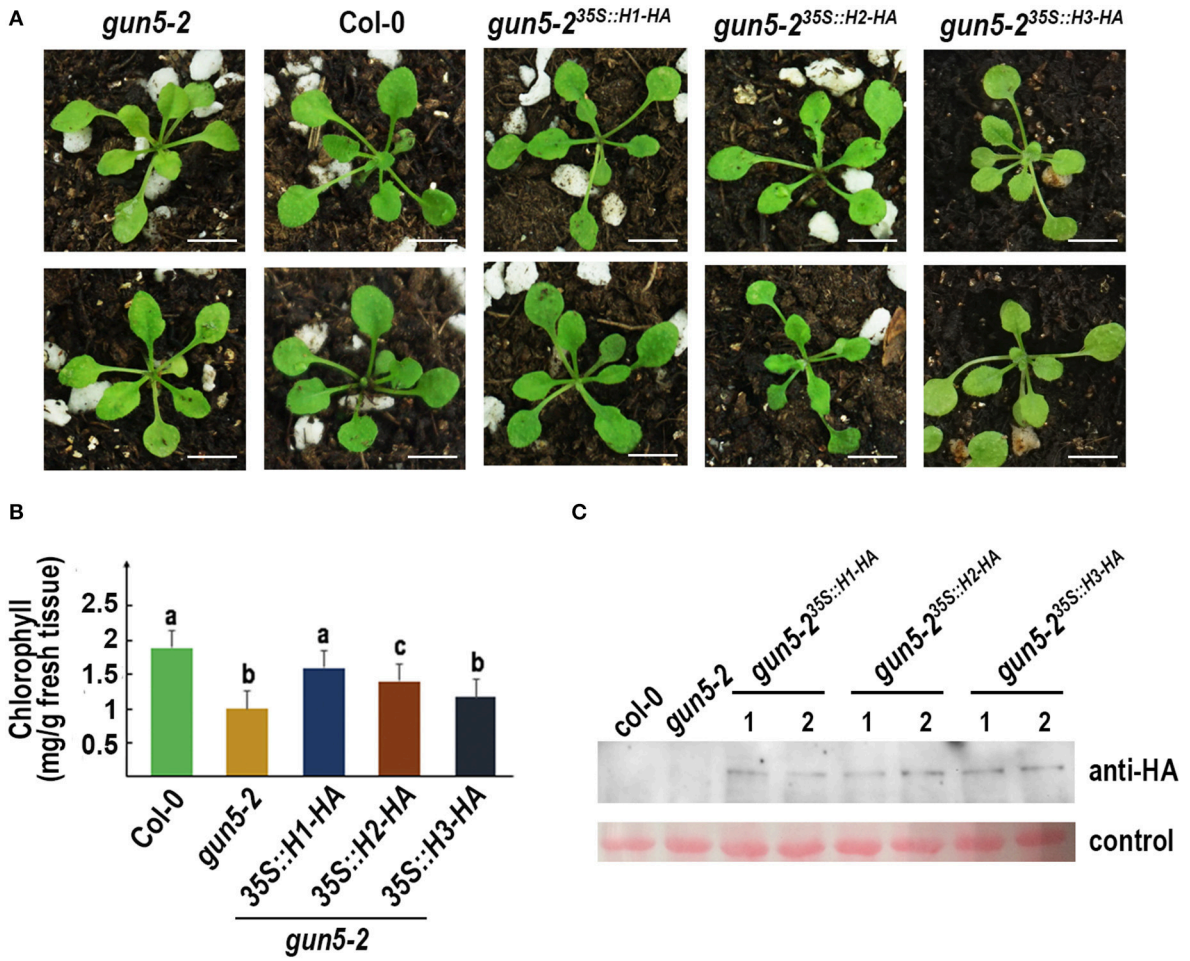

FIGURE 6 | Phenotypes of *Arabidopsis gun5-2* mutants carrying *GmChlH* genes. **(A)** 3-week old plants of *gun5-2* mutant (Col-0 background), Col-0, and transgenic *gun5-2* mutants carrying 35S-driven C-terminal *HA* fused *GmChlH1*, *GmChlH2*, and *GmChlH3*. Two independent transgenic lines are shown for each gene; **(B)** Chlorophyll contents in 3-week old plants from the lines present in **(A)**. Error bars indicate sd from three biological replications. Student *t*-test was performed for statistical analysis among all the lines; different letters represent statistically significant differences between transgenic plant and wild-type or mutant lines ($P < 0.05$); **(C)** Protein expression level of transgenes in the lines present in **(A)**. Western blot analysis was performed using HA tag antibody. The Ponceau S staining of Rubisco large subunit is used as the loading control. Scale bars = 5 mm.

(Figure S7) and produces viable pale green seedlings (**Figure 6A**). The 35S promoter-driven *HA* fused *GmChlH1*, *GmChlH2*, and *GmChlH3* were transformed into the homozygous *gun5-2* mutant. Transgenic plants carrying *35S::GmChlH1-HA* look as green as wild-type plants; however, transgenic plants carrying *35S::GmChlH2-HA* and *35S::GmChlH3-HA* show intermediate pale-green phenotypes (**Figure 6A**).

Results from a detailed chlorophyll analysis were consistent to the phenotypes (**Figure 6B**). The *gun5-2* plants expressing different GmChlHs had different chlorophyll levels. The chlorophyll content in $gun5\text{-}2^{35S::GmChlH1-HA}$ plants was highest, similar to that in wild types, and $gun5\text{-}2^{35S::GmChlH3-HA}$ plants had lowest amount of chlorophyll, which seemed a little higher than that in *gun5-2,* but without statistically significant difference (**Figure 6B**). As to $gun5\text{-}2^{35S::GmChlH2-HA}$ plants, the chlorophyll content was lower than that in $gun5\text{-}2^{35S::GmChlH1-HA}$ plants but higher than that in $gun5\text{-}2^{35S::GmChlH3-HA}$ plants (**Figure 6B**). However, western blot analysis exhibited that protein contents of three GmChlHs were similar in corresponding transgenic plants (**Figure 6C**), indicating that the failure of GmChlH2-HA and GmChlH3-HA to fully complement the *gun5-2* mutant phenotypes was not caused by a lack or lower of gene expression. These results imply that GmChlH1 is probably a full functional ChlH subunit, whereas GmChlH2 and GmChlH3 have lower chelatase activities.

CONCLUSION

In cyanobacterium and monocotyledon plants, each subunit of Mg-chelatase has only one isoform (Jensen et al., 1996; Sawers et al., 2006; Zhang et al., 2006; Muller et al., 2014), whereas most dicotyledons encodes 2 ChlI, 1 ChlD, and 1 ChlH subunits (Du et al., 2012; **Figure 1**). Soybean genome harbors 4 *GmChlI*, 2 *GmChlD*, and 3 *GmChlH* genes, and other legume species have 2 *ChlI*, 1 *ChlD*, and 2 *ChlH* genes (**Figures 1**, **2**). Phylogenetics analysis reveals that there are two gene duplication events occurring in the history of soybean Mg-chelatase, including one at the origin of the legume family, and the other one after speciation of soybean (**Figure 2**). The first round of gene duplication seems only apply to *GmChlI* and *GmChlH* genes. This is in an agreement with two recent major duplication events in soybean genome at 58 and 13 million years ago revealed by the soybean genome sequencing project (Schmutz et al., 2010).

Sequence alignment analysis (Figures S1–S3) and interaction assay (**Figure 4**; Figures S4–S6) indicate that the isoforms of each soybean Mg-chelatase subunit are likely functional proteins. Further ectopic expression of each Mg-chelatase subunit in *Arabidopsis* confirms that all of GmChlIs and GmChlDs have proper biochemical function because they can fully recover chlorophyll biosynthesis of the corresponding *Arabidopsis* mutants (**Figure 5**). However, the experiment also reveals that GmChlH2 and GmChlH3 are not as active as GmChlH1 in *Arabidopsis* (**Figure 6**). Even though GmChlH1, GmChlH2, and GmChlH3 are very similar in primary structure, the fine difference in their sequences could lead to a big change in enzyme activity.

Results from qRT-PCR and in silicon promoter analyses indicate that all soybean Mg-chelatase subunits are highly and similarly regulated by light, concerning the tissue specific expression patterns and the number of light response elements (**Tables 1**, **2**; **Figure 2**). Nevertheless, the expression levels are varied among different isoforms (**Figure 2**). Especially, the transcriptions of *GmChlI2a* and *GmChlI2b* are extremely low compared to *GmChlI1a* and *GmChlI1b* in photosynthetic tissues, indicating the latter two play the major role during active photosynthesis. Moreover, the elements responsive to environmental and growth conditions other than LREs are diverse in the promoters of all the subunit genes, indicating they are differentially regulated.

With respect to the sequence, biochemical function, and gene expression and regulation, we conclude that the paralogs of each soybean Mg-chelatase subunit are diverged in biological functions. The differently expressed and variously functional isoforms of the Mg-chelatase subunits may also suggest that there is a more complex regulatory mechanism to control chlorophyll content in soybean in order to response to different development stages and environmental stresses, and to optimize its light harvesting capacity and photosynthetic efficiency.

AUTHOR CONTRIBUTIONS

MX, AF, and DZ designed research. DZ, EC, XY, YoC, QY, YaC, and XL performed research. DZ, EC, XY, YoC, QY, YW, MX, and AF analyzed data. DZ, MX, and AF wrote the paper with contributions from all authors. All authors read and approved the manuscript.

FUNDING

This work was supported by the National Key R&D Program of China (2016YFD0101500 and 2016YFD0101503) and a Natural Sciences Foundation of China project (31371226) to MX, and a Shaanxi Science and Technology Project (2014KTCL02-03) to AF.

ACKNOWLEDGMENTS

We thank Dr. Hsou-min Li (Institute of Molecular Biology, Academia Sinica, Taipei, Taiwan) and Dr. Fang-Qing Guo (Institute of Plant Physiology & Ecology, Shanghai, China) for kindly providing us *Arabidopsis* mutants.

SUPPLEMENTARY MATERIAL

The Supplementary Material for this article can be found online at: https://www.frontiersin.org/articles/10.3389/fpls.2018.00720/full#supplementary-material

REFERENCES

Adhikari, N. D., Froehlich, J. E., Strand, D. D., Buck, S. M., Kramer, D. M., and Larkin, R. M. (2011). GUN4-porphyrin complexes bind the ChlH/GUN5 subunit of Mg-chelatase and promote chlorophyll biosynthesis in *Arabidopsis*. *Plant Cell* 23, 1449–1467. doi: 10.1105/tpc.110.082503

Ahmad, I., Khaliq, T., Ahmad, A., Basra, S. M. A., Hasnain, Z., and Ali, A. (2012). Effect of seed priming with ascorbic acid, salicylic acid and hydrogen peroxide on emergence, vigor and antioxidant activities of maize. *Afr. J. Biotechnol.* 11, 1127–1132. doi: 10.5897/AJB11.2266

Ainsworth, E. A., Yendrek, C. R., Skoneczka, J. A., and Long, S. P. (2012). Accelerating yield potential in soybean: potential targets for biotechnological improvement. *Plant Cell Environ.* 35, 38–52. doi: 10.1111/j.1365-3040.2011.02378.x

Bi, W., Wu, L., Coustry, F., de Crombrugghe, B., and Maity, S. N. (1997). DNA binding specificity of the CCAAT-binding factor CBF/NF-Y. *J. Biol. Chem.* 272, 26562–26572. doi: 10.1074/jbc.272.42.26562

Brzezowski, P., Richter, A. S., and Grimm, B. (2015). Regulation and function of tetrapyrrole biosynthesis in plants and algae. *Biochim. Biophys. Acta.* 1847, 968–985. doi: 10.1016/j.bbabio.2015.05.007

Campbell, B. W., Mani, D., Curtin, S. J., Slattery, R. A., Michno, J. M., Ort, D. R., et al. (2015). Identical substitutions in magnesium chelatase paralogs result in chlorophyll-deficient soybean mutants. *G3. (Bethesda)* 5, 123–131. doi: 10.1534/g3.114.015255

Chen, M., and Blankenship, R. E. (2011). Expanding the solar spectrum used by photosynthesis. *Trends Plant Sci.* 16, 427–431. doi: 10.1016/j.tplants.2011.03.011

Chen, X., Pu, H., Fang, Y., Wang, X., Zhao, S., Lin, Y., et al. (2015). Crystal structure of the catalytic subunit of magnesium chelatase. *Nat. Plants* 1:15125. doi: 10.1038/nplants.2015.125

Clough, S. J., and Bent, A. F. (1998). Floral dip: a simplified method for *Agrobacterium*-mediated transformation of *Arabidopsis thaliana*. *Plant J.* 16, 735–743. doi: 10.1046/j.1365-313x.1998.00343.x

Croce, R., and van Amerongen, H. (2014). Natural strategies for photosynthetic light harvesting. *Nat. Chem. Biol.* 10, 492–501. doi: 10.1038/nchembio.1555

Delmas, F., Sankaranarayanan, S., Deb, S., Widdup, E., Bournonvile, C., Bollier, N., et al. (2013). ABI3 controls embryo degreening through Mendel's I locus. *Proc. Natl. Acad. Sci. U.S.A.* 110, E3888–E3894. doi: 10.1073/pnas.1308114110

Deng, X. J., Zhang, H. Q., Wang, Y., He, F., Liu, J. L., Xiao, X., et al. (2014). Mapped clone and functional analysis of leaf-color gene *Ygl7* in a rice hybrid (*Oryza sativa* L. ssp. indica). *PLoS ONE* 9:e99564. doi: 10.1371/journal.pone.0099564

Dornbos, D. L. Jr., and Mullen, R. E. (1992). Soybean seed protein and oil contents and fatty acid composition adjustments by drought and temperature. *J. Am. Oil Chem. Soc.* 69, 228–231. doi: 10.1007/BF02635891

Du, S. Y., Zhang, X. F., Lu, Z., Xin, Q., Wu, Z., Jiang, T., et al. (2012). Roles of the different components of magnesium chelatase in abscisic acid signal transduction. *Plant Mol. Biol.* 80, 519–537. doi: 10.1007/s11103-012-9965-3

Egli, D. B. (2008). Soybean yield trends from 1972 to 2003 in mid-western USA. *Field Crops Res.* 106, 53–59. doi: 10.1016/j.fcr.2007.10.014

Fodje, M. N., Hansson, A., Hansson, M., Olsen, J. G., Gough, S., Willows, R. D., et al. (2001). Interplay between an AAA module and an integrin I domain may regulate the function of magnesium chelatase. *J. Mol. Biol.* 311, 111–122. doi: 10.1006/jmbi.2001.4834

Gibson, L. C., Marrison, J. L., Leech, R. M., Jensen, P. E., Bassham, D. C., Gibson, M., et al. (1996). A putative Mg chelatase subunit from *Arabidopsis thaliana* cv C24 (sequence and transcript analysis of the gene, import of the protein into chloroplasts, and *in situ* localization of the transcript and protein). *Plant Physiol.* 111, 61–71. doi: 10.1104/pp.111.1.61

Gräfe, S., Saluz, H. P., Grimm, B., and Hänel, F. (1999). Mg-chelatase of tobacco: the role of the subunit CHLD in the chelation step of protoporphyrin IX. *Proc. Natl. Acad. Sci. U.S.A.* 96, 1941–1946. doi: 10.1073/pnas.96.5.1941

Guan, C., Wang, X., Feng, J., Hong, S., Liang, Y., Ren, B., et al. (2014). Cytokinin antagonizes abscisic acid-mediated inhibition of cotyledon greening by promoting the degradation of ABSCISIC ACID INSENSITIVE5 protein in *Arabidopsis*. *Plant Physiol.* 164, 1515–1526. doi: 10.1104/pp.113.234740

Hansson, A., Willows, R. D., Roberts, T. H., and Hansson, M. (2002). Three semidominant barley mutants with single amino acid substitutions in the smallest magnesium chelatase subunit form defective AAA+ hexamers. *Proc. Natl. Acad. Sci. U.S.A.* 99, 13944–13949. doi: 10.1073/pnas.212504499

Huang, Y. S., and Li, H. M. (2009). *Arabidopsis* CHLI2 can substitute for CHLI1. *Plant Physiol.* 50, 636–645. doi: 10.1104/pp.109.135368

Jensen, P. E., Gibson, L. C., and Hunter, C. N. (1998). Determinants of catalytic activity with the use of purified I, D and H subunits of the magnesium protoporphyrin IX chelatase from *Synechocystis* PCC6803. *Biochem. J.* 334, 335–344. doi: 10.1042/bj3340335

Jensen, P. E., Gibson, L. C., Henningsen, K. W., and Hunter, C. N. (1996). Expression of the chlI, chlD, and chlH genes from the *Cyanobacterium synechocystis* PCC6803 in *Escherichia coli* and demonstration that the three cognate proteins are required for magnesium-protoporphyrin chelatase activity. *J. Biol. Chem.* 271, 16662–16667. doi: 10.1074/jbc.271.28.16662

Karger, G. A., Reid, J. D., and Hunter, C. N. (2001). Characterization of the binding of deuteroporphyrin IX to the magnesium chelatase H subunit and spectroscopic properties of the complex. *Biochemistry* 40, 9291–9299. doi: 10.1021/bi010562a

Khan, N. A., Syeed, S., Masood, A., Nazar, R., and Iqbal, N. (2010). Application of salicylic acid increases contents of nutrients and antioxidative metabolism in mungbean and alleviates adverse effects of salinity stress. *Int. J. Plant Biol.* 1:e1. doi: 10.4081/pb.2010.e1

Kim, S., Schlicke, H., Van, R. K., Karvonen, K., Subramaniam, A., Richter, A. S., et al. (2013). *Arabidopsis* chlorophyll biosynthesis: an essential balance between the methylerythritol phosphate and tetrapyrrole pathways. *Plant Cell* 25, 4984–4993. doi: 10.1105/tpc.113.119172

Kobayashi, K., Baba, S., Obayashi, T., Obayashi, T., Sato, M., Toyooka, K., et al. (2012). Regulation of root greening by light and auxin/cytokinin signaling in *Arabidopsis*. *Plant Cell* 24, 1081–1095. doi: 10.1105/tpc.111.092254

Koester, R. P., Skoneczka, J. A., Cary, T. R., Diers, B. W., and Ainsworth, E. A. (2014). Historical gains in soybean (*Glycine max* Merr.) seed yield are driven by linear increases in light interception, energy conversion, and partitioning efficiencies. *J. Exp. Bot.* 65, 3311–3321. doi: 10.1093/jxb/eru187

Lake, V., Olsson, U., Willows, R. D., and Hansson, M. (2004). ATPase activity of magnesium chelatase subunit I is required to maintain subunit D *in vivo*. *Eur. J. Biochem.* 271, 2182–2188. doi: 10.1111/j.1432-1033.2004.04143.x

Lescot, M., Déhais, P., Thijs, G., Marchal, K., Moreau, Y., Peer, Y. V. D., et al. (2002). PlantCARE, a database of plant *cis*-acting regulatory elements and a portal to tools for in silico analysis of promoter sequences. *Nucleic Acids Res.* 30, 325–327. doi: 10.1093/nar/30.1.325

Liu, X., Li, Y., and Zhong, S. (2017). Interplay between light and plant hormones in the control of *Arabidopsis* seedling chlorophyll biosynthesis. *Front. Plant Sci.* 8:1433. doi: 10.3389/fpls.2017.01433

Masuda, T. (2008). Recent overview of the Mg branch of the tetrapyrrole biosynthesis leading to chlorophylls. *Photosynth. Res.* 96, 121–143. doi: 10.1007/s11120-008-9291-4

Masuda, T., and Fujita, Y. (2008). Regulation and evolution of chlorophyll metabolism. *Photochem. Photobiol. Sci.* 7, 1131–1149. doi: 10.1039/b807210h

Masuda, T., and Goldsmith, P. D. (2009). World soybean production: area harvested, yield, and long-term projections. *Int. Food Agribus. Manag. Rev.* 12, 143–161.

Mochizuki, N., Brusslan, J. A., Larkin, R., Nagatani, A., and Chory, J. (2001). *Arabidopsis genomes uncoupled 5* (*GUN5*) mutant reveals the involvement of Mg-chelatase H subunit in plastid-to-nucleus signal transduction. *Proc. Natl. Acad. Sci. U.S.A.* 98, 2053–2058. doi: 10.1073/pnas.98.4.2053

Müller, A. H., Sawicki, A., Zhou, S., Tabrizi, S. T., Luo, M., Hansson, M., et al. (2014). Inducing the oxidative stress response in *Escherichia coli* improves the quality of a recombinant protein: magnesium chelatase ChlH. *Protein Exp. Purif.* 101, 61–67. doi: 10.1016/j.pep.2014.06.004

Nakayama, M., Masuda, T., Bando, T., Yamagata, H., Ohta, H., and Takamiya, K. (1998). Cloning and expression of the soybean chlH gene encoding a subunit of Mg-chelatase and localization of the Mg^{2+} concentration-dependent ChlH protein within the chloroplast. *Plant Cell Physiol.* 39, 275–284. doi: 10.1093/oxfordjournals.pcp.a029368

Nakayama, M., Masuda, T., Sato, N., Yamagata, H., Bowler, C., Ohta, H., et al. (1995). Cloning, subcellular localization and expression of *chlI*, a subunit of magnesium chelatase in soybean. *Biochem. Biophys. Res. Commun.* 215, 422–428. doi: 10.1006/bbrc.1995.2481

Natarajan, S., Luthria, D., Bae, H., Lakshman, D., and Mitra, A. (2013). Transgenic soybeans and soybean protein analysis: an overview. *J. Agric. Food Chem*. 61, 1736–1743. doi: 10.1021/jf402148e

Palmer, R. G., Hedges, B. R., Benavente, R. S., and Groose, R. W. (1989). *w4*-mutable line in soybean. *Dev. Genet*. 10, 542–551. doi: 10.1002/dvg.1020100613

Papenbrock, J., Mock, H., Kruse, E., and Grimm, B. (1999). Expression studies in tetrapyrrole biosynthesis: inverse maxima of magnesium chelatase and ferrochelatase activity during cyclic photoperiods. *Planta* 208, 264–273. doi: 10.1007/s004250050558

Pettigrew, W. T., Hesketh, D., Peters, D. B., and Woolley, T. (1989). Characterization of canopy photosynthesis of chlorophyll-deficient soybean isolines. *Crop Sci*. 29, 1024–1028. doi: 10.2135/cropsci1989.0011183X002900040040x

Ramachandra Reddy, A., Chaitanya, K. V., and Vivekanandan, M. (2004). Drought-induced responses of photosynthesis and antioxidant metabolism in higher plants. *J. Plant Physiol.* 161, 1189–1202. doi: 10.1016/j.jplph.2004.01.013

Sawers, R. J., Viney, J., Farmer, P. R., Bussey, R. R., Olsefski, G., Anufrikova, K., et al. (2006). The maize *Oil yellow1* (*Oy1*) gene encodes the I subunit of magnesium chelatase. *Plant Mol. Biol*. 60, 95–106. doi: 10.1007/s11103-005-2880-0

Schlueter, J. A., Lin, J. Y., Schlueter, S. D., VasylenkoSanders, I. F., Deshpande, S., Yi, J., et al. (2007). Gene duplication and paleopolyploidy in soybean and the implications for whole genome sequencing. *BMC Genomics* 8:330. doi: 10.1186/1471-2164-8-330

Schmutz, J., Cannon, S. B., Schlueter, J., Ma, J., Mitros, T., Nelson, W., et al. (2010). Genome sequence of the palaeopolyploid soybean. *Nature* 463, 178–183. doi: 10.1038/nature08670

Shoemaker, R. C., Schlueter, J., and Doyle, J. J. (2006). Paleopolyploidy and gene duplication in soybean and other legumes. *Curr. Opin. Plant Biol*. 9, 104–109. doi: 10.1016/j.pbi.2006.01.007

Sirijovski, N., Olsson, U., Lundqvist, J., Al-Karadaghi, S., Willows, R. D., and Hansson, M. (2006). ATPase activity associated with the magnesium chelatase H-subunit of the chlorophyll biosynthetic pathway is an artefact. *Biochem. J*. 400, 477–484. doi: 10.1042/BJ20061103

Slattery, R. A., VanLoocke, A., Bernacchi, C. J., Zhu, X. G., and Ort, D. R. (2017). Photosynthesis, light use efficiency, and yield of reduced-chlorophyll soybean mutants in field conditions. *Front. Plant Sci*. 8:549. doi: 10.3389/fpls.2017.00549

Stephenson, P. G., and Terry, M. J. (2008). Light signaling pathways regulating the Mg-chelatase branchpoint of chlorophyll synthesis during de-etiolation in *Arabidopsis thaliana*. *Photochem. Photobiol. Sci*. 7, 1243–1252. doi: 10.1039/b802596g

Tamura, K., Stecher, G., Peterson, D., Filipski, A., and Kumar, S. (2013). MEGA6: Molecular evolutionary genetics analysis version 6.0. *Mol. Biol. Evol*. 30, 2725–2729. doi: 10.1093/molbev/mst197

Toledo-Ortiz, G., Johansson, H., Lee, K. P., Bou-Torrent, J., Stewart, K., Steel, G., et al. (2014). The HY5-PIF regulatory module coordinates light and temperature control of photosynthetic gene transcription. *PLoS Genet*. 10:e1004416. doi: 10.1371/journal.pgen.1004416

Waadt, R., Schmidt, L. K., Lohse, M., Hashimoto, K., Bock, R., and Kudla, J. (2008). Multicolor bimolecular fluorescence complementation reveals simultaneous formation of alternative CBL/CIPK complexes in planta. *Plant J*. 56, 505–516. doi: 10.1111/j.1365-313X.2008.03612.x

Walker, B. J., Drewry, D. T., Slattery, R. A., VanLoocke, A., Cho, Y. B., and Ort, D. R. (2017). Chlorophyll can be reduced in crop canopies with little penalty to photosynthesis. *Plant Physiol*. 176, 1215–1232. doi: 10.1104/pp.17.01401

Walker, C. J., and Willows, R. D. (1997). Mechanism and regulation of Mg-chelatase. *Biochem. J*. 327, 321–333. doi: 10.1042/bj3270321

Wasternack, C., and Hause, B. (2013). Jasmonates: biosynthesis, perception, signal transduction and action in plant stress response, growth and development. *Ann. Bot.* 111, 1021–1058. doi: 10.1093/aob/mct067

Winter, D., Vinegar, B., Nahal, H., Ammar, R., Wilson, G. V., and Provart, N. (2007). An "electronic fluorescent pictograph" browser for exploring and analyzing large-scale biological data sets. *PLoS ONE* 2:e718. doi: 10.1371/journal.pone.0000718

Zhang, H., Li, J., Yoo, J. H., Yoo, S. C., Cho, S. H., Koh, H. J., et al. (2006). Rice *Chlorina-1* and *Chlorina-9* encode ChlD and ChlI subunits of Mg-chelatase, a key enzyme for chlorophyll synthesis and chloroplast development. *Plant Mol. Biol.* 62, 325–337. doi: 10.1007/s11103-006-9024-z

Zhong, S., Shi, H., Xue, C., Wei, N., Guo, H., and Deng, X. W. (2014). Ethylene-orchestrated circuitry coordinates a seedling's response to soil cover and etiolated growth. *Proc. Natl. Acad. Sci. U.S.A*. 111, 3913–3920. doi: 10.1073/pnas.1402491111

Zhu, X. G., Long, S. P., and Ort, D. R. (2010). Improving photosynthetic efficiency for greater yield. *Annu. Rev. Plant Biol*. 61, 235–261. doi: 10.1146/annurev-arplant-042809-112206

Conflict of Interest Statement: The authors declare that the research was conducted in the absence of any commercial or financial relationships that could be construed as a potential conflict of interest.

frontiers in Plant Science

METHODS
published: 18 August 2017
doi: 10.3389/fpls.2017.01444

A Rapid and Efficient Method to Obtain Photosynthetic Cell Suspension Cultures of *Arabidopsis thaliana*

*Simone Sello[1], Roberto Moscatiello[1], Nicoletta La Rocca[1], Barbara Baldan[1,2] and Lorella Navazio[1,2]**

[1] Department of Biology, University of Padova, Padova, Italy, [2] Botanical Garden, University of Padova, Padova, Italy

Photosynthetic cell suspension cultures are a useful experimental system to analyze a variety of physiological processes, bypassing the structural complexity of the plant organism *in toto*. Nevertheless, cell cultures containing functional chloroplasts are quite difficult to obtain, and this process is usually laborious and time-consuming. In this work a novel and rapid method to set up photosynthetic cell suspension cultures from the model plant *Arabidopsis thaliana* was developed. The direct germination of *Arabidopsis* seeds on a sucrose-containing agarized culture medium supplemented with 0.25 μg/ml 6-benzylaminopurine and 0.5 μg/ml 2,4-dichlorophenoxyacetic acid caused the straightforward formation of green calli at the level of seedling hypocotyls. The subsequent transfer of these calli in liquid culture medium containing the same concentrations of phytohormones and gradually decreasing sucrose levels allowed for the establishment of chloroplast-containing cell suspension cultures, containing functional chloroplasts, in a much faster way than previously described procedures. Pulse amplitude modulation analyses, measurements of oxygen evolution and electron transport rate, together with confocal and electron microscopy observations, confirmed the photosynthetic efficiency of these cell suspension cultures. The described procedure lends itself as a simple and effective way to obtain a convenient tool for a wide array of structural and functional studies on chloroplasts.

Keywords: *Arabidopsis thaliana*, green calli, chloroplasts, photosynthetic cell suspension cultures, phytohormones

OPEN ACCESS

Edited by:
Juliette Jouhet, UMR5168 Laboratoire de Physiologie Cellulaire Vegetale (LPCV), France

Reviewed by:
Jaideep Mathur, University of Guelph, Canada
Rosario Vera-Estrella, National Autonomous University of Mexico, Mexico

***Correspondence:**
Lorella Navazio
lorella.navazio@unipd.it

Specialty section:
This article was submitted to Plant Cell Biology, a section of the journal Frontiers in Plant Science

Received: *01 February 2017*
Accepted: *03 August 2017*
Published: *18 August 2017*

Citation:
Sello S, Moscatiello R, La Rocca N, Baldan B and Navazio L (2017) A Rapid and Efficient Method to Obtain Photosynthetic Cell Suspension Cultures of Arabidopsis thaliana. Front. Plant Sci. 8:1444. doi: 10.3389/fpls.2017.01444

INTRODUCTION

Plant cell suspension cultures are widely used as a useful and versatile experimental system to analyze complex plant physiological processes at the cellular and molecular level. By resolving the complexity of an *in toto* plant into its elementary units, suspension-cultured cells often represent a convenient tool to study a wide range of phenomena. This type of experimental system has been shown to be suitable to investigate many aspects of ion transport, secondary metabolite production, gene expression and defense responses (Ebel and Mithöfer, 1998; Hall, 2000; Moscatiello et al., 2006; González-Pérez et al., 2011; Wilson et al., 2014). In the field of signal transduction, cell suspension cultures have been shown to be an excellent mean to investigate calcium-mediated signaling events, by allowing the detection and amplification of even faint calcium signals, sometimes limited *in vivo* to only a particular tissue or cell type (Mithöfer et al., 1999; Lecourieux et al., 2005; Navazio et al., 2007a,b). Homogeneous plant cell

populations were also used to evaluate the translocating properties of cell-penetrating peptides, i.e., short cationic peptides that can be used as nanocarriers for the intracellular delivery of proteins (Zonin et al., 2011). Special types of cell cultures, containing for example specific members of the plastid family, may help to decipher molecular, physiological and metabolic mechanisms more easily than an *in toto* system, based on the use of entire seedlings. Unfortunately, due to so far elusive reasons, photoautotrophic cell cultures are quite difficult to obtain, and have been developed only for a restrict number of species (Roitsch and Sinha, 2002). Previous studies have already shown the advantages of working with cell cultures containing functional chloroplasts (Roitsch and Sinha, 2002; Hampp et al., 2012; Gutiérrez et al., 2014). The use of both heterotrophic and autotrophic cell suspension cultures in signaling studies has recently allowed the dissection of differential stimulus-specific calcium signals of non-green plastids *versus* chloroplasts (Sello et al., 2016).

In this work we describe a novel and rapid method to obtain *Arabidopsis thaliana* photosynthetic cell suspension cultures, i.e., containing chloroplasts as functional type of plastids. The time interval needed to establish such experimental system was found to be greatly reduced in comparison with traditionally used methods to set up photoautotrophic cell cultures (Loyola-Vargas and Vázquez-Flota, 2006; Mustafa et al., 2011; Hampp et al., 2012; Sello et al., 2016).

MATERIALS AND METHODS

Plant Material and Establishment of Photosynthetic Cultures

Arabidopsis thaliana ecotype Columbia (Col-0) seeds were surface sterilized for 60 s in a 70% ethanol, 0.05% Triton X-100 solution, 60 s in 100% ethanol and let dry on an autoclaved Whatman paper disk for at least 10 min. Twenty seeds were sown per cell culture dish (100 mm × 20 mm, Falcon, Corning, NY, United States), each containing 20 ml Murashige and Skoog (Murashige and Skoog, 1962) medium (MS Medium including vitamins, Prod. No. M0222, Duchefa Biochemie, Harlem, The Netherlands) supplemented with 3% sucrose, 0.25 μg/ml 6-benzylaminopurine (BAP), 0.5 μg/ml 2,4-dichlorophenoxyacetic acid (2,4-D), 0.8% plant agar, pH 5.5 and maintained in a growing chamber at 24°C with a 16/8 h light/dark cycle. After exactly 3 weeks, well-developed green calli, forming at the hypocotyl level, were cut and axenically transferred into 50 ml Erlenmeyer flasks (10 calli per flask) containing 10 ml MS medium supplemented with 2% sucrose, 0.25 μg/ml BAP, 0.5 μg/ml 2,4-D, pH 5.5 (pH 5.0 after autoclave). *In vitro* cultures were placed on a shaker at 80 rpm at 24°C under a relatively high illumination rate (110 μmol photons m^{-2} s^{-1}) under an unvaried 16/8 h light/dark photoperiod and renewed every week by transferring 1 packed cell volume (PCV) in 20 ml of MS medium containing the same concentrations of phytohormones as above and stepwise 50% less sucrose content. The growth curve of the cell cultures was determined as previously described (Moscatiello et al., 2013).

Light and Electron Microscopy Analyses

Observation of calli under a fluorescence stereomicroscope and of suspension-cultured cells by laser scanning confocal microscopy was carried out as previously described (Sello et al., 2016).

Transmission electron microscopy (TEM) analyses were carried as described by Zuppini et al. (2010).

Determination of Photosynthetic Pigments

Total chlorophylls and carotenoids were extracted in 80% acetone (v/v). Suspension-cultured cells (2 ml) in exponential growth phase were pelletted by centrifugation (1600 rpm for 2 min), the culture medium was removed and the fresh weight annotated. 80% (v/v) acetone (1 ml) was added and the samples were incubated at 4°C for 48 h in the dark. The supernatant obtained by centrifugation was spectrophotometrically analyzed and chlorophyll a and b, and carotenoid concentrations were calculated according to Wellburn (1994) and referred to g of fresh weight and total protein content (Zonin et al., 2011).

Pulse Amplitude Modulation (PAM) Analyses

Suspension-cultured cells (6-day-old) were placed in Petri dishes in a Closed FluorCam 800 MF (Photon Systems Instruments, Drasov, Czech Republic) and the maximum quantum yield of photosystem II (F_v/F_m, where F_v is the variable fluorescence given by the difference between the maximal (F_m) and the basal (F_0) fluorescence of chlorophyll) was analyzed and recorded.

Measurement of Oxygen Evolution

The measurements were performed at 25°C by using a Clark-type O_2 electrode (Hansatech, King's Lynn, United Kingdom). Suspension-cultured cells (6-day-old) in exponential growth phase were harvested by centrifugation and suspended in fresh culture medium. Their respiratory rate was measured in the dark while O_2 evolution was recorded after application of light with an intensity of 1500 μmol photons m^{-2} s^{-1} and in presence of 5 mM bicarbonate. Measurements were carried out in 2 ml total volume of cell culture. The total O_2 production was referred to g of cell fresh weight.

Measurement of Electron Transport Rate

Electron transport rate (ETR) of dark-adapted green cell suspension cultures was characterized monitoring PSII chlorophyll fluorescence at different light intensities. After 20 min of dark adaptation to completely oxidize the photosynthetic electron transport chain, samples were treated with actinic light of increasing intensity. After 60 s of each treatment a saturation pulse of 6000 μmol photons m^{-2} s^{-1} (600 ms) was used to assess the redox state of PSII. Every analysis lasted 15 min in total. During this protocol chlorophyll fluorescence was monitored using a Dual-PAM 100 (Walz). ETR was calculated as Y(II) × PPFD × 0.5 (Maxwell and Johnson, 2000).

Starch Detection and Quantitative Determination

Starch was detected by light microscopy observations after Lugol staining of photosynthetic cell suspension cultures and by TEM analyses. For starch quantitative determination, cells (>1 g fresh weight) were extensively washed with PBS (five times with 10 ml, each time followed by centrifugation at 450 *g* for 1 min). The cell pellet was ground in liquid nitrogen and starch concentration was measured by using a Starch Assay Kit (Sigma–Aldrich, St. Louis, MO, United States) according to manufacturer's instructions.

RESULTS

Arabidopsis thaliana seeds were surface sterilized and sown on Murashige and Skoog (MS) medium containing 3% sucrose, 0.8% plant agar and supplemented with

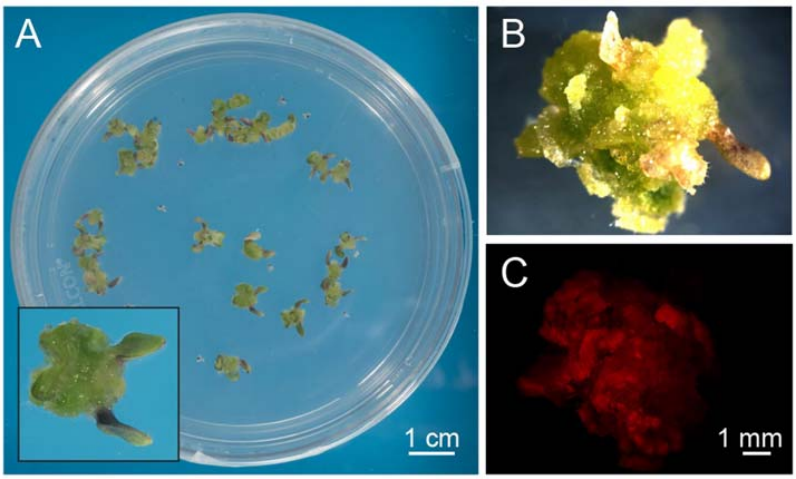

FIGURE 1 | Exogenous hormone-induced production of green calli from *Arabidopsis* seedlings. **(A)** Surface-sterilized seeds were plated on a cytokynin- and auxin-enriched agarized solid medium containing sucrose (MS, 0.8% agar, 3% sucrose, 0.25 μg/ml BAP, 0.5 μg/ml 2,4-D) that had a delaying effect on seedling growth and development. Insert: magnification of a well-developed callus originating from the dedifferentiation and proliferation of hypocotyl cells after 3 weeks of germination. **(B,C)** Observations at the fluorescence stereomicroscope of green calli **(B)**, displaying red autofluorescence of chlorophyll when excited with blue light **(C)**.

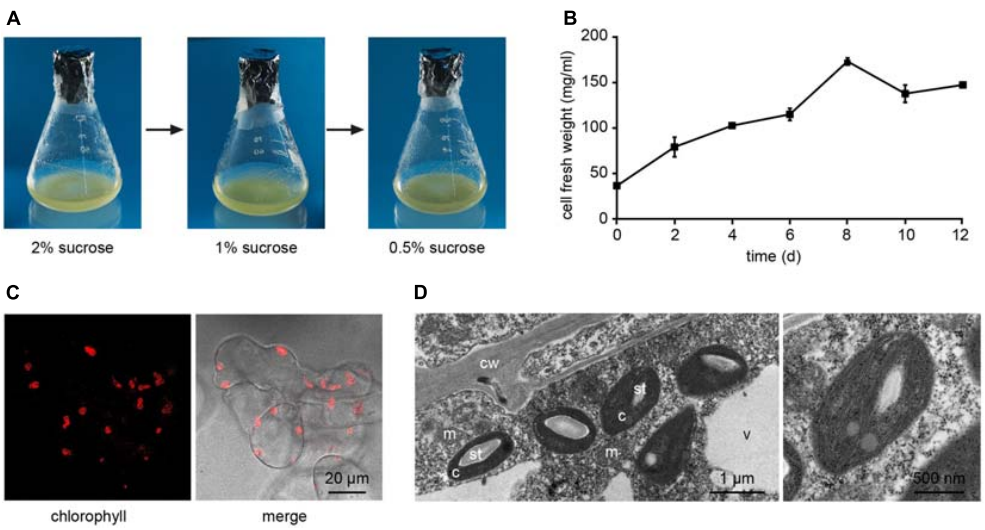

FIGURE 2 | Establishment of *Arabidopsis* photosynthetic cell suspension cultures. **(A)** Suspension-cultured cells were maintained in MS culture medium containing 0.25 μg/ml BAP and 0.5 μg/ml 2,4-D, and gradually reduced sucrose concentrations to stimulate the photosynthetic activity. **(B)** Growth curve of the photosynthetic cell suspension culture, after three sub-culturing steps in 0.5% sucrose-containing medium. Data are the means ± SE of three independent replicates for each time point. **(C)** Confocal microscopy analysis confirmed the presence of chloroplasts as functional type of plastids in the cell suspension cultures. **(D)** Ultrastructure of chloroplast-containing suspension-cultured cells. c, chloroplasts; cw, cell wall; m, mitochondria; st, starch; v, vacuole. In the image on the right the magnification of a chloroplast is shown.

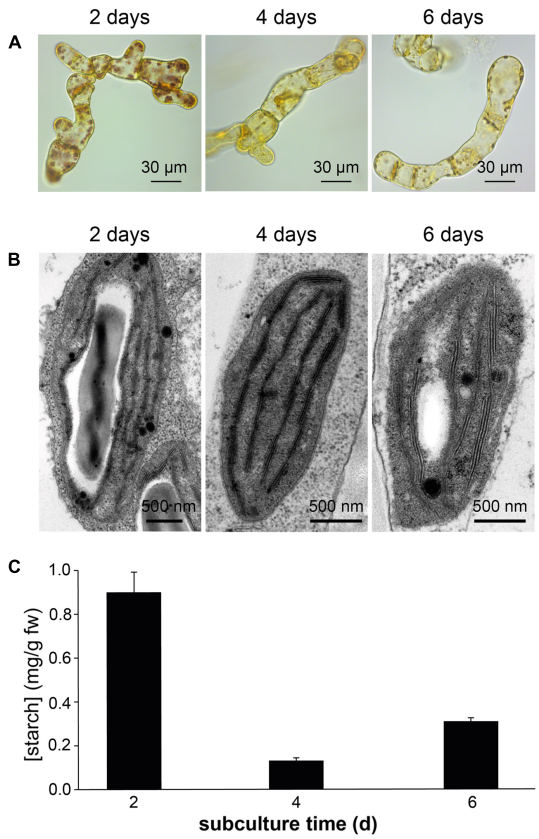

FIGURE 3 | Detection of starch in *Arabidopsis* photosynthetic cell cultures at different subculture times. Determinations of starch was carried out in suspension-cultured cells after 2, 4, and 6 days of subculture by Lugol staining **(A)**, TEM analyses **(B),** and a quantitative biochemical assay **(C)**.

0.25 µg/ml 6-benzylaminopurine (BAP) and 0.5 µg/ml 2,4-dichlorophenoxyacetic acid (2,4-D). We observed that, already after 1 week from sowing, the growth of *Arabidopsis* seedlings was slowed down, with the subsequent progressive formation of a green mass of dedifferentiated cells at the hypocotyl level (**Figure 1A**). After 3 weeks well-developed green calli, exhibiting evident chlorophyll autofluorescence (**Figures 1B,C**), were axenically separated from the root and cotyledons, cut in small pieces with a sterilized sharp blade, and transferred into liquid MS medium containing 2% sucrose and the same concentrations of phytohormones described above. In particular, cell suspension cultures were initiated by transferring 10 green calli (0.14 ± 0.01 g fresh weight, $n = 12$) into 50 ml Erlenmeyer flasks containing 10 ml of liquid medium. Cell suspension cultures were renewed every week by transferring 1 PCV in 20 ml of MS medium containing stepwise 50% less sucrose content, in order to stimulate photosynthetic activity. In particular, sucrose concentration was gradually reduced from 2 to 1% and then to 0.5% (w/v) every 2–3 weeks (**Figure 2A**). Once stabilized in the lowest sucrose concentration condition, a growth curve for the newly established photosynthetic culture cell line was determined. The fresh weight of the cell cultures was found to increase about five times in 8 days, followed by a stationary phase lasting 4 more days (**Figure 2B**).

Confocal microscopy (**Figure 2C**) and TEM (**Figure 2D**) analyses of suspension-cultured log-phase cells demonstrated the presence of chloroplasts as functional type of plastids in the newly established green cultures. In particular, TEM analyses confirmed the good ultrastructural organization of the cells, with chloroplasts exhibiting grana, stroma lamellae and starch granules (**Figure 2D**). Light microscopy observations after Lugol staining (**Figure 3A**), TEM analyses (**Figure 3B**) and biochemical analyses based on a quantitative starch assay (**Figure 3C**) demonstrated that the relative abundance of starch changed with the age of the culture, being maximal after 2 days from subculturing, minimal after 4 days, and reaching an intermediate level after 6 days. Transitory starch, produced during the 16 h light period, was found to disappear after 8 h of dark (**Figure 4**). Although the total photosynthetic pigment content of the cell suspension cultures (**Figure 5A**) was found to be at slightly lower levels than in a previously published work in *Arabidopsis* (Hampp et al., 2012), pulse amplitude modulation (PAM)

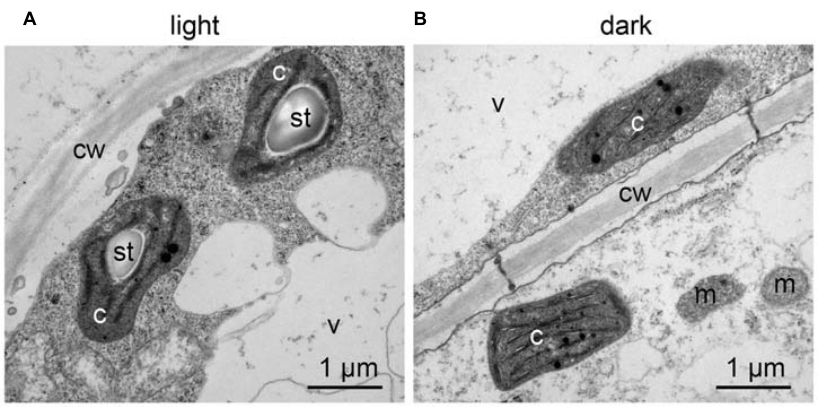

FIGURE 4 | Transitory starch accumulation in *Arabidopsis* photosynthetic cell cultures during the light/dark cycle. TEM observations were carried out: **(A)** at the end of the 16 h light phase; **(B)** at the end of the 8 h dark phase. c, chloroplasts; cw, cell wall; m, mitochondria; st, starch; v, vacuole.

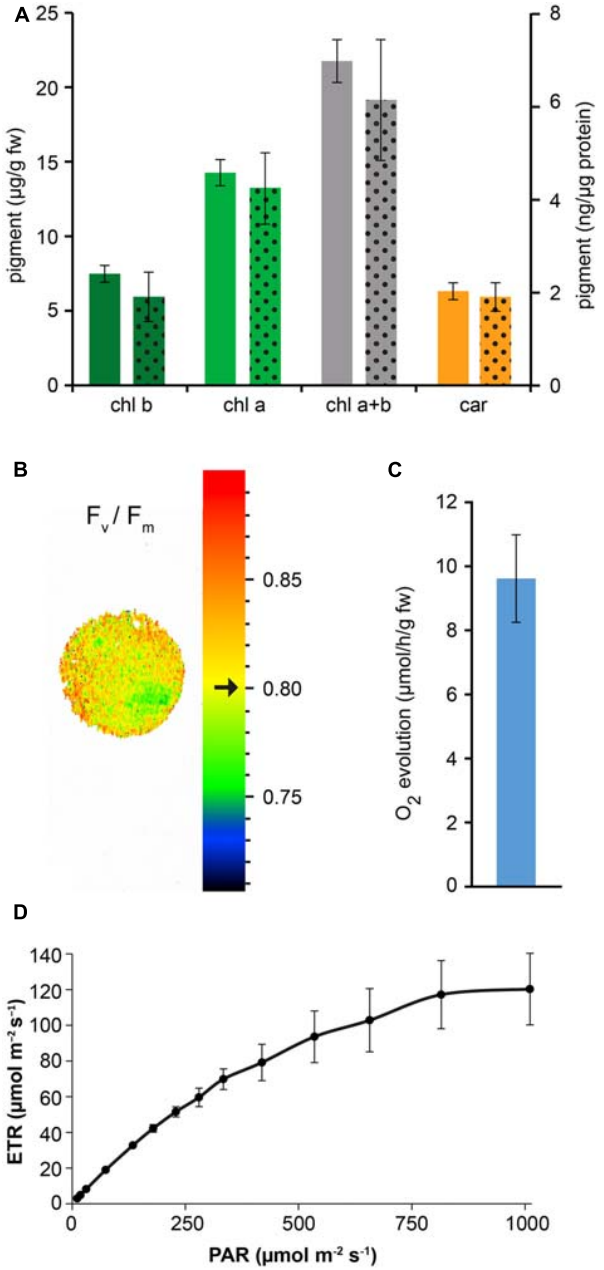

FIGURE 5 | Measurement of photosynthetic pigment content and photosynthetic activity of *Arabidopsis* cell suspension cultures. **(A)** Quantitative analysis of chlorophyll b (chl b), chlorophyll a (chl a) and total carotenoids (car). Full column values refer to the y axis on the left, dotted column values refer to the y axis on the right. Data are the means ± SE (n = 5). **(B)** PAM imaging analysis demonstrated a very good maximum quantum yield of photosystem II. Black arrow indicates a F_v/F_m mean value of 0.80 ± 0.01 (n = 3), representative for the displayed sample spot. **(C)** Quantitative analysis of O_2 evolution. Data are the means ± SE (n = 8). **(D)** Electron transport rate (ETR) at PSII. Data are the means ± SE (n = 3).

analyses (**Figure 5B**) and measurements of the rate of oxygen evolution (**Figure 5C**) demonstrated the good photosynthetic efficiency of our experimental system. Moreover, photosynthetic analyses were carried out on cell suspension cultures also with the aim to assess the ETR of PSII at different light intensities. This parameter gives an indication on PSII efficiency in using light, therefore demonstrating PSII functionality. **Figure 5D** shows that ETR gradually increases from 0 to nearly 120 µmol e^- m^{-2} s^{-1} at 811 µmol photons m^{-2} s^{-1}, following light intensity increase. Once reached this level, ETR is maintained at this steady-state also at 1000 µmol photons m^{-2} s^{-1}. These ETR values are similar to those reported in literature obtained from *Arabidopsis* leaves, indicating that PSII in our photosynthetic cell suspension cultures are functionally comparable with the photosynthetic apparatus in entire leaves (Munekage et al., 2008; Sperdouli and Moustakas, 2012).

When suspension-cultured cells were transferred from 0.5% sucrose-containing medium to sucrose-free medium, although exhibiting a decreased growth rate, they were still found to be characterized by a good F_v/F_m ratio (0.76 ± 0.01 at 0% sucrose *versus* 0.80 ± 0.01 at 0.5% sucrose; n = 3).

By applying our novel protocol, we were also able to set up heterotrophic cell suspension cultures directly from photoautotrophic ones, thus significantly shortening the required time interval. After obtaining photosynthetic cell suspension cultures, they were subcultured into MS medium, containing 0.25 µg/ml BAP 0.5 µg/ml 2,4-D, and supplemented with a high concentration of organic carbon (3% sucrose). Moreover, flasks were permanently wrapped in aluminum foil. After about 3 weeks, cells completely lost their ability to photosynthesize and plastids effectively turned from chloroplasts to amyloplasts, allowing for the obtainment of functional heterotrophic cell suspension cultures. The lack of chlorophyll autofluorescence (**Figure 6A**), together with the presence of evident Lugol-stained starch granules (**Figure 6B**) inside these organelles, whose ultrastructure appeared well-preserved (**Figure 6C**), confirmed the identity of these plastids as amyloplasts.

DISCUSSION

In this work a novel procedure to rapidly obtain photosynthetic *Arabidopsis* cell suspension cultures containing chloroplasts as functional type of plastids is presented. The novelty of this method relies on the initial germination of *Arabidopsis* seeds on a phytohormone-enriched medium, rather than on classical hormone-free media. The abnormal growth of *Arabidopsis* seedlings thus obtained, which is likely due to the crosstalk among endogenous and exogenous hormones, led to the dedifferentiation of cells and the formation of a well-evident green callus at the hypocotyl level after 3 weeks. The concentrations of phytohormones used (0.25 µg/ml BAP and 0.5 µg/ml 2,4-D) correspond to those traditionally employed to grow and maintain *Arabidopsis* heterotrophic cell suspension cultures (Moscatiello et al., 2013; Sello et al., 2016). In comparison with previously published methods (Mustafa et al., 2011; Hampp et al., 2012; Sello et al., 2016), the time frame needed to set up photoautotrophic cultures was found to be highly reduced (about 2–3 months *versus* 2 years). In a previously described more elaborate procedure, two-tiered flasks with a carbonate buffer in

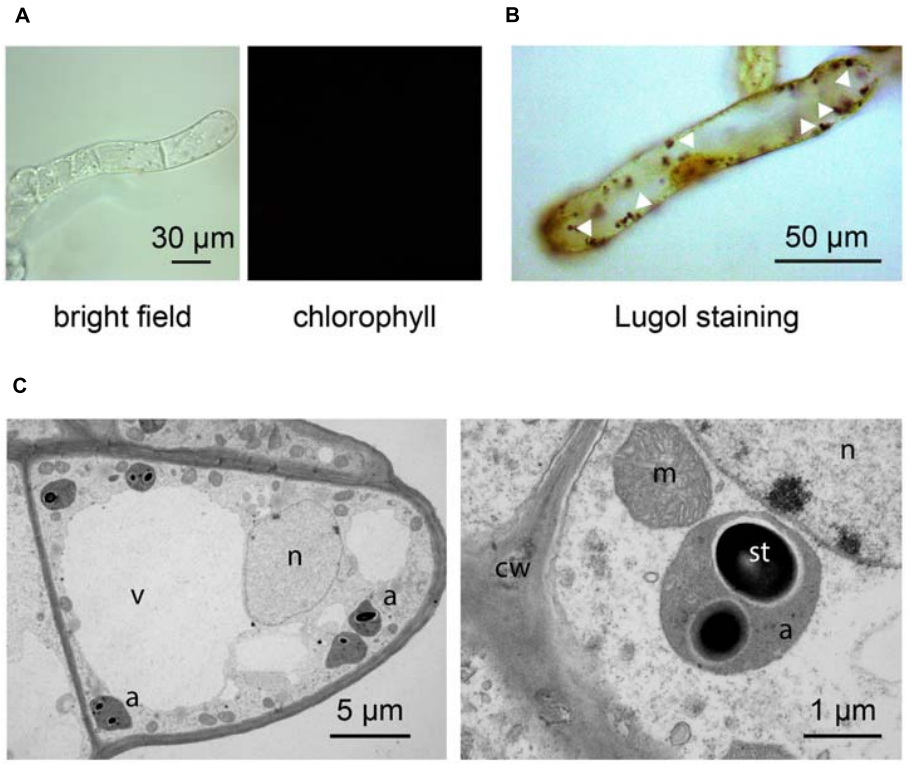

FIGURE 6 | Set up of *Arabidopsis* heterotrophic cell suspension culture, starting from the previously established photosynthetic culture. **(A,B)** Light microscopy observations of suspension-cultured cells, demonstrating the lack of any chlorophyll fluorescence signal **(A)**, as well as the presence of evident Lugol-stained starch granules (white arrowheads) **(B)**. **(C)** Ultrastructure of amyloplast-containing suspension-cultured cells. a, amyloplasts; cw, cell wall; m, mitochondria; n, nucleus; st, starch; v, vacuole.

the lower compartment were used to maintain about 2% CO_2 in the atmosphere (Hampp et al., 2012). In our experimental system, that more easily meets the standard basic equipment of every plant cell biology laboratory, cell suspension cultures were simply maintained in sterile Erlenmeyer flasks containing one-fifth volume of culture medium to ensure a proper aeration of the cell culture. Therefore, it is plausible that the comparatively lower concentration of pigments in our *in vitro* culture system may be due to a reduced rate of inorganic carbon availability. In agreement with this, we found that the presence of 0.5% sucrose in the medium was advisable to ensure a convenient cell growth rate (with a 7 days-subculture time), suitable to the performance of weekly experiments. Nevertheless, deprivation of sugar in the medium (0% sucrose) was not found to significantly alter the photosynthetic efficiency of the cell culture.

A diverse array of experiments can be conveniently performed in photosynthetic suspension-cultured cells, containing chloroplasts as unique type of plastids. For example, photoautotrophic cell cultures stably expressing the bioluminescent calcium reporter aequorin targeted to the chloroplast stroma were found to be an ideal experimental system to determine the specificity of organellar Ca^{2+} signaling (Sello et al., 2016).

Cell suspension cultures can also be useful as a valid alternative to *Arabidopsis* leaves as plant material source for the isolation of protoplasts. Indeed, protoplast isolation from cell suspension cultures is a quick, highly reproducible and straightforward procedure (Moscatiello et al., 2013) that typically gives high yields (from 10^5 to 10^6 protoplasts/ml of exponentially growing suspension-cultured cells). Similarly, intact chloroplasts can be directly isolated from cell suspension cultures, i.e., homogeneous cell populations that can be available every week in bulk quantities and with very reproducible conditions. Moreover, photosynthetic suspension-cultured cells and protoplasts are a convenient system to verify the localization of fluorescently tagged recombinant proteins targeted to different chloroplast sub-compartments (Sello et al., 2016; Navazio L., unpublished results).

The new protocol herewith described was found to be useful not only to rapidly obtain photoautotrophic cell suspension cultures, but also heterotrophic ones. Indeed, classical methods to set up *in vitro* cell cultures traditionally rely on the application of callus induction media to make hypocotyls and cotyledons dedifferentiate and generate calli. The complete procedure necessary to obtain rapidly proliferating cell suspension cultures containing non-green plastids involves a time-consuming procedure consisting of many different *in vitro* steps (Loyola-Vargas and Vázquez-Flota, 2006; Moscatiello et al., 2013; Barkla et al., 2014). An additional advantage of this method is that, by simply transferring the photosynthetic cultures from a

16 h light/8 h dark photoperiod to a condition of total darkness, in a culture medium containing a high concentration of sucrose (3%) as source of organic carbon, heterotrophic cell suspension cultures, containing amyloplasts rather than chloroplasts, can be easily and rapidly obtained, and maintained indefinitely *in vitro*.

CONCLUSION

The procedure described in this work may represent a useful and straightforward tool to quickly obtain *Arabidopsis* cell suspension cultures containing functional chloroplasts, i.e., a convenient experimental system for a wide array of studies aimed at the analysis of chloroplast structure and function.

AUTHOR CONTRIBUTIONS

LN conceived and designed the work. SS, RM, NLR, BB, and LN performed the experiments and analyzed the data. SS and LN wrote the paper. All authors participated in editing the manuscript and approved its final version.

FUNDING

This work was supported by Progetti di Ricerca di Ateneo 2012 (prot. CPDA127210), Ricerca Scientifica fondi quota EX 60% (prot. 60A06-2439/15) and Dotazione Ordinaria della Ricerca dipartimentale (DOR) 2016-2017 to LN.

ACKNOWLEDGMENTS

We thank Stefania Marcato and Anna Segalla for technical assistance. The Electron Microscopy Service of the Department of Biology of Padova (Italy) is gratefully acknowledged for skillful assistance.

REFERENCES

Barkla, B. J., Vera-Estrella, R., and Pantoja, O. (2014). Growing Arabidopsis in vitro: cell suspensions, in vitro culture, and regeneration. *Methods Mol. Biol.* 1062, 53–62. doi: 10.1007/978-1-62703-580-4_3

Ebel, J., and Mithöfer, A. (1998). Early events in the elicitation of plant defence. *Planta* 206, 335–348. doi: 10.1007/s004250050409

González-Pérez, S., Gutiérrez, J., García-García, F., Osuna, D., Dopazo, J., Lorenzo, Ó, et al. (2011). Early transcriptional defense responses in Arabidopsis cell suspension culture under high-light conditions. *Plant Physiol.* 156, 1439–1456. doi: 10.1104/pp.111.177766

Gutiérrez, J., González-Pérez, S., García-García, F., Daly, C. T., Lorenzo, Ó, Revuelta, J. L., et al. (2014). Programmed cell death activated by Rose Bengal in *Arabidopsis thaliana* cell suspension cultures requires functional chloroplasts. *J. Exp. Bot.* 65, 3081–3095. doi: 10.1093/jxb/eru151

Hall, R. D. (2000). Plant cell culture initiation, practical tips. *Mol. Biotechnol.* 16, 161–173. doi: 10.1385/MB:16:2:161

Hampp, C., Richter, A., Osorio, S., Zellnig, G., Sinha, A. K., Jammer, A., et al. (2012). Establishment of a photoautotrophic cell suspension culture of *Arabidopsis thaliana* for photosynthetic, metabolic, and signaling studies. *Mol. Plant* 5, 524–527. doi: 10.1093/mp/sss018

Lecourieux, D., Lamotte, O., Bourque, S., Wendehenne, D., Mazars, C., Ranjeva, R., et al. (2005). Proteinaceous and oligosaccharidic elicitors induce different calcium signatures in the nucleus of tobacco cells. *Cell Calcium* 38, 527–538. doi: 10.1016/j.ceca.2005.06.036

Loyola-Vargas, V. M., and Vázquez-Flota, F. (eds). (2006). "Plant cell culture protocols," in *Methods in Molecular Biology*, 2nd Edn, Vol. 318 (Totowa, NJ: Humana Press).

Maxwell, K., and Johnson, G. N. (2000). Chlorophyll fluorescence – a practical guide. *J. Exp. Bot.* 51, 659–668. doi: 10.1093/jxb/51.345.659

Mithöfer, A., Ebel, J., Bhagwat, A. A., Boller, T., and Neuhaus-Url, G. (1999). Transgenic aequorin monitors cytosolic calcium transients in soybean cells challenged with β-glucan or chitin elicitors. *Planta* 207, 566–574. doi: 10.1007/s004250050519

Moscatiello, R., Baldan, B., and Navazio, L. (2013). Plant cell suspension cultures. *Methods Mol. Biol.* 953, 77–93. doi: 10.1007/978-1-62703-152-3_5

Moscatiello, R., Mariani, P., Sanders, D., and Maathuis, F. J. M. (2006). Transcriptional analysis of calcium-dependent and calcium-independent signalling pathways induced by oligogalacturonides. *J. Exp. Bot.* 57, 2847–2865. doi: 10.1093/jxb/erl043

Munekage, Y. N., Genty, B., and Peltier, G. (2008). Effect of PGR5 impairment on photosynthesis and growth in *Arabidopsis thaliana*. *Plant Cell Physiol.* 49, 1688–1698. doi: 10.1093/pcp/pcn140

Murashige, T., and Skoog, F. (1962). A revised medium for rapid growth and bio assays with tobacco tissue cultures. *Physiol. Plant.* 15, 473–497. doi: 10.1111/j.1399-3054.1962.tb08052.x

Mustafa, N. R., de Winter, W., van Iren, F., and Verpoorte, R. (2011). Initiation, growth and cryopreservation of plant cell suspension cultures. *Nat. Protoc.* 6, 715–742. doi: 10.1038/nprot.2010.144

Navazio, L., Baldan, B., Moscatiello, R., Zuppini, A., Woo, S. L., Mariani, P., et al. (2007a). Calcium-mediated perception and defense responses activated in plant cells by metabolite mixtures secreted by the biocontrol fungus *Trichoderma atroviride*. *BMC Plant Biol.* 7:41.

Navazio, L., Moscatiello, R., Genre, A., Novero, M., Baldan, B., Bonfante, P., et al. (2007b). A diffusible signal from arbuscular mycorrhizal fungi elicits a transient cytosolic calcium elevation in host plant cells. *Plant Physiol.* 144, 673–681.

Roitsch, T., and Sinha, A. K. (2002). Application of photoautotrophic suspension cultures in plant science. *Photosynthetica* 40, 481–492. doi: 10.1023/A:1024332430494

Sello, S., Perotto, J., Carraretto, L., Szabò, I., Vothknecht, U. C., and Navazio, L. (2016). Dissecting stimulus-specific Ca^{2+} signals in amyloplasts and chloroplasts of *Arabidopsis thaliana* cell suspension cultures. *J. Exp. Bot.* 67, 3965–3974. doi: 10.1093/jxb/erw038

Sperdouli, I., and Moustakas, M. (2012). Spatio-temporal heterogeneity in *Arabidopsis thaliana* leaves under drought stress. *Plant Biol.* 14, 118–128. doi: 10.1111/j.1438-8677.2011.00473.x

Wellburn, A. R. (1994). The spectral determination of chlorophylls *a* and *b*, as well as total carotenoids, using various solvents with spectrophotometers of different resolution. *J. Plant Physiol.* 144, 307–313. doi: 10.1016/S0176-1617(11)81192-2

Wilson, S. A., Cummings, E. M., and Roberts, S. C. (2014). Multi-scale engineering of plant cell cultures for promotion of specialized metabolism. *Curr. Opin. Biotechnol.* 29, 163–170. doi: 10.1016/j.copbio.2014.07.001

Zonin, E., Moscatiello, R., Miuzzo, M., Cavallarin, N., Di Paolo, M. L., Sandonà, D., et al. (2011). TAT-mediated aequorin transduction: an alternative approach for effective calcium measurements in plant cells. *Plant Cell Physiol.* 52, 2225–2235. doi: 10.1093/pcp/pcr145

Zuppini, A., Gerotto, C., and Baldan, B. (2010). Programmed cell death and adaptation: two different types of abiotic stress response in a unicellular chlorophyte. *Plant Cell Physiol.* 51, 884–895. doi: 10.1093/pcp/pcq069

Conflict of Interest Statement: The authors declare that the research was conducted in the absence of any commercial or financial relationships that could be construed as a potential conflict of interest.

frontiers in Plant Science

METHODS
published: 29 August 2017
doi: 10.3389/fpls.2017.01503

Chloroplasts Isolation from *Chlamydomonas reinhardtii* under Nitrogen Stress

Miao Yang[1,2,3†], Jun-Peng Jiang[1,2†], Xi Xie[4], Ya-Dong Chu[1], Yan Fan[1,2], Xu-Peng Cao[1], Song Xue[1] and Zhan-You Chi[3]*

[1] Marine Bioengineering Group, Dalian Institute of Chemical Physics, Chinese Academy of Sciences, Dalian, China, [2] University of Chinese Academy of Sciences, Beijing, China, [3] School of Life Sciences and Biotechnology, Dalian University of Technology, Dalian, China, [4] Liaoning Ocean and Fisheries Science Research Institute, Dalian, China

Triacylglycerols are produced in abundance through chloroplast and endoplasmic reticulum pathways in some microalgae exposed to stress, though the relative contribution of either pathway remains elusive. Characterization of these pathways requires isolation of the organelles. In this study, an efficient and reproducible approach, including homogenous batch cultures of nitrogen-deprived algal cells in photobioreactors, gentle cell disruption using a simple custom-made disruptor with mechanical shear force, optimized differential centrifugation and Percoll density gradient centrifugation, was developed to isolate chloroplasts from *Chlamydomonas reinhardtii* subjected to nitrogen stress. Using this approach, the maximum limited stress duration was 4 h and the stressed cells exhibited 19 and 32% decreases in intracellular chlorophyll and nitrogen content, respectively. Chloroplasts with 48 – 300 μg chlorophyll were successfully isolated from stressed cells containing 10 mg chlorophyll. These stressed chloroplasts appeared intact, as monitored by ultrastructure observation and a novel quality control method involving the fatty acid biomarkers. This approach can provide sufficient quantities of intact stressed chloroplasts for subcellular biochemical studies in microalgae.

Keywords: ***Chlamydomonas*, chloroplast isolation, triacylglycerol, nitrogen stress, fatty acid biomarkers**

OPEN ACCESS

Edited by:
Juliette Jouhet, UMR5168 Laboratoire de Physiologie Cellulaire Vegetale (LPCV), France

Reviewed by:
Fabrice Franck, University of Liège, Belgium
Alistair McCormick, University of Edinburgh, United Kingdom

****Correspondence:***
Song Xue
xuesong@dicp.ac.cn

† These authors have contributed equally to this work.

Specialty section:
This article was submitted to Plant Physiology, a section of the journal Frontiers in Plant Science

Received: *18 June 2017*
Accepted: *14 August 2017*
Published: *29 August 2017*

Citation:
Yang M, Jiang J-P, Xie X, Chu Y-D, Fan Y, Cao X-P, Xue S and Chi Z-Y (2017) Chloroplasts Isolation from Chlamydomonas reinhardtii under Nitrogen Stress. Front. Plant Sci. 8:1503. doi: 10.3389/fpls.2017.01503

INTRODUCTION

The chloroplast is a specialized subcellular compartment of plant and algal cells that is derived from cyanobacteria through endosymbiosis (Moreira et al., 2000; Okamoto and Inouye, 2005). Through the process of photosynthesis, this organelle converts solar energy into biochemical energy, capturing environmental CO_2 and releasing O_2 (Engel et al., 2015). In addition to photosynthesis, multiple other processes occur in chloroplast, including biosyntheses of chlorophyll (Chl), amino acids, and fatty acids as well as membrane lipid assembly and trafficking (Baginsky and Gruissem, 2004; Block and Jouhet, 2015). Furthermore, chloroplast degradation and turnover and recycling of chloroplast nutrients play a crucial role in response to adverse environmental conditions, which is required to meet energetic demands and maintain homeostasis (Xie et al., 2015). Although chloroplasts have been

isolated from plants for analyses of tolerance to oxidative stresses, such as chilling, heat, osmotic and salt stress (Robinson et al., 1983; Heckathorn et al., 1998; Ling and Jarvis, 2016; Meng et al., 2016), such mechanistic studies in algae have been hampered by unavailable protocols for chloroplast isolation from stress-induced cells, especially microalgae.

In the past decade, *Chlamydomonas reinhardtii* has emerged as a model green microalga for investigations of many aspects of lipid metabolism (Li-Beisson et al., 2015), especially biosynthesis of the promising biofuel feedstock triacylglycerol (TAG) (Ruiz et al., 2016; Zienkiewicz et al., 2016). Increasing evidences reveal that parallel TAG biosynthesis pathways in the chloroplast and endoplasmic reticulum (ER) concomitantly exist in microalgae, especially the plastid pathways including *de novo* TAG biosynthesis and turnover of chloroplast membrane lipids into TAG (Goodson et al., 2011; Legeret et al., 2015; Goold et al., 2016; Xu et al., 2016; Balamurugan et al., 2017), which are distinct from the relatively known pathways present in higher plants and yeast (Xu et al., 2016). However, the specific contribution of the chloroplast and ER to TAG assembly remains ambiguous (Zienkiewicz et al., 2016). To date, there are abundant studies in *C. reinhardtii* involving the chloroplast than ER under normal growth conditions (Mason et al., 2006). As the chloroplastidic lipid remodeling that occurs in *C. reinhardtii* following stress conditions, nitrogen deprivation in particular, is proposed to be closely correlated to TAG synthesis (Li-Beisson et al., 2015; Du and Benning, 2016; Xu et al., 2016), it is essential to obtain stressed chloroplasts from this alga. Despite a brief mention by Fan et al. (2011), without any data presented, chloroplast isolation from stressed *C. reinhardtii* has yet to be achieved.

In general, the entire process of chloroplast isolation from microalgae consists of four major steps: algal cultivation, cell disruption, chloroplast purification and quality evaluation (Mason et al., 2006). In the past 50 years, distinct isolation methods have been employed to purify *C. reinhardtii* chloroplasts in different physiological states for different research purposes, including studies of photosynthetic activity (Klein et al., 1983; Mendiola-Morgenthaler et al., 1985), transport studies (Moroney et al., 1987; Mason et al., 1990) and metabolic enzyme characterization (Bollivar and Beale, 1995; Jans et al., 2008; Burgess et al., 2016). Nonetheless, these chloroplasts were all obtained from normally growing algal cells. Hence, there is a need to isolate intact chloroplasts from stressed *C. reinhardtii* cells to investigate the dynamic response of this crucial organelle to abiotic stress at a subcellular level; relevant analyses include characterization of subcellular TAG biosynthesis, remodeling of the chloroplastidic glycerolipidome and omics studies of chloroplastidic lipid droplets in microalgae. Regardless, it is well known that isolation of stressed chloroplasts is difficult due to the fact that chloroplasts undergo gradual degradation in response to stress (Xie et al., 2015; Zienkiewicz et al., 2016), which is characterized by disorganization of thylakoid membranes and accumulation of starch granules and lipid droplets (Warakanont et al., 2015). These alterations severely distort the microalgal chloroplast membrane structure (Fan et al., 2011; Preininger et al., 2015), similar to what occurs in plants (Meng et al., 2016; Woodson, 2016). Thus, it is difficult to ensure the integrity of stressed chloroplasts during isolation.

To address this issue, we developed a protocol for isolating nitrogen-stressed chloroplasts from *C. reinhardtii*. The protocol includes homogenous batch cultivation in PBRs with the maximum limited stress duration, gentle cell disruption with the aid of a custom-made disruptor, optimized purification involving centrifugations and novel quality assessment based on the fatty acid biomarker analysis.

MATERIALS AND METHODS

Microalgal Strains and Pre-cultures

A cell wall-less mutant of *C. reinhardtii* strain CC4326 was obtained from the Chlamydomonas Resource Center[1]. The cells were first grown on agar-solidified minimal medium (Mason et al., 2006) for 2 months at 50 μmol m^{-2} s^{-1} at 25°C. Algal patches were then transferred to 50 ml liquid minimal medium for 7 days to produce sufficient biomass (∼ 1 × 10^6 cells ml^{-1}) as a pre-inoculation culture, which was designated the 1stgeneration culture. The light cycle was set as 12 h light/12 h dark. The liquid cultures were centrifuged and added to fresh medium as the 2nd generation for another 7 days. Until the 4th generation, synchronous cultures were transferred on day 4 to photobioreactors (PBRs) at an initial cell density of ∼10^4 cells ml^{-1}. The 5th, 6th, and up to 10th generations were used as candidates for batch cultures for chloroplast isolation.

Batch Cultures in PBRs under Normal and Stress Conditions

Algal cultures were normally grown in minimal medium in PBRs (4.5 cm in diameter, 45 cm in height, 600 ml culture volume), bubbled with air (120 ml min^{-1}) containing 4% (v/v) CO_2 and illuminated from one side by cool white fluorescent tubes. Each experiment was independently repeated at least three times.

Pre-inoculated cells were utilized for two-stage cultures, including nitrogen-replete conditions for the first 4 days (the first 2 days under continuous illumination and the last 2 days under a 12-h light/12-h dark cycle) under a light intensity of 50 μmol m^{-2} s^{-1} followed by nitrogen-deprived conditions for 4 h at an irradiance of 100 μmol m^{-2} s^{-1}. The nitrogen starvation time was limited to 4 h based on prior experiments. N-replete cells were harvested at 4 h into the third light cycle by centrifugation for 5 min at 3000 × *g* and 4°C. A proportion of cultures with aliquots of cells containing 10 mg Chl were used for isolation of normal chloroplasts. The remaining pellet was washed once with nitrogen-free minimal medium using a fine paint brush, centrifuged as above, and transferred to the same medium before adjusting the optical density to ∼0.752. The cells were gradually stress-induced and sampled every hour for subsequent analysis. After 4 h of nitrogen deprivation, all the cells

[1]http://www.chlamycollection.org/

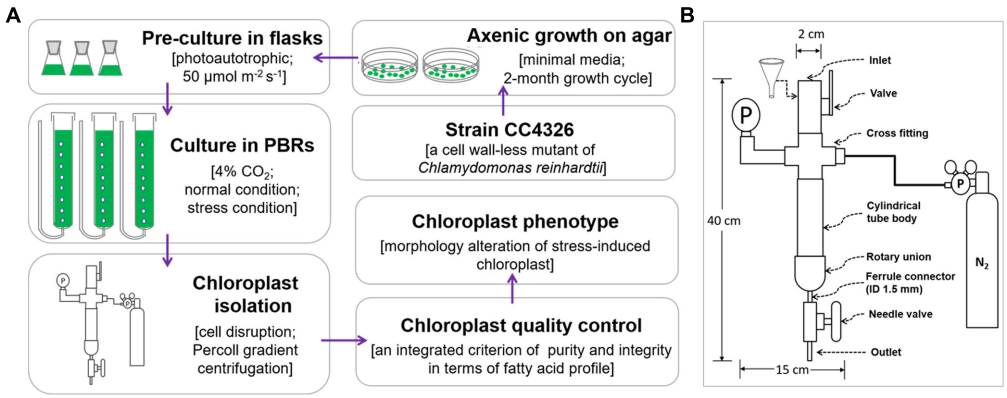

FIGURE 1 | The flow chart of chloroplast isolation from *C. reinhardtii*. **(A)** The whole process for chloroplast isolation from *C. reinhardtii*. **(B)** The structure diagram of the custom-made cell disruptor. ID means the inner diameter.

were collected (3000 × *g*, 5 min, 4°C) for isolating stress-induced chloroplasts.

Growth Measurement, Chl Quantification and Elemental Analysis

Cellular growth parameters, including optical density at 750 nm and cell concentration, were monitored using a spectrophotometer (Jasco v-530, Japan) and a hemacytometer, respectively. To determine biomass, ∼5 ml of culture were filtered onto a pre-weighed Whatman GF/C filter (47 mm diameter) and dried to a constant weight with a net biomass of more than 2 mg at 60°C. The illumination intensity was determined using a photosynthetically active radiation (PAR) detector (Optometer P9710 with PAR detector 3701, Gigahertz Optik Corporation, Germany). The photosystem II quantum yield, F_v/F_m, of the cells was measured using a Chl fluorometer (Water-PAM WALZ, Germany) according to the methods described by Yao et al. (2012).

For Chl determination, cells in 2 ml of culture were pelleted, followed by sonication in 2 ml of ethanol on ice. The pigment extracts were centrifuged at 8000 × *g* for 2 min, and the absorption of the supernatant was determined spectrophotometrically at 649 and 665 nm. The Chl concentration was calculated as Chl = 18.08 OD_{649} + 6.63 OD_{665}, according to the methods of Jespersen and Christoffersen (1987).

Quantification of microagal cell nitrogen was performed using a vario EL cube elemental analyzer (Elementar, Germany). 2∼4 mg of lyophilized biomass were accurately weighed using a Mettler Toledo XP6 microbalance (Mettler Toledo GmbH, Germany).

Chloroplast Isolation under Normal and Stress Conditions

All chloroplast isolation procedures were conducted at 4°C or on ice using a modified version (**Figure 1A**) of Mason et al.'s (2006) protocol. A fine paint brush was used to completely resuspend pelleted cells, and all centrifugations were performed using swing bucket rotors. Normally cultured cells with 10 mg Chl each were washed twice with 50 ml 50 mM HEPES-KOH (pH 7.5) (3000 × *g*, 5 min) to remove the small gelatinous particles surrounding the cells (Goyal et al., 1988) and to prevent the chloroplasts from clumping. Next, another 4 ml of wash buffer were used to resuspend the pellets. A custom-made disruptor (**Figure 1B**) of stainless steel was used to break the cells. From top to bottom, the device was composed of an inlet, a valve, a

TABLE 1 | Distinct yields and fatty acid methyl ester mass ratio (R) of chloroplasts isolated from *C. reinhardtii* under normal conditions.

Group	Condition	Yield (%)	*R*
N + 1	0.35 MPa; 750 × *g*, 2 min; 670 × *g*, 1 min	14 ± 1	7.36 ± 0.25
N + 2	0.35 MPa; 5000 × *g*, 2 min; 5000 × *g*, 1 min	30 ± 2	8.91 ± 0.34
N + 3	0.55 MPa; 750 × *g*, 2 min; 670 × *g*, 1 min	16 ± 2	7.22 ± 0.44
N + 4	0.55 MPa; 5000 × *g*, 2 min; 5000 × *g*, 1 min	26 ± 2	8.91 ± 0.43
N + 5	0.75 MPa; 750 × *g*, 2 min; 670 × *g*, 1 min	13 ± 1	7.54 ± 0.51
N + 6	0.75 MPa; 5000 × *g*, 2 min; 5000 × *g*, 1 min	28 ± 2	9.89 ± 0.50
N + cell	nd	nd	4.73 ± 0.27

N + 1, N + 2, N + 3, N + 4, N + 5, and N + 6 refer to normal chloroplasts isolated under six conditions. N + cell refers to cells cultured under normal conditions. The yield is calculated as "(chlorophyll content of isolated chloroplasts)/(chlorophyll content of the original cells) × 100%". R means the mass ratio of (16:4n3 + 18:3n3) to (18:3n6 + 18:4n3) and is calculated using the data of ***Figure 4A****. nd, not detected. Data are mean ± standard deviation of three measurement replicates from one independent experiment (n = 3).*

cross fitting, a pressure gage, a cylindrical tube body, a rotary union, a ferrule connector (inner diameter, 1.5 mm), a needle valve and an outlet. The cross fitting was connected to a standard high-pressure nitrogen tank equipped with a pressure gauge and a decompression valve. Before breaking the cells, the gas pressure was adjusted to the designated value (0.35, 0.55 or 0.75 MPa, **Tables 1**, **3**). Once the cell disruptor was prepared, 20 ml isolation buffer (0.3 M sorbitol, 50 mM HEPES-KOH [pH 7.5], 2 mM Na_2-EDTA [pH 8.0], 1 mM $MgCl_2$, 1% bovine serum albumin (BSA)) were added to the cell concentrates followed by prompt injection into the cylindrical tube body with the aid of a funnel (**Figure 1B**). The concentrated cells were disrupted by rapid extrusion through the cell disruptor under distinct pressures (0.35, 0.55, or 0.75 MPa, **Tables 1**, **3**). The flow rate was manually manipulated at ∼0.1 ml s^{-1}, and the pressates were collected into a 50-ml ice-cold centrifuge tube.

Several centrifugation conditions were tested to pellet chloroplasts (**Tables 1**, **3**). Every ∼12 ml of the pressates were centrifuged (750 or 5000 × *g*, 2 min) to pellet chloroplasts, whole cells and cell fragments. The pellet was resuspended in 2 ml chloroplast isolation buffer and then layered onto a discontinuous Percoll gradient (20%/45%/65%) followed by centrifugation at 4200 × *g* for 15 min. The chloroplast band between the 45 and 65% layers was pipetted into another round-bottom centrifuge tube, diluted with 10 ml chloroplast isolation buffer, and centrifuged at 670 or 5000 × *g* for 1 min to remove the Percoll or small particulates. The chloroplast pellet was finally resuspended in ≥250 μl of 50 mM HEPES-KOH (pH 8.0) and 0.3 M sorbitol. The collected chloroplast fraction was then used for Chl determination and subsequent analysis.

Fatty Acid Composition Analysis

Quantification of fatty acids was determined using one-step acid-catalyzed direct transesterification (Liu et al., 2015). Fresh cells or chloroplasts of no less than 300 μg dry biomass were transferred to a 10-ml flask; 5 ml 2% H_2SO_4-methanol (v/v, H_2SO_4/methanol) were added, and the mixtures were stirred at 70°C for 1 h with refluxing. After the mixtures were cooled to room temperature, 2 ml of hexane and 0.75 ml of distilled water were added, and then the mixtures were vortexed for 30 s. The upper hexane layer with fatty acid methyl esters (FAMEs) was analyzed by gas chromatography (Agilent 7890A GC) using triheptadecanoin as an internal standard. When necessary, the hexane extracts were concentrated under N_2. The mass of chloroplast fatty acid was normalized to the original cellular dry biomass, which was based on the Chl amount, and denoted as mg of fatty acids per g of the equivalent cellular dry biomass.

Immunoblotting Analysis

To ascertain the purity of the *C. reinhardtii* chloroplast preparation, each chloroplast fraction was tested for enrichment of specific marker proteins. Due to our focus on a pure chloroplast fraction free of ER, we used an ER marker protein, binding immunoglobulin protein (BIP) (Warakanont et al., 2015; Liu et al., 2016), to evaluate the purity. All chloroplast fractions were processed by immunoblotting, as described below. Fresh cells or chloroplast samples were initially resuspended in protein extraction buffer [50 mM Tris-HCl, pH 7.5, 0.15 M NaCl, 1 mM Na_2-EDTA, 1% NP-40, 10% glycerol and 1 mM phenylmethylsulfonyl fluoride (PMSF)] and then sonicated on ice to completely lyse the cells or chloroplasts. The lysate was centrifuged at 12,000 × *g* for 15 min at 4°C. The pellets were discarded, and the extracted proteins from equal amounts of cells and chloroplasts (3×10^6 cells or chloroplasts) were loaded and separated by 10% sodium dodecyl sulfate polyacrylamide gel electrophoresis (SDS-PAGE). The proteins were electroblotted onto polyvinylidene fluoride (PVDF) membranes in transfer buffer (60 mM Tris, 48 mM glycine, 1.6 mM SDS and 20% methanol) for 2 h at 200 mA, and the membranes were blocked for 2 h in phosphate-buffered saline/Tween 20 (PBST; 1.5 mM KH_2PO_4, 8 mM Na_2HPO_4, 0.1 M NaCl, 3 mM KCl, 0.05% Tween 20, v/v) with 5% (w/v) non-fat dried milk. The membranes were washed with PBST at room temperature for 5 min and then incubated overnight at 4°C with a specific primary antibody (SC-33757 Santa Cruz Biotechnology, Inc.,)[2] at a 1:200 dilution. Following equilibration for 1 h at room temperature, the incubated membranes were then washed three times with PBST at 15 min intervals. Goat anti-rabbit secondary antibodies conjugated with horseradish peroxidase (A0208 Beyotime Institute of Biotechnology[3]) at a 1:1000 dilution were incubated with the blots at room temperature for 2 h, followed by washing as described above. The blots were developed using DAB Horseradish Peroxidase Color Development Kit (P0203 Beyotime Institute of Biotechnology) for 15 min in the dark at room temperature.

Transmission Electron Microscopy

For transmission electron microscopy, pelleted chloroplasts or cells were fixed overnight in 2.5% (v/v) glutaraldehyde in chloroplast isolation buffer for chloroplasts or HEPES-KOH (pH 7.5) buffer for cells. After the cells and chloroplasts were embedded in 2% agarose, the samples were washed with the appropriate buffer three times at 15-min intervals and post-fixed for 2 h in 1% osmic acid (w/v) at 4°C. Following the washing procedure described above, the samples were dehydrated through an alcohol series (50∼90% alcohols) for 15 min each and finally rinsed 3 times with 100% ethanol at 10-min intervals. The samples were slowly infiltrated at 4°C with epoxy propane and epoxy resin for several changes and polymerized for 12 h at 37°C, for 24 h at 25°C and for 24 h at 60°C. Ultrathin sections were stained with 2% uranyl acetate for 30 min and lead citrate for 15 min and then observed under JEM-1200EX (**Figure 2C**, N+) and JEM-2100 (**Figure 2C**, N−) electron microscopes (JEOL Ltd., Tokyo, Japan) operated at 120 kV. Micrographs were obtained using an ANT camera system.

[2]http://www.scbt.com

[3]http://www.beyotime.com

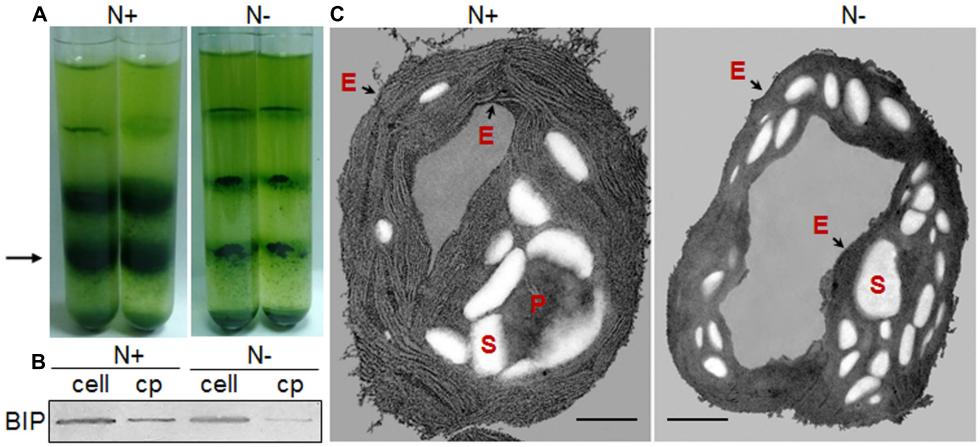

FIGURE 2 | Chloroplast morphology of *C. reinhardtii* in response to nitrogen stress. **(A)** Bands of chloroplasts in a Percoll gradient. A 3-ml aliquot of cell pressate was layered onto a discontinuous Percoll gradient, with 3 ml each of 20, 45, and 65%, top to bottom. Chloroplasts predominated at the 45–65% interface (black arrow). **(B)** Chloroplast fractions (cp) were compared with the whole-cell lysates (cell) based on an endoplasmic reticulum (ER) marker protein, binding immunoglobulin protein (BIP). **(C)** Ultrastructural alterations of the chloroplast following nitrogen starvation, showing the starch granules (S), pyrenoid (P) and the chloroplast envelope membrane (black arrows - E). Scale bar = 500 nm. N+ represents Group N + 6 under normal conditions; N- represents Group N-5 under nitrogen stress.

RESULTS

Chloroplast Isolation from *C. reinhardtii* under Normal Conditions

It is necessary to obtain sufficient amounts of homogenous cells before isolating chloroplasts from *C. reinhardtii* and thus, the synchronous batch cultures in PBRs were performed (see Materials and methods). These fully synchronized algal cells grew to mid-log phase after a normal culture of 100 h in PBRs (**Figure 1A**), during which the cell density increased from $\sim 10^4$ to 10^7 cells ml^{-1} (the OD_{750} increased from 0.01 to 1.15) and F_v/F_m (photosystem II quantum yield) was maintained at 0.747 ± 0.003 (**Figure 3**). In addition, the cell dry weight density and Chl concentration increased to 0.6 mg ml^{-1} and 20.11 μg ml^{-1}, respectively (**Figure 3**). At this time point, the algal cells were vigorous and sufficient enough for chloroplast isolation.

Further, Percoll discontinuous gradient centrifugation generated three layers between distinct gradients. Microscopy observation revealed that bands between 20 and 45% contained broken chloroplasts, e.g., thylakoid membranes, that bands between 45 and 65% contained mostly intact chloroplasts, and that bands below 65% contained unbroken cells (**Figure 2A**); these results agreed with the previous report (Mason et al., 2006). During the initial experiments, distinct disruption pressures resulted in distinct patterns of fragmentation, and some chloroplasts occurred in the upper band under distinct centrifugation conditions. To obtain high-quality chloroplasts with a high yield, purity and integrity, six conditions for chloroplast isolation were tested, including three disruption pressures and two centrifugation speeds for collecting pressates and chloroplasts (**Table 1**). Starting with a 500 ml uniform culture containing 10 mg Chl, the chloroplast yields under all six conditions ranged between 13 and 30% based on Chl recovery (**Table 1**). Moreover, the chloroplast yield under the higher rotation speed (5000 × *g* for 2 min, 5000 × *g* for 1 min, **Table 1**) was approximately 2- fold higher than that under the lower speed (750 × *g* for 2 min, 670 × *g* for 1 min, **Table 1**) at the same disruption pressure. Within range of disruption pressures from 0.35 to 0.75 MPa, the higher speed could yield more amounts of chloroplasts.

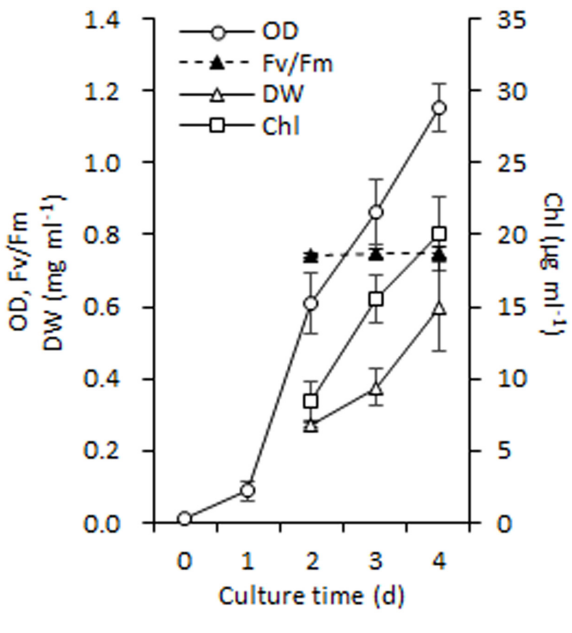

FIGURE 3 | Growth performance of *C. reinhardtii* in a photobioreactor under normal conditions. Data are the means of three independent experiments ($n = 3$). Error bars represent standard deviations. OD, Fv/Fm, DW and Chl refer to the optical density at 750 nm, photosystem II quantum yield, cellular dry weight and chlorophyll.

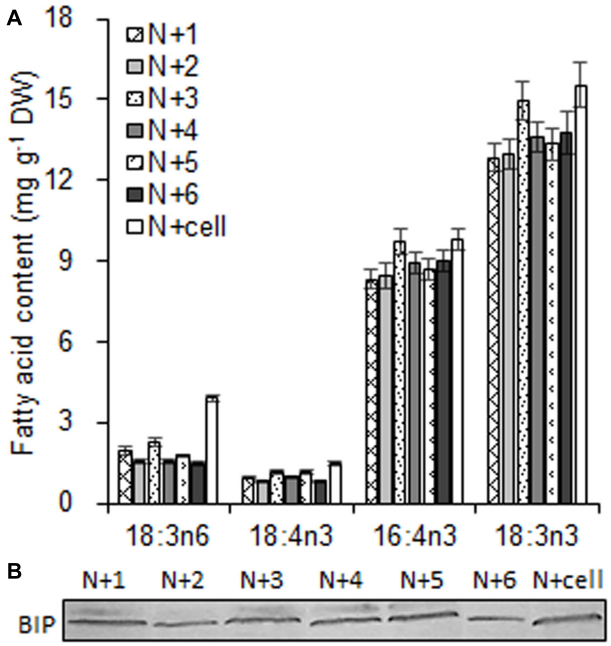

FIGURE 4 | The fatty acid biomarkers and immunoblotting analysis of chloroplasts isolated from *C. reinhardtii* under normal conditions. **(A)** The fatty acid biomarkers of chloroplasts was compared to that of the whole cells. **(B)** Western blotting for an endoplasmic reticulum (ER) marker protein, binding immunoglobulin protein (BIP), was conducted to detect ER contamination of the chloroplast fraction. N + 1, N + 3, and N + 5 refer to normal chloroplasts isolated after exposure to 0.35, 0.55, and 0.75 MPa, respectively, under the same rotation speeds of 750 g and subsequently 670 g. N + 2, N + 4, and N + 6 referred to normal chloroplasts isolated from 0.35, 0.55, and 0.75 MPa, respectively, under the same rotation speeds of 5000 × g and subsequently 5000 × *g*. N + cell refers to cells cultured under normal conditions. The cellular fatty acid content is denoted as mg of fatty acyl groups per g of the cellular biomass (DW). The mass of chloroplast fatty acid was normalized to the original cellular dry biomass, which was based on the chlorophyll (Chl) amount, and denoted as mg of fatty acids per g of the equivalent cellular dry biomass. The fatty acyl is expressed as number of carbons:number of double bonds with n-number, indicating the position of the double bond from the methyl end. Data are the means of three measurement replicates from one independent experiment (*n* = 3). Error bars represent standard deviations.

As the largest fraction of the algal lipidome (Horn and Benning, 2016), glycerolipids are specifically distributed into distinct subcellular membranes that execute unique functions (Moellering and Benning, 2011) and possess characteristic fatty acyl compositions (Trémolières, 1998). Therefore, the acyls of glycerolipids were analyzed for both the chloroplast and the entire cell. Four special fatty acids, i.e., 18:3n6, 18:4n3, 16:4n3, and 18:3n3 (number of carbons:number of double bonds with n-number, which indicates the position of the double bond from the methyl end), were found to be distributed in the chloroplast with distinct proportions (**Figures 4A**). The chloroplasts isolated under higher rotation speeds (Groups N + 2, 4, and 6) contained lower proportions of 18:3n6 (40, 40, and 38%) and 18:4n3 (57, 66, and 56%) of the whole cells (**Table 2**). In contrast, these chloroplasts had relatively higher proportions of 16:4n3 (86, 91, and 92%) and 18:3n3 (83, 88, and 88%). In particular, 18:3n6 and 18:4n3 are mainly limited to DGTS (diacylglycerol-*N, N, N*-trimethylhomoserine) and PE (phosphatidylethanolamine), which are the presumed signature lipids of extra-plastidic membranes, especially the ER (Giroud et al., 1988; Trémolières, 1998); 16:4n3 and 18:3n3 are exclusively enriched in MGDG (monogalactosyldiacylglycerol) and DGDG (digalactosyldiacylglycerol), which are the postulated signature lipids of the chloroplast (Giroud et al., 1988; Moellering and Benning, 2011). Based on the proposed principles (Giroud et al., 1988; Trémolières, 1998; Moellering and Benning, 2011), 18:3n6 and 18:4n3 can serve as negative biomarkers and 16:4n3 and 18:3n3 positive biomarkers of the isolated chloroplasts. In this study, their distribution ratios in the chloroplast were considered to represent the purity and integrity of this organelle in *C. reinhardtii*. Thus, the chloroplasts of Groups N + 2, 4, and 6 (**Table 1**) were presumed to contain more MGDG and DGDG and less DGTS and PE, indicating that these chloroplasts were of relatively higher integrity and purity. To further identify chloroplasts with higher quality, the mass ratios of (16:4n3 + 18:3n3) to (18:3n6 + 18:4n3), indicated as *R*, were compared. The results showed that the *R*-values of chloroplasts obtained from distinct isolation conditions were all greater than 7 and at least 1.5-fold of that in the whole cell, showing notable differences between the chloroplast and the whole cell. The highest *R*-value was observed for chloroplasts isolated under the highest pressure and centrifugation speed (Group N + 6, **Table 1**), reaching 9.89, which was twofold of that in the whole cell and assumed to be the chloroplasts with the best quality. In addition, these chloroplasts exhibited the weakest band of BIP, an ER marker, by western blotting, showing the lowest amount of ER (**Figure 4B**). Under transmission electron microscopy, the chloroplast was found to be morphologically intact, enclosed in the envelope membrane and with the central pyrenoid encircled by a starch sheath. Thus, high-quality chloroplasts had less than 38% of 18:3n6 and more

TABLE 2 | The percentage (%) of fatty acid biomarkers of chloroplasts in whole cells under normal conditions.

Fatty acid	Percentage (%)					
	N + 1	N + 2	N + 3	N + 4	N + 5	N + 6
18:3n6	50 ± 3	40 ± 2	59 ± 4	40 ± 2	45 ± 2	38 ± 2
18:4n3	64 ± 3	57 ± 3	78 ± 4	66 ± 4	80 ± 3	56 ± 3
16:4n3	85 ± 2	86 ± 5	99 ± 1	91 ± 5	89 ± 5	92 ± 5
18:3n3	83 ± 3	83 ± 2	96 ± 4	88 ± 4	86 ± 4	88 ± 4

The percentage of fatty acid biomarkers of chloroplasts in whole cells is calculated as "(the mass of fatty acyl group of chloroplasts) / (the mass of fatty acyl group of the whole cells) × 100%" according to the data of ***Figure 4A****. N + 1, N + 3, and N + 5 refer to normal chloroplasts isolated after exposure to 0.35, 0.55, and 0.75 MPa, respectively, under the same rotation speeds of 750 × g and subsequently 670 × g. N + 2, N + 4, and N + 6 refer to normal chloroplasts isolated after exposure to 0.35, 0.55, and 0.75 MPa, respectively, under the same rotation speeds of 5000 × g and subsequently 5000 × g. The fatty acid is expressed as number of carbons:number of double bonds with n-number, indicating the position of the double bond from the methyl end. Data are mean ± standard deviation of three measurement replicates from one independent experiment (n = 3).*

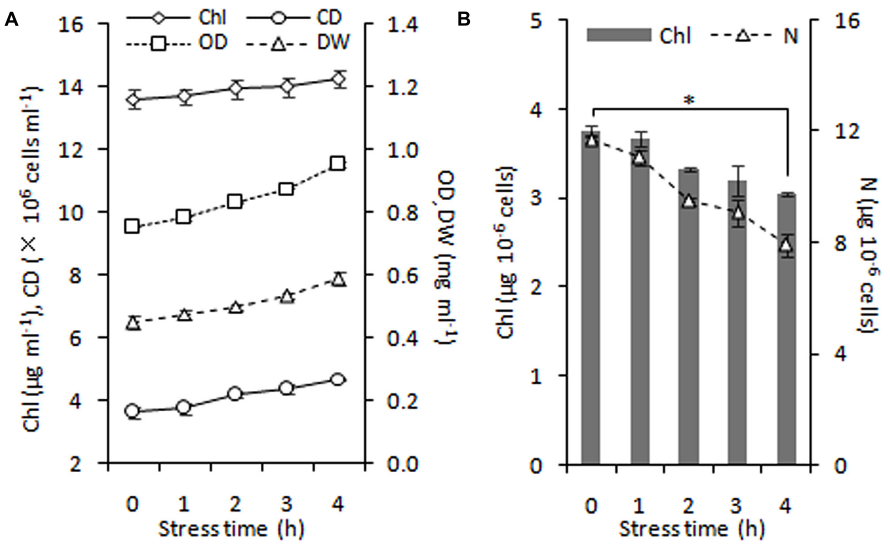

FIGURE 5 | Time course of growth performance of *C. reinhardtii* under nitrogen stress. **(A)** Changes in cell growth parameters in response to nitrogen stress. **(B)** Levels of intracellular chlorophyll (Chl) and nitrogen (N) content under nitrogen starvation. An asterisk denotes significant ($P < 0.05$) decreases of the cellular Chl and nitrogen content within 4 h of nitrogen stress. Data are the means of three independent experiments ($n = 3$). Error bars represent standard deviations. CD, OD and DW denote cell density, optical density at 750 nm and cellular dry weight.

than 88% of both 16:4n3 and 18:3n3 of that in the whole cell.

Chloroplast Isolation from Cells under Nitrogen Stress

During 4 h of exposure to nitrogen stress, there was a slight increase in cell density from 3.61 to 4.68 × 10^6 cells ml^{-1} (OD_{750} increased from 0.752 to 0.950), and the cellular dry weight density also showed an elevation from 0.45 to 0.59 mg ml^{-1} (**Figure 5A**). The cell dry weight remained unaltered (∼120 μg per million cells). The Chl concentration did not alter significantly, albeit exhibited a slight tendency to increase from 13.60 to 14.24 μg ml^{-1}. These gradual variations indicated that cell division occurred in the early stage of nitrogen stress. The Chl and nitrogen content of each cell decreased by 19% (calculate using Chl concentration and cell density) and 32% (**Figure 5B**), respectively, representing the stress levels of the algal cells. Further, the six conditions designed for the normal chloroplast isolation were applied to prepare nitrogen-stressed chloroplasts. Only 0.5–3% of chloroplasts were successfully isolated from stress-treated cells, a sharp decline of 80∼98% compared with normal chloroplasts (**Figure 2A**, **Table 3**), which indicated that the N-starvation conditions could only be imposed for at most 4 h. Thus, 4 h was set as the maximum limited stress duration for successful chloroplast isolation. In addition, the chloroplast yield from stress-induced cells was highest at low speeds (750 × *g* for 2 min and 670 × *g* for 1 min) (**Table 3**), which was opposite to that under normal conditions. It is likely that when the stronger centrifugation force acted on the less resistant cells, the chloroplast membranes were more easily destroyed, severely hindering isolation of stressed chloroplasts.

With respect to the proposed criteria involving the fatty acid biomarkers under normal conditions, the fatty acyl profiles of

TABLE 3 | Distinct yields and fatty acid methyl ester mass ratio (R) of chloroplasts isolated from *C. reinhardtii* under nitrogen stress.

Group	Condition	Yield (%)	*R*
N – 1	0.35 MPa; 750 × *g*, 2 min; 670 × *g*, 1 min	2.66 ± 0.11	8.97 ± 0.47
N – 2	0.35 MPa; 5000 × *g*, 2 min; 5000 × *g*, 1 min	0.59 ± 0.04	nd
N – 3	0.55 MPa; 750 × *g*, 2 min; 670 × *g*, 1 min	3.06 ± 0.14	9.24 ± 0.43
N – 4	0.55 MPa; 5000 × *g*, 2 min; 5000 × *g*, 1 min	2.00 ± 0.15	10.49 ± 0.57
N – 5	0.75 MPa; 750 × *g*, 2 min; 670 × *g*, 1 min	2.09 ± 0.16	11.29 ± 0.54
N – 6	0.75 MPa; 5000 × *g*, 2 min; 5000 × *g*, 1 min	0.48 ± 0.03	nd
N – cell	nd	nd	4.23 ± 0.28

N – 1, N – 2, N – 3, N – 4, N – 5, and N – 6 refer to stressed chloroplasts isolated from six conditions. N-cell refers to cells cultured under nitrogen stress. The yield is calculated as "(chlorophyll content of isolated chloroplasts)/(chlorophyll content of the corresponding cells) × 100%". R means the mass ratio of (16:4n3 + 18:3n3) to (18:3n6 + 18:4n3) and is calculated using the data of ***Figure 6****. nd, not detected. Data are mean ± standard deviation of three measurement replicates from one independent experiment (n = 3).*

stressed chloroplasts were further analyzed for quality evaluation (**Figure 6**). Due to the limitation of the minimum amount required for total fatty acid analysis (Liu et al., 2015), the fatty acyl compositions of chloroplasts from Groups N-2 and 6 were not determined. Lipid analysis showed that the isolated Group N-5 chloroplasts contained the lowest levels of negative fatty acid biomarkers (no more than 38% for both 18:3n6 and 18:4n3) and relatively high levels of positive fatty acid biomarkers (more than 90% for both 16:4n3 and 18:3n3; **Table 4**), resulting in the highest *R*-value (**Table 3**), which was postulated to be the chloroplasts with the best quality. Further, the quality of these chloroplasts were validated using Western blot and morphology observation. The stressed chloroplasts isolated from Group N-5 contained very low levels of ER, as revealed by the BIP marker test (**Figure 2B**) and retained good integrity as the normal chloroplasts (**Figure 2C**). Nevertheless, these chloroplasts were disorganized to some extent and exhibited less compactness, with some reduction of appressed regions of the thylakoids, which was consistent with the decrease in the Chl content of the stressed cells. In addition, starch granules significantly accumulated and were scattered among the thylakoid membranes, leading to the chloroplast being distorted and obscured. Taken together, sufficient amounts of chloroplasts were successfully isolated from *C. reinhardtii* cells following 4 h of nitrogen stress, and their purity and integrity remained uncompromised.

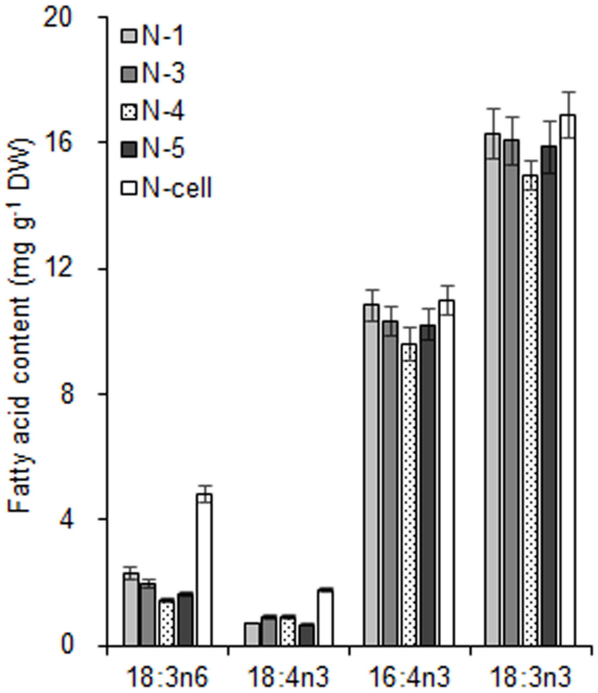

FIGURE 6 | The fatty acid biomarkers of chloroplasts isolated from *C. reinhardtii* in response to nitrogen stress. N-1, N-3, and N-5 refer to stressed chloroplasts isolated after exposure to 0.35, 0.55, and 0.75 MPa, respectively, under the same rotation speed 750 × *g* and subsequently 670 × *g*. N-4 refers to stressed chloroplasts isolated after exposure to 0.55 MPa, under 5000 × g and subsequently 5000 × g. N-cell refers to cells cultured under nitrogen stress. The cellular fatty acid content is denoted as mg of fatty acyl groups per g of the cellular biomass (DW). The mass of chloroplast fatty acid was normalized to the original cellular dry biomass, which was based on the chlorophyll (Chl) amount, and denoted as mg of fatty acids per g of the equivalent cellular dry biomass. The fatty acyl is expressed as number of carbons:number of double bonds with n-number, indicating the position of the double bond from the methyl end. Data are the means of three measurement replicates from one independent experiment (n = 3). Error bars represent standard deviations.

DISCUSSION

In response to nitrogen stress, the *C. reinhardtii* chloroplast plays a crucial role in TAG accumulation (Du and Benning, 2016; Xu et al., 2016). However, the contribution by chloroplasts in comparison to the ER with regard to TAG accumulation remains veiled. To help resolve this issue, it is imperative to obtain chloroplasts with high quality.

Homogenous Cultivation in PBRs Contributes to Reproducible Isolation of Chloroplasts

In previous studies, autotrophic or mixotrophic algal cultures are normally maintained in flasks, and the required volumes for chloroplast isolation are reportedly no more than 1 – 2 L (Bennoun, 1982; Bollivar and Beale, 1995; Mason et al., 2006). However, the culture volume for stressed chloroplast isolation is much higher than that under normal conditions because of the much lower isolation yield. In this case, cultivation in PBRs is a feasible approach to provide an adequate volume of stressed cells for chloroplast isolation. In the current study, uniform algal populations were obtained from cyclic subcultures in flasks and stable batch cultures in PBRs, which is vital to yielding abundant chloroplasts in similar physiological state. To a large extent, this process depends on a constant transferring cycle of liquid subculture in flasks (7 days in this study) under a synchronous light-dark cycle. In addition, *C. reinhardtii* propagates more slowly in minimal medium, even when supplemented with CO_2, compared with TAP medium, which contributes to the formation of a uniform culture. This autotrophic culture mode is able to prevent bacteria from frequent reproduction (Mason et al., 2006), especially at the initial growth phase when the cell density is low, i.e., $\sim 10^4$ cells ml^{-1} (**Figure 3**). Axenic culture derived from agar-solidified medium is also crucial to ensure vigorous growth of cells in flasks and PBRs.

The culture system in PBRs is stable and favorable for obtaining reproducible batch cultures. Moreover, the cell doubling time was notably reduced when the cultures were transferred into PBRs aerated with 4% CO_2 (see Materials and Methods). In this case, more chloroplasts could be isolated from more algal cultures in PBRs at one time, which is a time- and space-saving approach compared to flask culture. Based on a 500 ml algal culture containing 10 mg Chl, the stressed chloroplast yield was 0.5∼3%, containing 50 – 300 μg Chl and no more than 530 μg FAMEs (Supplemental Table S1). Chloroplast isolation under stress conditions largely relies on cyclic and stable pre-cultivation in flasks and PBRs, which serves as an essential assurance for isolating more homogenous chloroplasts.

TABLE 4 | The percentage (%) of fatty acid biomarkers of chloroplasts in whole cells under nitrogen stress.

Fatty acid	Percentage (%)			
	N – 1	N – 3	N – 4	N – 5
18:3n6	48 ± 2	41 ± 1	30 ± 2	34 ± 2
18:4n3	41 ± 1	51 ± 2	52 ± 2	38 ± 2
16:4n3	99 ± 4	94 ± 3	87 ± 3	93 ± 4
18:3n3	96 ± 3	95 ± 4	89 ± 3	94 ± 3

The percentage of fatty acid biomarkers of chloroplasts in whole cells is calculated as "(the mass of fatty acyl group of chloroplasts)/(the mass of fatty acyl group of the whole cells) × 100%" according to the data of ***Figure 6****. N-1, N-3, and N-5 refer to stressed chloroplasts after exposure to 0.35, 0.55, and 0.75 MPa, respectively, under the same rotation speed 750 × g and subsequently 670 × g. N-4 refers to stressed chloroplasts isolated after exposure to 0.55 MPa, under 5000 × g and subsequently 5000 × g. The fatty acid is expressed as number of carbons:number of double bonds with n-number, indicating the position of the double bond from the methyl end. Data are mean ± standard deviation of three measurement replicates from one independent experiment (n = 3).*

Cell Disruptor with Gentle Mechanical Shear Force is Vital to Keeping Chloroplast Intact

In addition to chemical lysis (Klein et al., 1983; Kreuzberg et al., 1987; Sultemeyer et al., 1988), mechanical methods through nitrogen decompression are often utilized to break cells for chloroplast isolation from *C. reinhardtii*. Although the Yeda press was widely used in the 1980s (Belknap and Togasaki, 1981; Mendiola-Morgenthaler et al., 1985; Goldschmidt-Clermont et al., 1989), it had less satisfactory results for cells grown photoautotrophically and tended to result in more ruptured chloroplasts (Moroney et al., 1987; Mason et al., 1991). Subsequently, a Bioneb nebulizer, available since the 1990s, became an alternative device for breaking cells (Bollivar and Beale, 1995; Jans et al., 2008; Burgess et al., 2016). In addition, a few custom-made devices (Naumann et al., 2005; Mason et al., 2006; Terashima et al., 2010) have been used to break *C. reinhardtii* cells. When Bioneb was applied to nitrogen-starved cells in our preliminary experiments, its mechanical shear force appeared to be so strong that we observed reduced integrity of stressed chloroplasts. Thus, a simple mechanical disruptor was designed (**Figure 1B**) to gently break stress-treated cells and release intact chloroplasts without strong mechanical force. Moreover, this device can be easily assembled and modified as needed. Its principle depends on nitrogen decompression. First, a massive amount of nitrogen is dissolved in concentrated cells in a stainless steel vessel under a designated pressure. When the gas pressure is controllably released from the needle valve, the nitrogen separates from the cells as expanding bubbles that stretch the membrane of each cell until they rupture, and multiple cell fragments including chloroplasts are then released from the disruptor. As this disruption device requires no electricity and generates no heat, the concentrated cells can be chilled to protect them from damage. The available volume of the cylinder tube body is 10 – 40 ml, and at most 15 mg Chl-containing cells can be broken at one time.

In this study, this custom-made disruptor produced 5 – 30% of normal chloroplasts (ranges of twelve independent tests), consistent with previous reports (Klein et al., 1983; Katzman et al., 1994; Mason et al., 2006). More importantly, it also generated 0.5 – 3% of stressed chloroplasts (ranges of seven independent tests). As an environmental sensor (Chan et al., 2016), the nitrogen-stressed chloroplasts became distorted, as determined by an decrease in appressed regions of the thylakoids and an increase in starch granules (**Figure 2C**), which were prone to result in broken chloroplasts and thought to be key limiting factors for yielding large amounts of intact chloroplasts (Klein et al., 1983; Fan et al., 2011). The physical features of the cell slurry, such as viscosity, cell density, particle size and settleability of the suspension, jointly affect the disruption level of the cells (Fleischer and Rouser, 1965; Chisti and Mooyoung, 1986). Additionally, the cell disruption process should be rapid; otherwise, the extruded chloroplast from a cell is likely to be ruptured (Moroney et al., 1987). It is suggested that a cell disruptor with similar principles of mild mechanical shear force on cells would be appropriate to gently break stress-induced cells and maintain good integrity of the chloroplast.

A Quality Control Method Involving the Fatty acid Biomarkers Is Feasible

Due to the different target applications of the isolated chloroplasts, the quality criteria also differ. Normally, the quality of *C. reinhardtii* chloroplasts involves three aspects, i.e., yield, purity and integrity (Mason et al., 2006). The yield is based on Chl recovery, and the purity or contamination depends on the presence of marker proteins in other sub-compartments, especially the mitochondria and cytosol, which are commonly less than 20% (Belknap, 1983; Klein et al., 1983; Kreuzberg et al., 1987). The fraction of isolated chloroplasts in this study was expected to be free of ER, the other essential organelle for TAG accumulation. Immunoblotting analyses revealed the slight ER contamination revealed by BIP detection, which were also reported in a previous study (Warakanont et al., 2015). Integrity is assessed by oxygen evolution using a ferricyanide assay, which is often more than 80% (Belknap, 1983; Kreuzberg et al., 1987). Furthermore, electron microscopy is often used to confirm the purity and integrity of chloroplasts (Klein et al., 1983; Mendiola-Morgenthaler et al., 1985; Mason et al., 2006). In our study, electron microscopy images showed that both the normal and stressed chloroplasts were largely intact. However, because of our aim to study subcellular lipid metabolism in *C. reinhardtii*, it was necessary to focus on chloroplast quality in terms of the lipid composition.

According to the proposed criteria based on the fatty acid biomarkers, the isolated chloroplasts with fewer proportions of 18:3n6 and 18:4n3 mainly in DGTS and PE and greater proportions of 16:4n3 and 18:3n3 mainly in MGDG and DGDG were likely to be less contaminated by ER and having relatively intact envelopes. The proposed criteria were deduced from a general principle, whereby the preferential distribution of fatty acids at the sn-2 position of glycerolipids reflects their biosynthetic origin from the ER or chloroplast in plants

(Roughan and Slack, 1982). Based on that, the chloroplast of *C. reinhardtii* was presumed to contain 14% DGTS, 11% PE, 97% MGDG and 97% DGDG (Giroud et al., 1988), indicating that a majority of DGTS and PE reside in the ER and that most MGDG and DGDG are present in the chloroplast of *C. reinhardtii*. However, what is the lowest proportion of 18:3n6 and 18:4n3 of DGTS and PE in ideal pure chloroplasts of *C. reinhardtii*? Janero and Barrnett (1981) detected 38% DGTS in chloroplast membranes. In this study, the 18:3n6 and 18:4n3 levels of DGTS and PE were no more than 38% and 16:4n3 and 18:3n3 levels of MGDG and DGDG were greater than 88% in the best quality chloroplasts (Groups N + 6 and N − 5) under normal and stress conditions, which were all close to the reported results. In addition, the immunoblotting analysis and ultrastructure observation further verified the purity and integrity of these chloroplasts. Therefore, it is feasible to monitor chloroplast quality using the fatty acid biomarkers, which are specifically localized in distinct subcellular compartments.

Stringent Culture Conditions and Prompt, Rapid Operations Facilitate Successful Chloroplast Isolation

Successful isolation of high-quality chloroplasts largely depends on stringent culture conditions and prompt, rapid operations. First, there are two vital points regarding the culture conditions. It is important to maintain a uniform culture through cyclic and stable subcultures in flasks and PBRs along with a synchronous light cycle, which can further facilitate uniform application during stress cultivation. Note that the degree of stress is equally critical for successful isolation, including the induction time, light intensity, inoculation density and other stress factors. It is critical to initially optimize the degree of stress, as excessive stress treatment can cause the cells to rupture more completely, thus making it more difficult to obtain intact chloroplasts. Second, the entire procedure of chloroplast isolation should be conducted quickly, consecutively and promptly. Once the concentrated cells are disrupted, any unnecessary delays can lead to distinct aggregation, which can lead to clump formation and disruption of the Percoll gradient, hindering the correct loading of subfractions into the corresponding gradient. It is also vital to resuspending the pellet gently and thoroughly using a fine paint brush. Insufficient resuspension is likely to result in aggregates, which can also prevent successful isolation.

CONCLUSION

In this study, starting with a 500 ml culture containing 10 mg Chl, stressed chloroplasts with 48 – 300 μg Chl were successfully isolated from *C. reinhardtii* cells. These chloroplasts appeared to be intact, as determined by the fatty acid biomarker analysis and ultrastructure observation. Homogenous batch cultures in PBRs and gentle cell disruption enabled the reproducible isolation of stressed chloroplasts. To the best of our knowledge, this is the first report of successful chloroplast isolation from microalgal cells under stress conditions, which can provide insight into the nature of stressed chloroplasts and offer available biomaterials for study of subcellular lipid metabolism in microalgae. Future work is necessary to isolate chloroplasts from microalgal cells following longer period of abiotic stress, which can facilitate understanding of subcellular biochemistry and biology of microalgae.

AUTHOR CONTRIBUTIONS

MY and SX conceived and designed the research. MY and J-PJ performed the experiments and analyzed data. MY, XX, and SX wrote the manuscript. Y-DC designed the cell disruptor. Y-DC and X-PC provided technical assistance. YF participated in algal cultivation. XX and Z-YC supervised specific experiments. All authors agreed on the manuscript.

FUNDING

This work was supported by the National Nature Science Foundation of China (21576253, 31470432 and 4140060435) and Liaoning Province Natural Science Foundation of China (201601387).

ACKNOWLEDGMENTS

We are very grateful to Prof. James V. Moroney (Louisiana State University) for generously providing us with useful and valuable advice on the isolation of chloroplasts. We would like to thank Jingxian Sun (Dalian Ocean University) for technical assistance in preparation of ultrathin sections and Chuanzhou Gao (Dalian Medical University) and Qike Jiang (Dalian Institute of Chemical Physics, Chinese Academy of Sciences) for access to the JEM-1200EX and JEM-2100 electron microscopes. We appreciate Dr. Peili Shen for helping with immunoblotting analysis.

SUPPLEMENTARY MATERIAL

The Supplementary Material for this article can be found online at: http://journal.frontiersin.org/article/10.3389/fpls.2017.01503/full#supplementary-material

REFERENCES

Baginsky, S., and Gruissem, W. (2004). Chloroplast proteomics: potentials and challenges. *J. Exp. Bot.* 55, 1213–1220. doi: 10.1093/jxb/erh104

Balamurugan, S., Wang, X., Wang, H. L., An, C. J., Li, H., Li, D. W., et al. (2017). Occurrence of plastidial triacylglycerol synthesis and the potential regulatory role of AGPAT in the model diatom *Phaeodactylum tricornutum*. *Biotechnol. Biofuels* 10, 97. doi: 10.1186/s13068-017-0786-0

Belknap, W. (1983). Partial purification of intact chloroplasts from *Chlamydomonas reinhardtii*. *Plant Physiol.* 72, 1130–1132. doi: 10.1104/pp.72.4.1130

Belknap, W., and Togasaki, R. K. (1981). *Chlamydomonas reinhardtii* cell preparation with altered permeability toward substrates of organellar reactions. *Proc. Natl. Acad. Sci. U.S.A.* 78, 2310–2314. doi: 10.1073/pnas.78.4.2310

Bennoun, P. (1982). Evidence for a respiratory chain in the chloroplast. *Proc. Natl. Acad. Sci. U.S.A.* 79, 4352–4356. doi: 10.1073/pnas.79.14.4352

Block, M. A., and Jouhet, J. (2015). Lipid trafficking at endoplasmic reticulum-chloroplast membrane contact sites. *Curr. Opin. Cell Biol.* 35, 21–29. doi: 10.1016/j.ceb.2015.03.004

Bollivar, D. W., and Beale, S. I. (1995). Formation of the isocyclic ring of chlorophyll by isolated *Chlamydomonas reinhardtii* chloroplasts. *Photosynth. Res.* 43, 113–124. doi: 10.1007/BF00042968

Burgess, S. J., Taha, H. S., Yeoman, J. A., Iamshanova, O., Chan, K. X., Boehm, M., et al. (2016). Identification of the elusive pyruvate reductase of *Chlamydomonas reinhardtii* chloroplasts. *Plant Cell Physiol.* 57, 82–94. doi: 10.1093/pcp/pcv167

Chan, K. X., Phua, S. Y., Crisp, P., Mcquinn, R., and Pogson, B. J. (2016). Learning the languages of the chloroplast: retrograde signaling and beyond. *Annu. Rev. Plant Bol.* 67, 25–53. doi: 10.1146/annurev-arplant-043015-111854

Chisti, Y., and Mooyoung, M. (1986). Disruption of microbial cells for intracellular products. *Enzyme Microb. Technol.* 8, 194–204. doi: 10.1016/0141-0229(86)90087-6

Du, Z. Y., and Benning, C. (2016). "Triacylglycerol accumulation in photosynthetic cells in plants and algae," in *Lipids in Plant and Algae Development*, eds Y. Nakamura and Y. Li-Beisson (Cham: Springer International Publishing), 179–205. doi: 10.1007/978-3-319-25979-6_8

Engel, B. D., Schaffer, M., Cuellar, L. K., Villa, E., Plitzko, J. M., and Baumeister, W. (2015). Native architecture of the *Chlamydomonas* chloroplast revealed by in situ cryo-electron tomography. *eLife* 4:e04889. doi: 10.7554/eLife.04889

Fan, J., Andre, C., and Xu, C. (2011). A chloroplast pathway for the *de novo* biosynthesis of triacylglycerol in *Chlamydomonas reinhardtii*. *FEBS Lett.* 585, 1985–1991. doi: 10.1016/j.febslet.2011.05.018

Fleischer, S., and Rouser, G. (1965). Lipids of subcellular particles. *J. Am. Oil. Chem. Soc.* 42, 588–607. doi: 10.1007/BF02541295

Giroud, C., Gerber, A., and Eichenberger, W. (1988). Lipids of *Chlamydomonas reinhardtii*. Analysis of molecular species and intracellular sites of biosynthesis. *Plant Cell Physiol.* 29, 587–595. doi: 10.1093/oxfordjournals.pcp.a077533

Goldschmidt-Clermont, M., Malnoe, P., and Rochaix, J. D. (1989). Preparation of *Chlamydomonas* chloroplasts for the *in vitro* import of polypeptide precursors. *Plant Physiol.* 89, 15–18. doi: 10.1104/pp.89.1.15

Goodson, C., Roth, R., Wang, Z. T., and Goodenough, U. (2011). Structural correlates of cytoplasmic and chloroplast lipid body synthesis in *Chlamydomonas reinhardtii* and stimulation of lipid body production with acetate boost. *Eukaryot. Cell* 10, 1592–1606. doi: 10.1128/EC.05242-11

Goold, H. D., Cuine, S., Legeret, B., Liang, Y., Brugiere, S., Auroy, P., et al. (2016). Saturating light induces sustained accumulation of oil in plastidal lipid droplets in *Chlamydomonas reinhardtii*. *Plant Physiol.* 171, 2406–2417. doi: 10.1104/pp.16.00718

Goyal, A., Betsche, T., and Tolbert, N. E. (1988). Isolation of intact chloroplasts from *Dunaliella tertiolecta*. *Plant Physiol.* 88, 543–546. doi: 10.1104/pp.88.3.543

Heckathorn, S. A., Downs, C. A., Sharkey, T. D., and Coleman, J. S. (1998). The small, methionine-rich chloroplast heat-shock protein protects photosystem II electron transport during heat stress. *Plant Physiol.* 116, 439–444. doi: 10.1104/pp.116.1.439

Horn, P. J., and Benning, C. (2016). The plant lipidome in human and environmental health. *Science* 353, 1228–1232. doi: 10.1126/science.aaf6206

Janero, D. R., and Barrnett, R. J. (1981). Cellular and thylakoid-membrane phospholipids of *Chlamydomonas reinhardtii* 137+. *J. Lipid Res.* 22, 1119–1125.

Jans, F., Mignolet, E., Houyoux, P., Cardol, P., Ghysels, B., Cuine, S., et al. (2008). A type II NAD(P)H dehydrogenase mediates light-independent plastoquinone reduction in the chloroplast of *Chlamydomonas*. *Proc. Natl. Acad. Sci. U.S.A.* 105, 20546–20551. doi: 10.1073/pnas.0806896105

Jespersen, A., and Christoffersen, K. (1987). Measurements of chlorophyll a from phytoplankton using ethanol as extraction solvent. *Arch. Hydrobiol.* 109, 445–454.

Katzman, G. L., Carlson, S. J., Marcus, Y., Moroney, J. V., and Togasaki, R. K. (1994). Carbonic anhydrase activity in isolated chloroplasts of wild-type and high-CO2-dependent mutants of *Chlamydomonas reinhardtii* as studied by a new assay. *Plant Physiol.* 105, 1197–1202. doi: 10.1104/pp.105.4.1197

Klein, U., Chen, C., Gibbs, M., and Plattaloia, K. A. (1983). Cellular fractionation of *Chlamydomonas reinhardii* with emphasis on the isolation of the chloroplast. *Plant Physiol.* 72, 481–487. doi: 10.1104/pp.72.2.481

Kreuzberg, K., Klock, G., and Grobheiser, D. (1987). Subcellular distribution of pyruvate-degrading enzymes in *Chlamydomonas reinhardtii* studied by an improved protoplast fractionation procedure. *Physiol. Plant.* 69, 481–488. doi: 10.1111/j.1399-3054.1987.tb09229.x

Legeret, B., Schulzraffelt, M., Nguyen, H. M., Auroy, P., Beisson, F., Peltier, G., et al. (2015). Lipidomic and transcriptomic analyses of *Chlamydomonas reinhardtii* under heat stress unveil a direct route for the conversion of membrane lipids into storage lipids. *Plant Cell Environ.* 39, 834–847. doi: 10.1111/pce.12656

Li-Beisson, Y., Beisson, F., and Riekhof, W. R. (2015). Metabolism of acyl-lipids in *Chlamydomonas reinhardtii*. *Plant J.* 82, 504–522. doi: 10.1111/tpj.12787

Ling, Q., and Jarvis, P. (2016). Analysis of protein import into chloroplasts isolated from stressed plants. *J. Vis. Exp.* 117, e:54717. doi: 10.3791/54717

Liu, J., Han, D., Yoon, K., Hu, Q., and Li, Y. (2016). Characterization of type 2 diacylglycerol acyltransferases in *Chlamydomonas reinhardtii* reveals their distinct substrate specificities and functions in triacylglycerol biosynthesis. *Plant J.* 86, 3–19. doi: 10.1111/tpj.13143

Liu, J., Liu, Y., Wang, H., and Xue, S. (2015). Direct transesterification of fresh microalgal cells. *Bioresour. Technol.* 176, 284–287. doi: 10.1016/j.biortech.2014.10.094

Mason, C. B., Bricker, T. M., and Moroney, J. V. (2006). A rapid method for chloroplast isolation from the green alga *Chlamydomonas reinhardtii*. *Nat. Protoc.* 1, 2227–2230. doi: 10.1038/nprot.2006.348

Mason, C. B., Manuel, L. J., and Moroney, J. V. (1990). A new chloroplast protein is induced by growth on low CO_2 in *Chlamydomonas reinhardtii*. *Plant Physiol.* 93, 833–836. doi: 10.1104/pp.93.2.833

Mason, C. B., Matthews, S., Bricker, T. M., and Moroney, J. V. (1991). Simplified procedure for the isolation of intact chloroplasts from *Chlamydomonas reinhardtii*. *Plant Physiol.* 97, 1576–1580. doi: 10.1104/pp.97.4.1576

Mendiola-Morgenthaler, L. R., Leu, S., and Boschetti, A. E. (1985). Isolation of biochemically active chloroplasts from *Chlamydomonas*. *Plant Sci.* 38, 33–39. doi: 10.1016/0168-9452(85)90076-7

Meng, F., Luo, Q., Wang, Q., Zhang, X., Qi, Z., Xu, F., et al. (2016). Physiological and proteomic responses to salt stress in chloroplasts of diploid and tetraploid black locust (*Robinia pseudoacacia* L.). *Sci. Rep.* 6:23098. doi: 10.1038/srep23098

Moellering, E. R., and Benning, C. (2011). Galactoglycerolipid metabolism under stress: a time for remodeling. *Trends Plant Sci.* 16, 98–107. doi: 10.1016/j.tplants.2010.11.004

Moreira, D., Guyader, H. L., and Philippe, H. (2000). The origin of red algae and the evolution of chloroplasts. *Nature* 405, 69–72. doi: 10.1038/35011054

Moroney, J. V., Kitayama, M., Togasaki, R. K., and Tolbert, N. E. (1987). Evidence for inorganic carbon transport by intact chloroplasts of *Chlamydomonas reinhardtii*. *Plant Physiol.* 83, 460–463.doi: 10.1104/pp.83.3.460

Naumann, B., Stauber, E. J., Busch, A., Sommer, F., and Hippler, M. (2005). N-terminal processing of Lhca3 is a key step in remodeling of the photosystem I-light-harvesting complex under iron deficiency in *Chlamydomonas reinhardtii*. *J. Biol. Chem.* 280, 20431–20441. doi: 10.1074/jbc.M414486200

Okamoto, N., and Inouye, I. (2005). A secondary symbiosis in progress. *Science* 310, 287. doi: 10.1126/science.1116125

Preininger, É. Kósa, A., Lõrincz, Z. S., Nyitrai, P., Simon, J., Böddi, B., et al. (2015). Structural and functional changes in the photosynthetic apparatus of *Chlamydomonas reinhardtii* during nitrogen deprivation and replenishment. *Photosynthetica* 53, 369–377. doi: 10.1007/s11099-015-0129-y

Robinson, S. P., Downton, W. J. S., and Millhouse, J. (1983). Photosynthesis and ion content of leaves and isolated chloroplasts of salt-stressed spinach. *Plant Physiol.* 73, 238–242. doi: 10.1104/pp.73.2.238

Roughan, P. G., and Slack, C. R. (1982). Cellular organization of glycerolipid metabolism. *Annu. Rev. Plant Physiol.* 33, 97–132. doi: 10.1146/annurev.pp.33.060182.000525

Ruiz, J. F., Olivieri, G., De, V. J. H., Bosma, R., Willems, P., Reith, J. H., et al. (2016). Towards industrial products from microalgae. *Energy Environ. Sci.* 9, 3036–3043. doi: 10.1039/C6EE01493C

Sultemeyer, D. F., Klock, G., Kreuzberg, K., and Fock, H. (1988). Photosynthesis and apparent affinity for dissolved inorganic carbon by cells and chloroplasts of

Chlamydomonas reinhardtii grown at high and low CO_2 concentrations. *Planta* 176, 256–260. doi: 10.1007/BF00392453

Terashima, M., Specht, M., Naumann, B., and Hippler, M. (2010). Characterizing the anaerobic response of *Chlamydomonas reinhardtii* by quantitative proteomics. *Mol. Cell. Proteomics* 9, 1514–1532. doi: 10.1074/mcp.M900421-MCP200

Trémolières, A. (1998). "Glycerolipids: composition, biosynthesis and function in *Chlamydomonas*," in *The Molecular Biology of Chloroplasts and Mitochondria in Chlamydomonas*, eds J. D. Rochaix and M. Goldschmidt-Clermont (Dordrecht: Springer), 415–431.

Warakanont, J., Tsai, C., Michel, E. J. S., Murphy, G. R., Hsueh, P. Y., Roston, R., et al. (2015). Chloroplast lipid transfer processes in *Chlamydomonas reinhardtii* involving a TRIGALACTOSYLDIACYLGLYCEROL 2 (TGD2) orthologue. *Plant J.* 84, 1005–1020. doi: 10.1111/tpj.13060

Woodson, J. D. (2016). Chloroplast quality control–balancing energy production and stress. *New Phytol.* 212, 36–41. doi: 10.1111/nph.14134

Xie, Q., Michaeli, S., Peledzehavi, H., and Galili, G. (2015). Chloroplast degradation: one organelle, multiple degradation pathways. *Trends Plant Sci.* 20, 264–265. doi: 10.1016/j.tplants.2015.03.013

Xu, C., Andre, C., Fan, J., and Shanklin, J. (2016). "Cellular organization of triacylglycerol biosynthesis in microalgae," in *Lipids in Plant and Algae Development*, eds Y. Nakamura and Y. Li-Beisson (Cham: Springer International Publishing), 207–221.

Yao, C., Ai, J., Cao, X., Xue, S., and Zhang, W. (2012). Enhancing starch production of a marine green microalga *Tetraselmis subcordiformis* through nutrient limitation. *Bioresour. Technol.* 118, 438–444. doi: 10.1016/j.biortech.2012.05.030

Zienkiewicz, K., Du, Z., Ma, W., Vollheyde, K., and Benning, C. (2016). Stress-induced neutral lipid biosynthesis in microalgae - molecular, cellular and physiological insights. *Biochim. Biophys. Acta* 1861, 1269–1281. doi: 10.1016/j.bbalip.2016.02.008

Conflict of Interest Statement: The authors declare that the research was conducted in the absence of any commercial or financial relationships that could be construed as a potential conflict of interest.

frontiers in Plant Science

METHODS
published: 05 December 2017
doi: 10.3389/fpls.2017.02079

A Reliable and Non-destructive Method for Monitoring the Stromal pH in Isolated Chloroplasts Using a Fluorescent pH Probe

Pai-Hsiang Su[1,2]* *and Yen-Hsun Lai*[2]

[1] *Agricultural Biotechnology Research Center, Academia Sinica, Taipei, Taiwan,* [2] *Biotechnology Center in Southern Taiwan, Academia Sinica, Tainan, Taiwan*

The proton gradient established by the pH difference across a biological membrane is essential for many physiological processes, including ATP synthesis and ion and metabolite transport. Currently, ionophores are used to study proton gradients, and determine their importance to biological functions of interest. Because of the lack of an easy method for monitoring the proton gradient across the inner envelope membrane of chloroplasts (ΔpH_{env}), whether the concentration of ionophores used can effectively abolish the ΔpH_{env} is not proven for most experiments. To overcome this hindrance, we tried to setup an easy method for real-time monitoring of the stromal pH in buffered, isolated chloroplasts by using fluorescent pH probes; using this method the ΔpH_{env} can be calculated by subtracting the buffer pH from the measured stromal pH. When three fluorescent dyes, BCECF-AM [2′,7′-bis-(2-carboxyethyl)-5-(and-6)-carboxyfluorescein acetoxymethyl ester], CFDA-SE [5(6)-Carboxyfluorescein diacetate succinimidyl ester] and SNARF-1 carboxylic acid acetate succinimidyl ester were incubated with isolated chloroplasts, BCECF-AM and CFDA-SE, but not the ester-formed SNARF-1 were taken up by chloroplasts and digested with esterase to release high levels of fluorescence. According to its relatively higher pKa value (6.98, near the physiological pH of the stroma), BCECF was chosen for further development. Due to shielding of the excitation and emission lights by chloroplast pigments, the ratiometric fluorescence of BCECF was highly dependent on the concentration of chloroplasts. By using a fixed concentration of chloroplasts, a highly correlated standard curve of pH to the BCECF ratiometric fluorescence with an *r*-square value of 0.98 was obtained, indicating the reliability of this method. Consistent with previous reports, the light-dependent formation of ΔpH_{env} can be detected ranging from 0.15 to 0.33 pH units upon illumination. The concentration of the ionophore nigericin required to collapse the ΔpH_{env} was then studied. The establishment of a non-destructive method of monitoring the stromal pH will be valuable for studying the roles of the ΔpH_{env} in chloroplast physiology.

Keywords: BCECF, chloroplast, fluorescent pH probe, nigericin, proton gradient, ionophore

OPEN ACCESS

Edited by:
Rebecca L. Roston, University of Nebraska–Lincoln, United States

Reviewed by:
Alexander Tikhonov, Moscow State University, Russia
Kees Venema, Consejo Superior de Investigaciones Científicas (CSIC), Spain

***Correspondence:**
Pai-Hsiang Su
kennedy@gate.sinica.edu.tw

Specialty section:
This article was submitted to Plant Physiology, a section of the journal Frontiers in Plant Science

Received: *15 September 2017*
Accepted: *21 November 2017*
Published: *05 December 2017*

Citation:
Su P-H and Lai Y-H (2017) A Reliable and Non-destructive Method for Monitoring the Stromal pH in Isolated Chloroplasts Using a Fluorescent pH Probe. Front. Plant Sci. 8:2079. doi: 10.3389/fpls.2017.02079

INTRODUCTION

Proton (H^+) gradients across biological membranes provide the driving force for ATP synthesis and for secondary active transport of solutes between cellular compartments, which maintain different pHs for optimal biochemical reactions (Reid et al., 1966; Avron, 1977; Shingles et al., 1996; Cruz et al., 2001; Neuhaus and Trentmann, 2014; Hohner et al., 2016). The measurement of the pH of different subcellular compartments is essential for determining the proton gradient across the membranes. Many methods have been developed to trace cellular and organelle pHs, including weak-acid/base indicators, nuclear magnetic resonance, pH microelectrodes, pH-sensitive dyes, and fluorescent probes and proteins (Iles, 1981; Loiselle and Casey, 2010). All methods currently used for measuring intracellular pH have their own advantages and technical limitations. Among them, fluorescent pH probes are a cost-effective and non-destructive way to determine the pH of intracellular compartments by spectrometric or image fluorescence, and are widely used in many organisms for real-time monitoring of intracellular pH (Grant and Acosta, 1997; Scott and Allen, 1999; Alvarez-Leefmans et al., 2006; Loiselle and Casey, 2010; Sundaresan et al., 2015).

In plant cells, the optimal cytoplasm pH for physiological activities is a neutral pH of around 7.2 to 7.4; the apoplast and vacuole have acidic pH ranging from 5 to 7; the thylakoid lumen has a more dynamic and highly acidic environment that changes with light/dark cycles. The mitochondrial matrix and chloroplast stroma need to keep a relatively basic environment around pH 8 for optimization of biochemical reactions occurring in these two compartments (Shen et al., 2013; Hohner et al., 2016). Consequently, proton gradients are formed across the membranes separating different compartments, and are maintained by H^+-transporting electron transfer chain (photosynthetic light reaction and respiratory oxidative phosphorylation) or by H^+-pumping fueled by ATP or pyrophosphate hydrolysis (H^+-ATPase or H^+-pyrophosphatase) (Kurkdjian and Guern, 1989).

Methods for determining the pH of most cellular and organelle compartments are well established and are used to assess the importance of pH and proton gradients for particular biological functions. However, to date, an easy and reliable method for real-time monitoring of the chloroplast stromal pH is still lacking. It is widely accepted that the stromal pH can increase from pH 7 in the dark to pH 8 upon illumination, which is required to fully activate the enzymes for carbon fixation (Berkowitz and Wu, 1993). Upon illumination, a proton gradient of 0.12–0.36 pH units across the inner envelope membrane (ΔpH_{env}) can be formed in isolated chloroplasts. The value can be determined with a destructive method called silicon oil microcentrifugation by monitoring the distribution of the radioactive weak acid [^{14}C]-5-5′-dimethyloxazolidine-2,4-dione across the chloroplast envelope (Heldt et al., 1973; Robinson, 1985; Wu and Berkowitz, 1992; Heiber et al., 1995).

Additionally, ionophores such as nigericin and carbonyl cyanide m-chlorophenyl hydrazone (CCCP) can be used to collapse the proton gradients for the assessment of the importance of the proton gradients on membrane activity (Nishio and Whitmarsh, 1991). The concentrations of ionophores required to diminish a particular membrane proton gradient need to be determined empirically because different membrane systems have different lipid compositions, H^+-translocating machinery and microenvironments to respond to the action of ionophores (Kasianowicz et al., 1984). Owing to the difficulty and technical limitations, chloroplast stromal pH is rarely determined experimentally. Instead, the levels of ionophores routinely used in other membrane systems are adopted directly without demonstrating the ionophores' ability to completely collapse the proton gradient.

Here we report the development of an easy and reliable method for continuous and real-time monitoring of the stromal pH using a ratiometric fluorescent pH probe, BCECF [2′,7′-bis-(2-carboxyethyl)-5-(and-6)-carboxyfluorescein]. Compared to the traditional destructive silicon oil filtration technique, the advantages of our method are that it is easy, cost-effective and non-destructive, and can be used in real-time. It is, therefore, ideal for conducting continuous measurements in live organelles.

MATERIALS AND METHODS

Reconstruction of a Fluorescence Spectrometer to Add Compatible Actinic Light

The commercial fluorescence spectrometer model FP-8300 equipped with an ETC-815 thermostat cuvette holder with stirrer and CSP-829 sample compartment lid with syringe port was purchased from Jasco International, Japan. To measure the light-dependent behavior of chloroplasts after fluorescent dye uptake, the introduction of a compatible actinic light is required. A red LED actinic light (0.5 Watts, peaking at 628 nm, emission spectrum shown in Supplementary Figure S1) was delivered 180° from the excitation beam and 90° from the emission detector. To eliminate the interference of strong actinic illumination on the excitation photons, a 550 nm Techspec Shortpass Filter (Edmund Optics, United States) was placed in front of the entrance hole of a cuvette holder. The overall light-path design, module assembly and machine validation are described in detail in the section "Results."

Plant Materials and Chloroplast Isolation

Pea chloroplasts were isolated from 8- to 10-day-old pea seedlings grown on vermiculite in a growth chamber at 22°C under a light intensity of 200 μmol/m^2/s. A continuous Percoll gradient was prepared by mixing half volume of Percoll reagent (GE Healthcare) and half volume of 2× grinding (GR) buffer, and by centrifuging at 38,000 × *g* for 30 min in a fixed angle rotor (RA20A2 rotor, Himac CR22G2; Hitachi Koki, Tokyo). A 1× GR buffer containing 50 mM Hepes-KOH pH 7.3, 330 mM sorbitol, 1 mM $MgCl_2$, 1 mM $MnCl_2$, 2 mM EDTA, and 0.1% BSA. About 20 g of young shoots was ground in a blender at low speed for 15 s, three times in GR buffer and spun at 3,000 × *g* for 3 min, and the pelleted chloroplasts were resuspended in 2 to 3 ml of GR buffer,

then centrifuged on a preformed continuous Percoll gradient for organelle fractionation at 3,900 × *g* for 13 min at 4°C (SX4250 Swinging-Bucket Rotor, Beckman Coulter, United States). The intact chloroplast fraction near the bottom of the tube was retrieved, put in a new tube and washed with GR buffer twice. Finally, isolated chloroplasts were resuspended in GR buffer at a concentration of 1 mg/ml chlorophyll, and stored on ice in the dark until use.

Uptake and Digestion of Esterified Fluorescent pH Probes

To determine the intracellular or intra-organellar pH by fluorescent pH probes, generally, their non-fluorescent and membrane permeable esterified forms are incubated with cells or organelles. After loading into the cells or organelles, their ester bonds are digested by endogenous esterase to release fluorescent free forms that are not membrane permeable. For our experiments, three commonly used pH indicators BCECF (pKa ∼6.98), CFDA [5(6)-carboxyfluorescein diacetate; pKa ∼6.5] and SNARF-1 (seminaphthorhodafluors; pKa ∼7.5) were tested. Their uptake ability and digestibility were evaluated by feeding isolated chloroplasts of 0.5 mg/ml chlorophyll with their ester derivatives BCECF-AM (acetoxymethyl ester) (B1170, Molecular Probes), CFDA-SE (*N*-succinimidyl ester) (Cat#21888, Sigma) and SNARF-1 carboxylic acid acetate succinimidyl ester (S22801, Molecular Probes), respectively, at concentrations of 20, 80, and 80 μM, for 20 min at RT and then 10 min on ice. Thereafter, intact chloroplasts were re-isolated by a 40% Percoll cushion, washed once with GR buffer and checked by a fluorescence spectrometer (FP-8300, Jasco, Japan) or a laser confocal microscope (LSM710, Zeiss, Germany). Parameters used are described in the figure legends. To determine the sub-organellar distribution of BCECF, intact chloroplasts were lysed in hypotonic buffer containing 50 mM Hepes-KOH pH 8.0, 50 mM NaCl and 4 mM $MgCl_2$ on ice for 3 min. The lysed chloroplasts were centrifuged at 3,000 × *g* for 3 min to separate the stromal fraction (supernatant) and the thylakoid lumen-containing membrane fraction (pellet). The resultant pellet was washed once with hypotonic buffer and centrifuged again. Two supernatant fractions were combined and clarified with centrifugation at 7,500 × *g* for 5 min. Two pellet fractions were resuspended in hypotonic buffer and combined. The BCECF signal was measured by the fluorescence spectrometer. An equal amount of chloroplasts that had not been incubated with BCECF was added to the stromal fraction to equalize the chlorophyll background with the pellet fraction before measurement.

Establishment of the pH-Fluorescence Correlation Standard Curve and Measurements of Proton Gradients

Stromal pH measurements with BCECF are made by determining the ratio of emission intensity at 535 nm when the dye is excited at 490 nm (pH-dependent) vs. when the dye is excited at 440 nm (pH-independent isosbestic point). *In situ* measurements of BCECF ratiometric fluorescence was conducted in 50 mM Hepes-Tris buffer of pH 6.8, 7.2, 7.6 and 8.0 containing 330 mM sorbitol, 15 mM KCl and 1 μM nigericin (N7143, Sigma). For each measurement, the fluorescence of chloroplasts of the same concentration without BCECF was measured as a background. The ratio of the fluorescence intensity is a sigmoidal function of the $[H^+]$ between pH 4 and 9 with an essentially linear mid region from pH 6 to 8 (James-Kracke, 1992). To simplify the conversion of ratio-metric fluorescence intensity to the stromal pH, the standard curve was established with simple linear regression.

Optimizing the Measurement Parameters of the Fluorimeter for Continuous Reading

Chloroplasts are very sensitive to light. Even in dim light, a photosynthetic light reaction may be triggered. The 9-Amionoacridine (9-AA) fluorescence quenching is routinely used to determine of the formation of a proton gradient across the thylakoid membrane (ΔpH_{thy}) upon illumination (Evron and McCarty, 2000; Theg and Tom, 2011). Here we optimized the measurement parameters (including excitation beam width and data reading interval) of the FP-8300 fluorescence spectrometer by determining the effect of measuring light on 9-AA fluorescence quenching. One milliliter chloroplast suspension of 0.1 mg/ml chlorophyll in GR buffer containing 5 μM 9-AA and 20 μM methyl viologen (as an electron acceptor) was mixed continuously in 1-ml stirred quartz cuvette at 25°C. The 9-AA fluorescence was monitored at 455 nm emission wavelength while it was excited at 400 nm. Fluorescence of the chloroplast suspension without the addition of 9-AA was measured as background.

Real-Time Monitoring of the Light Dependent Increase in Stromal pH and the Effect of Nigericin on Collapsing the ΔpH_{env}

To verify that our method can be used for continuous and real-time monitoring of the stromal pH in live chloroplasts, the fluctuation of the stromal pH upon illumination was determined continuously. One milliliter of BCECF-loaded chloroplast suspension of 0.1 mg/ml chlorophyll in GR buffer containing 5 mM $NaHCO_3$, 0.25 mM NaH_2PO_4, 1,000 units of catalase (as a scavenger of H_2O_2 produced in the light to protect chloroplasts from damage) was mixed continuously in 1-ml stirred quartz cuvette at 25°C. After a few minutes pre-equilibration, the ratiometric fluorescence of F490/440 was determined as described above. Red actinic light was delivered during 180–420 s in an 800-s time period. The fluorescence of the chloroplast suspension without BCECF was determined as background to normalize the reads. The data was collected every 5 s and the excitation shutter was opened only when the data were being collected. To test whether nigericin can collapse the light-dependent formation of the ΔpH_{env}, 5 μl of 0.2 mM nigericin was injected into the illuminated chloroplast suspension to make a final concentration at 1 μM through the syringe pore of CSP-829 sample compartment lid.

RESULTS

Light-Path Design for the Introduction of Actinic Light

To measure the light-dependent pH change in isolated chloroplasts, we modified a commercial fluorescence spectrometer to add actinic light. The light-path arrangement is shown in **Figure 1A**. A LED actinic light (4 chip Piranha red LED module, peaks at 628 nm, 0.5 Watts) was placed 180° from the excitation beam and 90° from the emission detector. To eliminate the interference of strong actinic illumination on the excitation photons, a 550 nm Techspec Shortpass Filter (Edmund Optics, United States) was placed in the front of the entrance hole of the cuvette holder. Side-by-side comparison of the interference of the actinic light on the dye fluorescence with or without the shortpass filter was conducted to validate our setup. As shown in **Figures 1B,C**, the emitted fluorescence intensities of BCECF and 9-Amionoacridine (9-AA) dropped significantly upon illumination without the use of a 550 nm shortpass filter. After the attachment of the shortpass filter, the phenomenon was totally eliminated. It should be noted that there was a 4–5% reduction in the fluorescence intensity when the shortpass filter was added because the coated filter has about 95–96% transmission efficacy.

Uptake of Fluorescent pH Probes by Isolated Chloroplasts

We next incubated isolated pea chloroplasts with three esterified pH-sensitive fluorescent probes, BCECF-AM, CFDA-SE, and SNARF-1 carboxylic acid acetate succinimidyl ester.

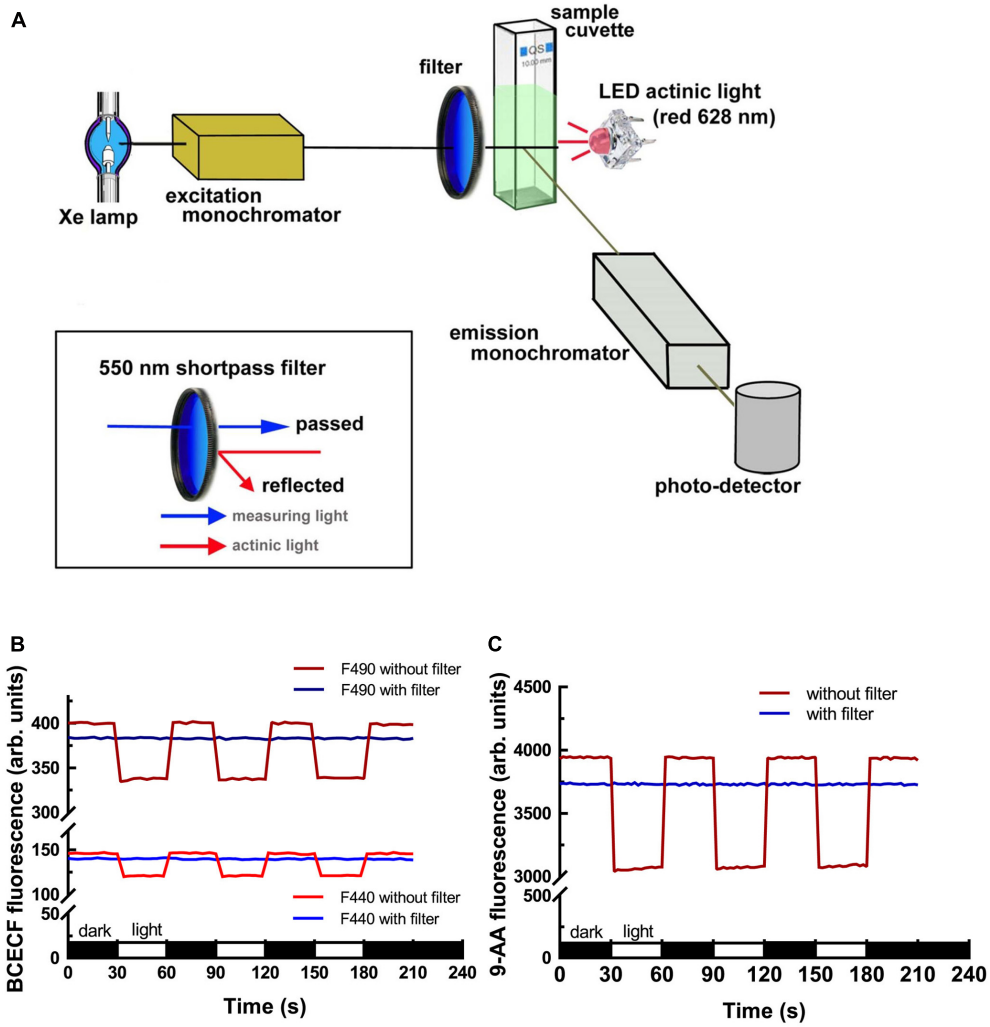

FIGURE 1 | Fluorescence spectrometer modification and validation. **(A)** Illustration of the light-path and module assembly for the introduction of actinic light for measuring the light-dependent behavior of chloroplasts. Attachment of a 550 nm shortpass filter in the front of the cuvette facing the excitation beam is critical for reducing the interference of strong actinic light on excitation photons. Measurements of BCECF **(B)** and 9-AA **(C)** fluorescence showed that the use of the 550 nm shortpass filter can eliminate the interference of actinic light on the excitation photons. Without the 550 nm shortpass filter, the emitted fluorescence of BCECF and 9-AA dropped upon illumination. After adding the shortpass filter the emitted fluorescence became constant.

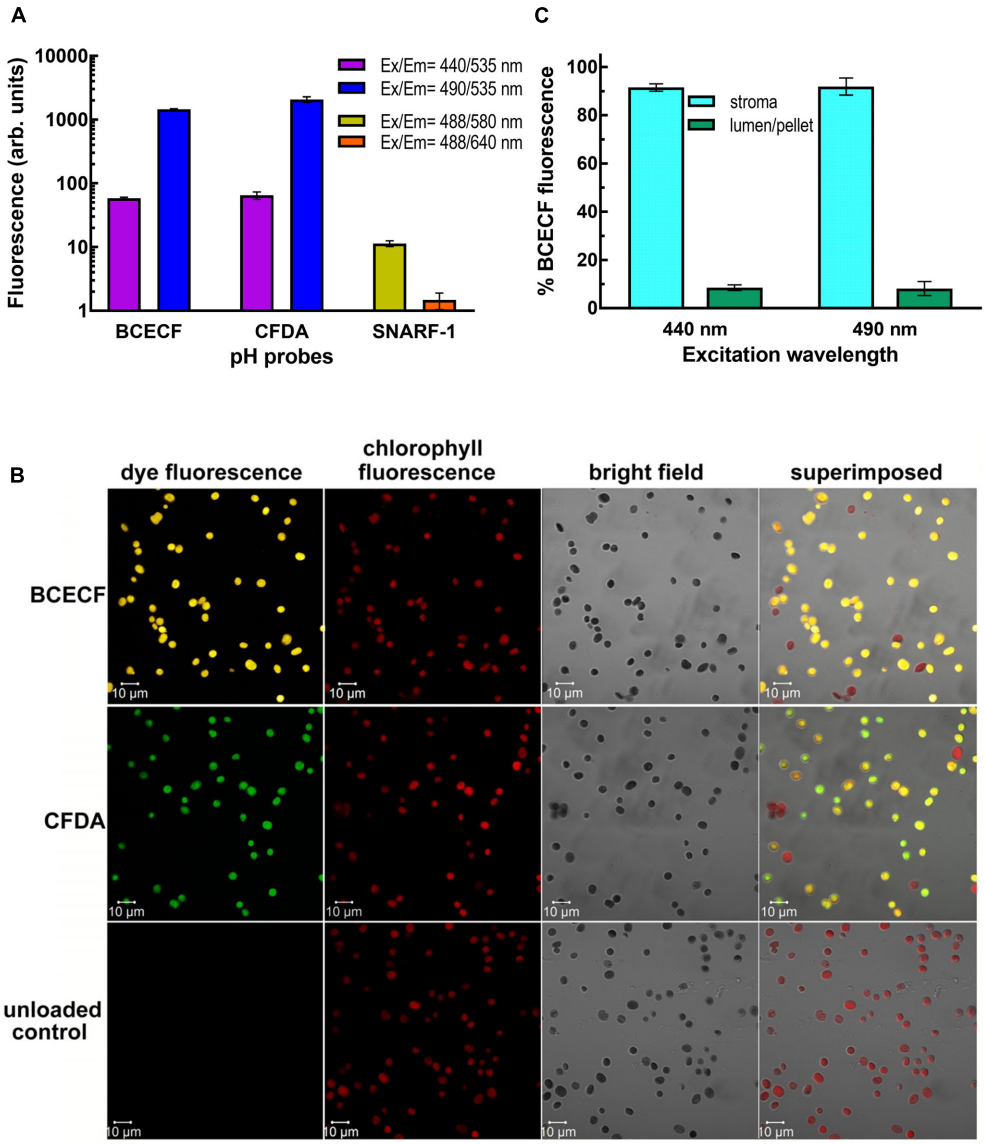

FIGURE 2 | Uptake and digestion of fluorescent pH dyes by isolated chloroplasts. **(A)** Fluorescence of the dye-loaded chloroplasts of 0.1 mg/ml chlorophyll was measured by a fluorescence spectrometer. For BCECF and CFDA, emission at 535 nm was detected when the dyes were excited at 440 and 490 nm. For SNARF-1, emission at 580 and 640 nm was detected when the dye was excited at 488 nm. **(B)** BCECF- and CFDA-loaded chloroplasts were visualized with Plan-Apochromat 63× oil (NA1.4) objective by Zeiss LSM710 laser confocal microscopy. When chloroplasts were excited with Argon laser at 488 nm, the fluorescence emitted at 515–555, 510–540, and 680–797 nm was collected by Quasar spectral detector as BCECF, CFDA, and chlorophyll fluorescence signals, respectively. The percentages of BCECF and CFDA-stained chloroplasts were 84.7 ± 4.5 and 83.9 ± 4, respectively. **(C)** BCECF-loaded chloroplasts were fractionated into the stroma and the thylakoid-lumen-containing membrane pellet fractions by centrifuging hypotonically lysed chloroplasts. An equal amount of chloroplasts that had not been incubated with BCECF was added to the stroma-containing supernatant to equalize the chlorophyll background before measurements. Percentage of BCECF fluorescence at 535 nm in each fraction when excited at 440 or 490 nm is presented. Data are means of three biological repeats ± SD.

After incubation for 20 min at room temperature and then 10 min on ice, the probe-loaded intact chloroplasts were re-isolated through a 40% Percoll cushion. If the non-fluorescent esterified probes could enter the chloroplasts, the probes should be digested to their fluorescent forms by the endogenous esterases. The fluorescence of the probes was monitored by the fluorimeter. Ratiometric measurements are critical to eliminate distortions of data caused by photobleaching and variations in probe loading and retention, as well as by instrumental factors such as illumination stability (O'Connor and Silver, 2007; Han and Burgess, 2010). Dual fluorescence values, one for pH-sensitive wavelengths and the other for pH-insensitive isosbestic point, have to be detected side-by-side. As shown in **Figure 2A**, BCECF-AM and CFDA-SE-fed chloroplasts produced high levels of fluorescence from the probes, indicating that the probes were taken up and digested by esterases. Only a

very low level of SNARF-1 fluorescence can be detected at an intensity of about 11 and 1.5 arbitrary units at the emission wavelength at 580 and 640 nm, respectively. This result suggests that either SNARF-1 carboxylic acid acetate succinimidyl ester could not be taken up by chloroplasts or could not be digested by chloroplast esterases. We, therefore, isolated the stromal fraction from SNARF-1-incubated chloroplasts and found that a significant level of SNARF-1 fluorescence can be detected in the chlorophyll-free stromal fraction (Supplementary Figure S2). This result suggests that SNARF-1 fluorescence was concealed, possibly because of shielding of the exciting and emitted lights by pigments in the thylakoid. Particularly, its emitted light at 640 nm would be strongly re-absorbed by chlorophyll. To confirm that the fluorescent probes had been taken up by chloroplasts, fluorescent images of BCECF- and CFDA-loaded chloroplasts were visualized by laser confocal microscopy. Their fluorescence signals showed an even distribution inside the chloroplasts overlapping with the images of chlorophyll auto-fluorescence (**Figure 2B**).

Considering its relatively higher pKa value of 6.98 (near the physiological pH of stroma) and its good intracellular retention (Han and Burgess, 2010), BCECF was chosen for further development of real-time monitoring of the stromal pH. We first checked whether BCECF was also taken up into the thylakoid lumen, which would interfere with the readout on determining the stromal pH by the fluorescent probe. Fractionation of BCECF-loaded chloroplasts demonstrated that BCECF fluorescence was almost located in the stroma and was little found in the thylakoid lumen (**Figure 2C**). Sub-organellar distribution of a luminal soluble protein plastocyanin indicated that the majority of thylakoid lumen was kept intact during fractionation (Supplementary Figure S3). Taken together, lumen-resident BCECF may have little interference on pH determining, but it nearly can be ignored due to its extremely low amount.

Establishment of a pH Standard Curve by Ratiometric Fluorescence Measurements

Measurements of pH with BCECF are generally made by determining the pH-dependent emission intensity ratio (ratiometric fluorescence) detected at 535 nm when the probe is excited at 490 nm (pH-dependent) vs. the emission intensity when the probe is excited at 440 nm (pH-independent isosbestic point). *In situ* calibration is performed to first establish a standard curve representing the correlation between the ratiometric fluorescence and the pH of the samples under study. This is important because different cellular compartments have different microenvironments that will have different effects on the signal intensity. In chloroplasts, the ratiometric fluorescence is also tremendously affected by endogenous pigments of chloroplasts. Not only may the excitation beam be absorbed by chlorophylls but also the emitted fluorescence may be absorbed by chlorophyll *b* and carotenoids owing to overlapping wavelengths. As shown in **Figure 3A**, BCECF fluorescence was highly attenuated in chloroplast suspensions compared to BCECF in buffer without chloroplasts. The BCECF fluorescence in chloroplast suspension of 0.1 mg/ml chlorophyll showed about 260- and 55-fold reductions when BCECF was excited at 440 and 490 nm, respectively. This result suggests that higher interference occurred at the excitation beam at 440 nm, for which the chlorophyll has a relatively higher absorbance. To demonstrate the overall interference of chloroplast pigments on BCECF fluorescence, the full excitation spectra of BCECF affected by chloroplast suspensions were determined. It was shown that the reduction ratio of BCECF signal was highly dependent on the chlorophyll levels and the chloroplast absorption spectrum (Supplementary Figures S4A–C). Their reduction ratio was increased with the increase of the chloroplast absorbance, supporting that a relative higher reduction of BCECF signal at 440 nm is resulted from a relative higher chloroplast absorbance at 440 nm (by comparing with 490 nm). In addition, as shown in Supplementary Figure S4D, BCECF in chloroplast suspensions remained the signature of a ratiometric dye, having the pH-insensitive isosbestic point (at 440 nm) and the pH-sensitive wavelengths (usually detected at 490 nm). Without chloroplast pigment interference, the ratiometric fluorescence of BCECF changed depending on the pH, but was not affected by its concentration. When we serially diluted free BCECF in buffer from 1 to 1/8×, a constant ratiometric fluorescence (F490/F440) value of 5.5 was detected (**Figure 3B**). However, the ratiometric value of BCECF-loaded chloroplasts increased with increasing chloroplast concentration owing to the interference of chloroplast pigments (**Figure 3C**), i.e., the ratiometric fluorescence is highly dependent on the chlorophyll levels. Therefore *in situ* calibration should be conducted at a fixed concentration of chloroplast suspension.

According to this consideration, we conducted the *in situ* calibration by measuring the F490/F440 of BCECF from the chloroplast suspension. Isolated pea chloroplasts were incubated with BCECF-AM for 20 min at room temperature and then 10 min on ice, and the probe-loaded intact chloroplasts were re-isolated and resuspended to 0.1 mg/ml chlorophyll in 50 mM Hepes-Tris buffer of pH 6.8, 7.2, 7.6, or 8.0 and 330 mM sorbitol, 15 mM KCl and 1 μM nigericin. Nigericin was added to collapse all the proton gradients so the pH of chloroplasts was equal to the pH of the buffer. For each measurement, the fluorescence of chloroplasts of the same concentration without BCECF was also measured as a background. As reported previously, the ratio of the fluorescence intensity is a sigmoidal function of the $[H^+]$ between pH 4 and 9 with an essentially linear mid region from pH 6 to 8 (James-Kracke, 1992). To simplify the conversion of ratiometric fluorescence intensity to stromal pH, the standard curve was established with simple linear regression instead. As shown in **Figure 3D**, a coefficient of *r*-square of 0.98 was obtained, indicating a good correlation between the BCECF ratiometric fluorescence and the stromal pH and demonstrating the feasibility of our method.

A Light-Dependent Formation of ΔpH_{env} in Isolated Chloroplasts

Upon illumination, light-dependent electron transfer on the thylakoid membrane drives the movement of H^+ from the

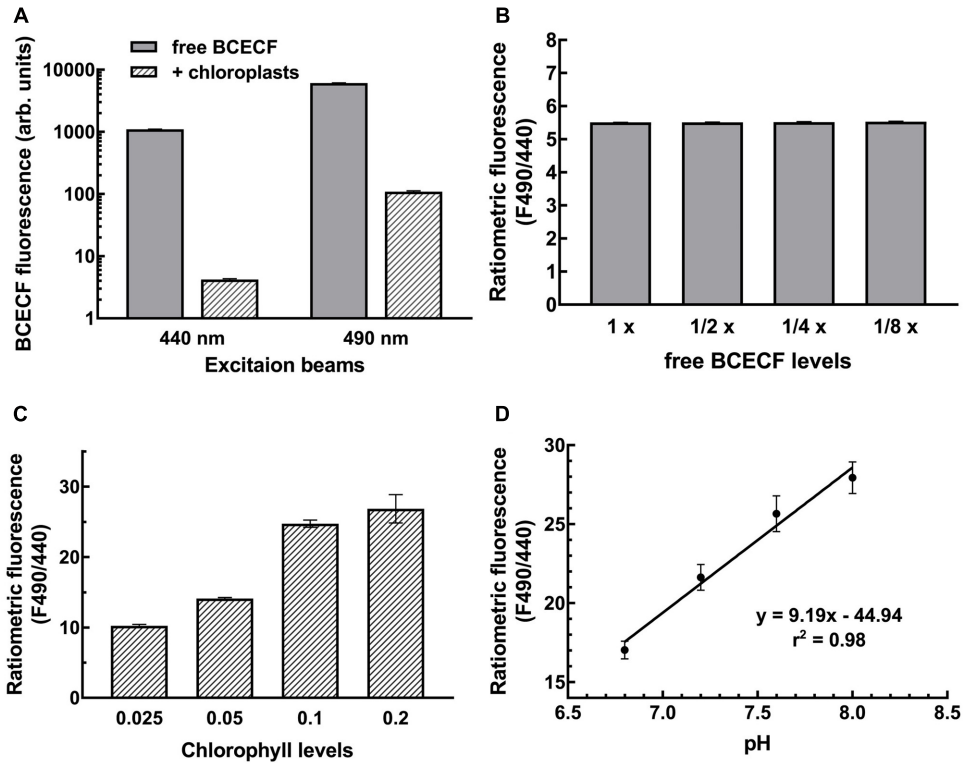

FIGURE 3 | Establishment of the BCECF pH-fluorescence standard curve. **(A)** Chloroplasts attenuated the BCECF fluorescence. Fluorescence was dramatically reduced when chloroplasts were added into the BCECF-containing buffer. **(B)** A serial dilution of free BCECF in grinding buffer was made, and their ratiometric fluorescence value was determined. **(C)** Ratiometric fluorescence of BCECF-loaded chloroplasts was determined at a serial concentration of chloroplasts ranging from 0.025 to 0.2 mg/ml chlorophyll. **(D)** *In situ* measurements of BCECF ratiometric fluorescence was conducted at a fixed concentration of chloroplasts of 0.1 mg/ml chlorophyll. The pH-fluorescence standard curve was established by linear regression between pH 6.8 to 8.0.

stroma to the thylakoid lumen, which acidifies the luminal space and alkalizes the stromal compartment, and builds up not only the ΔpH_{thy} between the thylakoid lumen and the stroma, but also the ΔpH_{env} between the stroma and the cytosol. To test if our fluorescent BCECF method is capable of measuring the stromal pH in buffered isolated chloroplasts in real time, the fluctuation of the stromal pH in response to actinic light was continuously determined. A typical result of the light-dependent increase in the stromal pH is shown in **Figure 4**. The stromal pH increased sharply upon illumination, and reached a plateau in less than 1 min. The higher pH was maintained at continuous actinic light, and then declined gradually after the light was turned off. From three independent experiments, a light-dependent formation of the ΔpH_{env} can be detected reproducibly and the calculated ΔpH_{env} ranged from 0.15 to 0.33 pH units, averaging 0.25 pH units (**Table 1**), which is comparable with previous reports determined by the silicon oil microcentrifugation (see Supplementary Table S1). Furthermore, addition of 1 μM nigericin under continuous actinic light caused a decline in stromal pH to the level before the light was turned on (**Figure 5**), indicating that 1 μM nigericin under these conditions was sufficient to completely collapse the ΔpH_{env}.

It should be noted that the amount of excitation light at 440 and 490 nm for exciting BCECF should be minimalized as much as possible to avoid activating the photosynthetic light reaction. According to the absorption spectra of chlorophylls, the light wavelengths at 400, 440, and 490 may have a comparable level of actinic effect on photosynthesis. The 9-AA fluorescence quenching excited at 400 nm is a sensitive way to determine the light-dependent formation of the ΔpH_{thy}. We therefore performed the measurement in order to find the best balance point between good BCECF fluorescence and low photosynthetic light reaction activation. As shown in Supplementary Figure S5, a 2.5 nm bandwidth and 5-s data interval had a high level of 9-AA fluorescence while only producing 9-AA quenching of 6%. Widening the excitation beam bandwidth and shortening the reading interval resulted in quenching as high as 30%. Therefore, a good tradeoff was obtained by setting the excitation bandwidth to 2.5 nm, reading the fluorescence every 5 s for 1 s and opening the excitation shutter only when reading the data. Under these conditions there was a good balance between reducing the actinic effect and keeping a high level of fluorescence; and the actinic effect can reach an equilibrium in less than 30 s as indicated by a continuous measurement of 9-AA fluorescence quenching (Supplementary Figure S5).

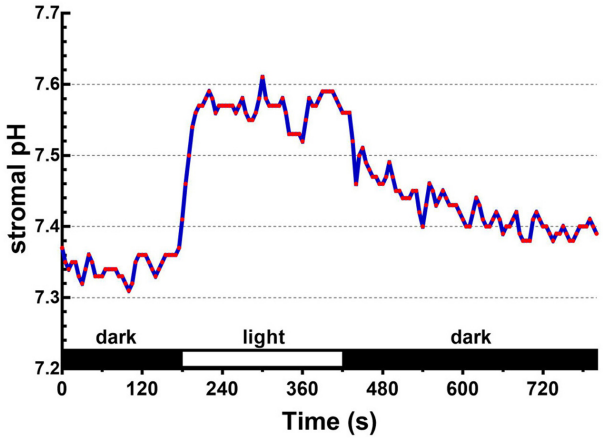

FIGURE 4 | Light-dependent changes in the stromal pH can be continuously monitored. The ratiometric fluorescence of BCECF-loaded chloroplasts of 0.1 mg/ml chlorophyll was continuously measured at 5-s intervals over an 800-s period. Red actinic light was delivered between 180 and 420 s. The stromal pH was calculated through the established standard curve as shown in **Figure 3D**. Each red circle represents a datum point.

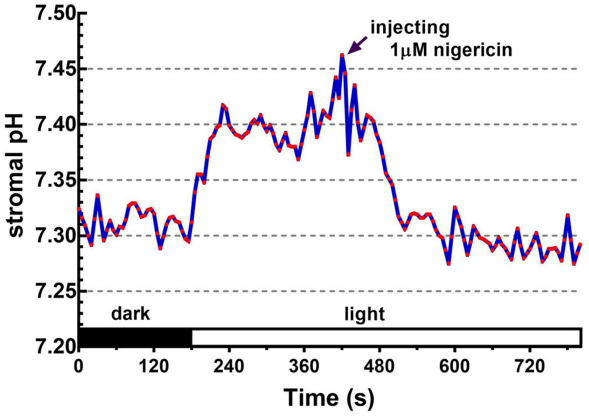

FIGURE 5 | Effect of nigericin on collapsing the light-dependent formation of the ΔpH_{env}. The ratiometric fluorescence of BCECF-loaded chloroplasts of 0.1 mg/ml chlorophyll was continuously measured at 5-s intervals over an 800-s period. The red actinic light was turned on at 180 s. After the formation of light-dependent ΔpH_{env}, nigericin was injected into the chloroplast suspension with a final concentration of 1 μM at 420 s as indicated by the arrow. Each red circle represents a datum point.

TABLE 1 | Measured stromal pH (pH_{str}) and calculated proton gradient across the inner envelope membranes (ΔpH_{env}) of isolated chloroplasts from three independent experiments.

Experiment#	Dark pH_{str}	Light pH_{str}	pH_{str} increase upon illumination	ΔpH_{env} in the light
1	7.30	7.45	0.15	0.15
2	7.32	7.63	0.31	0.33
3	7.34	7.57	0.23	0.27
Mean	7.32	7.55	0.23	0.25
SD	0.02	0.09	0.08	0.09

In all experiments, the stromal pH was determined by the ratiometric fluorescence of the BCECF-loaded chloroplasts of 0.1 mg/ml chlorophyll in a buffered medium of pH 7.3. The pH_{str} increase was calculated by substrating the dark pH_{str} from the light pH_{str}. The ΔpH_{env} was calculated by substrating the buffered medium pH (7.3) from the light pH_{str}.

DISCUSSION

Intracellular and organellar pHs are easily measured by fluorescent molecular probes or pH-sensitive fluorescent proteins with spectrometric or image fluorescence in many organisms (Sano et al., 2010; Shen et al., 2013). A plant organelle pH detection system based on modified pH-sensitive fluorescent proteins expressed in particular cellular compartments has been reported for Arabidopsis suspension cells (Shen et al., 2013). Unfortunately, the pH of the chloroplast stroma could not be determined because the auto-fluorescence signal of chlorophyll influenced the emission signal intensity of the pH sensor protein in light-cultured Arabidopsis PSB-L suspension cells. Plastid stromal pH could only be determined from PSB-D suspension cells incubated in the dark. It was shown that the pH value of the plastid stroma of dark-incubated PSB-D suspension cells was 7.2, which is near the cytosolic pH (around 7.3). There was almost no detectable proton gradient across the inner envelope membrane of plastids under these conditions, probably due to the fact that the plastids in the suspension-cultured cells were not fully functional because sugars were provided in the culture medium (Shen et al., 2013). These results highlight the difficulty in measuring the stromal pH of green chloroplasts due to the interference from the chlorophyll fluorescence (Yin et al., 1990; Shen et al., 2013).

Here we established an easy and reliable method for real-time monitoring of the stromal pH by the ratiometric fluorescence measurement of the pH-sensitive dye BCECF in isolated chloroplasts. The following requirements should be noted. First, because the absorption spectrum of chlorophylls overlapped with the BCECF excitation wavelengths of 440 and 490 nm, the excitation energy available to BCECF is attenuated in chloroplast suspension. Furthermore BCECF emitted fluorescence may be partially absorbed by chlorophyll *b* and carotenoids. Hence the chloroplast concentration in each sample has to be the same to equalize the interference from the chloroplast pigments (**Figure 3**). In addition, standard curves should be obtained using chloroplasts isolated from plants grown under the same conditions as the samples being studied because plants grown under different conditions would have different pigment compositions. Second, the excitation light bandwidth and shutter opening and data collection time of the fluorescence spectrometer should be set to achieve a good tradeoff between having a sufficient fluorescence signal and minimalizing the actinic effect of the excitation light on photosynthesis. In our case, narrowing the bandwidth of the excitation light to 2.5 nm, and opening the shutter only when reading the data at 5-s time interval achieved good results with the fluorescence spectrometer FP-8300 (see Supplementary Figure S5). Third, a short-pass filter in front of a sample cuvette in the path of the excitation beam is required when determining the light-dependent pH change

of chloroplasts. A short-pass filter is essential to eliminate the interference of the strong actinic light on the excitation beam (**Figure 1**). With the above optimization, a BCECF fluorescence vs. stromal pH standard curve with a high correlation coefficient ($r^2 = 0.98$) was successfully established, indicating the reliability of our method in measuring the stromal pH in buffered isolated chloroplasts. Compared to the traditional silicon oil filtration technique, our method is easy, cost-effective, and non-destructive and can be conducted in real-time. One of the most difficult parts of the silicon oil filtration technique is the determination of the accurate sizes of stromal and thylakoid luminal spaces, which is not necessary with our method.

It has long been accepted that the cytoplasm and the chloroplast stroma have a neutral pH close to 7, but upon illumination the stroma is alkalized up to pH 8 as a consequence of H^+-pumping into the thylakoid lumen. This suggests that a proton gradient between the cytosol and the stroma is established under light (Hohner et al., 2016). By our method, the increase of stromal pH upon illumination can be continuously monitored in real-time (**Figure 4**), providing a powerful tool for studying chloroplast physiology. Establishment of the ΔpH_{env} can be routinely detected upon illumination. The value is about 0.15–0.33 pH units, which is comparable with previous reports determined by the silicon oil filtration method (Heldt et al., 1973; Wu and Berkowitz, 1992; Heiber et al., 1995). It should be noted that our non-destructive method provides more detailed information than the single-point silicon oil filtration technique. The decline in the stromal pH after turning off the actinic light was gradual and took few minutes, implying the existence of an intricate buffering system that controls the homeostasis of stromal pH. The pH decline does not seem to depend solely on the H^+-transportation on the thylakoid membrane, since the light-dependent 9-AA quenching (representing the ΔpH_{thy}) is always recovered quite fast (Köster and Heber, 1982; Theg and Tom, 2011).

CONCLUSION

We have setup and validated a reliable method for the continuous, non-destructive, real-time stromal pH measurement in living chloroplasts, which will provide an important tool for future study of topics such as regulation of stromal pH changes and the importance of the ΔpH_{env}.

AUTHOR CONTRIBUTIONS

Y-HL contributed to the isolation of intact chloroplasts and the operation of laser confocal microscopy. P-HS designed the experiments, performed fluorescence spectrometer measurements, data processing and manuscript writing.

FUNDING

This work was supported by the funding of Academia Sinica to P-HS.

ACKNOWLEDGMENTS

The authors thank Dr. Hsou-min Li for careful reading the manuscript, and Ms. Miranda Loney for English editing.

SUPPLEMENTARY MATERIAL

The Supplementary Material for this article can be found online at: https://www.frontiersin.org/articles/10.3389/fpls.2017.02079/full#supplementary-material

REFERENCES

Alvarez-Leefmans, F. J., Herrera-Perez, J. J., Marquez, M. S., and Blanco, V. M. (2006). Simultaneous measurement of water volume and pH in single cells using BCECF and fluorescence imaging microscopy. *Biophys. J.* 90, 608–618. doi: 10.1529/biophysj.105.069450

Avron, M. (1977). Energy transduction in chloroplasts. *Annu. Rev. Biochem.* 46, 143–155. doi: 10.1146/annurev.bi.46.070177.001043

Berkowitz, G. A., and Wu, W. (1993). Magnesium, potassium flux and photosynthesis. *Magnes. Res.* 6, 257–265.

Cruz, J. A., Sacksteder, C. A., Kanazawa, A., and Kramer, D. M. (2001). Contribution of electric field ($\Delta\Psi$) to steady-state transthylakoid proton motive force (*pmf*) in vitro and in vivo. control of *pmf* parsing into $\Delta\Psi$ and ΔpH by ionic strength. *Biochemistry* 40, 1226–1237. doi: 10.1021/bi0018741

Evron, Y., and McCarty, R. E. (2000). Simultaneous measurement of ΔpH and electron transport in chloroplast thylakoids by 9-aminoacridine fluorescence. *Plant Physiol.* 124, 407–414. doi: 10.1104/pp.124.1.407

Grant, R. L., and Acosta, D. (1997). Ratiometric measurement of intracellular pH of cultured cells with BCECF in a fluorescence multi-well plate reader. *In Vitro Cell. Dev. Biol. Anim.* 33, 256–260. doi: 10.1007/s11626-997-0044-z

Han, J., and Burgess, K. (2010). Fluorescent indicators for intracellular pH. *Chem. Rev.* 110, 2709–2728. doi: 10.1021/cr900249z

Heiber, T., Steinkamp, T., Hinnah, S., Schwarz, M., Flugge, U. I., Weber, A., et al. (1995). Ion channels in the chloroplast envelope membrane. *Biochemistry* 34, 15906–15917. doi: 10.1021/bi00049a005

Heldt, W. H., Werdan, K., Milovancev, M., and Geller, G. (1973). Alkalization of the chloroplast stroma caused by light-dependent proton flux into the thylakoid space. *Biochim. Biophys. Acta* 314, 224–241. doi: 10.1016/0005-2728(73)90137-0

Hohner, R., Aboukila, A., Kunz, H. H., and Venema, K. (2016). Proton gradients and proton-dependent transport processes in the chloroplast. *Front. Plant Sci.* 7:218. doi: 10.3389/fpls.2016.00218

Iles, R. (1981). Measurement of intracellular pH. *Biosci. Rep.* 1, 687–699. doi: 10.1007/BF01116466

James-Kracke, M. R. (1992). Quick and accurate method to convert BCECF fluorescence to pHi: calibration in three different types of cell preparations. *J. Cell. Physiol.* 151, 596–603. doi: 10.1002/jcp.1041510320

Kasianowicz, J., Benz, R., and McLaughlin, S. (1984). The kinetic mechanism by which CCCP (carbonyl cyanide m-chlorophenylhydrazone) transports protons across membranes. *J. Membr. Biol.* 82, 179–190. doi: 10.1007/BF01868942

Köster, S., and Heber, U. (1982). Light scattering and quenching of 9-aminoacridine fluorescence as indicators of the phosphorylation state of the adenylate system in intact spinach chloroplasts. *Biochim. Biophys. Acta* 680, 88–94. doi: 10.1016/0005-2728(82)90319-X

Kurkdjian, A., and Guern, J. (1989). Intracellular pH: measurement and importance in cell activity. *Annu. Rev. Plant Physiol. Plant Mol. Biol.* 40, 271–303. doi: 10.1146/annurev.pp.40.060189.001415

Loiselle, F. B., and Casey, J. R. (2010). Measurement of intracellular pH. *Methods Mol. Biol.* 637, 311–331. doi: 10.1007/978-1-60761-700-6_17

Neuhaus, H. E., and Trentmann, O. (2014). Regulation of transport processes across the tonoplast. *Front. Plant Sci.* 5:460. doi: 10.3389/fpls.2014.00460

Nishio, J. N., and Whitmarsh, J. (1991). Dissipation of the proton electrochemical potential in intact and lysed chloroplasts I. electrical potential. *Plant Physiol.* 95, 522–528. doi: 10.1104/pp.95.2.522

O'Connor, N., and Silver, R. B. (2007). Ratio imaging: practical considerations for measuring intracellular Ca^{2+} and pH in living cells. *Methods Cell Biol.* 81, 415–433. doi: 10.1016/S0091-679X(06)81019-8

Reid, R. A., Moyle, J., and Mitchell, P. (1966). Synthesis of adenosine triphosphate by a protonmotive force in rat liver mitochondria. *Nature* 212, 257–258. doi: 10.1038/212257a0

Robinson, S.P. (1985). The involvement of stromal ATP in maintaining the pH gradient across the chloroplast envelope in the light. *Biochim. Biophys. Acta* 806, 187–194. doi: 10.1016/0005-2728(85)90096-9

Sano, T., Kutsuna, N., and Hasezawa, S. (2010). Improved cytoplasmic pH measurements in SNARF-1 stained plant cells by image processing. *Plant Signal. Behav.* 5, 406–408. doi: 10.4161/psb.5.4.10804

Scott, A. C., and Allen, N. S. (1999). Changes in cytosolic pH within Arabidopsis root columella cells play a key role in the early signaling pathway for root gravitropism. *Plant Physiol.* 121, 1291–1298. doi: 10.1104/pp.121.4.1291

Shen, J., Zeng, Y., Zhuang, X., Sun, L., Yao, X., Pimpl, P., et al. (2013). Organelle pH in the *Arabidopsis* endomembrane system. *Mol. Plant* 6, 1419–1437. doi: 10.1093/mp/sst079

Shingles, R., Roh, M. H., and McCarty, R. E. (1996). Nitrite transport in chloroplast inner envelope vesicles (I. direct measurement of proton-linked transport). *Plant Physiol.* 112, 1375–1381. doi: 10.1104/pp.112.3.1375

Sundaresan, S., Philosoph-Hadas, S., Riov, J., Belausov, E., Kochanek, B., Tucker, M. L., et al. (2015). Abscission of flowers and floral organs is closely associated with alkalization of the cytosol in abscission zone cells. *J. Exp. Bot.* 66, 1355–1368. doi: 10.1093/jxb/eru483

Theg, S. M., and Tom, C. (2011). Measurement of the ΔpH and electric field developed across Arabidopsis thylakoids in the light. *Methods Mol. Biol.* 775, 327–341. doi: 10.1007/978-1-61779-237-3_18

Wu, W., and Berkowitz, G. A. (1992). Stromal pH and photosynthesis are affected by electroneutral K^+ and H^+ exchange through chloroplast envelope ion channels. *Plant Physiol.* 98, 666–672. doi: 10.1104/pp.98.2.666

Yin, Z. H., Neimanis, S., Wagner, U., and Heber, U. (1990). Light-dependent pH changes in leaves of C3 plants I. recording pH changes in various cellular compartments by fluorescent probes. *Planta* 182, 244–252. doi: 10.1007/BF00197118

Conflict of Interest Statement: The authors declare that the research was conducted in the absence of any commercial or financial relationships that could be construed as a potential conflict of interest.

frontiers in Plant Science

PERSPECTIVE
published: 29 June 2017
doi: 10.3389/fpls.2017.01145

FtsH2-Dependent Proteolysis of EXECUTER1 Is Essential in Mediating Singlet Oxygen-Triggered Retrograde Signaling in *Arabidopsis thaliana*

*Vivek Dogra[1], Jianli Duan[1], Keun Pyo Lee[1], Shanshan Lv[2], Renyi Liu[2] and Chanhong Kim[1]**

[1] Laboratory of Photosynthesis and Stress Signaling, Center for Excellence in Molecular Plant Sciences, Shanghai Center for Plant Stress Biology, Chinese Academy of Sciences, Shanghai, China, [2] Shanghai Center for Plant Stress Biology, Chinese Academy of Sciences, Shanghai, China

Photosystem II reaction center (PSII RC) and light-harvesting complex inevitably generate highly reactive singlet oxygen ($^1O_2$) that can impose photo-oxidative damage, especially when the rate of generation exceeds the rate of detoxification. Besides being toxic, $^1O_2$ has also been ascribed to trigger retrograde signaling, which leads to nuclear gene expression changes. Two distinctive molecular components appear to regulate $^1O_2$ signaling: a volatile signaling molecule β-cyclocitral (β-CC) generated upon oxidation of β-carotene by $^1O_2$ in PSII RC assembled in grana core, and a thylakoid membrane-bound FtsH2 metalloprotease that promotes $^1O_2$-triggered signaling through the proteolysis of EXECUTER1 (EX1) proteins associated with PSII in grana margin. The role of FtsH2 protease in $^1O_2$ signaling was established recently in the conditional *fluorescent* (*flu*) mutant of *Arabidopsis thaliana* that generates $^1O_2$ upon dark-to-light shift. The *flu* mutant lacking functional FtsH2 significantly impairs $^1O_2$-triggered and EX1-mediated cell death. In the present study, the role of FtsH2 in the induction of $^1O_2$ signaling was further clarified by analyzing the FtsH2-dependent nuclear gene expression changes in the *flu* mutant. Genome-wide transcriptome analysis showed that the inactivation of FtsH2 repressed the majority (85%) of the EX1-dependent $^1O_2$-responsive genes (SORGs), providing direct connection between FtsH2-mediated EX1 degradation and $^1O_2$-triggered gene expression changes. Furthermore, the overlap between β-CC-induced genes and EX1-FtsH2-dependent genes was very limited, further supporting the coexistence of two distinctive $^1O_2$ signaling pathways.

Keywords: $^1O_2$, retrograde signaling, EXECUTER 1, FtsH2 protease, β-carotene, β-cyclocitral, chloroplast

OPEN ACCESS

Edited by:
Fei Yu,
Northwest A&F University, China

Reviewed by:
John Froehlich,
Michigan State University, United States
Aigen Fu,
Northwest University, United States

****Correspondence:***
Chanhong Kim
chanhongkim@sibs.ac.cn

Specialty section:
This article was submitted to Plant Cell Biology, a section of the journal Frontiers in Plant Science

Received: *13 February 2017*
Accepted: *15 June 2017*
Published: *29 June 2017*

Citation:
Dogra V, Duan J, Lee KP, Lv S, Liu R and Kim C (2017) FtsH2-Dependent Proteolysis of EXECUTER1 Is Essential in Mediating Singlet Oxygen-Triggered Retrograde Signaling in Arabidopsis thaliana. Front. Plant Sci. 8:1145. doi: 10.3389/fpls.2017.01145

BACKGROUND

Under a multitude of environmental factors, altered levels of reactive oxygen species (ROS) in chloroplasts, which have long been implicated with damaging of macromolecules, appear to trigger certain signaling cascades leading to nuclear gene expression changes via a process known as retrograde signaling (Apel and Hirt, 2004). The transcriptional reprogramming seems to be essential for plants to sustain and adapt to the environmental changes. Among various ROS,

chloroplasts generate $^1O_2$ during oxygenic photosynthesis at the active PSII RC residing in the grana core (appressed grana region) of the thylakoids (Triantaphylidès et al., 2008). In order to minimize the photo-oxidative damage caused by $^1O_2$, plants utilize molecular components residing in PSII RC, such as β-carotene and D1 protein, to quench $^1O_2$ (Triantaphylidès et al., 2008). Oxidation of D1 protein leads to PSII damage, which subsequently undergoes disassembly and reassembly processes through the proteolysis of the damaged D1 proteins by ATP-dependent hexameric FtsH metalloprotease and the concurrent *de novo* synthesis of D1 proteins, respectively (Kato and Sakamoto, 2009; Kato et al., 2012).

$^1O_2$ has also been reported to trigger chloroplast-to-nucleus retrograde signaling, which is manifested by altered nuclear gene expression, acclimation response and programmed cell death (PCD) (op den Camp et al., 2003; Wagner et al., 2004; Lee et al., 2007; Kim et al., 2008, 2012; Ramel et al., 2012, 2013; Wang et al., 2016). Because $^1O_2$ has an extremely short lifespan (∼200 ns) in a cellular environment (Li et al., 2012; Telfer, 2014), it is unlikely to serve as a signaling molecule. Therefore, chloroplasts may contain $^1O_2$ sensor(s) to translate the levels of $^1O_2$, either by self-oxidation or by monitoring the oxidation of other molecule(s), to subsequent changes in cellular processes. As $^1O_2$ is generated in PSII, it is reasonable to assume that $^1O_2$ sensor might be physically associated with PSII. Accordingly, the PSII components, such as D1 protein and β-carotene have long been supposed to act as primary scavengers of $^1O_2$ (Triantaphylidès and Havaux, 2009). Even though the degradation product of D1 has been shown to control the synthesis of D1 in cyanobacteria (Stelljes and Koenig, 2007), there is no evidence to support that the degradation product of D1 acts as a signaling molecule in plants.

In contrast, strong evidence has been found to support that β-carotene, a primary quencher of $^1O_2$ and a constituent of PSII RC, is a $^1O_2$ sensor. β-cyclocitral (β-CC), a volatile oxidized derivatives of β-carotene, has been found to act as a signaling molecule in Arabidopsis wild-type plants exposed to excess light stress (Ramel et al., 2013). Moreover, plants treated with β-CC upregulate a set of $^1O_2$-responsive genes (SORGs) (Ramel et al., 2012) identified previously using conditional Arabidopsis *flu* mutant generating $^1O_2$ upon dark-to-light shift (op den Camp et al., 2003). In addition, β-CC has also been implicated with the acclimation responses in *chlorina 1* (*ch1*) mutant lacking light-harvesting complex (LHC) of PSII, in which the level of $^1O_2$ under light stress was escalated (Ramel et al., 2013). Although the volatile can diffuse freely into the nucleus, the molecular mechanism underlying the β-CC-mediated transcriptional reprogramming is largely unknown. Nonetheless, the earlier genetic screen using the unicellular green alga *Chlamydomonas reinhardtii* uncovered Methylene Blue Sensitivity 1 (MBS1), a small Zinc finger protein, as a mediator of $^1O_2$ signaling (Shao et al., 2013). While the MBS1 protein is present in both cytosol and nucleus under normal conditions, it concentrates in specific stress granules and processing bodies under oxidative stress (Shao et al., 2013). A recent study revealed that MBS1 was upregulated in wild-type Arabidopsis plants under β-CC treatment even in normal light conditions, which led to gene expression changes for photo-acclimation (Shumbe et al., 2017). However, a further study is needed to show whether MBS1 can directly bind to DNA or requires other mediators to alter the nuclear gene expression.

Another distinct $^1O_2$ signaling has been identified earlier in Arabidopsis *flu* mutant (op den Camp et al., 2003). In the dark, FLU protein acts as a negative feedback regulator of tetrapyrrole synthesis in Mg^{2+}-branch. As the reduction of protochlorophyllide (Pchlide) to chlorophyllide is catalyzed by light-dependent enzyme protochlorophyllide oxidoreductase (POR), the *flu* mutant overaccumulates Pchlide in the dark. As a potent photosensitizer, the accumulated Pchlide upon illumination absorbs light energy and subsequently transfers the absorbed light energy to stable molecular oxygen, resulting in the formation of highly reactive $^1O_2$ in chloroplasts (Meskauskiene et al., 2001). The *flu* mutant, therefore, offers a conditional system that allows generating $^1O_2$ in a controlled and non-invasive manner (op den Camp et al., 2003). Various studies using the *flu* mutant revealed that the chloroplast-generated $^1O_2$ can induce the nuclear gene expression changes and PCD (op den Camp et al., 2003; Lee et al., 2007). The previous genetic screen using *flu* mutant has revealed that nuclear-encoded and chloroplast-targeted protein EX1 mediates the $^1O_2$-triggered stress responses (Wagner et al., 2004). Inactivation of EX1 significantly abolishes the $^1O_2$-induced cell death and nuclear gene expression changes in *flu* mutant (Wagner et al., 2004; Lee et al., 2007). Besides EX1, its close homolog EXECUTER2 (EX2) has also been implicated with mediating $^1O_2$ signaling. While inactivation of EX1 significantly attenuates the SORGs, inactivation of both EX1 and EX2 leads to almost complete repression of SORGs (Lee et al., 2007). In addition, EX1 and EX2 also appear to regulate the local and systemic gene expression changes in response to high light stress (Carmody et al., 2016).

Initially, it was contemplated that the two signaling cascades might be dependent on each other. However, in *ch1* mutant the β-CC was found to relay the signal under photoinhibitory conditions in an EX1-independent manner (Ramel et al., 2012), implying that the two signaling cascades might be independent. Considering that both signaling events are instigated from PSII, it is obscure how these two signaling events are triggered independently. This seeming paradox was resolved in our recent study in which EX1 proteins were found mainly in 'grana margin' where the repair of PSII and the chlorophyll synthesis happen, implying that EX1-mediated $^1O_2$ signaling is initiated in grana margin rather than the grana core (Wang et al., 2016). The study has also shown that light-adapted *flu* plants accumulated Pchlide in the dark almost evenly in different fractions across the thylakoid membrane, such as grana core, grana margin, and stroma lamellae (Wang et al., 2016). Given that *ex1/flu* abrogates the $^1O_2$-triggered stress responses including growth inhibition and cell death, $^1O_2$ generated in either grana core or stroma lamellae may not irreversibly damage the photosynthetic apparatus.

Protein immunoprecipitation (IP) coupled with mass spectrometry (MS) unveiled a group of proteins potentially forming the EXECUTER complex in grana margin, including enzymes involved in chlorophyll biosynthesis, PSII RC proteins

and FtsH proteases (Wang et al., 2016). Because EX1 is associated with PSII and FtsH protease, upon $^1O_2$ generation, EX1 possibly undergoes similar oxidative post-translational modification as PSII RC proteins including D1 and CP43 (Dreaden et al., 2012). If the oxidation occurs in EX1, the modified EX1 by $^1O_2$ may become a target of FtsH protease, which is shown to be the case of D1 (Kato and Sakamoto, 2009). This proteolysis of EX1 may lead to the release of a signal that might be a part of EX1 complex or EX1 itself. Indeed, FtsH2-dependent proteolysis of EX1 in response to $^1O_2$ and the concurrent induction of cell death are shown to be attenuated in the FtsH2-defecient *flu* mutant, namely *var2*/*flu*, implying that the proteolysis of EX1 is crucial for initiating the retrograde signaling (Wang et al., 2016). To investigate the underlying molecular mechanisms, we examined the effect of EX1 proteolysis on the induction of SORGs in *flu* mutant.

EXPERIMENTAL RESULTS

Identification of a True Set of SORGs

In earlier studies, the SORGs identified in *flu* mutant (Danon et al., 2006; Laloi et al., 2007; Lee et al., 2007) were employed to address the probable activation of $^1O_2$ signaling in various mutants and wild-type plants under photooxidative stress conditions (e.g., Ramel et al., 2013). Afterward, the detection of the rapid loss of chloroplast integrity following $^1O_2$ burst, as evidenced by the appearance of stroma proteins into cytosol (Kim et al., 2012; Chen et al., 2015), prompted us to redefine SORGs as a group of genes that were upregulated prior to the loss of chloroplast integrity (Chen et al., 2015) (399 genes; Supplementary Table S1). In addition, in all of those previous transcriptome data, the confounding effect of dark on the gene expression changes was not excluded. Hence, in the present study, we carried out RNA-seq-based gene expression analysis in 5-day-old seedlings of *flu* and FtsH2-deficient *var2*/*flu*, initially grown under continuous light (LL), and then subjected to 4 hours dark (4hD) followed by re-illumination for 30 (L'30) and 60 min (L'60). Samples harvested at the end of dark were included as additional control to exclude genes upregulated in the dark. As a result, we found that a large proportion (215 genes, 53%) of previously identified SORGs (399) appeared to be upregulated in the dark followed by a gradual repression during re-illumination (**Figure 1A**). These genes were reclassified as dark-induced genes (DIGs) and were excluded from the SORGs, together with 26 more genes that were either not expressed or significantly changed in the expression. The remaining 168 SORGs were thus considered as early $^1O_2$-responsive genes (hereafter ESORGs) (**Figure 1A** and Supplementary Table S2). The 168 ESORGs include *SIGMA FACTOR BINDING PROTEIN 1* (*SIB1*), *WRKY33* (*WRKY DNA-BINDING PROTEIN 33*), *WRKY40* (*WRKY DNA-BINDING PROTEIN 40*), *ETHYLENE RESPONSE FACTOR 104* (*ERF104*), *MAP KINASE KINASE 9* (*MKK9*), *SENESCENCE ASSOCIATED GENE 20* (*SAG20*), *TOLL/INTERLEUKIN-1 RECEPTOR-LIKE* (*TIR*) and many other stress-responsive genes (**Figure 1A** and Supplementary Table S2). This set of true ESORGs was used for further comparative analysis between *flu* and *var2*/*flu*.

FtsH2 Is Essential for the Induction of ESORGs

The comparison of transcriptome profiles of *flu* and *var2*/*flu* revealed that approximately 85% of ESORGs (142 out of 168 genes) were repressed in *var2*/*flu* as compared to *flu* (**Figures 1B,C** and Supplementary Table S3). In an earlier study, only three SORGs, namely *SIB1*, *WRKY33* and *WRKY40*, were shown to be upregulated not only in wild-type seedlings under photoinhibitory condition (Chen et al., 2015) but also in *flu* mutant upon dark-to-light shift in EX1/EX2-dependent manner. Hence, these genes were considered as $^1O_2$-specific and EX1/EX2-dependent genes (**Figure 1D**). The RNA-seq result was further validated by quantitative real time PCR (qRT-PCR) using these genes (**Figure 1E**). In consistent with the phenotype of *var2*/*flu* seedlings, which appear to be more tolerant to $^1O_2$ as compared to *flu* mutant seedlings (Wang et al., 2016), the global gene expression levels were less responsive to $^1O_2$ in *var2*/*flu* seedlings than in *flu* seedlings. The repressed expression of ESORGs following re-illumination and the concurrent attenuation of stress responses suggest that FtsH2 is a positive regulator of EX1-mediated $^1O_2$ signaling in *flu* mutant.

Comparative Analysis of β-CC-Induced and EX1-FtsH2-Dependent SORGs

Previous studies have established the role of β-CC in $^1O_2$-triggered acclimation responses (Ramel et al., 2012, 2013), whereas the EX1-mediated $^1O_2$ signaling has been mainly attributed to PCD in young seedlings and growth inhibition in mature plants (Wagner et al., 2004; Kim et al., 2012). In a very recent study, however, the role of EX1 and EX2 in an acclimation response to high light-induced transcriptional reprogramming has also been demonstrated (Carmody et al., 2016). To get insight into these distinctive cascades, we compared the β-CC-induced SORGs and EX1-FtsH2-dependent ESORGs, with the aim to explain the common and distinct molecular characteristics and enlighten their coexistence. Plants treated with β-CC for 4 h under normal light conditions exhibited a rapid reprogramming of nuclear gene expression, resulting in the altered expression of around 380 genes with at least twofold up- or down-regulation (Ramel et al., 2012). Among these 380 genes, the upregulated genes (292) are considered as β-CC-induced SORGs (Supplementary Table S4). Comparative analysis revealed that β-CC-induced (292) and EX1-FtsH2-dependent (142) genes shared only a small number of genes (20) (**Figure 2**). The shared genes include above-mentioned $^1O_2$-responsive genes, such as *WRKY33*, *WRKY40,* and *SIB1*. However, the expressions of these genes were comparatively higher in *flu* mutant (Supplementary Table S5). Taken together, these results further support the coexistence of the two independent $^1O_2$-signalings in Arabidopsis. Considering that $^1O_2$-specific and EX1/EX2-dependent genes including *WRKY33*, *WRKY40* and *SIB1*, appear to be upregulated in response to β-CC, we cannot

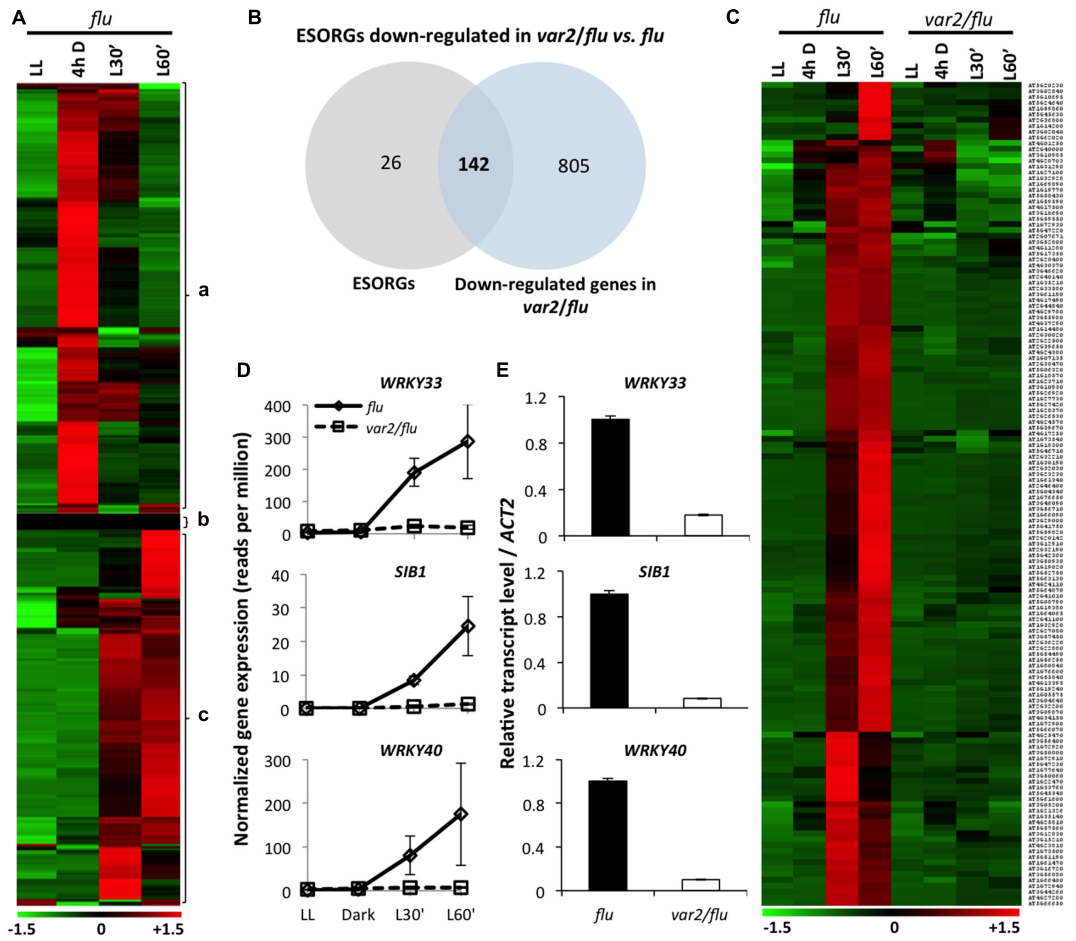

FIGURE 1 | FtsH2 is an integral component of EX1-mediated $^1O_2$ signaling. RNA- seq-based comparison of gene expression was performed in 5-day-old *var2/flu* and *flu* seedlings that were initially grown under continuous light (LL), transferred to dark for 4 hours (4 h D), and then re-exposed to light for 30 (L30′) and 60 min (L60′). **(A)** Heat map reclassified the expression of previously reported SORGs. After excluding 215 genes induced during dark incubation (a) and 26 genes that either exhibited no expression or were not expressed differentially (b), 168 true ESORGs (c) were identified. **(B,C)** *Venn diagram* and heat map revealed that the majority (142 genes; 85%) of ESORGs were downregulated in *var2/flu* in comparison to *flu* upon dark-to-light shift. **(D)** Expression of $^1O_2$-specific and EX1/EX2-dependent genes *SIB1*, *WRKY33* and *WRKY40* in *var2/flu* and *flu*. The average values and standard error of the normalized gene expression (reads per million; rpm) of three independent biological samples obtained by RNA-seq analysis were shown. **(E)** Validation of RNA-seq using those selected genes **(D)** by qRT-PCR. Results represent means of three independent biological replicates. *Actin2* was used as a control for normalization.

rule out the possibility that these two signaling cascades may share a certain downstream component to regulate those shared genes.

SUMMARY AND FUTURE DIRECTIONS

In summary, our previous study revealed the important role of ATP-dependent FtsH metalloprotease, assembled in thylakoid membrane and functioning in PSII repair cycle, in the induction of EX1-mediated stress response upon $^1O_2$ generation in chloroplast. The FtsH protease is co-localized with EX1 in grana margin where the PSII repair process undergoes, and it coordinates the retrograde signaling by promoting the proteolytic degradation of EX1 proteins through a yet unknown mechanism (**Figure 2**). FtsH-dependent EX1 degradation was found to occur upon $^1O_2$ burst in chloroplast, which possibly triggers the signaling. In agreement, inactivation of FtsH2, a subunit of the FtsH protease complex, appears to considerably compromise the proteolysis of EX1 and the concurrent $^1O_2$-triggered PCD in Arabidopsis *flu* mutant. Furthermore, the loss of FtsH2 in *flu* resulted in the repression of the majority of SORGs. β-CC-induced and EX1-FtsH2-dependent SORGs are largely distinct, sharing relatively a very small portion of genes. These results provide compelling evidence that chloroplasts may operate two distinctive $^1O_2$ signaling: one operated in grana core by β-carotene and one in grana margin by the coordination of EX1 and FtsH2 (**Figure 2**). Based on this foundation, further investigation on EX1-FtsH2-dependent signaling is needed in order answer questions such as (i) what is the source of $^1O_2$ in the grana margin? (ii) how EX1 senses and mediates this signaling in coordination with FtsH2? (iii) what is the genuine signaling

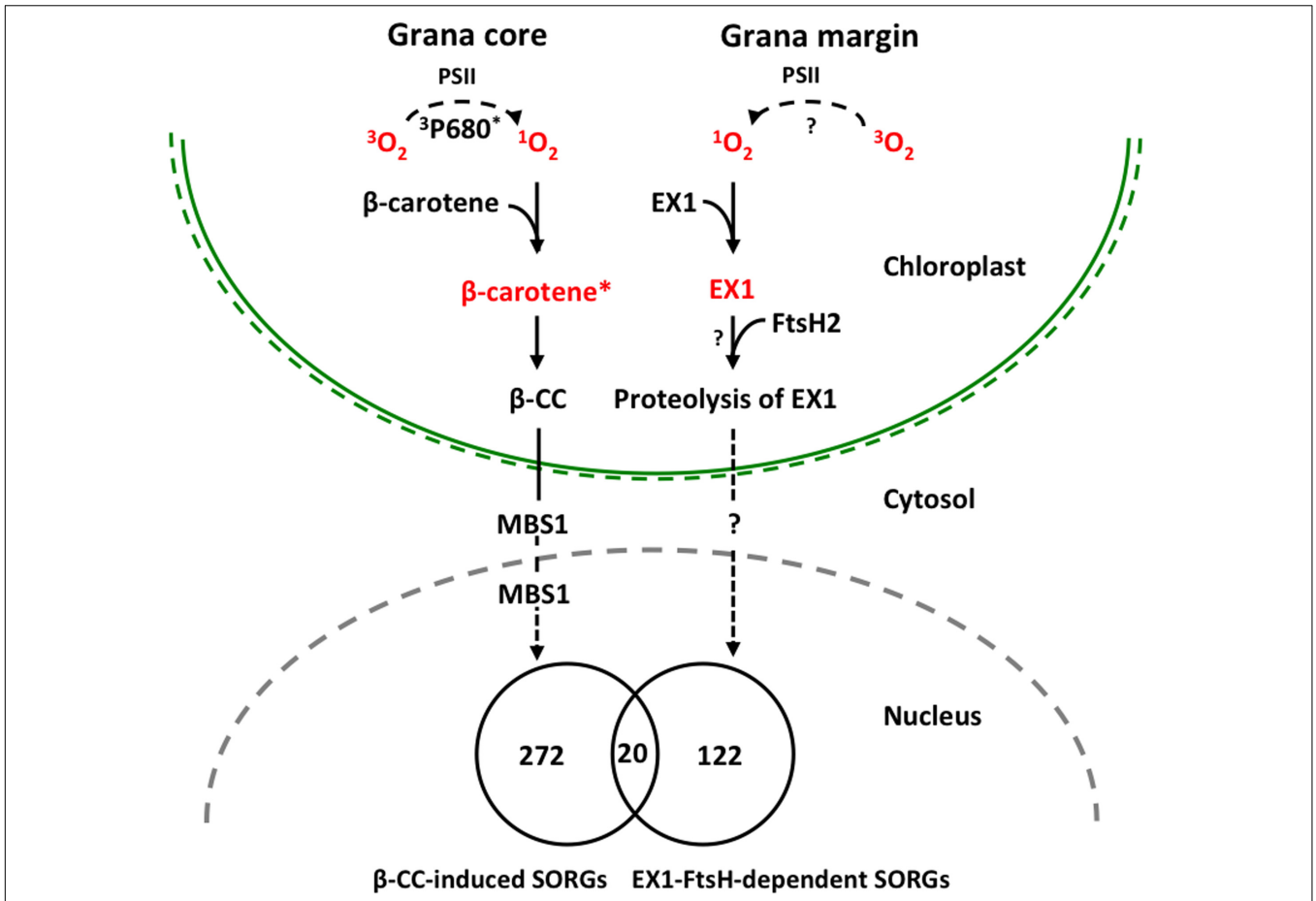

FIGURE 2 | Proposed model illustrating $^1O_2$-triggered EX1-independent and EX1-dependent chloroplast-to-nucleus retrograde signaling pathways. Under severe light stress, β-carotene from PSII RC enriched in grana core acts as a sensor of $^1O_2$ generated by the excited triplet P680 chlorophyll (^{3}P680*) through the energy transfer from ^{3}P680* to stable oxygen molecule (^{3}O2). The subsequent oxidation of β-carotene (β-carotene*) by $^1O_2$ concomitantly release β-CC, a volatile oxidized derivative, which functions as a messenger involved in the $^1O_2$ signaling pathway. MBS1 protein, a zinc finger protein located in cytoplasm and nucleus, acts downstream of β-CC. In grana margin, EX1 may sense $^1O_2$ generated through an as yet unknown process and initiates $^1O_2$ signaling in an FtsH2-dependent manner. FtsH2-dependent proteolysis of EX1 appears to be essential in the induction of nuclear gene expression changes. β-CC-induced and EX1-FtsH2-dependent SORGs are reasonably distinct as evidenced that these transcriptomes share relatively a very small portion of genes, signifying the coexistence of these two $^1O_2$ signaling cascades in plants.

molecule that is generated upon EX1 proteolysis? (**Figure 2**). Furthermore, the reasons for the coexistence of two distinctive $^1O_2$-triggered retrograde signaling pathways in plants are still unknown, which probably opens new perspectives of research in this direction.

MATERIALS AND METHODS

Plant Materials, Growth Conditions, and RNA Isolation

Seedlings of *flu* and *var2*/*flu* mutant lines (Wang et al., 2016), all in the Columbia-0 (Col-0) background, were grown under continuous light (40 μmol photons m^{-2} s^{-1}) at 20 ± 1°C on 0.6% agar plates containing ½ MS medium and 1xGamborg vitamins. Total RNA was isolated using RNA easy Plant mini kit (Qiagen, Germany). DNase I (Qiagen, Germany) treatment was performed to remove potential DNA contamination. RNA was examined by a Nano Photometer spectrophotometer (Implen, Westlake Village, CA, United States) for RNA purity. Qubit RNA Assay Kit in Qubit 2.0 Flurometer (Life Technologies, Foster City, CA, United States) was used to measure RNA concentration, and RNA Nano 6000 Assay Kit of the Bioanalyzer 2100 system (Agilent Technologies, Santa Clara, CA, United States) was used to evaluate RNA integrity. Only RNA samples that passed the quality control were used for RNA-Seq analyses. Three biological replicates were subject to RNA-Seq based gene expression analysis for each genotype/treatment.

RNA-seq Library Construction, Sequencing, and Analysis

RNA-seq libraries were constructed using the NEBNext Ultra Directional RNA Library Prep Kit for Illumina (NEB, Ipswich,

MA, United States) following manufacturer's instructions. RNA-seq libraries were sequenced on an Illumina HiSeq 2500 platform to generate 100 bp paired-end reads as described previously (Zhao et al., 2016). Lowly expressed genes were removed and genes with an expression level of at least 1 transcripts per million (TPM) in at least three samples were selected for differential expression analysis. The R package edgeR, which uses counts per gene in different samples from HTSeq-count as input and performs data normalization using the trimmed mean of M-values (TMM) method, was used to identify differentially expressed genes (DEGs). The genes with at least twofold change in expression and the false discovery rate (FDR) of less than 0.05 were considered to be differentially expressed. Gene expression levels were normalized to TPM according to the total number of mapped clean reads in each of library. The log2 values of normalized expression levels were used to build expression matrix and subsequent clustering and visualization was conducted using Multi-Experiment Viewer (MeV 4.9.0).

qRT-PCR Analysis

Quantitative real time PCR assays were performed with samples that were collected independently of samples used for RNA-Seq analysis. Three biological replicates were used for each genotype/treatment. RNAs were treated with RQ1 RNase-Free DNase (Promega) and reverse-transcribed using Improm II reverse transcriptase (Promega) and oligo(dT)15 primer (Promega) according to the manufacturer's recommendations. The qRT-PCR was performed by using the QuantStudio^{TM} 6 Flex Real-Time PCR System (Applied Biosystems) and iTaq Universal SYBR Green PCR master mix (Bio-Rad). Relative transcript levels were calculated by the comparative delta-Ct method and normalized to the *ACT2* (At3g18780) gene transcript level. The primers used in this study were designed by Primer Express Software for Real-time PCR, Version 3.0 (Applied Biosystems) and the primer sequences are included in Supplementary Table S6.

AUTHOR CONTRIBUTIONS

VD, KL, JD, and CK planned and designed the research; VD, JD, and KL performed research; SL and VD analyzed RNA-seq data; and VD, RL, and CK wrote the paper.

ACKNOWLEDGMENTS

We acknowledge the Core Facility of Genomics, Shanghai Center for Plant Stress Biology (PSC) for carrying out RNA sequencing. This research was supported by the 100-Talents Program from the Chinese Academy of Sciences (CAS) to CK and RL and by National Natural Science Foundation of China (NSFC) Grant 31570264 to CK.

SUPPLEMENTARY MATERIAL

The Supplementary Material for this article can be found online at: http://journal.frontiersin.org/article/10.3389/fpls.2017.01145/full#supplementary-material

REFERENCES

Apel, K., and Hirt, H. (2004). Reactive oxygen species: metabolism, oxidative stress, and signal transduction. *Annu. Rev. Plant Biol.* 55, 373–399.

Carmody, M., Crisp, P. A., D'Alessandro, S., Ganguly, D., Gordon, M., Havaux, M., et al. (2016). Uncoupling high light responses from singlet oxygen retrograde signaling and spatial-temporal systemic acquired acclimation in Arabidopsis. *Plant Physiol.* 171, 1734–1749.

Chen, S., Kim, C., Lee, J. M., Lee, H. A., Fei, Z., Wang, L., et al. (2015). Blocking the QB-binding site of photosystem II by tenuazonic acid, a non-host-specific toxin of *Alternaria alternata*, activates singlet oxygen-mediated and EXECUTER-dependent signalling in *Arabidopsis*. *Plant Cell Environ.* 38, 1069–1080. doi: 10.1111/pce.12462

Danon, A., Coll, N. S., and Apel, K. (2006). Cryptochrome-1-dependent execution of programmed cell death induced by singlet oxygen in *Arabidopsis thaliana*. *Proc. Natl. Acad. Sci. U.S.A.* 103, 17036–17041.

Dreaden, K. T. M., Rexroth, S., and Barry, B. A. (2012). Light-Induced oxidative stress, *N*-formylkynurenine, and oxygenic photosynthesis. *PLoS ONE* 7:e42220. doi: 10.1371/journal.pone.0042220

Kato, Y., and Sakamoto, W. (2009). Protein quality control in chloroplasts: a current model of D1 protein degradation in the photosystem II repair cycle. *J. Biochem.* 146, 463–469. doi: 10.1093/jb/mvp073

Kato, Y., Sun, X., Zhang, L., and Sakamoto, W. (2012). Cooperative D1 degradation in the photosystem II repair mediated by chloroplastic proteases in Arabidopsis. *Plant Physiol.* 159, 1428–1439. doi: 10.1104/pp.112.199042

Kim, C., Meskauskiene, R., Apel, K., and Laloi, C. (2008). No single way to understand singlet oxygen signalling in plants. *EMBO Rep.* 9, 435–439. doi: 10.1038/embor.2008.57

Kim, C., Meskauskiene, R., Zhang, S., Lee, K. P., Ashok, M. L., Blajecka, K., et al. (2012). Chloroplasts of *Arabidopsis* are the source and a primary target of a plant-specific programmed cell death signaling pathway. *Plant Cell* 24, 3026–3039. doi: 10.1105/tpc.112.100479

Laloi, C., Stachowiak, M., Pers-Kamczyc, E., Warzych, E., Murgia, I., and Apel, K. (2007). Cross-talk between singlet oxygen- and hydrogen peroxide-dependent signaling of stress responses in *Arabidopsis thaliana*. *Proc. Natl. Acad. Sci. U.S.A.* 104, 672–677.

Lee, K. P., Kim, C., Landgraf, F., and Apel, K. (2007). EXECUTER1- and EXECUTER2-dependent transfer of stress-related signals from the plastid to the nucleus of *Arabidopsis thaliana*. *Proc. Natl. Acad. Sci. U.S.A.* 104, 10270–10275.

Li, H., Melo, T. B., Arellano, J. B., and Naqvi, K. R. (2012). Temporal profile of the singlet oxygen emission endogenously produced by photosystem II reaction centre in an aqueous buffer. *Photosynth. Res.* 112, 75–79. doi: 10.1007/s11120-012-9739-4

Meskauskiene, R., Nater, M., Goslings, D., Kessler, F., op den Camp, R., and Apel, K. (2001). FLU: a negative regulator of chlorophyll biosynthesis in *Arabidopsis thaliana*. *Proc. Natl. Acad. Sci. U.S.A.* 98, 12826–12831.

op den Camp, R., Przybyla, D., Ochsenbein, C., Laloi, C., Kim, C., Danon, A., et al. (2003). Rapid induction of distinct stress responses after the release of singlet oxygen in *Arabidopsis*. *Plant Cell* 15, 2320–2332.

Ramel, F., Birtic, S., Ginies, C., Soubgou-Taconnat, L., Triantaphylidès, C., and Havaux, M. (2012). Carotenoid oxidation products are stress signals that mediate gene responses to singlet oxygen in plants. *Proc. Natl. Acad. Sci. U.S.A.* 109, 5535–5540. doi: 10.1073/pnas.1115982109

Ramel, F., Ksas, B., Akkari, E., Mialoundama, A. S., Monnet, F., Krieger-Liszkay, A., et al. (2013). Light-induced acclimation of the *Arabidopsis chlorina1* mutant to singlet oxygen. *Plant Cell* 25, 1445–1462. doi: 10.1105/tpc.113.109827

Shao, N., Duan, G. Y., and Bock, R. (2013). A mediator of singlet oxygen responses in *Chlamydomonas reinhardtii* and *Arabidopsis* identified by a luciferase-based genetic screen in algal cells. *Plant Cell* 25, 4209–4226. doi: 10.1105/tpc.113.117390

Shumbe, L., D'Alessandro, S., Shao, N., Chevalier, A., Ksas, B., Bock, R., et al. (2017). METHYLENE BLUE SENSITIVITY 1 (MBS1) is required for acclimation of Arabidopsis to singlet oxygen and acts downstream of β-cyclocitral. *Plant Cell Environ.* 42, 216–226. doi: 10.1111/pce.12856

Stelljes, C., and Koenig, F. (2007). Specific binding of D1 protein degradation products to the *psbAI* promoter in *Synechococcus* sp. strain PCC 7942. *J. Bacteriol.* 189, 1722–1726.

Telfer, A. (2014). Singlet oxygen production by PSII under light stress: mechanism, detection and the protective role of β-carotene. *Plant Cell Physiol.* 55, 1216–1223. doi: 10.1093/pcp/pcu040

Triantaphylidès, C., and Havaux, M. (2009). Singlet oxygen in plants: production, detoxification and signaling. *Trends Plant. Sci.* 14, 219–228. doi: 10.1016/j.tplants.2009.01.008

Triantaphylidès, C., Krischke, M., Hoeberichts, F. A., Ksas, B., Gresser, G., Havaux, M., et al. (2008). Singlet oxygen is the major reactive oxygen species involved in photooxidative damage to plants. *Plant Physiol.* 148, 960–968. doi: 10.1104/pp.108.125690

Wagner, D., Przybyla, D., op den Camp, R., Kim, C., Landgraf, F., Lee, K. P., et al. (2004). The genetic basis of singlet oxygen-induced stress responses of *Arabidopsis thaliana*. *Science* 306, 1183–1185.

Wang, L., Kim, C., Xu, X., Piskeuwicz, U., Dogra, V., Singh, S., et al. (2016). $^1O_2$- and EXECUTER1-mediated signaling is initiated in grana margins and depends on FtsH2 protease. *Proc. Natl. Acad. Sci. U.S.A.* 113, E3792–E3800. doi: 10.1073/pnas.1603562113

Zhao, J., Li, Y., Ding, L., Yan, S., Liu, M., Jiang, L., et al. (2016). Phloem transcriptome signatures underpin the physiological differentiation of the pedicel, stalk and fruit of cucumber (*Cucumis sativus* L.). *Plant Cell Physiol.* 57, 19–34. doi: 10.1093/pcp/pcv168

Conflict of Interest Statement: The authors declare that the research was conducted in the absence of any commercial or financial relationships that could be construed as a potential conflict of interest.

frontiers in Plant Science

PERSPECTIVE
published: 20 November 2017
doi: 10.3389/fpls.2017.01991

Specific Distribution of Phosphatidylglycerol to Photosystem Complexes in the Thylakoid Membrane

Koichi Kobayashi, Kaichiro Endo and Hajime Wada*

Department of Life Sciences, Graduate School of Arts and Sciences, The University of Tokyo, Tokyo, Japan

The thylakoid membrane is the site of photochemical and electron transport reactions of oxygenic photosynthesis. The lipid composition of the thylakoid membrane, with two galactolipids, one sulfolipid, and one phospholipid, is highly conserved among oxygenic photosynthetic organisms. Besides providing a lipid bilayer matrix, thylakoid lipids are integrated in photosynthetic complexes particularly in photosystems I and II and play important roles in electron transport processes. Thylakoid lipids are differentially allocated to photosynthetic complexes and the lipid bilayer fraction, but distribution of each lipid in the thylakoid membrane is unclear. In this study, based on published crystallographic and biochemical data, we estimated the proportions of photosynthetic complex-associated and bilayer-associated lipids in thylakoid membranes of cyanobacteria and plants. The data suggest that ∼30 mol% of phosphatidylglycerol (PG), the only major phospholipid in thylakoid membranes, is allocated to photosystem complexes, whereas glycolipids are mostly distributed to the lipid bilayer fraction and constitute the membrane lipid matrix. Because PG is essential for the structure and function of both photosystems, PG buried in these complexes might have been selectively conserved among oxygenic phototrophs. The specific and substantial allocation of PG to the deep sites of photosystems may need a unique mechanism to incorporate PG into the complexes possibly in coordination with the synthesis of photosynthetic proteins and pigments.

Keywords: thylakoid membrane, monogalactosyldiacylglycerol, digalactosyldiacylglycerol, sulfoquinovosyldiacylglycerol, phosphatidylglycerol, lipid bilayer, photosystem I, photosystem II

OPEN ACCESS

Edited by:
Rebecca L. Roston, University of Nebraska–Lincoln, United States

Reviewed by:
Conrad Mullineaux, Queen Mary University of London, United Kingdom
Julian Eaton-Rye, University of Otago, New Zealand

****Correspondence:***
Koichi Kobayashi
kkobayashi@bio.c.u-tokyo.ac.jp

Specialty section:
This article was submitted to Plant Cell Biology, a section of the journal Frontiers in Plant Science

Received: *27 September 2017*
Accepted: *06 November 2017*
Published: *20 November 2017*

Citation:
Kobayashi K, Endo K and Wada H (2017) Specific Distribution of Phosphatidylglycerol to Photosystem Complexes in the Thylakoid Membrane. Front. Plant Sci. 8:1991. doi: 10.3389/fpls.2017.01991

INTRODUCTION

The thylakoid membrane is the site of photochemical and electron transport reactions in oxygenic phototrophs. In thylakoid membranes, glycerolipids form a bilayer matrix, in which photosynthetic protein–cofactor complexes such as photosystem I (PSI), photosystem II (PSII), cytochrome (Cyt) b_6/f complex and ATP synthase are embedded. The hydrophobic lipid bilayer prevents free diffusion of ions and allows for creating a proton gradient while enabling lateral diffusion of the photosynthetic complexes and the mobile electron carriers for efficient electron transport reactions.

The lipid composition of the thylakoid membrane is highly conserved among oxygenic phototrophs (Murata et al., 1981; Mendiola-Morgenthaler et al., 1985; Dorne et al., 1990).

Galactolipids, monogalactosyldiacylglycerol (MGDG) and digalactosyldiacylglycerol (DGDG), account for ∼50 and ∼30 mol% of total thylakoid lipids, respectively. Thylakoids contain another unique glycolipid, sulfoquinovosyldiacylglycerol (SQDG), which constitutes ∼10% of the total lipids. The remaining ∼10% is phosphatidylglycerol (PG), the only major phospholipid in thylakoids.

Each lipid class has a different physicochemical property depending on the nature of its head group. MGDG and DGDG are neutral lipids with uncharged polar head groups. MGDG has a cone-like shape with a small galactose head group and flexible poly-unsaturated fatty acid tails and thus tends to form a non-bilayer lipid phase in mixture with water (Shipley et al., 1973; Jouhet, 2013). By contrast, DGDG has a more bulky head group with two galactoses, which gives DGDG a cylindrical shape and allows for forming a bilayer lamellar phase. The MGDG/DGDG ratio strongly affects the phase behavior of the lipid bilayer and may be important for the structure and stability of the thylakoid membrane (Murphy, 1982; Demé et al., 2014). SQDG and PG, which are both bilayer lipids, have negative charge at neutral pH and are classified as acidic lipids. PG and SQDG are in part functionally redundant in both cyanobacteria and plant chloroplasts, as we describe later, presumably because of their common acidic properties in polar head groups.

Besides providing a lipid bilayer matrix, thylakoid lipids are integrated in PSII (Loll et al., 2005, 2007; Sakurai et al., 2006; Umena et al., 2011; Wei et al., 2016), Cyt b_6/f (Kurisu et al., 2003; Stroebel et al., 2003; Baniulis et al., 2009; Hasan et al., 2011), PSI (Jordan et al., 2001; Kubota et al., 2010; Qin et al., 2015; Mazor et al., 2017), and light-harvesting complexes (LHCs) (Liu et al., 2004; Standfuss et al., 2005; Wei et al., 2016) and play important roles in electron transport processes (Kobayashi et al., 2016b). Because these photosynthetic complexes account for large quantities of the thylakoid membrane, substantial amounts of lipids would be allocated to the complexes as structural components. Based on published crystallographic and biochemical data, we estimated the amount of photosynthetic complex-associated lipids and lipid composition in the thylakoid lipid bilayer. The results indicated a preferential distribution of PG to photosystems and a minor contribution to the thylakoid lipid bilayer in plant chloroplasts and cyanobacteria.

DISTRIBUTION OF LIPIDS IN THE THYLAKOID MEMBRANE IN CYANOBACTERIA

Jordan et al. (2001) first revealed the crystal structure of PSI from *Thermosynechococcus elongatus* at 2.5-Å resolution. In the PSI trimer, 1 MGDG and 3 PG molecules per monomer were identified. The same lipid configuration was observed in the PSI crystal structure of *Synechocystis* sp. PCC 6803 (Mazor et al., 2014). Meanwhile, crystallographic analysis of the PSII dimer from *Thermosynechococcus vulcanus*, the species closely related to *T. elongatus*, at 1.9-Å resolution identified 20 lipid molecules (6 MGDGs, 5 DGDGs, 4 SQDGs, and 5 PGs) and 3 unknown diglycerides per monomer (Umena et al., 2011). A similar lipid composition was revealed by lipid analysis of PSII dimers purified from *T. vulcanus* and *Synechocystis* sp. PCC 6803 (Sakurai et al., 2006), which supports the validity of these results.

From the data in Sakurai et al. (2006), we computed the molar ratio of each lipid to chlorophyll (Chl) in the thylakoid fraction from *T. vulcanus* (**Table 1**). Because of no available data for the total PSI and PSII content in *Thermosynechococcus* species, in this study, we used the data for PSI (7.5 mmol/mol Chl) and PSII (3.2 mmol/mol Chl) content in another thermophilic cyanobacterium *Synechococcus lividus* (Melis and Brown, 1980) for a rough estimation. Similar content in *Synechocystis* sp. PCC 6714 (Fujita and Murakami, 1987; Murakami et al., 1997) supports the validity of this assumption. In combination with the crystallographic data (Jordan et al., 2001; Umena et al., 2011), these biochemical data allowed us to estimate 1.3 and 2.8 mol% of total thylakoid lipids allocated to PSI and PSII, respectively (**Figure 1A**). Of note, ∼30% of total PG molecules is associated with photosystems, whereas only a small portion (∼3%) is allocated to photosystems for other lipid classes. As a result, PG accounts for only 4.6 mol% of total lipids outside photosystems, presumably mainly in the lipid bilayer fraction. These data demonstrate that PG, the only phospholipid in cyanobacteria, is preferentially allocated to photosystem complexes, whereas glycolipids predominantly constitute the lipid bilayer of the thylakoid membrane. We should note that because the PSI-to-PSII ratios in cyanobacteria flexibly change from ∼0.5 to ∼5 depending on growth conditions, particularly light quality and quantity (Fujita and Murakami, 1987; Samson et al., 1994; Murakami et al., 1997), the proportion of PG in photosystems may also range from ∼45 to ∼23 mol% of total thylakoid PG.

DISTRIBUTION OF LIPIDS IN THE THYLAKOID MEMBRANE IN PLANTS

Plants contain LHC antenna complexes in addition to core complexes in both PSI and PSII complexes. The crystal structure of the PSI–LHCI complex from pea at 2.8-Å resolution includes 10 lipid molecules (3 MGDGs, 1 DGDG, and 6 PGs) per monomer (Qin et al., 2015). Similar to *T. elongatus* PSI (Jordan et al., 2001), 1 MGDG, 1 DGDG, and 3 PG molecules were associated with the PSI core in pea. The more recent analysis of the pea PSI–LHCI complex at 2.6-Å resolution identified 27 lipid molecules (19 MGDGs, 4 DGDGs, and 4 PGs), mostly located between PSI and LHCI, in addition to the five lipids in the core region (Mazor et al., 2017).

Single-particle cryo-electron microscopic analysis of the C_2S_2-type PSII–LHCII supercomplex (C; PSII core complex, S; strongly associated LHCII trimer) from spinach at 3.2-Å resolution revealed 21 lipid molecules per monomeric complex (Wei et al., 2016). The lipid content (5 MGDGs, 4 DGDGs, 3 SQDGs, and 4 PGs) in the spinach PSII core is similar to that in *T. vulcanus* (Umena et al., 2011). In addition,

TABLE 1 | Lipid content in the thylakoid membrane and photosystem complexes.

				Thylakoid	PSI	PSII	Other
Cyanobacteria		PSI		7.52	–	–	–
		PSII		3.24	–	–	–
	Lipids		Total	2350	30.1 (4)	64.8 (20)	2230
			MGDG	1020	7.52 (1)	19.4 (6)	995
			DGDG	602	0 (0)	16.2 (5)	586
			SQDG	583	0 (0)	13.0 (4)	570
			PG	143	22.6 (3)	16.2 (5)	104
Plants		PSI		2.25	–	–	–
		PSII		2.99	–	–	–
	Lipids		Total	1950	72.0 (32)	89.7 (30)	1790
			MGDG	840	45.0 (20)	15.0 (5)	780
			DGDG	510	11.3 (5)	12.0 (4)	487
			SQDG	380	0 (0)	9.00 (3)	371
			PG	220	15.8 (7)	53.8 (18)	150

Data are expressed as mmol mol^{-1} chlorophyll. Data are derived or calculated from Melis and Brown (1980) for the content of photosystem I (PSI) and photosystem II (PSII) in a cyanobacterium (Synechococcus lividus), Sakurai et al. (2006) for each lipid content in the thylakoid membrane of a cyanobacterium (Thermosynechococcus vulcanus), Kirchhoff et al. (2002) for the content of PSI, PSII and each lipid in the thylakoid membrane of a plant (spinach). The figures in parentheses denote numbers of each lipid in PSI and PSII deduced from crystallographic analyses of PSI from Thermosynechococcus elongatus (Jordan et al., 2001), PSII from T. vulcanus (Umena et al., 2011), PSI-light harvesting complex (LHC) I from pea (Mazor et al., 2017), and PSII–LHCII from spinach (Wei et al., 2016).

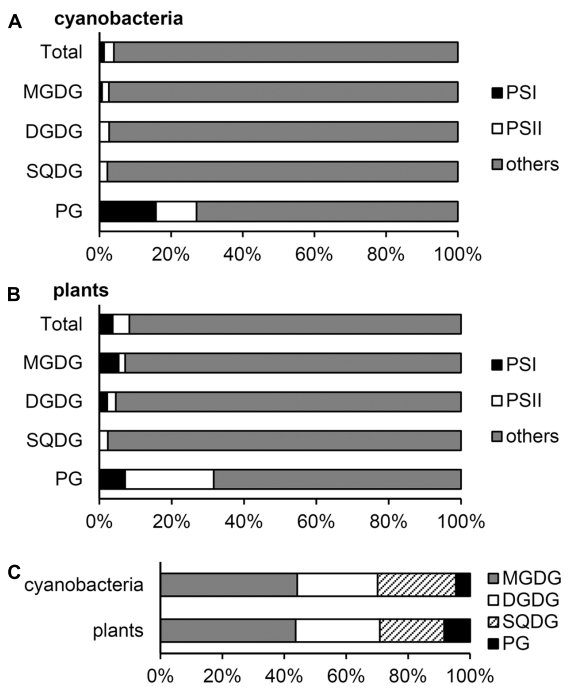

FIGURE 1 | Distribution of glycerolipids to photosystems and other fractions in the thylakoid membrane. **(A,B)** Distribution (mol%) of each lipid to photosystem I (PSI), photosystem II (PSII) and other thylakoid fractions in cyanobacteria **(A)** and plants **(B)**. **(C)** Lipid composition (mol%) of the thylakoid fraction outside photosystems. Lipid compositions are computed from the data in **Table 1**.

5 PG molecules were associated with the LHCII complex composed of 1 trimeric LHCII with 3 PGs, 1 monomeric CP26 with 1 PG, and 1 monomeric CP29 with 1 PG. X-ray crystallography analyses of the LHCII trimer from spinach at 2.7 Å (Liu et al., 2004) and from pea at 2.5 Å (Standfuss et al., 2005) both identified one PG molecule per monomer, which is consistent with the data in the C_2S_2-type PSII–LHCII supercomplex (Wei et al., 2016). By contrast, 2 DGDG molecules per monomer observed at the periphery of the crystallized LHCII trimers (Liu et al., 2004; Standfuss et al., 2005) were missing in the C_2S_2-type supercomplex. Because binding sites of DGDG differed between spinach and pea data, these DGDGs may be integrated into the LHCII trimer during crystallization processes. Besides the C_2S_2-type complex, other forms of the PSII–LHCII supercomplex such as $C_2S_2M_2$ type (M; moderately associated LHCII trimer) have been identified in plant thylakoids (Pan et al., 2013). Biochemical analysis revealed that a single PSII–LHCII unit contains 250 Chls on average (Ghirardi et al., 1986), which would correspond to 4 major LHCII trimers (12 subunits in total) and 3 minor monomeric LHCIIs, presumably CP24, CP26, and CP29, per PSII monomer (Peter and Thornber, 1991; Pan et al., 2013). This estimation is consistent with the 3.8-times higher amount of the LHCII trimer than the PSII monomer on a molar basis in spinach thylakoids (Kirchhoff et al., 2002). From these data, we assumed that PSII–LHCII complexes contain a total of 30 lipids (5 MGDGs, 4 DGDGs, 3 SQDGs, and 18 PGs) per PSII monomer, on average.

Although the relative abundance of PSI, PSII, and LHCII in plants greatly differs according to growth conditions, in this study, we estimated lipid content in photosystem complexes based on the data in spinach thylakoids (**Table 1**) (Kirchhoff et al., 2002). The estimation revealed that PSI–LHCI and PSII–LHCII contain 3.7 and 4.6 mol%, respectively, total lipids in the thylakoid membrane (**Figure 1B**). As in cyanobacteria, ∼30 mol% of total PG in the thylakoid membrane is allocated to photosystems in plant chloroplasts, and thus the contribution of

PG to other lipid fractions (8.4 mol%) is lower than that of SQDG (20.7 mol%) (**Figure 1C**).

DISTRIBUTION OF LIPIDS IN OTHER THYLAKOID FRACTIONS

The Cyt b_6/f complex mediates electron transfer from PSII to PSI and generates an electrochemical proton gradient across the thylakoid membrane together with water splitting in PSII. The crystal structure of the dimeric Cyt b_6/f complex has been determined for *Chlamydomonas reinhardtii* (Stroebel et al., 2003), *Mastigocladus laminosus* (Kurisu et al., 2003) and *Nostoc* sp. PCC 7120 (Baniulis et al., 2009). From these data, one SQDG molecule was identified with two synthetic phosphatidylcholine and four detergents per monomer. In addition, mass spectroscopy analysis of spinach Cyt b_6/f detected MGDG, DGDG, and PG along with SQDG (Hasan et al., 2011). Although two neutral lipids at the lumenal side were modeled as MGDGs in the *C. reinhardtii* Cyt b_6/f (Stroebel et al., 2003), one may be a DGDG molecule based on the mass spectroscopy data. Furthermore, the presence of stoichiometric amounts of PG and SQDG in spinach Cyt b_6/f suggests an equal amount of these anionic lipids in the structure (Hasan et al., 2011). Considering the content of Cyt b_6/f of ∼1.0 mmol/mol Chl in plants (Kirchhoff et al., 2002; Schöttler and Toth, 2014) and ∼5.0 mmol/mol Chl in cyanobacteria (Fujita and Murakami, 1987), we roughly estimated that 0.3 ∼ 0.9 mol% of total thylakoid lipids are integrated in the Cyt b_6/f complexes with stoichiometry of 1 MGDG, 1 DGDG, 1 SQDG, and 1 PG per monomer.

For ATP synthesis, ATP synthase uses a proton gradient across the thylakoid membrane. In animals, cardiolipin (diphosphatidylglycerol), the anionic lipid produced from PG and CDP-diacylglycerol, is an essential component of mitochondrial ATP synthase (Santiago et al., 1973; Laird et al., 1986). Computer simulations demonstrated that cardiolipin specifically and transiently interacts with the rotating c-ring of yeast ATP synthase (Duncan et al., 2016). In the thylakoid membrane, containing no cardiolipin, the anionic lipid PG or SQDG may be specifically associated with ATP synthase, although the lipid content in the thylakoid ATP synthase remains undetermined.

Considering the predominant amount of photosynthetic electron transport complexes in the thylakoid membrane (Yu et al., 1994; Herranen et al., 2004), lipids that do not integrate in these major complexes would be mostly allocated to the thylakoid lipid bilayer. We estimated that 92–95 mol% of the thylakoid lipid bilayer is composed of glycolipids (**Figure 1C**).

ROLE OF PG IN PHOTOSYSTEMS

In general, the primary role of membrane glycerolipids is to construct the lipid bilayer. In fact, most glycolipids in thylakoid are distributed to the lipid bilayer fraction as building blocks (**Figure 1**). However, our estimation revealed that ∼30 mol% of PG in the thylakoid membrane is allocated to photosystem complexes as a structural component in both cyanobacteria and plant chloroplasts, and the quantitative contribution of PG to the thylakoid lipid bilayer is low (5–8 mol%). Because loss of PG severely impairs photosynthetic electron transport in all oxygenic phototrophs examined to date (Kobayashi et al., 2016b), this lipid would specifically serve as an essential component of photosystems.

In the crystal structure of *T. vulcanus* PSII, all 5 PG molecules are deeply buried near the reaction center (Umena et al., 2011). Short-term depletion (3–7 days) of PG in *Synechocystis* sp. PCC 6803 cells caused loss of ∼3 PG molecules from PSII, accompanied by impaired electron transport from the primary (Q_A) to the secondary plastoquinone (Q_B) and destabilized oxygen-evolving complex (Sakurai et al., 2003, 2007). Moreover, site-directed mutations of PG-associated amino-acid residues of the D1 protein, which caused loss of about 1 PG molecule from the PSII complex, decreased electron transport activity and disordered PSII structures (Endo et al., 2015). These data demonstrate the essential roles of PSII-associated PG in structures and functions of the complex.

In contrast to the rapid inhibition of PSII by PG deficiency, PSI is affected only after a longer period (>2 weeks) of PG depletion (Domonkos et al., 2004), which may reflect more stable association of PG with PSI. Three PG molecules are integrated in the crystal structure of *T. elongatus* PSI (Jordan et al., 2001). One is buried near the reaction center, and the other two locate at the periphery. Decreased PSI activity and increased monomeric PSI complexes after long-term PG deficiency suggest an important role of PG in the activity and structural organization of PSI (Domonkos et al., 2004).

In plants, PG molecules are associated with the LHCI and LHCII complexes in addition to the photosystem core complexes (Liu et al., 2004; Standfuss et al., 2005; Qin et al., 2015; Wei et al., 2016; Mazor et al., 2017). Degradation of PG by phospholipase A2 treatment disassembled the LHCII trimer into the monomeric form (Nussberger et al., 1993; Kim et al., 2007). Moreover, PG deficiency in a *C. reinhardtii* mutant decreased trimeric LHCII level, but PG supplementation to the mutant partially recovered the phenotype (Dubertret et al., 1994). These findings indicate a crucial role of PG in structural organization of the LHCII trimer. In addition, in the pea PSI–LHCI complex, several PG molecules are located between PSI and LHCI with MGDGs and DGDGs (Mazor et al., 2017). Because lack of any of these lipids caused disorganization of PSI–LHCI complexes in *Arabidopsis thaliana* mutants (Ivanov et al., 2006; Kobayashi et al., 2013, 2016a), the lipid cluster observed between PSI and LHCI may specifically function to maintain the complex structure.

The preferential allocation of PG to the deep sites of both photosystems despite the low abundance of PG in the thylakoid lipid bilayer suggests a requirement of specific mechanisms to deliver PG molecules within the protein complexes. Kopečná et al. (2015) reported that loss of PG in the *Synechocystis* sp. PCC 6803 mutant strongly impaired synthesis of PSI proteins and Chls. The authors proposed that a PG-containing membrane microdomain may be required for the synthesis of these

components (Kopečná et al., 2015). Considering the low amount of PG in the thylakoid lipid bilayer, PG distribution may be restricted to a specific microdomain in the thylakoid membrane, where assembly of PG to protein–pigment complexes may take place along with synthesis of Chls and PSI.

ROLE OF PG OUTSIDE PHOTOSYSTEMS

Mutant analyses in *A. thaliana*, *C. reinhardtii* and several cyanobacteria revealed that loss of SQDG increased PG levels to maintain total anionic lipid content (Sato et al., 1995; Güler et al., 1996; Yu et al., 2002; Aoki et al., 2004; Endo et al., 2016). In *T. elongatus*, PG content was increased from 4 to 25 mol% by disruption of SQDG biosynthesis (Endo et al., 2016). Because photosystem-associated SQDG is only 3.7 mol% of the total SQDG level in *Thermosynechococcus* thylakoids (**Figure 1A**), PG produced in response to loss of SQDG would be mainly allocated to the lipid bilayer fraction. Although complete lack of SQDG alone has no or only weak effects in most photosynthetic organisms (Sato et al., 1995; Güler et al., 1996; Yu et al., 2002; Endo et al., 2016), a partial decrease in PG content along with lack of SQDG strongly impaired photosynthetic activity and growth (Güler et al., 1996; Yu and Benning, 2003; Endo et al., 2016). The result suggests an importance of maintained levels of total anionic lipids in thylakoids. Because SQDG is the major anionic lipid in the thylakoid lipid bilayer (**Figure 1C**), the main role of this lipid may be maintaining a certain level of anionic lipids in the membrane. By contrast, PG has more specific roles in photosystems. However, when SQDG content is decreased, PG content increases and would complement the role of SQDG in the lipid bilayer.

Under phosphate-limited conditions, PG content in *A. thaliana* decreased from ∼10 to ∼5 mol% of total membrane lipids, with SQDG content inversely increased from ∼6 to ∼11 mol% (Essigmann et al., 1998). Because photosystem-associated PG is indispensable for photosynthesis, PG molecules that are not integrated in the complexes may be preferentially degraded under phosphate limitation. This assumption is supported by the fact that phosphate limitation severely affected photosynthetic electron transport in PG-deficient *A. thaliana* mutants but not the wild type (Kobayashi et al., 2015). Thus, increased SQDG under phosphate limitation would mainly replace PG outside photosystem complexes. A similar relationship between PG and SQDG under phosphate limitation is observed in *S. elongatus* PCC 7942 (Güler et al., 1996) but not *Synechocystis* sp. PCC 6803 (Awai et al., 2007) or *T. elongatus* (Endo et al., 2016). PG content is substantially low in *T. elongatus* (∼4 mol%) as compared with *S. elongatus* (16.6 mol%) even under phosphate-sufficient conditions (Endo et al., 2016). Conversely, SQDG content is higher in *T. elongatus* (∼18 mol%) than *S. elongatus* (10.3 mol%). *T. elongatus* may already decrease PG content to a minimal level under phosphate-sufficient conditions and thus cannot further reduce PG content under limited phosphate. Use of glycolipids for the lipid bilayer reduces spending phosphate in the membrane, which would be advantageous for growth of photosynthetic organisms particularly under phosphate-limited conditions. The specific enrichment of PG in photosystems implies an indispensable role of this lipid, which presumably could not have been replaced by glycolipids during the long evolutionary processes of oxygenic photosynthetic organisms.

CONCLUSION

In both plants and cyanobacteria, one third of total PG molecules in thylakoids is specifically integrated with photosystems to fulfill its essential role in photosynthesis. By contrast, galactolipids mainly constitute the thylakoid lipid bilayer with the anionic glycolipid SQDG, which reduces the use of phosphate in the thylakoid membrane. The specific enrichment of PG in photosystems implies a particular mechanism to assemble PG into the deep sites of the complexes, which should be evaluated in future studies.

AUTHOR CONTRIBUTIONS

KK conceived the study, analyzed data, and wrote the manuscript. KE analyzed data and complemented the writing. HW supervised the study and complemented the writing.

FUNDING

This work was supported by the JSPS KAKENHI Grant Number 26711016.

REFERENCES

Aoki, M., Sato, N., Meguro, A., and Tsuzuki, M. (2004). Differing involvement of sulfoquinovosyl diacylglycerol in photosystem II in two species of unicellular cyanobacteria. *Eur. J. Biochem.* 271, 685–693. doi: 10.1111/j.1432-1033.2003.03970.x

Awai, K., Watanabe, H., Benning, C., and Nishida, I. (2007). Digalactosyldiacylglycerol is required for better photosynthetic growth of *Synechocystis* sp. PCC6803 under phosphate limitation. *Plant Cell Physiol.* 48, 1517–1523. doi: 10.1093/pcp/pcm134

Baniulis, D., Yamashita, E., Whitelegge, J. P., Zatsman, A. I., Hendrich, M. P., Hasan, S. S., et al. (2009). Structure-function, stability, and chemical modification of the cyanobacterial cytochrome b_6f complex from *Nostoc* sp. PCC 7120. *J. Biol. Chem.* 284, 9861–9869. doi: 10.1074/jbc.M809196200

Demé, B., Cataye, C., Block, M. A., Maréchal, E., and Jouhet, J. (2014). Contribution of galactoglycerolipids to the 3-dimensional architecture of thylakoids. *FASEB J.* 28, 3373–3383. doi: 10.1096/fj.13-247395

Domonkos, I., Malec, P., Sallai, A., Kovács, L., Itoh, K., Shen, G., et al. (2004). Phosphatidylglycerol is essential for oligomerization of photosystem I reaction center. *Plant Physiol.* 134, 1471–1478. doi: 10.1104/pp.103.037754

Dorne, A., Joyard, J., and Douce, R. (1990). Do thylakoids really contain phosphatidylcholine? *Proc. Natl. Acad. Sci. U.S.A.* 87, 71–74.

Dubertret, G., Mirshahi, A., Mirshahi, M., Gerard-Hirne, C., and Tremolieres, A. (1994). Evidence from *in vivo* manipulations of lipid composition in mutants that the Δ^3-*trans*-hexadecenoic acid-containing phosphatidylglycerol is involved in the biogenesis of the light-harvesting chlorophyll *a*/*b*-protein complex of *Chlamydomonas reinhardtii*. *Eur. J. Biochem.* 226, 473–482. doi: 10.1111/j.1432-1033.1994.tb20072.x

Duncan, A. L., Robinson, A. J., and Walker, J. E. (2016). Cardiolipin binds selectively but transiently to conserved lysine residues in the rotor of metazoan ATP synthases. *Proc. Natl. Acad. Sci. U.S.A.* 113, 8687–8692. doi: 10.1073/pnas.1608396113

Endo, K., Kobayashi, K., and Wada, H. (2016). Sulfoquinovosyldiacylglycerol has an essential role in *Thermosynechococcus elongatus* BP-1 under phosphate-deficient conditions. *Plant Cell Physiol.* 57, 2461–2471. doi: 10.1093/pcp/pcw159

Endo, K., Mizusawa, N., Shen, J.-R., Yamada, M., Tomo, T., Komatsu, H., et al. (2015). Site-directed mutagenesis of amino acid residues of D1 protein interacting with phosphatidylglycerol affects the function of plastoquinone Q_B in photosystem II. *Photosynth. Res.* 126, 385–397. doi: 10.1007/s11120-015-0150-9

Essigmann, B., Güler, S., Narang, R. A., Linke, D., and Benning, C. (1998). Phosphate availability affects the thylakoid lipid composition and the expression of *SQD1*, a gene required for sulfolipid biosynthesis in *Arabidopsis thaliana*. *Proc. Natl. Acad. Sci. U.S.A.* 95, 1950–1955.

Fujita, Y., and Murakami, A. (1987). Regulation of electron transport composition in cyanobacterial photosynthetic system: stoichiometry among photosystem I and II complexes and their light-harvesting antennae and cytochrome *b6/f* complex. *Plant Cell Physiol.* 28, 1547–1553.

Ghirardi, M. L., McCauley, S. W., and Melis, A. (1986). Photochemical apparatus organization in the thylakoid membrane of *Hordeum vulgare* wild type and chlorophyll *b*-less chlorina f2 mutant. *Biochim. Biophys. Acta* 851, 331–339. doi: 10.1016/0005-2728(86)90069-1

Güler, S., Seeliger, A., Härtel, H., Renger, G., and Benning, C. (1996). A null mutant of *Synechococcus* sp. PCC7942 deficient in the sulfolipid sulfoquinovosyl diacylglycerol. *J. Biol. Chem.* 271, 7501–7507. doi: 10.1074/jbc.271.13.7501

Hasan, S. S., Yamashita, E., Ryan, C. M., Whitelegge, J. P., and Cramer, W. A. (2011). Conservation of lipid functions in cytochrome *bc* complexes. *J. Mol. Biol.* 414, 145–162. doi: 10.1016/j.jmb.2011.09.023

Herranen, M., Battchikova, N., Zhang, P., Graf, A., Sirpiö, S., Paakkarinen, V., et al. (2004). Towards functional proteomics of membrane protein complexes in *Synechocystis* sp. PCC 6803. *Plant Physiol.* 134, 470–481. doi: 10.1104/pp.103.032326

Ivanov, A. G., Hendrickson, L., Krol, M., Selstam, E., Öquist, G., Hurry, V., et al. (2006). Digalactosyl-diacylglycerol deficiency impairs the capacity for photosynthetic intersystem electron transport and state transitions in *Arabidopsis thaliana* due to photosystem I acceptor-side limitations. *Plant Cell Physiol.* 47, 1146–1157. doi: 10.1093/pcp/pcj089

Jordan, P., Fromme, P., Witt, H. T., Klukas, O., Saenger, W., and Krauss, N. (2001). Three-dimensional structure of cyanobacterial photosystem I at 2.5 Å resolution. *Nature* 411, 909–917. doi: 10.1038/35082000

Jouhet, J. (2013). Importance of the hexagonal lipid phase in biological membrane organization. *Front. Plant Sci.* 4:494. doi: 10.3389/fpls.2013.00494

Kim, E.-H., Razeghifard, R., Anderson, J. M., and Chow, W. S. (2007). Multiple sites of retardation of electron transfer in Photosystem II after hydrolysis of phosphatidylglycerol. *Photosynth. Res.* 93, 149–158. doi: 10.1007/s11120-006-9126-0

Kirchhoff, H., Mukherjee, U., and Galla, H. J. (2002). Molecular architecture of the thylakoid membrane: lipid diffusion space for plastoquinone. *Biochemistry* 41, 4872–4882. doi: 10.1021/bi011650y

Kobayashi, K., Endo, K., and Wada, H. (2016a). Multiple impacts of loss of plastidic phosphatidylglycerol biosynthesis on photosynthesis during seedling growth of *Arabidopsis*. *Front. Plant Sci.* 7:336. doi: 10.3389/fpls.2016.00336

Kobayashi, K., Endo, K., and Wada, H. (2016b). "Roles of lipids in photosynthesis," in *Lipids in Plant and Algae Development*, eds Y. Nakamura and Y. Li-Beisson (Berlin: Springer International Publishing), 21–49. doi: 10.1007/978-3-319-25979-6_2

Kobayashi, K., Fujii, S., Sato, M., Toyooka, K., and Wada, H. (2015). Specific role of phosphatidylglycerol and functional overlaps with other thylakoid lipids in Arabidopsis chloroplast biogenesis. *Plant Cell Rep.* 34, 631–642. doi: 10.1007/s00299-014-1719-z

Kobayashi, K., Narise, T., Sonoike, K., Hashimoto, H., Sato, N., Kondo, M., et al. (2013). Role of galactolipid biosynthesis in coordinated development of photosynthetic complexes and thylakoid membranes during chloroplast biogenesis in Arabidopsis. *Plant J.* 73, 250–261. doi: 10.1111/tpj.12028

Kopečná, J., Pilný, J., Krynická, V., Tomčala, A., Kis, M., Gombos, Z., et al. (2015). Lack of phosphatidylglycerol inhibits chlorophyll biosynthesis at multiple sites and limits chlorophyllide reutilization in *Synechocystis* sp. strain PCC 6803. *Plant Physiol.* 169, 1307–1317. doi: 10.1104/pp.15.01150

Kubota, H., Sakurai, I., Katayama, K., Mizusawa, N., Ohashi, S., Kobayashi, M., et al. (2010). Purification and characterization of photosystem I complex from *Synechocystis* sp. PCC 6803 by expressing histidine-tagged subunits. *Biochim. Biophys. Acta* 1797, 98–105. doi: 10.1016/j.bbabio.2009.09.001

Kurisu, G., Zhang, H., Smith, J. L., and Cramer, W. A. (2003). Structure of the cytochrome b_6f complex of oxygenic photosynthesis: tuning the cavity. *Science* 302, 1009–1014. doi: 10.1126/science.1090165

Laird, D. M., Parce, J. W., Montgomery, R. I., and Cunningham, C. C. (1986). Effect of phospholipids on the catalytic subunits of the mitochondrial F0·F1-ATPase. *J. Biol. Chem.* 261, 14851–14856.

Liu, Z., Yan, H., Wang, K., Kuang, T., Zhang, J., Gui, L., et al. (2004). Crystal structure of spinach major light-harvesting complex at 2.72 Å resolution. *Nature* 428, 287–292. doi: 10.1038/nature02373

Loll, B., Kern, J., Saenger, W., Zouni, A., and Biesiadka, J. (2005). Towards complete cofactor arrangement in the 3.0 Å resolution structure of photosystem II. *Nature* 438, 1040–1044. doi: 10.1038/nature04224

Loll, B., Kern, J., Saenger, W., Zouni, A., and Biesiadka, J. (2007). Lipids in photosystem II: interactions with protein and cofactors. *Biochim. Biophys. Acta* 1767, 509–519. doi: 10.1016/j.bbabio.2006.12.009

Mazor, Y., Borovikova, A., and Nelson, N. (2017). The Structure of plant photosystem I super-complex at 2.8 Å resolution. *Nat. Plants* 3:e07433. doi: 10.7554/eLife.07433

Mazor, Y., Nataf, D., Toporik, H., and Nelson, N. (2014). Crystal structures of virus-like photosystem I complexes from the mesophilic cyanobacterium *Synechocystis* PCC 6803. *Elife* 3:e01496. doi: 10.7554/eLife.01496

Melis, A., and Brown, J. S. (1980). Stoichiometry of system I and system II reaction centers and of plastoquinone in different photosynthetic membranes. *Proc. Natl. Acad. Sci. U.S.A.* 77, 4712–4716. doi: 10.1073/pnas.77.8.4712

Mendiola-Morgenthaler, L., Eichenberger, W., and Boschetti, A. (1985). Isolation of chloroplast envelopes from *Chlamydomonas*. Lipid and polypeptide composition. *Plant Sci.* 41, 97–104.

Murakami, A., Kim, S.-J., and Fujita, Y. (1997). Changes in photosystem stoichiometry in response to environmental conditions for cell growth observed with the cyanophyte *Synechocystis* PCC 6714. *Plant Cell Physiol.* 38, 392–397. doi: 10.1093/oxfordjournals.pcp.a029181

Murata, N., Sato, N., Omata, T., and Kuwabara, T. (1981). Separation and characterization of thylakoid and cell envelope of the blue-green alga (cyanobacterium) *Anacystis nidulans*. *Plant Cell Physiol.* 22, 855–866.

Murphy, D. J. (1982). The importance of non-planar bilayer regions in photosynthetic membranes and their stabilisation by galactolipids. *FEBS Lett.* 150, 19–26. doi: 10.1016/0014-5793(82)81297-0

Nussberger, S., Dörr, K., Wang, D. N., and Kühlbrandt, W. (1993). Lipid-protein interactions in crystals of plant light-harvesting complex. *J. Mol. Biol.* 234, 347–356. doi: 10.1006/jmbi.1993.1591

Pan, X., Liu, Z., Li, M., and Chang, W. (2013). Architecture and function of plant light-harvesting complexes II. *Curr. Opin. Struct. Biol.* 23, 515–525. doi: 10.1016/j.sbi.2013.04.004

Peter, G. F., and Thornber, J. P. (1991). Biochemical composition and organization of higher plant photosystem II light-harvesting pigment-proteins. *J. Biol. Chem.* 266, 16745–16754.

Qin, X., Suga, M., Kuang, T., and Shen, J.-R. (2015). Structural basis for energy transfer pathways in the plant PSI-LHCI supercomplex. *Science* 348, 989–995. doi: 10.1126/science.aab0214

Sakurai, I., Hagio, M., Gombos, Z., Tyystjärvi, T., Paakkarinen, V., Aro, E.-M., et al. (2003). Requirement of phosphatidylglycerol for maintenance of photosynthetic machinery. *Plant Physiol.* 133, 1376–1384. doi: 10.1104/pp.103.026955

Sakurai, I., Mizusawa, N., Ohashi, S., Kobayashi, M., and Wada, H. (2007). Effects of the lack of phosphatidylglycerol on the donor side of photosystem II. *Plant Physiol.* 144, 1336–1346. doi: 10.1104/pp.107.098731

Sakurai, I., Shen, J.-R., Leng, J., Ohashi, S., Kobayashi, M., and Wada, H. (2006). Lipids in oxygen-evolving photosystem II complexes of cyanobacteria and higher plants. *J. Biochem.* 140, 201–209. doi: 10.1093/jb/mvj141

Samson, G., Herbert, S. K., Fork, D. C., and Laudenbach, D. E. (1994). Acclimation of the photosynthetic apparatus to growth irradiance in a mutant strain of *Synechococcus* lacking iron superoxide dismutase. *Plant Physiol.* 105, 287–294. doi: 10.1104/pp.105.1.287

Santiago, E., López-Moratalla, N., and Segovia, J. L. (1973). Correlation between losses of mitochondrial ATPase activity and cardiolipin degradation. *Biochem. Biophys. Res. Commun.* 53, 439–445. doi: 10.1016/0006-291X(73)90681-5

Sato, N., Tsuzuki, M., Matsuda, Y., Ehara, T., Osafune, T., and Kawaguchi, A. (1995). Isolation and characterization of mutants affected in lipid metabolism of *Chlamydomonas reinhardtii*. *Eur. J. Biochem.* 230, 987–993. doi: 10.1111/j.1432-1033.1995.0987g.x

Schöttler, M. A., and Toth, S. Z. (2014). Photosynthetic complex stoichiometry dynamics in higher plants: environmental acclimation and photosynthetic flux control. *Front. Plant Sci.* 5:188. doi: 10.3389/fpls.2014.00188

Shipley, G. G., Green, J. P., and Nichols, B. W. (1973). The phase behavior of monogalactosyl, digalactosyl, and sulphoquinovosyl diglycerides. *Biochim. Biophys. Acta* 311, 531–544. doi: 10.1016/0005-2736(73)90128-4

Standfuss, J., Terwisscha van Scheltinga, A. C., Lamborghini, M., and Kühlbrandt, W. (2005). Mechanisms of photoprotection and nonphotochemical quenching in pea light-harvesting complex at 2.5 Å resolution. *EMBO J.* 24, 919–928. doi: 10.1038/sj.emboj.7600585

Stroebel, D., Choquet, Y., Popot, J.-L., and Picot, D. (2003). An atypical haem in the cytochrome b_6f complex. *Nature* 426, 413–418. doi: 10.1038/nature02155

Umena, Y., Kawakami, K., Shen, J.-R., and Kamiya, N. (2011). Crystal structure of oxygen-evolving photosystem II at a resolution of 1.9 Å. *Nature* 473, 55–60. doi: 10.1038/nature09913

Wei, X., Su, X., Cao, P., Liu, X., Chang, W., Li, M., et al. (2016). Structure of spinach photosystem II–LHCII supercomplex at 3.2 Å resolution. *Nature* 534, 69–74. doi: 10.1038/nature18020

Yu, B., and Benning, C. (2003). Anionic lipids are required for chloroplast structure and function in *Arabidopsis*. *Plant J.* 36, 762–770. doi: 10.1046/j.1365-313X.2003.01918.x

Yu, B., Xu, C., and Benning, C. (2002). *Arabidopsis* disrupted in *SQD2* encoding sulfolipid synthase is impaired in phosphate-limited growth. *Proc. Natl. Acad. Sci. U.S.A.* 99, 5732–5737. doi: 10.1073/pnas.082696499

Yu, S. G., Stefansson, H., Romanowska, E., and Albertsson, P. Å. (1994). Two dimensional electrophoresis of thylakoid membrane proteins and its application to microsequencing. *Photosynth. Res.* 41, 475–486. doi: 10.1007/BF02183049

Conflict of Interest Statement: The authors declare that the research was conducted in the absence of any commercial or financial relationships that could be construed as a potential conflict of interest.

frontiers in Plant Science

HYPOTHESIS AND THEORY
published: 22 February 2018
doi: 10.3389/fpls.2018.00206

Dynamin-Like Proteins Are Potentially Involved in Membrane Dynamics within Chloroplasts and Cyanobacteria

*Ruven Jilly[1], Nadir Zaman Khan[2], Henrik Aronsson[3] and Dirk Schneider[1]**

[1] Institute of Pharmacy and Biochemistry, Johannes Gutenberg University Mainz, Mainz, Germany, [2] Department of Biotechnology, University of Malakand, Malakand, Pakistan, [3] Department of Biological and Environmental Sciences, University of Gothenburg, Gothenburg, Sweden

Dynamin-like proteins (DLPs) are a family of membrane-active proteins with low sequence identity. The proteins operate in different organelles in eukaryotic cells, where they trigger vesicle formation, membrane fusion, or organelle division. As discussed here, representatives of this protein family have also been identified in chloroplasts and DLPs are very common in cyanobacteria. Since cyanobacteria and chloroplasts, an organelle of bacterial origin, have similar internal membrane systems, we suggest that DLPs are involved in membrane dynamics in cyanobacteria and chloroplasts. Here, we discuss the features and activities of DLPs with a focus on their potential presence and activity in chloroplasts and cyanobacteria.

Keywords: dynamin, thylakoid membrane, membrane fusion, membrane biogenesis, cyanobacteria, chloroplasts

OPEN ACCESS

Edited by:
Rebecca L. Roston, University of Nebraska–Lincoln, United States

Reviewed by:
William Zerges, Concordia University, Canada
Wataru Sakamoto, Okayama University, Japan

****Correspondence:***
Dirk Schneider
dirk.schneider@uni-mainz.de

Specialty section:
This article was submitted to Plant Physiology, a section of the journal Frontiers in Plant Science

Received: *27 October 2017*
Accepted: *02 February 2018*
Published: *22 February 2018*

Citation:
Jilly R, Khan NZ, Aronsson H and Schneider D (2018) Dynamin-Like Proteins Are Potentially Involved in Membrane Dynamics within Chloroplasts and Cyanobacteria. Front. Plant Sci. 9:206. doi: 10.3389/fpls.2018.00206

CHLOROPLASTS AND CYANOBACTERIA CONTAIN TWO INNER MEMBRANE SYSTEMS

Cyanobacteria and eukaryotic chloroplasts are evolutionary deeply connected, as primordial eukaryotic organisms had engulfed cyanobacterial ancestors in an endosymbiotic event. Incorporation of the bacteria into the cell metabolism finally resulted in development of a new organelle, the chloroplast, and the first oxygenic photosynthetic eukaryotes arose (reviewed in greater detail in Hohmann-Marriott and Blankenship, 2011; Jensen and Leister, 2014). During the course of evolution, several metabolic functions were lost in this newly developed organelle, and many genes of cyanobacterial origin were transferred from the new organelle into the genome of the host eukaryote (Martin and Herrmann, 1998; Martin et al., 2002; Kleine et al., 2009). Nevertheless, the ultrastructure of cyanobacteria and chloroplasts is still very similar, and the process of oxygenic photosynthesis as well as the proteins and cofactors involved therein are largely conserved (Hohmann-Marriott and Blankenship, 2011). In both cyanobacteria and chloroplasts, the components of the photosynthetic electron transport chain are localized within a specialized and unique internal membrane system, the thylakoid membranes (TMs). While the TM system is a completely separated and enclosed membrane system in chloroplasts and cyanobacteria, the exact fine structure of TMs can differ. In chloroplasts, TMs typically form multiple membrane stacks, which are connected by unstacked

TMs, called grana and stroma lamellae, respectively (Adam et al., 2011), whereas TMs are organized in a sheet-like structure in cyanobacterial cells. However, the detailed TM arrangement can vary significantly in cyanobacterial strains (Herrero and Flores, 2008).

The structure of the TM system is highly dynamic in plant chloroplasts, and the amounts as well as the subcellular organization of TMs alter in response to changing environmental conditions (Chuartzman et al., 2008; Kirchhoff et al., 2011; Herbstova et al., 2012; Iwai et al., 2015). It has been stated that the dynamics observed in plant chloroplasts can essentially only be explained by the existence of a protein machinery that controls membrane fission and fusion processes (Chuartzman et al., 2008; Kirchhoff et al., 2011; Herbstova et al., 2012), analogous to the machineries involved in fusion of other organelle membranes, such as the ER, the Golgi apparatus, and the mitochondria (e.g., reviewed by Bonifacino, 2014). In fact, membrane connections and membrane fusion/fission processes have already been discussed for a long time (Nickelsen et al., 2011; Karim and Aronsson, 2014; Rast et al., 2015), but experimental evidence still is scarce. While described in chloroplasts, TM dynamics are essentially not studied in cyanobacteria yet. In cyanobacteria, individual TM layers appear to be as interconnected as in chloroplasts, and individual TM layers fuse and form "holes," which are discussed to be required for intracellular transport (Nevo et al., 2007; Liberton et al., 2011a,b). Thus, the structure of TMs is most likely as dynamic in cyanobacteria as in chloroplasts. However, in contrast to chloroplasts, where TMs potentially develop *de novo* from the chloroplast inner envelope membrane (Muehlethaler and Frey-Wyssling, 1959; Morré et al., 1991), in cyanobacteria TMs do probably not form *de novo* but assemble from existing structures (Barthel et al., 2013).

DYNAMIN(-LIKE) PROTEINS ARE INVOLVED IN MEMBRANE REMODELING PROCESSES IN PROKARYOTES AND EUKARYOTES

Dynamin-like proteins (DLPs) [also called, dynamin-related proteins (DRPs)] are involved in diverse membrane-related processes in prokaryotic and eukaryotic cells, involving membrane fusion, membrane scission, membrane protection, and/or membrane stabilization (**Figure 1**). DLPs are members of a protein superfamily of GTPases. To separate DLPs from other GTPases, such as Ras-like GTPases involved in signal transduction, proliferation and survival of cells, DLPs are also entitled "large GTPases" (Praefcke and McMahon, 2004; Lu et al., 2016). The first identified member of the dynamin family, MxA and its yeast homolog Vps1 were found being involved in virus resistance, vacuolar protein sorting, fission of endosomal membranes and in endocytic events (Staeheli et al., 1986; Smaczynska-de Rooij et al., 2010; Chi et al., 2014). Simultaneously, the founder of the dynamin superfamily, the prototypical dynamin protein (Dyn), was shown to be crucial for the scission of clathrin-coated endocytic vesicles from eukaryotic plasma membranes (Shpetner and Vallee, 1989; Hinshaw and Schmid, 1995). Upon triggering membrane fission, MxA and Dyn form dimers that interacts head to tail, resulting in formation of inactive tetramers. In presence of lipids, the structure reorganizes resulting in rearrangement of this auto-inhibitory structure, and the GTP hydrolysis rate of Dyn increases from 2.6 to 105 min^{-1} (Song et al., 2004; Reubold et al., 2015). The mechanistic details of this GTP-driven process are described in more detail elsewhere (Praefcke and McMahon, 2004; Antonny et al., 2016). However, besides the prototypical Dyn protein, a group of related DLPs is active in/at different eukaryotic organelles. E.g., the *Drosophila melanogaster* DLP Atlastin and its yeast counterpart Sey1p are required for fusion of ER membranes (Hu et al., 2009; Orso et al., 2010), and the yeast protein Dnm1 and its mammalian homolog Drp1 are involved in mitochondria scission (Smirnova et al., 2001; Legesse-Miller et al., 2003; Ingerman et al., 2005; Mears et al., 2011; Ugarte-Uribe et al., 2014). Similar to Dyn, the GTPase activity of Drp1 also increases in presence of lipids (Bustillo-Zabalbeitia et al., 2014; Reubold et al., 2015). The DLPs Mitofusin and FZO mediate fusion of the mitochondrial outer membrane, whereas OPA1 and Mgm1 are involved in fusion of the mitochondrial inner membrane system (Hermann et al., 1998; Santel and Fuller, 2001; Frezza et al., 2006; Meeusen et al., 2006).

As in yeast, *Drosophila* and mammals, DLPs are also present in plants and are currently best characterized in *Arabidopsis thaliana*. The DLP ARC5 is localized at the outer membrane of chloroplasts and is involved in chloroplast division (Gao et al., 2003), whereas FZL was found at the stromal side of the chloroplasts envelope and the TM (Gao et al., 2006). This issue makes FZL unique, because it is the only plant DLP within chloroplasts. Potential chloroplast DLPs, their subcellular localizations and potential activities are introduced and further discussed in more detail below (see section "DLPs in *Arabidopsis thaliana*").

While DLPs are also predicted to exist in prokaryotes, this protein family was ignored for a long time in these organisms. About 10 years ago, the structure and (*in vitro*) activity of the first DLP was described, and the protein of the cyanobacterium *Nostoc punctiforme* was named "bacterial dynamin-like protein" (BDLP, hereafter named *Nos*DLP) (Low and Löwe, 2006). While the exact *in vivo* function of this protein is still to be resolved, *Nos*DLP behaves like other DLPs *in vitro* (Low et al., 2009; Bramkamp, 2012). While DLPs are rather common in cyanobacteria and some species encode multiple DLPs (as further outlined below), further representatives are not experimentally studied yet. Recently, two additional BDLPs were identified and partly analyzed. DynA of *Bacillus subtilis* can mediate membrane fusion *in vitro* (Bürmann et al., 2011), and as there is no obvious need for membrane fusion processes in *B. subtilis,* the *in vivo* activity of DynA was proposed to involve repair of disordered membranes (de Sousa Borges and Scheffers, 2016; Sawant et al., 2016). It was suggested that environmental stress (e.g., induced by phage infection or antibiotics) results in membrane pore formation, and DynA is recruited to these stressed membrane regions where it oligomerizes and fuses

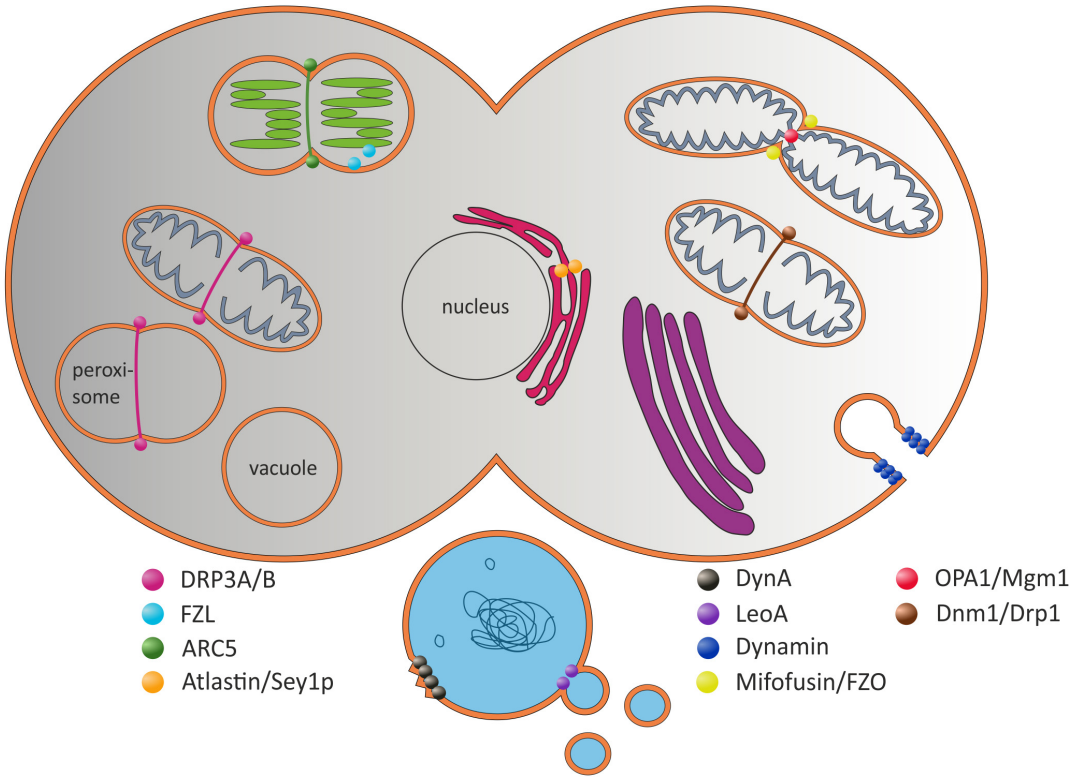

FIGURE 1 | Selected (B)DLPs and their proposed *in vivo* functions. The prototypical Dyn protein is involved in the formation of clathrin-coated vesicles at the plasma membrane (Hinshaw and Schmid, 1995). Dnm1-like proteins are involved in mitochondrial scission. ARC5 is involved in chloroplast division (Smirnova et al., 2001; Gao et al., 2003; Mears et al., 2011). Atlastin/Sey1p are potentially involved in ER fusion, whereas Mitofusin/FZO fuse the inner and OPA1/Mgm1 the outer mitochondrial membranes (Hermann et al., 1998; Santel and Fuller, 2001; Frezza et al., 2006; Meeusen et al., 2006; Hu et al., 2009; Orso et al., 2010). The plant FZL protein is localized at the chloroplast inner envelope and the TM (Gao et al., 2006). In prokaryotic cells, DynA is proposed to be involved in membrane protection and/or membrane repair, and LeoA has been suggested being a component of a vesicle release system (Michie et al., 2014; Sawant et al., 2016).

opposite bilayer patches in order to seal the membrane (Sawant et al., 2016). Furthermore, the *Escherichia coli* DLP LeoA was suggested to be involved in secretion of toxin-containing vesicles (Brown and Hardwidge, 2007; Michie et al., 2014). More recently two new BDLPs, DynA and DynB, were described to play a key role in a multiprotein cell division complex in *Streptomyces venezuelae* (Schlimpert et al., 2017). DynB is anchored to the cytoplasmic membrane where it interacts with DynA. Both BDLPs colocalize with the tubulin-like GTPase FtsZ and they might be involved, together with additional proteins, in the formation of sporulation septa during cell division (Schlimpert et al., 2017).

All thus far analyzed BDLPs hydrolyze GTP with much lower rates than eukaryotic DLPs (LeoA does not show any GTPase activity) and their GTP hydrolysis rates are typically not affected by lipids (Low and Löwe, 2006; Bürmann et al., 2011; Michie et al., 2014). However, being characteristic for DLPs, *Nos*DLP homodimerizes in its GDP-bound state via its GTPase domain, and in presence of GTP and lipids, the protein self-assembles around liposomes and forms lipid tubes (Low and Löwe, 2006). The *B. subtilis* DynA is an internally fused protein containing two BDLP subunits, and thus, this protein works per definition as a dimer. Consequently, it shows nucleotide independent self-assembly on liposomes (Bürmann et al., 2011). As for LeoA, homo-dimerization has not been shown, suggesting that activation via heterodimerization with LeoBC is crucial (Michie et al., 2014).

Besides these few BDLPs being studied to some extent, the physiological function of DLPs is not clarified in bacteria yet. It is interesting to notice that in chloroplasts and cyanobacteria, both having similar internal membrane systems, membrane dynamics are observed (as discussed above), albeit no clear machinery is yet defined mediating membrane remodeling. Thus, it is not unlikely that BDLPs are involved in membrane dynamics in both chloroplasts and cyanobacteria.

COMMON STRUCTURAL ELEMENTS AND DOMAINS OF (B)DLPs

All (B)DLPs have a very similar domain structure (**Figure 2A**). Typically, a (B)DLP has a G-domain with the GTPase activity, followed by a middle (MID) domain, a region needed for membrane interaction (MI domain) and a GTPase effector domain (GED). The structure of all DLPs is dominated by α-helices, and individual helices often form helical bundle

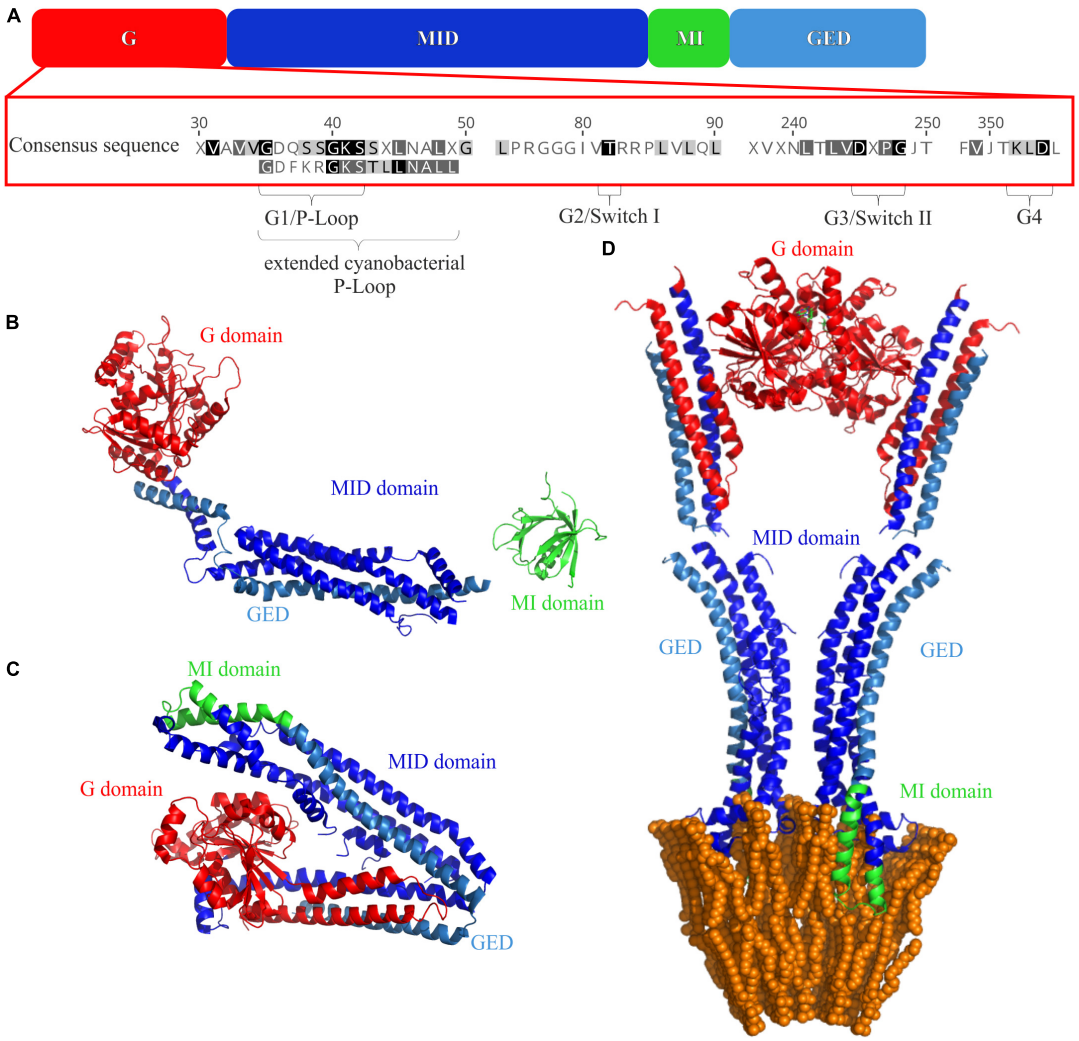

FIGURE 2 | Domain structures of (B)DLPs. **(A)** The G domain carries the GTPase activity, the MID domain is crucial for protein oligomerization, the membrane binding MI domain and the GED are also involved in protein oligomerization. The crystal structures of **(B)** monomeric Dyn G397D ΔPRD (PDB 3ZVR) (Ford et al., 2011), **(C)** *Nos*DLP in its GDP-bound closed monomeric form (PDB 2J69) (Low and Löwe, 2006), and **(D)** an open *Nos*DLP dimer (GDP-bound) anchored in a tubulated lipid bilayer (PDB 2W6D) (Low et al., 2009). The G-domain is colored red, the MID domain in blue and the GED in light blue. The MI domains are highlighted in green.

structures. The only highly conserved sequence of (B)DLPs is the G-domain, which is usually located at a (B)DLP N-terminus (**Figure 2A**). It harbors the GTPase domain and contains the amino acid motifs highly conserved in (B)DLPs. Like other GTPases, all (B)DLP share four motifs in the GTP binding/hydrolysis side: G1 or the P-Loop (GxxxxGKS/T), G2 or Switch I (T/S), G3 or Switch II (DxxG), and G4 (RD or N/TxxD). The G1 motif is involved in β-phosphate and Mg^{2+}-binding. While the G2 and G3 (D) motifs are also involved in Mg^{2+}-binding, they additionally interact with the γ-phosphate of GTP. The G4 motif is also involved in GTP binding but less conserved in (B)DLPs.

In contrast to the G-domain, the remaining (B)DLP domains can vary strongly in their amino acid sequence, but are similar in their function. Often, these domains cannot be identified by sequence comparison and/or homology searches but solely by functional studies.

The MID domain is structurally defined by the presence of α-helical bundles (**Figure 2**), which are crucial for mediating oligomerization of (B)DLPs (Low and Löwe, 2006; Low et al., 2009; Gao et al., 2010; Faelber et al., 2013; Fröhlich et al., 2013; Reubold et al., 2015).

Since (B)DLPs are membrane-active proteins, they harbor one or more MI domains that interact with biological membranes, and these MI domains usually follow the MID domain. However, while membrane interaction is a key feature of DLPs and the basis for membrane remodeling, the exact mode of membrane interaction is not conserved, and different (B)DLPs interact differently with membranes. FZO/Mitofusin, OPA1/Mgm1 as well as Atlastin are anchored to membranes

via transmembrane helices. In contrast, the prototypical Dyn interacts with membrane surfaces via the pleckstrin homology (PH) domain, which binds specifically to phosphatidylinositol lipids (Zheng et al., 1996). The DLP MxA harbors a disordered membrane binding loop (L4), and Dnm1 or the yeast homolog Drp1 uses the B insert loop that binds specifically to cardiolipin-enriched bilayers (Mitchell et al., 2013; Bustillo-Zabalbeitia et al., 2014). Furthermore, in EHD2, a polybasic motif was shown to mediate membrane interaction, and in GBP1, a specific Cys residue can be enzymatically isoprenylated, resulting in membrane anchoring (Nantais et al., 1996; Daumke et al., 2007; Vestal and Jeyaratnam, 2011). In case of DynA and *Nos*DLP, the membrane interacting domain is called *paddle domain* (P), and it is named Tip in case of LeoA. The P/Tip domain is dominated by hydrophobic amino acids that mediate interactions with membrane surfaces (Low and Löwe, 2006; Low et al., 2009; Bürmann et al., 2011; Michie et al., 2014).

With only a few exceptions (GBP1 and Atlastin), the GTPase effector domain (GED) follows the MI domain (**Figure 2**). The GED is also part of a helical bundle, and in Dyn, MxA and *Nos*DLP, the GED is additionally involved in the formation of higher-ordered structures (Schumacher and Staeheli, 1998; Chappie et al., 2009; Low et al., 2009).

Furthermore, besides the above described domains, additional domains might exist with more specialized functions.

In summary, all (B)DLPs appear to share three key features: (i) All (B)DLPs oligomerize and form higher ordered structures (Daumke and Praefcke, 2016). While in case of eukaryotic DLPs homo-oligomerization controls the GTPase activity, heterodimerization might be crucial for the activity of BDLPs (Bramkamp, 2012; Michie et al., 2014). (ii) All (B)DLPs are membrane-active and are involved in remodeling nearly every kind of cellular membrane system (reviewed in Bramkamp, 2012; Antonny et al., 2016; Daumke and Praefcke, 2016). For several DLPs it has been shown that they oligomerize *in vitro* and form helical structures around liposomes in the presence of a non-hydrolysable GTP analog, resulting in formation of tube-like membrane structures (Hinshaw, 2000; Low and Löwe, 2006; Bürmann et al., 2011; Mears et al., 2011; Shah et al., 2014; Ugarte-Uribe et al., 2014). (iii) (B)DLPs display a high sequence variability. Besides the G-domain, other domains can typically not be easily predicted in new classes of (B)DLPs and must be experimentally identified.

DLPs IN *Arabidopsis thaliana*

In the model plant *A. thaliana,* 16 DLPs (or DRPs) are encoded. Based on their amino acid sequence and domain structure, these proteins can be grouped in six subfamilies, DRP1-DRP6 (Hong et al., 2003; Backues et al., 2010; Bednarek and Backues, 2010). When using the dynamin signature domain DYN1 (PF00350) for identification of DRPs in *A. thaliana*, combined with the literature and the plant subcellular localization integrative predictor (PSI[1]) (Liu et al., 2013), six DRPs are identified with a putative chloroplast localization. Five of these are designated DRPs in the literature; AtDRP1a/AtADL1a (At5g42080), AtDRP3a/AtADL2a (At4g33650), AtDRP3b/AtADL2b (At2g14120), AtDRP5A (At1g53140), and AtDRP5B/AtARC5 (At3g19720), whereas one is named fuzzy onion (FZO)-like protein (FZL). AtDRP1a/AtADL1a, AtDRP3a/AtADL2a, and AtDRP3b/AtADL2b all contain the GTPase (DYN1, PF00350), the dynamin MID region (DYN2, PF01031) and the GTPase-effector domain (GED, PF02212) (Miyagishima et al., 2008; Heymann and Hinshaw, 2009). The proteins AtDRP5A and AtDRP5B/AtARC5 additionally contain a pleckstrin homology domain (PH, PF00169) that binds to membrane phospholipids. In contrast, the FZL protein (At1g03160) contains solely the DYN1 signature domain.

AtDRP1a/AtADL1a is one of five proteins in the DRP1 subfamily. AtDRP1a/AtADL1a was found in TMs and was suggested to be involved in vesicle formation inside chloroplasts due to impaired chloroplast development including reduced amount of chloroplast membranes (Park et al., 1998). However, AtDRP1a/AtADL1a was also identified at the cell plate (Lauber et al., 1997). This apparent discrepancy was explained by a shortcoming of the antibody used in the study of Park et al. (1997). While the antibody was expected to recognize the GTPase domain of AtDRP1a/AtADL1a, the GTPase domains of DLPs are generally highly conserved (as discussed above), and thus the antibody could well have detected other DLPs besides AtDRP1a/AtADL1a (Kang et al., 2001). Subsequent studies have further challenged the assumption of chloroplast localization, as AtDRP1a/AtADL1a is targeted to other cellular compartments and was shown to have other roles (Kang et al., 1998, 2003; Collings et al., 2008; Konopka and Bednarek, 2008; Fujimoto et al., 2010; Yoshinari et al., 2016). The protein is targeted to the cell plate during cytokinesis (Kang et al., 1998), and in mutants lacking AtDRP1a/AtADL1a, an unusual plasma membrane accumulation is observed. This seems to inhibit efficient targeting and fusion of exocytic vesicles to the cell surface, which disturbs cell wall production (Kang et al., 2003). Moreover, the protein has also been shown to have a role in endocytic events at the plasma membrane, possibly associated with formation of clathrin-coated vesicles (Collings et al., 2008; Konopka and Bednarek, 2008; Fujimoto et al., 2010; Yoshinari et al., 2016). Thus, AtDRP1 is currently not considered to be active in chloroplasts.

AtDRP3a/AtADL2a has also been predicted to be localized in chloroplasts. A GFP-tagged version of the *A. thaliana* DRP3a has been shown to be chloroplast-localized in soybean and tobacco, where the N-terminal 35 amino acid residues were shown to be sufficient for chloroplast targeting (Kang et al., 1998). However, in a later study a GFP-DRP3a fusion protein was observed in mitochondria rather than in chloroplasts and was shown to be involved in mitochondrial division (Arimura et al., 2004). Moreover, AtDRP3 has also been partially targeted to peroxisomes where it has been suggested to have an essential role in peroxisome fission and replication (Lingard et al., 2008; Zhang and Hu, 2009; Mano et al., 2011). Thus, although an AtDRP3 mutant displays slow growth and a pale color at the seedling stage (Zhang and Hu, 2009), AtDRP3a less likely functions inside

[1]http://bis.zju.edu.cn/psi/

chloroplasts, but instead the protein localizes to mitochondria and peroxisomes.

AtDRP3b, also known as "Arabidopsis dynamin-like 2b" (ADL2b), shares 76% sequence identity with AtDRP3a/AtADL2a (Hong et al., 2003). While the protein is predicted (by the plant subcellular tool PSI) to be chloroplast-localized, is has so far not been shown to be targeted to chloroplasts. Instead, it has been identified in mitochondria and peroxisomes where it is suggested to support mitochondrial and peroxisomal division, respectively (Arimura and Tsutsumi, 2002; Fujimoto et al., 2009; Zhang and Hu, 2009). The phenotype of a mutant is similar to a AtDRP3a mutant, i.e., retarded growth and pale colored at the seedling stage (Zhang and Hu, 2009). While both, AtDRP3a/AtADL2a and AtDRP3b/AtADL2b, are suggested to be involved in mitochondrial as well as in peroxisomal division, in mitochondria the proteins have redundant functions while in peroxisomes they appear to have more distinct functions (Fujimoto et al., 2009).

Similar to AtDRP3b, the PSI tool predicts the DRP5 subfamily member AtDRP5a to be targeted to chloroplasts, although this localization has yet to be confirmed experimentally. The phenotype of mutant plants shows retarded seedling growth with no altered chloroplast (Miyagishima et al., 2008). Thus, there is currently no clear link to chloroplasts except for a putative localization prediction. Instead, AtDRP5a has been identified via GFP-tagging and immunoblot analyses in the cytosol of meristematic and meristemoid cells, and the protein is mainly found within dividing cells and suggested to be involved in cytokinesis (Miyagishima et al., 2008).

AtDRP5b is localized in both chloroplasts and peroxisomes, and mutant plants show retarded plant growth with yellowish leaves and enlarged and dumbbell-shaped chloroplasts (Gao et al., 2003; Zhang and Hu, 2010). AtDRP5b, also known as "accumulation and replication of chloroplasts 5" (ARC5), has no predicted signal sequence-mediating protein import into chloroplasts, albeit it clearly localizes to this organelle. However, AtDRP5b/ARC5 is found at the outer chloroplasts envelope membrane facing the cytosol, where it is enrolled in division ring construction at the late stage of the chloroplast division (Pyke and Leech, 1994; Gao et al., 2003; Miyagishima et al., 2006). The protein is recruited to the plastid division site by two plastid division proteins (PDV1 and PDV2), which also regulate the GTPase activity of AtDRP5b/ARC5 (Gao et al., 2013; Holtsmark et al., 2013). However, AtDRP5b is also present in peroxisomes as revealed by bimolecular fluorescence complementation and co-immunoprecipitation assays, and when the AtDRP5b gene was mutated, impaired peroxisome division and function was observed (Zhang and Hu, 2010).

The *A. thaliana* protein AtFZL is related to fuzzy onion (FZO) proteins that are part of the dynamin superfamily of remodeling GTPases. FZO is a protein that is located in the outer mitochondria membrane where it is involved in fusion of opposing outer mitochondrial membranes in animals and fungi (Koshiba, 2004; Meeusen, 2004). However, the *A. thaliana* FZL protein shows low homology both to the Mitofusin domain found in the FZO family as well as to the dynamin domain (DYN1). Despite some sequence homology and similarities with FZO in respect of existing domains and their arrangement (GTPase, coiled-coil, transmembrane helices), absence of AtFZL does not affect mitochondria morphology in *A. thaliana* but instead the morphology of chloroplasts (Gao et al., 2006). AtFZL is located inside the chloroplasts at the TM but also at the chloroplast inner envelope (Gao et al., 2006). It is believed to be anchored to these membranes via two transmembrane domains located within the C-terminal part of the protein, leaving the GTPase and coiled-coil domains protruding into the chloroplast stroma (Gao et al., 2006). Whether the AtFZL operates in a similar fashion as the classical FZO, i.e., whether it brings two membranes into close contact resulting in membrane fusion, is currently unknown. However, such an activity is indicated and an involvement of AtFZL in the transport of lipids between the inner envelope and the TM has been suggested, since vesicles appear to not fuse in plants lacking AtFZL (Gao et al., 2006) and since the chloroplasts show a disorganized TM morphology. Thus, AtFZL likely is a membrane-remodeling GTPase, involved in TM biogenesis and dynamics in chloroplasts (Gao et al., 2006).

Thus, out of the six predicted DRPs, evidence for chloroplast localization and function is only strong for AtDRP5b and AtFZL. However, as AtDRP5b is localized at the outer envelope membrane, AtFZL is the one remaining that could facilitate membrane remodeling, potentially involving fission and fusion of vesicles budding off from the inner envelope membrane and being targeted to the TM (Kroll et al., 2001; Wang et al., 2004; Garcia et al., 2010; Tanz et al., 2012; Armbruster et al., 2013; Karim and Aronsson, 2014; Karim et al., 2014). Thus, DRPs can be important to secure a dynamic but organized thylakoid network in chloroplasts.

DLPs ARE CONSERVED IN CYANOBACTERIA

The BDLP of the cyanobacterium *N. punctiforme* has been characterized to some extent. As typical for DLPs, the smallest structural unit of this BDLP appears to be a dimer, which can further self-assemble (Low and Löwe, 2006; Low et al., 2009). *Nos*DLP is thought to mediate membrane fusion by inducing formation of highly curved membrane regions (Low and Löwe, 2006). After GTP-binding, *Nos*DLP self-oligomerizes *in vitro* around a membrane and forces the membrane into a tube-like structure with high curvature, similar to the prototypical eukaryotic Dyn protein that is involved in vesicle fission. After GTP hydrolyzes, *Nos*DLP is released from the lipid, and adjacent membrane regions spontaneously fuse (Low et al., 2009). A *Nos*DLP-GFP fusion protein was found in the cell periphery in *N. punctiforme* as well as in rare ring-like structures at the cell septa (Low and Löwe, 2006), highlighting that the protein is interacting with membranes and is membrane-active. Nevertheless, the *in vivo* function of this protein is still unclear.

To obtain further information about potential cyanobacterial BDLPs (hereafter named cBDLPs to distinguish them from other bacteria DLPs), we searched the *pfam* database (dynamin_N

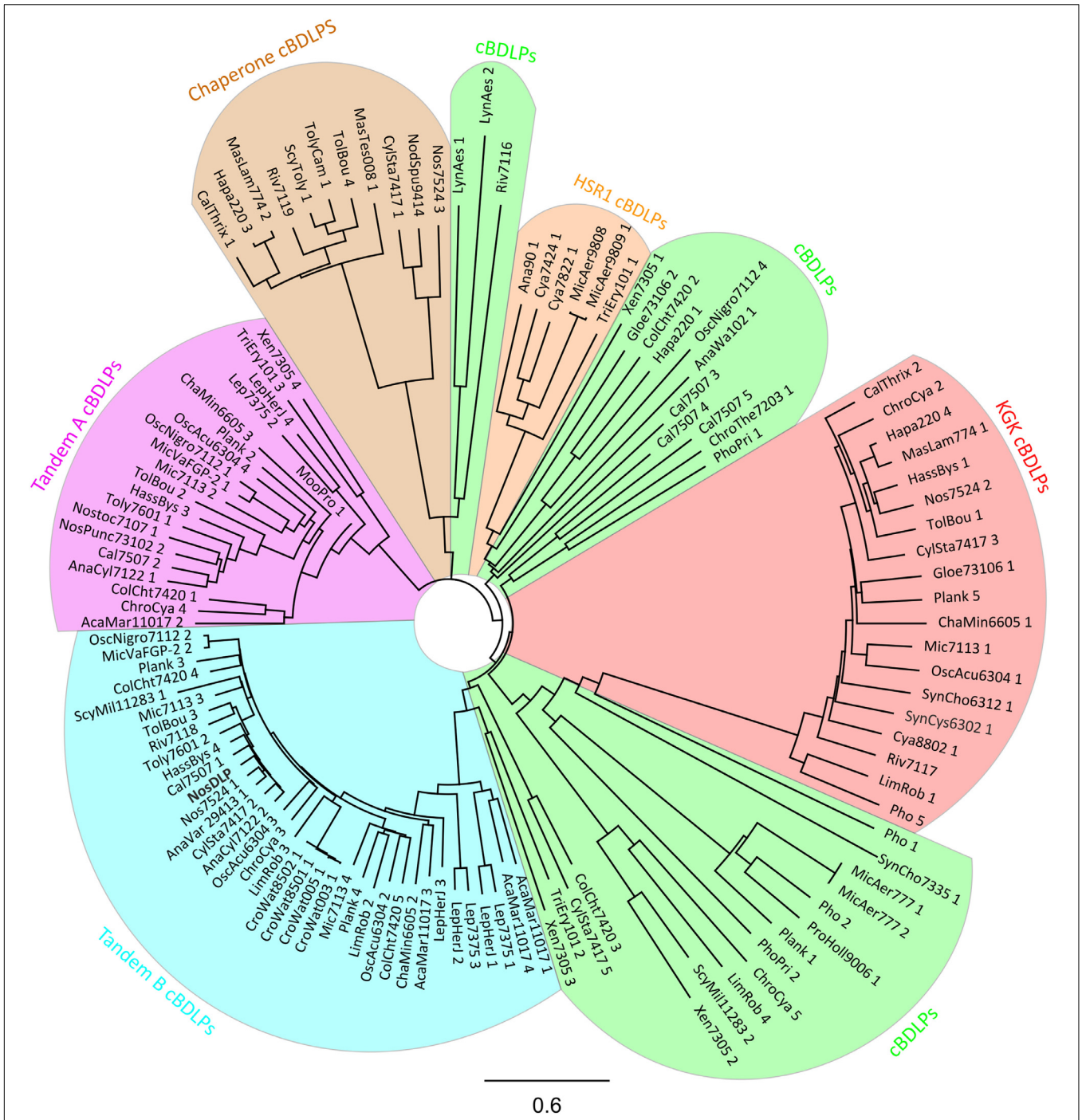

FIGURE 3 | Phylogenetic tree of 121 cBDLPs encoded in 56 cyanobacteria species (including *Nos*DLP). The DLP discussed in the text is shown in bold. The name of the potential dynamins is abbreviated. For full information about the strain, the gene name and the gene locus, view the **Supplementary Data Sheet S1**. The cBDLPs can be classified into six different clades, depending on their sequence and genomic environment: the *KGK* clade (red), the *HSR1* clade (orange), and the *chaperone* clade (brown). Upstream of the *Tandem A* (pink) clade, another cBDLP (*Tandem B*, light blue) is encoded. cBDLPs (green) could not be classified further and thus, represents a group of diverse cBDLPs. It is worth mentioning that boundaries between the *cBDLPs* clade and the *Tandem B* or *HSR1* clades, respectively, are not sharp and it might be that proteins share characteristics of both clades. Furthermore, while Xen7305 3 does not show significant sequence similarity to Tandem B members, downstream of this gene, the Tandem A protein Xen7305 4 is encoded. The here described group characteristics refer to the majority of the cBDLPs but do not represent every encoded protein. For further details, view the **Supplementary Data Sheet S1**. The phylogenetic tree (model: jukes-cantor, neighbor-joining) was created by a full-length multiprotein sequence alignment (Geneious global alignment, Matrix Blosum62) implemented in the software Geneious version 11.0.4 (http://www.geneious.com; Kearse et al., 2012). The cyanobacterial sequences were obtained from "cyanobase" (Nakamura et al., 1998; Fujisawa et al., 2017).

family PF00350), for cyanobacterial proteins carrying a dynamin GTPase domain, the only key marker for DLPs. Based on this analysis, 279 potential cBDLPs were identified being encoded in 74 different cyanobacterial species. However, we further limited our results and removed small GTPases, which sometimes also have a predicted dynamin GTPase domain. Finally, we ended up with 121 genes that likely encode BDLPs in 56 different cyanobacterial strains (**Figure 3** and **Supplementary Data Sheet S1**). It should be noted that due to the rather rigid search, we might have overlooked some cBDLPs. While all potential cBDLPs have a highly conserved dynamin-like GTPase domain within the N-terminal protein region, we did not limit our search to the identification of other known domains, since the sequences of these domains are typically not conserved (as discussed above). However, nearly all of the cBDLP sequences have an extended and conserved P-loop region within the G-domain: beside the common GxxxxGKS/T P-loop motif, cBDLPs have an additional L/INALL/I motif, which extends the P-loop motif to GxxxxGKS/TxL/INALL/I.

Unfortunately, none of the predicted cDLPs share a high sequence identity with the AtFZL protein in chloroplasts. However, based on a phylogenetic analysis we categorized the identified cBDLPs into six groups, where the sequences of individual cBDLPs are highly conserved within the defined clades but clearly differ in between the clades (**Figure 3**). Interestingly, the genetic context of some cBDLP is conserved in some clades and proteins are, e.g., part of conserved gene clusters (**Supplementary Data Sheet S1**).

Within the first cBDLP group, typically a KGK domain protein is encoded downstream of the cBDLP. Members of the KGK protein family (PF08872) are small cyanobacterial proteins (around 120 amino acids) that contain a KGK domain (Finn et al., 2014). Unfortunately, the precise function of this domain is enigmatic, albeit this domain potentially mediates protein–protein interactions. The second cBDLP group is termed *Tandem B* cBDLPs, and the only yet characterized cBLPD, the BDLP of *N. punctiforme*, belongs to this group (Low and Löwe, 2006). Upstream of the encoding gene, a second cBDLP is encoded (clade *Tandem A*), and thus, translation of the clustered genes likely results in expression of two different BDLPs. While it has been shown that *Nos*DLP forms homodimers, its GTPase activity was not at all affected by homo-oligomerization and/or lipid binding. Therefore, it has already been suggested that hetero-oligomerization with another, different BDLP might control the activity of this BDLP in a way, as observed in the case of eukaryotic DLPs (DeVay et al., 2009; Michie et al., 2014). Based on our analyses, the Tandem A representative of *N. punctiforme* is a likely candidate. Noteworthy, the sequences of the Tandem A and Tandem B cBDLPs differ substantially.

In the *HSR1 group* of cBDLPs, a potential protein of the HSR1 protein family is encoded downstream of the cBDLP. HSR1-releated proteins are not well-characterized GTP-binding proteins that, however, have no apparent GTPase enzymatic function (Finn et al., 2017). Thus, the cyanobacterial HSR1 proteins encoded adjacent of the cBDLPs potentially have a regulatory function. In the *chaperone group*, conserved proteins carrying a DnaK domain are encoded downstream of the respective cBLDP. DnaK proteins belong to the group of Hsp70 chaperones (Mayer and Bukau, 2005; Young, 2010; Mayer, 2013), and thus, here the activity of a membrane remodeling DLP is linked to the activity of an Hsp70 chaperone. In fact, membrane activity of Hsp70 members has been described in recent years (Armijo et al., 2014; Mahalka et al., 2014). In humans, selected Hsp70 proteins have been suggested to, e.g., carry immunogenic peptides for antigen presentation (Haug et al., 2005), and thus, DnaK-like proteins encoded in the vicinity of a cBDLP might be involved in protein sorting during membrane remodeling processes.

The remaining cBDLPs are not significantly related to one another and could not be further categorized (named *cBDLP* in **Figure 3**).

ARE (B)DLPs INVOLVED IN TM BIOGENESIS AND DYNAMICS IN CHLOROPLAST AND CYANOBACTERIA?

At least one DLP is present in chloroplasts and the activity of the FZL protein has been linked to membrane biogenesis and dynamics (Gao et al., 2006). As discussed before, DLPs are also encoded in cyanobacteria and at least the *Nos*DLP can remodel membranes resulting in membrane fission (Low et al., 2009). However, the exact *in vivo* function of (B)DLPs in chloroplasts and cyanobacteria still is enigmatic. Clearly, membrane disruption would be deleterious in chloroplasts as well as in cyanobacteria, e.g., disruption of TMs would result in a breakdown of the electrochemical gradient across the TM. Thus, it is feasible to propose a membrane protective function of the DLPs and a crucial role in the repair of ruptured membrane regions, as suggested, e.g., for the BDLP of *B. subtilis* (Sawant et al., 2016). However, in cyanobacteria different proteins and

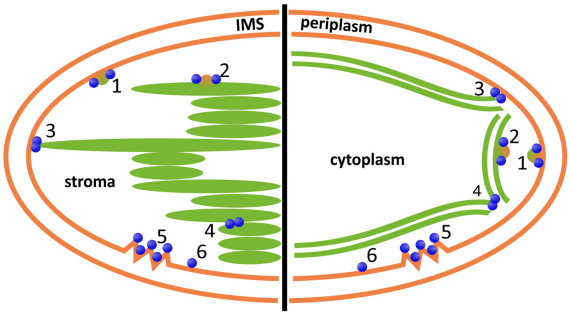

FIGURE 4 | Potential involvement of DLPs in chloroplast **(left)** and cyanobacterial **(right)** inner membrane dynamics. DLPs might be involved in vesicle formation, release or fusion at the chloroplast inner envelope or the cyanobacterial cytoplasmic membrane, respectively (1), or at the TMs (2); the fusion of the inner envelope or cytoplasmic membrane, respectively, with the TM system (3); and/or the fusion/constriction of individual TM layers (4). Moreover, DLPs are potentially involved in membrane repair (5) and/or membrane protection (6). IMS, inter membrane space. Note that DLPs located outside of the chloroplast, involving AtDRP5B/ARC5, are excluded.

systems are described that are suggested to be involved in membrane stabilization and membrane repair, involving small heat shock proteins and the PspA system (Torok et al., 2001; Nitta et al., 2005; Manganelli and Gennaro, 2017). Thus, the DLPs might have acquired additional functions in chloroplasts and cyanobacteria.

In recent years, evidence has accumulated indicating that membrane fusion and fission events are involved in TM development and dynamics in chloroplasts and cyanobacteria (Chuartzman et al., 2008; Kirchhoff et al., 2011; Herbstova et al., 2012; Nevo et al., 2012; Iwai et al., 2015). As spontaneous, uncontrolled membrane fusion would be deleterious to organisms, defined fusion and fission machineries likely control such remodeling processes (Chuartzman et al., 2008). However, proteins involved in membrane dynamics in chloroplast and cyanobacteria still need to be better characterized and more need to be identified. In bioinformatic analyses, several genes have been identified that code for putative chloroplast-localized proteins with homology to proteins involved in the secretory pathway, operating in the cytoplasm of eukaryotic cells, and some of these proteins are also conserved in cyanobacterial genomes (Nakai et al., 1993; Srivastava et al., 2005; Keller and Schneider, 2013; Khan et al., 2013; Paul et al., 2014). Nevertheless, potential involvement of these proteins in TM biogenesis and/or maintenance has only sparsely been shown experimentally yet, and it appears to be rather unlikely that vesicle fission and fusion is regulated identical in chloroplasts as in the secretory pathway. However, some of the identified (putative) membrane-active proteins might fulfill similar functions in chloroplasts as in the secretory pathway but work together with other, chloroplast- and cyanobacteria-specific proteins. Such chloroplast and cyanobacteria-specific proteins likely involve the recently identified Vipp1/IM30 protein (Kroll et al., 2001; Westphal et al., 2001), a protein that can fuse membranes in presence of Mg^{2+}, at least *in vitro* (Hennig et al., 2015). Moreover, IM30-depleted chloroplasts and cyanobacteria have a significantly reduced TM network (Kroll et al., 2001; Fuhrmann et al., 2009). Within the secretory pathway, several small GTPases are involved in vesicle formation and fission (Hutagalung and Novick, 2011; Barlowe and Miller, 2013), and involvement of the small GTPases AR1 and CPRabA5e in TM biogenesis has been shown in *A. thaliana* (Garcia et al., 2010; Karim et al., 2014). Since especially dynamin-like GTPases are directly associated with membrane remodeling processes in many eukaryotic organelles, it appears possible that DLPs are also involved in membrane biogenesis and/or remodeling processes in chloroplasts and cyanobacteria. In fact, FZL has been suggested to mediate contact of two adjacent membranes in *A. thaliana* chloroplasts, finally resulting in membrane fusion (Gao et al., 2006). The here presented analysis clearly demonstrates that DLPs are also highly abundant in cyanobacteria. However, thus far solely the DLP of the cyanobacterium *N. punctiforme* has been studied to some extent. The *in vitro* analyses clearly indicate that the protein behaves like the classical Dyn and thus might be involved in vesicle fission in cyanobacteria. Nevertheless, we initially expected to identify a prototypical cDLP in our analysis that is conserved in all cyanobacterial species. Surprisingly, we did not identify such a candidate; rather, while most cyanobacterial genomes encode at least one cDLP, the proteins belong to different clades. Thus, the sequences of cBDLPs are highly variable. While the exact physiological function of the cyanobacterial proteins is enigmatic, it is reasonable to assume that proteins with a membrane remodeling activity will be involved in membrane dynamics in chloroplasts and cyanobacteria. The exact physiological function of the proteins, i.e., their involvement in processes such as membrane protection, membrane repair, membrane fission and/or membrane fusion, however, still needs to be established. Nevertheless, the *in vivo* observation of FZL being involved in TM dynamics and vesicle fusion and the *in vitro* observation of *Nos*DLP behaving like the prototypical Dyn clearly indicates a crucial membrane-active role of DLPs in chloroplasts and cyanobacteria. Based on the described membrane activities of DLPs and on the need of membrane remodeling processes, in **Figure 4** we summarize a potential involvement of DLPs in chloroplasts and cyanobacteria. We hope this article will stimulate future research on the involvement of this membrane-active protein family in membrane dynamics in chloroplasts and cyanobacteria.

AUTHOR CONTRIBUTIONS

All authors listed have made a substantial, direct and intellectual contribution to the work and approved it for publication.

FUNDING

This work was funded by the Max Planck Graduate Center at the Max Planck Institutes and the University of Mainz (to RJ and DS) and by the Carl Trygger Foundation (HA).

SUPPLEMENTARY MATERIAL

The Supplementary Material for this article can be found online at: https://www.frontiersin.org/articles/10.3389/fpls.2018.00206/full#supplementary-material

DATA SHEET S1 | Cyanobacterial species.

REFERENCES

Adam, Z., Charuvi, D., Tsabari, O., Knopf, R. R., and Reich, Z. (2011). Biogenesis of thylakoid networks in angiosperms: knowns and unknowns. *Plant Mol. Biol.* 76, 221–234. doi: 10.1007/s11103-010-9693-5

Antonny, B., Burd, C., De Camilli, P., Chen, E., Daumke, O., Faelber, K., et al. (2016). Membrane fission by dynamin: what we know and what we need to know. *EMBO J.* 35, 2270–2284. doi: 10.15252/embj.201694613

Arimura, S., and Tsutsumi, N. (2002). A dynamin-like protein (ADL2b), rather than FtsZ, is involved in Arabidopsis mitochondrial division.

Proc. Natl. Acad. Sci. U.S.A. 99, 5727–5731. doi: 10.1073/pnas.082663299

Arimura, S. I., Aida, G. P., Fujimoto, M., Nakazono, M., and Tsutsumi, N. (2004). Arabidopsis dynamin-like protein 2a (ADL2a), like ADL2b, is involved in plant mitochondrial division. *Plant Cell Physiol.* 45, 236–242. doi: 10.1093/pcp/pch024

Armbruster, U., Labs, M., Pribil, M., Viola, S., Xu, W., Scharfenberg, M., et al. (2013). Arabidopsis CURVATURE THYLAKOID1 proteins modify thylakoid architecture by inducing membrane curvature. *Plant Cell* 25, 2661–2678. doi: 10.1105/tpc.113.113118

Armijo, G., Okerblom, J., Cauvi, D. M., Lopez, V., Schlamadinger, D. E., Kim, J., et al. (2014). Interaction of heat shock protein 70 with membranes depends on the lipid environment. *Cell Stress Chaperones* 19, 877–886. doi: 10.1007/s12192-014-0511-x

Backues, S. K., Korasick, D. A., Heese, A., and Bednarek, S. Y. (2010). The *Arabidopsis* dynamin-related protein2 family is essential for gametophyte development. *Plant Cell* 22, 3218–3231. doi: 10.1105/tpc.110.077727

Barlowe, C. K., and Miller, E. A. (2013). Secretory protein biogenesis and traffic in the early secretory pathway. *Genetics* 193, 383–410. doi: 10.1534/genetics.112.142810

Barthel, S., Bernát, G., Seidel, T., Rupprecht, E., Kahmann, U., and Schneider, D. (2013). Thylakoid membrane maturation and PSII activation are linked in greening Synechocystis sp. PCC 6803 cells. *Plant Physiol.* 163, 1037–1046. doi: 10.1104/pp.113.224428

Bednarek, S. Y., and Backues, S. K. (2010). Plant dynamin-related protein families DRP1 and DRP2 in plant development. *Biochem. Soc. Trans.* 38, 797–806. doi: 10.1042/BST0380797

Bonifacino, J. S. (2014). Vesicular transport earns a Nobel. *Trends Cell Biol.* 24, 3–5. doi: 10.1016/j.tcb.2013.11.001

Bramkamp, M. (2012). Structure and function of bacterial dynamin-like proteins. *Biol. Chem.* 393, 1203–1214. doi: 10.1515/hsz-2012-0185

Brown, E. A., and Hardwidge, P. R. (2007). Biochemical characterization of the enterotoxigenic *Escherichia coli* LeoA protein. *Microbiology* 153, 3776–3784. doi: 10.1099/mic.0.2007/009084-0

Bürmann, F., Ebert, N., van Baarle, S., and Bramkamp, M. (2011). A bacterial dynamin-like protein mediating nucleotide-independent membrane fusion. *Mol. Microbiol.* 79, 1294–1304. doi: 10.1111/j.1365-2958.2011.07523.x

Bustillo-Zabalbeitia, I., Montessuit, S., Raemy, E., Basañez, G., Terrones, O., and Martinou, J. C. (2014). Specific interaction with cardiolipin triggers functional activation of dynamin-related protein 1. *PLoS One* 9:e102738. doi: 10.1371/journal.pone.0102738

Chappie, J. S., Acharya, S., Liu, Y. W., Leonard, M., Pucadyil, T. J., and Schmid, S. L. (2009). An intramolecular signaling element that modulates dynamin function in vitro and in vivo. *Mol. Biol. Cell* 20, 3561–3571. doi: 10.1091/mbc.E09-04-0318

Chi, R. J., Liu, J., West, M., Wang, J., Odorizzi, G., and Burd, C. G. (2014). Fission of SNX-BAR-coated endosomal retrograde transport carriers is promoted by the dynamin-related protein Vps1. *J. Cell Biol.* 204, 793–806. doi: 10.1083/jcb.201309084

Chuartzman, S. G., Nevo, R., Shimoni, E., Charuvi, D., Kiss, V., Ohad, I., et al. (2008). Thylakoid membrane remodeling during state transitions in Arabidopsis. *Plant Cell* 20, 1029–1039. doi: 10.1105/tpc.107.055830

Collings, D. A., Gebbie, L. K., Howles, P. A., Hurley, U. A., Birch, R. J., Cork, A. H., et al. (2008). Arabidopsis dynamin-like protein DRP1A: a null mutant with widespread defects in endocytosis, cellulose synthesis, cytokinesis, and cell expansion. *J. Exp. Bot.* 59, 361–376. doi: 10.1093/jxb/erm324

Daumke, O., Lundmark, R., Vallis, Y., Martens, S., Butler, P. J. G., and McMahon, H. T. (2007). Architectural and mechanistic insights into an EHD ATPase involved in membrane remodelling. *Nature* 449, 923–927. doi: 10.1038/nature06173

Daumke, O., and Praefcke, G. J. K. (2016). Invited review: mechanisms of GTP hydrolysis and conformational transitions in the dynamin superfamily. *Biopolymers* 105, 580–593. doi: 10.1002/bip.22855

de Sousa Borges, A., and Scheffers, D. J. (2016). Bacterial dynamin as a membrane puncture repair kit. *Environ. Microbiol.* 18, 2298–2301. doi: 10.1111/1462-2920.13218

DeVay, R. M., Dominguez-Ramirez, L., Lackner, L. L., Hoppins, S., Stahlberg, H., and Nunnari, J. (2009). Coassembly of Mgm1 isoforms requires cardiolipin and mediates mitochondrial inner membrane fusion. *J. Cell Biol.* 186, 793–803. doi: 10.1083/jcb.200906098

Faelber, K., Gao, S., Held, M., Posor, Y., Haucke, V., Noé, F., et al. (2013). Oligomerization of dynamin superfamily proteins in health and disease. *Prog. Mol. Biol. Transl. Sci.* 117, 411–443. doi: 10.1016/B978-0-12-386931-9.00015-5

Finn, R. D., Attwood, T. K., Babbitt, P. C., Bateman, A., Bork, P., Bridge, A. J., et al. (2017). InterPro in 2017-beyond protein family and domain annotations. *Nucleic Acids Res.* 45, D190–D199. doi: 10.1093/nar/gkw1107

Finn, R. D., Bateman, A., Clements, J., Coggill, P., Eberhardt, R. Y., Eddy, S. R., et al. (2014). Pfam: the protein families database. *Nucleic Acids Res.* 42, D222–D230. doi: 10.1093/nar/gkt1223

Ford, M. G. J., Jenni, S., and Nunnari, J. (2011). The crystal structure of dynamin. *Nature* 477, 561–566. doi: 10.1038/nature10441

Frezza, C., Cipolat, S., Martins de Brito, O., Micaroni, M., Beznoussenko, G. V., Rudka, T., et al. (2006). OPA1 controls apoptotic cristae remodeling independently from mitochondrial fusion. *Cell* 126, 177–189. doi: 10.1016/j.cell.2006.06.025

Fröhlich, C., Grabiger, S., Schwefel, D., Faelber, K., Rosenbaum, E., Mears, J., et al. (2013). Structural insights into oligomerization and mitochondrial remodelling of dynamin 1-like protein. *EMBO J.* 32, 1280–1292. doi: 10.1038/emboj.2013.74

Fuhrmann, E., Gathmann, S., Rupprecht, E., Golecki, J., and Schneider, D. (2009). Thylakoid membrane reduction affects the photosystem stoichiometry in the cyanobacterium Synechocystis sp. PCC 6803. *Plant Physiol.* 149, 735–744. doi: 10.1104/pp.108.132373

Fujimoto, M., Arimura, S. I., Mano, S., Kondo, M., Saito, C., Ueda, T., et al. (2009). Arabidopsis dynamin-related proteins DRP3A and DRP3B are functionally redundant in mitochondrial fission, but have distinct roles in peroxisomal fission. *Plant J.* 58, 388–400. doi: 10.1111/j.1365-313X.2009.03786.x

Fujimoto, M., Arimura, S.-I., Ueda, T., Takanashi, H., Hayashi, Y., Nakano, A., et al. (2010). Arabidopsis dynamin-related proteins DRP2B and DRP1A participate together in clathrin-coated vesicle formation during endocytosis. *Proc. Natl. Acad. Sci. U.S.A.* 107, 6094–6099. doi: 10.1073/pnas.0913562107

Fujisawa, T., Narikawa, R., Maeda, S.-I., Watanabe, S., Kanesaki, Y., Kobayashi, K., et al. (2017). CyanoBase: a large-scale update on its 20th anniversary. *Nucleic Acids Res.* 45, D551–D554. doi: 10.1093/nar/gkw1131

Gao, H., Kadirjan-Kalbach, D., Froehlich, J. E., and Osteryoung, K. W. (2003). ARC5, a cytosolic dynamin-like protein from plants, is part of the chloroplast division machinery. *Proc. Natl. Acad. Sci. U.S.A.* 100, 4328–4333. doi: 10.1073/pnas.0530206100

Gao, H., Sage, T. L., and Osteryoung, K. W. (2006). FZL, an FZO-like protein in plants, is a determinant of thylakoid and chloroplast morphology. *Proc. Natl. Acad. Sci. U.S.A.* 103, 6759–6764. doi: 10.1073/pnas.0507287103

Gao, S., von der Malsburg, A., Paeschke, S., Behlke, J., Haller, O., Kochs, G., et al. (2010). Structural basis of oligomerization in the stalk region of dynamin-like MxA. *Nature* 465, 502–506. doi: 10.1038/nature08972

Gao, Y., Liu, H., An, C., Shi, Y., Liu, X., Yuan, W., et al. (2013). Arabidopsis FRS4/CPD25 and FHY3/CPD45 work cooperatively to promote the expression of the chloroplast division gene ARC5 and chloroplast division. *Plant J.* 75, 795–807. doi: 10.1111/tpj.12240

Garcia, C., Khan, N. Z., Nannmark, U., and Aronsson, H. (2010). The chloroplast protein CPSAR1, dually localized in the stroma and the inner envelope membrane, is involved in thylakoid biogenesis. *Plant J.* 63, 73–85. doi: 10.1111/j.1365-313X.2010.04225.x

Haug, M., Dannecker, L., Schepp, C. P., Kwok, W. W., Wernet, D., Buckner, J. H., et al. (2005). The heat shock protein Hsp70 enhances antigen-specific proliferation of human CD4+ memory T cells. *Eur. J. Immunol.* 35, 3163–3172. doi: 10.1002/eji.200535050

Hennig, R., Heidrich, J., Saur, M., Schmu, L., Roeters, S. J., Hellmann, N., et al. (2015). IM30 triggers membrane fusion in cyanobacteria and chloroplasts. *Nat. Commun.* 6:7018. doi: 10.1038/ncomms8018

Herbstova, M., Tietz, S., Kinzel, C., Turkina, M. V., and Kirchhoff, H. (2012). Architectural switch in plant photosynthetic membranes induced by light stress. *Proc. Natl. Acad. Sci. U.S.A.* 109, 20130–20135. doi: 10.1073/pnas.1214265109

Hermann, G. J., Thatcher, J. W., Mills, J. P., Hales, K. G., Fuller, M. T., Nunnari, J., et al. (1998). Mitochondrial fusion in yeast requires the transmembrane GTPase Fzo1p. *J. Cell Biol.* 143, 359–373. doi: 10.1083/jcb.143.2.359

Herrero, A., and Flores, E. (2008). *The Cyanobacteria: Molecular Biology, Genomics, and Evolution*. Poole: Caister Academic Press.

Heymann, J. A. W., and Hinshaw, J. E. (2009). Dynamins at a glance. *J. Cell Sci.* 122, 3427–3431. doi: 10.1242/jcs.051714

Hinshaw, J. E. (2000). Dynamin and its role in membrane fission. *Annu. Rev. Cell Dev. Biol.* 16, 483–519. doi: 10.1146/annurev.cellbio.16.1.483

Hinshaw, J. E., and Schmid, S. L. (1995). Dynamin self-assembles into rings suggesting a mechanism for coated vesicle budding. *Nature* 374, 190–192. doi: 10.1038/374190a0

Hohmann-Marriott, M. F., and Blankenship, R. E. (2011). Evolution of photosynthesis. *Annu. Rev. Plant Biol.* 62, 515–548. doi: 10.1146/annurev-arplant-042110-103811

Holtsmark, I., Lee, S., Lunde, K. A., Auestad, K., Maple-Grødem, J., and Møller, S. G. (2013). Plastid division control: The PDV proteins regulate DRP5B dynamin activity. *Plant Mol. Biol.* 82, 255–266. doi: 10.1007/s11103-013-0059-7

Hong, Z., Bednarek, S. Y., Blumwald, E., Hwang, I., Jurgens, G., Menzel, D., et al. (2003). A unified nomenclature for Arabidopsis dynamin-related large GTPases based on homology and possible functions. *Plant Mol. Biol.* 53, 261–265. doi: 10.1023/B:PLAN.0000007000.29697.81

Hu, J., Shibata, Y., Zhu, P. P., Voss, C., Rismanchi, N., Prinz, W. A., et al. (2009). A class of dynamin-like GTPases involved in the generation of the tubular ER network. *Cell* 138, 549–561. doi: 10.1016/j.cell.2009.05.025

Hutagalung, A. H., and Novick, P. J. (2011). Role of Rab GTPases in membrane traffic and cell physiology. *Physiol. Rev.* 91, 119–149. doi: 10.1152/physrev.00059.2009

Ingerman, E., Perkins, E. M., Marino, M., Mears, J. A., McCaffery, J. M., Hinshaw, J. E., et al. (2005). Dnm1 forms spirals that are structurally tailored to fit mitochondria. *J. Cell Biol.* 170, 1021–1027. doi: 10.1083/jcb.200506078

Iwai, M., Yokono, M., and Nakano, A. (2015). Visualizing structural dynamics of thylakoid membranes. *Sci. Rep.* 4:3768. doi: 10.1038/srep03768

Jensen, P. E., and Leister, D. (2014). Chloroplast evolution, structure and functions. *F1000Prime Rep.* 6:40. doi: 10.12703/P6-40

Kang, B. H., Busse, J. S., and Bednarek, S. Y. (2003). Members of the Arabidopsis dynamin-like gene family, ADL1, are essential for plant cytokinesis and polarized cell growth. *Plant Cell* 15, 899–913. doi: 10.1105/tpc.009670

Kang, B. H., Busse, J. S., Dickey, C., Rancour, D. M., and Bednarek, S. Y. (2001). The Arabidopsis cell plate-associated dynamin-like protein, ADL1Ap, is required for multiple stages of plant growth and development. *Plant Physiol.* 126, 47–68. doi: 10.1104/pp.126.1.47

Kang, S. G., Jin, J. B., Piao, H. L., Pih, K. T., Jang, H. J., Lim, J. H., et al. (1998). Molecular cloning of an Arabidopsis cDNA encoding a dynamin-like protein that is localized to plastids. *Plant Mol. Biol.* 38, 437–447. doi: 10.1023/A:1006099718761

Karim, S., Alezzawi, M., Garcia-Petit, C., Solymosi, K., Khan, N. Z., Lindquist, E., et al. (2014). A novel chloroplast localized Rab GTPase protein CPRabA5e is involved in stress, development, thylakoid biogenesis and vesicle transport in Arabidopsis. *Plant Mol. Biol.* 84, 675–692. doi: 10.1007/s11103-013-0161-x

Karim, S., and Aronsson, H. (2014). The puzzle of chloroplast vesicle transport - involvement of GTPases. *Front. Plant Sci.* 5:472. doi: 10.3389/fpls.2014.00472

Kearse, M., Moir, R., Wilson, A., Stones-Havas, S., Cheung, M., Sturrock, S., et al. (2012). Geneious basic: an integrated and extendable desktop software platform for the organization and analysis of sequence data. *Bioinformatics* 28, 1647–1649. doi: 10.1093/bioinformatics/bts199

Keller, R., and Schneider, D. (2013). Homologs of the yeast Tvp38 vesicle-associated protein are conserved in chloroplasts and cyanobacteria. *Front. Plant Sci.* 4:467. doi: 10.3389/fpls.2013.00467

Khan, N. Z., Lindquist, E., Aronsson, H., Preisinger, C., and Fuchs, E. (2013). New putative chloroplast vesicle transport components and cargo proteins revealed using a bioinformatics approach: an Arabidopsis model. *PLoS One* 8:e59898. doi: 10.1371/journal.pone.0059898

Kirchhoff, H., Hall, C., Wood, M., Herbstova, M., Tsabari, O., Nevo, R., et al. (2011). Dynamic control of protein diffusion within the granal thylakoid lumen. *Proc. Natl. Acad. Sci. U.S.A.* 108, 20248–20253. doi: 10.1073/pnas.1104141109

Kleine, T., Maier, U. G., and Leister, D. (2009). DNA transfer from organelles to the nucleus: the idiosyncratic genetics of endosymbiosis. *Annu. Rev. Plant Biol.* 60, 115–138. doi: 10.1146/annurev.arplant.043008.092119

Konopka, C. A., and Bednarek, S. Y. (2008). Comparison of the dynamics and functional redundancy of the Arabidopsis dynamin-related isoforms DRP1A and DRP1C during plant development. *Plant Physiol.* 147, 1590–1602. doi: 10.1104/pp.108.116863

Koshiba, T. (2004). Structural basis of mitochondrial tethering by mitofusin complexes. *Science* 305, 858–862. doi: 10.1126/science.1099793

Kroll, D., Meierhoff, K., Bechtold, N., Kinoshita, M., Westphal, S., Vothknecht, U. C., et al. (2001). VIPP1, a nuclear gene of *Arabidopsis thaliana* essential for thylakoid membrane formation. *Proc. Natl. Acad. Sci. U.S.A.* 98, 4238–4242. doi: 10.1073/pnas.061500998

Lauber, M. H., Waizenegger, I., Steinmann, T., Schwarz, H., Mayer, U., Hwang, I., et al. (1997). The Arabidopsis KNOLLE protein is a cytokinesis-specific syntaxin. *J. Cell Biol.* 139, 1485–1493. doi: 10.1083/jcb.139.6.1485

Legesse-Miller, A., Massol, R. H., and Kirchhausen, T. (2003). Constriction and Dnm1p recruitment are distinct processes in mitochondrial fission. *Mol. Biol. Cell* 14, 1953–1963. doi: 10.1091/mbc.E02-10-0657

Liberton, M., Austin, J. R., Berg, R. H., and Pakrasi, H. B. (2011a). Unique thylakoid membrane architecture of a unicellular N2-fixing Cyanobacterium revealed by electron tomography. *Plant Physiol.* 155, 1656–1666. doi: 10.1104/pp.110.165332

Liberton, M., Austin, J. R., Berg, R. H., and Pakrasi, H. B. (2011b). Insights into the complex 3-D architecture of thylakoid membranes in unicellular cyanobacterium Cyanothece sp. ATCC 51142. *Plant Signal. Behav.* 6, 566–569. doi: 10.4161/psb.6.4.14946

Lingard, M. J., Gidda, S. K., Bingham, S., Rothstein, S. J., Mullen, R. T., and Trelease, R. N. (2008). Arabidopsis PEROXIN11c-e, FISSION1b, and DYNAMIN-RELATED PROTEIN3A Cooperate in Cell Cycle-Associated Replication of Peroxisomes. *Plant Cell* 20, 1567–1585. doi: 10.1105/tpc.107.057679

Liu, L., Zhang, Z., Mei, Q., and Chen, M. (2013). PSI: a comprehensive and integrative approach for accurate plant subcellular localization prediction. *PLoS One* 8:e75826. doi: 10.1371/journal.pone.0075826

Low, H. H., and Löwe, J. (2006). A bacterial dynamin-like protein. *Nature* 444, 766–769. doi: 10.1038/nature05312

Low, H. H., Sachse, C., Amos, L. A., and Löwe, J. (2009). Structure of a bacterial dynamin-like protein lipid tube provides a mechanism for assembly and membrane curving. *Cell* 139, 1342–1352. doi: 10.1016/j.cell.2009.11.003

Lu, S., Jang, H., Gu, S., Zhang, J., and Nussinov, R. (2016). Drugging ras GTPase: a comprehensive mechanistic and signaling structural view. *Chem. Soc. Rev.* 45, 4929–4952. doi: 10.1039/C5CS00911A

Mahalka, A. K., Kirkegaard, T., Jukola, L. T. I., Jäättelä, M., and Kinnunen, P. K. J. (2014). Human heat shock protein 70 (Hsp70) as a peripheral membrane protein. *Biochim. Biophys. Acta* 1838, 1344–1361. doi: 10.1016/j.bbamem.2014.01.022

Manganelli, R., and Gennaro, M. L. (2017). Protecting from envelope stress: variations on the phage-shock-protein theme. *Trends Microbiol.* 25, 205–216. doi: 10.1016/j.tim.2016.10.001

Mano, S., Nakamori, C., Fukao, Y., Araki, M., Matsuda, A., Kondo, M., et al. (2011). A defect of peroxisomal membrane protein 38 causes enlargement of peroxisomes. *Plant Cell Physiol.* 52, 2157–2172. doi: 10.1093/pcp/pcr147

Martin, W., and Herrmann, R. G. (1998). Gene transfer from organelles to the nucleus: how much, what happens, and why? *Plant Physiol.* 118, 9–17. doi: 10.1104/pp.118.1.9

Martin, W., Rujan, T., Richly, E., Hansen, A., Cornelsen, S., Lins, T., et al. (2002). Evolutionary analysis of Arabidopsis, cyanobacterial, and chloroplast genomes reveals plastid phylogeny and thousands of cyanobacterial genes in the nucleus. *Proc. Natl. Acad. Sci. U.S.A.* 99, 12246–12251. doi: 10.1073/pnas.182432999

Mayer, M. P. (2013). Hsp70 chaperone dynamics and molecular mechanism. *Trends Biochem. Sci.* 38, 507–514. doi: 10.1016/j.tibs.2013.08.001

Mayer, M. P., and Bukau, B. (2005). Hsp70 chaperones: cellular functions and molecular mechanism. *Cell. Mol. Life Sci.* 62, 670–684. doi: 10.1007/s00018-004-4464-6

Mears, J. A., Lackner, L. L., Fang, S., Ingerman, E., Nunnari, J., and Hinshaw, J. E. (2011). Conformational changes in Dnm1 support a contractile mechanism for mitochondrial fission. *Nat. Struct. Mol. Biol.* 18, 20–26. doi: 10.1038/nsmb.1949

Meeusen, S. (2004). Mitochondrial fusion intermediates revealed in Vitro. *Science* 305, 1747–1752. doi: 10.1126/science.1100612

Meeusen, S., DeVay, R., Block, J., Cassidy-Stone, A., Wayson, S., McCaffery, J. M., et al. (2006). Mitochondrial inner-membrane fusion and crista maintenance requires the dynamin-related GTPase Mgm1. *Cell* 127, 383–395. doi: 10.1016/j.cell.2006.09.021

Michie, K. A., Boysen, A., Low, H. H., Møller-Jensen, J., and Löwe, J. (2014). LeoA, B and C from enterotoxigenic *Escherichia coli* (ETEC) are bacterial dynamins. *PLoS One* 9:e107211. doi: 10.1371/journal.pone.0107211

Mitchell, P. S., Emerman, M., and Malik, H. S. (2013). An evolutionary perspective on the broad antiviral specificity of MxA. *Curr. Opin. Microbiol.* 16, 493–499. doi: 10.1016/j.mib.2013.04.005

Miyagishima, S., Froehlich, J. E., and Osteryoung, K. W. (2006). PDV1 and PDV2 mediate recruitment of the dynamin-related protein ARC5 to the plastid division site. *Plant Cell* 18, 2517–2530. doi: 10.1105/tpc.106.045484

Miyagishima, S., Kuwayama, H., Urushihara, H., and Nakanishi, H. (2008). Evolutionary linkage between eukaryotic cytokinesis and chloroplast division by dynamin proteins. *Proc. Natl. Acad. Sci. U.S.A.* 105, 15202–15207. doi: 10.1073/pnas.0802412105

Morré, D. J., Selldén, G., Sundqvist, C., and Sandelius, A. S. (1991). Stromal low temperature compartment derived from the inner membrane of the chloroplast envelope. *Plant Physiol.* 97, 1558–1564. doi: 10.1104/pp.97.4.1558

Muehlethaler, K., and Frey-Wyssling, A. (1959). Development and structure of proplastids. *J. Biophys. Biochem. Cytol.* 6, 507–512.

Nakai, M., Sugita, D., Omata, T., and Endo, T. (1993). Sec-Y protein is localized in both the cytoplasmic and thylakoid membranes in the Cyanobacterium Synechococcus PCC7942. *Biochem. Biophys. Res. Commun.* 193, 228–234. doi: 10.1006/BBRC.1993.1613

Nakamura, Y., Kaneko, T., Hirosawa, M., Miyajima, N., and Tabata, S. (1998). CyanoBase, a www database containing the complete nucleotide sequence of the genome of Synechocystis sp. strain PCC6803. *Nucleic Acids Res.* 26, 63–67. doi: 10.1093/nar/26.1.63

Nantais, D. E., Schwemmle, M., Stickney, J. T., Vestal, D. J., and Buss, J. E. (1996). Prenylation of an interferon-gamma-induced GTP-binding protein: the human guanylate binding protein, huGBP1. *J. Leukoc. Biol.* 60, 423–431. doi: 10.1002/jlb.60.3.423

Nevo, R., Charuvi, D., Shimoni, E., Schwarz, R., Kaplan, A., Ohad, I., et al. (2007). Thylakoid membrane perforations and connectivity enable intracellular traffic in cyanobacteria. *EMBO J.* 26, 1467–1473. doi: 10.1038/sj.emboj.7601594

Nevo, R., Charuvi, D., Tsabari, O., and Reich, Z. (2012). Composition, architecture and dynamics of the photosynthetic apparatus in higher plants. *Plant J.* 70, 157–176. doi: 10.1111/j.1365-313X.2011.04876.x

Nickelsen, J., Rengstl, B., Stengel, A., Schottkowski, M., Soll, J., and Ankele, E. (2011). Biogenesis of the cyanobacterial thylakoid membrane system - an update. *FEMS Microbiol. Lett.* 315, 1–5. doi: 10.1111/j.1574-6968.2010.02096.x

Nitta, K., Suzuki, N., Honma, D., Kaneko, Y., and Nakamoto, H. (2005). Ultrastructural stability under high temperature or intensive light stress conferred by a small heat shock protein in cyanobacteria. *FEBS Lett.* 579, 1235–1242. doi: 10.1016/j.febslet.2004.12.095

Orso, G., Pendin, D., Liu, S., Tosetto, J., Moss, T. J., Faust, J. E., et al. (2010). Homotypic fusion of ER membranes requires the dynamin-like GTPase Atlastin. *Nature* 464, 942–942. doi: 10.1038/nature08886

Park, J. M., Cho, J. H., Kang, S. G., Jang, H. J., Pih, K. T., Piao, H. L., et al. (1998). A dynamin-like protein in *Arabidopsis thaliana* is involved in biogenesis of thylakoid membranes. *EMBO J.* 17, 859–867. doi: 10.1093/emboj/17.4.859

Park, J. M., Kang, S. G., Pih, K. T., Jang, H. J., Piao, H. L., Yoon, H. W., et al. (1997). A dynamin-like protein, ADL1, is present in membranes as a high-molecular -mass complex in Arabidopsis thaliana. *Plant Physiol.* 115, 763–771. doi: 10.1104/pp.115.2.763

Paul, P., Simm, S., Mirus, O., Scharf, K. D., Fragkostefanakis, S., and Schleiff, E. (2014). The complexity of vesicle transport factors in plants examined by orthology search. *PLoS One* 9:e97745. doi: 10.1371/journal.pone.0097745

Praefcke, G. J. K., and McMahon, H. T. (2004). The dynamin superfamily: universal membrane tubulation and fission molecules? *Nat. Rev. Mol. Cell Biol.* 5, 133–147. doi: 10.1038/nrm1313

Pyke, K. A., and Leech, R. M. (1994). A genetic analysis of chloroplast division and expansion in *Arabidopsis thaliana*. *Plant Physiol.* 104, 201–207. doi: 10.1104/pp.110.160382

Rast, A., Heinz, S., and Nickelsen, J. (2015). Biogenesis of thylakoid membranes. *Biochim. Biophys. Acta* 1847, 821–830. doi: 10.1016/j.bbabio.2015.01.007

Reubold, T. F., Faelber, K., Plattner, N., Posor, Y., Ketel, K., Curth, U., et al. (2015). Crystal structure of the dynamin tetramer. *Nature* 525, 404–408. doi: 10.1038/nature14880

Santel, A., and Fuller, M. T. (2001). Control of mitochondrial morphology by a human mitofusin. *J. Cell Sci.* 114, 867–874.

Sawant, P., Eissenberger, K., Karier, L., Mascher, T., and Bramkamp, M. (2016). A dynamin-like protein involved in bacterial cell membrane surveillance under environmental stress. *Environ. Microbiol.* 18, 2705–2720. doi: 10.1111/1462-2920.13110

Schlimpert, S., Wasserstrom, S., Chandra, G., Bibb, M. J., Findlay, K. C., Flärdh, K., et al. (2017). Two dynamin-like proteins stabilize FtsZ rings during *Streptomyces* sporulation. *Proc. Natl. Acad. Sci. U.S.A.* 114, E6176–E6183. doi: 10.1073/pnas.1704612114

Schumacher, B., and Staeheli, P. (1998). Domains mediating intramolecular folding and oligomerization of MxA GTPase. *J. Biol. Chem.* 273, 28365–28370. doi: 10.1074/jbc.273.43.28365

Shah, C., Hegde, B. G., Morén, B., Behrmann, E., Mielke, T., Moenke, G., et al. (2014). Structural insights into membrane interaction and caveolar targeting of dynamin-like EHD2. *Structure* 22, 409–420. doi: 10.1016/j.str.2013.12.015

Shpetner, H. S., and Vallee, R. B. (1989). Identification of dynamin, a novel mechanochemical enzyme that mediates interactions between microtubules. *Cell* 59, 421–432. doi: 10.1016/0092-8674(89)90027-5

Smaczynska-de Rooij, I. I., Allwood, E. G., Aghamohammadzadeh, S., Hettema, E. H., Goldberg, M. W., and Ayscough, K. R. (2010). A role for the dynamin-like protein Vps1 during endocytosis in yeast. *J. Cell Sci.* 123, 3496–3506. doi: 10.1242/jcs.070508

Smirnova, E., Griparic, L., Shurland, D.-L., and van der Bliek, A. M. (2001). Dynamin-related protein Drp1 is required for mitochondrial division in mammalian cells. *Mol. Biol. Cell* 12, 2245–2256. doi: 10.1091/mbc.12.8.2245

Song, B. D., Leonard, M., and Schmid, S. L. (2004). Dynamin GTPase domain mutants that differentially affect GTP binding, GTP hydrolysis, and clathrin-mediated endocytosis. *J. Biol. Chem.* 279, 40431–40436. doi: 10.1074/jbc.M407007200

Srivastava, R., Pisareva, T., and Norling, B. (2005). Proteomic studies of the thylakoid membrane of Synechocystis sp. PCC 6803. *Proteomics* 5, 4905–4916. doi: 10.1002/pmic.200500111

Staeheli, P., Haller, O., Boll, W., Lindenmann, J., and Weissmann, C. (1986). Mx protein: Constitutive expression in 3T3 cells transformed with cloned Mx cDNA confers selective resistance to influenza virus. *Cell* 44, 147–158. doi: 10.1016/0092-8674(86)90493-9

Tanz, S. K., Kilian, J., Johnsson, C., Apel, K., Small, I., Harter, K., et al. (2012). The SCO2 protein disulphide isomerase is required for thylakoid biogenesis and interacts with LCHB1 chlorophyll a/b binding proteins which affects chlorophyll biosynthesis in Arabidopsis seedlings. *Plant J.* 69, 743–754. doi: 10.1111/j.1365-313X.2011.04833.x

Torok, Z., Goloubinoff, P., Horvath, I., Tsvetkova, N. M., Glatz, A., Balogh, G., et al. (2001). Synechocystis HSP17 is an amphitropic protein that stabilizes heat-stressed membranes and binds denatured proteins for subsequent chaperone-mediated refolding. *Proc. Natl. Acad. Sci. U.S.A.* 98, 3098–3103. doi: 10.1073/pnas.051619498

Ugarte-Uribe, B., Müller, H. M., Otsuki, M., Nickel, W., and García-Sáez, A. J. (2014). Dynamin-related protein 1 (Drp1) promotes structural intermediates of membrane division. *J. Biol. Chem.* 289, 30645–30656. doi: 10.1074/jbc.M114.575779

Vestal, D. J., and Jeyaratnam, J. A. (2011). The guanylate-binding proteins: emerging insights into the biochemical properties and functions of this family of large interferon-induced guanosine triphosphatase. *J. Interfereon Cytokine Res.* 31, 89–97. doi: 10.1089/jir.2010.0102

Wang, Q., Sullivan, R. W., Kight, A., Henry, R. L., Huang, J., Jones, A. M., et al. (2004). Deletion of the chloroplast-localized Thylakoid formation1 gene product in Arabidopsis leads to deficient thylakoid formation and variegated leaves. *Plant Physiol.* 136, 3594–3604. doi: 10.1104/pp.104.049841

Westphal, S., Heins, L., Soll, J., and Vothknecht, U. C. (2001). Vipp1 deletion mutant of Synechocystis: a connection between bacterial phage shock and thylakoid biogenesis? *Proc. Natl. Acad. Sci. U.S.A.* 98, 4243–4248. doi: 10.1073/pnas.061501198

Yoshinari, A., Fujimoto, M., Ueda, T., Inada, N., Naito, S., and Takano, J. (2016). DRP1-dependent endocytosis is essential for polar localization and boron-induced degradation of the borate transporter BOR1 in *Arabidopsis thaliana*. *Plant Cell Physiol.* 57, 1985–2000. doi: 10.1093/pcp/pcw121

Young, J. C. (2010). Mechanisms of the Hsp70 chaperone system. *Biochem. Cell Biol.* 88, 291–300. doi: 10.1139/o09-175

Zhang, X., and Hu, J. (2009). Two small protein families, DYNAMIN-RELATED PROTEIN3 and FISSION1, are required for peroxisome fission in Arabidopsis. *Plant J.* 57, 146–159. doi: 10.1111/j.1365-313X.2008.03677.x

Zhang, X., and Hu, J. (2010). The Arabidopsis chloroplast division protein DYNAMIN-RELATED PROTEIN5B also mediates peroxisome division. *Plant Cell* 22, 431–442. doi: 10.1105/tpc.109.071324

Zheng, J., Cahill, S. M., Lemmon, M. A., Fushman, D., Schlessinger, J., and Cowburn, D. (1996). Identification of the binding site for acidic phospholipids on the PH domain of dynamin: implications for stimulation of GTPase activity. *J. Mol. Biol.* 255, 14–21. doi: 10.1006/jmbi.1996.0002

Conflict of Interest Statement: The authors declare that the research was conducted in the absence of any commercial or financial relationships that could be construed as a potential conflict of interest.

Advantages of publishing in Frontiers

OPEN ACCESS
Articles are free to read for greatest visibility and readership

FAST PUBLICATION
Around 90 days from submission to decision

HIGH QUALITY PEER-REVIEW
Rigorous, collaborative, and constructive peer-review

TRANSPARENT PEER-REVIEW
Editors and reviewers acknowledged by name on published articles

Frontiers
Avenue du Tribunal-Fédéral 34
1005 Lausanne | Switzerland

Visit us: www.frontiersin.org
Contact us: info@frontiersin.org | +41 21 510 17 00

REPRODUCIBILITY OF RESEARCH
Support open data and methods to enhance research reproducibility

DIGITAL PUBLISHING
Articles designed for optimal readership across devices

FOLLOW US
@frontiersin

IMPACT METRICS
Advanced article metrics track visibility across digital media

EXTENSIVE PROMOTION
Marketing and promotion of impactful research

LOOP RESEARCH NETWORK
Our network increases your article's readership